UNCLASSIFIED

AD NUMBER
AD384924
CLASSIFICATION CHANGES
TO: **UNCLASSIFIED**
FROM: **CONFIDENTIAL**
LIMITATION CHANGES
TO: **Approved for public release; distribution is unlimited.**
FROM: **Distribution authorized to U.S. Gov't. agencies only; Administrative/Operational Use; AUG 1967. Other requests shall be referred to U.S. Army Aviation Materiel Laboratories, Fort Eustis, VA.**
AUTHORITY
USAAML Notice dtd 17 Oct 1968; USAAML ltr dtd 12 Feb 1971

THIS PAGE IS UNCLASSIFIED

UNCLASSIFIED

AD 384924

AD

USAAVLABS TECHNICAL REPORT 67-30
ELEMENT DESIGN AND DEVELOPMENT OF SMALL CENTRIFUGAL COMPRESSOR (U)
VOLUME II

By
A. D. Welliver
J. Acurio

August 1967

U. S. ARMY AVIATION MATERIEL LABORATORIES
FORT EUSTIS, VIRGINIA

CONTRACT DA 44-177-AMC-173(T)
THE BOEING COMPANY
SEATTLE, WASHINGTON

This material contains information affecting the national defense of the United States within the meaning of the Espionage Laws (18 U.S.C. 793 and 794), the transmission

Downgraded from CONFIDENTIAL to UNCLASSIFIED and will appear in TAB 69-5 dated 1 March 1969 (cited in letter from DDC-TS dated 23 January 1969)

Fred J. Galante
Fred J. Galante PFS 24 January 1969

In addition to security requirements which apply to this document and must be met, each transmittal outside the agencies of the US Government must have prior approval of US Army Aviation Materiel Laboratories, Fort Eustis, Virginia 23604.

UNCLASSIFIED

Copy 10 of 96 Copies

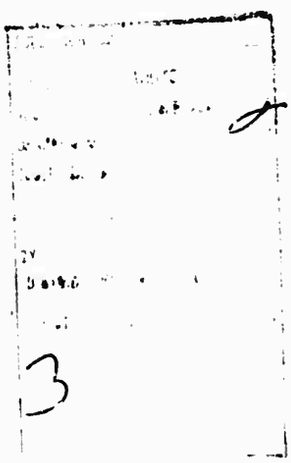
Disclaimers

When Government drawings, specifications, or other data are used for any purpose other than in connection with a definitely related Government procurement operation, the United States Government thereby incurs no responsibility nor any obligation whatsoever; and the fact that the Government may have formulated, furnished, or in any way supplied the said drawings, specifications, or other data is not to be regarded by implication or otherwise as in any manner licensing the holder or any other person or corporation, or conveying any rights or permission, to manufacture, use, or sell any patented invention that may in any way be related thereto.

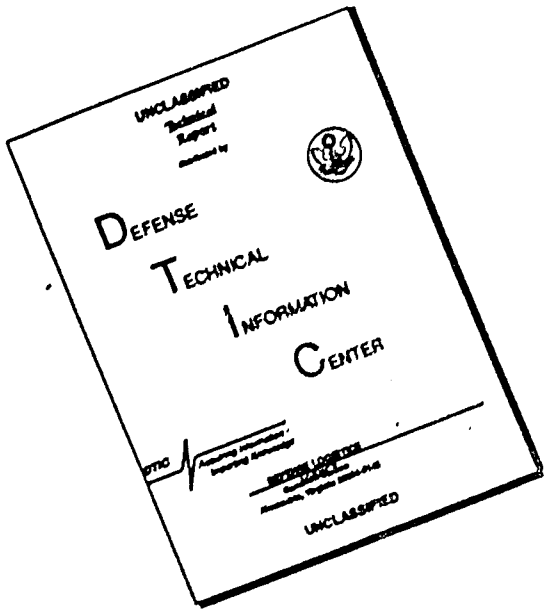
Trade names cited in this report do not constitute an official endorsement or approval of the use of such commercial hardware or software.

Disposition Instructions

When this report is no longer needed, Department of the Army organizations will destroy it in accordance with the procedures given in AR 380-5.



DISCLAIMER NOTICE



THIS DOCUMENT IS BEST QUALITY AVAILABLE. THE COPY FURNISHED TO DTIC CONTAINED A SIGNIFICANT NUMBER OF PAGES WHICH DO NOT REPRODUCE LEGIBLY.

UNCLASSIFIED

DEPARTMENT OF THE ARMY
U. S. ARMY AVIATION MATERIEL LABORATORIES
FORT EUSTIS, VIRGINIA 23604

(U) This Command has reviewed this report and concurs with the conclusions contained herein. The findings and recommendations as outlined in this report will be further considered and defined in a subsequent research report entitled "Design and Development of Small, Single-Stage Centrifugal Compressor."

MISSING PAGE NUMBERS ARE BLANK

UNCLASSIFIED

UNCLASSIFIED

Task 1M121401D14413
Contract DA-44-177-AMC-173(T)
USAAVLABS Technical Report 67-30
August 1967
TR-67-30-Vol-2
50 pp

ELEMENT DESIGN AND DEVELOPMENT OF SMALL CENTRIFUGAL COMPRESSOR (U).

VOLUME II

(Final Report)

D4-3434-Vol-2

by

A. D. Welliver and
J. Acurio

Prepared by

The Boeing Company
Seattle, Washington

This material contains information affecting the national defense of the United States within the meaning of the Espionage Laws (18 U.S.C. 793 and 794), the transmission or revelation of which in any manner to an unauthorized person is prohibited by law.

for

U. S. ARMY AVIATION MATERIEL LABORATORIES

FORT EUSTIS, VIRGINIA

In addition to security requirements which apply to this document and must be met, each transmittal outside the agencies of the US Government must have prior approval of US Army Aviation Materiel Laboratories, Fort Eustis, Virginia 23604.

UNCLASSIFIED

Downgraded 3 years
declassified after 12 years
DoD Dir 5200.10

UNCLASSIFIED

UNCLASSIFIED

Individual pages of Appendixes I and X are unclassified; however, when compiled in complete appendixes, such material is classified as confidential.

UNCLASSIFIED

UNCLASSIFIED

(U) CONTENTS

Appendix		Page
I	IMPELLER RADIAL-EQUILIBRIUM DESIGN.	1
	1.0 General Information	2
	1.1 Purpose	2
	1.2 Assumptions	2
	1.3 Limitations	2
	2.0 Procedure	3
	2.1 Nomenclature	3
	2.2 Method	12
	2.3 Results	37
	3.0 Input Preparation and Output Description	38
	3.1 Input-Data Preparation	38
	3.2 Output Description	44
	3.3 Sample Case	45
	4.0 Operating Information	45
	4.1 Program and Data Setup	45
	4.2 Run Information	62
	5.0 Programming Information	64
	5.1 Flow Diagrams	64
	5.2 Program Routines	78
	5.3 Program Listing	80

CONTENTS (Continued)

Appendix		Page
II	IMPELLER STRESS AND VIBRATION ANALYSIS.	125
	1.0 Discussion	130
	2.0 MF-1 Impeller Analysis	134
	3.0 MF-2 Impeller Analysis	144
	4.0 MF-3 Impeller Analysis	156
	5.0 RF-1 Impeller Analysis	168
	6.0 Workhorse Impeller Analysis	178
III	TEST-RIG DEVELOPMENT	187
	1.0 Introduction	190
	2.0 Diffuser Test Sections	190
	2.1 Bearing System	190
	2.2 Rotor Dynamics Analysis	195
	2.3 Modifications	200
	2.4 Conclusions	202
	3.0 Impeller Test Sections	202
	3.1 Bearing System	202
	3.2 Rotor Dynamics Analyses	206
	3.3 Modifications	209
	3.4 Conclusions	216

CONTENTS (Continued)

Appendix		Page
IV	SPIN-PIT TESTING	219
	1.0 Background and Introduction	220
	2.0 Boeing Spin-Pit Facility	220
	3.0 Impeller Spin Tests	221
	4.0 Discussion	223
	4.1 Residual Imbalance	223
	4.2 Impeller-To-Shaft Fit	224
	4.3 Axial Clamping Load	224
	4.4 Extraneous Excitations	224
	5.0 Conclusions and Recommendations	233
V	MODAL BALANCE	235
	1.0 General Information	237
	2.0 Instrumentation	238
	3.0 Procedure	238
	3.1 Trial and Error Method	238
	3.2 Analytical Method	244
VI	VIBRATORY-STRESS TEST OF WORKHORSE IMPELLER	247
	1.0 Summary	249
	2.0 Discussion	249

CONTENTS (Continued)

Appendix		Page
	2.1 Rig Components and Instrumentation Equipment	249
	2.2 Procedure	250
	2.3 Results	260
	3.0 Conclusions	263
VII	WAKE INTERACTION EFFECTS AND PERFORMANCE CHARACTERISTICS OF STAGNATION-TYPE THERMOCOUPLE	267
	1.0 Summary, Conclusions, and Outline of Analysis	271
	1.1 Summary	271
	1.2 Recommendations and Conclusions	271
	1.3 Outline of Analysis	271
	2.0 Steady-State Probe Behavior	272
	2.1 Conclusions	281
	2.2 Recommendations	281
	3.0 Equilibrium Temperature of an Isolated Probe in a High-Frequency Intermittent Flow	282
	3.1 The Effect of High-Frequency Fluctuations	282
	3.2 The Low-Velocity Heat-Transfer Problem — Energy-Balance Relations	285
	3.3 Estimate of the Jet- and Wake-Flow Conditions Affecting the Temperature-Measuring Problem	289
	3.4 The Effect of Velocity Fluctuations on the Heat-Transfer Coefficient	289

CONTENTS (Continued)

Appendix — Page

3.5 The Effect of Fluctuations in the Angle of Incidence of the Stream 290

3.6 The High-Velocity Heat-Transfer Problem 290

3.7 Simplifications Based on $h_1 = h_2$ and $\rho_1 V_1 = \rho_2 V_2$ . . . 292

4.0 The Effect of Wake Fluid Entrainment and Probe Position . . 292

VIII INSTRUMENTATION RESEARCH 299

1.0 Introduction 301

1.1 Objective 301

1.2 Scope 301

2.0 Measurement of Blade-to-Shroud Running Clearance . . . 301

2.1 Goals 301

2.2 Research and Development Effort 301

3.0 Measurement of Total Pressure in the Presence of Unsteady Flow. 311

3.1 Goals 311

3.2 Research Effort 311

4.0 Measurement of Torque at Rotational Speeds to 60,000 RPM . . 319

4.1 Research Effort 319

4.2 Conclusions 321

5.0 Accurate Measurement of Total Temperature in Compressor Diffuser Passages 322

5.1 Research Effort 322

5.2 Conclusions 330

CONTENTS (Continued)

Appendix		Page
IX	COMPUTER PRINTOUT OF DIFFUSER DATA — STATIC PRESSURES	335
X	SCHLIEREN PHOTOGRAPHS	379
	1.0 Objectives	380
	2.0 Method	380
	3.0 Results	384
XI	INLET-MACH-NUMBER EFFECTS ON SUBSONIC DIFFUSER PERFORMANCE	417
	1.0 Literature Surveys of Subsonic Diffusers	419
	2.0 Evaluation of Inlet-Mach-Number Effects	419
	2.1 Effect of Inlet Mach Number on Group A Diffusers	423
	2.2 Effect of Inlet Mach Number on Group B Diffusers	423
	2.3 Effect of Inlet Mach Number on Group C Diffusers	426
	3.0 Summary	426
XII	STRAIGHT DIFFUSER PERFORMANCE AT HIGH INLET MACH NUMBERS	429
	1.0 Introduction	432
	2.0 Experimental Procedure	436
	2.1 Geometrical Parameters	437
	2.2 Flow Parameters	443

CONTENTS (Continued)

Appendix		Page
	2.3 Flow Measurements	444
	2.4 Flow Unsteadiness	452
3.0	Results and Discussion	452
	3.1 C_p Versus Inlet Mach Number	453
	3.2 C_p Supercritical Flow Conditions	463
	3.3 Comparison of Present Data with Low Mach Number Data of Reneau — C_p Versus 2θ	463
	3.4 C_p Versus B and Aspect Ratio at High Inlet Mach Numbers	467
4.0	Recommendations	472
	4.1 High Mach Number Diffuser Map	472
	4.2 Low Mach Number Data	472
	4.3 Resolving Unsteady Character of Mass Flow Rate	473
	4.4 Inlet Boundary-Layer Velocity Profile	473
5.0	Uncertainty Analysis	473
6.0	Conclusions	477

(U) LIST OF ILLUSTRATIONS

Figure		Page
	APPENDIX I	
1	Impeller Meridional View	13
2	Angle Sign Conventions	14
	APPENDIX II	
3	Blade and Disk Metal Temperature Calculations	131
4	Goodman Diagram	133
5	Disk and Blade Profile of MF-1	135
6	Temperature Distribution of MF-1	135
7	Natural Frequencies of MF-1 Blades	136
8	Campbell Diagram for MF-1	137
9	Blade Stress Calculations for MF-1	138
10	MF-1 Impeller-Blade Force, Weight, and Inertia	139
11	Blade-Root Stress, Temperature, and Safety Factor for MF-1	140
12	Impeller Flow Area of MF-1	141
13	Disk Calculations for MF-1	143
14	Disk and Blade Profile of MF-2	145
15	Temperature Distribution of MF-2	145
16	Natural Frequencies of MF-2 Blades	146
17	Revised Natural Frequencies of MF-2 Blades	147
18	Campbell Diagram for MF-2	148
19	Blade Stress Calculations for MF-2	149

LIST OF ILLUSTRATIONS (Continued)

Figure		Page
20	MF-2 Impeller-Blade Force, Weight, and Inertia	150
21	Blade-Root Stress, Temperature, and Safety Factor for MF-2	151
22	Impeller Flow Area of MF-2	153
23	Disk Calculations for MF-2	155
24	Disk and Blade Profile of MF-3	157
25	Temperature Distribution of MF-3	157
26	Natural Frequencies of MF-3 Blades	158
27	Natural Frequencies of Modified MF-3 Blades	159
28	Campbell Diagram for MF-3	160
29	Blade Stress Calculations for MF-3	161
30	MF-3 Impeller-Blade Force, Weight, and Inertia	162
31	Blade-Root Stress, Temperature, and Safety Factor for MF-3	163
32	Impeller Flow Area of MF-3	165
33	Disk Calculations for MF-3	167
34	Disk and Blade Profile of RF-1	169
35	Temperature Distribution of RF-1	169
36	Natural Frequencies of RF-1 Blades	170
37	Campbell Diagram for RF-1	171
38	Blade Stress Calculations of RF-1	172
39	RF-1 Impeller-Blade Force, Weight, and Inertia	173
40	Blade-Root Stress, Temperature, and Safety Factor for RF-1	174

LIST OF ILLUSTRATIONS (Continued)

Figure		Page
41	Impeller Flow Area of RF-1	175
42	Disk Calculations for RF-1	177
43	Disk and Blade Profile of Workhorse Impeller	179
44	Temperature Distribution of Workhorse Impeller	180
45	Natural Frequencies of Workhorse Impeller Blades	181
46	Campbell Diagram for Workhorse Impeller	182
47	Blade Stress Calculations for Workhorse Impeller	183
48	Workhorse Impeller-Blade Force, Weight, and Inertia	184
49	Blade-Root Stress, Temperature, and Safety Factor for Workhorse Impeller	185
50	Disk Calculations for Workhorse Impeller	186
	APPENDIX III	
51	Variation of Speed Ratio with Sommerfeld Number for Full-Floating Journal Bearing	194
52	Bearing Stiffness Versus Rotor Speed	198
53	Shaft Mode Shapes	199
54	Diffuser Rig Rotor System	201
55	Impeller Shaft Arrangements	203
56	MF-1 Rotor Force Diagram	205
57	MF-2 Rotor Force Diagram	207
58	Critical Speed Versus Bearing Stiffness	208
59	MF-1 Vibration Levels	210

Figure		Page
60	MF-1 Clearance Changes	212
61	Effects of Viscous Damping	213
	APPENDIX IV	
62	Spin-Pit Facility	220
63	MF-2 Impeller (Spin-Pit Installation)	222
64	MF-2 Impeller (Spin-Pit Speed Record)	225
65	Spin-Pit Drive Quill Shaft After Attempted Proof Spin of Impeller MF-2	226
66	Spin-Pit Drive Turbine Lower Bearing After Attempted Proof Spin of Impeller MF-2	227
67	Impeller MF-2 After Attempted Proof Spin	229
68	Upper (Rear) Face of Impeller MF-2 After Attempted Proof Spin	230
69	Broken Arbor at the Upper End of Impeller MF-2 After Attempted Proof Spin	231
70	Broken Arbor at the Lower End of Impeller MF-2 After Attempted Proof Spin	232
	APPENDIX V	
71	Shaft-Bending Schematic	238
72	Proximity Probe	239
73	Proximity-Probe Installation	240
74	Amplitude-Phase Relationship	241
75	Typical Modal-Balance Weights	242

Figure		Page
76	Impeller With Modal-Balance Weight	243
77	Shaft-Displacement Sketch	245
78	Phase Angle Versus Rotational Speed	245
79	Shaft-Displacement Diagram	245
	APPENDIX VI	
80	Bench-Test Strain-Gage Locations	253
81	Campbell Diagram	256
82	Maximum Vibratory-Stress Points	257
83	Rig-Test Strain-Gage Locations	258
84	Test Equipment Instrumentation	259
85	Data Reduction Method	261
86	Expanded Oscillograph Trace	262
87	Campbell Diagram	264
88	Compressor Map	265
	APPENDIX VII	
89	Sketch of Temperature Probe	272
90	Variation in Overall Probe-Recovery Factor	278
91	Annular-Control Volume (Jet and Wake)	295

LIST OF ILLUSTRATIONS (Continued)

Figure		Page
	APPENDIX VIII	
92	Gated-Beam Proximity Detection System (Schematic Diagram)	303
93	Detail of Water-Cooled Sensor Adapter	305
94	Eddy-Current Clearance-Probe Data	309
95	Actuated Rub Sensor Data and Eddy-Current Clearance-Probe Data	310
96	Rectangular-Wave Pressure Pulsation	312
97	Effect of Pressure Pulse Shape on Root-Mean Balance Pressure	314
98	Pressure Probes Tested	316
99	Supersonic Duct (Temperature-Recovery Calibration Facility)	323
100	Temperature Recovery Data	325
101	Temperature Probes	326
102	Slotted-Shield Total-Temperature-Probe Data	327
103	Miniature Total-Temperature-Probe Data	328
104	Total-Temperature-Probe Mounting Tower	329
	APPENDIX IX	
105	Test Points	336
106	Diffuser Static-Pressure Instrumentation, DI-1	341
107	Diffuser Static-Pressure Instrumentation, DI-1	345
108	Diffuser Static-Pressure Instrumentation, DI-1	349

LIST OF ILLUSTRATIONS (Continued)

Figure		Page
109	Diffuser Static-Pressure Instrumentation, DI-1-2 . . .	353
110	Diffuser Static-Pressure Instrumentation, DI-1-3 . . .	357
111	Diffuser Static-Pressure Instrumentation, DI-2	363
112	Diffuser Static-Pressure Instrumentation, DI-X1 . . .	367
113	Diffuser Static-Pressure Instrumentation, DI-X1-2 and DI-X1-3	373
114	Diffuser Static-Pressure Instrumentation, DI-2-2 . . .	377
	APPENDIX X	
115	Impeller-Blade Positions for Schlieren Photographs . . .	381
116	Time-Delay Calibration	382
117	Test Points	384
118	Schlieren Photograph of DI-2 (Test Number 3312, Impeller Position = 16 Degrees, Impeller Speed = 46,000 rpm, Data Point 5)	386
119	Schlieren Photograph of DI-2 (Test Number 3312, Impeller Position = 12 Degrees, Impeller Speed = 46,000 rpm, Data Point 5)	387
120	Schlieren Photograph of DI-2 (Test Number 3312, Impeller Position = 8 Degrees, Impeller Speed = 46,000 rpm, Data Point 5)	388
121	Schlieren Photograph of DI-2 (Test Number 3312, Impeller Position = 4 Degrees, Impeller Speed = 46,000 rpm, Data Point 5)	389
122	Schlieren Photograph of DI-2 (Test Number 3312, Impeller Position = 0 Degrees, Impeller Speed = 46,000 rpm, Data Point 5)	390

LIST OF ILLUSTRATIONS (Continued)

Figure		Page
123	Schlieren Photograph of DI-2 (Test Number 3312, Impeller Speed = 46,000 rpm, Data Point 3)	391
124	Schlieren Photograph of DI-2 (Test Number 3312, Impeller Speed = 46,000 rpm, Data Point 7)	392
125	Schlieren Photograph of DI-1 (Test Number 3311, Impeller Speed = 15,000 rpm, Data Point 5)	393
126	Schlieren Photograph of DI-1 (Test Number 3311, Impeller Speed = 20,000 rpm, Data Point 5)	394
127	Schlieren Photograph of DI-1 (Test Number 3311, Impeller Speed = 25,000 rpm, Data Point 5)	395
128	Schlieren Photograph of DI-1 (Test Number 3311, Impeller Speed = 30,000 rpm, Data Point 5)	396
129	Schlieren Photograph of DI-1 (Test Number 3311, Impeller Speed = 35,000 rpm, Data Point 5)	397
130	Schlieren Photograph of DI-1 (Test Number 3311, Impeller Speed = 46,000 rpm, Data Point 5)	398
131	Schlieren Photograph of DI-1 (Test Number 3317, Impeller Speed = 50,000 rpm, Data Point 5)	399
132	Schlieren Photograph of DI-2 (Test Number 3312, Impeller Speed = 20,000 rpm, Data Point 5)	400
133	Schlieren Photograph of DI-2 (Test Number 3312, Impeller Speed = 25,000 rpm, Data Point 5)	401
134	Schlieren Photograph of DI-2 (Test Number 3312, Impeller Speed = 30,000 rpm, Data Point 5)	402
135	Schlieren Photograph of DI-2 (Test Number 3312, Impeller Speed = 35,000 rpm, Data Point 5)	403
136	Schlieren Photograph of DI-2 (Test Number 3312, Impeller Speed = 39,000 rpm, Data Point 5)	404

LIST OF ILLUSTRATIONS (Continued)

Figure		Page
137	Schlieren Photograph of DI-2 (Test Number 3313, Impeller Speed = 46,000 rpm, Data Point 5)	405
138	Schlieren Photograph of DI-3 (Test Number 3314, Impeller Speed = 25,000 rpm)	406
139	Schlieren Photograph of DI-3 (Test Number 3314, Impeller Speed = 46,000 rpm, Data Point 2)	407
140	Schlieren Photograph of DI-3 (Test Number 3314, Impeller Speed = 46,000 rpm, Data Point 3)	408
141	Schlieren Photograph of DI-3 (Test Number 3314, Impeller Speed = 46,000 rpm, Data Point 5)	409
142	Schlieren Photograph of DI-3 (Test Number 3314, Impeller Speed = 46,000 rpm, Data Point 7)	410
143	Schlieren Photograph of DI-1-2 (Test Number 3319, Impeller Speed = 50,000 rpm, Data Point 5)	411
144	Schlieren Photograph of DI-X1 (Test Number 3315, Impeller Speed = 50,000 rpm, Data Point 5)	412
145	Schlieren Photograph of DI-X1-2 (Test Number 3318, Impeller Speed = 50,000 rpm, Data Point 5)	413
146	Schlieren Unit	414
147	Schlieren Schematic Diagram	415

APPENDIX XI

148	Typical Variation of Pressure-Recovery Coefficient Versus Inlet Mach Number.	421
149	Velocity Profiles of Normal and Separating Boundary Layers	421
150	Flow-Regime Map	422

LIST OF ILLUSTRATIONS (Continued)

Figure		Page
151	Locus of Maximum Pressure Recovery Versus System Geometry	424
152	Critical Inlet Mach Number Versus Inlet Blockage Ratio	425
	APPENDIX XII	
153	Characteristic Grouping of Diffuser Data (C_p Versus Inlet Mach Number at Fixed Geometry)	433
154	Flow-Regime Map, Inlet Mach Number Group Classification	434
155	Critical Inlet Mach Number Versus Blockage Ratio . . .	435
156	Flow Arrangement and Measurement Techniques	438
157	Diffuser Test Section (5.7 Aspect Ratio).	439
158	Nozzle and Diffuser Block Dimensions (5.7 Aspect Ratio)	440
159	Diffuser Test Section (0.25 Aspect Ratio)	441
160	Nozzle and Diffuser Block Geometry (0.25 Aspect Ratio Tests, L/W = 15)	442
161	Centerline Stagnation Pressure Change (3.5-Inch-Long Throat).	446
162	Straight Diffuser Performance (Pressure Ratio Versus Axial Distance for Various Backpressures, 0.25 Aspect Ratio, $2\theta = 6°$, $L_{throat} = 0.125$ Inch) . . .	447
163	Straight Diffuser Performance (Pressure Ratio Versus Axial Distance For Various Backpressures, 0.25 Aspect Ratio, $2\theta = 6°$, $L_{throat} = 1.625$ Inch) . . .	448
164	Straight Diffuser Performance (Pressure Ratio Versus Axial Distance For Various Backpressures, 0.25 Aspect Ratio, $2\theta = 6°$, $L_{throat} = 3.5$ Inches) . . .	450

LIST OF ILLUSTRATIONS (Continued)

Figure		Page
165	Straight Diffuser Performance (C_p Versus Mach Number)	454
166	Straight Diffuser Performance (C_p Versus Mach Number)	455
167	Straight Diffuser Performance (C_p Versus Mach Number)	456
168	Straight Diffuser Performance (C_p Versus Mach Number)	457
169	Straight Diffuser Performance (C_p Versus Mach Number)	458
170	Straight Diffuser Performance (C_p Versus Mach Number)	459
171	Straight Diffuser Performance (C_p Versus Mach Number)	460
172	Straight Diffuser Performance (C_p Versus Mach Number)	461
173	Straight Diffuser Performance (C_p Versus Mach Number)	462
174	Straight Diffuser Performance (Pressure Recovery Versus Divergence Angle, L/W = 10)	464
175	Straight Diffuser Performance (Pressure Recovery Versus Divergence Angle, L/W = 15)	465
176	Straight Diffuser Performance (Pressure Recovery Versus Divergence Angle, L/W = 15)	466
177	Straight Diffuser Performance (Blockage Versus Divergence Angle With Pressure Recovery as Parameter)	469

LIST OF ILLUSTRATIONS (Continued)

Figure		Page
178	Straight Diffuser Performance (Blockage Versus Divergence Angle With Pressure Recovery as Parameter)	470
179	Straight Diffuser Performance	471

(U) TABLES

Table		Page
	APPENDIX III	
I	Compressor Critical Speeds	215
	APPENDIX VII	
II	Compressor Data for the General Test Case of the Workhorse Impeller Supplied by the Contractor	284
	APPENDIX X	
III	Time Delay in Microseconds	383
	APPENDIX XI	
XI	Reference Data and Symbols	420

UNCLASSIFIED

(C) APPENDIX I (U)

IMPELLER RADIAL-EQUILIBRIUM DESIGN (U)

ABSTRACT (U)

This program is used to perform a two-dimensional axisymmetrical design analysis of the fluid flow in radial rotors. Given inlet, geometry, recovery and flow-angle information, the program can be used to solve for radial equilibrium at stations normal to the meridional streamlines of a compressor. Temperatures, pressures, and vector diagrams are program outputs.

UNCLASSIFIED

UNCLASSIFIED

1.0 GENERAL INFORMATION

The program is written in FORTRAN IV for use on the SRU 1107 computer.

1.1 PURPOSE

The purpose of this program is to facilitate the radial equilibrium analysis of the fluid flow in radial- and mixed-flow impellers for given design conditions. The radial-equilibrium equation is solved at stations normal to the meridional streamlines of an impeller.

The total inlet conditions, exit-flow-angle distribution, recovery distribution, and the impeller geometry are inputs to the program. The design results printed out consist of temperatures, pressures, velocities, and angles determined at equilibrium streamlines for the inlet and downstream normal stations. The equilibrium results are used to compute blade surface velocities, which are also program outputs.

1.2 ASSUMPTIONS

1) The fluid is nonviscous but compressible.

2) Flow is axisymmetrical.

3) The meridional angle, γ', is constant along any normal streamline, and $0° < \gamma' < 90°$.

4) Real fluid losses are accounted for by using relative, total-pressure-recovery factors.

5) The impeller blades are composed of radial blade elements.

1.3 LIMITATIONS

1) The blade and flow angles are the same inside the channel, up to the station at which slip begins.

2) Boundary-layer blockage is constant at any normal station, but variable metal blockage is used.

3) The meridional distance is constant along any streamline and is measured along the mean line.

4) Relative velocities inside the impeller are subsonic.

5) There is a maximum of 20 stations, including the inlet and exit stations.

UNCLASSIFIED

UNCLASSIFIED

2.0 PROCEDURE

2.1 NOMENCLATURE

The A-, C-, and V-arrays are used in routine IMPEL, which computes conditions at the normal stations. The nomenclature for these arrays is given below. When different from those used in the program, the units correspond to the dimensions used for input and output data.

Program Symbol	Math Symbol	Units	Description
A			IMPEL storage array
AC	A_c	$in.^2$	Actual area check
ACCEL	A_{ccel}	ft/sec^2	Acceleration due to first two terms of dp/dn equation
AK	γ		Specific heat ratio
ALPHA, A (121-125)	α	deg	Absolute fluid-flow angle
AMASS, C (21-25)	W_a	lbm/sec	Mass flow rate, input
AREA, A (1-5)	A	$in.^2$	Actual annulus area
A8256-260), V (11-15)	A_{ann}	$in.^2$	Blocked annulus area
A (236-240)	A'_{ann}	$in.^2$	Adjusted A_{ann}
A (219)	$A_{ann,\ T}$	$in.^2$	Total A_{ann}
A(218)	$A'_{ann,\ T}$	$in.^2$	Total A'_{ann}
A (66-70)	$(A/A^*)_3$		Relative isentropic area ratio

UNCLASSIFIED

CONFIDENTIAL

Program Symbol	Math Symbol	Units	Description
A (146-150)	$(A/A^*)_4$		Absolute isentropic area ratio
	$(A/A^*)'_3$		Adjusted $(A/A^*)_3$
	α''	deg	Wrap angle
BETA, A (56-60)	β	deg	Relative fluid-flow angle
BLADES, V (23)	B		Number impeller blades
BLF, V (8)	BLF		Total blockage factor
BLFOUT	BLF_{exit}		Exit blockage factor
	BLF_{BL}		Boundary-layer factor
	BLF_m		Metal-blockage factor
C			IMPEL storage array
CF			Indicates if curvature will be used at inlet
DDMARG	$(\frac{2\pi R}{B} - t)\, V_{t4}$	in. fps	Angular momentum of blade-surface velocities
DERIV1	dR/dZ		First derivative of radius with respect to axial distance
DERIV2	d^2R/dZ^2	$in.^{-1}$	Second derivative of radius with respect to axial distance
DGR	0.01745329	rad/deg	Geometric conversion factor
DPDN, A (191-195)	dP_3/dn	m. Hg/in.	First derivative of static pressure with respect to normal distance

CONFIDENTIAL

Program Symbol	Math Symbol	Units	Description
A (46-50)	$d\alpha''/dZ$	deg/in.	First derivative of wrap angle with respect to axial distance
A (451-500)	$d\alpha''/dZ$	deg/in.	$d\alpha''/dZ$ table
	dV_T/dm	ft/in.-sec	First derivative of tangential velocity with respect to meridional distance
A (176-180)	F_N	ft/sec^2	Component of blade force per unit mass in normal direction
GAMMA, A (204), V (4)	γ'	deg	Meridional fluid-flow angle, measured from axis of rotation
GC	g	$\frac{lbm\text{-}ft}{lbf\text{-}sec^2}$	Gravitational constant, 32.17
GIVM	W_{aT}	lbm/sec	Total given mass flow rate
GRID			Storage array for TALL14 plots
HGPSI	2.03593	in. Hg/psi	Pressure conversion factor
HJ	J	ft-lbf/Btu	Work conversion factor, 778.2
HS	h_s	Btu/lbm	Static enthalpy
HRT, A (21-25)	h_T	Btu/lbm	Relative total enthalpy
HT, A (161-165)	h_T	Btu/lmb	Absolute total enthalpy
	H	in.	Normal blade height
KSLIP	k_{slip}		Slip station

Program Symbol	Math Symbol	Units	Description
K2	k		Station number, one at inlet
A (241-245)	M'_3		Adjusted M_3
NOMODE			Storage array for TALL14 plots
NORMLS	norm		Number of normals past inlet
NPLOT			Plot logical indicator
NS, V (10)			Number of stations, NORMLS + 1
NSLIP	n_{slip}		Slip station, if input
NTITLE			Title storage array
NXY			Number of points in input curve
A (213)	ω	rad/sec	Rotational speed
PHI	ϕ	deg	Blade angle
PI	π		Geometric constant, 3.14159
PLOTDX		in.	X-axis plot interpolation, x
PS, A (86-90)	p_s	in. Hg	Static pressure
PRT, C (6-10) A (36-40)	P_T	in. Hg	Relative total pressure
PT, A (151-155)	P_T	in. Hg	Absolute total pressure
A (196-200)	P'_{S3}	in. Hg	Present adjusted relative static pressure

Program Symbol	Math Symbol	Units	Description
A (261-265)	$P'_{S3,\ previous}$	in. Hg	Previous P'_{S3}
A (31-25)	P_{r3}		Relative pressure function
A (166-170)	P_{r4}		Absolute pressure function
Q			Equivalent to V-array
QMASS	$\dot{M}$	lbm/sec	Computed mass flow rate
R	R	$\frac{\text{ft-lbf}}{\text{lbm-°R}}$	Gas constant for air, 53.35
RAD		rad/deg	Same as DGR
RADIUS, A (11-15), C (1-5)	R	in.	Radial distance from axis, streamlines are rms of tubes
RCURV A (181-185)	R_c	in.	Radius of curvature
REC, V (16-20)	R_{ec}		Relative pressure recovery
	R_{ec_i}		Inducer recovery
	δR_{ec}		Recovery correction factor
RHO	ρ_T	lbm/in.^3	Total mass density
RIN	R	in.	Inlet mean radius
RPM, C (26)	N	rpm	Rotational speed
A (186-190)	ρ	lbm/in.^3	Static mass density
SLIP, V (9)			Slip logic indicator

Program Symbol	Math Symbol	Units	Description
SLIPFC	K_{slip}		Velocity slip factor input, usually about 1.4
	t_{hub}	in.	Blade thickness at hub measured in plane normal to axis of rotation
	t_{tip}	in.	Blade thickness at tip measured in plane normal to axis of rotation
TABLE, TAB 2	$f( )$		Indicates a table interpolation of degree one, except for geometry (third degree) table look-ups
TS, A (91-95)	T_s	°R	Static temperature
TRT, A (26-30), C (16-20)	T_T	°R	Relative total temperature
TT, A (156-160)	T_T	°R	Absolute total temperature
U, A (16-20)	U	fps	Wheel speed
V			IMPEL storage array
V, A (126-130)	V	fps	Absolute total velocity
VCR	V_{cr}	fps	Critical velocity
VP	V_P	fps	Pressure blade surface velocity
VPW	$V_P/V_{2,\ mean}$		Normalized pressure velocity
VR	V_r	fps	Absolute radial velocity
VS	V_s	fps	Suction blade-surface velocity

Program Symbol	Math Symbol	Units	Description
VSND, A (96-100)	a	fps	Sonic velocity
VSW	$V_s/V_{2,\ mean}$	fps	Normalized suction velocity
VTW	$V_s/V_{2,\ mean}$		Normalized total relative velocity
VU, A (116-120)	V_T	fps	Absolute tangential velocity
VVSND, A (131-135)	M		Absolute Mach number
VX	V_x	fps	Absolute axial velocity
W, A (101-105)	V	fps	Relative total velocity
WM, A (106-110)	V_m	fps	Relative meridional velocity
WR	V_r	fps	Relative radial velocity
WU, C (11-15), A (111-115)	V_T	fps	Relative tangential velocity
XBLF		in.	Independent array of n for BLF = f (n) and α_3 = f (n)
XLØC (1, K2)	Z_{hub}	in.	Axial distance to normal intersection with hub
XLØC, V (6), A (41-45)	Z	in.	Axial distance
XMD, V (21)	m	in.	Meridional distance from inlet along mean line
XND, A (61-65)	n	in.	Normal distance from hub
XRC		in.	Independent array of n for R_c = f (n)

Program Symbol	Math Symbol	Units	Description
XVAL			Independent variable array for input tables
YVAL		rad	Dependent array of α_3 for $\alpha_3 = f(n)$
YBLF			Dependent array of BLF for BLF = f (n)
YRC		in.	Dependent array of R_c for $R_c = f(n)$
YVAL			Dependent variable array for input tables
ZTIPG	$z_{tip,\ guess}$	in.	First guess of axial distance to normal intersection with the tip
XLØC (4, K2), A (401, 450)	Z_{mean}	in.	Axial distance to normal intersection with mean line
X	$\alpha'3$	rad	Relative fluid-flow angle based on Ø

Subscripts	Description
1	Inlet absolute
2	Inlet relative (to moving blade row)
3	Exit (or normal) relative
4	Exit (or normal) absolute
exit	Exit station (or last normal)
hub	Impeller hub
inlet	Inlet station
j	Streamline (or streamtube), j = 1 for hub streamtube

Subscripts	Description (Continued)
k	Station, k = 1 for inlet station, k = 20 for discharge station
m	Meridional direction, or mean line
mean	Mean line, that curve dividing the total annulus area in half
r	Radial direction
S	Static
slip	Slip station (where slip begins)
T	Total, or tangential direction
tip	Impeller tip
x	Axial direction
1	Hub streamtube
2	Second streamtube
.	.
.	.
.	.
5	Tip streamtube
1	Inlet station
2	Second station (first normal station)
.	.
.	.
.	.
20	Twentieth station

2.2 METHOD

The 5-streamtube approach is used, and the method of analysis for radial equilibrium downstream from the inlet is that developed in NACA Report 1082.* Radial equilibrium at the impeller inlet is established for the given inlet flow rates by using the methods of Swan.** Geometric dependent calculations are made for each normal station. The resulting inlet relative conditions and geometry are used, together with given recovery and fluid angle information, to solve the radial-equilibrium equation at each station along a streamline normal to the meridional plane.

See Figures 1 and 2 for the definitions of geometry and sign conventions. The functional notation, $y = f(x)$, indicates that x and y are in tabular form; the degree of interpolation is noted for $f(\ )$ in Section 2.1 of this appendix. The streamtube subscript is j, where $j = 1$ at the hub streamtube; k is the station subscript, where $k = 1$ at the inducer inlet. For clarity, the equations do not have the unit conversion factors, such as DGR and HGPSI, included. The last normal station downstream from the inlet is considered to be the exit.

2.2.1 INLET CALCULATIONS

Five streamtubes of equal area are assumed initially. The velocity profile is varied until a total mass flow balance is attained. If streamtube continuity is not satisfied, the streamtube areas are adjusted, and a total mass balance is again attained. This process and the velocity equation ensure radial equilibrium. The given information at the inlet is:

1) Mass-flow rate per streamtube, $W_{a,j}$;

2) Total-temperature schedule, $T_{T1} = f(R)$;

3) Total-pressure schedule, $P_{T1} = f(R)$;

4) Absolute-fluid-flow-angle schedule, $\alpha_1 = f(R)$;

5) Total-blockage schedule, $BLF_1 = f(R)$;

---

*J.T. Hamrick, A. Ginsberg, and W.M. Osborn, Method of Analysis for Compressible Flow Through Mixed-Flow Centrifugal Impellers of Arbitrary Design, NACA Report 1082 (Supersedes NACA TN 2165), 1952.

**W.C. Swan, A Practical Engineering Solution of the Three Dimensional Flow in Transonic Type Axial Flow Compressors, WADC TR 58-57, 1959.

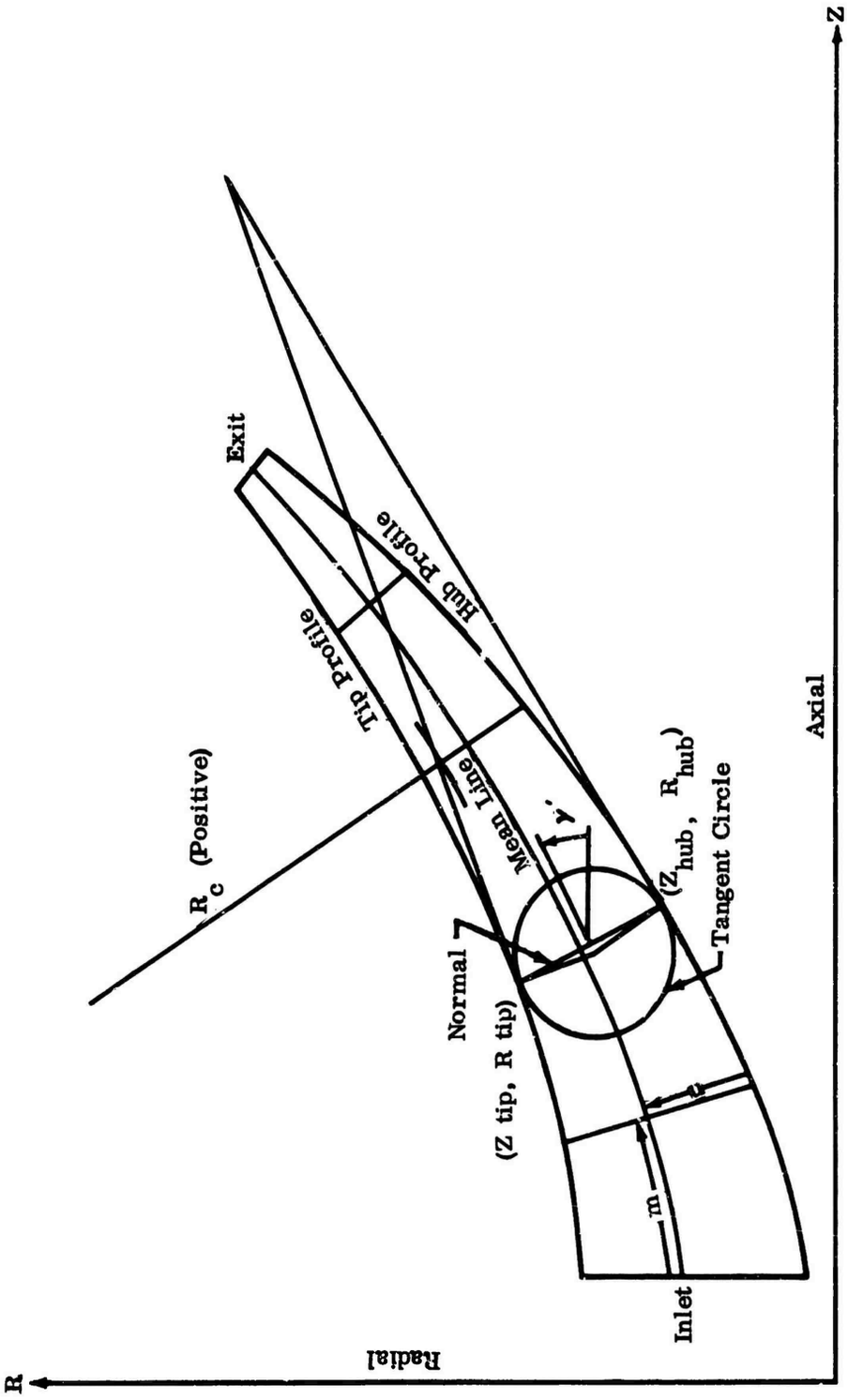


Figure 1. Impeller Meridional View.

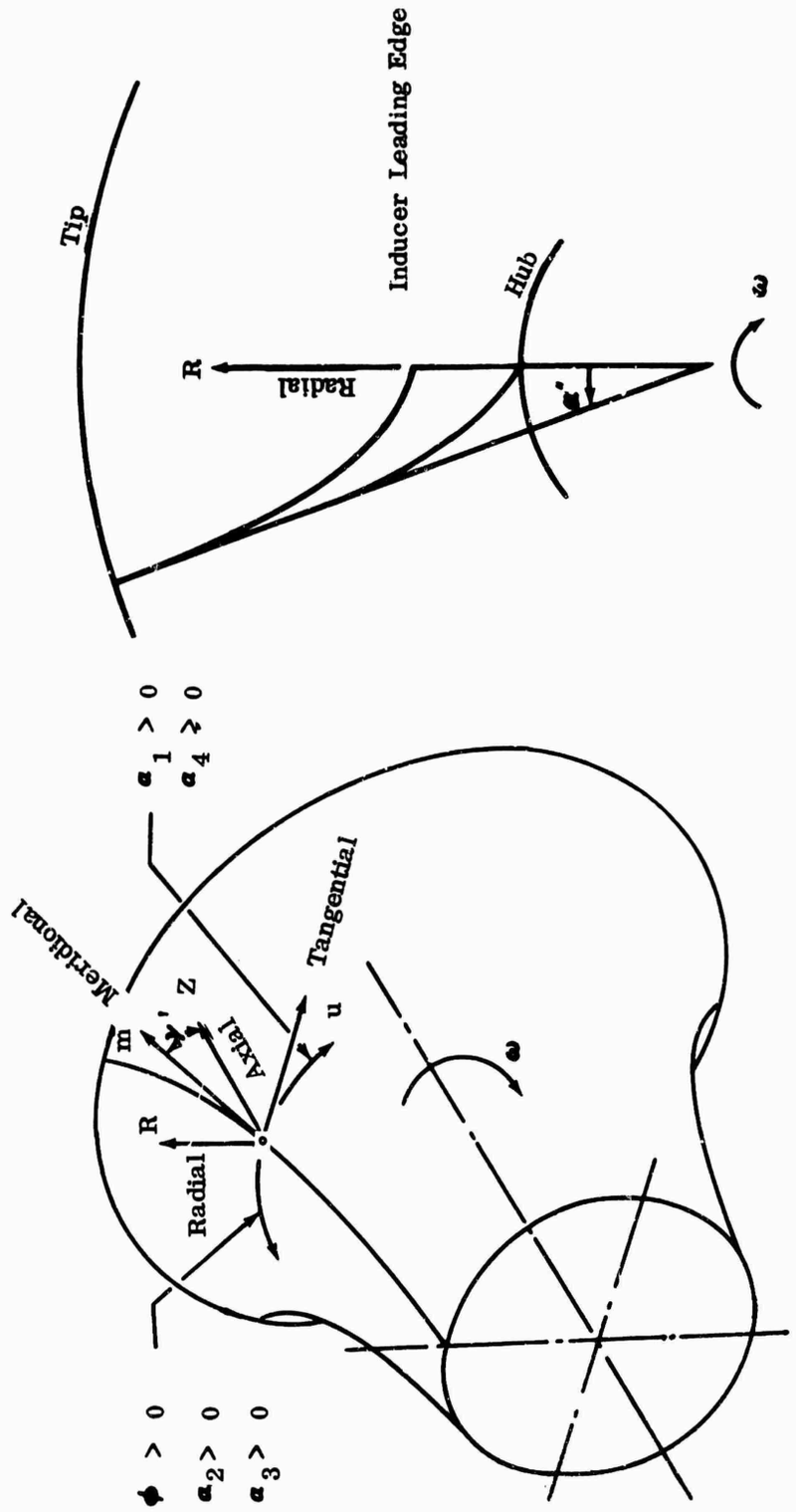


Figure 2. Angle Sign Conventions.

6) Hub- and tip-radius schedules, $R = f(z)$;

7) Station location, Z_1;

8) Rotational speed, N;

9) Thermodynamic tables, $h = f(T)$ and $\gamma = f(T)$.

Equal-Area Streamtubes

$$R_{hub} = f(Z_1) \tag{1}$$

$$R_{tip} = f(Z_1) \tag{2}$$

$$A_T = \pi (R_{tip}^2 - R_{hub}^2) \tag{3}$$

$$A_j = A_T/5 \tag{4}$$

$$R_{hub,1} = R_{hub} \tag{5}$$

$$R_{tip,j} = \sqrt{A_j/\pi + R_{hub,j}^2} \tag{6}$$

$$R_j = \sqrt{(R_{tip,j}^2 + R_{hub,j}^2)/2} \tag{7}$$

$$R_{hub,j+1} = R_{tip,j} \qquad \text{for } j = 1,2,3,4,5. \tag{8}$$

Radial Derivatives

$R_j +$ and $R_j -$ are determined as above at stations downstream and upstream, respectively, from the inducer inlet.

$$\left(\frac{dR}{dz}\right)_j = \left(\frac{R^+ - R^-}{2\ \Delta\ X}\right)_j \qquad \Delta X = 0.1 \text{ inch} \qquad (9)$$

$$\left(\frac{d^2R}{dz^2}\right)_j = \left(\frac{R^+ - 2R + R^-}{\Delta X^2}\right)_j \qquad (10)$$

Scheduled Input

$$T_{T1,j} = f(z_1) \qquad (11)$$

$$P_{T1,j} = f(z_1) \qquad (12)$$

$$\alpha_{1,j} = f(z_1) \qquad (13)$$

$$BLF_{1,j} = f(z_1) \qquad (14)$$

Velocity Profile

$V_{X1,\ hub}$ is assumed to be initially 600 fps when the bisection and Newton methods are used.

$$V_{T1,j} = V_{X1,}\ \cos\ \alpha_{1,j} \qquad (15)$$

$$\gamma = f\ \left\{\left(T_{T1,j+1} = T_{T1,j}\right)\right\}\ /2 \qquad (16)$$

$$c_j = 2\ \gamma\ R/J(\gamma\ -1) \qquad (17)$$

$$\Delta R_j = R_{j+1} - R_j \qquad (18)$$

$$a_j = gc \quad J(T_{T1,j+1} + T_{T1,j}) \tag{19}$$

$$b_j = \frac{R}{J} \ln \left\{ \frac{(T_{T1,j+1}/T_{T1,j})}{P_{T1,j+1}/P_{T1,j}} \quad \frac{\gamma}{\gamma+1} \right\} \tag{20}$$

$$h_{T1,j} = f\left(T_{T1,j}\right) \tag{21}$$

$$C1 = V^2_{X1,j} \left\{ 1 + \frac{b}{c} \left[1 + \left(\frac{dR}{dZ}\right)^2 \right] + \frac{d^2R}{dZ^2} \quad \Delta R \right\}_j - a_j b_j \tag{22}$$

$$C2 = 2 g_c J\left(h_{T1,j+1} - h_{T1,j}\right) \tag{23}$$

$$C3 = V^2_{T1,j+1} \left\{ \left(\frac{b}{c}\right) - 2 + \frac{R_j}{R_j+1} \right\} + V^2_{T1,j} \left\{ \left(\frac{b}{c}\right)_j + 2 - \frac{R_{j+1}}{R_j} \right\} \tag{24}$$

$$C4 = 1 - \left(\frac{b}{c}\right)_j \left\{ 1 + \left(\frac{dR}{dZ}\right)^2_{j+1} \right\} - 9\left(\frac{d^2R}{dZ^2}\right)_{j+1} \Delta R_j \tag{25}$$

$$V^2_{X1,j+1} = \frac{C1 + C2 + C3}{C4} \qquad \text{for } j = 1, 2, 3, 4. \tag{26}$$

Total Mass Balance

$$M_j = \left(BLF_1 \frac{\rho V_{X1}}{\rho_T V_{crl}} \quad \rho_T \quad V_{crl} A \right)_j \tag{27}$$

$$\dot{M}_T = \sum_{j=1}^{5} \dot{M}_j \tag{28}$$

$$\frac{\rho V_{X1}}{\rho_T V_{crl}} = \left(\frac{V_{X1}}{V_{crl}}\right)_j \left\{1 - \frac{\gamma - 1}{\gamma + 1}\left(\frac{V_{X1}}{V_{crl}}\right)^2 \left[1 + \tan^2\alpha_1 + \left(\frac{dR}{dZ}\right)^2\right]\right\}_j^{\frac{1}{\gamma - 1}} \tag{29}$$

$$\gamma = f(T_{T1,j}) \tag{30}$$

$$V_{crl,j} = \sqrt{\gamma g R \frac{2T_{T1,i}}{\gamma - 1}} \tag{31}$$

$$\rho_{T,j} = \left(\frac{P_{TL}}{R\ T_{T1}}\right)_j \tag{32}$$

$$W_{aT} = \sum_{j=1}^{5} W_{a,j} \tag{33}$$

If $\left|\dot{M}_T - W_{aT}\right| < 0.005$, a total mass balance has been achieved and a check on streamtube continuity is made; otherwise, a new velocity profile is computed based on a new $V_{X1,hub}$ (see Velocity Profile section of this appendix).

Streamtube Mass Balance

$$A_{c,j} = A_j W_{a,j}/M_j \tag{34}$$

If $\left|A_{c,\,j} - A_j\right| < 0.01$ for j = 1, 2, 3, 4, 5, complete radial equilibrium has been attained; otherwise, a streamline shift is made as shown below and the process is repeated beginning with the steps in the Scheduled Input section.

$$R_{hub,\,1} = R_{hub} \tag{5}$$

$$R_{tip,\,j} = \sqrt{(A_c/\pi + R_{hub}^2)_j} \tag{35}$$

$$\delta R_j = (R_{tip} - R_{hub})_j \tag{36}$$

$$R_{hub,\,j+1} = R_{tip,\,j} \quad \text{for } j = 1, 2, 3, 4, 5 \tag{8}$$

$$\Delta R_T = R_{tip} - R_{hub} \tag{37}$$

$$\delta R_T = \sum_{j=1}^{5} \delta R_j \tag{38}$$

$$\Delta R_j = \delta R_j \frac{\Delta R_T}{\delta R_T} \tag{39}$$

$$R_j = \sqrt{\left|R_{hub}^2 + (R_{hub} + \Delta R)^2\right|_j / 2} \tag{40}$$

$$A_j = \pi\left\{(R_{hub} + \Delta R)^2 - R_{hub}^2\right\}_j \tag{41}$$

$$R_{hub,\,j+1} = R_{tip,\,j} \quad \text{for } j = 1, 2, 3, 4, 5. \tag{8}$$

Return to the steps in the Scheduled Input section.

Additional Calculations

After complete equilibrium is established, the following inlet calcu. tions are made:

$$T_{S1,j} = T_{T1,j} \left\{1 - \frac{\gamma - 1}{\gamma + 1} \left(\frac{V_1}{V_{crl}}\right)^2\right\} \quad ; \gamma_r + (T_{T1,j}) \tag{42}$$

$$V_{r1,j} = \left(\frac{dR}{dz}\right)_j V_{X1,j} \tag{43}$$

$$V_{1,j} = \sqrt{(V_{rl}^2 + V_{X1}^2 + V_{T1}^2)_j} \tag{44}$$

$$P_{S1,j} = P_{T1,j} \left\{\left(\frac{T_{S1}}{T_{T1}}\right)^{\frac{\gamma}{\gamma - 1}}\right\}, \gamma = f\left\{(T_{S1} + T_{T1})_j / 2\right\} \tag{45}$$

$$a_{1,j} = \sqrt{\gamma g_c R T_{S1,j}} \; \gamma = f(T_{S1,j}) \tag{46}$$

$$M_{1,j} = \left(\frac{V_1}{a_1}\right)_j \tag{47}$$

$$U_{1,j} = \pi R_j N/360 \tag{48}$$

$$V_{T2,j} = (U_1 - V_{T1})_j \tag{49}$$

$$V_{X2,j} = V_{X1,j} \tag{50}$$

$$V_{r2,j} = V_{r1,j} \tag{51}$$

$$V_{2,j} = \sqrt{\left(V_{r2}^{\ 2} + V_{X2}^{\ 2} + V_{r2}^{\ 2}\right)}_{j} \tag{52}$$

$$M_{2,j} = \left(\frac{V_2}{a_1}\right)_j \tag{53}$$

$$\alpha_{2,j} = \tan^{-1}\left(\frac{V_{T2}}{V_{X2}}\right)_j \tag{54}$$

$$V_{M2,j} = \sqrt{\left(V_{X2}^{\ 2} + V_{r2}^{\ 2}\right)}_{j} \tag{55}$$

$$h_{s1,j} = f(T_{s,j}) \tag{56}$$

$$h_{T2,j} = \left(h_{s1} + V_2/2\, g_c\, J\right)_j \tag{57}$$

$$T_{T2,j} = f(h_{T2,j}) \tag{58}$$

$$P_{T2,j} = \left(\frac{T_{T2}}{T_{S1}}\right)^{\frac{\gamma}{\gamma - 1}} P_{T1,j}, \qquad \gamma = f\left\{(T_{r2} + T_{S1})/2\right\} \tag{59}$$

$$R_{c,j} = \frac{\left\{1 + \left(\frac{dR}{dz}\right)_j^2\right\}^{1.5}}{\left(\frac{d^2R}{dz^2}\right)_j} \tag{60}$$

2.2.2 GEOMETRIC CALCULATIONS

At each station downstream from the inlet, the intersections of the normal stations with the hub and tip profiles in the meridional plane are determined first. The initial streamtube areas, the meridional angle, the mean line, and meridional distances, and the radius of curvature schedules can then be calculated. Schedules for the relative pressure recoveries and blockage factors are next developed at each normal station. The above preliminary information is used, together with input information, to solve the radial equilibrium equation at each station, as described in Section 2.2.3 of this appendix. The given information relevant to calculations in this section is listed below:

1) Hub profile, $R_{hub} = f(z)$;

2) Tip profile, $R_{tip} = f(z)$;

3) Exit total blockage, BLF;

4) Inducer streamtube recovery schedules, $R_{ec_{i,j}} = f(M_2)$;

5) Recovery correction schedule, $\delta R_{ec} = f(H)$;

6) Axial distance to stations at the hub, $Z_{hub,k}$;

7) Axial distance (approximate) to stations at the tip, $Z_{tip\ guess,\ k}$;

8) Number of impeller blades, B ;

9) Blade thickness schedules, $t_{hub} = f(z)$ and $t_{tip} = f(z)$;

10) Radius of curvature schedules, $R_{C_{hub}} = f(Z)$ and $R_{C_{tip}} = f(Z)$.

Normal Determination

Refer to the reference* for a detailed development of the equations. The normal station passing through a known point (Z_{hub}, R_{hub}) is found, which satisfies the tangent circle criterion (see Figure 1). The iterative algorithm uses a third-degree exact polynomial fit to determine profile slopes. The tip point ($Z_{tip\ guess}$, R_{tip}) provides a starting point in the iteration. After the stations normal to the streamlines have been determined, the following information is known:

*See second footnote, page 12.

$$(Z_{hub},\ R_{hub})_k$$

$$(Z_{tip},\ R_{tip})_k$$

$$\gamma'_k = \tan^{-1}\left(\frac{Z_{hub} - Z_{tip}}{R_{tip} - R_{hub}}\right)_k \tag{61}$$

where: k = station number (at inlet k = 1).

Station Geometry

$$A_T = \pi(R_{tip}^2 - R_{hub}^2)/\cos\gamma' \tag{62}$$

$$A_j = A_T/5 \tag{4}$$

$$R_{hub,1} = R_{hub} \tag{5}$$

$$R_{tip,j} = \sqrt{(\cos\gamma'/\pi + R_{hub}^2)_j} \tag{63}$$

$$R_j = \sqrt{(R_{tip}^2 + R_{hub}^2)_j/2} \tag{7}$$

$$n_j = (R_j - R_{hub})/\cos\gamma' \tag{64}$$

$$R_{hub,j+1} = R_{tip,j} \quad \text{for } j = 1, 2, 3, 4, 5 \tag{8}$$

$$Z_j = Z_{tip} + \tan\gamma'(R_{tip} - R_j) \tag{65}$$

$$R_m = R_3 \tag{66}$$

$$Z_m = Z_3 \tag{67}$$

$$n_m = n_3 \tag{68}$$

The R_c versus n schedule at each station is constructed by computing R_c at the hub and tip.

$$R_{C_{hub}} = f\left(Z_{hub}\right) \tag{69}$$

$$R_{C_{tip}} = f\left(Z_{tip}\right) \tag{70}$$

With the hub and tip radii of curvature being used, the streamline R_c values are obtained by linear interpolation of normal distance. After the above geometric calculations have been made, the meridional distance, m , from the inlet to each station is determined by linear (station-to-station) integration along the mean-line points (Z_m, R_m).

Station Recovery and Blockage Schedules

$$BLF_{metal} = \frac{A - (H \cdot \bar{t} \cdot B)}{A} = 1 - \frac{\bar{t} \cdot B}{2\,\bar{R}} \tag{71}$$

$$\bar{R} = (R_{hub} + R_{tip})/2 \tag{72}$$

$$\bar{t} = (t_{hub} + t_{tip})/2 \tag{73}$$

$$BLF_{BL,\,exit} = \frac{BLF_{exit}}{BLF_{metal,\ exit,\ mean}} \tag{74}$$

$$BLF_{BL,\,in.} = \frac{BLF_{i,\,mean}}{BLF_{metal,\,in.,mean}} \tag{75}$$

BLF_{BL} at each station is determined by linear interpolation of meridional distance and is assessed in a one-dimensional analysis.

$$BLF_{BL,\,K} = \frac{BLF_{BL,\,exit} - BLF_{BL,\,in.}}{m_{exit}} m_k + BLF_{BL,\,in.} \tag{76}$$

BLF_{metal} is determined for streamtubes at each station, and a total blockage schedule, BLF = f(n), is computed for each station.

$$BLF_{k,j} = \left(BLF_{metal,\,k,j}\right)\left(BLF_{BL,k}\right) \tag{77}$$

k = station number

j = streamline number (1, 2, 3, 4, 5)

$$A_{ann,k,j} = A_{k,j}\, BLF_{k,j} \tag{78}$$

$$\delta R_{ec_j} = f\left(\frac{n_j}{n_{tip}}\, 100\right)_{exit} \tag{79}$$

$$R_{ec_{i,j}} = f(M_{2,j}) \tag{80}$$

$$R_{ec_{exit,\,j}} = R_{ec_{i,j}}\, \delta R_{ec_j} \tag{81}$$

The streamtube recovery distributions are calculated by linear interpolation from a recovery of one at the inlet to the respective streamtube recovery at the exit as a function of meridional distance.

$$R_{ec_{k,j}} = -\frac{R_{ec_{exit,j}} - 1}{m_{exit}} m_k + 1 \qquad (82)$$

2.2.3 IMPELLER NORMAL CALCULATIONS

In general, the methods developed by Hamrick, et al* are followed. The radial-equilibrium equation to be solved is:

$$\frac{dP_3}{dn} = \rho\left(\frac{12V_{T4}^2}{R}\cos\gamma' - \frac{12V_{M4}^2}{R_c} - F_N\right) \qquad (83)$$

The static-pressure change in the direction normal to the mean line and in the meridional plane is equated to the force per unit volume due to rotation about the impeller axis, plus the centrifugal force per unit volume due to the curvilinear paths of the fluid particles, plus the component of the blade surface force per unit volume normal to the meridional streamline.

The general outline of the iterative method of solution is now described. An initial area distribution is assumed, and solution is obtained for the vector triangles (Vectors 3 and 4) at the station of interest. This gives a schedule of static pressure versus normal distance. The radial equilibrium is used to adjust the static-pressure schedule about the mean-line static-pressure value. If the static-pressure values do not agree with those calculated, area distribution is adjusted and the calculations are repeated.

The blade-surface velocities are computed at each station after the radial equilibrium for all stations has been established. The method proposed by Stanitz and Prian** is used.

The information given for the impeller normal station calculations is computed as shown in Sections 2.2.1 or 2.2.2, or is used as data input as follows:

1) Metal blade angle schedule, $\phi = f(z_m)$;

2) Station number, n_{slip}, at which $\alpha_3 = 0$ and slip begins, and which may be downstream from the last normal if no slip is expected;

---

*(See footnote, page 12)

**J.D. Stanitz, and V.D. Prian, A Rapid Approximate Method for Determining Velocity Distribution on Impeller Blades of Centrifugal Compressors, NACA TN 2421, July 1951.

3) If n_{slip} is not specified, a constant K_{slip} (approximately 1.4) is used as input data, which the program compares with $(V_2/V_3)_{mean}$ to determine where slip begins;

4) Thermodynamic table, $P_r = f(T)$;

5) Exit relative fluid-flow angle schedule, $\alpha_{3,exit} = f(\%H)$, required if slip is expected upstream from the last normal station (impeller exit).

Vector Diagrams

$$A_{ann,T} = \sum_{j=1}^{5} A_{ann,j} \tag{84}$$

After the first iteration, the blockage factor becomes $BLF_m = f(n_j)$:

$$A_j = A_{ann,j}/BLF_j \tag{85}$$

$$R_{tip,1} = \sqrt{\cos \gamma' \, A_1/\pi + R_{hub}^2} \tag{86}$$

$$R_{tip,j} = \sqrt{\cos \gamma' \, A_j/\pi + R_{tip,j-1}^2}, \quad j = 2,3,4,5 \tag{87}$$

$$R_1 = \sqrt{\left(R_{hub}^2 + R_{tip,1}^2\right)/2} \tag{88}$$

$$R_j = \sqrt{\left(R_{tip,j-1}^2 + R_{tip,j}^2\right)/2} \tag{89}$$

$$n_j = (R_j - R_{hub})/12 \cos \gamma', \quad U_{4,j} = \pi N R_j/360 \tag{90}$$

$$h_{T3,j} = h_{T2,j} + (U_{4,j}/223.77)^2 \cdot \left\{ 1 - \left(\frac{R_{inlet,j}}{R_j} \right)^2 \right\} \tag{91}$$

$$T_{T3,j} = f(h_{T3,j}) \tag{92}$$

$$P_{r3,j} = f(T_{T3,j}) \tag{93}$$

$$P_{T3,j} = P_{T2,j} \; R_{ec,j} \; P_{r3,j}/P_{r2,j} \tag{94}$$

$$Z_i = Z_{hub} - \left(R_j - R_{hub}\right)\tan \gamma' \tag{95}$$

The following steps were used in calculating impeller slip.

Step a) α_3 Before Slip — A schedule of $\left(\frac{d\alpha'}{dz}\right)_m = f(z_m)$ is constructed.

$$\left(\frac{d\alpha''}{dz}\right)_{k,m} = \frac{\tan \phi_k}{R_{k,m} \cos \gamma'_k} \tag{96}$$

$$\phi_k = f(z_{k,m}) \tag{97}$$

$$k = 1, 2, ---, \text{norm} + 1$$

m means one-dimensional

$$\left(\frac{d\alpha''}{dz}\right)_j = f(z_j) \tag{98}$$

$$\alpha_{3,j} = \tan^{-1} \left\{R_j \left(\frac{d\alpha''}{dz}\right)_j \cos \gamma'\right\} \tag{99}$$

$\alpha_{3,j} = \alpha_{3,j}$ and is always computed.

Step b) α_3 at Slip — If n_{slip} is specified, α_3 at that station is zero; $alpha_{3,j}$ = zero.

Step c) α_3 After Slip — If K_{slip} is specified, the program defines the station at which slip begins to become $\left(\frac{V_2}{V_3}\right)_{mean} \geq K$ slip. After slip, α_3 is computed by linear interpolation of $\alpha_{3,exit}$ as a function of meridional distance from the point of the slip.

$$\alpha_{3,\ exit,\ j} = f\left(\frac{n_j}{n_{tip}}\ 100\right)_{exit} \tag{100}$$

$$\alpha_{3,k,j} = \frac{\left(\alpha_{3,\ exit} - \alpha_{3,\ slip_j}\right)}{(m_{exit} - m_{slip})} (M_k - M_{slip}) + \alpha_{3,\ slip,\ j} \tag{101}$$

where:

k = present station number.

If n_{slip} is specified, $\alpha_{3,\ slip,\ j} = O$; otherwise, the $\alpha_{3,\ slip,\ j}$ values are as computed in Step a) above.

Relative Mach Number Calculation

Step a) —
$$(A/A^*)_{3,j} = \frac{K\ P_{T3,j}\ A_{ann,j} \cos\ \alpha_{3,j}}{W_{a,j}\sqrt{T_{T3,j}}} \tag{102}$$

$$K = .49118\left[\frac{\gamma g}{R}\left(\frac{2}{\gamma+1}\right)^{\frac{\gamma+1}{\gamma-1}}\right]^{1/2},\quad \gamma = f(T_{TI})_{mean}. \tag{103}$$

On the first d P_{s3}/dn iteration, the $(A/A^*)_{3,j}$ values are compared to 1. If all the $(A/A^*)_{3,j}$ values are greater than or equal to 1, skip to Step c) below. If the average is less than 1, the input is considered to be invalid, a message is printed, and the calculations for the present normal are terminated. If the average $(A/A^*)_3$, which is represented by $\overline{(A/A^*)_3}$, is equal to or greater than 1, the assumed streamtube-area distribution is adjusted as follows:

Step b) —

$$A'_{ann,j} = A_{ann,j} \frac{\overline{(A/A^*)_3}}{(A/A^*)_{3,j}} \tag{104}$$

$$A'_{ann,T} = \sum_{j=1}^{5} A'_{ann,j} \tag{105}$$

$$A_{ann,j} = A'_{ann,j} \frac{A_{ann,T}}{A'_{ann,T}} \tag{106}$$

Calculations begin again with the steps in the Vector Diagrams section.

Step c) — Iterate to solve the equations in Step d) for $M_{3,j}$ and γ ; solve for $M_{3,j}$ by using bisection and by assuming $\gamma = 1.4$ initially.

Step d) —

$$\left(\frac{A}{A^*}\right)_{3,j} = \frac{1}{M_{3,j}} \left\{ \frac{2}{\gamma+1} \left[1 + \frac{\gamma-1}{2} M_{3,j}^2 \right] \right\}^{\frac{\gamma+1}{2(\gamma-1)}} \tag{107}$$

$$\left(\frac{T_S}{T_{T3,j}}\right) = \left(1 + \frac{\gamma-1}{2} M_{3,j}^2\right)^{-1} \tag{108}$$

$$T_{S3,j} = \left(\frac{T_S}{T_{T3,j}}\right) T_{T3,j} \tag{109}$$

$$\gamma'' = f(T_{S3,j}) \tag{110}$$

If $|\gamma'' - \gamma| < 0.0005$, check $\left(\frac{A}{A^*}\right)'_{3,j}$; otherwise, let $\gamma = \gamma''$ and return to Step d) above. If $\left|\left(\frac{A}{A^*}\right)_{3,j} - \left(\frac{A}{A^*}\right)'_{3,j}\right| < 0.0005$, compute $\left(\frac{P_S}{P_T}\right)_{3,j}$; otherwise, adjust $M_{3,j}$ by using bisection and reuse Step d).

$$\left(\frac{P_S}{P_T}\right)_{3,j} = \left\{\left[1 + \frac{\gamma-1}{2} M_{3,j}^2\right]^{\frac{\gamma}{\gamma-1}}\right\}^{-1} \tag{111}$$

$$P_{S3,j} = P_{T3,j}\left(\frac{P_S}{P_T}\right)_{3,j} \tag{112}$$

$$a_{3,j} = \sqrt{\gamma g R T_{S3,j}}, \quad \gamma = 1.4 \tag{113}$$

$$V_{3,j} = M_{3,j} \; a_{3,j} \tag{114}$$

$$V_{M3,j} = V_{3,j} \cos \alpha_{3,j} \tag{115}$$

$$V_{T3,j} = V_{3,j} \sin \alpha_{3,j} \tag{116}$$

$$V_{T4,j} = U_{3,j} - V_{T3,j} \tag{117}$$

$$\alpha_{4,j} = \tan^{-1}\left(\frac{V_{T4}}{V_{M3}}\right)_j \tag{118}$$

$$V_{4,j} = V_{M3,j}/\cos \alpha_{4,j} \tag{119}$$

$$M_{4,j} = V_{4,j}/a_{3,j} \tag{120}$$

$$T_{S4,j} = T_{S3,j} \tag{121}$$

Step e) — Solve the equations in Step e) for $(A/A^*)_{4,j}$ and γ. Four successive replacement iterations are used to solve for γ, assuming that $\gamma = 1.4$ initially.

$$\left(\frac{A}{A^*}\right)_{4,j} = \frac{1}{M_{4,j}}\left\{\frac{2}{\gamma+1}\left(\frac{T_T}{T_S}\right)_{4,j}\right\}^{\frac{\gamma+1}{2(\gamma-1)}} \tag{122}$$

where:

$$\left(\frac{T_S}{T_T}\right)_{4,j} = \left(1 + \frac{\gamma-1}{2} M^2_{4,j}\right) \tag{123}$$

$$T_{T4,j} = T_{S4,j}\Big/\left(\frac{T_S}{T_T}\right)_{4,j} \tag{124}$$

$$\gamma = f(T_{T4})_{mean} \tag{125}$$

Return to Step e) if this is not the fourth iteration; otherwise, compute $(P_S/P_T)_{4,j}$.

$$\left(\frac{P_S}{P_T}\right)_{4,j} = \left\{\left(\frac{T_T}{T_S}\right)_{4,j}^{\frac{\gamma}{\gamma-1}}\right\}^{-1} \tag{126}$$

$$P_{S4,j} = P_{S3,j} \tag{127}$$

$$P_{T4,j} = P_{S4,j} \Big/ \left(\frac{P_S}{P_I}\right)_{4,j} \tag{128}$$

$$h_{T4,j} = f\left(T_{T4,j}\right) \tag{129}$$

$$P_{r4,j} = f\left(T_{T4,j}\right) \tag{130}$$

Radial-Equilibrium Equation

The equations used in the radial-equilibrium calculations are:

$$\omega = 2\,\pi\,N/60 \tag{131}$$

and at the first normal station, $k = 2$, and,

$$\left(\frac{d\,V_T}{dm}\right)_j = \left(\frac{V_{T2} - V_{T3,k}}{M_k - M_{k-1}}\right)_j 12 \tag{132}$$

otherwise,

$$\left(\frac{d\,V_T}{dm}\right)_j = \left(\frac{V_{T3,\,k-1} - V_{T3,\,k}}{M_k - M_{k-1}}\right)_j 12 \tag{133}$$

$$F_{N,j} = V_{3,j} \sin \alpha'_{3,j} \sin \gamma' \tan \gamma' \left\{ 2\,\omega + \left(\frac{d\,V_T}{dm}\right)_j \frac{1}{\sin \gamma'} - \frac{V_{3,j}\,12}{R_j} \sin \alpha'_{3,j} \right\} \tag{134}$$

$$R_{c,j} = f(n_j) \tag{135}$$

$$\rho_j = \frac{P_{S,3}}{R\,T_{S,3}} \tag{136}$$

The radial-equilibrium equation is:

$$\left(\frac{dP_3}{dn}\right)_j = \rho_j \left[\frac{-12\,V^2_{m3,j}}{R_{c,j}} + \frac{12\,V^2_{T3,j}}{R_j}\cos\ ' - F_{N,j}\right] \tag{137}$$

The solution of the exit vectors has given 5 points on the curve, $P_{S3} = f(n)$. The slopes, $\frac{dP_S}{dn}$, found by using the radial-equilibrium equation are used to adjust the P_{S3} curve about the point (n_{mean}, $P_{S3,\ mean}$). The static-pressure values at n_j from the adjusted curve are $P'_{S3,j}$ where:

$$P'_{S3,3} = P_{S3,3} \tag{138}$$

$$P'_{S3,2} = P'_{S3,3} - \frac{(n_3 - n_2)}{2}\left[\left(\frac{dP_3}{dn}\right)_3 + \left(\frac{dP_3}{dn}\right)_3\right] \tag{139}$$

$$P'_{S3,1} = P'_{S3,2} - \frac{(n_2 - n_1)}{2}\left[\left(\frac{dP_3}{dn}\right)_2 + \left(\frac{dP_3}{dn}\right)_1\right] \tag{140}$$

$$P'_{S3,4} = P'_{S3,3} + \frac{n_4 - n_3}{2}\left[\left(\frac{dP_3}{dn}\right)_4 + \left(\frac{dP_3}{dn}\right)_3\right] \tag{141}$$

$$P'_{S3,5} = P'_{S3,4} + \frac{n_5 - n_4}{2}\left[\left(\frac{dP_3}{dn}\right)_5 + \left(\frac{dP_3}{dn}\right)_4\right] \tag{142}$$

If this is the first iteration, continue to Step a) below; otherwise, compare the P'_{S3} values with the P_{S3} values. If

$$\left| P'_{S3} - P_{S3} \right|_j / P_{S3} \leq 0.002 \tag{143}$$

the radial-equilibrium iteration is considered converged, and the logic proceeds to Step c) below. Otherwise, the following area adjustments are made in Step a) below.

Step a)–If $\left(\frac{P_{T3}}{P'_{S3}}\right)_j \leq 1$ for any streamline, j, decrease all $P'_{S3,j}$ by 0.5 continually until the inequality is satisfied: $\gamma = f(T_{T4})_{mean}$.

$$M'_{3,j} = \left\{ \left[\left(\frac{P_{T3}}{P'_{S3}} \right)^{\frac{\gamma - 1}{\gamma}} - 1 \right] 2 \Big/ (\gamma - 1) \right\}^{1/2} \tag{144}$$

$$(A/A^*)'_{3,j} = \frac{1}{M'_3} \left\{ \frac{2}{\gamma + 2} \left[1 + \frac{\gamma - 1}{2} \left(M'_3 \right)^2 \right] \right\}^{\frac{\gamma + 1}{2(\gamma - 1)}} \tag{145}$$

$$A'_{ann,j} = (A/A^*)'_{3,j} A_{ann,j} / (A/A^*)_{3,j} \tag{146}$$

$$A'_{ann,T} = \sum_{j=1}^{5} A'_{ann,j} \tag{147}$$

If $\left| A'_{ann,T} - A_{ann,T} \right| / A_{ann,T} \leq 0.003$, continue to Step b); otherwise, make the following adjustments:

$$\text{Const} = -0.02 P'_{S3,\,mean} \frac{A'_{ann,\,T} - A_{ann,\,T}}{A_{ann,\,T}} \tag{148}$$

$$P'_{S3,\,j} = P'_{S3,\,j} + \text{Const.} \tag{149}$$

The logic now returns to Step a).

Step b) —

$$A_{ann,\,j} = A'_{ann,\,j} \left(\frac{A_{ann,\,T}}{A'_{ann,\,T}} \right) \tag{150}$$

This ends one radial-equilibrium iteration; return to the calculations in the Vector Diagrams section of this appendix.

Step c) — The acceleration is computed:

$$A_{ccel,\,j} = \left(\frac{12 V_{T4}^2}{R} \cos \gamma' - \frac{12 V_{M3}^2}{R_C} \right)_j \tag{151}$$

Blade-Surface Velocities

The blade-surface velocities are calculated after radial equilibrium has been found for each station. The metal blade angle of the blade pressure surface at any station is assumed to be equal to that of the blade suction surface.*

$$\Delta V_r = \frac{1}{2} \cos \alpha_3 \frac{d}{m} \left[\left(\frac{2 \pi R}{B} - t \right) V_{T4} \right]. \tag{152}$$

After vector diagrams have been found that satisfy radial equilibrium at each normal station downstream from the inlet, the following relationship is known:

*See second footnote, page 26.

$$\left(\frac{2\pi R}{B} - t\right) V_{T4} = f(m) \tag{153}$$

The blade-surface velocities are calculated at each station as follows:

$$\left[\left(\frac{2\pi R}{B} - t\right) V_{T4,j}\right]^{-} = f(m_j - \Delta m), \quad \Delta m = 0.02 \tag{154}$$

$$\left[\left(\frac{2\pi R}{B} - t\right) V_{T4,j}\right]^{+} = f(m_j + \Delta m) \tag{155}$$

$$\frac{d}{dm}\left[\left(\frac{2\pi R}{B} - t\right) V_{T4,j}\right] = \left[\frac{f(m_j = \Delta m) - f(m_j - \Delta m)}{2\Delta m}\right] \tag{156}$$

$$V_{S,j} = V_{3,j} + \Delta V_{r,j} \tag{157}$$

$$V_{P,j} = V_{3,j} - \Delta V_{r,j} \tag{158}$$

$$(V_S/V_2)_j = V_{S,j}/V_{2,mean} \tag{159}$$

$$(V_P/V_2)_j = V_{P,j}/V_{2,mean} \tag{160}$$

$$(V/V_2)_j = V_{3,j}/V_{2,mean} \tag{161}$$

2.3 RESULTS

The inlet calculations were checked against hand calculations; the geometry calculations were checked graphically.

3.0 INPUT PREPARATION AND OUTPUT DESCRIPTION

3.1 INPUT-DATA PREPARATION

Input data are regulated by alphabetic control cards. The data for each control card must follow a specified sequence. However, a control card and associated data need not appear in any particular sequence, except for the CONSTANTS data, which must appear before the Z(HUB) and Z(TIP GUESS) data, and the BEGIN COMPUTE card, which must be the last card for any set of data that defines the impeller. Multiple impellers or cases can be run by altering only the changed data, followed by a BEGIN COMPUTE card. The program uses a seven-digit or character field. All data are read in 10E7.0 format, and all control cards and the title card are read in 16A5 format. All input data are on punched cards. The following control cards are valid:

TITLE;

CONSTANTS;

MASS FLOW RATES;

Z(HUB) AT NORMALS;

Z(TIP GUESS) AT NORMALS;

TABLE;

GEOMETRY PLOT;

BEGIN COMPUTE;

END PLOT.

All numerical input data must have decimal points. A complete explanation of the input data format is presented on the following pages.

Card No.	Field No.	Symbol	Description
1	1	TITLE	Control card indicating that a title card follows.
2	1-11		Comment: This information will be printed as a heading in each output page.
1	1-2	CONSTANTS	Control card indicating that constant data follow.
	3-11		Comment: This will be printed with input data for identification.

Card No.	Field No.	Symbol	Description
2	1	N	Shaft speed, rpm.
	2	B	No. impeller blades.
	3	norm	No. stations downstream from the inlet, $1 \leq norm \leq 19$; at least one required.
	4	CF	= 0 for using radial derivations at inlet; = 1 for setting these to zero.
	5	Z_{inlet}	Axial distance to inlet, in.
	6	BLF_{exit}	Exit total blockage, where last normal is considered the exit.
	7	n_{slip}	Station no. at which slip begins, where inlet station no. is 1. If $n_{slip} = 0$, the program will use k_{slip} to determine the slip station. If $n_{slip} > norm + 1$, slippage will not occur.
	8	k_{slip}	Factor program used to determine station at which slip begins (see Vector Diagrams section of this appendix).
1	1-3	MASS FLOW RATES	Control card indicating that mass flow rates follow.
	4-11		Comment.
2	1	W_{a1}	Mass flow rate, lbm/sec, for hub streamtube.
	2	W_{a2}	Mass flow rate, lbm/sec, for Streamtube 2.
	3	W_{a3}	Mass flow rate, lbm/sec, for Streamtube 3.
	4	W_{a4}	Mass flow rate, lbm/sec, for Streamtube 4.

Card No.	Field No.	Symbol	Description
	5	W_{a5}	Mass flow rate, lbm/sec, for tip streamtube.
1	1-3	Z(HUB)AT NORMALS	Control card indicating Z_{hub} values follow.
	4-11		Comment.
2	1	$Z_{hub,1}$	Axial distance, in., to intersection of hub profile and first normal downstream from inlet.
	2	$Z_{hub,2}$	Axial distance, in., to intersection of hub profile and second normal.
		$Z_{hub,norm}$	Axial distance, in., to intersection of hub profile and exit normal.

NOTE: The last normal is considered the exit. At least one Z_{hub} is required. These two cards must follow CONSTANTS card.

1	1-4	Z(TIP GUESS) AT NORMALS	Control card indicating that $Z_{tip\ guess}$ values follow.
	5-11		Comment.
2	1	$Z_{tip\ guess,1}$	First estimate of axial distance, in., to intersection of tip profile and first normal (see Normal Determination section).
	2	$Z_{tip\ guess,2}$	First estimate of axial distance, in., to intersection of tip profile and second normal.
		$Z_{tip\ guess,norm}$	First estimate of axial distance, in., to intersection of tip profile and exit normal.

NOTE: These two cards must follow CONSTANTS cards.

1	1	TABLE	Control card indicating that table data follow.

Card No.	Field No.	Symbol	Description
	2-11		Comment.
2	1	n_{tab}	Table no., $1 \leq n_{tab} \leq 20$.
	2	n_{pts}	No. points in this table, $2 \leq n_{pts} \leq 50$, except for input tables 4 and 5, then $4 \leq n_{pts} \leq 50$.
3	1	X_1	Independent argument.
	2	Y_1	Dependent argument corresponding to X_1.
		Xn_{tab}	
		Yn_{tab}	
1	1-2	GEOMETRY PLOT	Control card indicating that geometry plot is desired (see Section 3.2 of this appendix).
	3-11		Comment.
2	1	X_{grid}	Length, in., of Z plot scale; $1 \leq X_{grid} \leq 50$.
	2	Y_{grid}	Length, in., of R plot scale, $1 \leq Y_{grid} \leq 9.5$.
	3	ΔX	Axial increment, in., used for profile interpolations.
1	1-2	BEGIN COMPUTE	Control card indicating that all data for 1 case have been given and computation is beginning.
1	1-2	END PLOT	Control card indicating that the plotting generated by the previous GEOMETRY PLOT card is ended; the END PLOT card must follow a BEGIN COMPUTE card and cause the program to rewind and sign off the plot tape.

TEN FIELD, SEVEN DIGIT CRD FORMAT

1 — 7	8 — 14	15 — 21	22 — 28	29 — 35	36 — 42	43 — 49	50 — 56	57 — 63	64 — 70	71	72	IDENT — 80
TITLE												
(comment)												
CONSTANTS												
N	B	norm	CF	Z_{inlet}	BLF_{exit}	n_{slip}	k_{slip}					
MASS FLOW RATES												
W_{a1}	W_{a2}	W_{a3}	W_{a4}	W_{a5}								
Z(HUB) AT NORMALS												
Z_{hub1}	Z_{hub2}											
	. . . .		$Z_{hub\,norm}$									
Z(TIP GUESS) AT NORMALS												
$Z_{tip\,guess1}$	$Z_{tip\,guess2}$											
	. . . .		$Z_{tip\,guess\,norm}$									
TABLE												
n_{tab}	n_{pts}											
X_1	Y_1	X_2	Y_2	. . .								
					. . .							
					. . .	X_{npts}	Y_{npts}					
GEOMETRY PLOT												
X_{grid}	Y_{grid}	ΔX										
BEGIN COMPUTE												
END PLOT						NAME		DATE		PAGE	OF	

CONFIDENTIAL

A list of the tables needed for the program is given below. Independent variables must be input data in either increasing or decreasing order.

Table	Dependent Variable	Independent Variable	Comment
1	h(lbm)	T(°R)	For air at low pressure
2	P_r	T(°R)	For air at low pressure
3		T(°R)	For air at low pressure
4	R_{hub}(in.)	Z(in.)	Hub profile (minimum four points)
5	R_{tip}(in.)	Z(in.)	Tip profile (minimum four points)
6	T_{T1}(in. Hg)	R(in.)	Inlet pressure
7	T_{Ti}(°R)	R(in.)	Inlet temperature
8	BLF_1	R(in.)	Inlet total blockage
9	α_1(deg)	R(in.)	Inlet absolute flow angle
10	t_{hub}(in.)	Z(in.)	Hub blade thickness must include inlet t_{hub} measured in plane normal to axis of rotation
11	t_{tip}(in.)	Z(in.)	Tip blade thickness must include inlet t_{tip} measured in plane normal to axis of rotation
12	ϕ(deg)	Z_m(in.)	Blade angle, from inlet to exit
13	$\alpha_{3, exit}$(deg)	% H(from hub)	Exit relative flow angle: input if slip is to occur upstream from exit normal
14	δR_{ec}	% H (from hub)	Recovery correction factor vs % H at exit

Table	Dependent Variable	Independent Variable	Comment
15	$R_{ec_{i1}}$	M_2	Inducer recovery for hub tube
16	$R_{ec_{i2}}$	M_2	Inducer recovery for second tube
17	$R_{ec_{i3}}$	M_2	Inducer recovery for third tube
18	$R_{ec_{i4}}$	M_2	Inducer recovery for fourth tube
19	$R_{ec_{i5}}$	M_2	Inducer recovery for tip tube
20	$R_{c,hub}$(in.)	Z(in.)	Radius of curvature for hub profile
21	$R_{c,tip}$(in.)	Z(in.)	Radius of curvature for tip profile

All tables must have at least 2 points, and Tables 4 and 5 must have at least 4 points. Except for Tables 4 and 5, all table look-ups are accomplished by using linear interpolation across small segments. Third-degree polynomial interpolation is used for the hub and tip profiles (see Tables 4 and 5).

Third-degree interpolation involves finding the third-degree polynomial passing through the 4 points nearest the value of interest. This method is used to calculate numerically the derivatives dR/dZ and d^2R/dZ^2 in the normal finding and to determine the radius of curvature at the inlet. The interpolated curve will pass through the input points, but care must be taken in defining the profiles so that the interpolated curves observed on the plot have the desired smoothness and curvature. To ensure a straight-line segment, 4 points should be inserted as input data. Smooth curves should be represented with points that are spaced about evenly with points closer together where the curvature is greatest. Several points should be given to define the curves upstream from the inlet and downstream from the exit normal.

3.2 OUTPUT DESCRIPTION

Input data are printed out as they are read. Computed results for each station are output data, with 1 page of output data per station. The case title, station number, and streamtube numbers are printed, as are the data labels and units.

When a Tally plot is specified, the program generates a labeled plot of points for the following 9 curves: hub profile, tip profile, interpolated (third-degree) hub profile, interpolated (third-degree) tip profile, and 5 streamlines. The plot is titled and the axes are labeled.

3.3 SAMPLE CASE

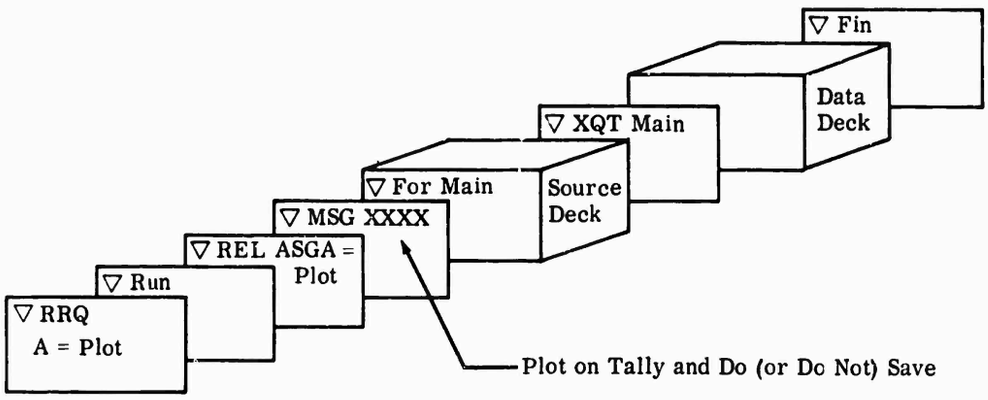
The following 3 pages list the input data deck, and are followed by the corresponding program output data.

4.0 OPERATING INFORMATION

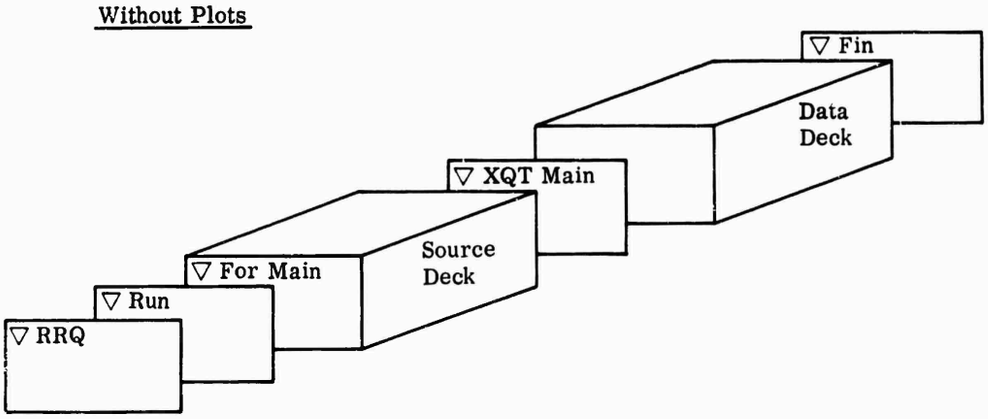
4.1 PROGRAM AND DATA SETUP

The deck setups for the SRU 1107 computer are shown below. If more than 1 plot is needed, the plot tape should be saved.

With Tally Plots



Without Plots



```
- XQT MAIN
TITLE
AS 2496 TEST CASE
CONSTANTS
57000. 22.    7.     0.     0.     .88    5.     0.
MASS FLOW RATES
.4     .4     .4     .4     .4
Z(HUB) AT NORMALS
.83    1.685  2.485  3.08   3.442  3.55   3.653
Z(TIP GUESS) AT NORMALS
.8     1.5    2.2    2.7    3.2    3.3    3.5
TABLE 1        H=F(T) FOR AIR
1.     50.
100.   23.74  125.   29.72  150.   35.71  175.   41.69  200.   47.67
225.   53.66  250.   59.64  275.   65.62  300.   71.61  325.   77.59
350.   83.57  375.   89.55  400.   95.53  425.   101.52 450.   107.50
475.   113.50 500.   119.48 525.   125.47 550.   131.46 575.   137.47
600.   143.47 650.   155.50 700.   167.56 750.   179.66 800.   191.81
850.   204.01 900.   216.26 950.   228.58 1000.  240.98 1050.  253.45
1100.  265.99 1150.  278.61 1200.  291.30 1250.  304.08 1300.  316.94
1350.  329.88 1400.  342.90 1450.  356.00 1500.  369.17 1550.  382.42
1600.  395.74 1700.  422.59 1800.  449.72 1900.  477.09 2000.  504.71
3000.  790.68 4000.  1088.265000.  1392.876000.  1702.996500.  1858.44
TABLE 2        PR=F(T) FOR AIR
2.     44.
420.   .5760  440.   .6776  460.   .7923  480.   .9182  500.   1.059
520.   1.2147 540.   1.386  560.   1.5742 580.   1.78   600.   2.005
620.   2.249  640.   2.514  660.   2.801  680.   3.111  700.   3.446
720.   3.806  740.   4.193  760.   4.607  780.   5.051  800.   5.526
820.   6.033  840.   6.573  860.   7.149  880.   7.761  900.   8.411
920.   9.102  940.   9.834  960.   10.61  980.   11.43  1000.  12.298
1020.  13.215 1040.  14.182 1060.  15.203 1080.  16.278 1100.  17.413
1120.  18.604 1140.  19.858 1160.  21.18  1180.  22.56  1200.  24.01
1220.  25.53  1240.  27.13  1260.  28.80  1280.  30.55
TABLE 3        K=F(T) FOR AIR
3.     35.
300.   1.4024 350.   1.4023 400.   1.4020 450.   1.4016 500.   1.4010
550.   1.4000 600.   1.3989 650.   1.3975 700.   1.3960 750.   1.3941
800.   1.3920 850.   1.3897 900.   1.3870 950.   1.3842 1000.  1.3810
1050.  1.3776 1100.  1.3741 1150.  1.3710 1200.  1.3679 1250.  1.3649
1300.  1.3620 1350.  1.3590 1400.  1.356  1450.  1.3536 1500.  1.3504
1550.  1.3477 1600.  1.3453 1650.  1.3429 1700.  1.3405 1750.  1.3381
1800.  1.3361 1850.  1.3341 1900.  1.3320 1950.  1.3301 2000.  1.3282
TABLE 4 R(HUB)=F(Z)
4.     9.
-.4    1.176  .41    1.187  1.26   1.285  2.105  1.56   2.825  2.097
3.292  2.839  3.5    3.439  3.653  4.01   3.75   4.373
TABLE 5 R(TIP)=F(Z)
5.     9.
-.4    1.964  .384   1.977  1.136  2.046  1.854  2.22   2.461  2.510
2.996  3.008  3.256  3.512  3.471  4.068  3.6    4.403
TABLE 6 PT1=F(R)
6.     2.
1.     29.62  2.     29.62
```

```
TABLE 7 TT1=F(R)
7.      2.
1.      519.7   2.      519.7
TABLE 8 BLF1=F(R)
8.      2.
1.      .9      2.      .9
TABLE 9 ALPHA1=F(R)
9.      2.
1.      0.      2.      0.
TABLE 10 T(HUB)=F(Z)
10.     15.
0.      .046    .2      .079    .41     .100    .833    .110    1.26    .120
1.69    .130    2.102   .130    2.484   .125    2.824   .124    3.083   .116
3.292   .103    3.441   .093    3.5     .083    3.55    .078    3.653   .048
TABLE 11 T(TIP)=F(Z)
11.     15.
0.      .046    .193    .043    .284    .038    .768    .035    1.138   .032
1.508   .03     1.854   .028    2.162   .026    2.462   .026    2.743   .025
2.996   .025    3.184   .025    3.256   .025    3.325   .025    3.471   .025
TABLE 12 PHI=F(Z-MID)
12.     7.
0.      50.     .4      44.7    .8      37.9    1.96    19.7    2.913   1.5
3.148   0.      3.562   0.
TABLE 13 ALPHA(EXIT)=F(PERCENT BLADE HEIGHT)
13.     12.
10.     42.5    28.     32.5    34.     30.     38.     29.4    44.     29.
50.     29.     56.     29.1    60.     29.2    64.     29.6    68.     30.5
80.     37.5    100.    49.5
TABLE 14 REC CORR FACTOR=F(PERCENT BLADE HEIGHT)
14.     2.
0.      .95     100.    .95
TABLE 15 INDUCER REC1=F(M2)
15.     6.
.35     .98     .45     .979    .55     .973    .65     .964    .75     .951
.85     .936
TABLE 16 INDUCER REC2=F(M2)
16.     6.
.4      .99     .5      .99     .6      .986    .7      .98     .8      .972
.9      .962
TABLE 17 INDUCER REC3=F(M2)
17.     6.
.45     .996    .55     .995    .65     .991    .75     .986    .85     .98
.95     .974
TABLE 18 INDUCER REC4=F(M2)
18.     6.
.5      .987    .6      .982    .7      .974    .8      .964    .9      .953
1.      .940
TABLE 19 INDUCER REC5=F(M2)
19.     6.
.55     .965    .65     .952    .75     .936    .85     .917    .95     .896
1.05    .874
TABLE 20  HUB RC=F(X)
20.     7.
.83     5.55    1.7     2.85    2.5     1.75    3.1     2.15    3.4     7.5
```

```
3.55    21.25  3.65    100.
TABLE 21  TIP RC=F(X)
21.     7.
.75     6.65   1.5     3.8     2.15    2.25    2.75    1.3     3.2     4.65
3.3     13.2   3.5     70.
GEOMETRY PLOT
12.4    9.50   .0050
BEGIN COMPUTE
END PLOT
- FIN
```

000118

IMPELLER RADIAL EQUILIBRIUM DESIGN PROGRAM INPUT

TITLE

AS 2496 TEST CASE

CONSTANTS

57000.0	22.	7.	8.	.0000	.8800	5.	.0000

MASS FLOW RATES

.4000	.4000	.4000	.4000	.4000

Z(HUB) AT NORMALS

.8300	1.6850	2.4850	3.0000	3.4920	3.5500	3.6530

Z(TIP GUESS) AT NORMALS

.8000	1.5000	2.2000	2.7000	3.2000	3.3000	3.5000

TABLE 1 RHO=F(T) FOR AIR PRINT

1.	50.								
100.0000	23.7400	125.0000	29.7200	150.0000	35.7100	175.0000	41.6900	200.0000	47.6700
225.0000	53.6600	250.0000	59.6400	275.0000	65.6200	300.0000	71.6100	325.0000	77.5900
350.0000	83.5700	375.0000	89.5500	400.0000	95.5300	425.0000	101.5200	450.0000	107.5000
475.0000	113.5000	500.0000	119.4800	525.0000	125.4700	550.0000	131.4600	575.0000	137.4700
600.0000	143.4700	650.0000	155.5000	700.0000	167.5600	750.0000	179.6600	800.0000	191.8100
850.0000	204.0100	900.0000	216.2600	950.0000	228.5800	1000.0000	240.9800	1050.0000	253.4500
1100.0000	265.9900	1149.9999	278.6100	1200.0000	291.3000	1250.0000	304.0800	1300.0000	316.9400
1350.0000	329.8800	1399.9999	342.9000	1450.0000	356.0000	1500.0000	369.1700	1549.9999	382.6200
1600.0000	395.7400	1699.9999	422.5900	1800.0000	449.7100	1900.0000	477.0900	2000.0000	504.7100
3000.0000	790.6000	4000.0000	1088.2600	5000.0000	1392.8699	5999.9999	1702.9899	6500.0000	1858.4400

TABLE 2 PRS=F(T) FOR AIR PRINT

2.	44.								
420.0000	.5760	440.0000	.6776	460.0000	.7923	480.0000	.9182	500.0000	1.0590
520.0000	1.2147	540.0000	1.3860	560.0000	1.5742	580.0000	1.7800	600.0000	2.0050
620.0000	2.2490	640.0000	2.5140	660.0000	2.8010	680.0000	3.1110	700.0000	3.4460
720.0000	3.8060	740.0000	4.1930	760.0000	4.6070	780.0000	5.0510	800.0000	5.5260
820.0000	6.0330	840.0000	6.5730	860.0000	7.1490	880.0000	7.7610	900.0000	8.4110
920.0000	9.1020	940.0000	9.8340	960.0000	10.6100	980.0000	11.4300	1000.0000	12.2980
1020.0000	13.2150	1039.9999	14.1820	1060.0000	15.2030	1080.0000	16.2780	1100.0000	17.4130
1120.0000	18.6040	1140.0000	19.8585	1160.0000	21.1800	1179.9999	22.5600	1200.0000	24.0100
1219.9999	25.5300	1240.0000	27.1340	1259.9999	28.8080	1280.0000	30.5500		

TABLE 3 K=F(T) FOR AIR PRINT

3.	35.								
300.0000	1.4024	350.0000	1.4023	400.0000	1.4020	450.0000	1.4016	500.0000	1.4010
550.0000	1.4000	600.0000	1.3989	650.0000	1.3975	700.0000	1.3960	750.0000	1.3941
800.0000	1.3920	850.0000	1.3897	900.0000	1.3870	950.0000	1.3842	1000.0000	1.3810
1050.0000	1.3776	1100.0000	1.3741	1149.9999	1.3710	1200.0000	1.3679	1250.0000	1.3649

1300.0000	1.3620	1350.0000	1.3590	1399.9999	1.3560	1450.0000	1.3536	1500.0000	1.3504
1549.9999	1.3477	1600.0000	1.3453	1650.0000	1.3429	1699.9999	1.3405	1750.0000	1.3381
1800.0000	1.3361	1849.9999	1.3341	1900.0000	1.3320	1950.0000	1.3301	2000.0000	1.3282

TABLE 4 R(HUB)=F(Z)

4.		9.							
-.4000	1.1760	.4100	1.1870	1.2600	1.2850	2.1050	1.5600	2.8250	2.0970
3.2920	2.8390	3.5000	3.4390	3.6530	4.0100	3.7500	4.3730		

TABLE 5 R(TIP)=F(Z)

5.		9.							
-.4000	1.9440	.3840	1.9770	1.1360	2.0460	1.8540	2.2200	2.4610	2.5100
2.9960	3.0080	3.2560	3.5120	3.4710	4.0600	3.6000	4.4030		

TABLE 6 PT1=F(R)

6.		2.	
1.0000	29.6200	2.0000	29.6200

TABLE 7 TT1=F(R)

7.		2.	
1.0000	519.7000	2.0000	519.7000

TABLE 8 RLF1=F(R)

8.		2.	
1.0000	.9000	2.0000	.9000

TABLE 9 ALPHA1=F(R)

9.		2.	
1.0000	.0000	2.0000	.0000

TABLE 10 Y(HUB)=F(Z)

10.		15.							
.0000	.0460	.2000	.0790	.3100	.1000	.8330	.1100	1.2600	.1200
1.6900	.1300	2.1020	.1300	2.4840	.1250	2.8240	.1240	3.0830	.1160
3.2920	.1050	3.4410	.0930	3.5000	.0830	3.5500	.0780	3.6530	.0480

TABLE 11 Y(TIP)=F(Z)

11.		15.							
.0000	.0460	.1930	.0430	.3840	.0380	.7680	.0350	1.1360	.0320
1.5080	.0300	1.8540	.0280	2.1620	.0260	2.4620	.0260	2.7430	.0250
2.9960	.0250	3.1840	.0250	3.2560	.0250	3.3250	.0250	3.4710	.0320

TABLE 12 PHI=F(Z-MID)

12.		7.							
.0000	56.0000	.4000	44.7000	.8000	37.9000	1.9600	19.7000	2.9130	1.0000
3.1480	.0000	3.5420	.0000						

TABLE 13 ALPHA(EXIT)=F(PERCENT BLADE HEIGHT)

CONFIDENTIAL

```
                13.       12.
          10.0000   42.5000   28.0000   32.5000   34.0000   30.0000   38.0000   29.4000   44.0000   29.0000
          50.0000   29.0000   56.0000   29.1000   60.0000   29.2000   64.0000   29.6000   68.0000   30.5000
          80.0000   37.5000  100.0000   49.5000

TABLE 14 REC CORR FACTOR=F(PERCENT BLADE HEIGHT)
                14.       2.
            .0000     .9500  100.0000     .9500

TABLE 15 INDUCER REC1=F(M2)
                15.       6.
            .3500     .9800     .4500     .9790     .5500     .9730     .6500     .9640     .7500     .9510
            .8500     .9360

TABLE 16 INDUCER REC2=F(M2)
                16.       6.
            .4000     .9900     .5000     .9900     .6000     .9860     .7000     .9800     .8000     .9720
            .9000     .9620

TABLE 17 INDUCER REC3=F(M2)
                17.       6.
            .6500     .9960     .5500     .9950     .6500     .9910     .7500     .9840     .8500     .9400
            .9500     .9740

TABLE 18 INDUCER REC4=F(M2)
                18.       6.
            .5000     .9870     .6000     .9820     .7000     .9740     .8000     .9640     .9000     .9530
           1.0000     .9400

TABLE 19 INDUCER REC5=F(M2)
                19.       6.
            .5500     .9650     .6500     .9520     .7500     .9360     .8500     .9170     .9500     .4960
           1.0500     .8700

TABLE 20  HUB RC=F(X)
                20.       7.
            .0300    5.5500    1.7000    2.8500    2.5000    1.7500    3.1000    2.1500    3.4000    7.5000
           3.3500   21.2500    3.6500  100.0000

TABLE 21  TIP RC=F(X)
                21.       7.
            .7500    6.6500    1.5000    3.6000    2.1500    2.2500    2.7500    1.3000    3.2000     .6000
           3.3000   13.2000    3.5000   70.0000

GEOMETRY PLOT
               12.00      9.50      .0050

BEGIN COMPUTE
```

CONFIDENTIAL

IMPELLER RADIAL EQUILIBRIUM DESIGN RESULTS FOR STATION 1

AS 2496 TEST CASE

STREAMTUBE	HUB	1	2	3	4	5	TIP
DISTANCES(INCHES)							
AXIAL	.000	.000	.000	.000	.000	.000	.000
RADIAL	1.177	1.279	1.462	1.623	1.769	1.904	1.967
MERIDIONAL				.000			
RADIUS OF CURVATURE	10.97	17.95	19.98	20.61	21.47	22.11	22.34
ACTUAL AREA(SQ IN)		1.579	1.569	1.561	1.554	1.548	7.609
BLOCKAGE FACTOR		.900	.900	.900	.900	.900	
TEMPERATURES(DEG R)							
TOTAL		519.7	519.7	519.7	519.7	519.7	
STATIC		486.2	485.5	485.0	484.5	484.1	
RELATIVE TOTAL		553.5	563.8	574.0	584.2	594.4	
PRESSURES(IN HG)							
TOTAL		29.62	29.62	29.62	29.62	29.62	
STATIC		23.47	23.36	23.26	23.16	23.11	
RELATIVE TOTAL		36.91	39.38	41.94	44.61	47.39	
MACH NUMBERS							
ABSOLUTE		.586	.592	.598	.602	.606	
RELATIVE		.831	.897	.957	1.014	1.067	
ANGLES(DEGREES)							
MERIDIONAL				.61			
ABSOLUTE FLUID		.00	.00	.00	.00	.00	
RELATIVE FLUID		45.10	48.64	51.36	53.56	55.37	
ABS VELOCITIES(FT/SEC)							
TOTAL		634.0	640.2	645.4	649.9	653.9	
TANGENTIAL		.0	.0	.0	.0	.0	
SOUND		1081.3	1080.6	1080.0	1079.4	1078.9	
WHEEL	585.2	636.1	727.1	807.4	880.0	946.9	978.5
REL VELOCITIES(FT/SEC)							
TOTAL		898.1	968.7	1033.6	1094.0	1150.8	
MERIDIONAL		634.0	640.2	645.4	649.9	653.9	
TANGENTIAL		636.1	727.1	807.4	880.0	946.9	

CONFIDENTIAL

IMPELLER RADIAL EQUILIBRIUM DESIGN RESULTS FOR STATION 2

AS 2496 TEST CASE

STREAMTUBE	HUB	1	2	3	4	5	TIP
DISTANCES(INCHES)							
AXIAL	.830	.817	.796	.781	.769	.758	.756
RADIAL	1.219	1.353	1.564	1.716	1.841	1.950	2.000
NORMAL	.0000	.1353	.3465	.4993	.6248	.7345	.7852
MERIDIONAL				.789			
RADIUS OF CURVATURE	5.55	5.74	6.03	6.24	6.41	6.56	6.63
ACTUAL AREA(SQ IN)		2.187	1.684	1.464	1.341	1.278	1.258
BLOCKAGE FACTOR		.737	.816	.861	.892	.916	
TEMPERATURES(DEG R)							
TOTAL		563.4	570.5	575.0	578.7	582.5	
STATIC		533.9	534.9	535.5	536.3	538.1	
RELATIVE TOTAL		557.5	570.1	580.4	589.5	598.8	
PRESSURES(IN HG)							
TOTAL		38.57	40.49	41.64	42.41	42.88	
STATIC		31.95	32.31	32.44	32.49	32.49	
RELATIVE TOTAL		37.16	38.39	43.08	45.29	47.01	
MACH NUMBERS							
ABSOLUTE		.526	.577	.608	.629	.642	
RELATIVE		.670	.678	.647	.794	.796	
ANGLES(DEGREES)							
MERIDIONAL				5.64			
BLADE				30.10			
ABSOLUTE FLUID		40.90	36.84	34.39	32.86	32.19	
RELATIVE FLUID		32.21	36.39	39.21	41.40	43.22	
ABS VELOCITIES(FT/SEC)							
TOTAL		595.3	654.8	689.3	713.5	730.2	
TANGENTIAL		389.7	392.1	389.4	387.2	389.0	
SOUND		1132.2	1133.2	1133.9	1134.6	1136.7	
WHEEL	686.3	673.2	777.8	853.4	915.6	969.8	994.9
REL VELOCITIES(FT/SEC)							
TOTAL		531.8	650.2	734.1	799.0	848.1	
MERIDIONAL		458.8	523.4	568.9	599.3	618.0	
TANGENTIAL		283.5	385.7	464.1	528.4	580.8	
SURFACE VEL(FT/SEC)							
SUCTION		584.4	716.6	808.2	879.6	934.8	
PRESSURE		479.3	583.8	660.1	718.4	761.3	
SUCTION/V2 MEAN		.565	.693	.782	.851	.904	
PRESSURE/V2 MEAN		.464	.565	.639	.695	.737	
REL TOTAL/V2 MEAN		.515	.629	.710	.773	.820	
ACCEL(FT/SEC SQ)		.9167+06	.6287+06	.4329+06	.3084+06	.2289+06	
RECOVERY		.9821	.9858	.9876	.9828	.9714	
DP/DN(IN HG/FT)		25.81	13.98	9.45	-.78	-4.83	

CONFIDENTIAL

IMPELLER RADIAL EQUILIBRIUM DESIGN RESULTS FOR STATION 3

AS 2496 TEST CASE

STREAMTUBE	HUB	1	2	3	4	5	TIP
DISTANCES(INCHES)							
AXIAL	1.685	1.649	1.592	1.554	1.524	1.498	1.486
RADIAL	1.388	1.523	1.727	1.863	1.972	2.068	2.113
NORMAL	.0000	.1485	.3528	.4930	.6060	.7054	.7519
MERIDIONAL				1.587			
RADIUS OF CURVATURE	2.90	3.08	3.34	3.52	3.67	3.79	3.85
ACTUAL AREA(SQ IN)		2.569	1.751	1.429	1.295	1.227	8.268
BLOCKAGE FACTOR		.722	.807	.853	.885	.911	
TEMPERATURES(DEG R)							
TOTAL		597.4	612.0	620.9	629.3	637.7	
STATIC		555.0	559.7	562.0	566.0	571.1	
RELATIVE TOTAL		567.5	581.2	591.2	599.8	607.8	
PRESSURES(IN HG)							
TOTAL		46.55	51.02	53.91	55.80	57.21	
STATIC		35.93	37.27	38.00	38.47	38.85	
RELATIVE TOTAL		38.85	42.52	45.36	47.17	48.29	
MACH NUMBERS							
ABSOLUTE		.620	.685	.725	.749	.765	
RELATIVE		.334	.438	.509	.546	.566	
ANGLES(DEGREES)							
MERIDIONAL				15.39			
BLADE				25.73			
ABSOLUTE FLUID		59.62	54.49	51.29	50.35	50.43	
RELATIVE FLUID		21.18	24.69	27.86	28.96	30.63	
ABS VELOCITIES(FT/SEC)							
TOTAL		715.6	794.6	842.5	873.3	895.9	
TANGENTIAL		617.3	646.8	637.5	672.4	690.6	
SOUND		1154.3	1159.2	1161.7	1165.8	1171.0	
WHEEL	690.2	757.6	859.8	926.6	980.8	1028.5	1030.8
REL VELOCITIES(FT/SEC)							
TOTAL		388.1	508.8	591.6	637.0	663.3	
MERIDIONAL		361.8	461.5	526.8	557.3	570.7	
TANGENTIAL		140.2	212.2	269.1	308.4	337.9	
SURFACE VEL(FT/SEC)							
SUCTION		465.8	597.9	689.2	742.4	777.7	
PRESSURE		318.3	418.1	494.0	531.5	548.8	
SUCTION/V2 MEAN		.451	.578	.667	.718	.752	
PRESSURE/V2 MEAN		.308	.404	.478	.514	.531	
REL TOTAL/V2 MEAN		.375	.491	.572	.616	.642	
ACCEL(FT/SEC SQ)		.2384+07	.2036+07	.1739+07	.1637+07	.1638+07	
RECOVERY		.9648	.9718	.9758	.9638	.9423	
DP/DN(IN HG/FT)		82.56	66.84	52.84	44.69	41.68	

IMPELLER RADIAL EQUILIBRIUM DESIGN RESULTS FOR STATION 4

AS 2496 TEST CASE

STREAMTUBE	HUB	1	2	3	4	5	TIP
DISTANCES(INCHES)							
AXIAL	2.485	2.427	2.336	2.279	2.224	2.176	2.153
RADIAL	1.774	1.873	2.026	2.129	2.215	2.295	2.335
NORMAL	.8888	.1143	.2922	.4125	.5120	.6055	.6525
MERIDIONAL				2.379			
RADIUS OF CURVATURE	1.77	1.85	1.98	2.07	2.14	2.21	2.25
ACTUAL AREA(SQ IN)		2.618	1.749	1.402	1.313	1.337	1.425
BLOCKAGE FACTOR		.764	.824	.860	.887	.910	
TEMPERATURES(DEG R)							
TOTAL		655.8	673.4	684.9	696.2	708.9	
STATIC		584.2	590.0	593.4	599.7	608.8	
RELATIVE TOTAL		591.9	604.2	613.9	620.7	628.1	
PRESSURES(IN HG)							
TOTAL		63.84	70.45	75.17	78.18	80.53	
STATIC		42.22	44.21	45.36	46.23	47.11	
RELATIVE TOTAL		45.28	48.84	50.85	52.14	52.56	
MACH NUMBERS							
ABSOLUTE		.786	.845	.882	.901	.911	
RELATIVE		.257	.347	.407	.418	.399	
ANGLES(DEGREES)							
MERIDIONAL				30.78			
BLADE				13.05			
ABSOLUTE FLUID		71.[illegible]	66.29	63.39	63.42	65.25	
RELATIVE FLUID		9.45	12.16	14.03	15.57	17.07	
ABS VELOCITIES(FT/SEC)							
TOTAL		931.3	1005.3	1052.7	1081.1	1101.2	
TANGENTIAL		881.4	920.5	961.2	966.8	1000.0	
SOUND		1184.4	1190.2	1193.6	1200.0	1209.0	
WHEEL	882.6	931.4	1007.5	1059.8	1101.6	1141.6	1161.7
REL VELOCITIES(FT/SEC)							
TOTAL		304.8	413.5	486.1	502.1	482.3	
MERIDIONAL		300.4	404.2	471.6	483.7	461.1	
TANGENTIAL		58.[illegible]	87.1	117.8	134.8	141.6	
SURFACE VEL(FT/SEC)							
SUCTION		972.3	579.5	655.0	674.7	661.7	
PRESSURE		137.3	247.5	317.2	329.6	302.9	
SUCTION/V2 MEAN		.457	.561	.634	.653	.640	
PRESSURE/V2 MEAN		.133	.239	.307	.319	.293	
REL TOTAL/V2 MEAN		.285	.400	.470	.486	.467	
ACCEL(FT/SEC SQ)		.3698+07	.3327+07	.3004+07	.3045+07	.3342+07	
RECOVERY		.9482	.9573	.9626	.9559	.9138	
DP/DN(IN HG/FT)		146.36	127.70	108.60	106.58	117.57	

CONFIDENTIAL

IMPELLER RADIAL EQUILIBRIUM DESIGN RESULTS FOR STATION 5

AS 2499 TEST CASE

STREAMTUBE	HUB	1	2	3	4	5	TIP
DISTANCES(INCHES)							
AXIAL	3.000	3.037	2.981	2.900	2.842	2.776	2.739
RADIAL	2.438	2.454	2.617	2.568	2.616	2.671	2.701
NORMAL	.0000	.0560	.1444	.2344	.3094	.3951	.4426
MERIDIONAL				3.198			
RADIUS OF CURVATURE	2.14	2.03	1.85	1.70	1.56	1.48	1.32
ACTUAL AREA(SQ IN)		1.713	1.361	1.194	1.098	1.089	7.114
BLOCKAGE FACTOR		.000	.030	.053	.074	.092	
TEMPERATURES(DEG R)							
TOTAL		705.2	777.9	788.8	788.7	818.6	
STATIC		632.8	634.4	636.8	644.8	657.3	
RELATIVE TOTAL		643.6	686.8	655.4	668.5	664.4	
PRESSURES(IN HG)							
TOTAL		107.53	115.89	122.39	124.99	123.68	
STATIC		90.79	96.22	97.36	98.68	89.73	
RELATIVE TOTAL		98.18	61.23	63.44	63.65	62.71	
MACH NUMBERS							
ABSOLUTE		1.034	1.074	1.102	1.104	1.098	
RELATIVE		.397	.392	.383	.383	.265	
ANGLES(DEGREES)							
MERIDIONAL				88.21			
BLADE				1.67			
ABSOLUTE FLUID		73.30	70.88	69.68	71.35	73.94	
RELATIVE FLUID		.00	.00	.00	.00	.00	
ABS VELOCITIES(FT/SEC)							
TOTAL		1270.4	1325.8	1342.2	1373.5	1369.6	
TANGENTIAL		1220.6	1252.8	1277.4	1301.3	1328.6	
SOUND		1232.3	1234.2	1236.5	1244.8	1254.2	
WHEEL	1292.8	1220.6	1252.8	1277.4	1301.3	1328.6	1363.6
REL VELOCITIES(FT/SEC)							
TOTAL		366.3	433.9	473.1	439.8	332.8	
MERIDIONAL		366.3	433.9	473.1	439.8	332.8	
TANGENTIAL		.0	.0	.0	.0	.0	
SURFACE VEL(FT/SEC)							
SUCTION		630.8	687.6	729.2	685.8	587.4	
PRESSURE		181.8	180.2	225.9	193.9	78.1	
SUCTION/V2 MEAN		.618	.669	.697	.663	.568	
PRESSURE/V2 MEAN		.099	.176	.219	.188	.076	
REL TOTAL/V2 MEAN		.304	.429	.458	.425	.322	
ACCEL(FT/SEC SQ)		.3071+07	.3562+07	.3303+07	.3409+07	.4130+07	
RECOVERY		.9287	.9434	.9305	.9283	.8858	
DP/DN(IN HG/FT)		198.18	177.82	163.48	178.61	203.99	

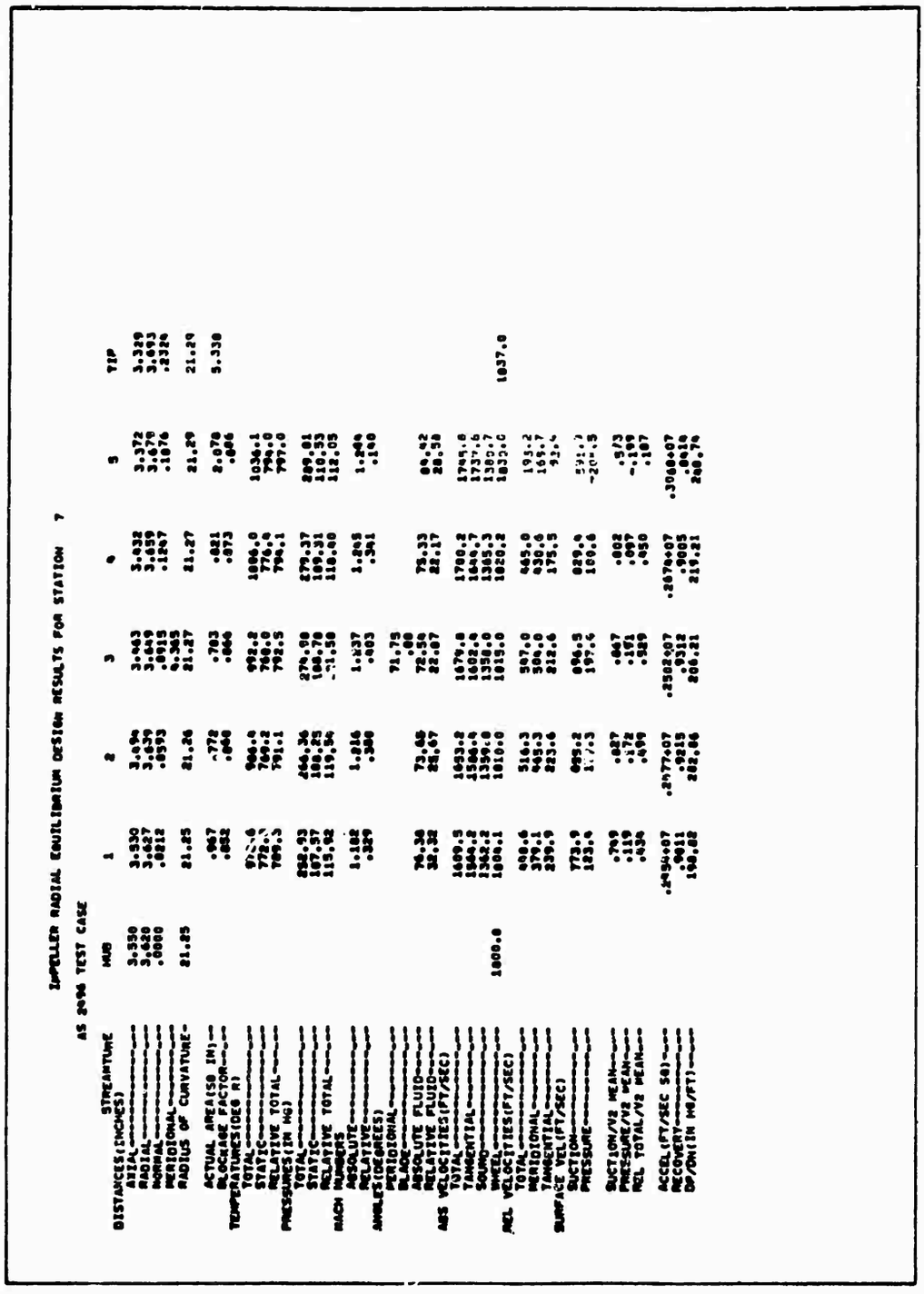
CONFIDENTIAL

IMPELLER RADIAL EQUILIBRIUM DESIGN RESULTS FOR STATION 6

AS 2496 TEST CASE

STREAMTUBE	HUB	1	2	3	4	5	TIP
DISTANCES(INCHES)							
AXIAL	3.002	3.017	3.371	3.331	3.291	3.227	3.184
RADIAL	3.259	3.262	3.281	3.296	3.312	3.338	3.355
NORMAL	.0000	.0273	.0768	.1192	.1625	.2320	.2780
MERIDIONAL				3.991			
RADIUS OF CURVATURE	11.[illegible]	10.68	9.47	8.43	7.37	5.66	4.53
ACTUAL AREA(SQ IN)		1.117	.916	.837	.762	1.941	5.771
BLOCKAGE FACTOR		.839	.851	.861	.872	.888	
TEMPERATURES(DEG R)							
TOTAL		907.8	916.4	921.6	930.8	948.7	
STATIC		723.6	721.3	720.9	726.6	743.3	
RELATIVE TOTAL		738.2	748.6	742.7	744.9	748.4	
PRESSURES(IN HG)							
TOTAL		199.26	205.16	211.41	212.42	213.73	
STATIC		83.99	86.80	87.47	88.15	89.37	
RELATIVE TOTAL		92.29	95.31	97.20	95.31	91.14	
MACH NUMBERS							
ABSOLUTE		1.149	1.184	1.202	1.199	1.193	
RELATIVE		.329	.369	.392	.336	.168	
ANGLES(DEGREES)							
MERIDIONAL				68.26			
BLADE				.00			
ABSOLUTE FLUID		78.87	72.71	71.70	74.36	82.44	
RELATIVE FLUID		22.23	17.24	15.63	15.70	20.62	
ABS VELOCITIES(FT/SEC)							
TOTAL		1514.4	1558.6	1580.8	1586.2	1595.4	
TANGENTIAL		1483.3	1488.1	1500.8	1527.3	1581.5	
SOUND		1318.0	1316.8	1315.6	1322.7	1335.8	
WHEEL	1617.7	1622.7	1631.9	1639.7	1647.7	1660.5	1668.9
REL VELOCITIES(FT/SEC)							
TOTAL		421.5	449.1	515.5	448.8	224.2	
MERIDIONAL		390.2	443.3	496.5	428.2	209.8	
TANGENTIAL		159.5	145.8	138.9	120.4	79.0	
SURFACE VEL(FT/SEC)							
SUCTION		726.9	790.7	816.4	751.6	554.2	
PRESSURE		116.2	179.6	214.7	138.1	-105.7	
SUCTION/V2 MEAN		.703	.765	.790	.727	.536	
PRESSURE/V2 MEAN		.112	.174	.208	.134	-.102	
REL TOTAL/V2 MEAN		.408	.469	.499	.430	.217	
ACCEL(FT/SEC SQ)		.2746+07	.2728+07	.2686+07	.2831+07	.3237+07	
RECOVERY		.9094	.9282	.9371	.9098	.8558	
DP/DK(IN HG/FT)		190.05	191.23	189.82	190.26	225.73	

CONFIDENTIAL



IMPELLER RADIAL EQUILIBRIUM DESIGN RESULTS FOR STATION 7

AS 2096 TEST CASE

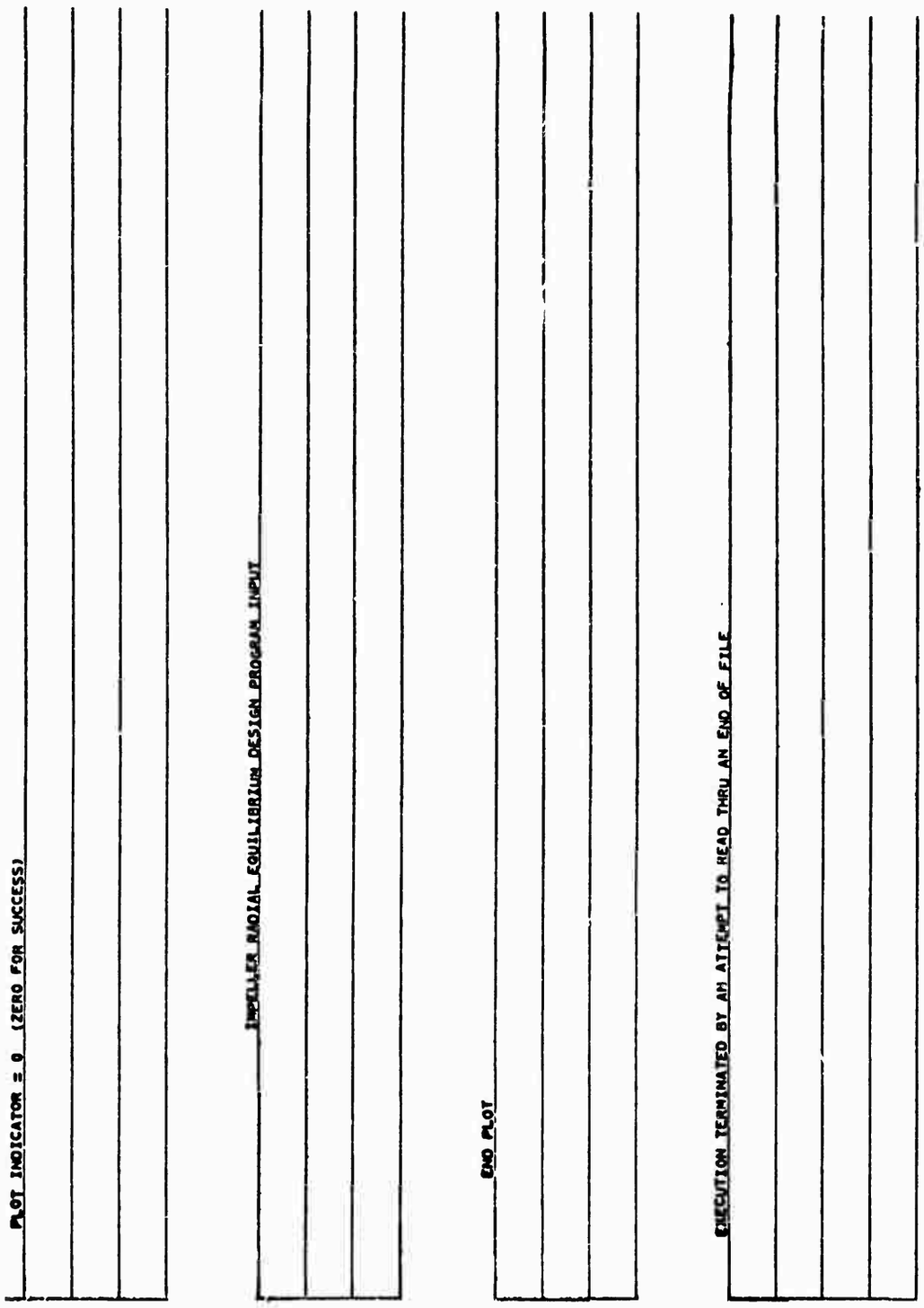
STREAMTUBE	HUB	1	2	3	4	5	TIP
DISTANCES(INCHES)							
AXIAL	3.330	3.530	3.494	3.463	3.432	3.372	3.329
RADIAL	3.620	3.627	3.634	3.649	3.659	3.678	3.693
NORMAL	.0000	.0812	.0593	.0313	.1267	.1076	.2326
MERIDIONAL				.0363			
RADIUS OF CURVATURE	21.25	21.26	21.26	21.27	21.27	21.29	21.29
ACTUAL AREA(SQ IN)		.967	.772	.703	.821	2.078	5.338
BLOCKAGE FACTOR		.852	.890	.866	.873	.846	
TEMPERATURES(DEG R)							
TOTAL		959.4	964.4	962.2	1064.0	1036.1	
STATIC		778.1	766.2	760.0	776.4	796.0	
RELATIVE TOTAL		959.4	964.4	962.2	794.1	797.0	
PRESSURES(IN HG)		799.3	791.1	782.5			
TOTAL		858.93	866.36	870.98	879.37	889.81	
STATIC		187.57	180.25	168.78	189.31	110.53	
RELATIVE TOTAL		119.82	119.36	71.58	110.80	112.05	
MACH NUMBERS							
ABSOLUTE		1.102	1.216	1.237	1.265	1.244	
RELATIVE		.829	.380	.803	.341	.100	
ANGLES(DEGREES)							
MERIDIONAL				71.75			
BLADE				.00			
ABSOLUTE FLUID		76.38	73.68	72.56	73.33	80.42	
RELATIVE FLUID		32.32	28.67	22.07	22.17	20.58	
ABS VELOCITIES(FT/SEC)							
TOTAL		1699.5	1693.2	1679.8	1700.2	1745.6	
TANGENTIAL		1644.2	1588.4	1602.4	1640.7	1737.6	
SOUND		1342.2	1339.0	1358.0	1305.3	1380.7	
WHEEL	1000.0	1000.1	1010.0	1019.0	1020.2	1033.0	1037.0
REL VELOCITIES(FT/SEC)							
TOTAL		898.6	516.3	507.0	445.0	193.2	
MERIDIONAL		379.1	469.3	500.0	430.6	165.7	
TANGENTIAL		239.9	223.6	212.6	175.5	93.4	
SURFACE VEL(FT/SEC)							
SUCTION		773.9	695.2	696.5	829.6	531.2	
PRESSURE		123.6	177.3	197.6	180.6	-20.5	
SUCTION/V2 MEAN		.799	.827	.847	.882	.573	
PRESSURE/V2 MEAN		.119	.172	.191	.097	-.199	
REL TOTAL/V2 MEAN		.436	.490	.389	.450	.187	
ACCEL(FT/SEC SQ)		.2494+07	.2477+07	.2582+07	.2674+07	.3068+07	
RECOVERY		.9011	.9215	.9312	.9005	.8010	
DF/ON(IN HG/FT)		190.88	202.86	206.21	219.21	260.76	

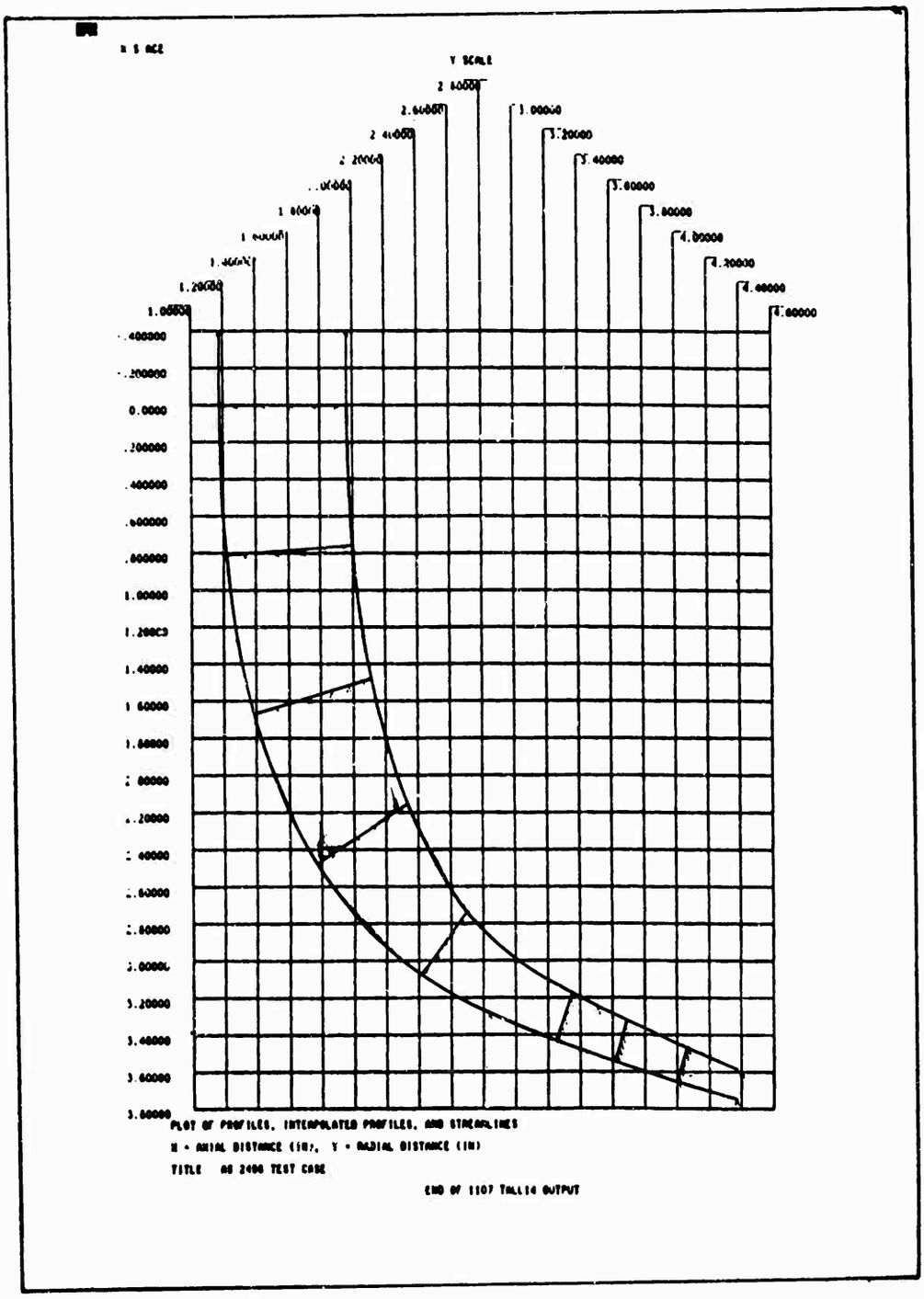
IMPELLER RADIAL EQUILIBRIUM DESIGN RESULTS FOR STATION 8

AS 2496 TEST CASE

STREAMTUBE	HUB	1	2	3	4	5	TIP
DISTANCES(INCHES)							
AXIAL	3.653	3.637	3.608	3.585	3.562	3.509	3.471
RADIAL	4.010	4.015	4.024	4.032	4.039	4.056	4.068
NORMAL	.0000	.0178	.0669	.0711	.0959	.1506	.1920
MERIDIONAL				4.767			
RADIUS OF CURVATURE	182.36	98.77	92.96	87.36	82.69	78.51	61.81
ACTUAL AREA(SQ IN)		.857	.651	.576	.483	2.105	4.072
BLOCKAGE FACTOR		.872	.875	.877	.880	.885	
TEMPERATURES(DEG R)							
TOTAL		1058.1	1065.5	1074.9	1093.8	1101.2	
STATIC		830.6	826.1	824.8	833.4	853.5	
RELATIVE TOTAL		849.4	850.9	852.1	853.3	856.1	
PRESSURES(IN HG)							
TOTAL		333.72	351.26	366.99	375.57	406.89	
STATIC		137.57	138.33	138.78	139.16	140.50	
RELATIVE TOTAL		148.99	153.72	156.26	151.39	141.99	
MACH NUMBERS							
ABSOLUTE		1.207	1.248	1.273	1.288	1.339	
RELATIVE		.341	.392	.419	.358	.123	
ANGLES(DEGREES)							
MERIDIONAL				72.89			
BLADE				-.08			
ABSOLUTE FLUID		70.12	73.91	73.42	76.24	85.76	
RELATIVE FLUID		63.14	34.49	29.56	29.00	36.68	
ABS VELOCITIES(FT/SEC)							
TOTAL		1784.9	1749.2	1790.3	1821.3	1917.2	
TANGENTIAL		1648.9	1688.8	1715.9	1769.1	1912.6	
SOUND		1612.2	1588.3	1586.6	1614.6	1631.5	
WHEEL	1994.6	1997.2	2001.7	2005.9	2009.2	2017.5	2023.7
REL VELOCITIES(FT/SEC)							
TOTAL		681.8	552.5	587.2	695.2	376.7	
MERIDIONAL		351.8	455.4	510.9	633.1	141.6	
TANGENTIAL		328.8	312.9	289.5	290.1	105.5	
SURFACE VEL(FT/SEC)							
SUCTION		781.8	883.7	993.8	863.7	368.8	
PRESSURE		180.9	221.4	238.7	126.7	-215.4	
SUCTION/V2 MEAN		.756	.885	.913	.836	.858	
PRESSURE/V2 MEAN		.175	.214	.223	.123	-.208	
REL TOTAL/V2 MEAN		.665	.535	.568	.679	.171	
ACCEL(FT/SEC SQ)		.2516+07	.2561+07	.2630+07	.8882+07	.3287+07	
RECOVERY		.8918	.9142	.9269	.8913	.8268	
DP/DN(IN HG/FT)		243.54	256.19	258.88	272.36	318.99	

CONFIDENTIAL


PLOT INDICATOR = 0 (ZERO FOR SUCCESS)
IMPELLER RADIAL EQUILIBRIUM DESIGN PROGRAM INPUT
END PLOT
EXECUTION TERMINATED BY AN ATTEMPT TO READ THRU AN END OF FILE


X SCALE
Y SCALE
PLOT OF PROFILES, INTERPOLATED PROFILES, AND STREAMLINES
X = AXIAL DISTANCE (IN), Y = RADIAL DISTANCE (IN)
TITLE AS 2400 TEST CASE
END OF 1107 TALLIE OUTPUT

4.2 RUN INFORMATION

A normal run is ended by attempting to read another case and by reading the end of file. The program may terminate the execution of a station and may print out the accumulated results and a diagnostic routine. The program diagnostic routine and originating routines are listed below.

MAIN

"THE FOLLOWING CONTROL CARD IS IN ERROR XXXX." This is caused by an incorrect control card or by a misplaced control card. Execution is attempted.

"PLOT INDICATOR = XX (ZERO FOR SUCCESS)." This is printed after an attempt to plot. If the number is zero, the plot was a success.

IMPEL

"THE TABLE LOOK-UP ON DA/DZ HAS FAILED FOR STATION XX." This refers to the computation of α_3 from $\frac{d\alpha''}{dz} - f(Z_m)$ in the Vector Diagrams section of this appendix and is caused by an error in input, probably in Table 12, reference page 43. The A-array is also printed, and execution for station XX is terminated.

"AT STREAMLINE X, STATION XX, A/A STAR FAILED TO CONVERGE." This refers to the M_3 bisection iteration of the Vector Diagrams section; it is printed after 20 iterations and is caused by bad inputs. It also refers to the adjustment of the initial area distribution in the Vector Diagrams section; it is printed after 10 adjustments, or, if the average $A/A^* < 1$, it is caused by bad inputs. The A-array is dumped, and execution for station XX is terminated.

"K FAILED TO CONVERGE AT STATION XX." This refers to the iteration on γ included in the M_3 solution of the Vector Diagrams section; it is printed after 10^3 iterations and is caused by bad input. The A-array is dumped, and execution is continued.

"AT STATION XX PS3 PRIME FAILED TO CONVERGE." This refers to the radial-equilibrium iteration in the Radial-Equilibrium Equation section of this appendix; it is printed after 20 iterations and it is caused by extreme inputs. The A-array is dumped, and execution is continued using the non-equilibrium results.

"PS3 PRIME ADJUSTMENT OF A ANN PRIME FAILED TO CONVERGE AT STATION XX." This is printed if the number of P'_{S3} adjustments in the Radial-Equilibrium Equation section have reached 300 during one dP_{S3}/dn iteration. The

A-array is printed, and execution is continued; the non-equilibrium results are used.

INLET

"THE AXIAL VELOCITY SQUARED IS XXX, AT STATION XX, STREAMLINE X, WHEN THE HUB VELOCITY EQUALS XXX." This indicates difficulty in the total mass balance iteration of the Velocity Profile section, which is caused by extreme inlet conditions. The program makes automatic adjustments and attempts a solution.

"THE PROGRAM WAS UNABLE TO OBTAIN A VELOCITY PROFILE THAT WOULD GIVE A MASS BALANCE AT STATION XX, EPS M = XX COMPUTED M = XX GIVEN M = XXX." This is caused by bad inputs associated with the inlet in the Total Mass Balance section, and the execution of this case is terminated.

"THE PROGRAM WAS UNABLE TO OBTAIN A CORRECT SET OF STREAMLINE POSITIONS AT STATION XX NO. INCORRECT X." This is caused by extreme inputs for the inlet (see Streamtube Mass Balance section), but remaining calculations are attempted.

CHORD

"THE NUMBER OF ITERATIONS ON SLOPES HAS EXCEEDED 100 AND THE ITERATION IS DISCONTINUED: XHUB YHUB HSLOPE XTIP YTIP TSLOPE ANGC XXX XXX XXX XXX XXX XXX XXX XXX."

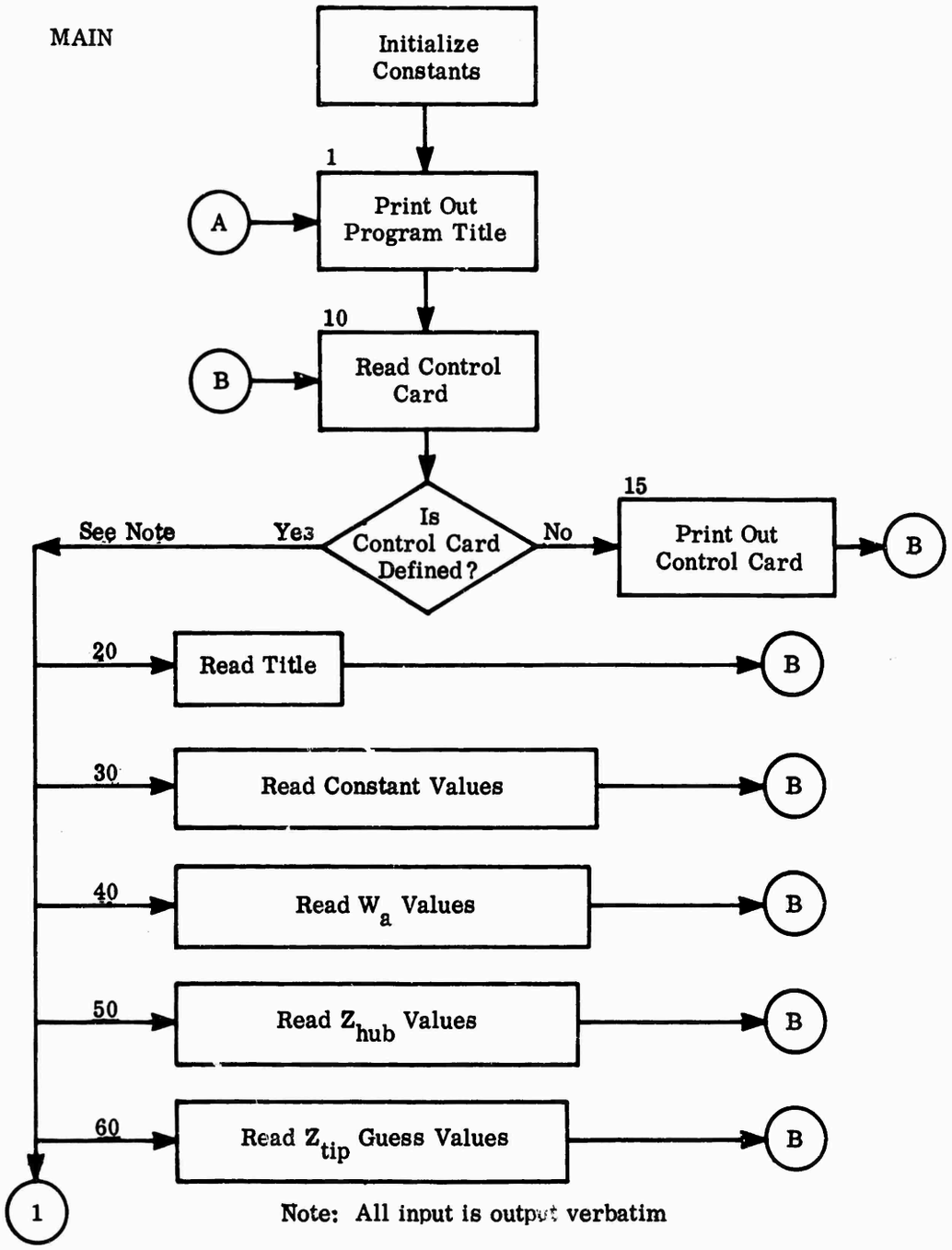
"AFTER 25 ITERATIONS CANNOT CONVERGE ON MIDSLOPE: X-GUESS Y-GUESS Y-PP X-HUB YHUB HSLOPE XTIP YTIP TSLOPE XXX XXX XXX XXX XXX XXX XXX XXX." These are caused by irregular hub or tip profiles, or a bad $Z_{\text{tip guess}}$. The results may still be usable and execution is attempted.

Average run time for a geometric plot of 15 stations is 2:00 minutes; it is 1:30 minutes without a plot. About 0:30 minute of this time is used for compilation, and this amount of time can be saved by placing the program complex file on magnetic tape or drum.

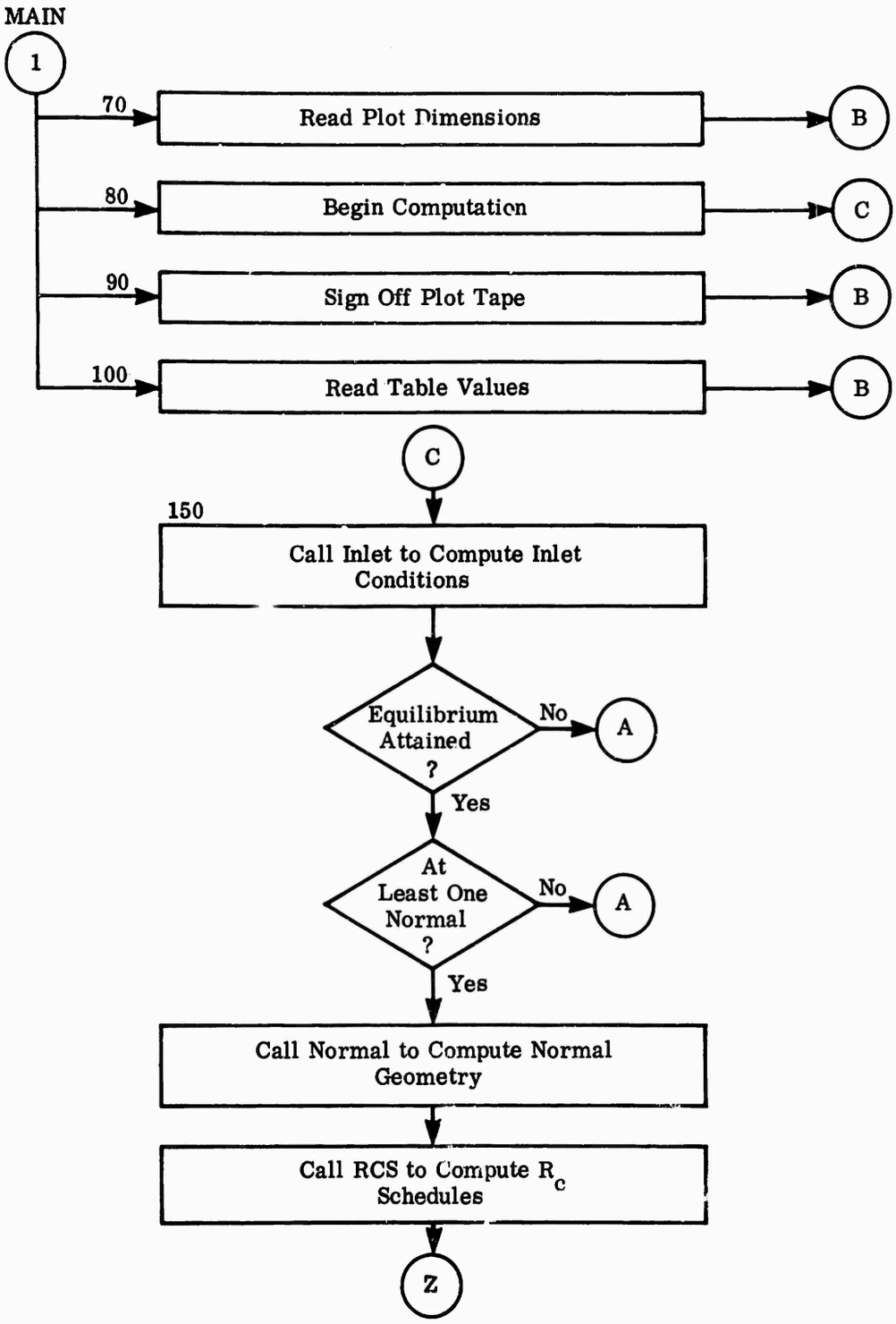
5.0 PROGRAMMING INFORMATION

5.1 FLOW DIAGRAMS

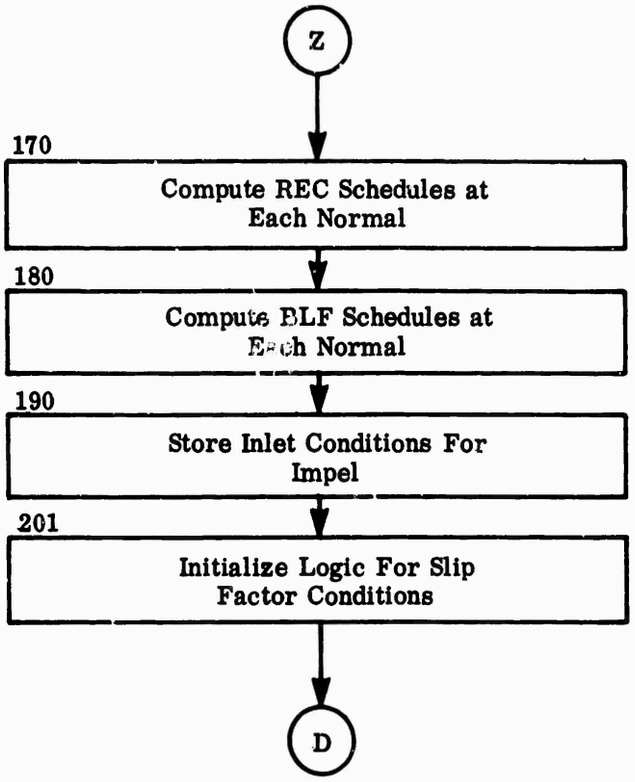
MAIN



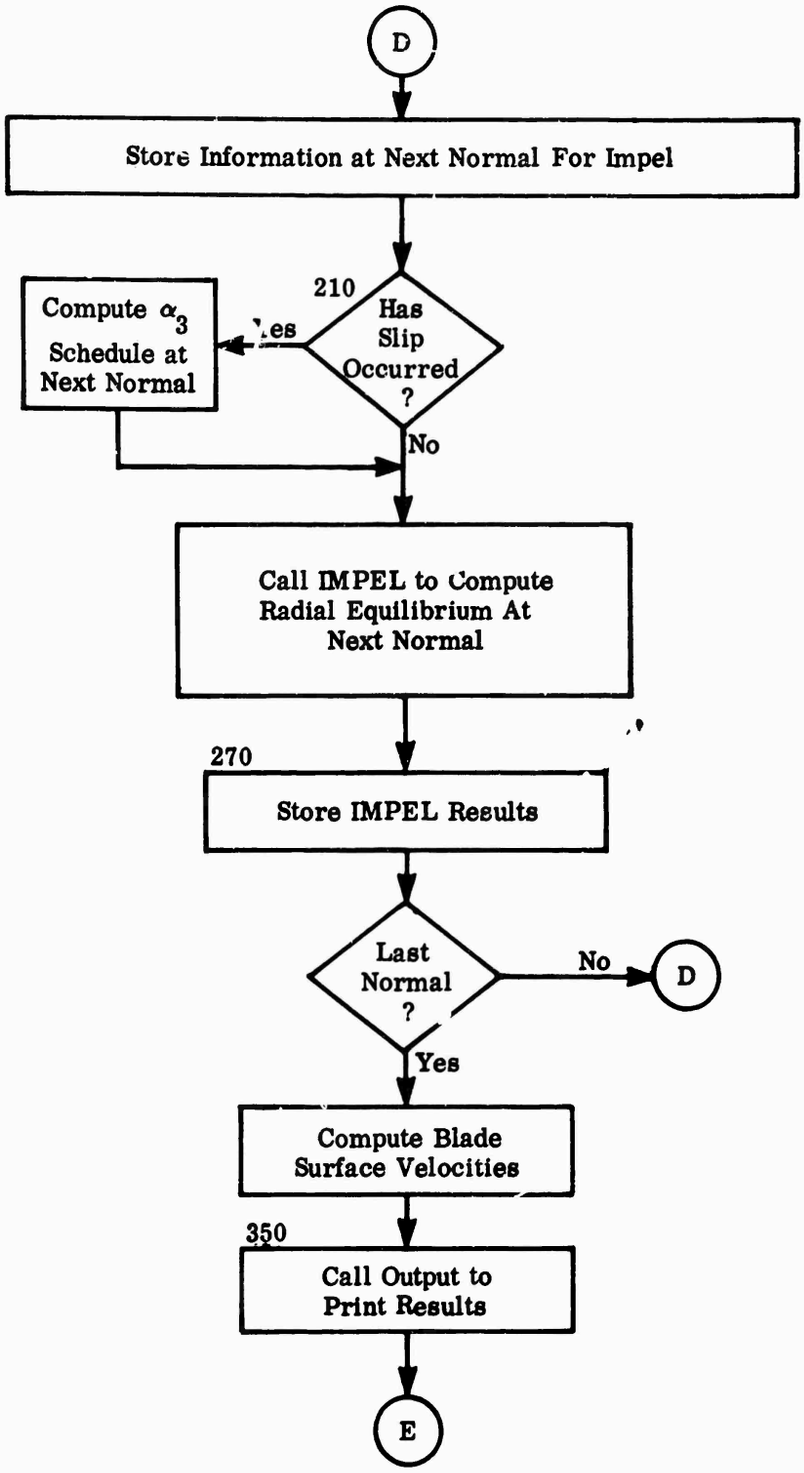
Note: All input is output verbatim


MAIN
1
70
Read Plot Dimensions
B
80
Begin Computation
C
90
Sign Off Plot Tape
B
100
Read Table Values
B
C
150
Call Inlet to Compute Inlet Conditions
Equilibrium Attained ?
No
A
Yes
At Least One Normal ?
No
A
Yes
Call Normal to Compute Normal Geometry
Call RCS to Compute R_c Schedules
Z

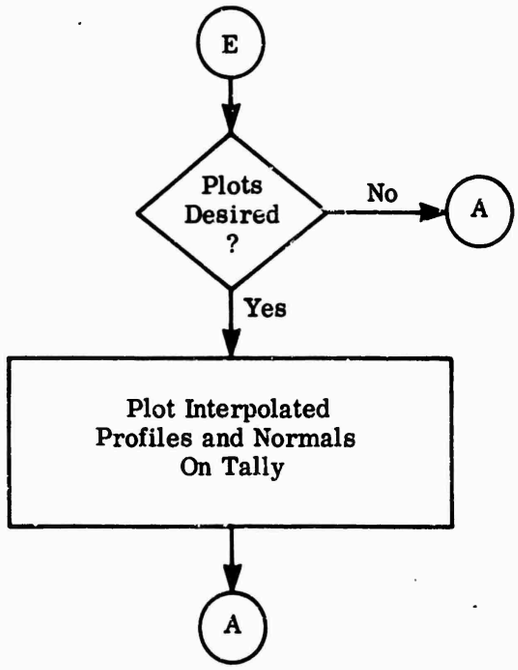
MAIN


Z
170
Compute REC Schedules at Each Normal
180
Compute BLF Schedules at Each Normal
190
Store Inlet Conditions For Impel
201
Initialize Logic For Slip Factor Conditions
D

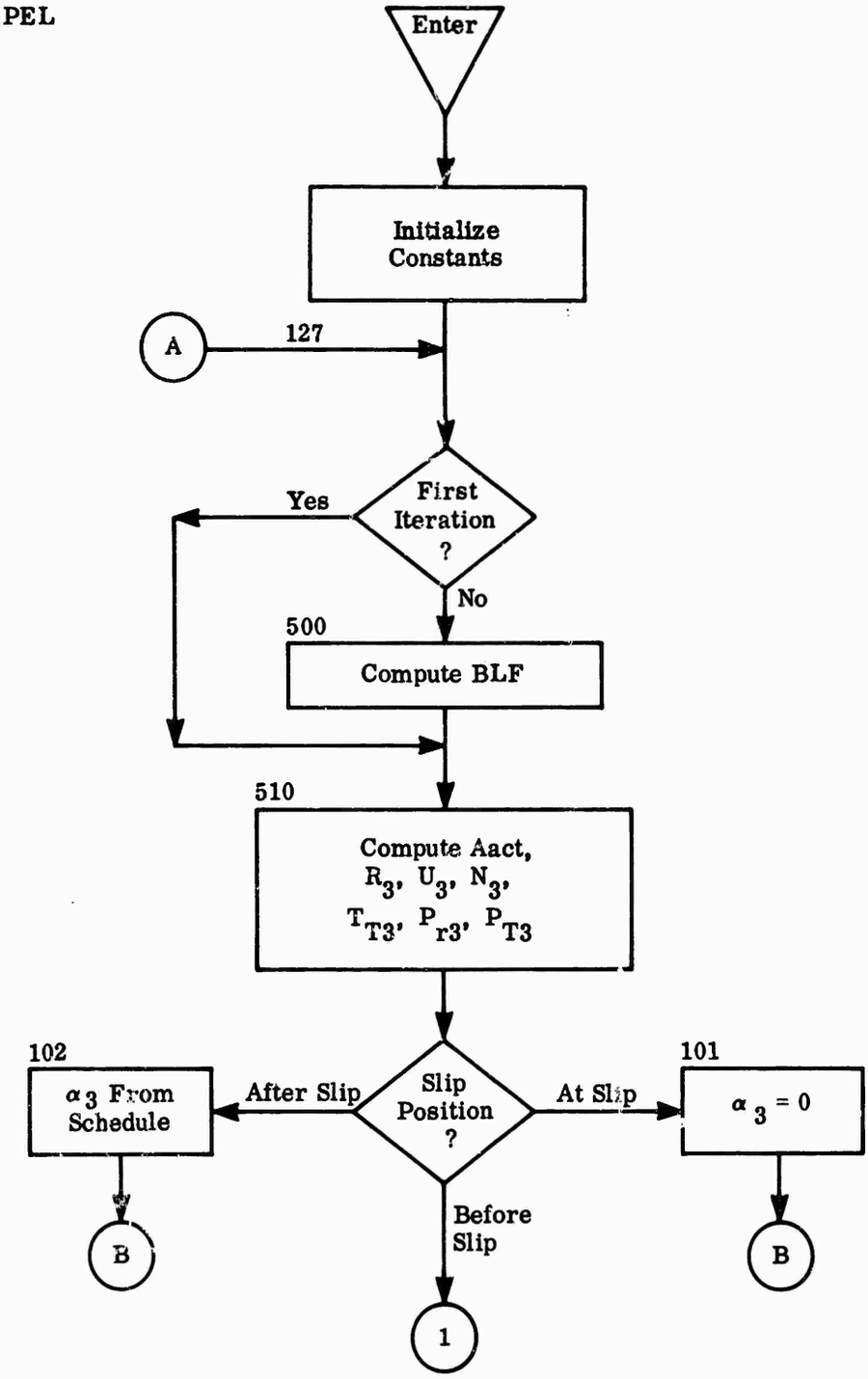
MAIN


D
Store Information at Next Normal For Impel
210
Has Slip Occurred ?
Yes
Compute α_3 Schedule at Next Normal
No
Call IMPEL to Compute Radial Equilibrium At Next Normal
270
Store IMPEL Results
Last Normal ?
No
D
Yes
Compute Blade Surface Velocities
350
Call Output to Print Results
E

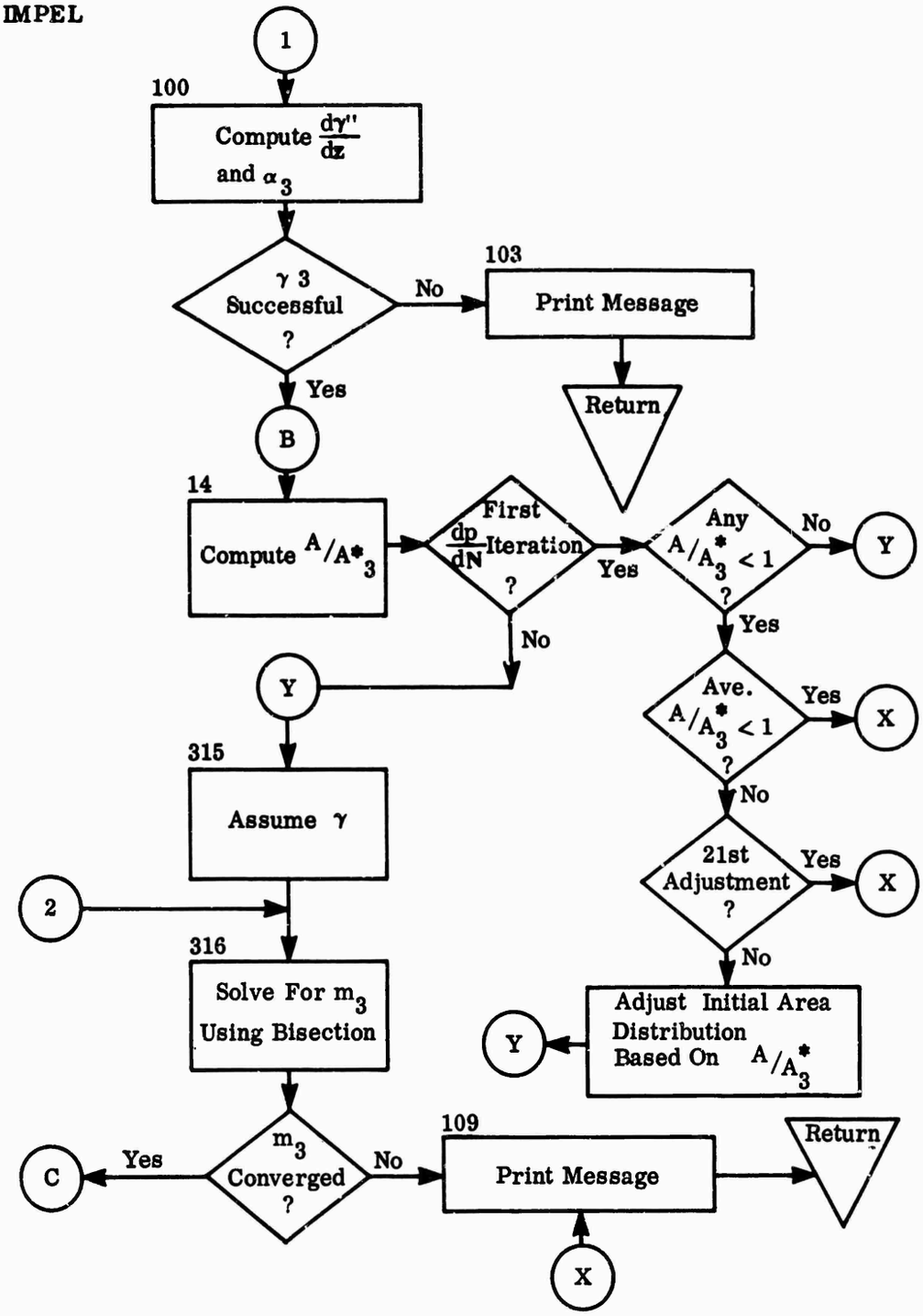
MAIN


E
Plots Desired ?
No
A
Yes
Plot Interpolated Profiles and Normals On Tally
A

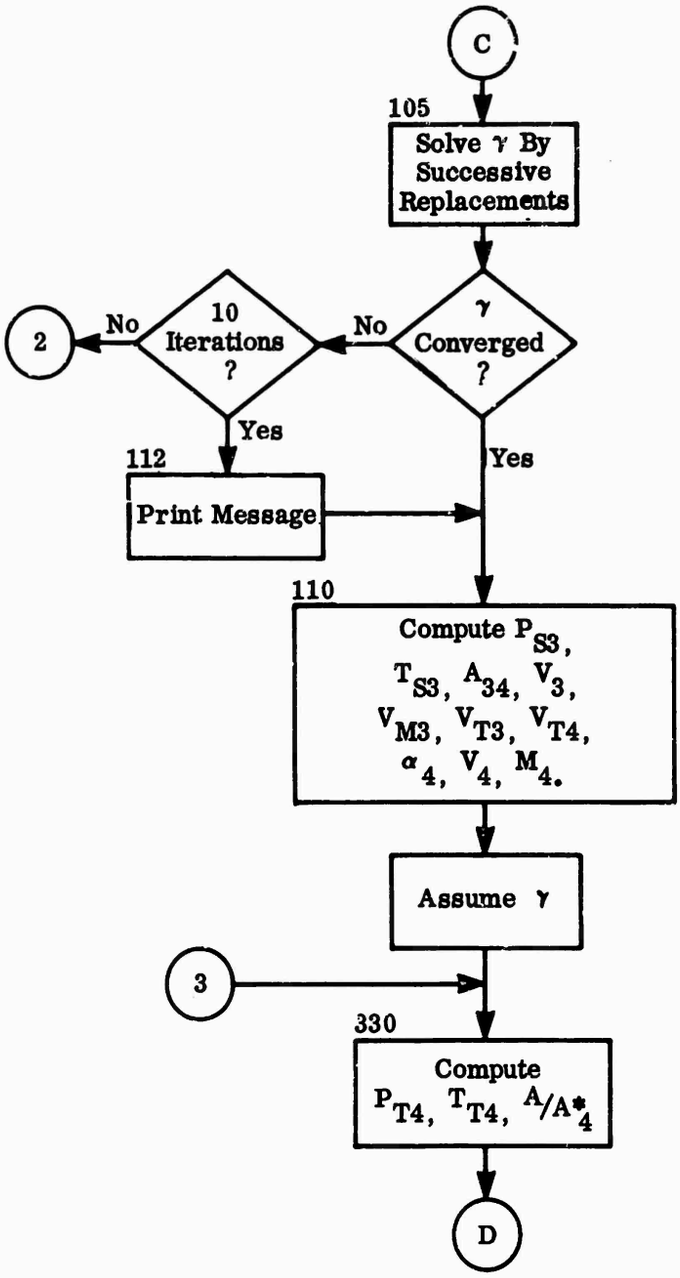
IMPEL

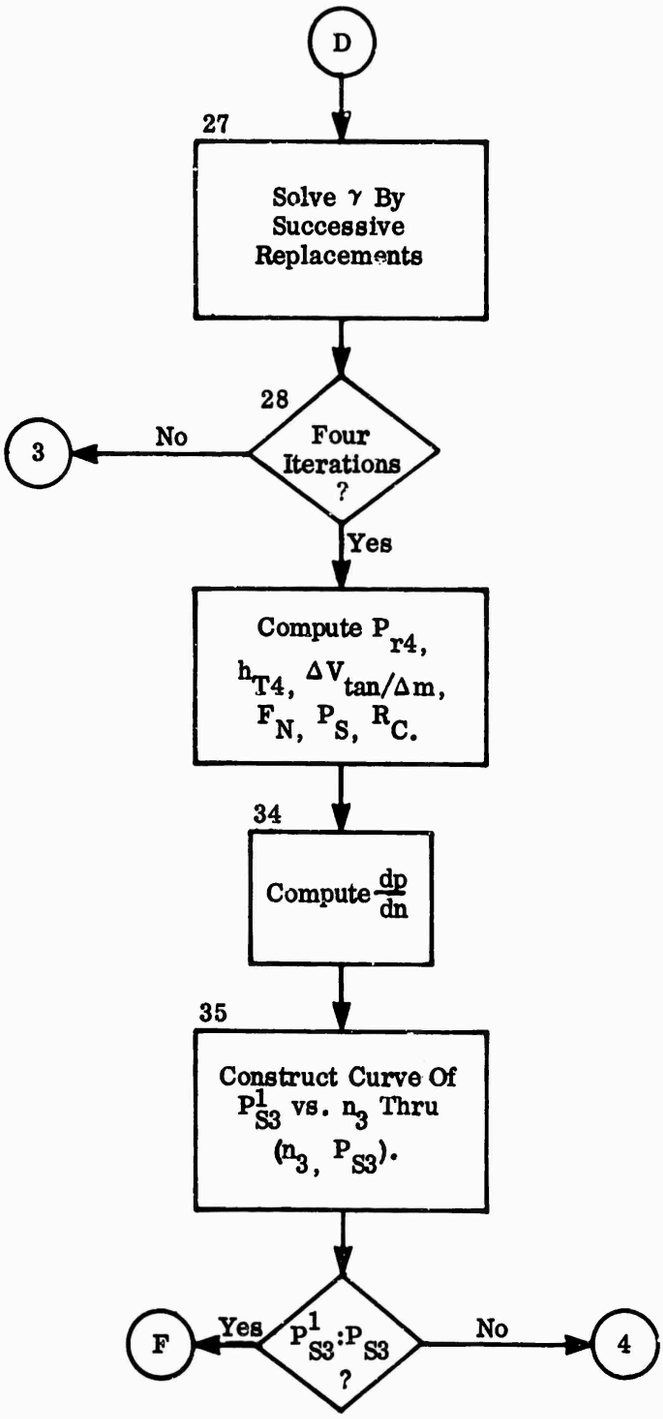

Enter
Initialize Constants
A
127
First Iteration ?
Yes
No
500
Compute BLF
510
Compute Aact, R_3, U_3, N_3, T_{T3}, P_{r3}, P_{T3}
Slip Position ?
After Slip
At Slip
Before Slip
102
α_3 From Schedule
101
$\alpha_3 = 0$
B
B
1

IMPEL

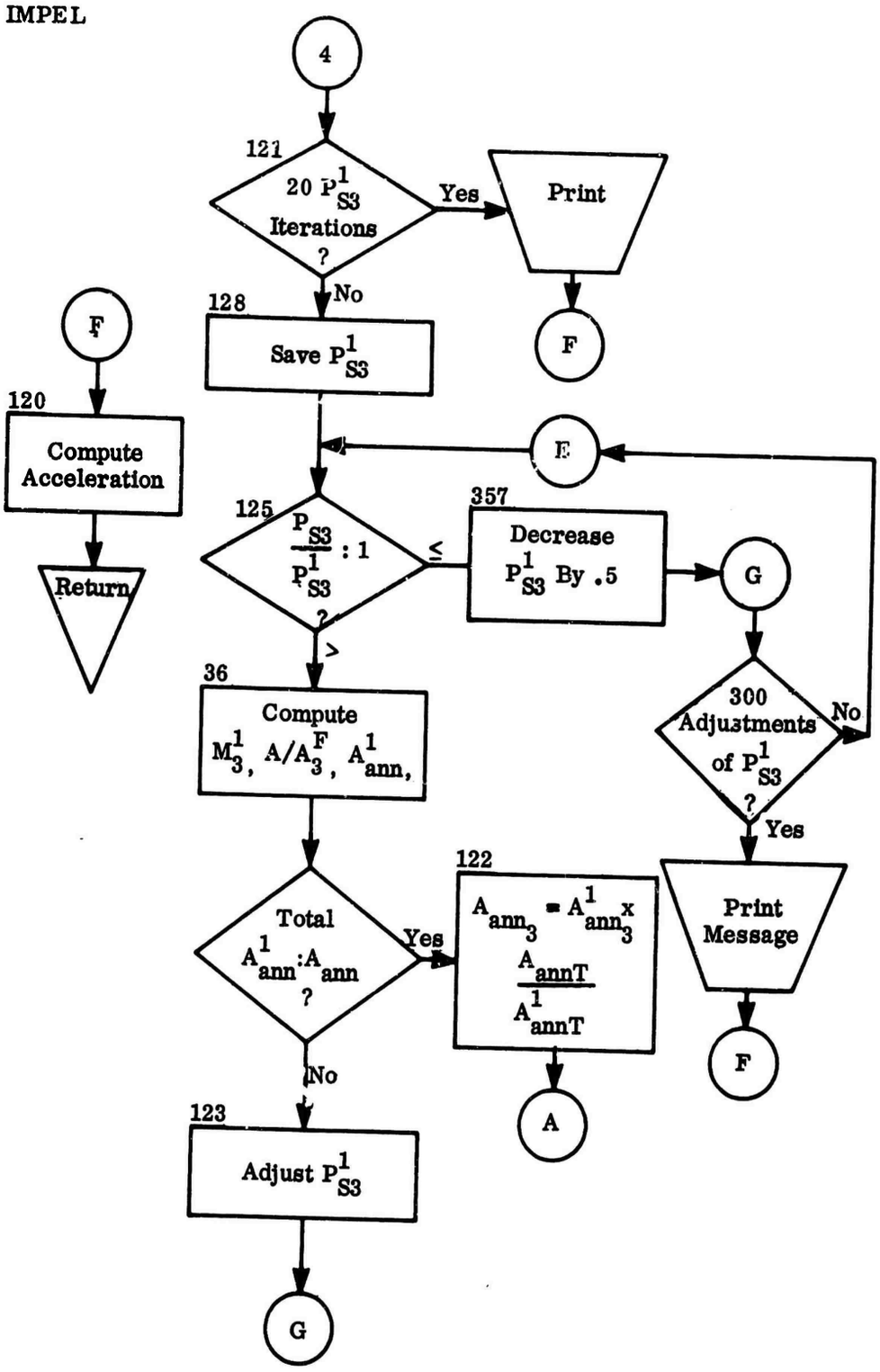

1
100
Compute $\frac{d\gamma''}{dz}$ and α_3
γ 3 Successful ?
No
103
Print Message
Return
Yes
B
14
Compute A/A^*_3
First $\frac{dp}{dN}$ Iteration ?
Yes
Any $A/A^*_3 < 1$?
No
Y
Yes
No
Y
Ave. $A/A^*_3 < 1$?
Yes
X
315
Assume γ
No
21st Adjustment ?
Yes
X
2
No
316
Solve For m_3 Using Bisection
Adjust Initial Area Distribution Based On A/A^*_3
Y
109
Return
m_3 Converged ?
Yes
C
No
Print Message
X

IMPEL

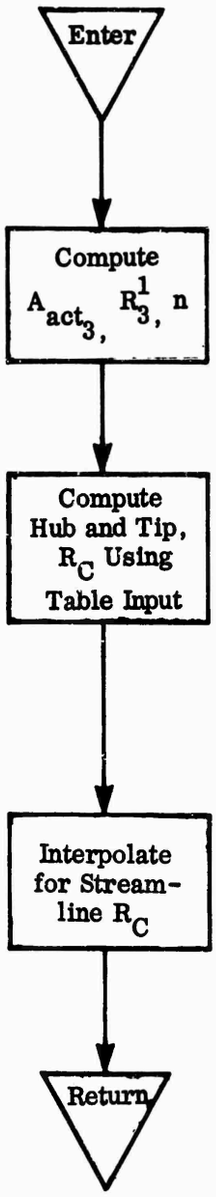

C
105
Solve γ By Successive Replacements
γ Converged ?
No
10 Iterations ?
No
2
Yes
112
Print Message
Yes
110
Compute P_{S3}, T_{S3}, A_{34}, V_3, V_{M3}, V_{T3}, V_{T4}, α_4, V_4, M_4.
Assume γ
3
330
Compute P_{T4}, T_{T4}, A/A^*_4
D


D
27
Solve γ By Successive Replacements
28
Four Iterations ?
No
3
Yes
Compute P_{r4}, h_{T4}, $\Delta V_{tan}/\Delta m$, F_N, P_S, R_C.
34
Compute $\frac{dp}{dn}$
35
Construct Curve Of P^1_{S3} vs. n_3 Thru (n_3, P_{S3}).
P^1_{S3}:P_{S3} ?
Yes
F
No
4

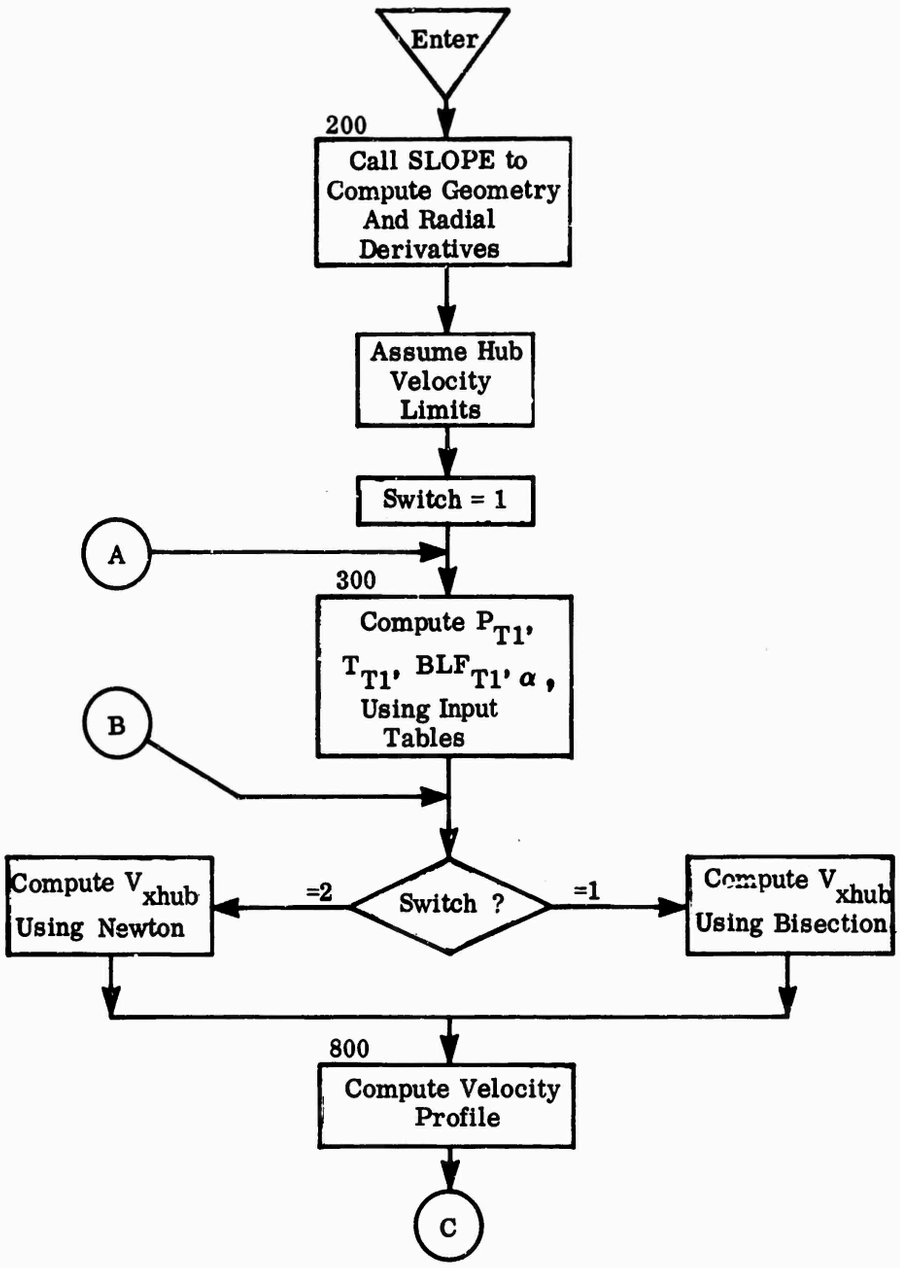
IMPEL


4
121
20 P^1_{S3} Iterations ?
Yes
Print
No
128
Save P^1_{S3}
F
F
120
Compute Acceleration
Return
E
125
$\frac{P_{S3}}{P^1_{S3}}$: 1 ?
≤
357
Decrease P^1_{S3} By .5
G
>
36
Compute M^1_3, A/A^F_3, A^1_{ann},
300 Adjustments of P^1_{S3} ?
No
Yes
Print Message
F
Total A^1_{ann}:A_{ann} ?
Yes
122
$A_{ann_3} = A^1_{ann_3} x \frac{A_{annT}}{A^1_{annT}}$
A
No
123
Adjust P^1_{S3}
G

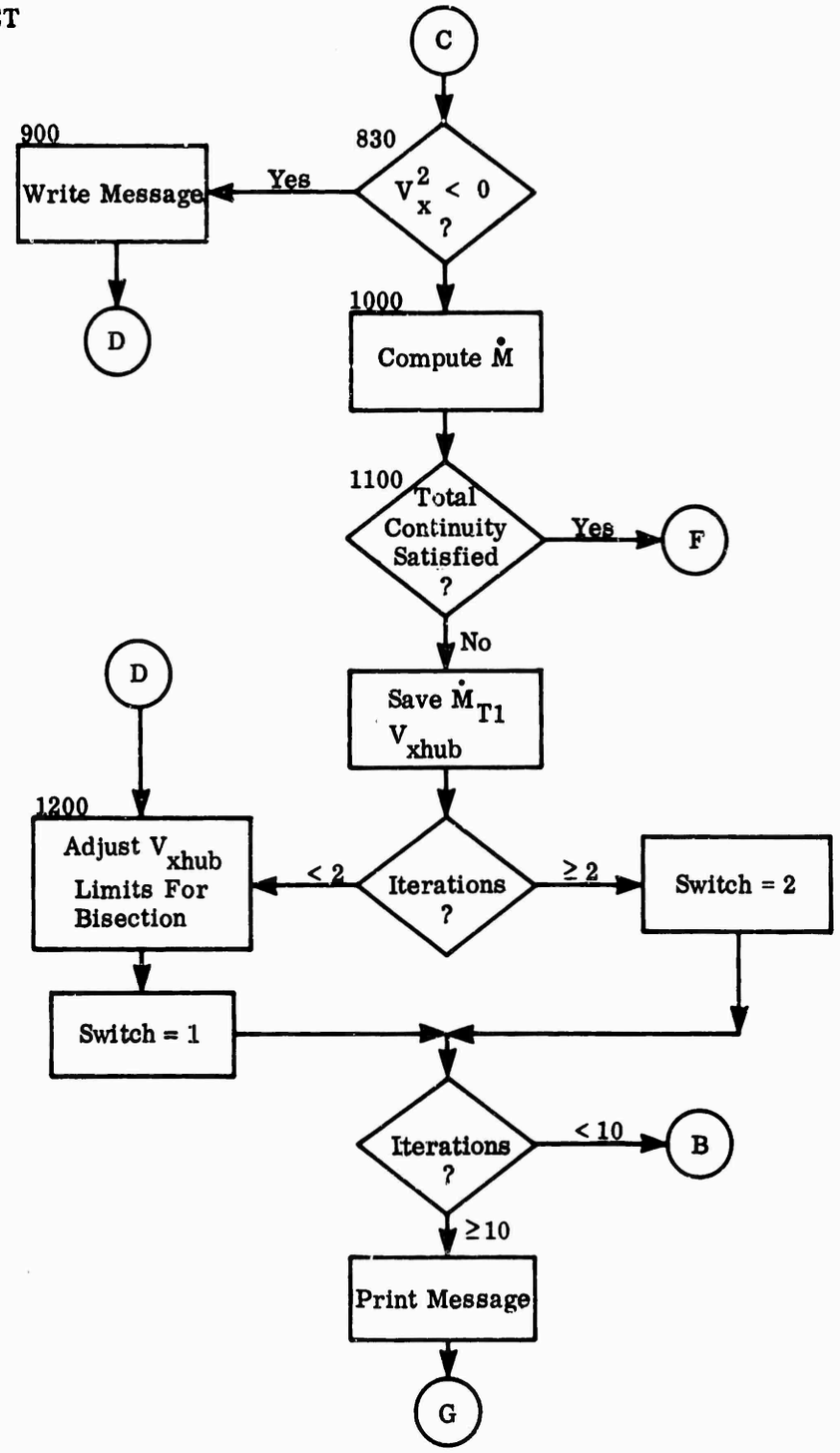
RCS


Enter
Compute
A_{act_3}, R_3^1, n
Compute
Hub and Tip,
R_C Using
Table Input
Interpolate
for Stream-
line R_C
Return

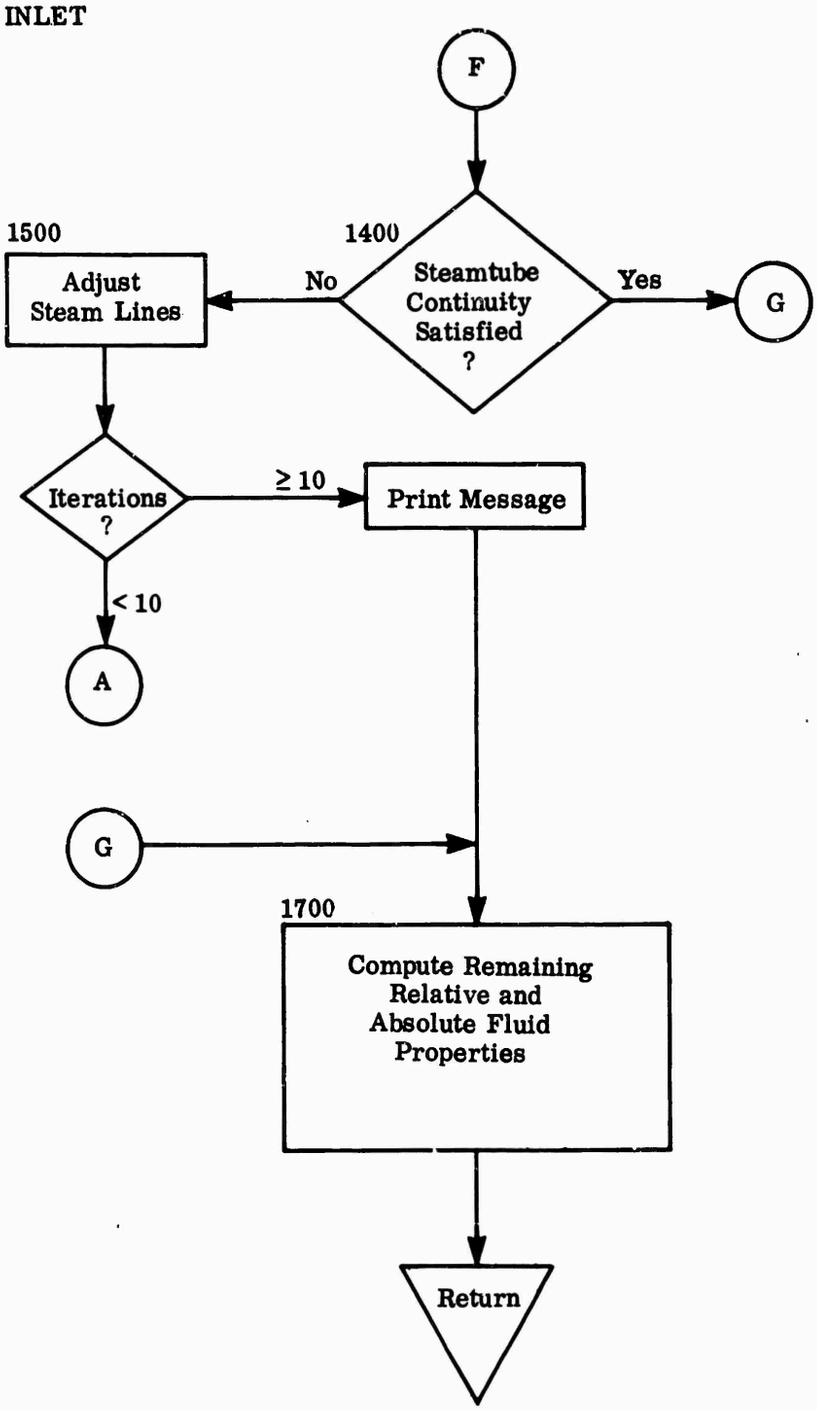
INLET


Enter
200
Call SLOPE to Compute Geometry And Radial Derivatives
Assume Hub Velocity Limits
Switch = 1
A
300
Compute P_{T1}, T_{T1}, BLF_{T1}, α, Using Input Tables
B
Compute V_{xhub} Using Newton
=2
Switch ?
=1
Compute V_{xhub} Using Bisection
800
Compute Velocity Profile
C

INLET


C
830
$V_x^2 < 0$?
Yes
900
Write Message
D
1000
Compute $\dot{M}$
1100
Total Continuity Satisfied ?
Yes
F
No
D
Save $\dot{M}_{T1}$ V_{xhub}
1200
Adjust V_{xhub} Limits For Bisection
< 2
Iterations ?
≥ 2
Switch = 2
Switch = 1
Iterations ?
< 10
B
≥ 10
Print Message
G

INLET


F
1400
Steamtube Continuity Satisfied ?
No
Yes
G
1500
Adjust Steam Lines
Iterations ?
≥ 10
Print Message
< 10
A
G
1700
Compute Remaining Relative and Absolute Fluid Properties
Return

5.2 PROGRAM ROUTINES

This section describes the functions of each routine, its calling sequence, and the routines used in this computer program.

MAIN

MAIN accomplishes input, control, and some intermediate calculations. MAIN references INLET, CHORD, RCS, IMPEL, OUTPUT, TALL14, TALLZZ, TABLE, TAB2, SQRT, ATAN, and COS.

IMPEL (K2)

IMPEL computes the impeller-station conditions that satisfy radial equilibrium in the meridional plane along the normal. IMPEL references TABLE, TAB2, SQRT, SIN, COS, TAN, ATAN, and ATAN2.

K2 = Station number.

INLET (K2)

INLET computes the inducer-inlet relative conditions along a radial line in the meridional plane to verify that the conditions satisfy radial equilibrium INLET references SLOPE, TABLE, TAB2, SORT, SQRT, ATAN, ATAN2, TAN, and ALOG.

K2 = Station number.

RCS (K2, XLOC, RADIUS, GAMMA, DX, AREA, XND, and BLF)

RCS computes streamtubes of equal area and the radius of curvature schedule along a normal. RCS refers NORMAL, TABLE, COS, SQRT, and TAN.

K2	=	station number
XLOC	=	radial distance
GAMMA	=	meridional angle
DX	=	change in axial distance used for derivatives
AREA	=	actual annulus area
XND	=	normal distance
RADIUS	=	average streamtube radius
BLF	=	blockage factor

SLOPE (XHUB, DX, RADIUS, AREA, CF, DERIV1, DERIV2)

SLOPE computes streamtubes of equal area along a radial line and the first and second radial derivatives of the streamlines. SLOPE references TABLE and SQRT.

XHUB	=	axial distance to a radial station
DX	=	change in axial distance used for derivatives
RADIUS	=	radial distance
AREA	=	actual annulus area
CF	=	0 if derivatives are to be computed
CF	=	1 if not
DERIV1	=	first radial derivative
DERIV2	=	second radial derivative

OUTPUT

OUTPUT prints out the calculated streamtube results at each station.

CHORD (XHUB, TIPG, HX, HY, TX, TY, NH, NT, K, XTIP, RTIP, and SLOPE)

CHORD computes the normal in an annulus cross section of a duct that satisfies the tangent circle criterion. CHORD references TAB2, ATAN, TAN, and SQRT.

XHUB	=	station-hub axial distance
XTIPG	=	guess as to station-tip axial distance
XTIP	=	station-tip axial distance
RTIP	=	station-tip radial distance
HX	=	array of hub Z-values
HY	=	array of hub R-values
TX	=	array of tip Z-values
TY	=	array of tip R-values
NH	=	number of hub points

NT = number of tip points

SLOPE = the angle that the normal angle makes with Z-axis

SORT (TX, TY, and NT)

SORT sorts a single table by increasing values of the independent variable.

TX = independent variable array

TY = dependent variable array

NT = number of points to be sorted

TABLE (NT and ARG)

TABLE performs a single table look-up and references TAB2.

NT = table number

ARG = argument

TAB2 (X, Y, NX, NDEG, ARG, and IE)

TAB2 performs a multidegree interpolation of a single table using Aitkins exact polynomial fit algorithm.

X = independent variable array

Y = dependent variable array

NX = number of points in table

NDEG = degree of interpolation

ARG = independent argument

IE = 1 for success

IE = 2 for overflow

IE = 3 for failure

5.3 PROGRAM LISTING

```
0    FOR MAIN                                                    2496A002
COMPILATION BY UNIVAC 1108 FORTRAN-IV DATED     NOV. 23,1965 F4008
THIS COMPILATION WAS DONE ON 19 AUG 66 AT 17:37:00

MAIN PROGRAM          ENTRY POINT 000000

STORAGE USED (BLOCK, NAME, LENGTH)

        0001   *CODE   002324
        0000   *DATA   010422
        0002   *BLANK  004735
        0003   RC      000170
        0004   IMPELR  002335
        0005   BLOCK   010757


EXTERNAL REFERENCES (BLOCK, NAME)

        0006   TALLZZ
        0007   INLET
        0010   CHORD
        0011   TABLE
        0012   RCS
        0013   SQRT
        0014   IMPEL
        0015   TAB2
        0016   COS
        0017   OUTPUT
        0020   TALL18
        0021   NWDU$
        0022   NIO2$
        0023   NRDU$
        0024   NIO1$
        0025   NERR2$
        0026   NEXP6$
        0027   NSTOP$

STORAGE ASSIGNMENT FOR VARIABLES (BLOCK, TYPE, RELATIVE LOCATION, NAME)

0001 000014 1L    0001 000020 10L   0001 000450 100L  0000 010226 1000F 0000 010240 1001F
0000 010241 1002F 0000 010243 1003F 0000 010245 1004F 0000 010255 1005F 0000 010264 1006F
0000 010267 1007F 0000 010272 1008F 0000 010275 1009F 0001 002155 1016G 0001 002172 1024G
0001 002217 1036G 0001 002304 1047G 0001 000025 135G  0001 000033 142G  0001 000555 150L
0001 000072 154G  0001 000624 156L  0001 000104 164G  0001 000115 172G  0001 000077 20L
0001 000126 200G  0001 001274 201L  0001 001313 202L  0000 010302 2020F 0000 010334 2030F
0001 001315 205L  0001 001350 208L  0001 000140 210G  0001 001415 210L  0001 001426 211L
0001 001433 213L  0001 001457 220L  0001 001467 221L  0001 000207 227G  0001 001521 230L
0001 000220 235G  0001 000232 245G  0001 001556 250L  0001 000243 253G  0001 001565 260L
0001 000254 261G  0001 001575 261L  0001 001612 270L  0001 000271 271G  0001 000302 277G
0001 000133 30L   0001 000313 305G  0001 000330 315G  0001 000341 323G  0001 000352 331G
0001 000400 347G  0001 000424 356G  0001 000436 374G  0001 002065 375L  0001 000225 40L
0001 002102 400L  0001 000515 415G  0001 000530 424G  0001 000546 434G  0001 000573 451G
0001 000615 463G  0001 000641 477G  0001 000261 50L   0001 000743 513G  0001 001014 522G
0001 001016 525G  0001 001122 542G  0001 001143 547G  0001 001175 562G  0001 000220 60L
```

CONFIDENTIAL

CONFIDENTIAL


```
0001   001326 6176    0001   001360 625G    0001   001452 645G    0001   001513 656G    0001   001531 666G
0001   000357 70L     0001   001646 721G    0001   001774 760G    0001   001776 763G    0001   000417 80L
0001   000431 90L     0001   002317 900L    0004 R 000000 A       0005 R 000000 ACCEL   0000 R 010174 AK
0005 R 000214 ALPHA   0005 R 000430 AMASS   0005 R 000644 AREA    0005 R 001060 BETA    0000 R 010172 BIN
0000 R 010152 BLADES  0004 R 000764 BLF     0000 R 010171 BLFM    0000 R 010154 BLFOUT  0000 R 010173 BOUT
0004 R 001200 C       0005 R 001274 CF      0000 R 01017C CONST   0016 R 000000 COS     0000 R 000202 DATA
0000 R 000000 DDMARG  0005   001275 DERIV1   0005   001511 DERIV2  0005 R 001725 DGR     0005 R 001726 DPDN
0000 R 010205 DV      0004 R 001262 GAMMA   0005 R 002142 GC      0005   002143 GIVM    0000 R 010100 GRID
0005 R 002144 HGPSI   0005 R 002145 HJ      0000 I 010150 I       0000 I 010213 IBAD    0000 I 010203 IE
0000 I 010147 J       0000 I 010206 JHUB    0000 I 010207 JTIP    0000 I 010175 JUMP    0000 I 010176 JUMP1
0000 I 010177 JUMP2   0000 I 010212 K       0000 I 010201 KSLIP   0000 I 010164 K2      0000 I 000144 LIBRAY
0000 I 010162 N       0000 I 010210 NHUB    0000 I 010113 NOMODE  0000 I 010153 NORMLS   0000 I 010151 NPLOT
0005 I 002146 NS      0000 I 010155 NSLIP   0000 I 010211 NTIP    0005 I 002147 NTITLE  0000 I 000156 NWORD
0000 I 010163 NX      0002 I 000000 NXY     0005 R 002173 PHI     0005 R 002217 PI      0000 R 010157 PLOTDX
0005 R 002220 PRT     0005 R 002434 PS      0005 R 002650 PT      0004 R 001522 Q       0005 R 003064 R
0004 R 001306 RADIUS  0005 R 003065 RCURV   0005 R 003301 REC     0005 R 003515 RIN     0000 R 010165 RLAST
0005 R 003516 RPM     0000 R 010156 SLIPFC  0000 R 010167 SLOPE   0013 R 000000 SQRT    0011 R 000000 TABLE
0000 R 010160 TABNO   0015 R 000000 TAB2    0005 R 003517 TRT     0005 R 003733 TS      0005 R 004147 TT
0005 R 004363 TX      0005   004407 TY      0005 R 004433 U       0005 R 004647 V       0005 R 005063 VP
0005 R 005277 VPW     0005   005513 VR      0005 R 005727 VS      0005 R 006143 VSND    0005 R 006357 VSW
0004 R 000000 VTW     0005 R 006573 VU      0005 R 007007 VVSND   0005   007223 VX      0005 R 007437 W
0005 R 007653 WM      0005 R 010303 WU      0005 R 010067 WVSND   0000 R 000240 X       0004 R 001604 XBLF
0004 R 001750 XLOC    0005 R 010517 XMD     0000 R 010161 XN      0005 R 010543 XND     0003   000000 XRC
0002 R 000031 XVAL    0000 R 010200 XYZ     0000 R 010214 X10     0000 R 010216 X11     0000 R 010220 X12
0000 R 010222 X13     0000 R 010224 X14     0000 R 004160 Y       0004 R 002164 YAL     0004 R 002171 YBLF
0003 R 000074 YRC     0002 R 002373 YVAL    0000 R 010202 Y1      0000 R 010215 Y10     0000 R 010217 Y11
0000 R 010221 Y12     0000 R 010223 Y13     0000 R 010225 Y14     0000 R 010204 Y2      0000 R 000214 ZTIPG
0000 R 010166 ZZZZ
```

```
00100     1.  C                                                                    2496A004
00100     2.  C     IMPELLER RADIAL EQUILIBRIUM DESIGN, AS2496, BY R. CURNOW       2496A006
00100     3.  C     FOR L. WINSLOW                                                 2496A008
00100     4.  C                                                                    2496A010
00101     5.        COMMON/RC/XRC(3,20),YRC(3,20)                                  2496A012
00103     6.        COMMON NXY(25),XVAL(50,25),YVAL(50,25)                         2496A014
00104     7.        COMMON/IMPELR/A(500)      ,BLF(20,7)      ,C(50)       ,     2496A016
00104     8.       *GAMMA(20)     ,RADIUS(20,7)  ,Q(50)        ,XBLF(5,20)  ,     2496A018
00104     9.       *XLOC(20,7)    ,YAL(5)        ,YBLF(5,20)                     2496A020
00105    10.        COMMON/BLOCK/ ACCEL(20,7)    ,ALPHA(20,7)    ,AMASS(20,7) ,     2496A022
00105    11.       *AREA(20,7)    ,BETA(20,7)    ,CF             ,DERIV1(20,7)  ,     2496A024
00105    12.       *DERIV2(20,7)  ,DGR           ,DPDN(20,7)     ,GC    ,GIVM   ,     2496A026
00105    13.       *HGPSI,HJ,NS   ,NTITLE(20)    ,PHI(20) ,PI    ,PRT(20,7)     ,     2496A028
00105    14.       *PS(20,7)      ,PT(20,7)      ,R              ,RCURV(20,7)   ,     2496A030
00105    15.       *REC(20,7)     ,RIN   ,RPM    ,TRT(20,7)      ,TS(20,7)      ,     2496A032
00105    16.       *TT(20,7)      ,TX(20)        ,TY(20)         ,U(20,7)       ,     2496A034
00105    17.       *V(20,7)       ,VP(20,7)      ,VPW(20,7)      ,VR(20,7)      ,     2496A036
00105    18.       *VS(20,7)      ,VSND(20,7)    ,VSW(20,7)      ,VU(20,7)      ,     2496A038
00105    19.       *VVSND(20,7)   ,VX(20,7)      ,W(20,7)        ,WM(20,7)      ,     2496A040
00105    20.       *WVSND(20,7)   ,WU(20,7)      ,XMD(20)        ,XND(20,7)           2496A042
00106    21.        DIMENSION DDMARG(20,5),VTW(20,5)                              2496A044
00107    22.        EQUIVALENCE (VTW(1,1),A(1))                                   2496A046
00110    23.        DIMENSION LIBRAY(10),NWORD(20),DATA(10),ZTIPG(20)             2496A048
00111    24.        DIMENSION X(1000,2),Y(1000,2),GRID(11),NOMODE(28)             2496A050
00112    25.        DATA (GRID(J),J=1,11)/2*5.,7.,0.,9.5,6*0./,(NOMODE(J),J=1,19)/ 2496A052
00112    26.       *18*-7,1/                                                      2496A054
```

CONFIDENTIAL

```
00115   27.          DATA (LIBRAY(I),I=1,9)/5HTITLE,5HCONSI,5HMASS ,5HZLIVR,5HZLIP,
00115   28.         *5HTABLE,5HGEOME,5HBEGIN,5HEND */                                  2496A056
00117   29.          DATA NPLOT/1/                                                      2496A058
00117   30.    C                                                                        2496A060
00117   31.    C     INITIALIZE CONSTANTS                                             2496A062
00121   32.          GC=32.17                                                         2496A064
00122   33.          MJ=778.2                                                         2496A066
00123   34.          R=53.35                                                          2496A068
00124   35.          PI=3.14159                                                       2496A070
00125   36.          DGR=.01745329                                                    2496A072
00126   37.          HGPSI=2.03593                                                    2496A074
00127   38.    1     CONTINUE                                                         2496A076
00130   39.          WRITE(6,1000)                                                    2496A078
00130   40.    C                                                                      2496A080
00130   41.    C     READ IN A CONTROL WORD                                           2496A082
00132   42.   10     CONTINUE                                                         2496A084
00133   43.          READ(5,1001)(NWORD(I),I=1,16)                                    2496A086
00133   44.    C                                                                      2496A088
00133   45.    C     DETERMINE IF THE WORD IS DEFINED IN THE LIBRARY                  2496A090
00141   46.          DO 15 I=1,9                                                      2496A092
00144   47.          IF(NWORD(1).EQ.LIBRAY(I)) GO TO (20,30,40,50,60,100,70,80,90),I  2496A094
00146   48.   15     CONTINUE                                                         2496A096
00146   49.    C                                                                      2496A098
00146   50.    C     PRINT OUT ILLEGAL DATA CONTROL CARD                              2496A100
00146   51.          WRITE(6,1004)                                                    2496A102
00150   52.          WRITE(6,1003)(NWORD(I),I=1,16)                                   2496A104
00152   53.          GO TO 10                                                         2496A106
00160   54.    C                                                                      2496A108
00160   55.    C     READ IN TITLE CARD                                               2496A110
00160   56.   20     CONTINUE                                                         2496A112
00162   57.          READ(5,1001)(NTITLE(I),I=1,16)                                   2496A114
00170   58.          WRITE(6,1003)(NWORD(I),I=1,16)                                   2496A116
00176   59.          WRITE(6,1003)(NTITLE(I),I=1,16)                                  2496A118
00204   60.          GO TO 10                                                         2496A120
00204   61.    C                                                                      2496A122
00204   62.    C     READ IN CONSTANTS                                                2496A124
00205   63.   30     CONTINUE                                                         2496A126
00206   64.          READ(5,1002)(DATA(I),I=1,8)                                      2496A128
00214   65.          RPM=DATA(1)                                                      2496A130
00215   66.          BLADES=DATA(2)                                                   2496A132
00216   67.          NORMLS=DATA(3)                                                   2496A134
00217   68.          CF=DATA(4)                                                       2496A136
00220   69.          XLOC(1,1)=DATA(5)                                                2496A138
00221   70.          BLFOUT=DATA(6)                                                   2496A140
00222   71.          NSLIP=DATA(7)                                                    2496A142
00223   72.          SLIPFC=DATA(8)                                                   2496A144
00224   73.          NS=NORMLS+1                                                      2496A146
00225   74.          WRITE(6,1003)(NWORD(I),I=1,16)                                   2496A148
00233   75.          WRITE(6,1005)(DATA(I),I=1,8)                                     2496A150
00241   76.          GO TO 10                                                         2496A152
00241   77.    C                                                                      2496A154
00241   78.    C     READ IN MASS FLOW RATES                                          2496A156
00242   79.   40     CONTINUE                                                         2496A158
00243   80.          READ(5,1002)(AMASS(1,I),I=1,5)                                   2496A160
00251   81.          WRITE(6,1003)(NWORD(I),I=1,16)                                   2496A162
00257   82.          WRITE(6,1006)(AMASS(1,I),I=1,5)                                  2496A164
00265   83.          GO TO 10                                                         2496A166
00265   84.    C                                                                      2496A168
                                                                                     2496A170
```

```
00265    65.   C     READ IN Z(HUB) VALUES                                  2496A172
00266    66.   50    CONTINUE                                               2496A174
00267    67.         READ(5,1002)(XLOC(I,1),I=2,NS)                         2496A176
00275    68.         WRITE(6,1003)(NWORD(I),I=1,16)                         2496A178
00303    69.         WRITE(6,1006)(XLOC(I,1),I=2,NS)                        2496A180
00311    90.         GO TO 10                                               2496A182
00311    91.   C                                                            2496A184
00311    92.   C     READ IN Z(TIP GUESS) VALUES                            2496A186
00312    93.   60    CONTINUE                                               2496A188
00313    94.         READ(5,1002)(ZTIPG(I),I=1,NORMLS)                      2496A190
00321    95.         WRITE(6,1003)(NWORD(I),I=1,16)                         2496A192
00327    96.         WRITE(6,1006)(ZTIPG(I),I=1,NORMLS)                     2495A194
00335    97.         GO TO 10                                               2496A196
00335    98.   C                                                            2496A198
00335    99.   C     READ IN PLOT DIMENSIONS                                2496A200
00336   100.   70    CONTINUE                                               2496A202
00337   101.         READ(5,1002)GRID(3),GRID(5),PLOTDX                     2496A204
00344   102.         NPLOT=2                                                2496A206
00345   103.         WRITE(6,1003)(NWORD(I),I=1,16)                         2496A208
00353   104.         WRITE(6,1007)GRID(3),GRID(5),PLOTDX                    2496A210
00360   105.         GO TO 10                                               2496A212
00360   106.   C                                                            2496A214
00360   107.   C     BEGIN COMPUTATION                                      2496A216
00361   108.   80    CONTINUE                                               2496A218
00362   109.         WRITE(6,1003)(NWORD(I),I=1,16)                         2496A220
00370   110.         GO TO 150                                              2496A222
00370   111.   C                                                            2496A224
00370   112.   C     SIGN OFF GEOMETRY PLOT TAPE                            2496A226
00371   113.   90    CONTINUE                                               2496A228
00372   114.         WRITE(6,1008)(NWORD(I),I=1,16)                         2496A230
00400   115.         NPLOT=1                                                2496A232
00401   116.         CALL TALLZZ(1)                                         2496A234
00402   117.         GO TO 10                                               2496A236
00402   118.   C                                                            2496A238
00402   119.   C     READ IN TABLE DATA                                     2496A240
00403   120.   100   CONTINUE                                               2496A242
00404   121.         READ(5,1002)TABNO,XN                                   2496A244
00410   122.         N=TABNO                                                2496A246
00411   123.         NX=XN                                                  2496A248
00412   124.         NXY(N)=NX                                              2496A250
00413   125.         READ(5,1002)(XVAL(I,N),YVAL(I,N),I=1,NX)               2496A252
00422   126.         WRITE(6,1003)(NWORD(I),I=1,16)                         2496A254
00430   127.         WRITE(6,1009)TABNO,XN,(XVAL(I,N),YVAL(I,N),I=1,NX)     2496A256
00441   128.         GO TO 10                                               2496A258
00441   129.   C                                                            2496A260
00441   130.   C     COMPUTE INLET CONDITIONS                               2496A262
00442   131.   150   CONTINUE                                               2496A264
00443   132.         K2=1                                                   2496A266
00444   133.         CALL INLET(K2)                                         2496A268
00445   134.         XMD(1)=0.                                              2496A270
00446   135.         RLAST=RIN                                              2496A272
00447   136.         XMD(1)=0.                                              2496A274
00450   137.         DO 155 J=1,5                                           2496A276
00453   138.         PT(1,J)=PT(1,J)*HGPSI                                  2496A278
00454   139.         PS(1,J)=PS(1,J)*HGPSI                                  2496A280
00455   140.         PRT(1,J)=PRT(1,J)*HGPSI                                2496A282
00456   141.         ALPHA(1,J)=ALPHA(1,J)/DGR                              2496A284
00457   142.         BETA(1,J)=BETA(1,J)/DGR                                2496A286
```


CONFIDENTIAL

```
00460  143.     155  CONTINUE                                                    2496A288
00462  144.          DO 156 J=1,7                                                2496A290
00465  145.          IF(ABS(RCURV(1,J)).GT.0.1)  GO TO 156                       2496A292
00467  146.          RCURV(1,J)=10000.                                           2496A294
00470  147.     156  CONTINUE                                                    2496A296
00472  148.          IF(K2.LT.1) GO TO 900                                       2496A298
00474  149.          IF(NS.EQ.1) GO TO 900                                       2496A300
00474  150.     C                                                                2496A302
00474  151.     C    COMPUTE THE GEOMETRY OF THE NORMALS                         2496A304
00476  152.          DO 160 J=2,NS                                               2496A306
00501  153.          ZZZZ=ZTIPG(J-1)                                             2496A308
00502  154.          CALL CHORD(XLOC(J,1),ZZZZ      ,XVAL(1,4),YVAL(1,4),XVAL(1,5),
00502  155.         *YVAL(1,5),NXY(4),NXY(5),3,XLOC(J,7),RADIUS(J,7),SLOPE)      2496A312
00503  156.          GAMMA(J)=(SLOPE-90.)*DGR                                    2496A314
00504  157.          RADIUS(J,1)=TABLE(4,XLOC(J,1))                              2496A316
00505  158.          CALL RCS(J,XLOC,RADIUS,GAMMA,0.05,AREA,XND,BLF)             2496A318
00506  159.          XMD(J)=SQRT((XLOC(J,4)-XLOC(J-1,4))**2+(RADIUS(J,4)-RLAST)**2) 2496A320
00506  160.         *+XMD(J-1)                                                   2496A322
00507  161.          RLAST=RADIUS(J,4)                                           2496A324
00510  162.     160  CONTINUE                                                    2496A326
00510  163.     C                                                                2496A328
00510  164.     C    COMPUTE THE RECOVERIES                                      2496A330
00512  165.          DO 170 J=1,5                                                2496A332
00515  166.          REC(NS,J)=TABLE(J+19,WSND(1,J))*TABLE(14,XND(NS,J+1)/       2496A334
00515  167.         *XND(NS,7)*100.)                                             2496A336
00516  168.          TX(J)=(REC(NS,J)-1.)/XMD(NS)                                2496A338
00517  169.     170  CONTINUE                                                    2496A340
00521  170.          DO 180 K2=2,NS                                              2496A342
00524  171.          DO 180 J=1,5                                                2496A344
00527  172.          REC(K2,J)=TX(J)*XMD(K2)+1.                                  2496A346
00530  173.     180  CONTINUE                                                    2496A348
00530  174.     C                                                                2496A350
00530  175.     C    COMPUTE THE BLOCKAGE FACTORS                                2496A352
00533  176.          CONST=2.*PI/BLADES                                          2496A354
00534  177.          BLFW=(AREA(1,6)-((RADIUS(1,7)-RADIUS(1,1))*(TABLE(10,XLOC(1,1)) 2496A356
00534  178.         *+TABLE(11,XLOC(1,1)))/2.*BLADES))/ARLA(1,6)                 2496A358
00535  179.          BIN=BLF(1,3)/BLFM                                           2496A360
00536  180.          BLFM=(AREA(NS,6)-(XND(NS,7)*(TABLE(10,XLOC(NS,1))+TABLE     2496A362
00536  181.         *(11,XLOC(NS,7)))/2.*BLADES))/AREA(NS,6)                     2496A364
00537  182.          BOUT=BLFOUT/BLFM                                            2496A366
00[illegible]  183.          TX(1)=(BOUT-BIN)/XMD(NS)                            2496A368
00541  184.          DO 190 K2=2,NS                                              2496A370
00544  185.          TX(2)=TABLE(10,XLOC(K2,1))                                  2496A372
00545  186.          TX(3)=(TABLE(11,XLOC(K2,7))-TX(2))/XND(K2,7)                2496A374
00546  187.          DO 190 J=1,5                                                2496A376
00551  188.          TX(5)=XND(K2,J+1)*TX(3)+TX(2)                               2496A378
00552  189.          BLFM=1.-TX(5)*BLADES/2./PI/BLF(K2,J)                        2496A380
00553  190.          BLF(K2,J)=(TX(1)*XMD(K2)+BIN)*BLFM                          2496A382
00554  191.          XBLF(J,K2)=XND(K2,J+1)                                      2496A384
00555  192.          YBLF(J,K2)=BLF(K2,J)                                        2496A386
00556  193.     190  CONTINUE                                                    2496A388
00556  194.     C                                                                2496A390
00556  195.     C    COMPUTE RADIAL EQUILIBRIUM AT IMPELLER NORMALS              2496A392
00561  196.          DO 200 J=1,5                                                2496A394
00564  197.          C(J)=RADIUS(1,J+1)                                          2496A396
00565  198.          C(J+5)=PRT(1,J)                                             2496A398
00566  199.          C(J+15)=TRT(1,J)                                            2496A400
00567  200.          C(J+20)=AMASS(1,J)                                          2496A402
```

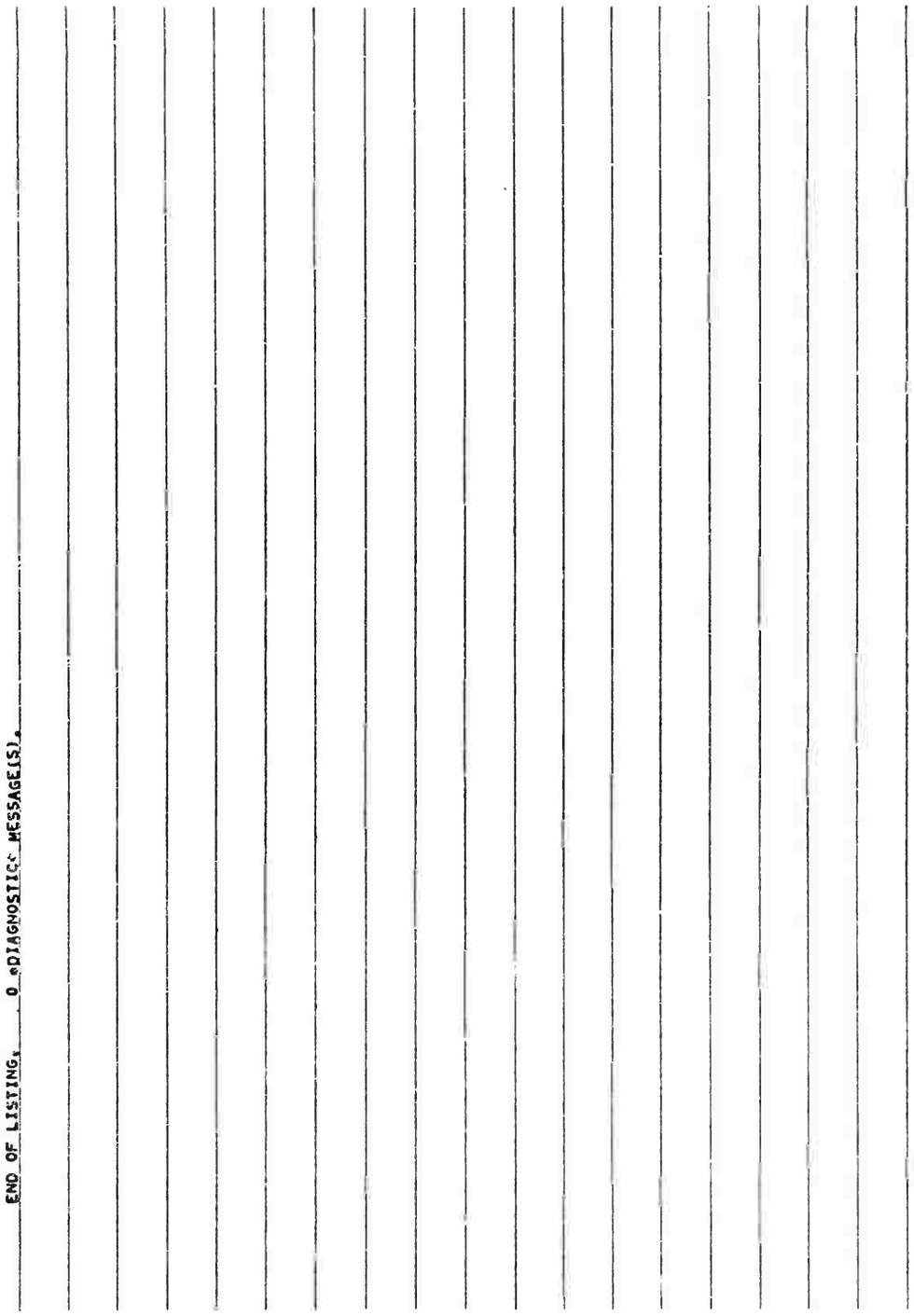
```
00570   201.    200   CONTINUE                                                    2496A404
00572   202.          C(26)=RPM                                                   2496A406
00573   203.          AK=TABLE(3,TT(1,3))                                         2496A408
00574   204.          C(27)=SQRT(AK*GC/R*(2./(AK+1.))**((AK+1.)/(AK-1.)))*.49118  2496A410
00574   205.    C                                                                 2496A412
00574   206.    C     Q ARRAY IS V ARRAY IN IMPEL                                 2496A414
00575   207.          Q(22)=W(1,3)                                                2496A416
00576   208.          Q(23)=BLADES                                                2496A418
00577   209.          Q(10)=FLOAT(NS)                                             2496A420
00577   210.    C                                                                 2496A422
00600   211.          JUMP=1                                                      2496A424
00601   212.          IF(NSLIP.LT.1)JUMP=2                                        2496A426
00603   213.          GO TO (201,202),JUMP                                        2496A428
00604   214.    201   JUMP1=1                                                     2496A430
00605   215.          IF(NSLIP.EQ.2)JUMP1=2                                       2496A432
00607   216.          IF(NSLIP.EQ.1)JUMP1=3                                       2496A434
00611   217.          GO TO 205                                                   2496A436
00612   218.    202   JUMP2=1                                                     2496A438
00613   219.    205   Q(9)=1.                                                     2496A440
00614   220.          IF(NSLIP.GT.NS) GO TO 208                                   2496A442
00616   221.          DO 206 J=1,5                                                2496A444
00621   222.    206   BETA(NS,J)=TABLE(13,XND(NS,J+1)/XND(NS,7)*100.)             2496A446
00623   223.    208   CONTINUE                                                    2496A448
00623   224.    C                                                                 2496A450
00623   225.    C                                                                 2496A452
00624   226.          DO 300 K2=2,NS                                              2496A454
00627   227.          Q(1)=RADIUS(K2,1)                                           2496A456
00630   228.          Q(2)=RADIUS(K2,7)                                           2496A458
00631   229.          Q(3)=FLOAT(K2-1)                                            2496A460
00632   230.          Q(4)=GAMMA(K2)/DGR                                          2496A462
00633   231.          Q(5)=FLOAT(K2)                                              2496A464
00634   232.          Q(6)=XLOC(K2,1)                                             2496A466
00634   233.    C                                                                 2496A468
00634   234.    C     DETERMINE RELATIVE SLIP POSITION                            2496A470
00635   235.          GO TO (210,220),JUMP                                        2496A472
00636   236.    210   GO TO (230,211,213),JUMP1                                   2496A474
00637   237.    211   Q(9)=2.                                                     2496A476
00640   238.          JUMP1=3                                                     2496A478
00641   239.          GO TO 230                                                   2496A480
00642   240.    213   Q(9)=3.                                                     2496A482
00643   241.          XYZ=(XMD(K2)-XMD(NSLIP))/(XMD(NS)-XMD(NSLIP))               2496A484
00644   242.          DO 214 J=1,5                                                2496A486
00647   243.    214   YAL(J)=XYZ*BETA(NS,J)                                       2496A488
00651   244.          GO TO 230                                                   2496A490
00652   245.    220   GO TO (230,221),JUMP2                                       2496A492
00653   246.    221   Q(9)=3.                                                     2496A494
00654   247.          XYZ=(XMD(K2)-XMD(KSLIP))/(XMD(NS)-XMD(KSLIP))               2496A496
00655   248.          DO 222 J=1,5                                                2496A498
00660   249.    222   YAL(J)=(XYZ*(BETA(NS,J)-BETA(KSLIP,J))+BETA(KSLIP,J))       2496A500
00662   250.    230   CONTINUE                                                    2496A502
00663   251.          Q(7)=(XMD(K2)-XMD(K2-1))/12.                                2496A504
00664   252.          Q(8)=BLF(K2,3)                                              2496A506
00665   253.          DO 240 J=1,5                                                2496A508
00670   254.          Q(J+10)=RO(K2-1,J)                                          2496A510
00671   255.          Q(J+10)=AREA(K2,J)*BLF(K2,J)                                2496A512
00672   256.    240   Q(J+15)=REC(K2,J)                                           2496A514
00674   257.          Q(21)=XMD(K2)                                               2496A516
00675   258.          CALL IMPEL(K2)                                              2496A518
```


CONFIDENTIAL

```
00676   259.          GO TO (250,260),JUMP                                    2496A520
00677   260.   250    IF((K2+1).EQ.NSLIP) JUMP1=2                             2496A522
00701   261.          GO TO 270                                               2496A524
00702   262.   260    GO TO (261,270),JUMP2                                   2496A526
00703   263.   261    IF(W(1,3)/A(103).LT.SLIPFC) GO TO 270                   2496A528
00705   264.          KSLIP=K2                                                2496A530
00706   265.          JUMP2=2                                                 2496A532
00707   266.          GO TO 270                                               2496A534
00710   267.   270    CONTINUE                                                2496A536
00711   268.          RCURV(K2,1)=YRC(1,K2)                                   2496A538
00712   269.          RCURV(K2,7)=YRC(3,K2)                                   2496A540
00713   270.          U(K2,1)=PI*RPM*RADIUS(K2,1)/360.                        2496A542
00714   271.          U(K2,7)=PI*RPM*RADIUS(K2,7)/360.                        2496A544
00715   272.          GAMMA(K2)=GAMMA(K2)/DGR                                 2496A546
00716   273.          PHI(K2)=TABLE(12,XLOC(K2,4))                            2496A548
00717   274.          TX(K2)=XMD(K2)                                          2496A550
00720   275.          DO 300 J=1,5                                            2496A552
00723   276.          AREA(K2,J)=A(J)                                         2496A554
00724   277.          RADIUS(K2,J+1)=A(J+10)                                  2496A556
00725   278.          U(K2,J+1)=A(J+15)                                       2496A558
00726   279.          TRT(K2,J)=A(J+25)                                       2496A560
00727   280.          PRT(K2,J)=A(J+35)                                       2496A562
00730   281.          XLOC(K2,J+1)=A(J+40)                                    2496A564
00731   282.          BETA(K2,J)=A(J+55)                                      2496A566
00732   283.          XMD(K2,J+1)=A(J+60)*12.                                 2496A568
00733   284.          WVSND(K2,J)=A(J+70)                                     2496A570
00734   285.          PS(K2,J)=A(J+85)                                        2496A572
00735   286.          TS(K2,J)=A(J+90)                                        2496A574
00736   287.          VSND(K2,J)=A(J+95)                                      2496A576
00737   288           W(K2,J)=A(J+100)                                        2496A578
00740   289.          WM(K2,J)=A(J+105)                                       2496A580
00741   290.          WU(K2,J)=A(J+110)                                       2496A582
00742   291.          VU(K2,J)=A(J+115)                                       2496A584
00743   292.          ALPHA(K2,J)=A(J+120)                                    2496A586
00744   293.          V(K2,J)=A(J+125)                                        2496A588
00745   294.          VVSND(K2,J)=A(J+130)                                    2496A590
00746   295.          PT(K2,J)=A(J+150)                                       2496A592
00747   296.          TT(K2,J)=A(J+155)                                       2496A594
00750   297.          RCURV(K2,J+1)=A(J+180)*12.                              2496A596
00751   298.          DPDN(K2,J)=A(J+190)                                     2496A598
00752   299.          ACCEL(K2,J)=A(J+315)                                    2496A600
00753   300.          DDMARG(K2,J)=VU(K2,J)*(RADIUS(K2,J+1)*CONST-(XMD(K2,J+1)*TABLE(11,2496A602
00753   301.         *XLOC(K2,7))+TABLE(10,XLOC(K2,1))*(XMD(K2,7)-XMD(K2,J+1)))/XMD(K2,72496A604
00753   302.         *))                                                     2496A606
00754   303.   300    CONTINUE                                                2496A608
00754   304.   C                                                             2496A610
00754   305.   C      COMPUTE THE SURFACE VELOCITIES                          2496A612
00757   306.          DO 350 K2=2,NS                                          2496A614
00762   307.          DO 350 J=1,5                                            2496A616
00765   308.          Y1=TAB2(TX,DDMARG(1,J),NS,1,XMD(K2)-0.02 ,IE)           2496A618
00766   309.          Y2=TAB2(TX,DDMARG(1,J),NS,1,XMD(K2)+0.02 ,IE)           2496A620
00767   310.          DV= 12.5*COS(BETA(K2,J)*DGR)*(Y2-Y1)                    2496A622
00770   311.          VS(K2,J)=W(K2,J)+DV                                     2496A624
00771   312.          VP(K2,J)=W(K2,J)-DV                                     2496A626
00772   313.          VSW(K2,J)=VS(K2,J)/W(1,3)                               2496A628
00773   314.          VPW(K2,J)=VP(K2,J)/W(1,3)                               2496A630
00774   315.          VTW(K2,J)=W(K2,J)/W(1,3)                                2496A632
00775   316.   350    CONTINUE                                                2496A634
```


CONFIDENTIAL

```
00775  317.      C
00775  318.      C     PRINT OUT RESULTS
01000  319.  375  CONTINUE
01001  320.      CALL OUTPUT
01002  321.      NS=NORMLS+1
01003  322.      GO TO (1,400),NPLOT
01003  323.      C
01003  324.      C     PLOT OUT GEOMETRY
01004  325.  400 CONTINUE
01005  326.      JHUB=NXY(4)
01006  327.      JTIP=NXY(5)
01007  328.      NHUB=(XVAL(JHUB,4)-XVAL(1,4))/PLOTDX+2.
01010  329.      NTIP=(XVAL(JTIP,5)-XVAL(1,5))/PLOTDX+2.
01011  330.      X(1,1)=XVAL(1,4)
01012  331.      X(1,2)=XVAL(1,5)
01013  332.      Y(1,1)=YVAL(1,4)
01014  333.      Y(1,2)=YVAL(1,5)
01015  334.      DO 410 J=2,NHUB
01020  335.      X(J,1)=X(J-1,1)+PLOTDX
01021  336.  410 Y(J,1)=TABLE(4,X(J,1))
01023  337.      DO 420 J=2,NTIP
01026  338.      X(J,2)=X(J-1,2)+PLOTDX
01027  339.  420 Y(J,2)=TABLE(5,X(J,2))
01031  340.      NOMODE(1)=NHUB
01032  341.      NOMODE(3)=NTIP
01033  342.      NOMODE(5)=NXY(4)
01034  343.      NOMODE(7)=NXY(5)
01035  344.      DO 460 J=1,5
01040  345.      K=2*J+7
01041  346.  460 NOMODE(K)=NS
01043  347.      IBAD=-1
01044  348.      CALL TALL14(GRID,NOMODE,1,IBAD,4,X(1,1),Y(1,1),X(1,2),Y(1,2),
01044  349.     *XVAL(1,4),YVAL(1,4),XVAL(1,5),YVAL(1,5),XLOC(1,2),
01044  350.     *RADIUS(1,2),XLOC(1,3),RADIUS(1,3),XLOC(1,4),RADIUS(1,4),
01044  351.     *XLOC(1,5),RADIUS(1,5),XLOC(1,6),RADIUS(1,6),X10,Y10,X11,Y11,
01044  352.     *X12,Y12,X13,Y13,X14,Y14,60)
01045  353.      WRITE(1,2020)(NTITLE(K),K=1,16)
01053  354.      WRITE(6,2030) IRAD
01056  355.      GO TO 1
01057  356.  900 CONTINUE
01060  357.      NS=1
01061  358.      GO TO 375
01062  359.  1000 FORMAT(1H120X,48HIMPELLER RADIAL EQUILIBRIUM DESIGN PROGRAM INPUT)
01063  360.  1001 FORMAT(16A5)
01064  361.  1002 FORMAT(10F7.0)
01065  362.  1003 FORMAT(//6X,16A5)
01066  363.  1004 FORMAT(//39H THE FOLLOWING CONTROL CARD IS IN ERROR )
01067  364.  1005 FORMAT(10X,F11.1,3F11.0,2F11.4,F11.0,F11.4)
01070  365.  1006 FORMAT(10X,10F11.4)
01071  366.  1007 FORMAT(10X,2F11.2,F11.4)
01072  367.  1008 FORMAT(1H1,5X,16A5)
01073  368.  1009 FORMAT(10X,2F11.0/(10X,10F11.4))
01074  369.  2020 FORMAT(10X,57HPLOT OF PROFILES, INTERPOLATED PROFILES, AND STREAML
01074  370.     *INES  /1H /10X,53HX = AXIAL DISTANCE (IN),  Y = RADIAL DISTANCE (I
01074  371.     *N)    /1H /10X,8HTITLE     ,16A5)
01075  372.  2030 FORMAT(1H1,16HPLOT INDICATOR =  ,I2,20H  (ZERO FOR SUCCESS) )
01076  373.      END
```


END OF LISTING, 0 *DIAGNOSTIC* MESSAGE(S).

CONFIDENTIAL


```
@     FOR INLET                                                    2496B002
COMPILATION BY UNIVAC 1108 FORTRAN-IV DATED     NOV..23,1965 F4008
THIS COMPILATION WAS DONE ON 19 AUG 66 AT 17:37:05


     SUBROUTINE INLET     ENTRY POINT 001354

     STORAGE USED (BLOCK, NAME, LENGTH)

          0001   *CODE   001401
          0000   *DATA   000334
          0002   *BLANK  004735
          0003   RC      000170
          0004   IMPELR  002335
          0005   BLOCK   010757


     EXTERNAL REFERENCES (BLOCK, NAME)

          0006   SLOPE
          0007   ATAN
          0010   TABLE
          0011   TAB2
          0012   TAN
          0013   ALOG
          0014   SQRT
          0015   SQRT
          0016   ATAN2
          0017   NEXP6$
          0020   NWDU$
          0021   NIO1$
          0022   NIO2$


     STORAGE ASSIGNMENT FOR VARIABLES (BLOCK, TYPE, RELATIVE LOCATION, NAME)

     0001   000407 1000L      0001   000563 1200L      0001   000570 1210L      0001   000015 122G      0001   000575 1220L
     0001   000601 1299L      0000   000201 1310F      0001   000622 1400L      0001   000643 1410L      0001   000061 144G
     0001   000065 150G       0000   000235 1610F      0001   000140 164G       0001   000754 1700L      0001   000165 177G
     0001   000202 205G       0001   000415 247G       0001   000631 332G       0001   000710 356G       0001   000763 400G
     0001   000152 610L       0001   000163 615L       0001   000367 900L       0000   000154 910F       0004 R 000000 A
     0000 R 000000 AC         0005   000000 ACCEL      0000 R 000127 AK         0000 R 000130 AK1        0013 R 000000 ALOG
     0005 R 000214 ALPHA      0005 R 000430 AMASS      0005 R 000644 AREA       0007 R 000000 ATAN       0016 R 000000 ATAN2
     0000 R 000131 B          0005 R 001060 BETA       0004 R 000764 BLF        0004 R 001200 C          0005 R 001274 CF
     0000 R 000133 C1         0000 R 000134 C2         0000 R 000135 C3         0000 R 000136 C4         0000 R 000137 DEN
     0005 R 001275 DERIV1     0005 R 001511 DERIV2     0005 R 001725 DGR        0005   001726 DPDN       0000 R 000132 DR
     0000 R 000104 EPSM       0004 R 001252 GAMMA      0005 R 002142 GC         0005 R 002143 GIVM       0005 R 002144 HGPSI
     0005 R 002145 HJ         0000 R 000153 HRT        0000 R 000152 HS         0000 R 000066 HT         0000 I 000122 IA
     0000 I 000125 IB         0000 I 000126 IE         0000 I 000147 IND        0000 I 000124 ITRAT      0000 I 000111 J
     0000 I 000112 JGO        0000 I 000141 JP1        0000 I 000105 K1         0000 I 000123 NGO        0000 I 000107 NM1
     0005   002146 NS         0005   002147 NTITLE     0000 I 000106 NTUBES     0002   000000 NXY        0005   002173 PHI
     0005 R 002217 PI         0005 R 002220 PRT        0005 R 002434 PS         0005 R 002650 PT         0004   001522 Q
     0000 R 000075 QMASS      0005 R 003064 R          0004 R 001306 RADIUS     0000 R 000150 RC         0005 R 003065 RCURV
     0005   003301 REC        0000 R 000143 RHO        0000 R 000113 RHUB       0000 R 000115 RHUB1      0005 R 003515 RIN
     0005 R 003516 RPM        0000 R 000114 RTIP       0000 R 000116 RTIP1      0000 R 000146 RVRVCR     0014 R 000000 SQRT
     0000 R 000110 STUBES     0010 R 000000 TABLE      0011 R 000000 TAB2       0012 R 000000 TAN        0000 R 000117 TDR
```

CONFIDENTIAL

CONFIDENTIAL


```
0000 R 000151 TDRC      0000 R 000142 TMASS     0005 R 003517 TRT       0005 R 003733 TS        0005 R 004147 TT
0005   004363 TX        0005   003407 TY        0005 R 004433 U         0005 R 004647 V         0000 R 000144 VCR
0000 R 000121 VLL       0005   005063 VP        0005   005277 VPW       0005 R 005513 VR        0005   005727 VS
0005 R 006143 VSND      0000 R 000140 VSQ       0005   006357 VSW       0005 R 006573 VU        0000 R 000120 VUL
0005 R 007007 VVSND     0005 R 007223 VX        0000 R 000145 VXVCR     0005 R 007437 W         0005 R 007653 WM
0005 R 005513 WR        0005 R 010303 WU        0005 R 010067 WVSND     0004   001604 XBLF      0004 R 001750 XLOC
0005   010517 XMD       0005   010543 XND       0003   000000 XRC       0000 R 000007 XTMASS    0002   000031 XVAL
0000 R 000033 XWX       0004   002164 YAL       0004   002171 YBLF      0003   000075 YRC       0002   002373 YVAL
0000 R 000057 ZDR
```

```
00101     1.          SUBROUTINE INLET(K2)                                                                  24968004
00101     2.    C                                                                                           24968006
00101     3.    C     THIS ROUTINE COMPUTES THE INLET CONDITIONS                                            24968008
00101     4.    C                                                                                           24968010
00103     5.          COMMON/RC/XRC(3,20),YRC(3,20)                                                         24968012
00104     6.          COMMON NXY(25),XVAL(50,25),YVAL(50,25)                                                24968014
00105     7.          COMMON/IMPELR/A(500)          ,BLF(20,7)      ,C(50)          ,                   24968016
00105     8.         *GAMMA(20)     ,RADIUS(20,7)  ,Q(50)          ,XBLF(5,20)     ,                   24968018
00105     9.         *XLOC(20,7)    ,YAL(5)        ,YBLF(5,20)                                            24968020
00106    10.          COMMON/BLOCK/ ACCEL(20,7)    ,ALPHA(20,7)    ,AMASS(20,7)    ,                   24968022
00106    11.         *AREA(20,7)    ,BETA(20,7)    ,CF             ,DERIV1(20,7)   ,                   24968024
00106    12.         *DERIV2(20,7) ,DGR            ,DPSN(20,7)     ,GC    ,GIVM    ,                   24968026
00106    13.         *HGPSI,HJ,NS  ,NTITLE(20)     ,PHI(20) ,PI    ,PRT(20,7)      ,                   24968028
00106    14.         *PS(20,7)      ,PT(20,7)      ,R              ,RCURV(20,7)    ,                   24968030
00106    15.         *REC(20,7)     ,RIN   ,RPM    ,TRT(20,7)      ,TS(20,7)       ,                   24968032
00106    16.         *TT(20,7)      ,TX(20)        ,TY(20)         ,U(20,7)        ,                   24968034
00106    17.         *V(20,7)       ,VP(20,7)      ,VPW(20,7)      ,VR(20,7)       ,                   24968036
00106    18.         *VS(20,7)      ,VSND(20,7)    ,VSW(20,7)      ,VU(20,7)       ,                   24968038
00106    19.         *VVSND(20,7)   ,VX(20,7)      ,W(20,7)        ,WM(20,7)       ,                   24968040
00106    20.         *WVSND(20,7)   ,WU(20,7)      ,XMD(20)        ,XND(20,7)                          24968042
00107    21.          DIMENSION AC(7),WR(20,7),XTMASS(20),XWX(20),ZDR(7),HT(7)                              24968044
00110    22.          DIMENSION GMASS(7)                                                                    24968046
00111    23.          EQUIVALENCE (VR,WR)                                                                   24968048
00112    24.          DATA EPSM/.005/,K1/1/,NTUBES/5/,NM1/4/,STUBES/5./                                     24968050
00112    25.    C                                                                                           24968052
00112    26.    C                                                                                           24968054
00112    27.    C***INITIALIZE                                                                              24968056
00120    28.          GIVM=0.                                                                               24968058
00121    29.          DO 100 J=1,5                                                                          24968060
00124    30.          GIVM=GIVM+AMASS(1,J)                                                                  24968062
00125    31.    100   CONTINUE                                                                              24968064
00125    32.    C                                                                                           24968066
00125    33.    C     JGO=0 AND 1 FOR NORMAL AND ERROR RETURNS                                              24968068
00127    34.          JGO=0                                                                                 24968070
00127    35.    C                                                                                           24968072
00127    36.    C***ASSUME STREAMLINES BASED ON EQUAL AREAS AND COMPUTE DERIVATIVES                          24968074
00130    37.    200   CONTINUE                                                                              24968076
00131    38.          CALL SLOPE(XLOC(1,1),0.05,RADIUS,AREA,CF,DERIV1,DERIV2)                               24968078
00132    39.          RIN=RADIUS(1,4)                                                                       24968080
00133    40.          RHUB=RADIUS(1,1)                                                                      24968082
00134    41.          RTIP=RADIUS(1,7)                                                                      24968084
00135    42.          RHUB1=RHUB                                                                            24968086
00136    43.          RTIP1=RTIP                                                                            24968088
00137    44.          TDR=RTIP-RHUB                                                                         24968090
00140    45.          GAMMA(1)=ATAN(DERIV1(1,4))                                                            24968092
```

CONFIDENTIAL

```
00140    46.  C                                                          24968094
00140    47.  C***ASSUME LIMITS FOR HUB VELOCITY                         24968096
00141    48.        VUL=1200.                                            24968098
00142    49.        VLL=0.                                               24968100
00142    50.  C                                                          24968102
00143    51.        DO 1599 IA=1,10                                      24968104
00143    52.  C                                                          24968106
00143    53.  C***COMPUTE INLET TOTAL PRESSURE FROM INPUT OF P=F(R)       24968108
00146    54.  300   CONTINUE                                            24968110
00147    55.        DO 399 J=1,NTUBES                                    24968112
00152    56.        PT(1,J)=TABLE(6,RADIUS(1,J+1))/HGPSI                 24968114
00153    57.        TT(1,J)=TABLE(7,RADIUS(1,J+1))                       24968116
00154    58.        BLF(1,J)=TABLE(8,RADIUS(1,J+1))                      24968118
00155    59.        ALPHA(1,J)=TABLE(9,RADIUS(1,J+1))*DGR                24968120
00156    60.        HT(J)=TABLE(1,TT(1,J))                               24968122
00157    61.  399   CONTINUE                                            24968124
00157    62.  C                                                          24968126
00161    63.        NGO=1                                                24968128
00162    64.        ITRAT=0                                              24968130
00162    65.  C                                                          24968132
00163    66.        DO 1299 IB=1,10                                      24968134
00163    67.  C                                                          24968136
00163    68.  C***COMPUTE HUB VELOCITY BASED ON ASSOCIATED LIMITS        24968138
00166    69.  600   CONTINUE                                            24968140
00167    70.        IF(NGO.EQ.2) GO TO 610                               24968142
00171    71.        VX(K2,1)=(VUL+VLL)/2.0                               24968144
00172    72.        GO TO 615                                            24968146
00173    73.  610   CONTINUE                                            24968148
00174    74.        VX(K2,1)=TAB2(XTMASS,XWX,ITRAT,1,GIVM,IE)            24968150
00175    75.  615   CONTINUE                                            24968152
00176    76.        DO 800 J=1,5                                         24968154
00201    77.        VU(1,J)=TAN(ALPHA(1,J))*VX(1,J)                      24968156
00202    78.  800   CONTINUE                                            24968158
00202    79.  C                                                          24968160
00202    80.  C***COMPUTE THE VELOCITY PROFILE                           24968162
00204    81.        DO 899 J=1,NM1                                       24968164
00207    82.        A=GC*HJ*(TT(K2,J+1)+TT(K2,J))                        24968166
00210    83.        AK=TABLE(3,(TT(1,J+1)+TT(1,J))/2.)                   24968168
00211    84.        AK1=AK/(AK-1.0)                                      24968170
00212    85.        B=R/HJ*ALOG((TT(K2,J+1)/TT(K2,J))**AK1/(PT(K2,J+1)/PT(K2,J)))  24968172
00213    86.        C=2.0*R*AK/(HJ*(AK-1.0))                             24968174
00214    87.        DR=RADIUS(1,J+2)-RADIUS(1,J+1)                       24968176
00215    88.        C1=VX(1,J)**2*(1.+B/C*(1.+DERIV1(1,J+1)**2)+DERIV2(1,J+1)*DR)-A*B  24968178
00216    89.        C2=2.*GC*HJ*(HT(J+1)-HT(J))                          24968180
00217    90.        C3=VU(1,J+1)**2*(B/C-2.+RADIUS(1,J+1)/RADIUS(1,J+2))+VU(1,J)**2  24968182
00217    91.       **(B/C+2.-RADIUS(1,J+2)/RADIUS(1,J+1))                24968184
00220    92.        C4=1.-B/C*(1.+DERIV1(1,J+2)**2)                      24968186
00221    93.        DEN=C4-DERIV2(1,J+2)*DR                              24968188
00222    94.        VSQ=(C1+C2+C3)/DEN                                   24968190
00222    95.  C                                                          24968192
00222    96.  C***IS THE VELOCITY SQUARED NEGATIVE                       24968194
00223    97.  830   CONTINUE                                            24968196
00224    98.        IF(VSQ.LT.0.) GO TO 900                              24968198
00226    99.        VX(K2,J+1)=SQRT(VSQ)                                 24968200
00227   100.  899   CONTINUE                                            24968202
00231   101.        GO TO 1000                                           24968204
00231   102.  C                                                          24968206
00231   103.  C***PRINT DIAGNOSTIC MESSAGE                               24968208
```

CONFIDENTIAL

```
00231   104.   C                                                                    24960210
00232   105.   900   CONTINUE                                                       24960212
00233   106.         JP1=J+1                                                        24960214
00234   107.         WRITE(6,910)VSQ,K1,JP1,VX(K2,1)                                24960216
00242   108.   910   FORMAT(//31H THE AXIAL VELOCITY SQUARED IS  ,E11.4,12H  AT STATION24960218
00242   109.        1  ,I2,12H, STREAMLINE  ,I2,31H, WHEN THE HUB VELOCITY EQUALS  ,F8.24960220
00242   110.        22)                                                            24960222
00243   111.         GO TO 1210                                                     24960224
00243   112.   C                                                                    24960226
00243   113.   C***COMPUTE MASS FLOW RATE BASED ON VELOCITY PROFILE                 24960228
00244   114.   1000  CONTINUE                                                       24960230
00245   115.         TMASS = 0.0                                                    24960232
00246   116.         DO 1099 J=1,NTUBES                                             24960234
00251   117.         AK=TABLE(3,TT(1,J))                                            24960236
00252   118.         RHO=PT(K2,J)/R/TT(K2,J)                                        24960238
00253   119.         VCR=SQRT(AK*GC*R*2.0*TT(K2,J)/(AK+1.0))                        24960240
00254   120.         VXVCR=VX(K2,J)/VCR                                             24960242
00255   121.         AK1=(AK-1.0)/(AK+1.0)                                          24960244
00256   122.         RVRVCR=VXVCR*(1.0-AK1*VXVCR**2*(1.0+TAN(ALPHA(K2,J))**2+DERIV1(K2,24960246
00256   123.        *J+1)**2))**(1./(AK-1.))                                       24960248
00257   124.         QMASS(J)=BLF(1,J)*RVRVCR*RHO*VCR*AREA(1,J)                     24960250
00260   125.         TMASS=TMASS+QMASS(J)                                           24960252
00261   126.         AC(J)=AMASS(1,J)/BLF(K2,J)/RVRVCR/RHO/VCR                      24960254
00262   127.   1099  CONTINUE                                                       24960256
00262   128.   C                                                                    24960258
00262   129.   C***IS OVERALL CONTINUITY SATISFIED                                  24960260
00264   130.   1100  CONTINUE                                                       24960262
00265   131.         IF(ABS(TMASS-GIVM) .LT. EPSM)  GO TO 1400                      24960264
00267   132.         ITRAT=ITRAT+1                                                  24960266
00270   133.         XWX(ITRAT)=VX(K2,1)                                            24960268
00271   134.         XTMASS(ITRAT)=TMASS                                            24960270
00272   135.         IF(ITRAT.LT.2) GO TO 1200                                      24960272
00274   136.         CALL SORT(XTMASS,XWX,ITRAT)                                    24960274
00275   137.         NGO=2                                                          24960276
00276   138.         GO TO 1299                                                     24960278
00276   139.   C                                                                    24960280
00276   140.   C***ADJUST THE HUB VELOCITY LIMITS                                   24960282
00277   141.   1200  CONTINUE                                                       24960284
00300   142.         IF(TMASS.GT.GIVM) GO TO 1220                                   24960286
00300   143.   C                                                                    24960288
00300   144.   C     INCREASE HUB VELOCITY                                          24960290
00302   145.   1210  CONTINUE                                                       24960292
00303   146.         VLL=VX(K2,1)                                                   24960294
00304   147.         NGO=1                                                          24960296
00305   148.         GO TO 1299                                                     24960298
00305   149.   C                                                                    24960300
00305   150.   C     DECREASE HUB VELOCITY                                          24960302
00306   151.   1220  CONTINUE                                                       24960304
00307   152.         VUL=VX(K2,1)                                                   24960306
00310   153.         NGO=1                                                          24960308
00311   154.   1299  CONTINUE                                                       24960310
00311   155.   C                                                                    24960312
00311   156.   C***PRINT DIAGNOSTIC MESSAGE                                         24960314
00313   157.   1300  CONTINUE                                                       24960316
00314   158.         WRITE(6,1310) K1,EPSM,TMASS,GIVM                               24960318
00322   159.   1310  FORMAT(//1X,94HTHE PROGRAM WAS UNABLE TO OBTAIN A VELOCITY PROFILE24960320
00322   160.        1 THAT WOULD GIVE A MASS BALANCE AT STATION   I2  /6X,7HEPS M = F7.24960322
00322   161.        24,3X,12HCOMPUTED M = F7.4,3X,9HGIVEN M = F7.4  )               24960324
```


CONFIDENTIAL

CONFIDENTIAL


```
00323   162.          JGO=1                                                    24968326
00324   163.          GO TO 1700                                               24968328
00324   164.    C                                                              24968330
00324   165.    C***IS STREAMTUBE CONTINUITY SATISFIED                         24968332
00325   166.    1400  CONTINUE                                                 24968334
00326   167.          IND=0                                                    24968336
00327   168.          RHUB=RHUB1                                               24968338
00330   169.          TDR=0                                                    24968340
00331   170.          DO 1499 J=1,NTUBES                                       24968342
00334   171.          IF(ABS(AC(J)-AREA(K2,J)) .LT. 0.010)  GO TO 1410         24968344
00336   172.          IND=IND+1                                                24968346
00337   173.    1410  CONTINUE                                                 24968348
00340   174.          RC=SQRT(AC(J)/PI+RHUB**2)                                24968350
00341   175.          ZDR(J)=RC-RHUB                                           24968352
00342   176.          TDR = TDR+ZDR(J)                                         24968354
00343   177.          RHUB=RC                                                  24968356
00344   178.    1499  CONTINUE                                                 24968358
00344   179.    C                                                              24968360
00346   180.          IF(IND.EQ.0) GO TO 1700                                  24968362
00346   181.    C                                                              24968364
00346   182.    C***ADJUST STREAMLINES BASED ON VELOCITY PROFILE               24968366
00350   183.    1500  CONTINUE                                                 24968368
00351   184.          VUL=VX(K2,1)+200.                                        24968370
00352   185.          VLL=VX(K2,1)-200.                                        24968372
00353   186.          TDRC=RTIP1-RHUB1                                         24968374
00354   187.          RHUB=RHUB1                                               24968376
00355   188.          DO 1599 J=1,NTUBES                                       24968378
00360   189.          ZDR(J)=ZDR(J)*TDRC/TDR                                   24968380
00361   190.          RADIUS(1,J+1)=SQRT((RHUB**2+(RHUB+ZDR(J))**2)/2.)        24968382
00362   191.          AREA(K2,J)=PI*((RHUB+ZDR(J))**2-RHUB**2)                 24968384
00363   192.          RHUB=RHUB+ZDR(J)                                         24968386
00364   193.    1599. CONTINUE                                                 24968388
00364   194.    C                                                              24968390
00364   195.    C***PRINT DIAGNOSTIC MESSAGE                                   24968392
00367   196.    1600  CONTINUE                                                 24968394
00370   197.          WRITE(6,1610) K1,IND                                     24968396
00374   198.    1610  FORMAT(//83H THE PROGRAM WAS UNABLE TO OBTAIN A CORRECT SET OF STR24968398
00374   199.         1EAMLINE POSITIONS AT STATION  I2. /6X,13HNO. INCORRECT  I4  )  24968400
00374   200.    C                                                              24968402
00374   201.    C***COMPUTE REMAINING INLET FLUID PROPERTIES                   24968404
00375   202.    1700  CONTINUE                                                 24968406
00376   203.          AREA(1,6)=0.                                             24968408
00377   204.          DO 1799 J=1,NTUBES                                       24968410
00402   205.          AREA(1,6)=AREA(1,6)+AREA(1,J)                            24968412
00403   206.          XLOC(1,J+1)=XLOC(1,1)                                    24968414
00404   207.          RCURV(1,J+1)=(1.+DERIV1(1,J+1)**2)**1.5/DERIV2(1,J+1)    24968416
00405   208.          AK=TABLE(3,TT(K2,J))                                     24968418
00406   209.          AK1 = (AK-1.0)/(AK+1.0)                                  24968420
00407   210.          VR(1,J)=VX(1,J)*DERIV1(1,J+1)                            24968422
00410   211.          V(K2,J) = SQRT(VX(K2,J)**2+VU(K2,J)**2+VR(K2,J)**2)      24968424
00411   212.          VCR = SQRT(AK*GC*R*2.0*TT(K2,J)/(AK+1.0))                24968426
00412   213.          TS(1,J)=TT(1,J)*(1.-AK1*(V(1,J)/VCR)**2)                 24968428
00413   214.          AK=TABLE(3,TS(1,J))                                      24968430
00414   215.          VSND(K2,J)=SQRT(AK*GC*R*TS(K2,J))                        24968432
00415   216.          VVSND(K2,J)=V(K2,J)/VSND(K2,J)                           24968434
00416   217.          AK=TABLE(3,(TT(1,J)+TS(1,J))/2.)                         24968436
00417   218.          PS(K2,J)=PT(K2,J)*(TS(K2,J)/TT(K2,J))**(AK/(AK-1.))      24968438
00420   219.          U(1,J+1)=PI*RADIUS(1,J+1)*RPM/360.                       24968440
```

CONFIDENTIAL

```
00421   220.          WU(1,J)=U(1,J+1)-VU(1,J)                                  24968442
00422   221.          W(K2,J)=SQRT(VX(K2,J)**2+WU(K2,J)**2+WR(K2,J)**2)         24968444
00423   222.          WVSND(K2,J)=W(K2,J)/VSND(K2,J)                            24968446
00424   223.          WM(1,J)=SQRT(VX(1,J)**2+WR(1,J)**2)                       24968448
00425   224.          BETA(K2,J)=ATAN2(WU(K2,J),VX(K2,J))                       24968450
00426   225.          HS=TABLE(1,TS(1,J))                                       24968452
00427   226.          HRT=HS+W(1,J)**2/2./GC/HJ                                 24968454
00430   227.          TRT(1,J)=TABLE(-1 ,HRT)                                   24968456
00431   228.          AK=TABLE(3.,(TT(1,J)+TRT(1,J))/2.)                        24968458
00432   229.          PRT(1,J)=(TRT(1,J)/TT(1,J))**(AK/(AK-1.))*PT(1,J)         24968460
00433   230.   1799   CONTINUE                                                  24968462
00433   231.   C                                                               24968464
00435   232.          J=NTUBES+1                                                24968466
00436   233.          XLOC(1,J+1)=XLOC(1,1)                                     24968468
00437   234.          RCURV(1,J+1)=(1.+DERIV1(1,J+1)**2)**1.5/DERIV2(1,J+1)     24968470
00440   235.          U(1,J+1)=PI*RADIUS(1,J+1)*RPM/360.                        24968472
00441   236.          J=0                                                       24968474
00442   237.          RCURV(1,J+1)=(1.+DERIV1(1,J+1)**2)**1.5/DERIV2(1,J+1)     24968476
00443   238.          U(1,J+1)=PI*RADIUS(1,J+1)*RPM/360.                        24968478
00444   239.   1800   CONTINUE                                                  24968480
00444   240.   C                                                               24968482
00445   241.          IF(JGO.EQ.1)K2=-1                                         24968484
00447   242.          RETURN                                                    24968486
00450   243.          END                                                       24968488

        END OF LISTING.      0 *DIAGNOSTIC* MESSAGE(S).
```


CONFIDENTIAL

```
0    FOR SLOPE                                                    24968490
COMPILATION BY IBM/360 1108 FORTRAN-IV DATED    NOV. 23,1965 F4008
THIS COMPILATION DONE ON 10 AUG 66 AT 17:37:09


   SUBROUTINE SLOPE      ENTRY POINT 000206

   STORAGE USED (BLOCK, NAME, LENGTH)

      0001   ●CODE   000257
      0000   ●DATA   000130
      0002   ●BLANK  000000


   EXTERNAL REFERENCES (BLOCK, NAME)

      0003   TABLE
      0004   SQRT


   STORAGE ASSIGNMENT FOR VARIABLES (BLOCK, TYPE, RELATIVE LOCATION, NAME)

      0001  000023 I1IG        0001  000111 140G        0001  000113 143G        0001  000163 350L        0001  000165 395L
      0000 R 000256 A          0000 I 000372 I          0000 I 000071 J          0000 I 000065 K2         0000 I 000067 L
      0000 I 000066 M          0000 I 000063 NTUBES     0000 R 000062 PI         0000 R 000000 RH         0000 R 000050 RS
      0000 R 000012 RT         0004 R 000000 SQRT       0000 R 000064 STUBES     0003 R 000000 TABLE      0000 R 000070 X
      0000 R 000000 Z


00101     1.          SUBROUTINE SLOPE(XHUB,DX,RADIUS,AREA,CF,DERIV1,DERIV2)                                  24968492
00101     2.    C
00101     3.    C     SLOPE COMPUTES  FIRST AND SECOND RADIAL DERIVATIVES OF STREAMLINES                      24968494
00101     4.    C     OF STREAMTUBES OF EQUAL AREA                                                            24968496
00101     5.    C                                                                                             24968498
00103     6.          DIMENSION R(10),RT(10),Z(10),A(10),RS(10)                                               24968500
00104     7.          DIMENSION RADIUS(20,7),AREA(20,7),CF(11),DERIV1(20,7),DERIV2(120,7)                     24968502
00105     8.          DATA PI/3.14159/,NTUBES/5/,STUBES/5./,M/1/,H/.2/                                        24968504
00105     9.    C                                                                                             24968506
00105    10.    C     SET UP HUB AND TIP POINTS                                                               24968508
00114    11.    100   CONTINUE                                                                                24968510
00114    12.    C                                                                                             24968512
00115    13.          X=XHUB-DX                                                                               24968514
00116    14.          DO 199 J=1,M                                                                            24968516
00121    15.          Z(J)=X                                                                                  24968518
00122    16.          RH(J)=TABLE(4,X)                                                                        24968520
00123    17.          RT(J)=TABLE(5,X)                                                                        24968522
00124    18.          X=X+DX                                                                                  24968524
00125    19.          A(J)=(RT(J)**2-RH(J)**2)/STUBES                                                         24968526
00126    20.    199   CONTINUE                                                                                24968528
00130    21.          RADIUS(1,1)=RH(L)                                                                       24968530
00131    22.          RADIUS(1,7)=RT(L)                                                                       24968532
00132    23.          DERIV1(1,1)=(RH(3)-RH(1))/2./DX                                                         24968534
00133    24.          DERIV1(1,7)=(RT(3)-RT(1))/2./DX                                                         24968536
00134    25.          DERIV2(1,1)=(RH(3)-2.*RH(2)+RH(1))/DX**2                                                24968538
                                                                                                             24968540
```

CONFIDENTIAL

```
00135   26.          DERIV2(1,7)=(RT(3)-2.*RT(2)+RT(1))/DX**2                    24968542
00135   27.    C                                                                 24968544
00135   28.    C     SET UP STREAMLINE POINTS BASED ON EQUAL AREAS               24968546
00136   29.    200   CONTINUE                                                    24968548
00137   30.          DO 399 J=1,NTUBES                                           24968550
00142   31.          DO 299 I=1,M                                                24968552
00145   32.          RT(I)=SQRT(A(I)+RH(I)**2)                                   24968554
00146   33.          RS(I)=SQRT((RT(I)**2+RH(I)**2)/2.)                          24968556
00147   34.          RH(I)=RT(I)                                                 24968558
00150   35.    299   CONTINUE                                                    24968560
00152   36.          RADIUS(1,J+1)=RS(L)                                         24968562
00153   37.          AREA(K2,J)=A(L)*PI                                          24968564
00154   38.          IF(CF(K2).GT.0.) GO TO 350                                  24968566
00154   39.    C                                                                 24968568
00154   40.    C     COMPUTE THE RADIAL DERIVATIVE                               24968570
00156   41.    300   CONTINUE                                                    24968572
00157   42.          DERIV1(1,J+1)=(RS(3)-RS(1))/2./DX                           24968574
00160   43.          DERIV2(1,J+1)=(RS(3)-2.*RS(2)+RS(1))/DX**2                  24968576
00161   44.          GO TO 399                                                   24968578
00162   45.    350   CONTINUE                                                    24968580
00163   46.          DERIV1(1,J+1)=0.                                            24968582
00164   47.          DERIV2(1,J+1)=0.                                            24968584
00165   48.    399   CONTINUE                                                    24968586
00167   49.          RETURN                                                      24968588
00170   50.          END                                                         24968590

        END OF LISTING.      0 *DIAGNOSTIC* MESSAGE(S).
```


CONFIDENTIAL

CONFIDENTIAL


```
0     FOR SORT                                                    24968592
COMPILATION BY UNIVAC 1108 FORTRAN-IV DATED     NOV. 23,1965 F4008
THIS COMPILATION WAS DONE ON 19 AUG 66 AT 17:37:11

    SUBROUTINE SORT       ENTRY POINT 000065

    STORAGE USED (BLOCK, NAME, LENGTH)

          0001   *CODE   000114
          0000   *DATA   000022
          0002   *BLANK  000000

    STORAGE ASSIGNMENT FOR VARIABLES (BLOCK, TYPE, RELATIVE LOCATION, NAME)

     0001   000013 1106       0001   000022 1156       0001   000014 1136       0001   000052 1396       0000 I 000001 JJ1
     0000 I 000003 JJ2        0000 I 000004 JJ3        0000 I 000002 NT1        0000 I 000000 NT2        0000 R 000005 TEMP1
     0000 R 000006 TEMP2


00101     1.          SUBROUTINE SORT(TX,TY,NT)                                24968594
00101     2.    C                                                              24968596
00101     3.    C     SORT SORTS THE TX ARRAY IN INCREASING ORDER AND THE      24968598
00101     4.    C     TY ARRAY CORRESPONDINGLY                                 24968600
00101     5.    C                                                              24968602
00101     6.    C     NT IS THE NUMBER OF POINTS TO BE SORTED                  24968604
00101     7.    C                                                              24968606
00103     8.          DIMENSION TX(1),TY(1)                                    24968608
00104     9.          IF(NT.LT.2) RETURN                                       24968610
00106    10.          NT2=NT-1                                                 24968612
00107    11.          DO 139 JJ1=1,NT2                                         24968614
00112    12.    136   CONTINUE                                                 24968616
00113    13.          NT1=NT-JJ1                                               24968618
00114    14.          DO 139 JJ2=1,NT1                                         24968620
00117    15.          JJ3=JJ1+JJ2                                              24968622
00120  *DIAGNOSTIC*   THE TEST FOR EQUALITY BETWEEN NON-INTEGERS MAY NOT BE MEANINGFUL.
00120    16.          IF(TX(JJ1).LE.TX(JJ3))  GO TO 139                        24968624
00122    17.          TEMP1=TX(JJ1)                                            24968626
00123    18.          TEMP2=TY(JJ1)                                            24968628
00124    19.          TX(JJ1)=TX(JJ3)                                          24968630
00125    20.          TY(JJ1)=TY(JJ3)                                          24968632
00126    21.          TX(JJ3)=TEMP1                                            24968634
00127    22.          TY(JJ3)=TEMP2                                            24968636
00130    23.          GO TO 136                                                24968638
00131    24.    139   CONTINUE                                                 24968640
00134    25.          RETURN                                                   24968642
00135    26.          END                                                      24968644

       END OF LISTING.     1 *DIAGNOSTIC* MESSAGE(S).
```

CONFIDENTIAL

```
@     FOR IMPEL                                                    2496C002
COMPILATION BY UNIVAC 1108 FORTRAN-IV DATED     NOV. 23,1965 F4008
THIS COMPILATION WAS DONE ON 26 OCT 66 AT 12:17:34

   SUBROUTINE IMPEL     ENTRY POINT 002251

   STORAGE USED (BLOCK, NAME, LENGTH)

        0001   *CODE   002267
        0000   *DATA   000262
        0002   *BLANK  000000
        0003   RC      000170
        0004   IMPELR  002335


   EXTERNAL REFERENCES (BLOCK, NAME)

        0005   COS
        0006   TAB2
        0007   SQRT
        0010   TABLE
        0011   TAN
        0012   ATAN
        0013   SIN
        0014   ATAN2
        0015   NERR2S
        0016   NVDUS
        0017   N101S
        0020   N102S
        0021   *EXP6S


   STORAGE ASSIGNMENT FOR VARIABLES (BLOCK, TYPE, RELATIVE LOCATION, NAME)

0001   002171 1000L     0000   000035 1001F     0000   000047 1002F     0000   000064 1003F     0000   000074 1004F
0000   000102 1005F     0001   002121 1006L     0001   000622 101L      0001   002143 1017L     0001   000627 102L
0001   000540 103L      0001   002204 1033L     0001   000701 104L      0001   001130 105L      0001   002231 1050L
0001   001123 106L      0000   000120 1066F     0001   001125 109L      0001   001202 110L      0001   000042 1160
0001   002125 120L      0001   001706 121L      0001   002110 122L      0001   001700 125L      0001   000054 127L
0001   001737 128L      0001   001715 129L      0001   000066 1350      0001   000116 1446      0001   000273 1650
0001   000301 1736      0001   000321 2010      0001   000347 2106      0001   000370 2176      0001   000410 2256
0001   000457 2406      0001   000514 2500      0001   000553 2528      0001   000564 2728      0001   000572 3004
0001   002211 3000L     0001   000624 3110      0001   001031 315L      0001   000645 3230      0001   000667 3330
0001   000703 3426      0001   000733 3516      0001   001747 364L      0001   001003 3716      0001   001020 3776
0001   000665 4002L     0001   000056 4020L     0001   001033 404#      0001   001040 4126      0001   001046 4176
0001   001176 4376      0001   001232 4716      0001   001240 471L      0001   000507 501L      0001   001246 5056
0001   000107 510L      0001   001260 5136      0001   001266 5216      0001   001301 5276      0001   001314 5356
0001   001322 5436      0001   001337 5516      0001   001353 5576      0001   001362 5656      0001   001364 5716
0001   001436 6016      0001   001455 6136      0001   001476 6226      0001   001504 6306      0001   001532 6366
0001   001571 6446      0001   001601 6526      0001   001673 6656      0001   001730 7106      0001   001751 7256
0001   001762 7346      0001   001773 7456      0001   002051 7546      0001   002103 7706      0001   002112 7776
0001   000560 8L        0004 R 000000 A         0000 R 000024 AASB      0000 R 000000 AP        0000 R 000026 APT
0000 R 000016 AT        0012 R 000000 ATAN      0014 R 000000 ATAN2     0004 R 000764 BLF       0004 R 001200 C
0000 R 000033 CONST     0005 R 000000 COS       0004 R 001262 GAMMA     0000 I 000020 IE        0000 I 000023 INDY
0000 1 000022 IQ        0003 1 000025 IT        0000 I 000013 ITIME     0000 I 000021 J         0000 1 000032 JJ60
```

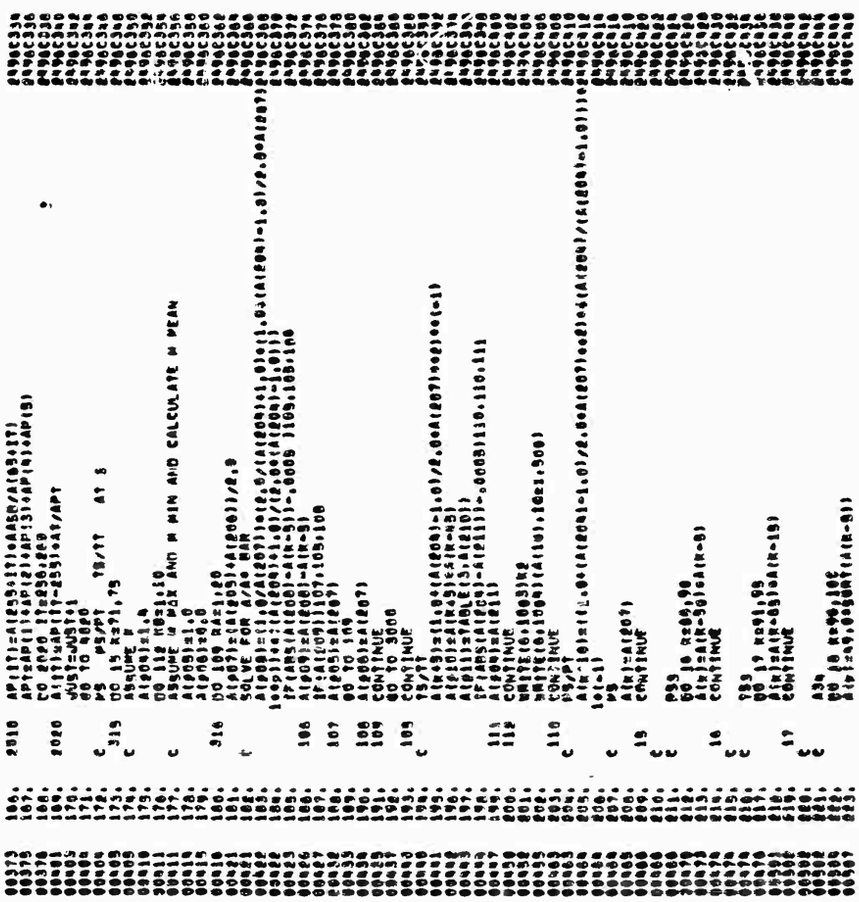
CONFIDENTIAL

```
0000 I 000017 JUST      0000 I 000015 K         0000 I 000030 KA        0000 1 000027 KB        0000 I 000031 KC
0000 1 000034 KD        0000 R 000014 RAD       0004 R 001306 RADIUS    0013 R 000000 SIN       0000 I 000012 SLIP
0007 R 000000 SQRT      0010 R 000000 TABLE     0006 R 000000 TAN2      0011 R 000000 TAN       0004 R 001522 V
0030 R 000005 X         0004 R 001604 XBLF      0004 R 001750 XLOC      0003 R 000000 XRC       0004 R 002164 YAL
0004 R 052171 YBLF      0003 R 000074 YRC
```

```
00101     1.          SUBROUTINE IMPEL(K2)                                                    2496C004
00101     2.    C                                                                             2496C006
00101     3.    C     IMPEL COMPUTES THE VELOCITY VECTORS SATISFYING RADIAL                   2496C008
00101     4.    C     EQUILIBRIUM ALONG AN IMPELLER NORMAL STATION                            2496C010
00101     5.    C                                                                             2496C012
00103     6.          COMMON/RC/XRC(3,20),YRC(3,20)                                           2496C014
00104     7.          COMMON/IMPELR/A(500)          ,BLF(20,7)      ,C(50)                    2496C016
00104     8.         *,APPA(20)     ,RADIUS(20,7)  ,V(50)          ,XBLF(5,20)               2496C018
00104     9.         *XLOC(20,7)    ,YAL(5)        ,YBLF(5,20)                                2496C020
00105    10.          DIMENSION AP(5),X(5)                                                    2496C022
00106    11.          INTEGER SLIP                                                            2496C024
00107    12.          ITIME=-1                                                                2496C026
00110    13.          RAD = .017453293                                                        2496C028
00110    14.    C     OPEGA                                                                   2496C030
00111    15.          A(213) = 2.0*3.14159*C(26)/60.                                          2496C032
00112    16.          A(201)=3.14159/COS(V(4)*.017453293)                                     2496C034
00113    17.          A(220) = 0.                                                             2496C036
00114    18.          A(219) = V(11)+V(12)+V(13)+V(14)+V(15)                                  2496C038
00115    19.          DO 40 K=256,260                                                         2496C040
00120    20.          A(K) = V(K-245)                                                         2496C042
00121    21.          A(K+5)=0.                                                               2496C044
00122    22.       40 CONTINUE                                                                2496C046
00124    23.          AT=A(256)+A(257)+A(258)+A(259)+A(260)                                   2496C048
00125    24.      127 CONTINUE                                                                2496C050
00126    25.          JUST=1                                                                  2496C052
00127    26.    4020  CONTINUE                                                                2496C054
00127    27.    C                                                                             2496C056
00127    28.    C     COMPUTE BLF                                                             2496C058
00130    29.          IF(A(220))510,510,500                                                   2496C060
00133    30.    500   CONTINUE                                                                2496C062
00134    31.          DO 505 K=1,5                                                            2496C064
00137    32.          BLF(K2,K)=TAB2(XBLF(1,K2),YBLF(1,K2),5,1,A(K+60),12,.1E)                2496C066
00140    33.    505   CONTINUE                                                                2496C068
00140    34.    C                                                                             2496C070
00140    35.    C     A ACT HUB                                                               2496C072
00142    36.    510   CONTINUE                                                                2496C074
00143    37.          DO 1 K=1,5                                                              2496C076
00146    38.          A(K)=A(K+255)/BLF(K2,K)                                                 2496C078
00147    39.       1  CONTINUE                                                                2496C080
00147    40.    C                                                                             2496C082
00147    41.    C     R T                                                                     2496C084
00151    42.          A(6)=SQRT(A(1)/A(201)+V(3)**2)                                          2496C086
00152    43.          A(7)=SQRT(A(2)/A(201)+A(6)**2)                                          2496C088
00153    44.          A(8)=SQRT(A(3)/A(201)+A(7)**2)                                          2496C090
00154    45.          A(9)=SQRT(A(4)/A(201)+A(8)**2)                                          2496C092
00155    46.          A(10)=SQRT(A(5)/A(201)+A(9)**2)                                         2496C094
00155    47.    C                                                                             2496C096
00155    48.    C     R 3                                                                     2496C098
00156    49.          A(11)=SQRT((V(1)**2+A(6)**2)/2.0)                                       2496C100
```

```
00157   50.          A(12)=SQRT((A(8)**2+A(7)**2)/2.0)                                  2496C102
00160   51.          A(13)=SQRT((A(7)**2+A(8)**2)/2.0)                                  2496C104
00161   52.          A(14)=SQRT((A(8)**2+A(9)**2)/2.0)                                  2496C106
00162   53.          A(15)=SQRT((A(9)**2+A(10)**2)/2.0)                                 2496C108
00162   54.                                                                             2496C110
00165   55.      C   U 3                                                                2496C112
00163   56.      C   A(202)=3.1e159*C(26)/360.                                          2496C114
00167   57.          DO 2 K=16,20                                                       2496C116
00170   58.          A(K)=A(202)*A(K-5)                                                 2496C118
00170   59.          CONTINUE                                                           2496C120
00170   60.      2   CONTINUE                                                           2496C122
00170   61.      C   W 3                                                                2496C124
00172   62.          DO 13 K=61,65                                                      2496C126
00175   63.          A(K)=(A(K-50)-V(1))/COS(V(6)*.017453293)/12.0                      2496C128
00176   64.     13   CONTINUE                                                           2496C130
00176   65.      C                                                                      2496C132
00176   66.      C   M T 3                                                              2496C134
00200   67.          DO 3 K=81,85                                                       2496C136
00203   68.          A(K)=TABLE(1,C(K-5))                                               2496C138
00204   69.          A(K)=A(203)*(A(K-5)/223.37)**2*(1.0-(C(K-20)/A(K-10))**2)          2496C140
00205   70.      3   CONTINUE                                                           2496C142
00205   71.      C                                                                      2496C144
00205   72.      C   T T 3  AND  P R 3                                                 2496C146
00207   73.          DO 4 K=26,30                                                       2496C148
00212   74.          A(K)=TABLE(1,A(K-5))                                               2496C150
00213   75.          A(K+5)=TABLE(2,A(K))                                               2496C152
00214   76.      4   CONTINUE                                                           2496C154
00214   77.      C                                                                      2496C156
00214   78.      C   P T 3                                                             2496C158
00216   79.          DO 5 K=36,40                                                       2496C160
00221   80.          A(K)=E(K-35)*(V(2)-A(K-5))/TABLE(2,C(K-20))                        2496C162
00221   81.      5   CONTINUE                                                           2496C164
00222   82.      C                                                                      2496C166
00222   83.      C   Z                                                                  2496C168
00224   84.          DO 6 K=41,45                                                       2496C170
00227   85.          A(K)=V(6)-(A(K-30)-V(1))*TAN(V(6)*.017453293)                      2496C172
00230   86.      6   CONTINUE                                                           2496C174
00230   87.      C                                                                      2496C176
00230   88.      C   SLIP DETERMINATION                                               2496C178
00230   89.      C   V(9)=1 BEFORE SLIP   =2 AT SLIP   =3 AFTER SLIP                   2496C180
00232   90.          SLIPEV(8)                                                          2496C182
00232   91.      C                                                                      2496C184
00233   92.    100   CONTINUE                                                           2496C186
00233   93.      C                                                                      2496C188
00233   94.      C   BUILD GA/02 TABLES                                                2496C190
00234   95.          JPIFIX(C(19))=900                                                  2496C192
00236   96.          IF(K2.GT.2)  GO TO 501                                             2496C194
00237   97.          DO 7 K=81,J,900.81                                                 2496C196
00241   98.          A(K)=XLOC(K+900.81)                                                2496C198
00243   99.          A(K+90)=TANTABLE(12,A(K))*RAD)/RADIUS(K+900.81)/                   2496C200
00243  100.         *COS(GAMMA(K+900))                                                  2496C202
00246  101.      7   CONTINUE                                                           2496C204
00246  102.      C                                                                      2496C206
00246  103.    501   CONTINUE                                                           2496C208
00246  104.      C   D ALPHA/02                                                       2496C210
00246  105.      C                                                                      2496C212
00247  106.          DO 8 K=84,90                                                       2496C214
00252  107.          A(K)=TABLE(1901),A(K51),J=900,3,A(K-3),IE)                         2496C216
```

```
      GO TO (8,103,103),IE                                              2496C220
103   CONTINUE                                                          2496C222
      WRITE(6,1001)K2                                                   2496C224
      WRITE(6,1004)(A(I0),I0=1,800)                                     2496C226
      RETURN                                                            2496C228
      CONTINUE                                                          2496C230
C                                                                       2496C232
C     TAN BETA                                                          2496C234
      DO 9 K=50,59                                                      2496C236
      A(K)=A(K-9)*A(K-8)                                                2496C238
9     CONTINUE                                                          2496C240
C                                                                       2496C242
C     ALPHA 3                                                           2496C244
      DO 10 K=50,68                                                     2496C246
      A(K)=ATAN(A(K-5)*COS(V(6)*.01745329))/.01745329                   2496C248
      B(K-95)=A(K)                                                      2496C250
10    CONTINUE                                                          2496C252
      GO TO (104,101,102),SLIP                                          2496C254
C                                                                       2496C256
C     AT SLIP                                                           2496C258
C     ALPHA 3                                                           2496C260
101   CONTINUE                                                          2496C262
      DO 11 K=50,60                                                     2496C264
      A(K)=0.                                                           2496C266
11    CONTINUE                                                          2496C268
      GO TO 104                                                         2496C270
C                                                                       2496C272
C     AFTER SLIP                                                        2496C274
C     ALPHA 3                                                           2496C276
102   CONTINUE                                                          2496C278
      IF(IPIK(V(10)),EQ.K2)  GO TO 4002                                 2496C280
      DO 12 K=50,60                                                     2496C282
      A(K)=TABLE1(B(K2),VAL,8,8,A(K+9),12,.1E)                          2496C284
12    CONTINUE                                                          2496C286
      GO TO 104                                                         2496C288
4002  CONTINUE                                                          2496C290
      DO 4003 K=50,60                                                   2496C292
      A(K)=TABLE1(3:A(K+9),1200./XRC(3),F.2))                           2496C294
4003  CONTINUE                                                          2496C296
104   CONTINUE                                                          2496C298
C                                                                       2496C300
C     A/A                                                               2496C302
      DO 14 K=60,70                                                     2496C304
      A(K)=(C(27)*A(K-30)*A(K+50)*COS(A(K-50)*.01745329))/(C(K-65)*SQRT(2496C306
     1(1(K-60)))                                                        2496C308
14    CONTINUE                                                          2496C310
C                                                                       2496C312
      INDY=0                                                            2496C314
      DO 4010 K=60,70                                                   2496C316
      IF(A(K).LT.1.)GO TO 4010  INDY=1                                  2496C318
4010  CONTINUE                                                          2496C320
      IF(INDY.LT.1) GO TO 315                                           2496C322
      IF(VJST.GE.20) GO TO 3000                                         2496C324
      IF(VJST.EQ.11) ITIME=ITIME+1                                      2496C326
      AAGE=(A(66)*A(67)*A(68)*A(69)*A(70))/5.                           2496C328
      IF(AASG.LT.1.0)  GO TO 3000                                       2496C330
      GO TO 315                                                         2496C332
```



```
00518  225.      18  CONTINUE                                                  2496C450
00510  225.      C                                                             2496C452
00510  226.      C     V3                                                      2496C454
00512  227.            DO 19 K=101,105                                         2496C456
00515  228.            A(K)=A(K-30)+A(K-5)                                     2496C458
00516  229.      19    CONTINUE                                                2496C460
00516  230.      C                                                             2496C462
00516  231.      C     V*3                                                     2496C464
00520  232.            DO 20 K=106,110                                         2496C466
00523  233.            A(K)=A(K-5)*COS(A(K-50)*.0174533293)                    2496C468
00523  234.      20    CONTINUE                                                2496C470
00528  235.      C                                                             2496C472
00528  236.      C     VT3                                                     2496C474
00526  237.            DO 21 K=111,115                                         2496C476
00531  238.            A(K)=A(K-10)+SIN(A(K-55)*.0174533293)                   2496C478
00532  239.      21    CONTINUE                                                2496C480
00532  240.      C                                                             2496C482
00532  241.      C     VT*                                                     2496C484
00535  242.            DO 22 K=116,120                                         2496C486
00537  243.            A(K)=A(K-100)-A(K-5)                                    2496C488
00540  244.      22    CONTINUE                                                2496C490
00540  245.      C                                                             2496C492
00540  246.      C     ALPHA *                                                 2496C494
00542  247.            DO 23 K=121,125                                         2496C496
00545  248.            A(K)=ATAN2(A(K-5)*A(K-15))/.0174533293                  2496C498
00545  249.      23    CONTINUE                                                2496C500
00546  250.      C                                                             2496C502
00546  251.      C     V*                                                      2496C504
00550  252.            DO 24 K=126,130                                         2496C506
00553  253.            A(K)=A(K-20)/COS(A(K-5)*.0174533293)                    2496C508
00554  254.      24    CONTINUE                                                2496C510
00554  255.      C                                                             2496C512
00554  256.      C     V*                                                      2496C514
00556  257.            DO 25 K=131,133                                         2496C516
00561  258.            A(K)=A(K-5)/A(K-35)                                     2496C518
00562  259.      25    CONTINUE                                                2496C520
00562  260.      C                                                             2496C522
00562  261.      C                                                             2496C524
00562  262.      C     ASSUME K                                                2496C526
00564  263.            A(212)=1.0                                              2496C528
00565  264.            DO 26 K=136,140                                         2496C530
00570  265.      330   TT/TS                                                   2496C532
00570  266.      C     A(K)=1.0+(A(212)-1.0)/2.0*A(K-5)**2                     2496C534
00573  267.      C     PT*PS                                                   2496C536
00573  268.      C     A(K+5)=A(K)**(A(212)/(A(212)-1.0))                      2496C538
00574  269.      C     A/A*                                                    2496C540
00574  270.            A(K+10)=(1.0/A(K-5))*((2.0/(A(212)+1.0))*A(K))**((A(212)+1.0)/(2.0*(A(212)-1.0)))*(A(212)+1.0)  2496C542
00575  271.           1*(A(212)-1.0))                                          2496C544
00575  272.      26   CONTINUE                                                2496C546
00576  273.                                                                   2496C548
00576  274.      C                                                            2496C550
00576  275.      C     PT*                                                     2496C552
00600  276.            DO 27 K=151,155                                         2496C554
00603  277.            A(K)=A(K-65)*A(K-10)                                    2496C556
00604  278.            A(K+5)=A(K-60)*A(K-15)                                  2496C558
00605  279.      27    CONTINUE                                                2496C560
00607  280.            A(212)=TABLE(3,A(198))                                  2496C562
00610  281.      28    CONTINUE                                                2496C564
```

```
00610  282.      C
00610  283.      C        ETA  PRN                                                                  24966564
00612  284.               DO 29 K=161,165                                                          24966568
00615  285.                 S(K)=TABLE(1,A(K-5))                                                   24966570
00616  286.                 A(K+5)=TABLE(2,A(K-5))                                                 24966572
00617  287.           29  CONTINUE                                                                 24966574
00617  288.      C                                                                                 24966576
00617  289.      C                                                                                 24966578
00617  290.      C        DELTA VT                                                                 24966580
00617  291.      C                                                                                 24966582
00621  292.               DO 30 K=171, 175                                                         24966584
00624  293.                 A(K) = C(K-160)-A(K-60)                                                24966586
00625  294.           30  CONTINUE                                                                 24966588
00625  295.      C                                                                                 24966590
00625  296.      C        FN                                                                       24966592
00627  297.               DO 32 K=176, 180                                                         24966594
00632  298.                 A(K) = A(K-75)*SIN(X(K-175)*RAD)*TAN(V(4)*RAD)*.5IN(V(4)*RAD)*       24966596
00632  299.                1((2.*A(213)-12.*A(K-75)*SIN(X(K-175)*RAD)/A(K-165)) +                24966598
00632  300.                2A(K-5)/V(7)/SIN(V(4)*RAD))                                           24966600
00633  301.           32  CONTINUE                                                                 24966602
00633  302.      C                                                                                 24966604
00633  303.      C        RADIUS OF CURVATURE                                                      24966606
00633  304.               DO 33 K=181, 185                                                         24966608
00635  305.                 A(K)=((YRC(3,K2)-YRC(1,K2))/(XRC(3,K2)-XRC(1,K2))*(A(K-120)*12.      24966610
00640  306.                *-XRC(1,K2))+YRC(1,K2))/12.                                           24966612
00641  307.           33  CONTINUE                                                                 24966614
00641  308.      C                                                                                 24966616
00641  309.      C        RHO S                                                                    24966618
00641  310.               DO 34 K=186, 190                                                         24966620
00643  311.                 A(K) = A(K-100)/(32.2*53.342*A(K-95))                                  24966622
00646  312.           34  CONTINUE                                                                 24966624
00647  313.                                                                                        24966626
00647  314.      C        DP/DN                                                                    24966628
00647  315.               DO 35 K=191, 195                                                         24966630
00651  316.                 A(K) = A(K-5)*(A(K-75)**2*P05(V(4)*.0174533293)*12.0/A(K-180)*A(K-82496.634
00654  317.                15)**2/A(K-10)-A(K-15))                                               24966636
00654  318.           35  CONTINUE                                                                 24966638
00655  319.      C                                                                                 24966640
00655  320.      C        P S 3 PRIME                                                              24966642
00657  321.               A(198) = A(88)                                                           24966644
00660  322.               A(197) = A(88)-(A(63)-A(62))*(A(193)+A(192))/2.0                         24966646
00661  323.               A(196) = A(197)-(A(62)-A(61))*(A(192)+A(191))/2.0                        24966648
00662  324.               A(199) = A(80)+(A(64)-A(63))*(A(193)+A(194))/2.0                         24966650
00663  325.               A(200) = A(199)+(A(65)-A(64))*(A(195)+A(194))/2.0                        24966652
00663  326.      C                                                                                 24966654
00664  327.               DO 39 K=196, 200                                                         24966656
00667  328.                 IF(ABS(A(K)-A(K-110))/A(K-110)-.002)39,39,121                          24966658
00672  329.           39  CONTINUE                                                                 24966660
00672  330.      C                                                                                 24966662
00672  331.      C                                                                                 24966664
00674  332.               GO TO 120                                                                24966666
00674  333.      C                                                                                 24966668
00675  334.          121  CONTINUE                                                                 24966670
00676  335.                 A(220)=A(220)+1.0                                                      24966672
00677  336.                 IF(A(220)-20.0) 128,128,129                                            24966674
00702  337.          129  CONTINUE                                                                 24966676
00703  338.               WRITE(6,1008)K2                                                          24966678
00706  339.               WRITE(6,1004)(A(IQ),IQ=1,500)                                            24966680
```

```
00714  340.          ITIME=-1                                                  2496C682
00715  341.          GO TO 120                                                 2496C684
00716  342.      128 CONTINUE                                                  2496C686
00716  343.      C                                                             2496C688
00716  344.      C     PT3/PS3 PRIME                                           2496C690
00717  345.            JJGO=0                                                  2496C692
00720  346.      125 CONTINUE                                                  2496C694
00721  347.          JJGO=JJGO+1                                               2496C696
00722  348.          IF(JJGO.EQ.300160 TO 1000                                 2496C698
00724  349.          DO 36 K=226, 230                                          2496C700
00727  350.          A(K) = A(K-190)/A(K-30)                                   2496C702
00730  351.          IF (A(K)-1.) 357, 357, 36                                 2496C704
00733  352.      357 DO 359 J=196, 200                                         2496C706
00736  353.          A(J) = A(J) -.5                                           2496C708
00737  354.      359 CONTINUE                                                  2496C710
00741  355.          GO TO 125                                                 2496C712
00742  356.       36 CONTINUE                                                  2496C714
00742  357.      C                                                             2496C716
00744  358.          DO 37 K=231, 235                                          2496C718
00744  359.      C     P PRIME                                                 2496C720
00747  360.      C     A(K+10)= SQRT((A(K-5)**(A(212)-1.0)/A(212))**2-2.6)/(A(212)-1.0))  2496C722
00747  361.      C     A/ASTAR PRIME                                           2496C724
00750  362.            A(K) = (1.0/A(K+10 ))**(2.0/(A(212)+1.0)*(1.0*(A(212)-1.0)*2.0*  2496C726
00750  363.           1A(K+10 )**2))**((A(212)+1.0)/2.0/(A(212)-1.0))           2496C728
00750  364.       37 CONTINUE                                                  2496C730
00751  365.      C                                                             2496C732
00751  366.      C     A ANN PRIME                                             2496C734
00753  367.            DO 38 K=236, 240                                        2496C736
00756  368.            A(K) = A(K-5)/A(K-170)*A(K+20)                          2496C738
00757  369.       38   CONTINUE                                                2496C740
00761  370.            A(218) = A(236)+A(237)+A(238)+A(239)+A(240)             2496C742
00761  371.      C                                                             2496C744
00761  372.      C     ANNULUS AREA COMPARISON                                 2496C746
00762  373.            IF(ABS(A(218)-A(219))/A(219)-.003)122,122,123           2496C748
00765  374.      123   CONTINUE                                                2496C750
00766  375.            CONST =   -.020*A(198)*(A(218)-A(219))/A(219)           2496C752
00767  376.            DO 41 K=196, 200                                        2496C754
00772  377.            A(K)=A(K)+CONST                                         2496C756
00773  378.       41   CONTINUE                                                2496C758
00775  379.            GO TO 125                                               2496C760
00775  380.      C                                                             2496C762
00776  381.      122 DO 43 K=1, 5                                              2496C764
01001  382.          A(K+235) = A(K+235)*A(219)/A(218)                         2496C766
01002  383.       43 CONTINUE                                                  2496C768
01002  384.      C                                                             2496C770
01004  385.          DO 46 K=261, 265                                          2496C772
01007  386.          A(K) = A(K-65)                                            2496C774
01010  387.       46 CONTINUE                                                  2496C776
01012  388.          GO TO 127                                                 2496C778
01012  389.      C                                                             2496C780
01013  390.      120 CONTINUE                                                  2496C782
01014  391.          IF(IFIX(A(220)).EQ.ITIME) GO TO 125                       2496C784
01014  392.      C     ACCELERATION=A N.TOT                                    2496C786
01016  393.            DO 131 K=316,320                                        2496C788
01021  394.            A(K)=12.*A(K-200)**2*COS(V(K)*RAD)/A(K-305)-A(K-210)**2/A(K-135)  2496C790
01022  395.       131  CONTINUE                                                2496C792
01022  396.      C                                                             2496C794
01024  397.      200   RETURN                                                  2496C796
```

```
01025  398.  1000  CONTINUE                                                  2496C7F8
01026  399.        WRITE(6,1005)K2                                           2496C800
01031  400.        WRITE(6,1004)(A(IQ),IQ=1,500)                             2496C802
01037  401.        GO TO 120                                                 2496L804
01040  402.  3000  CONTINUE                                                  2496C806
01041  403.        KO=K-70                                                   2496C808
01042  404.        WRITE(6,1002)KO,K2                                        2496C810
01046  405.        WRITE(6,1004)(A(IQ),IQ=1,500)                             2496C812
01054  406.        RETURN                                                    2496C814
01054  407.     C                                                            2496C816
01055  408.  1001  FORMAT(1HO,*8HTHE TABLE LOOKUP ON DA/DZ HAS FAILED FOR STATION,I312496C818
01056  409.  1002  FORMAT(1HO,13HAT STREAMLINE,I3,9H, STATION,I3,29H, A/A STAR FAILED2496C820
01056  410.       * TO CONVERGE)                                             2496C822
01057  411.  1003  FORMAT(1HO,31HK FAILED TO CONVERGE AT STATION,I3)         2496C824
01060  412.  1004  FORMAT(15H THE A ARRAY IS/(6X,10F11.*))                   2496C826
01061  413.  1005  FORMAT(72HoPS3 PRIME ADJUSTMENT OF A ANN PRIME TOTAL FAILED TO CON2496C828
01061  414.       *VERGE AT STATION    ,I3)                                 2496C830
01062  415.  1008  FORMAT(1HO,10HAT STATION,I3,29H PS3 PRIME FAILED TO CONVERGE)  2496C832
01063  416.        END                                                       2496C834

   END OF LISTING,     0 *DIAGNOSTIC* MESSAGE(S),          10 AUG 66  00:13:31    1  00053674   36    1  (DELETED)
      I*PEL   CODE    RELOCATABLE                                          0  00053740   14  139
```

```
@    FOR CHORD                                                    24690002
COMPILATION BY UNIVAC 1108 FORTRAN-IV DATED     NOV. 23,1965 F4008
THIS COMPILATION WAS DONE ON 19 AUG 66 AT 17:37:17


    SUBROUTINE CHORD      ENTRY POINT 000731

    STORAGE USED (BLOCK, NAME, LENGTH)

        0001   *CODE   001073
        0000   *DATA   000165
        0002   *BLANK  000000


    EXTERNAL REFERENCES (BLOCK, NAME)

        0003   TAB2
        0004   SQRT
        0005   ATAN
        0006   TAN
        0007   NWDU$
        0010   NIO1$
        0011   NIO2$


    STORAGE ASSIGNMENT FOR VARIABLES (BLOCK, TYPE, RELATIVE LOCATION, NAME)

    0000   000047 1000F     0000   000110 1001F     0001   000160 15L     0001   000621 2000L     0001   000272 25L
    0001   000332 35L       0001   000334 40L       0001   000372 45L     0001   000403 50L       0001   000434 55L
    0001   000571 60L       0001   000611 65L       0001   000632 66L     0001   000667 67L       0000 R 000033 ANGC
    0000 R 000035 ANGG      0000 R 000036 ANGX      0005 R 000000 ATAN     0000 R 000032 CTAN      0001 R 000000 DYDX
    0000 R 000034 GTAN      0000 R 000005 GUESSX    0000 R 000010 GUESSY   0000 R 000020 HSLOPE    0000 I 000011 IA
    0000 I 000015 IB        0000 I 000017 IC        0000 I 000024 ID       0000 I 000026 IE        0000 I 000031 IG
    0000 I 000043 IH        0000 I 000044 II        0000 I 000045 IJ       0000 I 000046 IK        0000 I 000006 INDX
    0000 I 000007 JNDX      0000 R 000000 RDN       0004 R 000000 SQRT     0003 R 000000 TAB2      0006 R 000000 TAN
    0000 R 000027 TSLOPE    0000 R 000012 XMH       0000 R 000021 XMT      0000 R 000040 XO        0000 R 000013 XPH
    0000 R 000022 XPT       0000 R 000037 XSLOPE    0000 R 000001 X1       0000 R 000003 X2        0000 R 000030 YHUB
    0000 R 000014 YMH       0000 R 000023 YMT       0000 R 000041 YO       0000 R 000016 YPH       0000 R 000042 YPP
    0000 R 000025 YPT       0000 R 000002 Y1        0000 R 000004 Y2


00100    1.   C    HX(I)     INDEPENDENT VARIABLE - HUB ARRAY                    -24690004
00100    2.   C    HY(I)     DEPENDENT VARIABLE - HUB ARRAY                      -24690006
00100    3.   C    TX(I)     INDEPENDENT VARIABLE - TIP ARRAY                    -24690008
00100    4.   C    TY(I)     DEPENDENT VARIABLE - TIP ARRAY                      -24690010
00100    5.   C    XMH       CURRENT HUB X-VALUE MINUS INCREMENT                 -24690012
00100    6.   C    XPH       CURRENT HUB X-VALUE PLUS INCREMENT                  -24690014
00100    7.   C    YMH       CURRENT HUB Y-VALUE MINUS INCREMENT                 -24690016
00100    8.   C    YPH       CURRENT HUB Y-VALUE PLUS INCREMENT                  -24690018
00100    9.   C    NH        NUMBER OF INDEPENDENT VARIABLES IN HUB ARRAY        -24690020
00100   10.   C    NT        NUMBER OF INDEPENDENT VARIABLES IN TIP ARRAY        -24690022
00100   11.   C    XMT       CURRENT TIP X-VALUE MINUS INCREMENT                 -24690024
00100   12.   C    XPT       CURRENT TIP X-VALUE PLUS  INCREMENT                 -24690026
00100   13.   C    YMT       CURRENT TIP Y-VALUE MINUS INCREMENT                 -24690028
```

CONFIDENTIAL

```
00100   14.   C     YPT          CURRENT TIP Y-VALUE PLUS INCREMENT                -2469D030
00100   15.   C     GUESS        AN ESTIMATE OF THE X-TIP VALUE CORRESPONDING TO THE -2469D032
00100   16.   C                  FIRST TABLE VALUE FOR X-HUB                       -2469D034
00100   17.   C     CTAN         TANGENT OF ANGLE OF DESIRED LINE COMPUTED BY FORMULA-2469D036
00100   18.   C     TSLOPE       SLOPE OF TANGENT LINE AT A POINT ON TIP PROFILE   -2469D038
00100   19.   C     HSLOPE       SLOPE OF TANGENT LINE AT A POINT ON HUB PROFILE   -2469D040
00100   20.   C     GTAN         TANGENT OF ANGLE OF DESIRED LINE FROM POINTS      -2469D042
00100   21.   C     ANGC         ARCTANGENT(CTAN)                                  -2469D044
00100   22.   C     ANGG         ARCTANGENT(GTAN)                                  -2469D046
00101   23.         SUBROUTINE CHORD(XHUB,GUESS,HX,HY,TX,TY,NH,NT,K,XTIP,YTIP,ANGANS) 2469D048
00103   24.         DIMENSION HX(1),HY(1),TX(1),TY(1)                               2469D050
00104   25.         DATA RDN/57.29578/                                              2469D052
00106   26.         DYDX(X1,Y1,X2,Y2)=(Y2-Y1)/(X2-X1)                               2469D054
00107   27.         GUESSX=GUESS                                                    2469D056
00110   28.         INDX=0                                                          2469D058
00111   29.         JNDX=0                                                          2469D060
00112   30.         GUESSY=TAB2(TX(1),TY(1),NT,K,GUESS,IA)                          2469D062
00113   31.         XMH=XHUB-0.05                                                   2469D064
00114   32.         XPH=XHUB+0.05                                                   2469D066
00115   33.         YMH=TAB2(HX(1),HY(1),NH,K,XMH,IB)                               2469D068
00116   34.         YPH=TAB2(HX(1),HY(1),NH,K,XPH,IC)                               2469D070
00117   35.         HSLOPE=DYDX(XMH,YMH,XPH,YPH)                                    2469D072
00120   36.         IF(ABS(YMH-YPH).LT.1.0E-04)HSLOPE=0.0                           2469D074
00122   37.         XMT=GUESS-0.05                                                  2469D076
00123   38.         XPT=GUESS+0.05                                                  2469D078
00124   39.         YMT=TAB2(TX(1),TY(1),NT,K,XMT,ID)                               2469D080
00125   40.         YPT=TAB2(TX(1),TY(1),NT,K,XPT,IE)                               2469D082
00126   41.         TSLOPE=DYDX(XMT,YMT,XPT,YPT)                                    2469D084
00127   42.         IF(ABS(YMT-YPT).LT.1.0E-04)TSLOPE=0.0                           2469D086
00131   43.         YHUB=TAB2(HX(1),HY(1),NH,K,XHUB,IG)                             2469D088
00132   44.      15 IF(ABS(TSLOPE)+ABS(HSLOPE).LT.0.001)GO TO 35                    2469D090
00134 *DIAGNOSTIC* THE TEST FOR EQUALITY BETWEEN NON-INTEGERS MAY NOT BE MEANINGFUL.
00134   45.         IF(HSLOPE.GE.0.0.AND.TSLOPE.GE.0.0.OR.HSLOPE.LE.0.0.AND.TSLOPE.LE. 2469D092
00134   46.        -0.0)GO TO 25                                                   2469D094
00136   47.         IF(ABS(HSLOPE).GT.ABS(TSLOPE))GO TO 25                          2469D096
00140   48.      30 CTAN=(SQRT((1.0+HSLOPE**2)*(1.0+TSLOPE**2))-1.0+HSLOPE*TSLOPE)/(HS2469D098
00140   49.        -LOPE+TSLOPE)                                                   2469D100
00141   50.         ANGC=ATAN(CTAN)*RDN                                             2469D102
00142   51.         IF(CTAN.LT.0.0)ANGC=ANGC+180.0                                  2469D104
00144   52.         GO TO 40                                                        2469D106
00145   53.      25 CTAN=-(SQRT((1.0+HSLOPE**2)*(1.0+TSLOPE**2))+1.0-HSLOPE*TSLOPE)/(H2469D108
00145   54.        -SLOPE+TSLOPE)                                                  2469D110
00146   55.         ANGC=ATAN(CTAN)*RDN                                             2469D112
00147   56.         IF(CTAN.LT.0.0)ANGC=ANGC+180.0                                  2469D114
00151   57.         GO TO 40                                                        2469D116
00152   58.      35 ANGC=90.0                                                       2469D118
00153   59.      40 IF(ABS(XHUB-GUESS).LT.0.001)GO TO 45                            2469D120
00155   60.         GTAN=DYDX(XHUB,YHUB,GUESS,GUESSY)                               2469D122
00156   61.         ANGG=ATAN(GTAN)*RDN                                             2469D124
00157   62.         IF(GTAN.LT.0.0)ANGG=ANGG+180.0                                  2469D126
00161   63.         GO TO 50                                                        2469D128
00162   64.      45 IF(ABS(ANGC-90.0).LT.1.0E-2)GO TO 60                            2469D130
00164   65.         ANGG=90.0                                                       2469D132
00165   66.      50 IF(ABS(ANGG-ANGC).LT.1.0E-1)GO TO 65                            2469D134
00167   67.         INDX=INDX+1                                                     2469D136
00170   68.         IF(INDX.GT.100)GO TO 66                                         2469D138
00172   69.         ANGX=0.5*(ANGC+ANGG)                                            2469D140
00173   70.         XSLOPE=TAN(ANGX/RDN)                                            2469D142
```

CONFIDENTIAL

```
00174   71.      55 XO=(XSLOPE*XHUB-TSLOPE*GUESS-YHUB+GUESSY)/(XSLOPE-TSLOPE)      24690144
00175   72.         YO=(XSLOPE*GUESSY-TSLOPE*YHUB+XSLOPE*TSLOPE*(XHUB-GUESS))/     24690146
00175   73.        -(XSLOPE-TSLOPE)                                                 24690148
00176   74.         YPP=TAB2(TX(1),TY(1),NT,K,XO,IH)                                24690150
00177   75.         JNDX=JNDX+1                                                     24690152
00200   76.         IF(JNDX.GT.25)GO TO 67                                          24690154
00202   77.         GUESS=XO                                                        24690156
00203   78.         GUESSY=YPP                                                      24690158
00204   79.         XMT=GUESS+0.05                                                  24690160
00205   80.         XPT=GUESS+0.05                                                  24690162
00206   81.         YMT=TAB2(TX(1),TY(1),NT,K,XMT,II)                               24690164
00207   82.         YPT=TAB2(TX(1),TY(1),NT,K,XPT,IJ)                               24690166
00210   83.         TSLOPE=DYDX(XMT,YMT,XPT,YPT)                                    24690168
00211   84.         IF(ABS(YMT-YPT).LT.1.0E-04)TSLOPE=0.0                           24690170
00213   85.         IF(ABS(YO-YPP).LT.0.001)GO TO 15                                24690172
00215   86.         GO TO 55                                                        24690174
00216   87.      60 XTIP=XHUB                                                       24690176
00217   88.         YTIP=TAB2(TX(1),TY(1),NT,K,XTIP,IK)                             24690178
00220   89.         ANGANS=ANGC                                                     24690180
00221   90.         GUESS =GUESSX                                                   24690182
00222   91.         RETURN                                                          24690184
00223   92.      65 CONTINUE                                                        24690186
00224   93.         IF(INDX.GT.0)  GO TO 2000                                       24690188
00226   94.         XO=GUESS                                                        24690190
00227   95.         YPP=GUESSY                                                      24690192
00230   96.   2000  CONTINUE                                                       24690194
00231   97.         XTIP=XO                                                         24690196
00232   98.         YTIP=YPP                                                        24690198
00233   99.         ANGANS=ANGC                                                     24690200
00234  100.         GUESS =GUESSX                                                   24690202
00235  101.         RETURN                                                          24690204
00236  102.      66 CONTINUE                                                        24690206
00237  103.         XTIP=XO                                                         24690208
00240  104.         YTIP=YPP                                                        24690210
00241  105.         ANGANS=ANGC                                                     24690212
00242  106.         GUESS =GUESSX                                                   24690214
00243  107.         WRITE (6,1000) XHUB,YHUB,HSLOPE,XTIP,YTIP,TSLOPE,ANGG,ANGC      24690216
00255  108.   1000 FORMAT(1H1, 85HTHE NUMBER OF ITERATIONS ON SLOPES HAS EXCEEDED 10024690218
00255  109.        -AND THE ITERATION IS DISCONTINUED      //1X, 81H      XHUB      YHUB 24690220
00255  110.        -  HSLOPE     XTIP     YTIP     TSLOPE     ANGG     ANGC    //    24690222
00255  111.         -(1X,10G10.4))                                                  24690224
00256  112.         RETURN                                                          24690226
00257  113.      67 CONTINUE                                                        24690228
00260  114.         XTIP=XO                                                         24690230
00261  115.         YTIP=YPP                                                        24690232
00262  116.         ANGANS=ANGC                                                     24690234
00263  117.         GUESS =GUESSX                                                   24690236
00264  118.         WRITE (6,1001) XO,YO,YPP,XHUB,YHUB,HSLOPE,XTIP,YTIP,TSLOPE      24690238
00277  119.   1001 FORMAT(1H1,47HAFTER 25 ITERATIONS CANNOT CONVERGE ON MIDSLOPE//1X,24690240
00277  120.        -90H  X-GUESS   Y-GUESS     Y-PP       X-HUB      Y-HUB     HSLOPE 24690242
00277  121.        -XTIP     Y-TIP    TSLOPE    //(1X,10G10.4))                     24690244
00300  122.         RETURN                                                          24690246
00301  123.         END                                                             24690248

      END OF LISTING,     1 *DIAGNOSTIC* MESSAGE(S).
```

```
0     FOR RCS                                                                    2469D250
COMPILATION BY UNIVAC 1108 FOR: AN-IV DATED     NOV. 23,1965 F4008
THIS COMPILATION WAS DONE ON 19 AUG 66 AT 17:37:20

    SUBROUTINE RCS        ENTRY POINT 000165

    STORAGE USED (BLOCK, NAME, LENGTH)

        C001   *CODE   000251
        0000   *DATA   000027
        0002   *BLANK  000000
        0003   RC      00017U

    EXTERNAL REFERENCES (BLOCK, NAME)

        0004   COS
        0005   SQRT
        0006   TAN
        0007   TABLE

    STORAGE ASSIGNMENT FOR VARIABLES (BLOCK, TYPE, RELATIVE LOCATION, NAME)

     0001   000043 116G      0001   000122 134G      0000 R 000001 A       0000 R 000002 AJ      0004 R 000020 COS
     0000 R 000006 COSG      0000 I 000004 J         0000 R 000000 PI      0000 R 000003 RHUB    0000 R 000005 RTIP
     0005 R 000000 SQRT      0007 R 000000 TABLE     0006 R 000000 TAN     0003 R 000000 XRC     0003 R 000074 YRC

00101     1.          SUBROUTINE RCS(K2,XLOC,RADIUS,GAMMA,DX,AREA,XND,BLF)          2469D252
00101     2.    C                                                                   2469D254
00101     3.    C     RCS COMPUTES STREAMTUBES OF EQUAL AREA ALONG A NORMAL         2469D256
00101     4.    C     AND RC=F(N)                                                   2469D258
00101     5.    C                                                                   2469D260
00103     6.          COMMON/RC/XRC(3,20),YRC(3,20)                                 2469D262
00104     7.          DIMENSION XLOC(20,7),RADIUS(20,7),GAMMA(20),AREA(20,7),XND(20,7)  2469D264
00105     8.          DIMENSION BLF(20,7)                                           2469D266
00105     9.    C                                                                   2469D268
00106    10.          DATA PI/3.14159/                                              2469D270
00106    11.    C     AREAS AND RADII                                               2469D272
00110    12.          A=(RADIUS(K2,7)**2-RADIUS(K2,1)**2)                           2469D274
00111    13.          AREA(K2,6)=PI*A/COS(GAMMA(K2))                                2469D276
00112    14.          AJ=AREA(K2,6)/5.                                              2469D278
00113    15.          A=A/5.                                                        2469D280
00114    16.          RHUB=RADIUS(K2,1)                                             2469D282
00115    17.          DO 100 J=1,5                                                  2469D284
00120    18.          AREA(K2,J)=AJ                                                 2469D286
00121    19.          RTIP=SQRT(A+RHUB**2)                                          2469D288
00122    20.          RADIUS(K2,J+1)=SQRT((RHUB**2+RTIP**2)/2.)                     2469D290
00123    21.          BLF(K2,J)=(RHUB+RTIP)/2.                                      2469D292
00124    22.          RHUB=RTIP                                                     2469D294
00125    23.          XLOC(K2,J+1)=XLOC(K2,7)+TAN(GAMMA(K2))*(RADIUS(K2,7)-RADIUS(K2,J+1  2469D296
00125    24.         1))                                                            2469D298
```


CONFIDENTIAL

CONFIDENTIAL

```
00126    25.   100   CONTINUE                                                    2469D300
00126    26.   C                                                                2469D302
00126    27.   C     RADII OF CURVATURE                                         2469D304
00130    28.         XRC(1,K2)=0.                                               2469D306
00131    29.         COSG=COS(GAMMA(K2))                                        2469D308
00132    30.         XND(K2,1)=0.                                               2469D310
00133    31.         DO 140 J=2,7                                               2469D312
00136    32.   140   XND(K2,J)=(RADIUS(K2,J)-RADIUS(K2,1))/COSG                 2469D314
00140    33.         XRC(2,K2)=XND(K2,4)                                        2469D316
00141    34.         XRC(3,K2)=XND(K2,7)                                        2469D318
00142    35.   300   CONTINUE                                                   2469D320
00143    36.         YRC(1,K2)=TABLE(20,XLOC(K2,1))                             2469D322
00144    37.         YRC(3,K2)=TABLE(21,XLOC(K2,7))                             2469D324
00145    38.         YRC(2,K2)=XRC(2,K2)*(YRC(3,K2)-YRC(1,K2))/XRC(3,K2)+YRC(1,K2; 2469D326
00146    39.   500   RETURN                                                     2469D328
00147    40.         END                                                        2469D330

        END OF LISTING.      0 *DIAGNOSTIC* MESSAGE(S).
```


CONFIDENTIAL

```
0     FOR OUTPUT                                                    2569D332
COMPILATION BY UNIVAC 1108 FORTRAN-IV DATED     NOV. 23,1965 F4008
THIS COMPILATION WAS DONE ON 19 AUG 66 AT 17:37:22


    SUBROUTINE OUTPUT    ENTRY POINT 000757

    STORAGE USED (BLOCK, NAME, LENGTH)

        0001   *CODE   000776
        0000   *DATA   000517
        0002   *BLANK  000000
        0003   IMPELR  002335
        0004   BLOCK   010757


    EXTERNAL REFERENCES (BLOCK, NAME)

        0005   NWDU$
        0006   NIO1$
        0007   NIO2$
        0010   NERR2$


    STORAGE ASSIGNMENT FOR VARIABLES (BLOCK, TYPE, RELATIVE LOCATION, NAME)

0001  000122 1L     0000  000003 10F    0001  000036 111G   0000  000017 12F    0001  000356 120G
0001  000076 132G   0000  000022 14F    0001  000106 140G   0001  000130 150G   0000  000040 16F
0001  000147 162G   0001  000157 170G   0001  000167 176G   0000  000044 18F    0001  000134 2L
0000  000052 20F    0001  000203 206G   0001  000213 214G   0000  000060 22F    0001  000223 222G
0001  000237 232G   0000  000066 24F    0001  000251 240G   0001  000263 246G   0001  000301 256G
0000  000075 26F    0001  000313 264G   0000  000103 28F    0001  000343 3L     0000  000112 30F
0001  000356 305G   0001  000370 313G   0000  000121 32F    0001  000406 323G   0001  000420 331G
0001  000432 337G   0000  000126 34F    0001  000444 345G   0001  000462 355G   0000  000135 36F
0001  000474 363G   0001  000506 371G   0000  000145 38F    0001  000352 4L     0000  000153 40F
0001  000536 403G   0001  000550 411G   0001  000562 417G   0000  000157 42F    0001  000574 425G
0001  000606 433G   0000  000166 44F    0001  000620 441G   0001  000632 447G   0001  000644 455G
0000  000175 46F    0000  000204 48F    0001  000524 5L     0000  000207 50F    0000  000216 52F
0000  000225 54F    0000  000231 56F    0000  000240 58F    0000  000247 60F    0000  000256 62F
0000  000265 64F    0000  000272 66F    0000  000301 68F    0001  000650 7L     0000  000310 70F
0000  000317 72F    0000  000325 74F    0000  000332 76F    0000  000341 78F    0000  000350 80F
0000  000357 82F    0000  000364 84F    0000  000373 86F    0000  000402 88F    0000  000411 90F
0000  000427 91F    0000  000420 92F    0000  000436 94F    0000  000445 95F    0003  000000 A
0004 R 000000 ACCEL  0004 R 000214 ALPHA  0004  000430 AMASS  0004 R 000644 AREA   0004 R 001060 BETA
0003 R 000764 BLF    0003  001200 C      0004  001274 CF     0004  001275 DERIV1  0004  001511 DERIV2
0004  001725 DGR    0004 R 001726 DPDN   0003 R 001262 GAMMA  0004  002142 GC     0004  002143 GIVM
0004  002144 HGPSI  0004  002145 HJ     0000 I 000002 I     0000 I 000001 J     0000 I 000000 JGO
0004 I 002146 NS     0004 I 002147 NTITLE  0004 R 002173 PHI  0004  002217 PI     0004 R 002220 PSI
0004 R 002434 PS     0004 R 002650 PT     0003  001522 Q     0004  003064 R      0003 R 001356 RADIUS
0004 R 003065 RCURV  0004 R 003301 REC    0004  003515 RIN   0004  003516 RPM    0004 R 003517 TRI
0004 R 003733 TS     0004 R 004147 TT     0004  004363 TX     0004  004407 TY     0004 R 004433 U
0004 R 004647 V      0004 R 005063 VP     0004 R 005277 VPW   0004  005513 VR     0004 R 005727 VS
0004 R 006143 VSND   0004 R 006357 VSW    0003 R 000000 VTW   0004 R 006573 VU     0004 R 007007 VVSND
0004  007223 VX     0004 R 007437 W      0004 R 007653 WM    0004 R 010303 WU     0004 R 010067 WVSND
0003  001604 XBLF   0003 R 001750 XLOC   0004 R 010517 XMD   0004 R 010543 XND    0003  002164 YAL
0003  002171 YBLF
```

CONFIDENTIAL

```
00101    1.      SUBROUTINE OUTPUT                                                
```

```
00351   58.          WRITE(6,74)                                                                    2469D448
00353   59.          WRITE(6,76)(W(J,I),I=1,5)                                                      2469D450
00361   60.          WRITE(6,78)(WM(J,I),I=1,5)                                                     2469D452
00367   61.          WRITE(6,80)(WU(J,I),I=1,5)                                                     2469D454
00375   62.          GO TO (5,7),JGO                                                                2469D456
00376   63.    5     CONTINUE                                                                       2469D458
00377   64.          WRITE(6,82)                                                                    2469D460
00401   65.          WRITE(6,84)(VS(J,I),I=1,5)                                                     2469D462
00407   66.          WRITE(6,86)(VP(J,I),I=1,5)                                                     2469D464
00415   67.          WRITE(6,88)(VSW(J,I),I=1,5)                                                    2469D466
00423   68.          WRITE(6,90)(VPW(J,I),I=1,5)                                                    2469D468
00431   69.          WRITE(6,91)(VTW(J,I),I=1,5)                                                    2469D470
00437   70.          WRITE(6,92)(ACCCL(J,I),I=1,5)                                                  2469D472
00445   71.          WRITE(6,94)(REC(J,I),I=1,5)                                                    2469D474
00453   72.          WRITE(6,96)(DPDN(J,I),I=1,5)                                                   2469D476
00461   73.    7     CONTINUE                                                                       2469D478
00462   74.          JGO=1                                                                          2469D480
00463   75.    8     CONTINUE                                                                       2469D482
00465   76.          RETURN                                                                         2469D484
00466   77.    10    FORMAT(1H1,29X,56HIMPELLER RADIAL EQUILIBRIUM DESIGN RESULTS FOR S2469D486
00466   78.         *TATION    ,I2)                                                                2469D488
00467   79.    12    FORMAT(1H0,23X,18A5)                                                           2469D490
00470   80.    14    FORMAT(1H0,14X,10HSTREAMTUBE,8X,3HHUB,10X,1H1,11X,1H2,11X,1H3,11X,2469D492
00470   81.         *1H4,11X,1H5,10X,3HTIP)                                                         2469D494
00471   82.    16    FORMAT(18H DISTANCES(INCHES))                                                  2469D496
00472   83.    18    FORMAT( 6X,20HAXIAL----------      ,7F12.3)                                    2469D498
00473   84.    20    FORMAT( 6X,20HRADIAL---------      ,7F12.3)                                    2469D500
00474   85.    22    FORMAT( 6X,20HNORMAL---------      ,7F12.4)                                    2469D502
00475   86.    24    FORMAT( 6X,20HMERIDIONAL---------  ,36X,F12.3)                                2469D504
00476   87.    26    FORMAT( 6X,20HRADIUS OF CURVATURE- ,7F12.2)                                    2469D506
00477   88.    28    FORMAT(/6X,20HACTUAL AREA(SQ IN)-- ,12X,6F12.3)                                2469D508
00500   89.    30    FORMAT( 6X,20HBLOCKAGE FACTOR----- ,12X,6F12.3)                                2469D510
00501   90.    32    FORMAT(20H TEMPERATURES(DEG R))                                                2469D512
00502   91.    34    FORMAT( 6X,20HTOTAL----------      ,12X,6F12.1)                                2469D514
00503   92.    36    FORMAT( 6X,20HSTATIC---------      ,12X,6F12.1)                                2469D516
00504   93.    38    FORMAT( 6X,20HRELATIVE TOTAL-----  ,12X,6F12.1)                                2469D518
00505   94.    40    FORMAT(17H PRESSURES(IN HG))                                                   2469D520
00506   95.    42    FORMAT( 6X,20HTOTAL----------      ,12X,6F12.2)                                2469D522
00507   96.    44    FORMAT( 6X,20HSTATIC---------      ,12X,6F12.2)                                2469D524
00510   97.    46    FORMAT( 6X,20HRELATIVE TOTAL-----  ,12X,6F12.2)                                2469D526
00511   98.    48    FORMAT(13H MACH NUMBERS)                                                       2469D528
00512   99.    50    FORMAT( 6X,20HABSOLUTE---------    ,12X,6F12.3)                                2469D530
00513  100.    52    FORMAT( 6X,20HRELATIVE---------    ,12X,6F12.3)                                2469D532
00514  101.    54    FORMAT(16H ANGLES(DEGREES))                                                    2469D534
00515  102.    56    FORMAT( 6X,20HMERIDIONAL---------  ,36X,F12.2)                                2469D536
00516  103.    58    FORMAT( 6X,20HBLADE----------      ,36X,F12.2)                                 2469D538
00517  104.    60    FORMAT( 6X,20HABSOLUTE FLUID-----  ,12X,6F12.2)                                2469D540
00520  105.    62    FORMAT( 6X,20HRELATIVE FLUID-----  ,12X,6F12.2)                                2469D542
00521  106.    64    FORMAT(23H ABS VELOCITIES(FT/SEC))                                             2469D544
00522  107.    66    FORMAT( 6X,20HTOTAL----------      ,12X,6F12.1)                                2469D546
00523  108.    68    FORMAT( 6X,20HTANGENTIAL-------    ,12X,6F12.1)                                2469D548
00524  109.    70    FORMAT( 6X,20HSOUND----------      ,12X,6F12.1)                                2469D550
00525  110.    72    FORMAT( 6X,20HWHEEL----------      ,7F12.1)                                    2469D552
00526  111.    74    FORMAT(23H REL VELOCITIES(FT/SEC))                                             2469D554
00527  112.    76    FORMAT( 6X,20HTOTAL----------      ,12X,6F12.1)                                2469D556
00530  113.    78    FORMAT( 6X,20HMERIDIONAL---------  ,12X,6F12.1)                                2469D558
00531  114.    80    FORMAT( 6X,20HTANGENTIAL---------  ,12X,6F12.1)                                2469D560
00532  115.    82    FORMAT(20H SURFACE VEL(FT/SEC))                                                2469D562
```

```
00533   116.    84    FORMAT( 6X,20HSUCTION-----------    ,12X,6F12.1)          24690564
00534   117.    86    FORMAT( 6X,20HPRESSURE----------    ,12X,6F12.1)          24690566
00535   118.    88    FORMAT(/6X,20HSUCTION/V2 MEAN-----  ,12X,6F12.3)          24690568
00536   119.    90    FORMAT( 6X,20HPRESSURE/V2 MEAN----  ,12X,6F12.3)          24690570
00537   120.    92    FORMAT(/6X,20HACCEL(FT/SEC SQ)----  ,12X,6E12.4)          24690572
00540   121.    91    FORMAT( 6X,20HREL TOTAL/V2 MEAN---  ,12X,6F12.3)          24690574
00541   122.    94    FORMAT( 6X,20HRECOVERY----------    ,12X,6F12.4)          24690576
00542   123.    96    FORMAT( 6X,20HDP/DN(IN HG/FT)-----  ,12X,6F12.2)          24690578
00543   124.          END                                                       24690580

        END OF LISTING.     0 *DIAGNOSTIC* MESSAGE(S).
```


CONFIDENTIAL

```
0     FOR TABLE                                                    2469D582
COMPILATION BY UNIVAC 1108 FORTRAN-IV DATED     NOV. 23,1965 F4008
THIS COMPILATION WAS DONE ON 19 AUG 66 AT 17:37:24

    FUNCTION TABLE        ENTRY POINT 000065

    STORAGE USED (BLOCK, NAME, LENGTH)

         0001   *CODE   000077
         0000   *DATA   000043
         0002   *BLANK  004735

    EXTERNAL REFERENCES (BLOCK, NAME)

         0003   TAB2

    STORAGE ASSIGNMENT FOR VARIABLES (BLOCK, TYPE, RELATIVE LOCATION, NAME)

     0001   000032 10L       0000 I 000032 I          0000 I 000033 IE        0000 I 000034 KT        0000 I 000001 NDEG
     0002 I 000000 NXY       0000 R 000000 TABLE      0003 R 000000 TAB2      0002 R 000031 XVAL      0002 R 002373 YVAL


00101     1.          FUNCTION TABLE(NT,ARG)                                  2469D584
00103     2.          COMMON NXY(25),XVAL(50,25),YVAL(50,25)                  2469D586
00104     3.          DIMENSION NDEG(25)                                      2469D588
00105     4.          DATA(NDEG(I),I=1,25)/3*1,3,3,20*1/                      2469D590
00107     5.          IF(NT .LT. 0 ) GO TO 10                                 2469D592
00111     6.          TABLE=TAB2(XVAL(1,NT),YVAL(1,NT),NXY(NT),NDEG(NT),ARG,IE)  2469D594
00112     7.          RETURN                                                  2469D596
00113     8.    10    KT=-NT                                                  2469D598
00114     9.          TABLE=TAB2(YVAL(1,KT),XVAL(1,KT),NXY(KT),NDEG(KT),ARG,IE)  2469D600
00115    10.          RETURN                                                  2469D602
00116    11.          END                                                     2469D604

        END OF 'ISTING.     0 *DIAGNOSTIC* MESSAGE(S).
```


CONFIDENTIAL

```
0     FOR TAB2                                                    2469D606
COMPILATION BY UNIVAC 1108 FORTRAN-IV DATED     NOV. 23,1965 F4008
THIS COMPILATION WAS DONE ON 19 AUG 66 AT 17:37:26

    FUNCTION TAB2         ENTRY POINT 000263

    STORAGE USED (BLOCK, NAME, LENGTH)

         0001   *CODE   000324
         0000   *DATA   000050
         0002   *BLANK  000000

    EXTERNAL REFERENCES (BLOCK, NAME)

         0003   OVERFL

    STORAGE ASSIGNMENT FOR VARIABLES (BLOCK, TYPE, RELATIVE LOCATION, NAME)

     0001   000211 100L      0001   000243 110L      0001   000054 123G      0001   000131 141G      0001   000145 150G
     0001   000154 154G      0001   000225 175G      0001   000072 20L       0001   000121 24L       0001   000124 30L
     0001   000206 40L       0001   000247 98L       0001   000251 99L       0000 I 000024 I         0000 I 000021 J
     0000 I 000022 K         0000 I 000023 LAST      0000 I 000030 M         0000 I 000025 N         0000 I 000017 ND2
     0000 I 000027 NN        0000 I 000016 NP1       0000 I 000020 NP1D2     0000 I 000015 NXM1      0000 I 000026 N1
     0000 R 000000 TAB2      0000 R 000001 XX        0000 R 000007 YY

00101    1.          FUNCTION TAB2(X,Y,NX,NDEG,ARG,IE)                          2469D608
00101    2.    C     SINGLE INTERPOLATION ROUTINE                               2469D610
00101    3.    C                                                                2469D612
00103    4.          DIMENSION XX(6), YY(6), X(1), Y(1)                         2469D614
00103    5.    C                                                                2469D616
00103    6.    C     X---INDEPENDENT VARIABLE ARRAY STORED IN CONSECUTIVE LOCATIONS 2469D618
00103    7.    C     Y---DEPENDENT VARIABLE ARRAY STORED IN CONSECUTIVE LOCATIONS 2469D620
00103    8.    C     NX---NUMBER OF X OR Y-VALUES IN THE TABLE                  2469D622
00103    9.    C     NDEG---THE DEGREE OF INTERPOLATION DESIRED                 2469D624
00103   10.    C     ARG---THE ARGUMENT FOR WHICH A CORRESPONDING VALUE OF Y WILL BE OB2469D626
00103   11.    C     IE---=1 FOR SUCCESS,=2 FOR OVERFLOW,=3 FOR INCORRECT CALLING 2469D628
00103   12.    C                                                                2469D630
00104   13.          NXM1=NX-1                                                  2469D632
00105   14.          NP1=NDEG+1                                                 2469D634
00105   15.    C                                                                2469D636
00105   16.    C     DETERMINE IF IT IS POSSIBLE TO GIVE THE DEGREE REQUESTED   2469D638
00105   17.    C                                                                2469D640
00106   18.          IF(NXM1-NDEG)98,110,2                                      2469D642
00106   19.    C                                                                2469D644
00111   20.     2    ND2=NDEG/2                                                 2469D646
00112   21.          NP1D2=NP1/2                                                2469D648
00113   22.          J=NP1D2+2                                                  2469D650
00114   23.          K=J                                                        2469D652
00115   24.          LAST = NX-NP1D2                                            2469D654
00115   25.    C                                                                2469D656
```


CONFIDENTIAL

```
00115   26.    C      IS THE ARRAY IN INCREASING ORDER                          24690658
00116   27.           IF(X(1).GT.X(2))  GO TO 100                               24690660
00116   28.    C                                                                24690662
00116   29.    C      THE ARRAY IS IN INCREASING ORDER                          24690664
00116   30.    C                                                                24690666
00116   31.    C      CHECK FOR EXTRAPOLATION                                   24690668
00120  *DIAGNOSTIC*  THE TEST FOR EQUALITY BETWEEN NON-INTEGERS MAY NOT BE MEANINGFUL.
00120   32.           IF(X(J-1).GE.ARG)  GO TO 110                              24690670
00120   33.    C                                                                24690672
00120   34.    C      DETERMINE WHAT POINTS THE ARGUMENT LIES BETWEEN           24690674
00120   35.    C                                                                24690676
00122   36.     10    DO 12 I=K,LAST                                            24690678
00125  *DIAGNOSTIC*  THE TEST FOR EQUALITY BETWEEN NON-INTEGERS MAY NOT BE MEANINGFUL.
00125   37.           IF(X(I).GE.ARG)  GO TO 20                                 24690680
00127   38.     12    J=J+1                                                     24690682
00127   39.    C                                                                24690684
00127   40.    C      EXTRAPOLATE ON FAR SIDE OF CURVE                          24690686
00127   41.    C                                                                24690688
00131   42.           J=NX                                                      24690690
00132   43.           GO TO 30                                                  24690692
00132   44.    C                                                                24690694
00132   45.    C      IS THE DEGREE OF INTERPOLATION ODD OR EVEN                24690696
00133   46.     20    IF(2*ND2.NE.NDEG)  GO TO 24                               24690698
00133   47.    C                                                                24690700
00133   48.    C      THE DEGREE OF INTERPOLATION IS EVEN                       24690702
00133   49.    C                                                                24690704
00135   50.           IF(ABS(X(J-1)-ARG).LT.ABS(X(J)-ARG))  J=J-1               24690706
00137   51.     24    J=J+ND2                                                   24690708
00137   52.    C                                                                24690710
00140   53.     30    DO 32 N=1,NP1                                             24690712
00143   54.           XX(N)=ARG-X(J)                                            24690714
00144   55.           YY(N)=Y(J)                                                24690716
00145   56.     32    J=J-1                                                     24690718
00145   57.    C                                                                24690720
00147   58.           DO 36 N=1,NDEG                                            24690722
00152   59.           N1=N+1                                                    24690724
00152   60.    C                                                                24690726
00153   61.           DO 36 NN=N1,NP1                                           24690728
00156   62.           YY(NN)=(YY(N)*XX(NN)-YY(NN)*XX(N))/(XX(NN)-XX(N))         24690730
00157   63.           CALL OVERFL(M)                                            24690732
00160   64.           IF(M.EQ.1)  GO TO 40                                      24690734
00162   65.     36    CONTINUE                                                  24690736
00162   66.    C                                                                24690738
00162   67.    C      INTERPOLATION WAS SUCCESSFUL RETURN                       24690740
00165   68.           IE=1                                                      24690742
00166   69.           TAB2=YY(NP1)                                              24690744
00167   70.           RETURN                                                    24690746
00167   71.    C                                                                24690748
00170   72.     40    IE=2                                                      24690750
00171   73.           GO TO 99                                                  24690752
00171   74.    C                                                                24690754
00171   75.    C      THE ARRAY IS IN DECREASING ORDER                          24690756
00171   76.    C                                                                24690758
00171   77.    C      CHECK FOR EXTRAPOLATION                                   24690760
00172  *DIAGNOSTIC*  THE TEST FOR EQUALITY BETWEEN NON-INTEGERS MAY NOT BE MEANINGFUL.
00172   78.     100   IF(ARG.GE.X(J-1))  GO TO 110                              24690762
00172   79.    C                                                                24690764
00174   80.           DO 104 I=K,LAST                                           24690766
```


CONFIDENTIAL

```
00177  *DIAGNOSTIC*  THE TEST FOR EQUALITY BETWEEN NON-INTEGERS MAY NOT BE MEANINGFUL.
00177     81.        IF(ARG.GE.X(I))  GO TO 20                                  2469D768
00201     82.   104  J = J+1                                                    2469D770
00201     83.   C                                                              2469D772
00203     84.        J=NX                                                       2469D774
00204     85.        GO TO 30                                                   2469D776
00204     86.   C                                                              2469D778
00205     87.   110  J=NDEG+1                                                  2469D780
00206     88.        GO TO 30                                                   2469D782
00206     89.   C    THE DEGREE REQUESTED IS TOO LARGE FOR THE DATA GIVEN       2469D784
00207     90.    98  IE=3                                                      2469D786
00210     91.    99  TAB2 = ARG                                                2469D788
00211     92.        RETURN                                                     2469D790
00212     93.        END                                                        2469D792

        END OF LISTING.     4 *DIAGNOSTIC* MESSAGE(S).
```


CONFIDENTIAL

```
* XQT MAIN

      BLANK COMMON.    163043    167777

      STARTING ADDRESS  014000

      CORE LIMITS 014000 047237    100000 134271

MAIN  /CODE
0  100000-110421
1  014000-016323

MPAUS/CODE
1  016324-016371

MEXPI/CODE
1  016372-016626
2  110422-110431

EXP   /CODE
1  016627-016671
2  110932-110951

ALOG  /CODE
1  016672-016736
2  110452-110504

MERRS /CODE
1  016737-017142
2  110505-110505

CHAREY/CODE
0  110506-110506

MINPT/CODE
1  017143-020061
2  110507-110563

MTAB3 /CODE
2  110564-112500

MFTV3 /CODE
1  020062-020105
```

```
NFWTS /CODE
1  020166-021011
2  112501-112614

MISTS/CODE
1  021012-021143
2  112615-112616

MOUTS /CODE
1  021144-022313
2  112617-112743

TALL2 /CODE
0  112744-113711
1  022314-030654

LIFTB /CODE
1  030655-030741

TALL3 /CODE
0  113712-114107
1  030742-032424

TAN   /CODE
1  032425-032450
2  114110-114115

ATAN  /CODE
1  032451-032535
2  114116-114157

OUTPUT/CODE
0  114160-114674
1  032536-033533

SINCOS/CODE
1  033534-035624
2  114677-114716

TAB2  /CODE
0  114717-114766
1  035625-035150

IPPEL /CODE
0  114767-115250
1  035151-036437

SQRT  /CODE
1  036440-036502
2  115281-115256

RCS   /CODE
0  115257-115305
1  036503-036753

TABLE /CODE
0  115306-115350
1  036754-037052
```

```
CHORD /CODE
0  115353-115534
1  037053-040104

INLET /CODE
0  115535-116070
1  040105-041505

SORT  /CODE
0  116071-116112
1  041506-041621

SLOPE /CODE
0  116113-116242
1  041622-042100

TAIL /CODE
0  116243-117561
1  042101-045655

NRLNOS/CODE
1  045656-045722

THRUS /CODE
0  117562-117665

TYPE  /CODE
0  117666-117702

EDATES/CODE
1  045723-046013

NTRAN /CODE
1  046014-047237
2  117703-120025

TSCRMS/CODE
0  120026-120263

TSWAPS/CODE
0  120264-120363

TINTLS/CODE
0  120364-120471

RC    /******
0  120472-120661

IMPELR/******
0  120662-123216

BLOCK /******
0  123217-134175

TALLCP/******
0  134176-134271
```

END OF ALLOCATION

(U) APPENDIX II

IMPELLER STRESS AND VIBRATION ANALYSIS

ABSTRACT

A discussion of the procedure and the results of the stress and vibration analyses are presented for the MF-1, MF-2, MF-3, RF-1, and workhorse impellers. The temperature distribution, Campbell diagram, natural-frequency calculations, and stress calculations are included for each impeller.

SYMBOLS

A	true flow area (in.^{2}), $A = A^1 \cos \phi$
A'	total geometric area less area blocked by blades (in.^{2}), $A' = A_T - A_B$
A_B	area blocked by blades (in.^{2}), $A_B = \frac{N}{2} h' \left(t_t + t_r\right)$
A_T	total geometric area (in.^{2}), $A_T = \pi h\left(r_1 + r_2\right)$
A_{td}	cross-sectional area of impeller disk (in.^{2})
E	modulus of elasticity (psi)
F', F_r'	blade radial force per inch of axial length (lb/in.)
F_{fu}	failure force based on ultimate stress (lb)
F_{fy}	failure force based on yield stress (lb)
F_{sr}	calculated blade pull (lb)
T_{td}	total disk force (lb)
F_{ts}	total blade force (lb)
F_{tw}	total wheel force (lb)
g	gravitational constant (32.17 ft/sec^2)
h	flow-passage height normal to mean flow path, includes clearance (in.)
h'	blade height normal to mean flow path (in.)

I'	blade mass moment of inertia per inch of axial length (lb-in. - sec^2 /in.)
I_{td}	total disk mass moment of inertia (lb-in.-sec^2)
I_{ts}	total blade mass moment of inertia (lb-in.-sec^2)
I_{tw}	total wheel mass moment of inertia (lb-in.-sec^2)
L_r	total meridional length along blade root (in.)
L_t	total meridional length along shroud (in.)
ℓ_r	meridional distance to point along blade root (in.)
ℓ_t	meridional distance to point along blade tip (in.)
N	rotational speed (rpm) or number of impeller blades
r	radius (in.)
r_r	root radius (in.)
r_t	tip radius (in.)
r_1	disk bore radius (in.)
r_2	impeller-hub radius at the inlet (in.)
r_3	impeller-tip radius at the exit (in.)
S_{as}	allowable stress (psi)
S_c	calculated blade-root stress (psi)

S_f failure stress (psi)

S_{root} local blade-root stress (psi)

S_{tan} average tangential disk stress (psi)

T metal temperature (° F)

T_a bore temperature at forward pilot (° F),

$$T_a = \frac{T_o + T_i}{2}$$

T_b bore temperature at rear pilot (° F)

T_d downstream disk-face temperature (° F),

$$T_d = T_b + \left(\frac{T_e - T_b}{r_3 - r_1}\right) r$$

T_e relative exit total temperature (° F)

T_i relative inlet total temperature (° F)

T_o ambient air inlet temperature (° F)

T_r metal temperature along the blade root (° F),

$$T_r = T_i + \left(\frac{T_e - T_i}{L_r}\right) \ell_r$$

T_t metal temperature along the blade tip (° F),

$$T_t = T_i + \left(\frac{T_e - T_i}{L_t}\right) \ell_t$$

T_u upstream disk-face temperature (° F),

$$T_u = T_a + \left(\frac{T_i - T_a}{r_2 - r_1}\right) r$$

t	axial length of disk element (in.)
t_r	blade thickness at the root (in.)
t_t	blade thickness at the tip (in.)
W'	weight of blade per inch of axial length (lb/in.)
W_{td}	total disk weight (lb)
W_{ts}	total blade weight (lb)
W_{tw}	total wheel weight (lb)
Z	axial distance (in.)
α	inclination of blade cross section (degrees)
γ	material density ($lb/in.^3$)
η_s	safety factor based on allowable stress
η_u	safety factor based on ultimate stress
η_y	safety factor based on yield stress
ϕ	angle between blade and meridional plane (degrees)
ω	angle velocity (radians/sec)

1.0 DISCUSSION

Impeller stress and vibration analyses were conducted through use of a series of computer programs developed during company-sponsored research. For initial stress checks, a preliminary scaled layout of the disk, blade, and shroud profile was prepared for each aerodynamic design. Blade-root and blade-tip dimensions, wrap angles, and inlet- and exit-gas temperatures were also provided. Temperature distribution for the blade and disk was then estimated from the aerodynamic design data. The procedures used were developed empirically for previous impeller designs.

The blade metal temperatures were assumed to vary linearly as functions of meridional length along the shroud and disk profiles as shown on Figure 3. For the blade tip along the shroud,

$$T_t = T_i + \left(\frac{T_e - T_i}{L_t}\right) \ell_t \tag{162}$$

and along the blade root,

$$T_r = T_i + \left(\frac{T_e - T_i}{L_r}\right) \ell_r \tag{163}$$

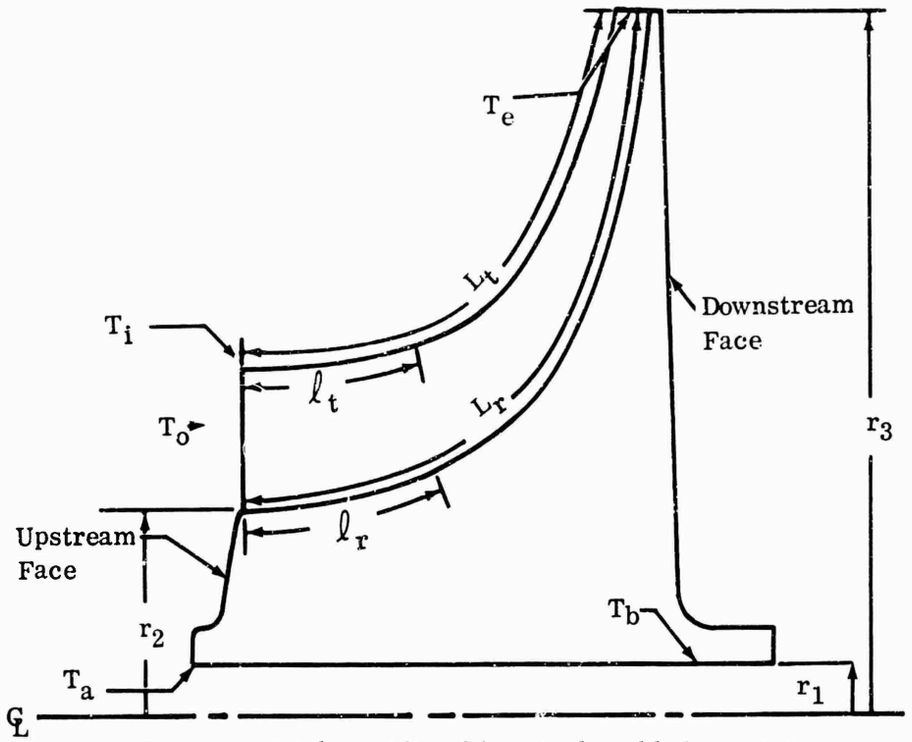
Similarly, the upstream and downstream disk-face temperatures were assumed to be linear functions of radius; thus,

$$T_u = T_a + \left(\frac{T_i - T_a}{r_2 - r_1}\right) r \tag{164}$$

and

$$T_d = T_b + \left(\frac{T_e - T_b}{r_3 - r_1}\right) r \tag{165}$$

The symbols used are described in Figure 3.



L_r = total meridional length along blade root (in.)

L_t = total meridional length along shroud (in.)

T_a = bore temperature at forward pilot, $\frac{T_o + T_i}{2}$

T_o = ambient air inlet temperature (°F)

T_i = relative inlet total temperature at shroud (°F)

T_e = relative exit total temperature (°F)

T_b = bore temperature at rear pilot (200°F assumed for journal bearing application; 300°F for oil-mist-lubricated ball bearing)

ℓ_r = distance to point along blade root (in.)

ℓ_t = distance to point along blade tip (in.)

r = radius (in.)

Figure 3. Blade and Disk Metal Temperature Calculations.

Blade natural frequencies were determined through a contractor-developed computer program with inputs from blade drawing tabulations of root and tip thickness, wrap angle, and axial location. Blade root and tip thickness were taken in a plane normal to the axis of the disk. The first 5 natural frequencies were calculated, and the results were plotted on a Campbell diagram. A Campbell diagram shows blade frequency versus shaft speed, and the orders are excitation caused by wakes or obstructions in the flow path. Each time the blade passes a wake the blade encounters a sharp change in pressure which causes the blade to deflect slightly. Because the number of wakes that the blade encounters is a linear function of shaft speed, the orders appear on the Campbell diagram as straight lines, fanning out from the origin. For example, if 4 inlet struts were used, each blade would feel the disturbance 4 times per revolution of the shaft; the order number, therefore, would be 4. Other potentially critical orders are caused by the inlet guide vanes and the diffuser passages. If the shaft speed and order frequency were to coincide with a blade natural frequency, the blade might vibrate and fail in a short time. Consequently, it is necessary to design a blade so that an order line and a natural-frequency line do not intersect at the design speed.

The blade radial force (F'_r), weight (W'_t), mass moment of inertia (I'), and root stress (S_c) were computed with the same design data as the blade-frequency calculation. Several representative stations along the blade, including a station at the exit tip, were chosen; independent plates or strips were assumed to exist at these points.

The thickness and height of the plates were the same as those of the blade at that station, and the length was assumed to be unity. The resulting calculated radial force, weight, and polar mass moment of inertia were plotted versus axial position of the calculation station. Integration of these plots yielded blade pull, F_{sr} (pounds-force), blade weight, W_{ts} (pounds-weight), and blade polar mass moment of inertia, I_{ts} (lb-in.-sec^2).

The calculated blade-root stress (s_c), blade-root temperature (T_r), allowable stress (s_{as}), and safety factor (η_s) to allowable stress were plotted versus axial length. The blade-root temperature was taken from the temperature distribution estimate, and the allowable stress was obtained from the material strength versus temperature curve. The material strength versus temperature curve has a built-in vibratory-stress margin, which is determined by discounting the yield or rupture curve by using a Goodman diagram (see Figure 4).

Two such material strength curves were used, 1 with a discount corresponding to ± 20,000 psi vibratory stress and one with a discount corresponding to ± 12,000 psi vibratory stress. The ± 20,000 psi vibratory stress is the maximum which can be allowed and still maintain design integrity in the inducer section of the impeller. Based on the contractor's experience with aluminum impellers, the maximum allowable vibratory stress must be reduced by 40 percent in the radial

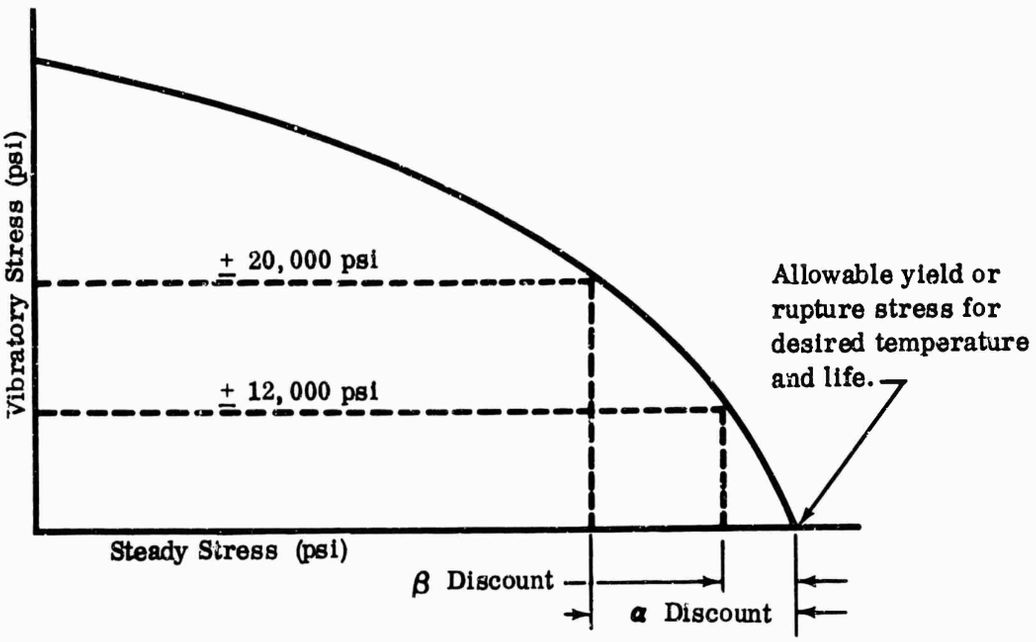


Figure 4. Goodman Diagram.

portion of the impeller. Even though the vibration characteristics of titanium are better than those of aluminum, the 40-percent reduction was used to provide a conservative design because of lack of titanium test data. Region α, defined as the first 25 percent of the blade root meridional length, is the impeller blade section with the allowable ± 20,000 psi vibratory stress. Region β is the remainder of the blade with an allowable vibratory stress of ± 12,000 psi. The aerodynamic blade load was assumed to be a negligible percentage of the total blade stress. Because the calculation of the blade-root stress does not consider shear stress between adjacent plates, which would distribute the stress more evenly along the blade root, the stress analysis of the blade is conservative.

The disk tangential force, cross-sectional area, weight, and polar mass moment of inertia were computed. The failure load was divided by the tangential force to determine a safety factor to failure. Failure was defined as minimum yield or minimum rupture stress. However, failure was not meant to be a disk burst. For steady-state operation, this safety factor must be at least 1.25 to minimum yield stress or to minimum rupture stress, whichever is least. For momentary overspeed conditions, the safety factor may be reduced to 1.10 to minimum yield stress or 1.25 to minimum ultimate stress, whichever is least.

2.0 MF-1 IMPELLER ANALYSIS

The life of the MF-1 impeller is not limited for operation at 62,700 rpm and 60° F inlet temperature if the vibratory stresses do not exceed ± 20,000 psi and ± 12,000 psi in the α and β regions of the blade, respectively. Figure 8 indicates that blade resonant conditions may exist at 35,700 and 47,000 rpm. If continuous operation is expected in these regions, an experimental vibration survey should be conducted to determine modifications that may be required.

The calculated minimum safety factors for steady-state operation at 62,700 rpm and an impeller inlet temperature of 60° F are as follows:

1) Blade safety factor is 3.42 to minimum 0.2-percent yield stress including ± 12,000 psi vibratory stress.

2) Disk safety factors are 1.44 to minimum 0.2-percent yield stress and 1.62 to minimum ultimate stress.

The calculated minimum safety factors for momentary operation at 71,500 rpm and an impeller inlet temperature of 60° F are as follows:

1) Blade safety factor is 2.66 to minimum 0.2-percent yield stress.

2) Disk safety factors are 1.10 to minimum 0.2-percent yield stress and 1.25 to minimum ultimate stress.

The weight of the impeller is 7.67 pounds, and the mass moment of inertia is 0.0899 lb-in.-sec^2.

Figures 5 through 13 present the results of stress and vibration analyses for the MF-1 impeller.

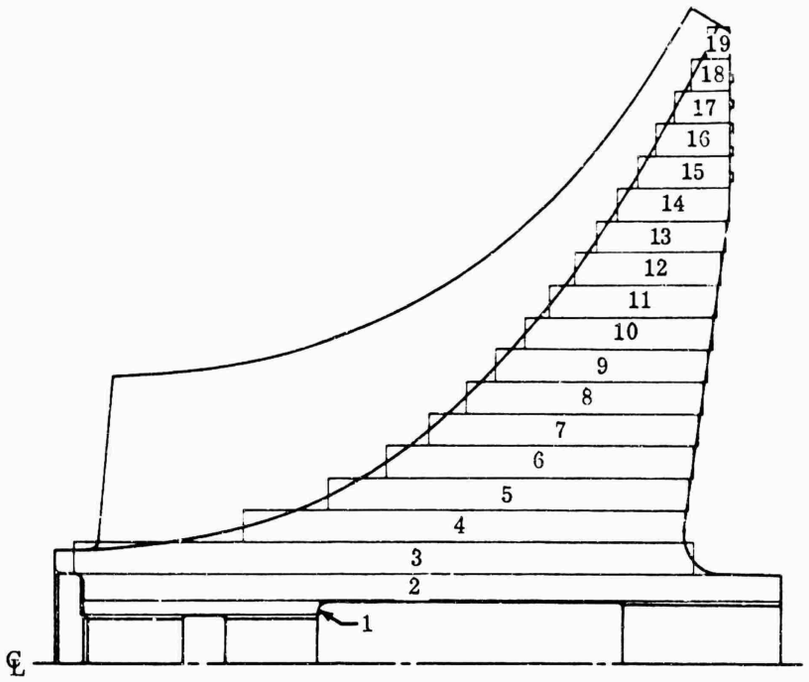


Figure 5. Disk and Blade Profile of MF-1.

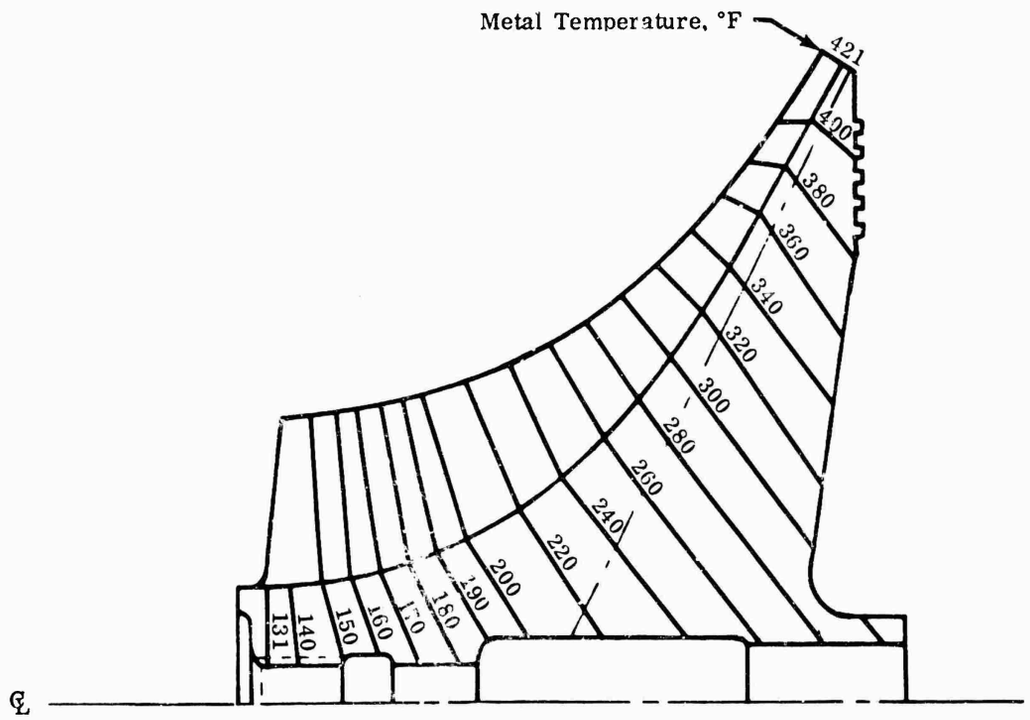


Figure 6. Temperature Distribution of MF-1.

Computer Input Data:

Title:

MF-1 Impeller Blade Natural Frequencies

Number of Drawing Stations	Material Const.		Blade Profile	Number of Nodes at General Z Station	Required Number of Modes
	Density γ	Modulus of Elasticity E			
	$(lb/in.^3)$	(psi)			
19	0.16	16,000,000	Linear	5	5

Computer Output Data:

Mode No.	Frequency, cps
1	4,697
2	9,385
3	12,406
4	16,380
5	17,987

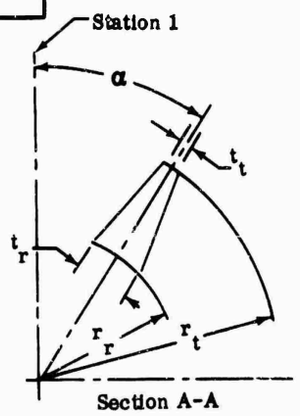
Information From Drawing :

Station No.	Axial Dist. Z	Tip Rad. r_t	Root Rad. r_r	Inclination α	Tip Thickness t_t	Root Thickness t_r
	in.	in.	in.	Degree	in.	in.
1	0	0.710	0.710	0	0.065	0.065
1a	0.100	1.748	0.715	4.8	0.050	0.062
2	0.490	1.780	0.759	22.6	0.051	0.113
2a	0.740	1.808	0.802	31.8	0.052	0.126
3	0.988	1.847	0.861	39.7	0.051	0.135
3a	1.235	1.899	0.938	46.4	0.052	0.139
4	1.476	1.963	1.029	52.4	0.054	0.142
4a	1.696	2.040	1.135	57.1	0.054	0.143
5	1.930	2.135	1.270	60.9	0.056	0.142
5a	2.144	2.238	1.416	63.3	0.051	0.138
6	2.360	2.356	1.586	65.9	0.047	0.130
7	2.550	2.476	1.762	67.3	0.044	0.122
8	2.750	2.623	1.968	68.5	0.042	0.113
9	2.924	2.772	2.162	69.0	0.040	0.104
10	3.110	2.945	2.389	69.3	0.039	0.096
11	3.424	3.300	2.822	69.3	0.035	0.080
12	3.712	3.690	3.268	69.3	0.029	0.066
13	3.946	4.036	3.668	69.3	0.025	0.053
14	4.100	3.950	3.950	69.3	0.045	0.045

Required Number of Node Distances

Z Distances for Node Stations, (In.)

0.	0.10	0.20	0.40	0.80	1.20	1.60	2.0	2.4	2.8
3.2	3.6	4.0	4.10						



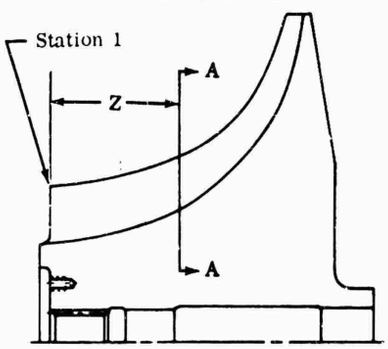


Figure 7. Natural Frequencies of MF-1 Blades.

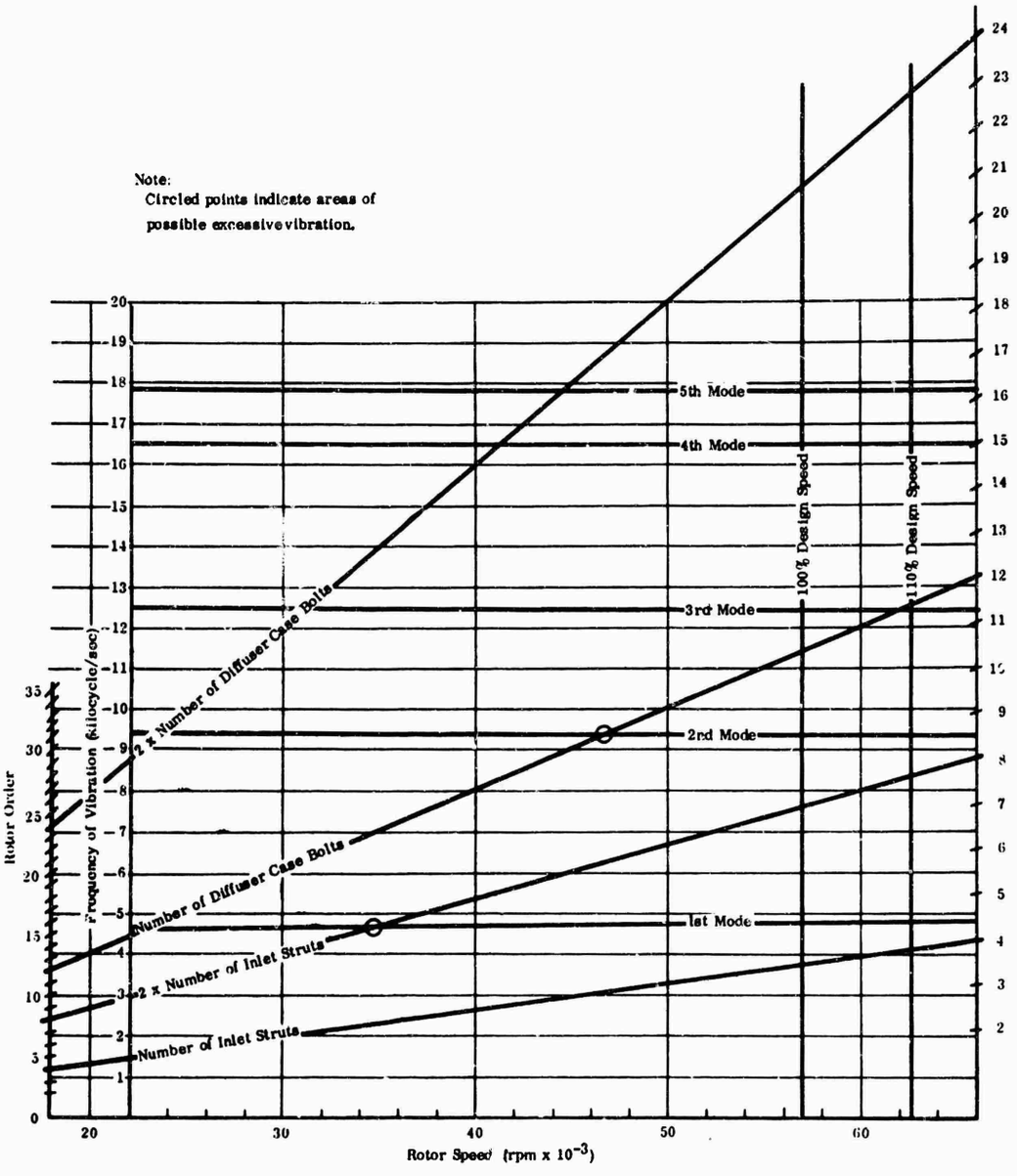


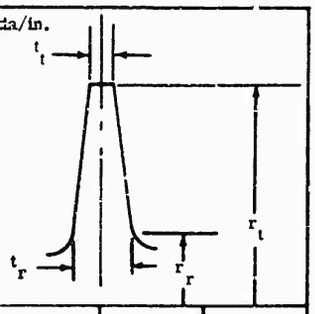
Figure 8. Campbell Diagram for MF-1.

Radial Flow Blade Root Stress, Force in., Weight/in., and Mass Moment of Inertia/in.

Material: Titanium, 6Al-4V $\omega = 0.1047 \times N$ radians/sec

Speed N, = 62,700 rpm Density, $\gamma = 0.160$ lb/in.^{3}
(10% overspeed)

$g = 386$ in./sec^2



Blade Station No.			1n	2	4	6	8	10	13
1	r_t	in.	1.748	1.780	1.963	2.356	2.623	2.945	4.036
2	r_r	in.	0.715	0.739	1.029	1.586	1.968	2.389	3.668
3	t_t	in.	0.050	0.051	0.054	0.047	0.042	0.039	0.025
4	t_r	in.	0.072	0.113	0.142	0.130	0.113	0.096	0.053
5	r_t^2	①^2	3.056	3.168	3.853	5.551	6.880	8.673	16.289
6	r_t^3	① x ⑤	5.342	5.639	7.564	13.078	18.046	25.542	65.744
7	r_r^2	②^2	0.511	0.576	1.059	2.515	3.873	5.707	13.454
8	r_r^3	② x ⑦	0.365	0.437	1.090	3.989	7.622	13.635	49.350
9	$r_t - r_r$	① - ②	1.033	1.021	0.934	0.770	0.655	0.556	0.368
10	$r_t^2 - r_r^2$	⑤ - ⑦	2.545	2.592	2.794	3.036	3.007	2.966	2.835
11	$r_t^3 - r_r^3$	⑥ - ⑧	4.977	5.202	6.474	9.089	10.424	11.907	16.394
12	$t_r - t_t$	④ - ③	0.022	0.062	0.090	0.083	0.071	0.057	0.028
13	$\frac{t_r - t_t}{r_t - r_r}$	⑫ + ⑨	0.021	0.061	0.096	0.108	0.108	0.103	0.076
14		⑬ x ②	0.015	0.046	0.09878	0.17129	0.21254	0.24607	0.27877
15		④ + ⑭	0.087	0.159	0.24078	0.30129	0.32554	0.34207	0.33177
16		⑮ x ⑩+2	0.111	0.206	0.33637	0.45736	0.48945	0.50728	0.47028
17		⑬ x ⑪+3	0.035	0.106	0.20716	0.32720	0.37526	0.40880	0.41531
18		⑯ - ⑰	0.076	0.100	0.12921	0.13016	0.11419	0.09843	0.05497
19	F_r'	$\frac{\gamma}{g}$ ⑱^2	1,3560	1,790	2,310	2,330	2,040	1,760	980
20	S_{root}	⑲ + ④	18,870	15,810	16,260	17,870	18,060	18,330	18,530
21	r_t	① x ⑥	9,339	10,036	14,848	30,812	47,334	75,221	265,343
22	r_r'	② x ⑧	0.261	0.332	1.122	6.327	15.000	32.574	181.016
23	$r_t^4 - r_r^4$	㉑ - ㉒	9.078	9.704	13.726	24.485	32.334	42.647	84.327
24	$t_r + t_t$	③ + ④	0.122	0.164	0.196	0.177	0.155	0.135	0.078
25		⑮ x ⑪+3	0.14433	0.2757	0.5196	0.9128	1.13114	1.35766	1.61300
26		⑬ x ㉓+4	0.04766	0.14799	0.32943	0.66110	0.87302	1.09816	1.60221
27		㉕ - ㉖	0.09667	0.12771	0.19017	0.25170	0.25812	0.25950	0.21079
28	$I' \times 10^4$	$\frac{\gamma}{g}$ ㉗	0.40	0.53	0.79	1.04	1.07	1.08	0.87
29		⑨ x ㉔	0.12603	0.16744	0.18306	0.13629	0.10153	0.07506	0.02870
30	$W' \times 10^2$	$\frac{\gamma}{2}$ ㉙	1.01	1.34	1.46	1.09	0.81	0.60	0.23

Figure 9. Blade Stress Calculations for MF-1.

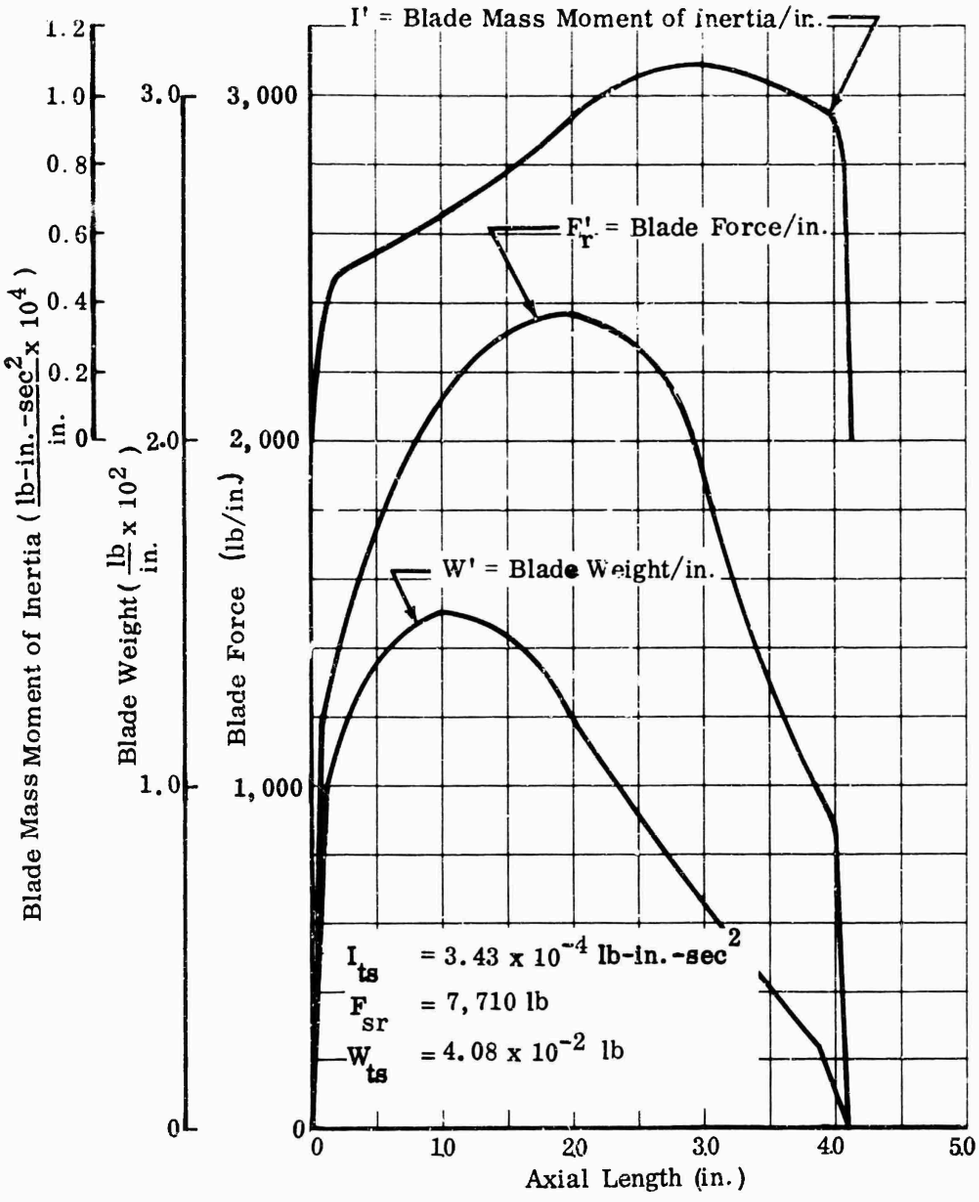


Figure 10. MF-1 Impeller-Blade Force, Weight, and Inertia.

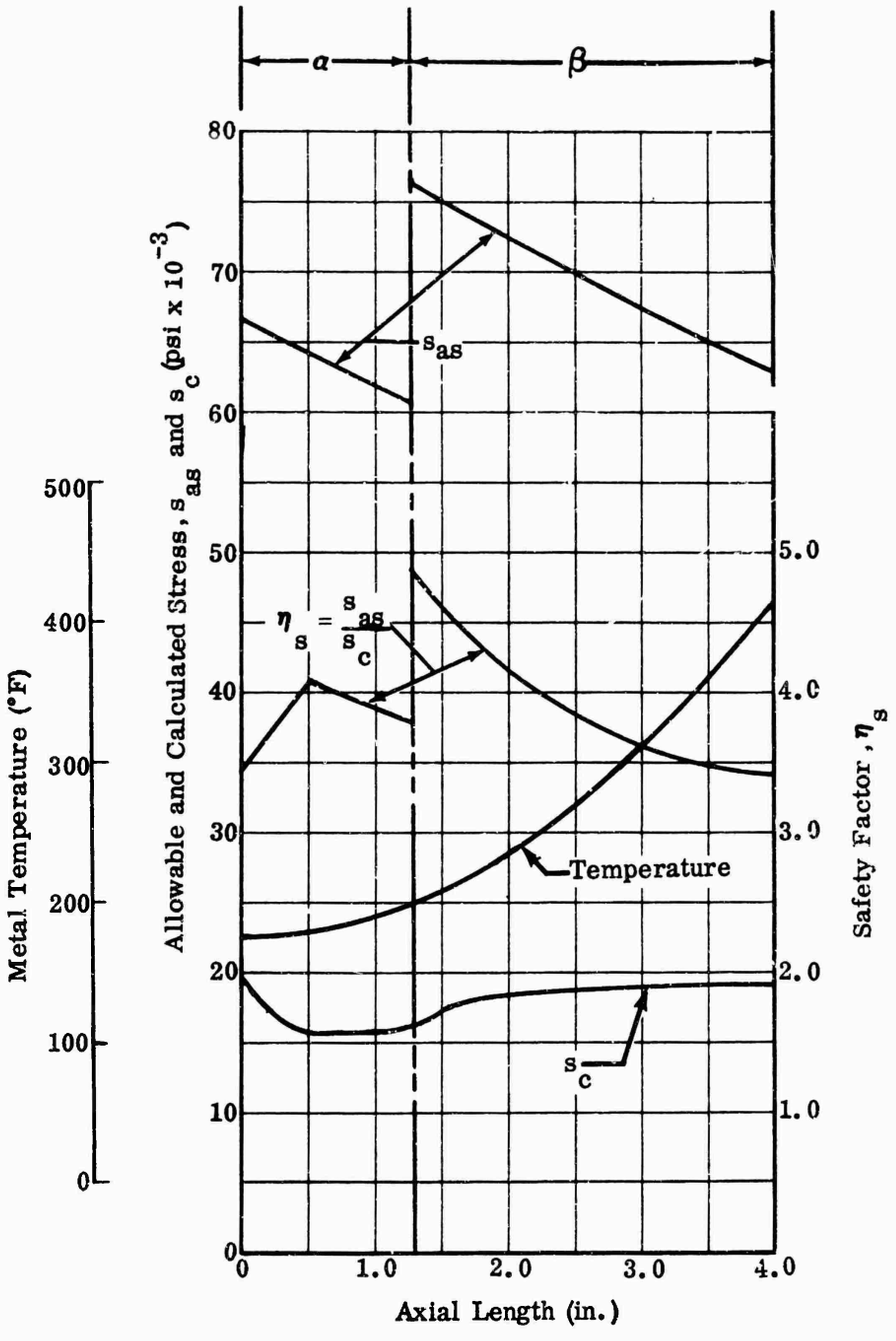


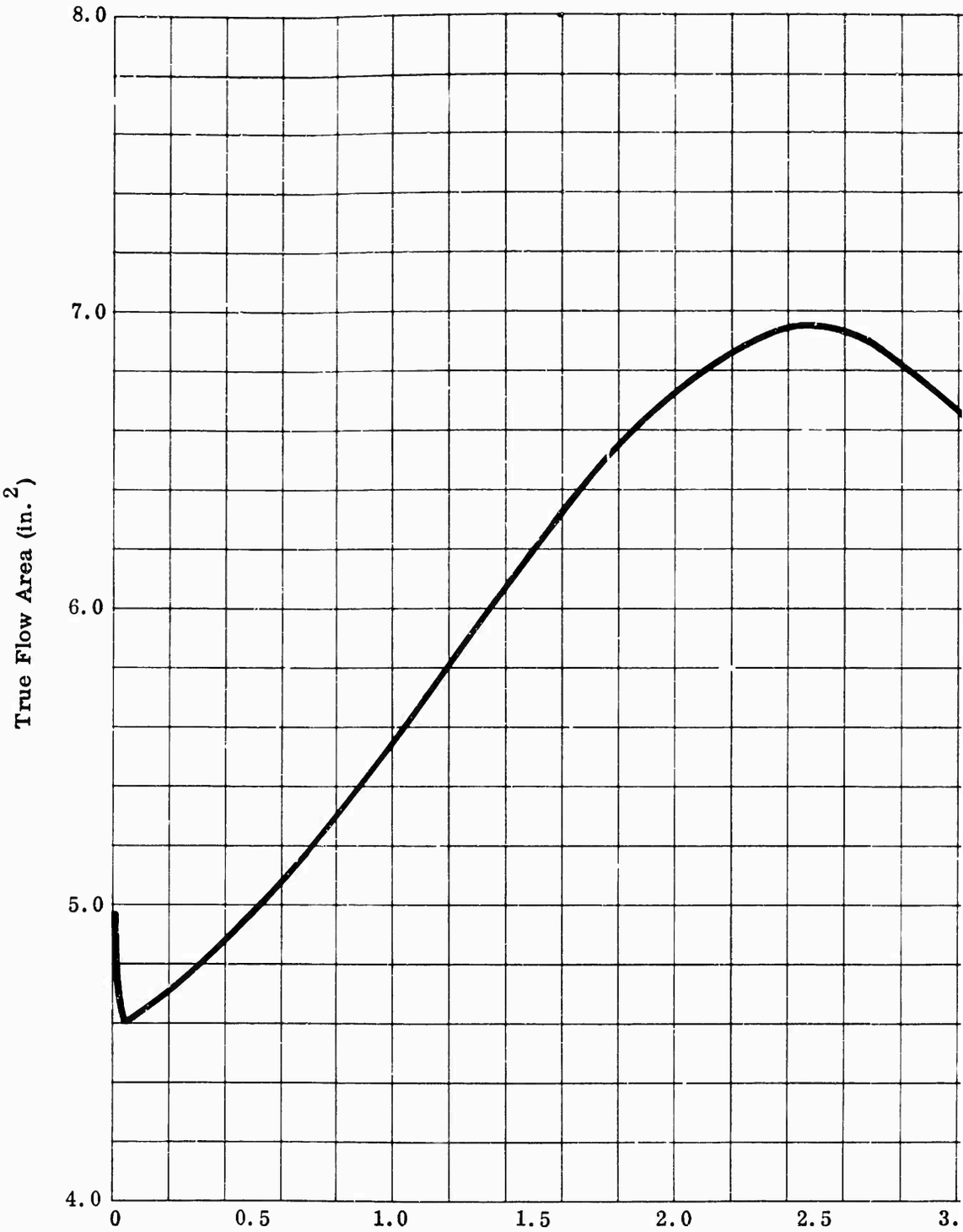
Figure 11. Blade-Root Stress, Temperature, and Safety Factor for MF-1.

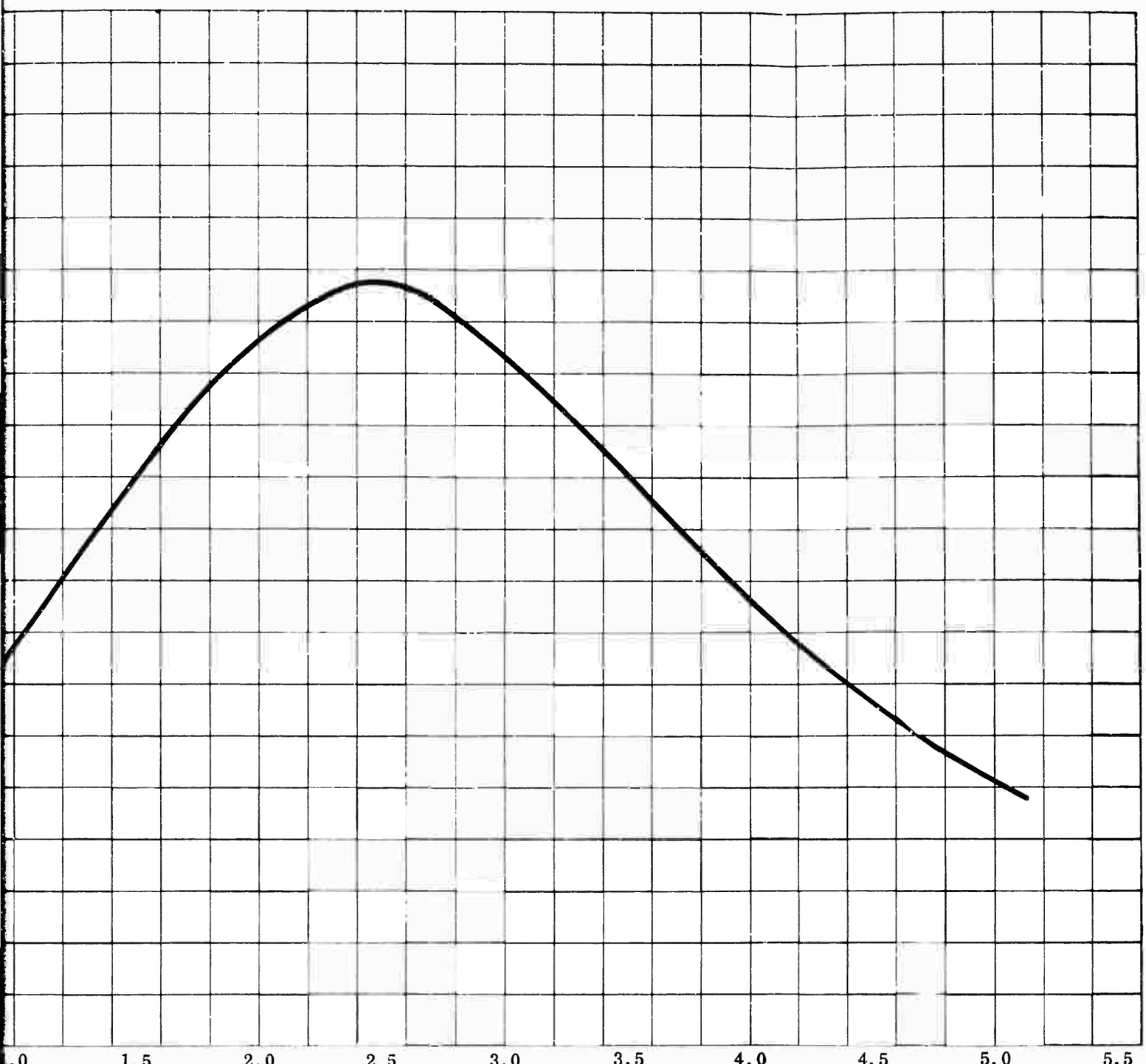
Flow Area Calculation

Sec.	h	r_1	r_2	A_T $\pi h (r_1+r_2)$	h'	t_t	t_r	A_B $\frac{N}{2} h' (t_t+t_r)$	A' $(A_T - A_B)$	ϕ	C
A	1.057	1.765	0.710	8.219	1.037			0.0	8.219	50.84	0
B	1.056	1.772	0.718	8.261	1.036	0.050	0.077	1.184	7.077	49.40	0
C	1.034	1.795	0.770	8.331	1.014	0.051	0.115	1.515	6.816	43.60	0
D	0.978	1.847	0.895	8.423	0.960	0.052	0.136	1.624	6.799	36.30	0
E	0.898	1.941	1.100	8.579	0.876	0.054	0.142	1.545	7.034	28.90	0
F	0.780	2.080	1.400	8.526	0.757	0.056	0.140	1.335	7.191	21.50	0
G	0.640	2.280	1.757	8.118	0.617	0.050	0.121	0.950	7.168	14.30	0
H	0.500	2.528	2.155	7.357	0.478	0.043	0.105	0.637	6.720	7.00	0
I	0.388	2.843	2.574	6.603	0.366	0.038	0.087	0.412	6.191	0.20	0
J	0.308	3.190	3.002	5.994	0.283	0.036	0.075	0.283	5.711	0	1
K	0.250	3.582	3.440	5.512	0.226	0.031	0.061	0.187	5.325	0	1
L	0.212	3.950	3.832	5.183	0.186	0.027	0.048	0.126	5.057	0	1

Figure 12. Impeller Flow Area of MF-1.

Cos ϕ	A / A' Cos ϕ
0.6315	5.190
0.6508	4.606
0.7242	4.936
0.8059	5.479
0.8755	6.158
0.9304	6.691
0.9690	6.946
0.9926	6.670
0.9999	6.190
1.0	5.711
1.0	5.325
1.0	5.057





Meridional Mean Flow Path (in.)

Disk Tangential Stress, Cross-Sectional Area, Weight
Mass Moment of Inertia, and Failure Load

Material: Titanium 6Al-4V

I_t = 3.43 x 10^{-4} lb-in.-sec^2

ω = 0.1047N radians/sec

Speed, N = 62,760 rpm (10% overspeed)

r_{-r} = [illegible] lb

Density, γ = 0.160 lb/$in.^3$

Number of Blades, n = 18

W_{ts} = 4.08x10^{-2} lb

g = 386 in./sec^2

								Failure Stress 0.2% Yield			Failure Stress Ultimate		
	(1)	(2)	(3)	(4)	(5)	(6)	(7)	(8)	(9)	(10)	(8)	(9)	(10)
Segment No.	r	Δr	t	(2) x (3)	(1) x (1)	(1) x (5)	(1) x (6)	T	S_f	(4) x (9)	T	S_f	(4) x (9)
	in.	in.	in.	$in.^2$	$in.^3$	$in.^4$	$in.^5$	°F	psi	lb	°F	psi	lb
1	0.3425	0.0850	1.570	0.1335	0.04572	0.01566	0.005	156	101,500	13,550	150	111,000	14,818
2	0.4675	0.1675	4.610	0.7722	0.36196	0.16967	0.079	211	95,500	73,745	211	106,000	[illegible]
3	0.6525	0.2000	4.120	0.8240	0.53766	0.35082	0.229	222	94,500	[illegible]	222	105,500	[illegible]
4	0.8525		2.925	0.7550	0.49771	0.42515	0.362	232	93,500	64,659	232	105,000	81,425
5	1.0525		2.390	0.4780	0.50310	0.52951	0.557	243	92,500	44,215	243	104,000	49,712
6	1.2525		2.040	0.4080	0.51102	0.64005	0.802	255	91,500	37,332	255	103,500	42,228
7	1.4525		1.790	0.3580	0.52000	0.75530	1.097	266	90,500	32,396	266	102,500	36,695
8	1.6525		1.575	0.3150	0.52054	0.86019	1.421	279	90,000	28,350	279	102,000	32,130
9	1.9525		1.405	0.2810	0.52053	0.96432	1.786	291	89,000	25,009	291	101,500	28,522
10	2.0525		1.245	0.2490	0.51107	1.04907	2.153	303	88,000	21,912	303	100,500	25,025
11	2.2525		1.105	0.2210	0.49780	1.12129	2.526	316	87,500	19,338	316	100,000	22,100
12	2.4525		0.975	0.1950	0.47824	1.17288	2.876	328	86,500	16,868	328	99,500	19,403
13	2.6525		0.855	0.1710	0.45358	1.20312	3.191	341	86,000	14,706	341	98,500	16,844
14	2.8525		0.740	0.1480	0.42217	1.20424	3.435	353	85,000	12,580	353	98,000	14,504
15	3.0525		0.620	0.1240	0.37851	1.15540	3.527	366	84,500	10,478	366	97,500	12,090
16	3.2525		0.500	0.1000	0.32525	1.05788	3.441	378	83,500	8,350	378	97,000	[illegible]
17	3.4525		[illegible]	0.0740	0.25549	[illegible]	3.045	390	83,000	6,142	390	96,000	7,104
18	3.6525	0.2000	0.255	0.0510	0.18628	0.68039	2.485	403	82,500	4,208	403	95,500	4,871
19	3.7475	0.1000	0.140	0.0280	0.10494	0.39335	1.515	414	82,000	2,181	414	95,000	2,527

A_{td}	2Σ(4)	11.03	$in.^2$
I_{td}	$[2\pi\gamma\omega^2 \div g]\Sigma$(6)	522.900	lb
I_{ts}	$F_{sr}^{xn} \div \pi$	44,199	lb
I_{tw}	I_{td} [illegible] I_{ts}	567.099	lb
I_{ts}	$[2\pi\gamma \div g]\Sigma$(7)	0.8992	lb-in-sec^2
I_{tw}	$I_{td}+nI_{ts}$	0.0961	lb-in-sec^2
W_{td}	$2\pi\gamma\Sigma$(5)	7.67	lb
W_{tw}	W_{td} + n [illegible] s	8.40	lb
η	[illegible] $\div W_{tw}$	1.44	-
η_u	$= F_{fy} \div F_{tw}$	1.62	-
S_{tan}	$= F_{tw} \div A_{td}$	51,400	psi

S_{tan} = Average Tangential Disk Stress

F_{fy} = 1.62x Σ(10) = 816,597

F_{fy} = 1.62 x Σ(10) = 920,942

S_f Failure Stress at Temperature, T

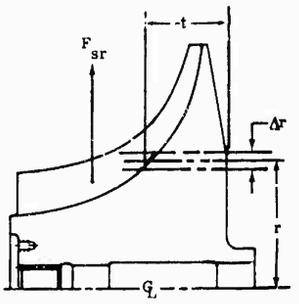


Figure 13. Disk Calculations for MF-1.

3.0 MF-2 IMPELLER ANALYSIS

This impeller is limited to 77,000 rpm for steady-state operation for the blade profile defined in Figure 16 due to the possibility of high vibratory stress at the 80,300 rpm design speed. By cutting the leading edge back in a straight line from the root at station no. 1 to the tip at station no. 3, as dimensioned in Figure 17, the maximum steady-state speed is increased to 80,300 rpm.

The calculated minimum safety factors for steady-state operation at 80,300 rpm and for an impeller inlet temperature of 60° F are as follows:

1) Blade safety factor is 1.95 to minimum 0.2-percent yield stress including ± 20,000 psi vibratory stress.

2) Disk safety factors are 1.34 to minimum 0.2-percent yield stress and 1.53 to minimum ultimate stress.

The calculated minimum safety factors for momentary operation at 88,600 rpm and for an impeller inlet temperature of 60° F are as follows:

1) Blade safety factor is 2.50 to minimum 0.2-percent yield stress.

2) Disk safety factors are 1.10 to minimum 0.2-percent yield stress and 1.25 to minimum ultimate stress.

The weight of the impeller is 5.24 pounds, and the mass moment of inertia is 0.0347 lb-in.-sec^2.

Figures 14 through 23 present the results of stress and vibration analyses for the MF-2 impeller.

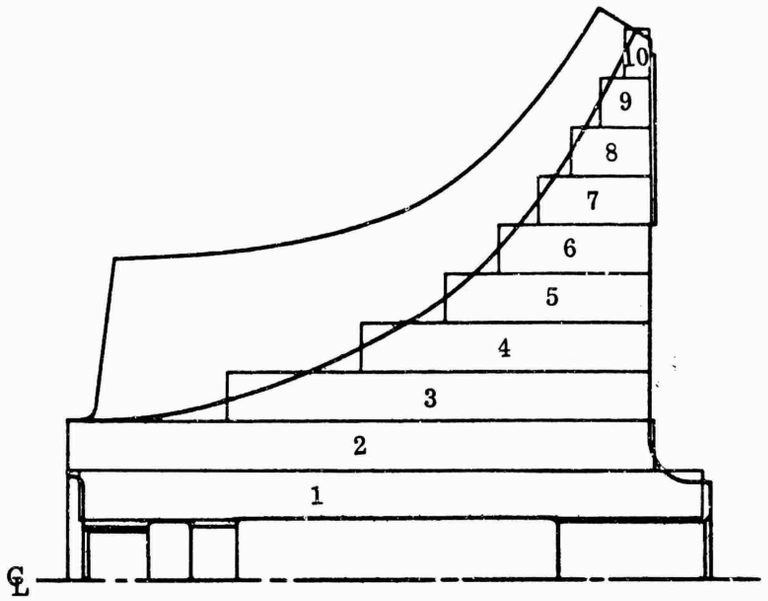


Figure 14. Disk and Blade Profile of MF-2.

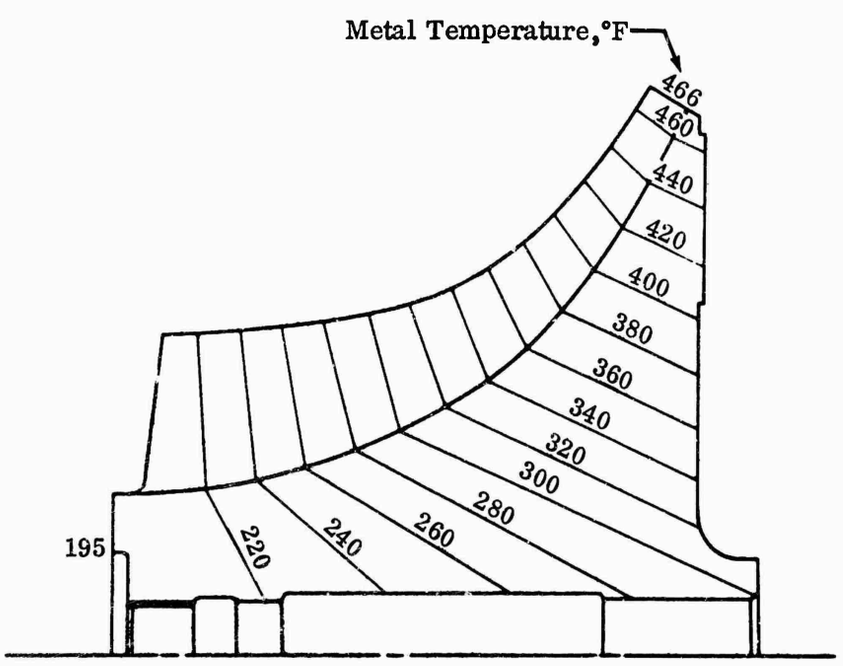


Figure 15. Temperature Distribution of MF-2.

Computer Input Data:

Title:

MF-2 Impeller Blade Natural Frequencies

Number of Drawing Stations	Material Const.		Blade Profile	Number of Nodes at General Z Station	Required Number of Modes
	Density γ	Modulus of Elasticity E			
	(lb/in.^{3})	(psi)			
15	0.160	16,000,000	Linear	5	5

Computer Output Data:

Mode No.	Frequency, cps
1	5,821
2	11,970
3	16,340
4	20,940
5	22,780

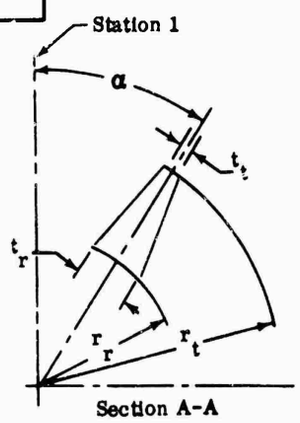
Information From Drawing :

Station No.	Axial Dist. Z	Tip Rad. r_t	Root Rad. r_r	Inclination α	Tip Thickness t_t	Root Thickness t_r
	in.	in.	in.	Degree	in.	in.
1	0	0.910	0.910	0	0.031	0.031
2	0.100	1.806	0.913	5.4	0.050	0.063
3	0.200	1.815	0.919	10.5	0.050	0.093
4	0.392	1.830	0.935	19.4	0.051	0.133
5	0.600	1.847	0.969	27.9	0.053	0.152
6	0.794	1.865	1.015	34.5	0.054	0.163
7	1.000	1.887	1.079	40.8	0.057	0.168
8	1.183	1.912	1.141	45.6	0.056	0.171
9	1.559	1.994	1.294	52.9	0.053	0.169
10	1.965	2.127	1.487	56.7	0.045	0.153
11	2.235	2.338	1.738	58.2	0.040	0.129
12	2.524	2.601	2.030	58.5	0.034	0.107
13	2.773	2.900	2.344	58.5	0.030	0.090
14	2.991	3.219	2.694	58.5	0.025	0.073
15	3.191	3.105	3.105	58.5	0.054	0.054

13 Required Number of Node Distances

Z Distances for Node Stations, (in.)

0	0.10	0.20	0.30	0.50	0.70	0.950	1.2	7.5	7.9
2.3	2.7	3.191							



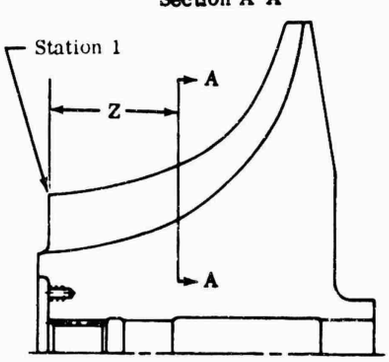


Figure 16. Natural Frequencies of MF-2 Blades.

Computer Input Data:

Title:

MF-2 Impeller - Modified Blade Natural Frequencies

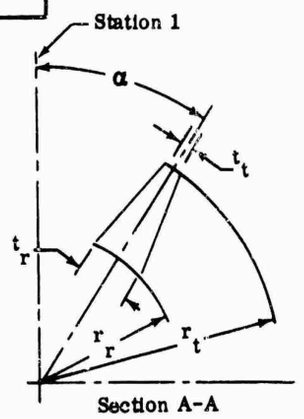
Number of Drawing Stations	Material Const. Density γ (lb/in.^{3})	Material Const. Modulus of Elasticity E (psi)	Blade Profile	Number of Nodes at General Z Station	Required Number of Modes
15	0.160	16,000,000	Linear	5	5

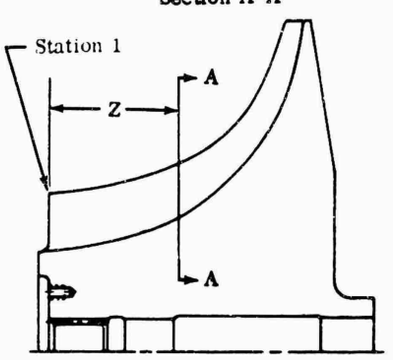
Computer Output Data:

Mode No.	Frequency, cps
1	5.970
2	11.760
3	16.240
4	19.260
5	21.870

Information From Drawing :

Station No.	Axial Dist. Z (in.)	Tip Rad. r_t (in.)	Root Rad. r_r (in.)	Inclination α (Degree)	Tip Thickness t_t (in.)	Root Thickness t_r (in.)
1	0	0.910	0.910	0	0.031	0.031
2	0.100	1.361	0.913	5.4	.041	0.063
3	0.200	1.815	0.919	10.5	0.050	0.093
4	0.392	1.830	0.935	19.4	0.051	0.133
5	0.600	1.847	0.969	27.9	0.053	0.152
6	0.794	1.865	1.015	34.5	0.054	0.163
7	1.000	1.887	1.079	40.8	0.057	0.168
8	1.183	1.912	1.141	45.6	0.056	0.171
9	1.559	1.994	1.294	52.9	0.053	0.169
10	1.905	2.127	1.487	56.7	0.045	0.153
11	2.235	2.338	1.738	58.2	0.040	0.129
12	2.524	2.601	2.030	58.5	0.034	0.107
13	2.773	2.900	2.344	58.5	0.030	0.090
14	2.991	3.219	2.694	58.5	0.025	0.073
15	3.191	3.105	3.195	58.5	0.054	0.054
13	Required Number of Node Distances					





Z Distances for Node Stations, (in.)

0	0.10	0.20	0.30	0.50	0.70	0.95	1.20	1.50	1.90
2.30	2.70	3.191							

Figure 17. Revised Natural Frequencies of MF-2 Blades.

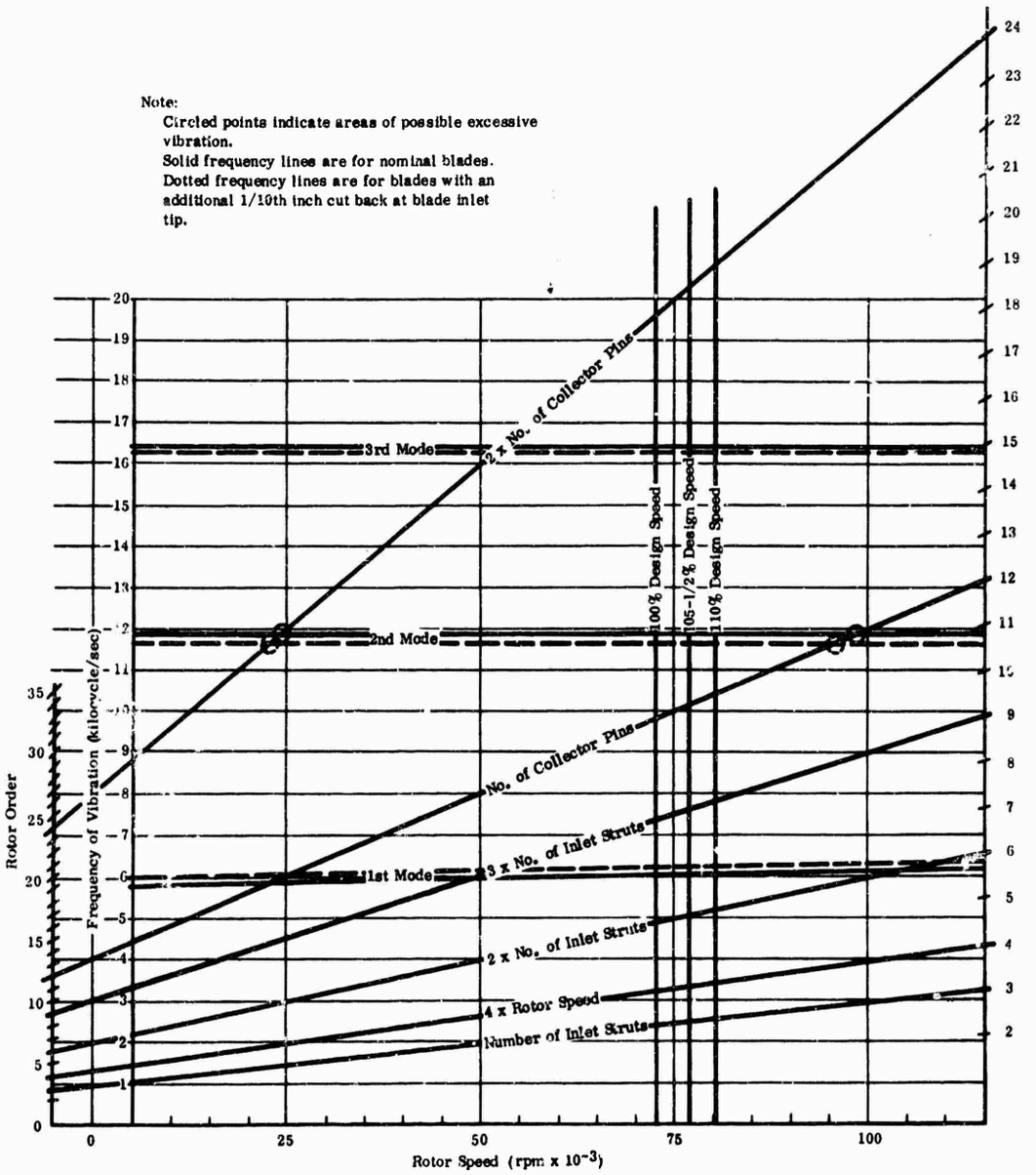
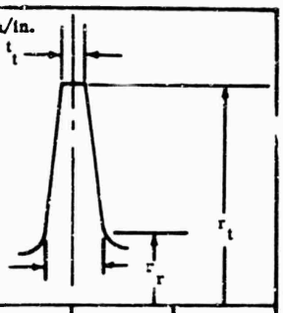


Figure 18. Campbell Diagram for MF-2.

Radial Flow Blade Root Stress, Force/in., Weight/in., and Mass Moment of Inertia/in.



Material: Titanium, 6Al-4V $\omega = 0.1047 \times N$ radians/sec^2

Speed, N = 80,300 rpm (10% overspeed) Density, $\gamma = 0.160$ lb/in.^{3}

$g = 386$ in./sec^2

Blade Station No.			2	3	5	9	10	12	14
1	r_t	in.	1.807	1.816	1.848	1.995	2.127	2.601	3.219
2	r_r	in.	0.913	0.918	0.969	1.295	1.488	2.030	2.694
3	t_t	in.	0.050	0.050	0.053	0.053	0.045	0.034	0.025
4	t_r	in.	0.063	0.093	0.152	0.169	0.153	0.107	0.073
5	r_t^2	①^2	3.2652	3.2979	3.4151	3.9800	4.5241	6.7652	10.3620
6	r_t^3	① x ⑤	5.9003	5.9869	6.3111	7.9401	9.6228	17.5963	33.3553
7	r_r^2	②^2	0.8336	0.8427	0.9390	1.6770	2.2141	4.1209	7.2576
8	r_r^3	② x ⑦	0.7610	0.7736	0.9099	2.1717	3.2946	8.3654	19.5521
9	$r_t - r_r$	① - ②	0.8940	0.898	0.879	0.700	0.639	0.571	0.525
10	$r_t^2 - r_r^2$	⑤ - ⑦	2.4316	2.4552	2.4761	2.303	2.310	2.6443	3.1044
11	$r_t^3 - r_r^3$	⑥ - ⑧	5.1393	5.2153	5.4012	5.7684	6.3282	9.2309	13.8032
12	$t_r - t_t$	④ - ③	0.013	0.043	0.099	0.116	0.108	0.0730	0.048
13	$\frac{t_r - t_t}{r_r - r_r}$	⑫ ÷ ⑨	0.0145	0.0479	0.1126	0.1657	0.1690	0.1278	0.0914
14		⑬ x ②	0.0132	0.0440	0.1091	0.2146	0.2515	0.2594	0.2462
15		④ + ⑭	0.0762	0.1370	0.2611	0.3836	0.4045	0.3664	0.3192
16		⑮ x ⑩ ÷ 2	0.0926	0.1681	0.3233	0.4417	0.4672	0.4844	0.4955
17		⑬ x ⑪ ÷ 3	0.0248	0.0833	0.2027	0.3186	0.3565	0.3932	0.4205
18		⑯ - ⑰	0.0678	0.0848	0.1206	0.1231	0.1107	0.0912	0.0750
19	F_r'	$\frac{\gamma\omega^2}{g}$ ⑱	1,990	2,480	3,530	3,610	3,240	2,670	2,200
20	S_{root}	⑲ + ④	31,530	26,720	23,250	21,340	21,200	24,970	30,100
21	r_t^4	① x ⑥	10.6616	10.8758	11.6629	15.8405	20.4677	45.7680	107.3717
22	r_r^4	② x ⑧	0.6948	0.7102	0.8808	2.8124	4.9024	16.9818	52.6734
23	$r_t^4 - r_r^4$	㉑ - ㉒	9.9670	10.1656	10.7821	13.0281	15.5053	28.7862	54.6973
24	$t_r + t_t$	③ + ④	0.113	0.143	0.205	0.222	0.198	0.141	0.098
25		⑯ x ⑪ ÷ 3	0.1305	0.2382	0.4701	0.7376	0.8533	1.1274	1.4687
26		㉓ x ㉓ ÷ 4	0.0361	0.1217	0.3035	0.5397	0.6576	0.9197	1.2498
27		㉕ - ㉖	0.0944	0.1165	0.1666	0.1979	0.1957	0.2077	0.2189
28	$I' \times 10^4$	$\frac{\gamma}{g}$ ㉗	0.39	0.48	0.69	0.83	0.81	0.86	0.91
29		⑨ x ㉔	0.1010	0.1284	0.1862	0.2314	0.1265	0.0805	0.0535
30	$W' \times 10^4$	$\frac{\gamma}{2}$ ㉙	0.81	1.03	1.44	1.24	1.01	0.84	0.41

Figure 19. Blade Stress Calculations for MF-2.

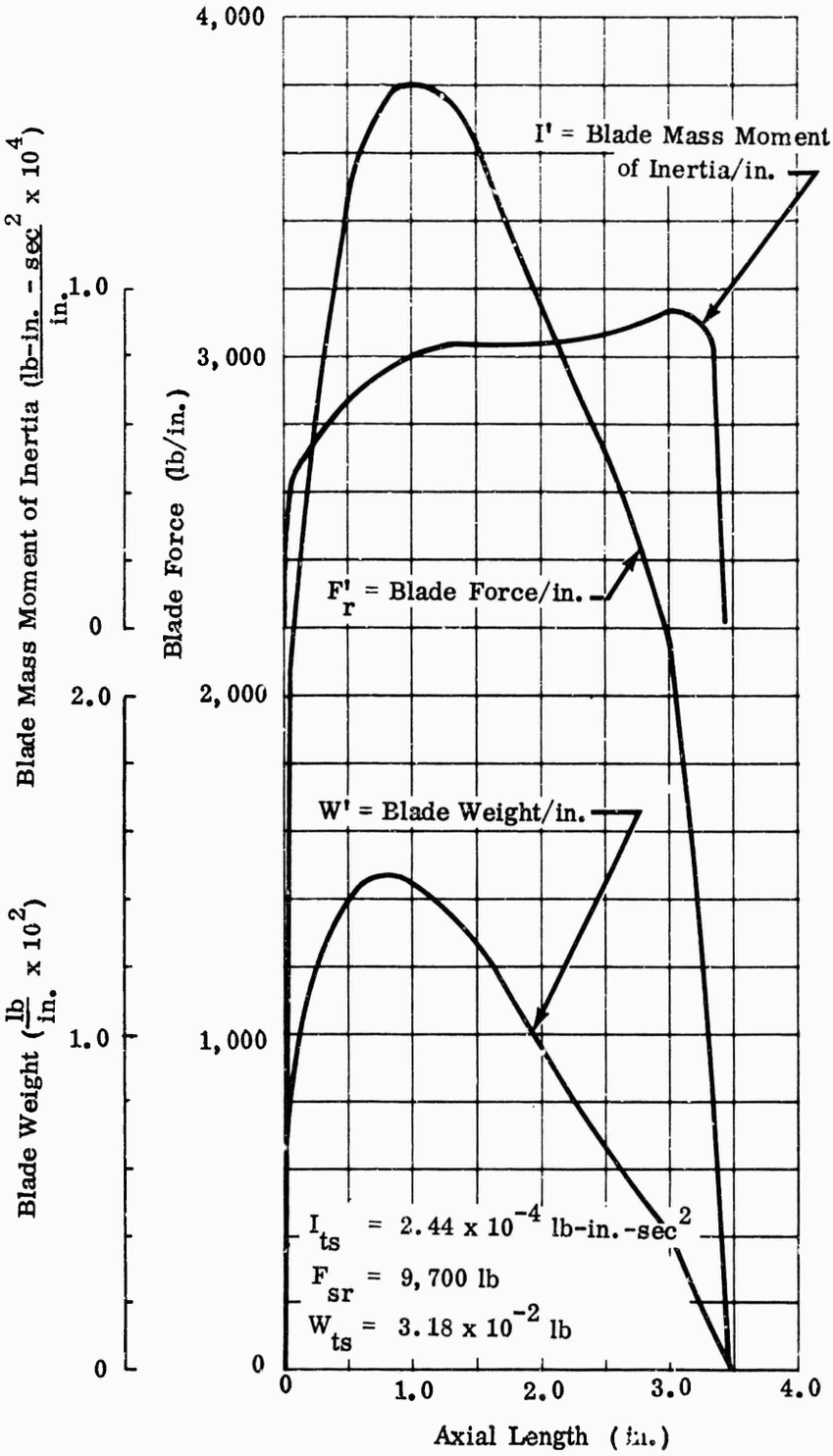


Figure 20. MF-2 Impeller-Blade Force, Weight, and Inertia.

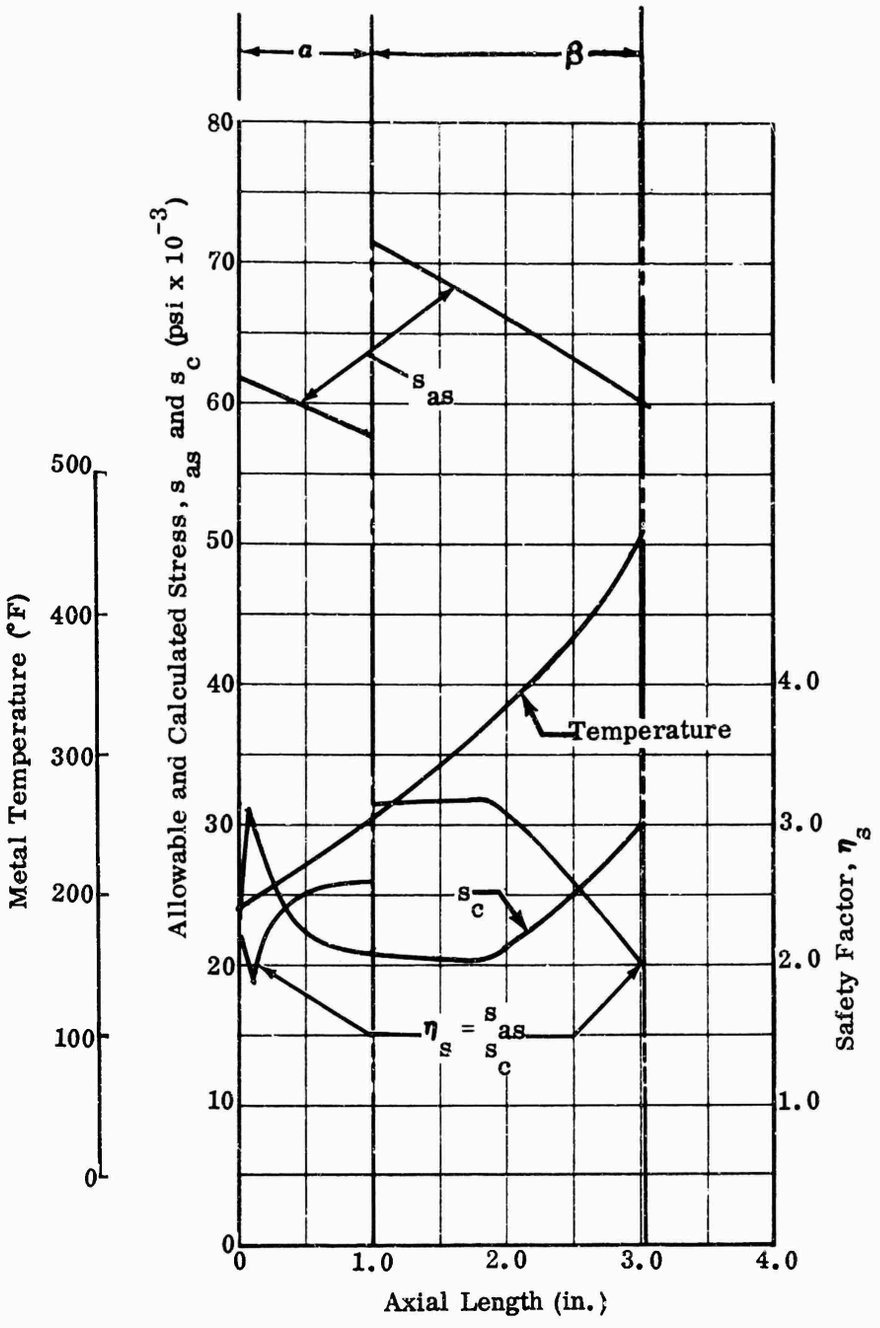
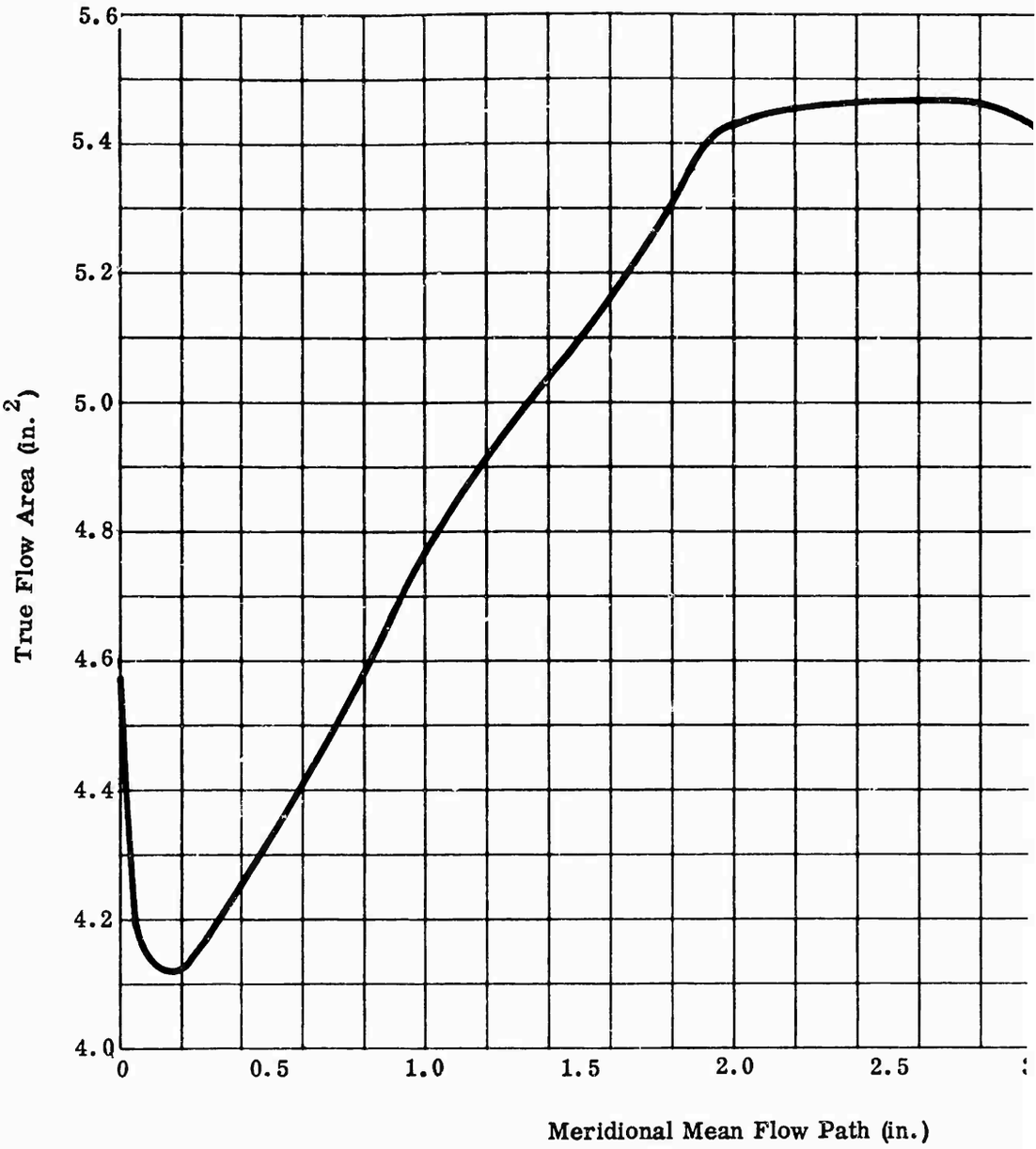


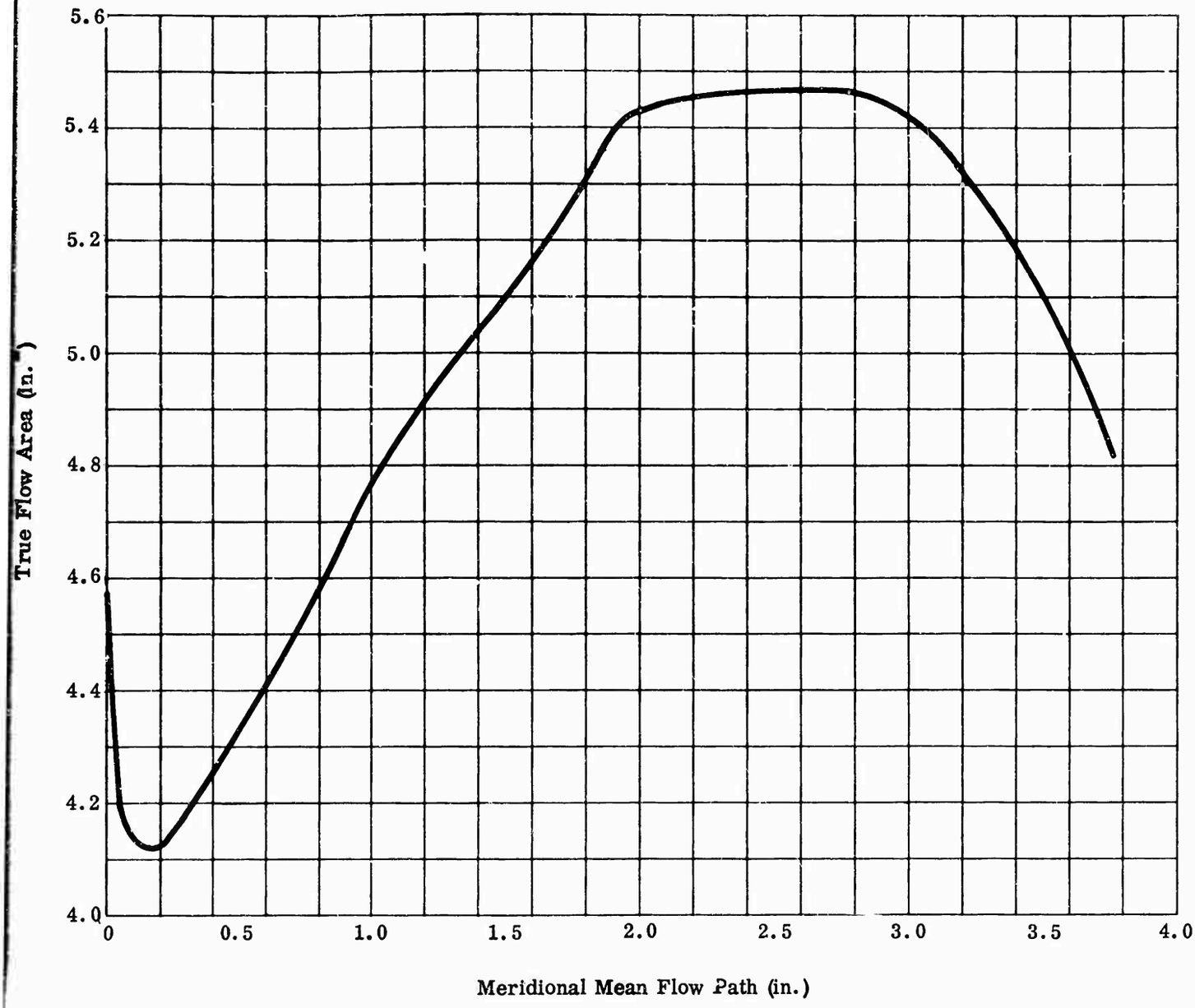
Figure 21. Blade-Root Stress, Temperature, and Safety Factor for MF-2.

Flow Area Calculation											
Sec.	h	r_1	r_2	A_T $\pi h (r_1 + r_2)$	h'	t_t	t_r	A_B $\frac{N}{2} h' (t_t + t_r)$	A' $(A_T - A_B)$	ϕ	C
A	0.909	1.819	0.910	7.793					7.795	54.00	0.
B	0.911	1.826	0.914	7.842	0.782	0.051	0.073	0.970	6.872	53.00	0.
C	0.915	1.834	0.920	7.917	0.894	0.050	0.100	1.341	6.576	51.20	0.
D	0.911	1.849	0.942	7.988	0.891	0.050	0.138	1.675	6.313	47.70	0.
E	0.852	1.880	1.038	7.810	0.832	0.053	0.165	1.814	5.996	40.20	0.
F	0.763	1.921	1.177	7.426	0.743	0.057	0.172	1.702	5.724	32.50	0.
G	0.670	1.987	1.356	7.037	0.650	0.054	0.165	1.424	5.613	23.65	0.
H	0.570	2.089	1.591	6.590	0.550	0.048	0.143	1.051	5.539	12.35	0
I	0.475	2.257	1.889	6.1869	0.455	0.041	0.117	0.719	5.468	4.30	0
J	0.404	2.489	2.218	5.974	0.384	0.037	0.097	0.515	5.459	0	1
K	0.340	2.767	2.562	5.692	0.320	0.032	0.079	0.355	5.337	0	1
L	0.294	2.993	2.831	5.379	0.274	0.029	0.066	0.260	5.119	0	1
M	0.279	3.075	2.933	5.266	0.259	0.028	0.061	0.230	5.036	0	1
N	0.265	3.153	3.020	5.139	0.245	0.027	0.058	0.208	4.931	0	1
O	0.251	3.230	3.105	5.000	0.231	0.025	0.054	0.182	4.813	0	1

Figure 22. Impeller Flow Area of MF-2.

Cos ϕ	A / A' Cos ϕ
0.58779	4.581
0.60182	4.136
0.62660	4.121
0.67301	4.249
0.76380	4.580
0.84339	4.828
0.91601	5.142
0.97686	5.411
0.99719	5.453
1.0000	5.459
1.0000	5.337
1.0000	5.119
1.0000	5.036
1.0000	4.931
1.0000	4.813




5.6
5.4
5.2
5.0
4.8
4.6
4.4
4.2
4.0
True Flow Area (in.²)
0
0.5
1.0
1.5
2.0
2.5
3.0
3.5
4.0
Meridional Mean Flow Path (in.)

Disk Tangential Force, Cross-Sectional Area, Weight, Mass Moment of Inertia, and Failure Load

Material: Titanium 6Al-4V

Speed, N = 80,300 rpm (10 % overspeed)

Number of Blades, n = 20

$I_{ts} = 2.44 \times 10^{-4}$ lb-in.-sec^2

$F_{sr} = 9700$ lb

$W_{ts} = 3.18 \times 10^{-2}$ lb

ω 0.1047N radians/sec

Density, γ 0.160 lb/in.^{3}

g 386 in./sec^2

								Failure Stress 0.2% Yield			Failure Stress Ultimate		
	(1)	(2)	(3)	(4)	(5)	(6)	(7)	(8)	(9)	(10)	(8)	(9)	(10)
Segment No.	r	Δr	t	(2) x (3)	(1) x (4)	(1) x (5)	(1) x (6)	T	S_f	(4) x (9)	T	S_f	(4) x (9)
	in.	in.	in.	in.^{2}	in.^{3}	in.^{4}	in.^{5}	F	psi	lb	F	psi	lb
1	0.470	0.275	3.710	1.0203	0.4795	0.2254	0.1059	255	91,600	93,459	255	103,300	105,397
2	0.745		3.495	0.9611	0.7160	0.5334	0.3974	277	90,000	86,499	277	102,000	98,032
3	1.020		2.530	0.6958	0.7097	0.7239	0.7384	300	88,200	61,370	300	100,00	70,137
4	1.295		1.730	0.4758	0.6162	0.7980	1.0334	327	86,600	41,204	327	99,300	47,247
5	1.570		1.230	0.3383	0.5311	0.8338	1.3091	353	85,000	28,756	353	98,000	33,153
6	1.845		0.915	0.2516	0.4642	0.8564	1.5801	376	83,800	21,084	376	96,900	24,3 0
7	2.120		0.680	0.1870	0.3964	0.8404	1.7816	397	82,700	15,465	397	96,000	17,952
8	2.395		0.480	0.1320	0.3161	0.7571	1.8131	420	81,500	10,758	420	95,500	12,606
9	2.670		0.310	0.0853	0.2278	0.6082	1.6239	441	80,500	6,867	441	94,000	8,018
10	2.945	0.275	0.150	0.0413	0.1216	0.3581	1.0546	461	79,800	3,296	461	93,100	3,845

A_{td}	2Σ (4)	8.3770	in.^{2}
F_{td}	$[(2\gamma\omega^2 \div g]\Sigma$(6)	382.930	lb
F_{ts}	$F_{sr} \times n \div \pi$	1.800	lb
F_{tw}	$F_{td} + F_{ts}$	444.730	lb
I_{td}	$[(2\pi\gamma) \div g]\ \Sigma$(7)	0.02978	lb-in-sec^2
I_{tw}	$I_{td} + nI_{ts}$	0.0347	lb-in-sec^2
W_{td}	$2\pi\gamma\Sigma$(5)	4.60287	lb
W_{tw}	$W_{td} + nW_{ts}$	5.24	lb
η_y	$F_{fy} \div F_{tw}$	1.34	-
η_u	$F_{fu} \div F_{tw}$	1.53	-
S_{tan}	$F_{tw} \div A_{td}$	53,100	psi

S_{tan} Average Tangential Disk Stress

$F_{fy} = 1.62 \times \Sigma$(10) = 597,388

$F_{fu} = 1.62 \times \Sigma$(10) = 681,643

S_f Failure Stress at Temperature, T

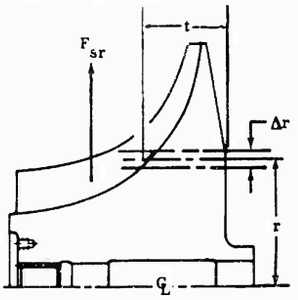


Figure 23. Disk Calculations for MF-2.

4.0 MF-3 IMPELLER ANALYSIS

The impeller is satisfactory for steady-state operation. Analysis of the configuration defined in Figure 26 indicated that excessive blade vibration might be encountered. The leading edge of the impeller blade was modified as defined in Figure 27. Frequency calculations were made for both configurations to serve as a guide for leading edge modifications. The circled points on Figure 28 indicate the regions of concern.

The blade stress analysis was based on dimensions of the preliminary design. These dimensions differ from those used in the blade frequency analyses (Figures 26 and 27) because the blade dimensions were modified slightly to change the frequencies to the proper range. The blade stresses were not recalculated for the new blade configurations because a check of the most highly stressed station showed that the revised dimensions produced lower stresses.

The minimum safety factors for steady-state operation at 65,000 rpm and for an impeller inlet temperature of 60° F are as follows:

1) Blade safety factor is 3.07 to minimum 0.2-percent yield stress including ± 20,000 psi vibratory stress.

2) Disk safety factors are 1.80 to minimum 0.2-percent yield stress and 2.02 to minimum ultimate stress.

The minimum safety factors for momentary operation at 82,600 rpm and an impeller inlet temperature of 60° F are as follows:

1) Blade safety factor is 2.68 to minimum 0.2-percent yield stress.

2) Disk safety factors are 1.11 to minimum 0.2-percent yield stress and 1.25 to minimum ultimate stress.

The weight of the impeller is 5.30 pounds, and the mass moment of inertia is 0.0450 lb-in.-sec^2.

Figures 24 through 33 present the results of stress and vibration analyses for the MF-3 impeller.

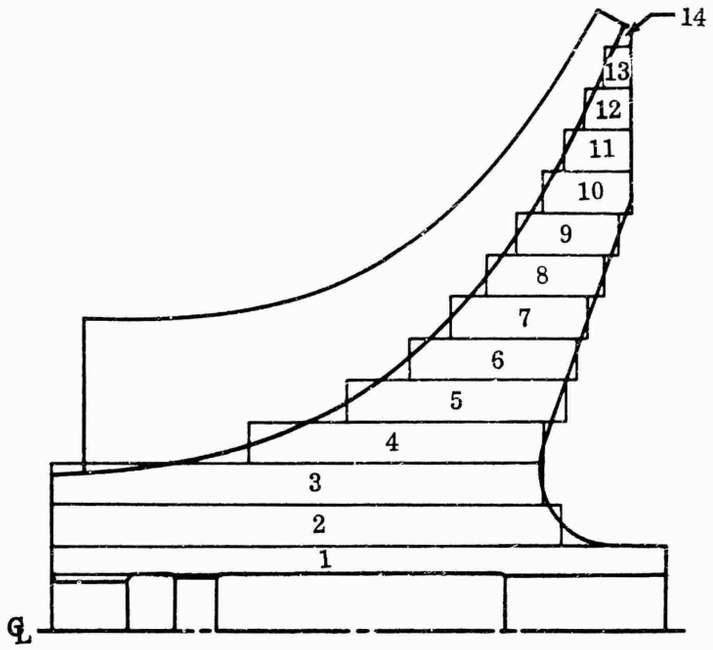


Figure 24. Disk and Blade Profile of MF-3.

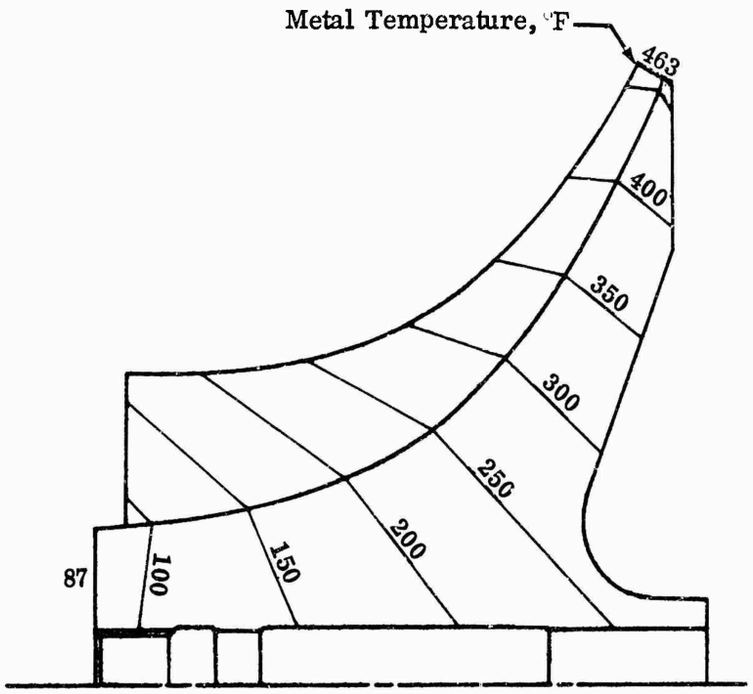


Figure 25. Temperature Distribution of MF-3.

Computer Input Data:

Title:

MF-3 Impeller Blade Natural Frequencies

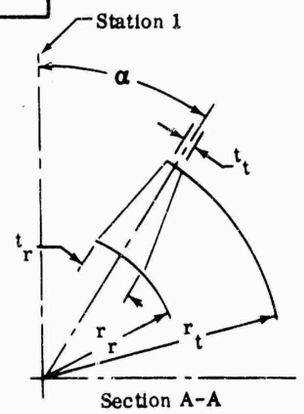
Number of Drawing Stations	Material Const.		Blade Profile	Number of Nodes at General Z Station	Required Number of Modes
	Density γ	Modulus of Elasticity E			
	$(lb/in.^3)$	(psi)			
15	0.160	15,870,000	Linear	5	5

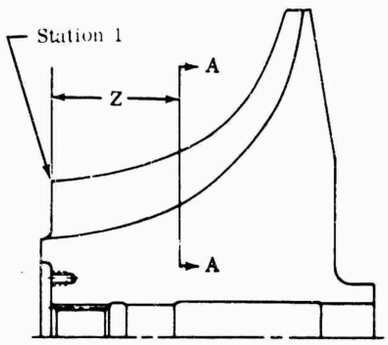
Computer Output Data

Mode No.	Frequency, cps
1	5.361
2	10.778
3	15.318
4	16.587
5	20.064

Information From Drawing :

Station No.	Axial Dist. Z	Tip Rad. r_t	Root Rad. r_r	Inclination α	Tip Thickness t_t	Root Thickness t_r
	in.	in.	in.	Degree	in.	in.
1	0.000	1.800	0.910	0.00	0.044	0.043
2	0.200	1.800	0.932	8.86	0.051	0.098
3	0.400	1.800	0.955	16.34	0.054	0.133
4	0.599	1.804	0.983	22.43	0.054	0.150
5	0.797	1.819	1.020	27.46	0.054	0.156
6	1.182	1.888	1.131	34.60	0.055	0.158
7	1.565	2.017	1.300	38.54	0.052	0.166
8	1.912	2.194	1.515	39.68	0.052	0.156
9	2.232	2.424	1.788	39.68	0.048	0.139
10	2.511	2.690	2.103	39.68	0.042	0.121
11	2.754	3.000	2.456	39.68	0.036	0.104
12	2.957	3.306	2.813	39.68	0.031	0.086
13	3.154	3.573	3.214	39.68	0.029	0.067
14	3.204	3.543	3.317	39.68	0.038	0.063
15	3.290	3.493	3.493	39.68	0.054	0.054
13	Required Number of Node Distances					





Z Distances for Node Stations, (in.)

0.0	0.1	0.2	0.3	0.5	0.7	0.95	1.2	1.6	2.0
2.4	2.8	3.29							

Figure 26. Natural Frequencies of MF-3 Blades.

Computer Input Data:

Title:

MF-3 Impeller Modified Blade Natural Frequencies

(.03" cut back)

Number of Drawing Stations	Material Const.		Blade Profile	Number of Nodes at General Z Station	Required Number of Modes
	Density γ	Modulus of Elasticity E			
	($lb/in.^3$)	(psi)			
16	0.160	15,879,000	Linear	5	5

Computer Output Data:

Mode No.	Frequency, cps
1	5.644
2	11.760
3	17.176
4	18.633
5	21.624

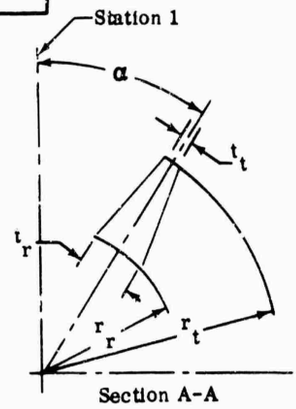
Information From Drawing :

Station No.	Axial Dist. Z	Tip Rad. r_t	Root Rad. r_r	Inclination α	Tip Thickness t_t	Root Thickness t_r
	in.	in.	in.	Degree	in.	in.
1	0.000	0.910	0.910	0.00	0.043	0.043
2	0.030	1.800	0.914	1.40	0.046	0.053
3	0.200	1.800	0.932	8.86	0.051	0.098
4	0.400	1.800	0.955	16.34	0.054	0.133
5	0.599	1.804	0.983	22.43	0.051	0.150
6	0.797	1.819	1.020	27.46	0.054	0.156
7	1.182	1.888	1.131	34.60	0.055	0.158
8	1.565	2.017	1.300	38.54	0.052	0.166
9	1.912	2.194	1.515	39.68	0.052	0.156
10	2.232	2.424	1.788	39.68	0.048	0.139
11	2.511	2.690	2.103	39.68	0.042	0.121
12	2.754	3.000	2.456	39.68	0.036	0.103
13	2.957	3.306	2.813	39.68	0.031	0.086
14	3.154	3.573	3.214	39.68	0.029	0.067
15	3.204	3.543	3.317	39.68	0.038	0.063
16	3.290	3.493	3.493	39.68	0.054	0.054

13 Required Number of Node Distances

Z Distances for Node Stations, (in.)

0.0	0.03	0.1	0.2	0.3	0.5	0.8	1.2	1.6	2.0
2.4	2.8	3.29							



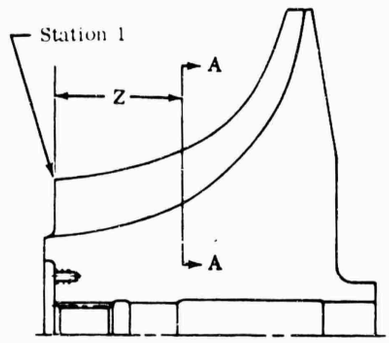


Figure 27. Natural Frequencies of Modified MF-3 Blades.

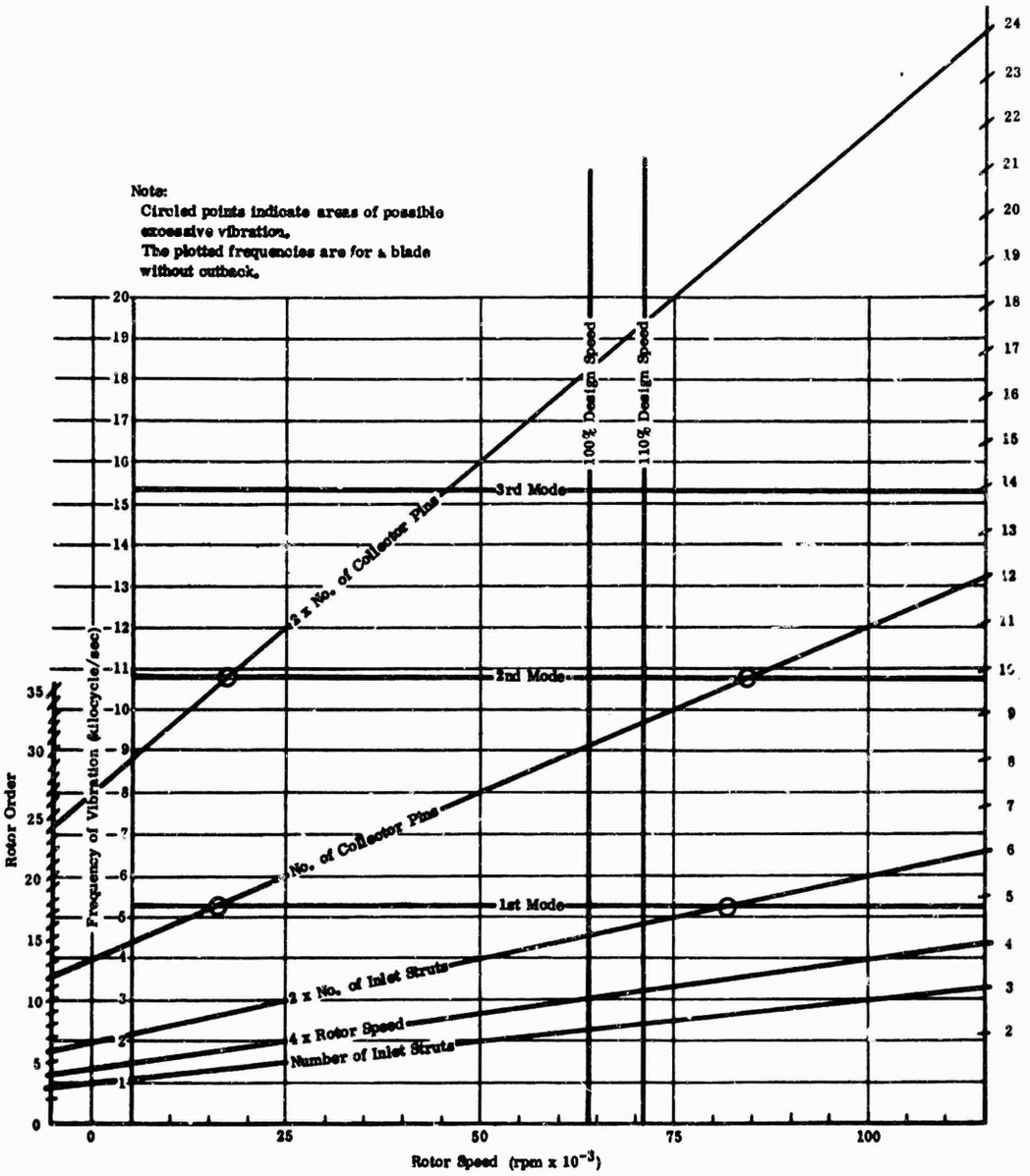
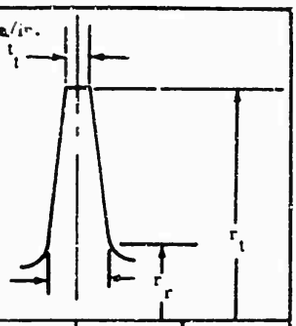


Figure 28. Campbell Diagram for MF-3.

Radial Flow Blade Root Stress, Force/in., Weight/in., and Mass Moment of Inertia/in.



Material: Titanium, 6Al-4V

Speed, N = 65,000 rpm Density, γ = 0.160 lb/in.^{3}

Blade Station No.			1	4t	7t	10t	13t	14	
Computer Input									
1	r_t	in.	1.800	1.801	1.964	2.541	3.472	3.543	
2	r_r	in.	0.910	0.977	1.232	1.928	3.030	3.315	
3	t_t	in.	0.044	0.054	0.052	0.045	0.028	0.038	
4	t_r	in.	0.049	0.147	0.164	0.130	0.074	0.062	
Computer Output									
1	F'	lb /in.	1,010	2,110	2,330	2,250	1,390	750	
2	S_{root}	lb /in.^{2}	23,460	14,340	14,210	17,310	18,820	12,080	
3	I'x 10^4	$\frac{\text{lb-in.-sec}^2}{\text{in.}}$	0.31	0.62	0.78	1.07	0.97	0.55	
4	W'x 10^2	lb /in.	0.62	1.32	1.26	0.86	0.36	0.18	

Figure 29. Blade Stress Calculations for MF-3.

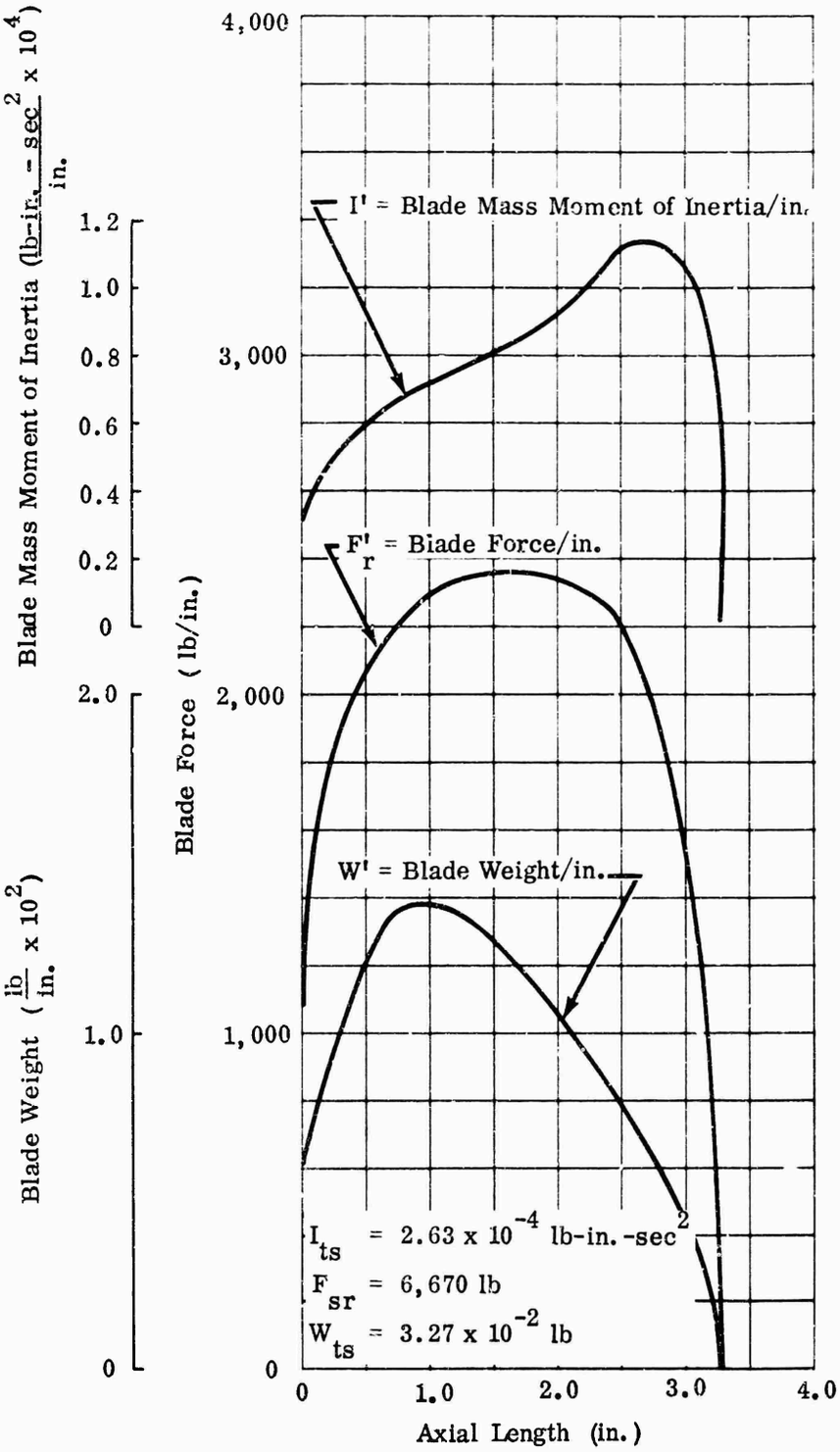


Figure 30. MF-3 Impeller-Blade Force, Weight, and Inertia.

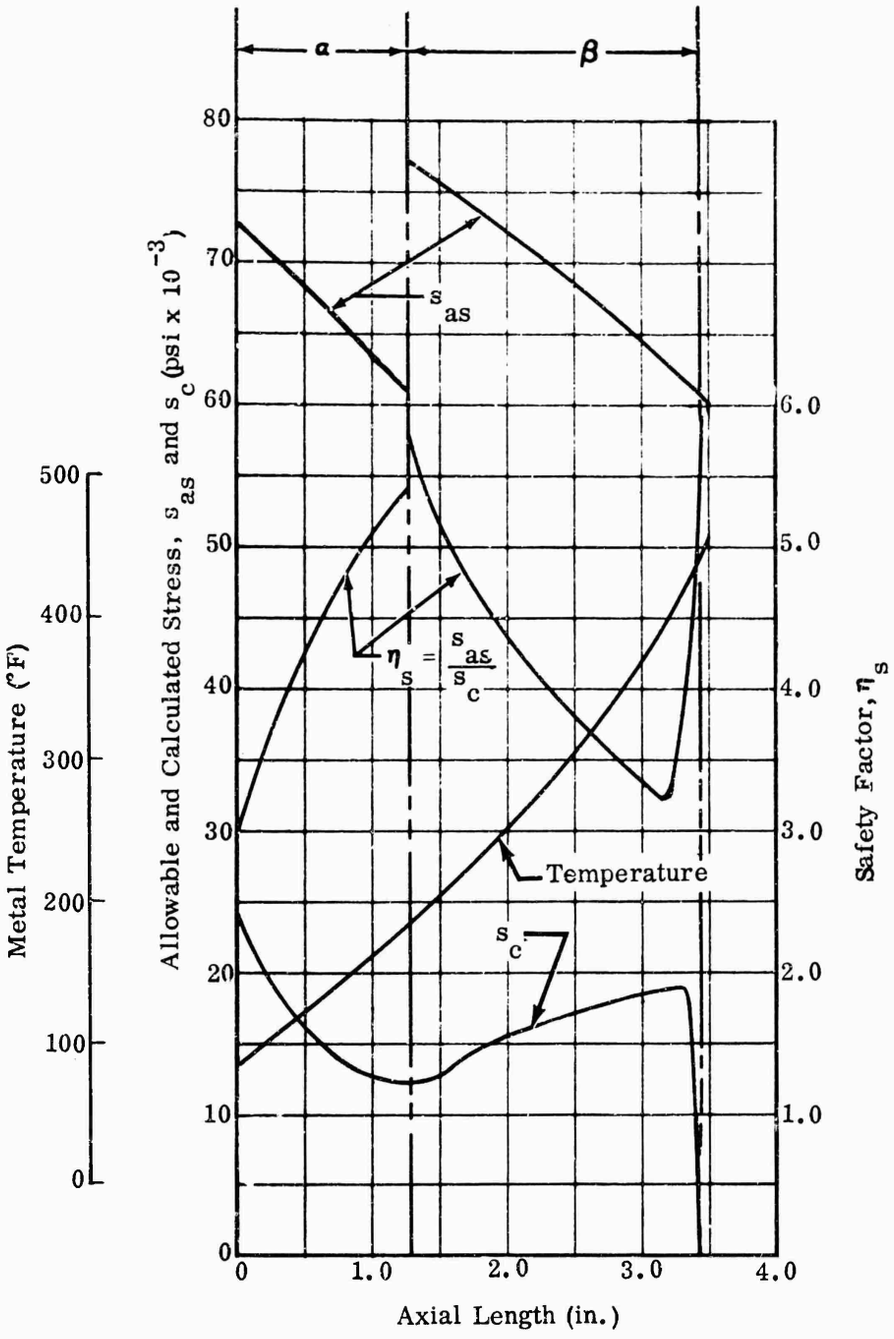
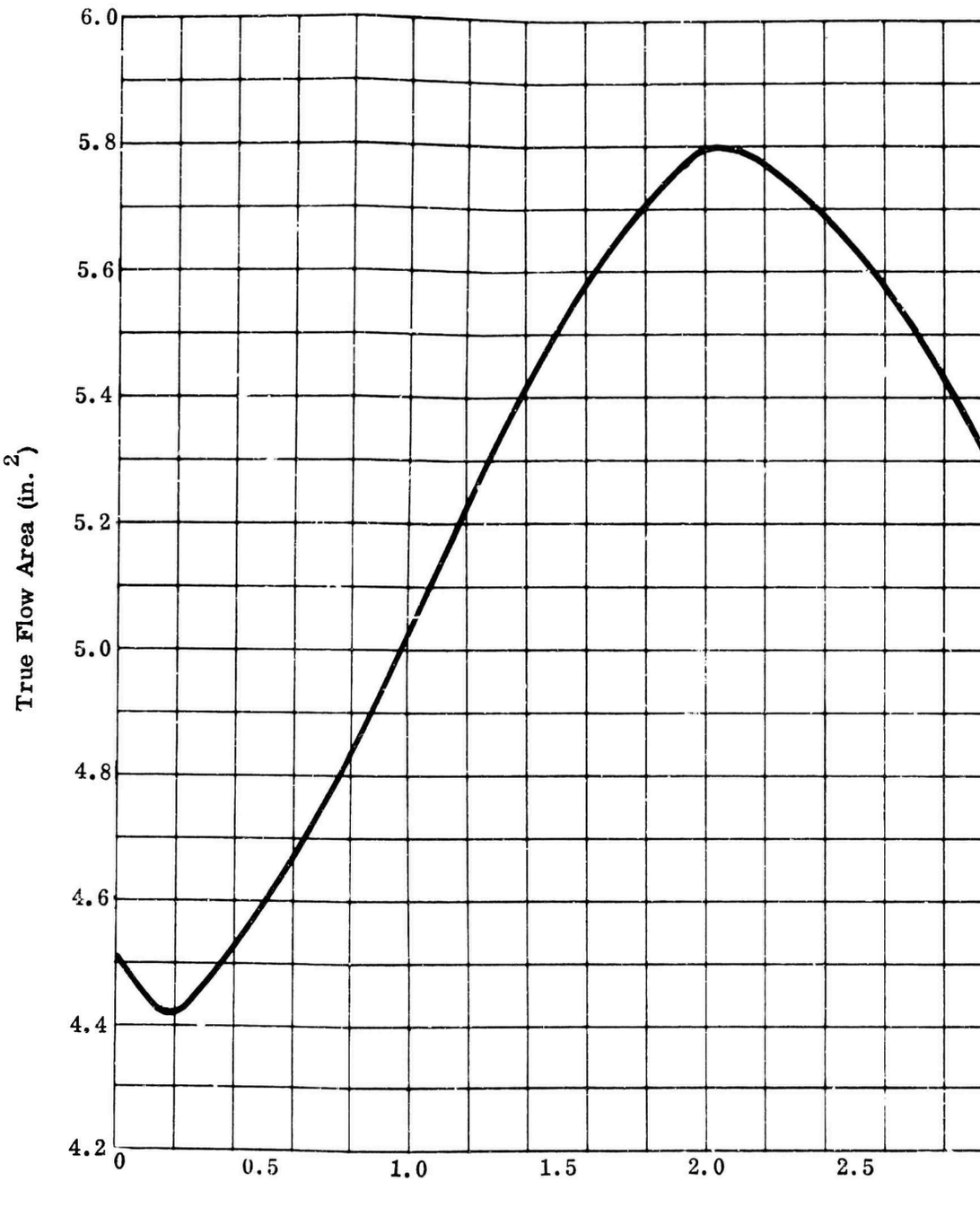


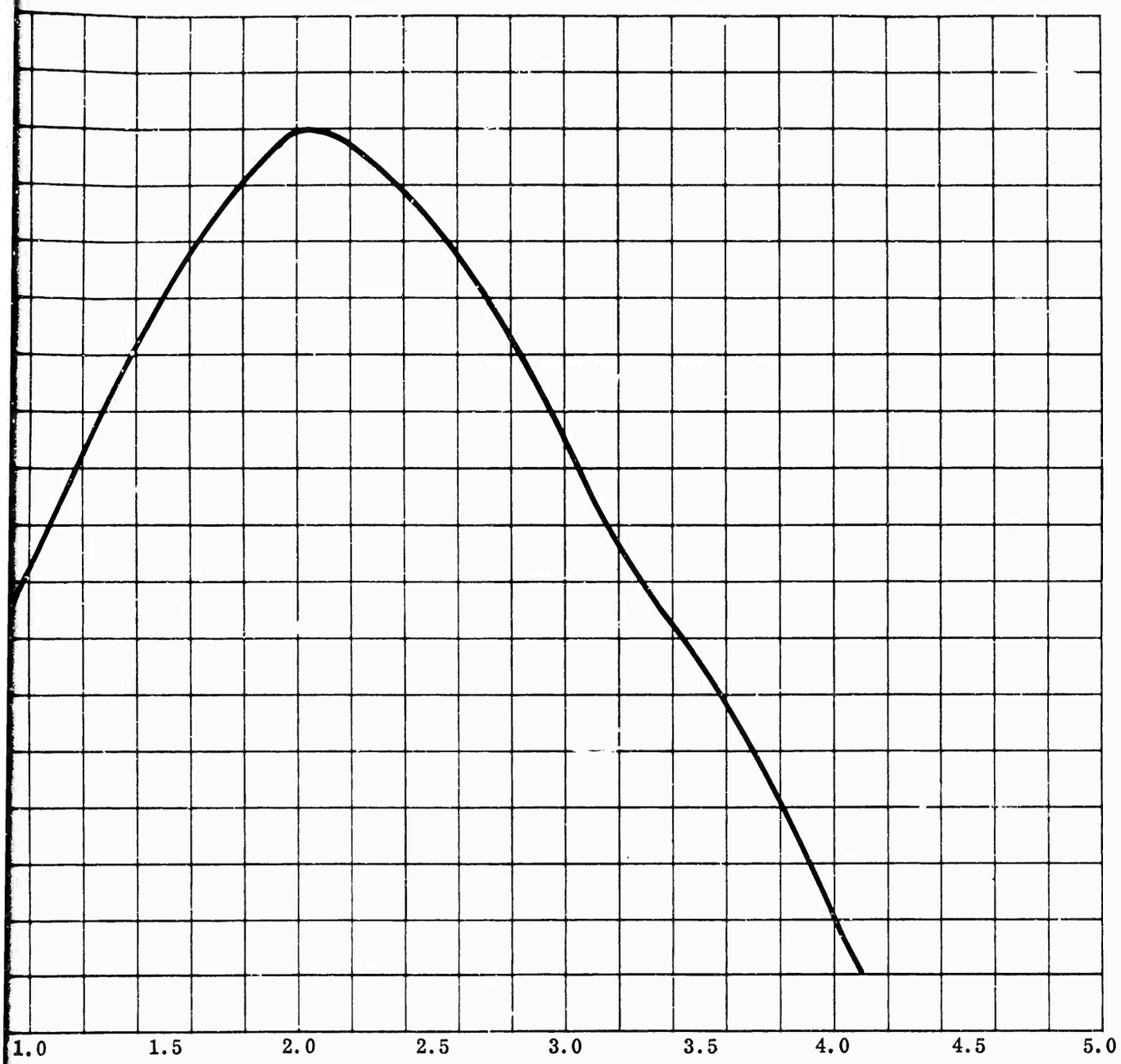
Figure 31. Blade-Root Stress, Temperature, and Safety Factor for MF-3.

Flow Area Calculation											
Sec.	h	r_1	r_2	A_T $\pi h (r_1 + r_2)$	h'	t_t	t_r	A_B $\frac{N}{2} h' (t_t+t_r)$	A' $(A_T - A_B)$	ϕ	
A	0.910	1.820	0.910	7.805	0.890	0.044	0.043	0.774	7.031	50.0	0.
B	0.888	1.820	0.932	7.677	0.868	0.049	0.101	1.302	6.375	46.1	0.
C	0.863	1.820	0.958	7.530	0.843	0.053	0.135	1.585	5.945	40.4	0.
D	0.835	1.821	0.991	7.380	0.815	0.054	0.152	1.679	5.701	35.1	0.
E	0.805	1.830	1.037	7.251	0.785	0.054	0.156	1.649	5.602	30.6	0.
F	0.739	1.883	1.181	7.110	0.719	0.055	0.162	1.560	5.550	20.0	0.
G	0.664	1.985	1.391	7.045	0.644	0.052	0.164	1.391	5.654	10.0	0.
H	0.580	2.130	1.655	6.900	0.560	0.051	0.147	1.109	5.791	0	1.
I	0.482	2.326	1.973	6.510	0.462	0.050	0.128	0.822	5.688	0	1.
J	0.391	2.568	2.318	6.000	0.371	0.045	0.109	0.571	5.429	0	1.
K	0.313	2.855	2.680	5.445	0.293	0.039	0.091	0.381	5.064	0	1.
L	0.257	3.181	3.051	5.032	0.237	0.033	0.074	0.254	4.778	0	1.
M	0.210	3.509	3.402	4.560	0.190	0.028	0.059	0.165	4.395	0	1.
N	0.200	3.593	3.493	4.450	0.180	0.026	0.054	0.144	4.306	0	1.

Figure 32. Impeller Flow Area of MF-3.

	Cos ϕ	A / A' Cos ϕ
	0.64279	4.519
	0.69340	4.420
	0.76154	4.527
	0.81815	4.664
	0.86074	4.822
	0.93969	5.215
	0.98481	5.568
	1.0000	5.791
	1.0000	5.688
	1.0000	5.429
	1.0000	5.064
	1.0000	4.778
	1.0000	4.395
	1.0000	4.306




1.0
1.5
2.0
2.5
3.0
3.5
4.0
4.5
5.0
Meridional Mean Flow Path (in.)

Disk Tangential Force, Cross-Sectional Area, Weight,
Mass Moment of Inertia, and Failure Loads

Material: Titanium 6Al-4V

Speed, N = 65,000 rpm

Number of Blades, n = 20

I_{ts} = 2.63 x 10^{-4}

F_{sr} = 6,670 lbs

W_{ts} = 3.27 x 10^{-2} lb

Density, γ = 0.160 lb/in.^{3}

Segment No.	r	r	t	ΔA				Failure Stress 0.2 Yield			Failure Stress Ultimate		
								(8)	(9)	(10)	(8)	(9)	(10)
			(4)					T	S_f	(4) x (9)	T	S_f	(4) x (9)
	in.	in.	in.	in.^{2}				°F	psi	lb	°F	psi	lb
1	0.400	0.160	3.550	0.600				176	98,860	59,300	176	108,800	65,250
2	0.600	0.240	3.110	0.744				181	98,200	73,250	181	108,300	80,850
3	0.840		2.990	0.718				200	96,300	69,100	200	107,000	76,750
4	1.080		1.800	0.432				231	93,600	40,450	231	104,900	45,400
5	1.320		1.330	0.319				264	90,800	29,000	264	102,800	32,800
6	1.560		1.030	0.247				290	89,000	22,000	290	101,200	25,000
7	1.800		0.840	0.202				315	87,300	17,630	315	100,000	20,200
8	2.040		0.720	0.173				338	85,800	14,850	338	98,700	17,080
9	2.280		0.630	0.151				358	84,600	12,780	358	97,700	14,770
10	2.520		0.550	0.132				378	83,600	11,030	378	96,700	12,780
11	2.760		0.420	0.101				398	82,500	8,325	398	95,800	9,670
12	3.000		0.390	0.070				418	81,500	5,700	418	95,000	6,650
13	3.240	0.240	0.170	0.041				438	80,600	3,300	438	94,100	3,860
14	3.420	0.120	0.100	0.012				455	80,000	959	455	93,500	1,120

Computer Calculated

A_{td}	7.89	in.^{2}
F_{td}	287,670	lb
F_{fy}	42,450	lb
F_{tw}	330,120	lb
W_{tw}	5.30	lb
I_{tw}	0.0450	lbs-in-sec^2
$\eta_y = F_{fy} \div F_{tw}$	1.80	—
$\eta_u = F_{fu} \div F_{tw}$	2.02	—
$S_{tan} = F_{tw} \div A_{td}$	41,900	psi
S_{tan} = Average Tangential Disk Stress		

F_{fu} = 1.62 x Σ(10) = 667,650

F_{fy} = 1.62 x Σ(7) = 595,632

S_f Failure Stress at Temperature, T

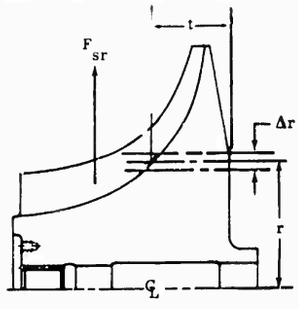


Figure 33. Disk Calculations for MF-3.

5.0 RF-1 IMPELLER ANALYSIS

The Campbell diagram, Figure 37, indicates that this impeller is satisfactory for steady-state operation to 60,000 rpm and for short intervals of operation to 62,700 rpm. Accurate natural frequencies should be determined by test. The impeller is safe for steady-state operation to 62,700 rpm if the natural frequencies are slightly higher or if the amplitudes are small enough to produce vibratory stresses within the design limits.

The calculated minimum safety factors for steady-state operation at 62,700 rpm and for an impeller inlet temperature of 60° F are as follows:

1) Blade safety factor is 2.20 to minimum 0.2-percent yield stress including ± 20,000 psi vibratory stress.

2) Disk safety factors are 1.74 to minimum 0.2-percent yield stress and 1.99 to minimum ultimate stress.

The calculated minimum safety factors for momentary operation at 68,970 rpm and for an impeller inlet temperature of 60° F are as follows:

1) Blade safety factor is 1.82 to minimum 0.2-percent yield stress.

2) Disk safety factors are 1.44 to minimum 0.2-percent yield stress and 1.64 to minimum ultimate stress.

The weight of the impeller is 7.20 pounds, and the mass moment of inertia is 0.0699 lb-in.-sec^2.

Figures 34 through 42 present the results of stress and vibration analyses for the RF-1 impeller.

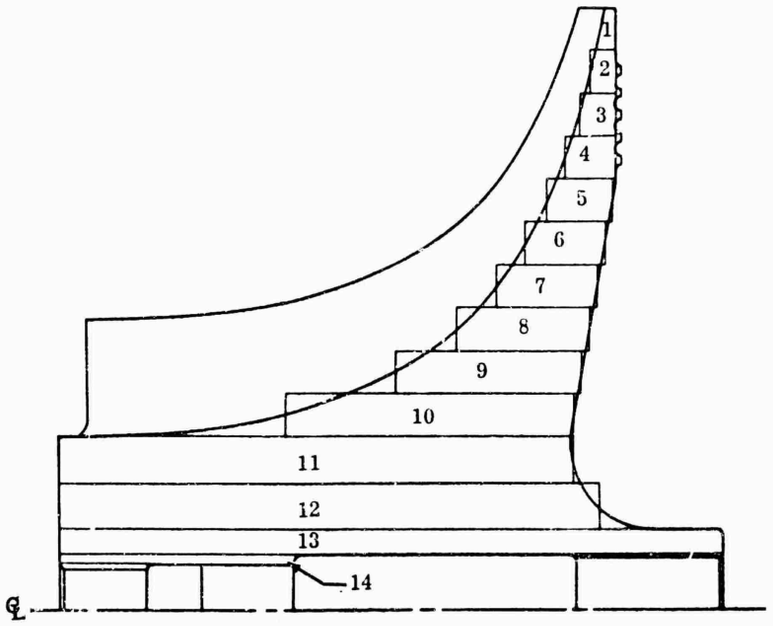


Figure 34. Disk and Blade Profile of RF 1.

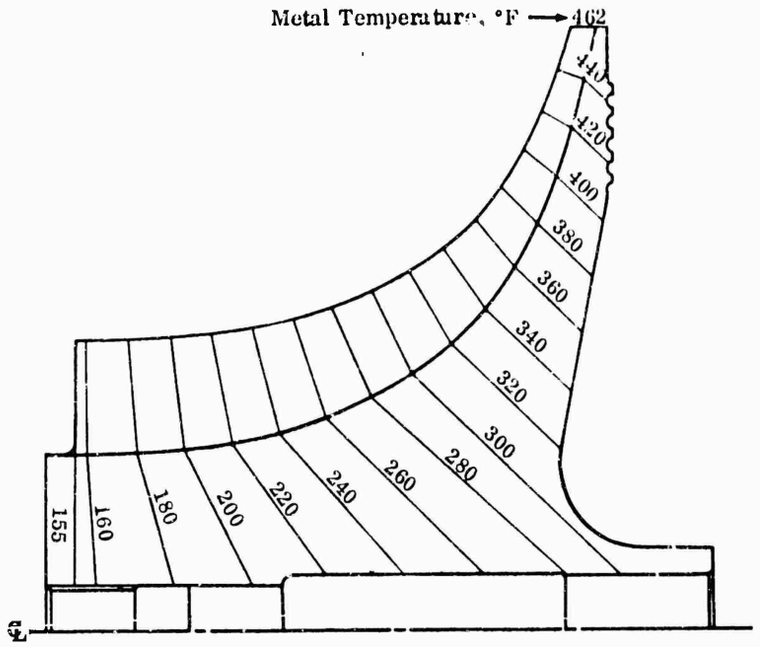


Figure 35. Temperature Distribution of RF-1.

Computer Input Data

Title

RF-1 Impeller Blade Natural Frequencies

Number of Drawing Stations	Material Const.		Blade Profile	Number of Nodes at General Z Station	Required Number of Modes
	Density γ	Modulus of Elasticity E			
	(lb/in.^{3})	(psi)			
17	0.160	16,000,000	Linear	5	5

Information From Drawing :

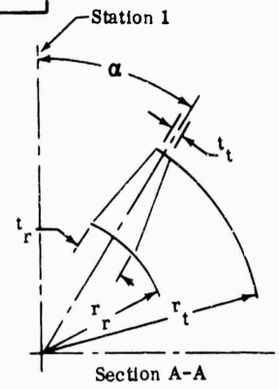
Station No.	Axial Dist. Z	Tip Rad. r_t	Root Rad. r_r	Inclination α	Tip Thickness t_t	Root Thickness t_r
	in.	in.	in.	Degree	in.	in.
1	0	1.918	1.179	0	0.045	0.054
2	0.200	1.951	1.181	8.15	0.043	0.077
3	0.400	1.957	1.187	15.57	0.039	0.110
4	0.800	1.981	1.215	27.73	0.035	0.145
5	1.196	2.031	1.272	37.25	0.031	0.157
6	1.583	2.120	1.361	44.10	0.029	0.165
7	1.960	2.211	1.500	49.55	0.027	0.165
8	2.315	2.111	1.676	52.95	0.026	0.155
9	2.658	2.623	1.909	54.88	0.026	0.136
10	2.913	2.868	2.197	55.61	0.025	0.118
11	3.118	3.197	2.550	55.71	0.025	0.113
12	3.320	3.588	2.888	55.71	0.025	0.161
13	3.385	3.768	3.040	55.71	0.025	0.100
14	3.413	3.936	3.216	55.71	0.025	0.094
15	3.476	4.010	3.347	55.71	0.025	0.090
16	3.562	4.010	3.655	55.71	0.034	0.075
17	3.662	4.010	4.010	55.71	0.045	0.045
18	Required Number of Node Distances					

Z Distances for Node Stations, (in.)

0	0.1	0.2	0.3	0.5	0.7	1.0	1.4	1.8	2.2
2.6	3.0	3.662							

Computer Output Data

Mode No.	Frequency, cps
1	1,892
2	9,785
3	12,755
4	15,196
5	16,360



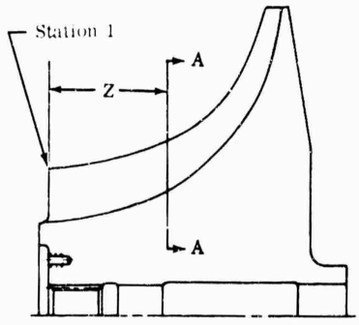


Figure 36. Natural Frequencies of RF-1 Blades.

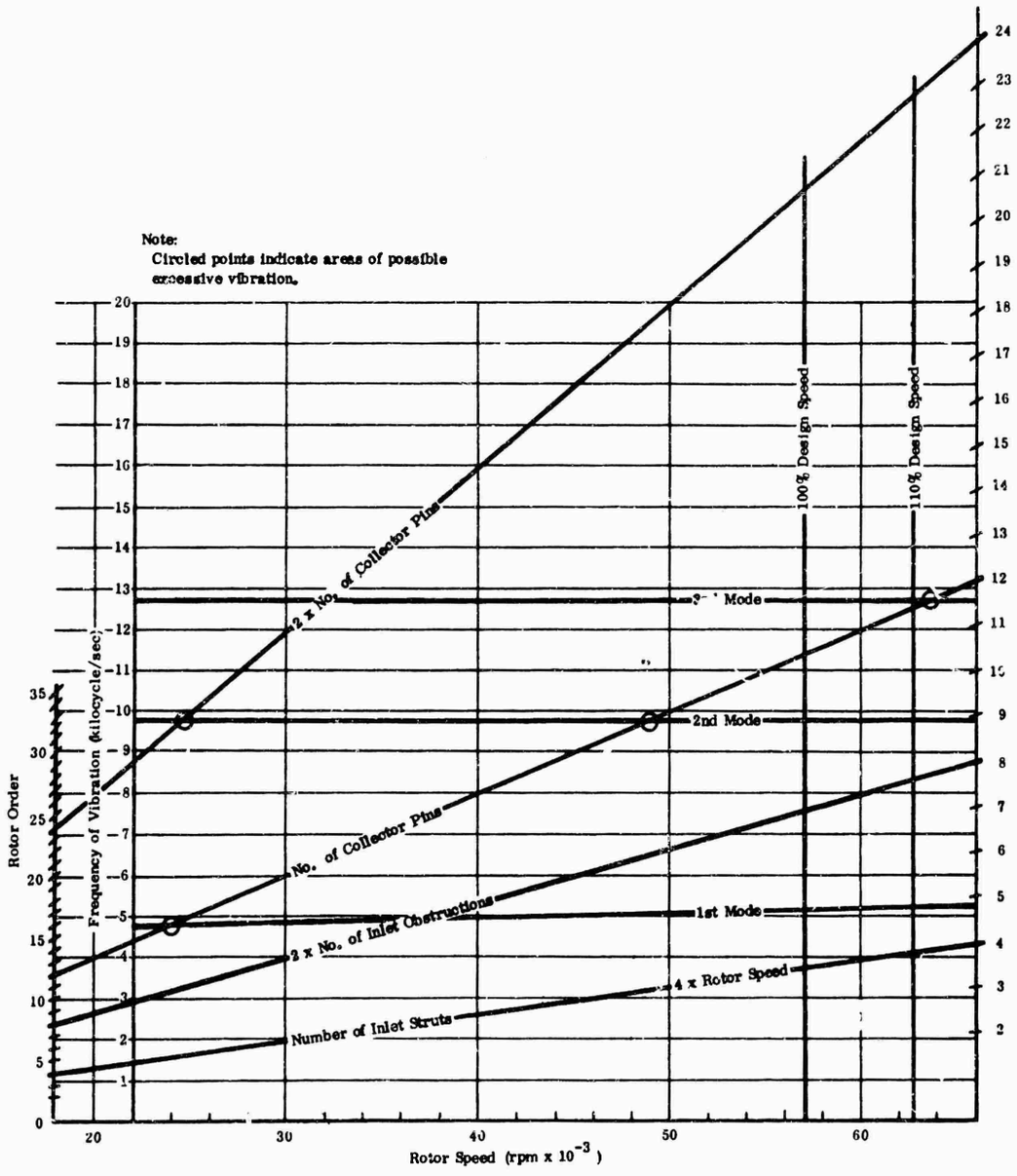


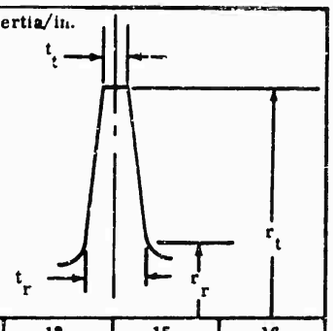
Figure 37. Campbell Diagram for RF-1.

Radial Flow Blade Root Stress, Force/in., Weight/in., and Mass Moment of Inertia/in.

Material: Titanium, 6Al-4V

Speed, N = 62,500 rpm (10% overspeed)

Density, γ = 0.160 lb/in.^{3}



Blade Station No.			1	4	10	11	13	15	16
Computer Input									
1	r_t	in.	1.948	1.981	2.868	3.197	3.768	4.040	4.04
2	r_r	in.	1.179	1.215	2.197	2.550	3.040	3.347	3.655
3	t_t	in.	0.045	0.035	0.025	0.025	0.025	0.025	0.034
4	t_r	in.	0.054	0.145	0.118	0.113	0.100	0.090	0.075
Computer Output									
1	F_r	lb/in.	1,050	1,860	2,100	2,220	2,690	2,570	1,420
2	S_{root}	lb/in.^{2}	19,424	12,832	17,758	19,675	26,913	28,523	18,393
3	$I' \times 10^4$	$\frac{\text{lb-in.-sec}^2}{\text{in.}}$	0.39	0.67	1.21	1.46	2.10	2.18	1.27
4	$W' \times 10^2$	lb/in.	0.61	1.10	0.77	0.71	0.73	0.64	0.34

Figure 38. Blade Stress Calculations of RF-1.

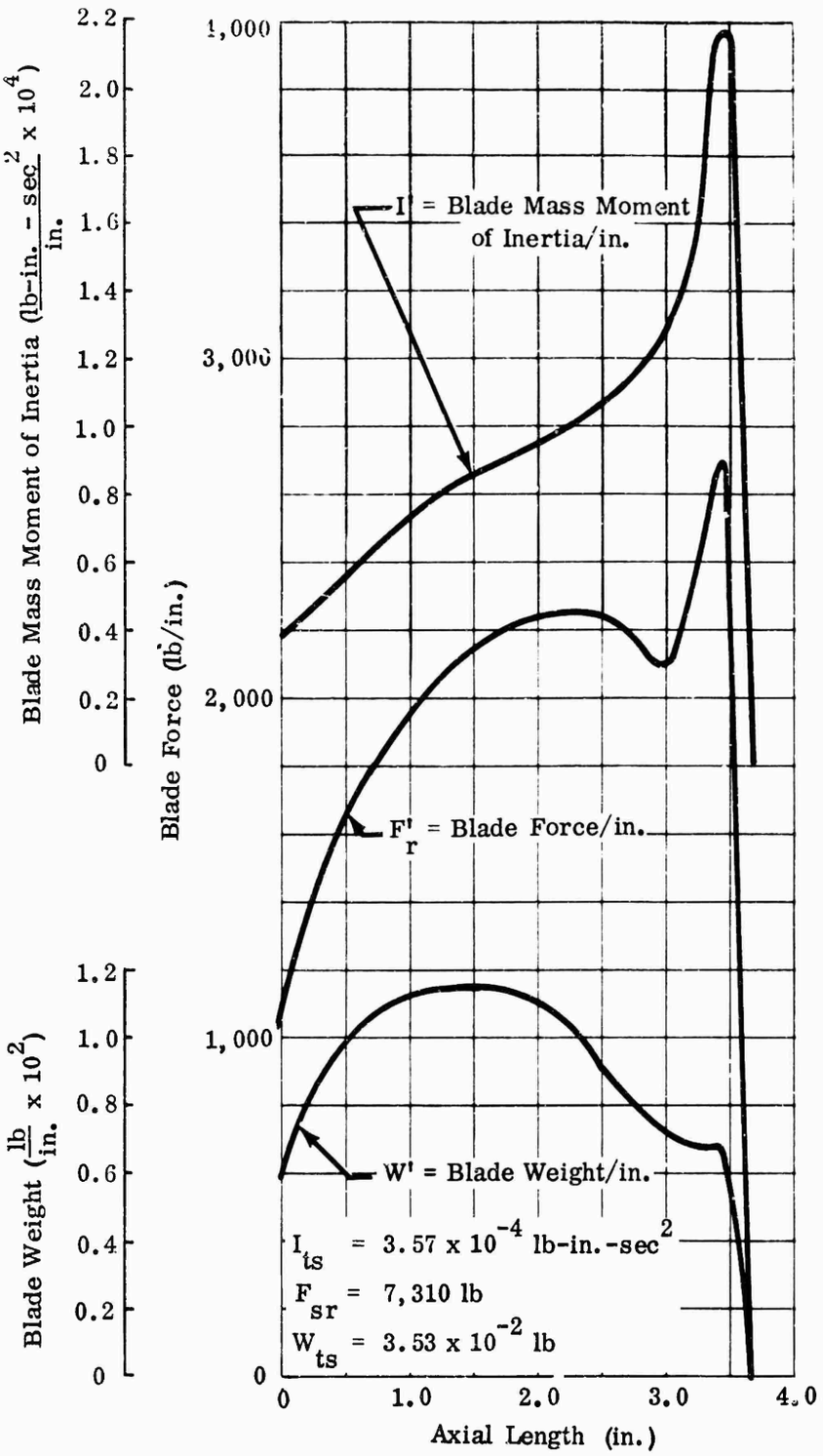


Figure 39. RF-1 Impeller-Blade Force, Weight, and Inertia.

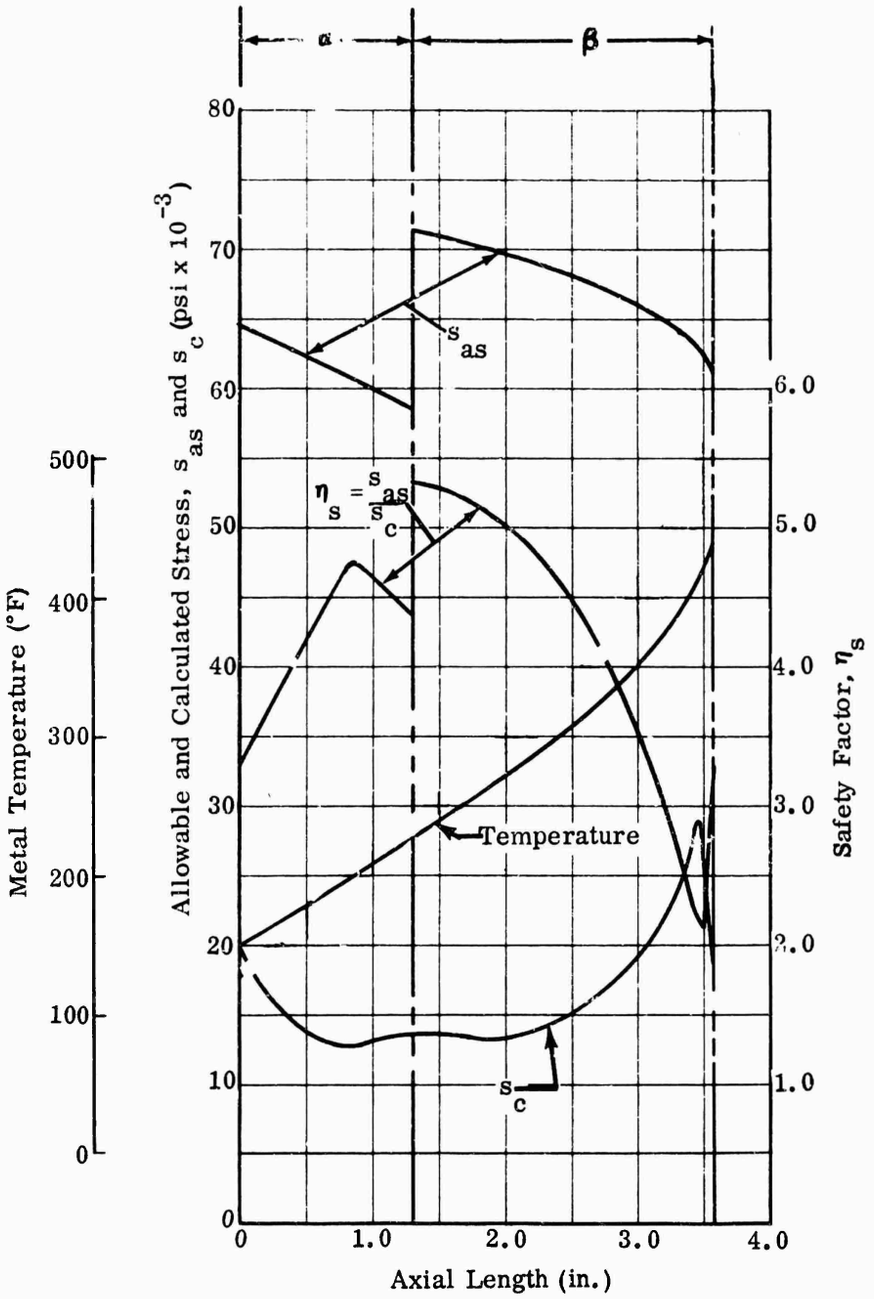
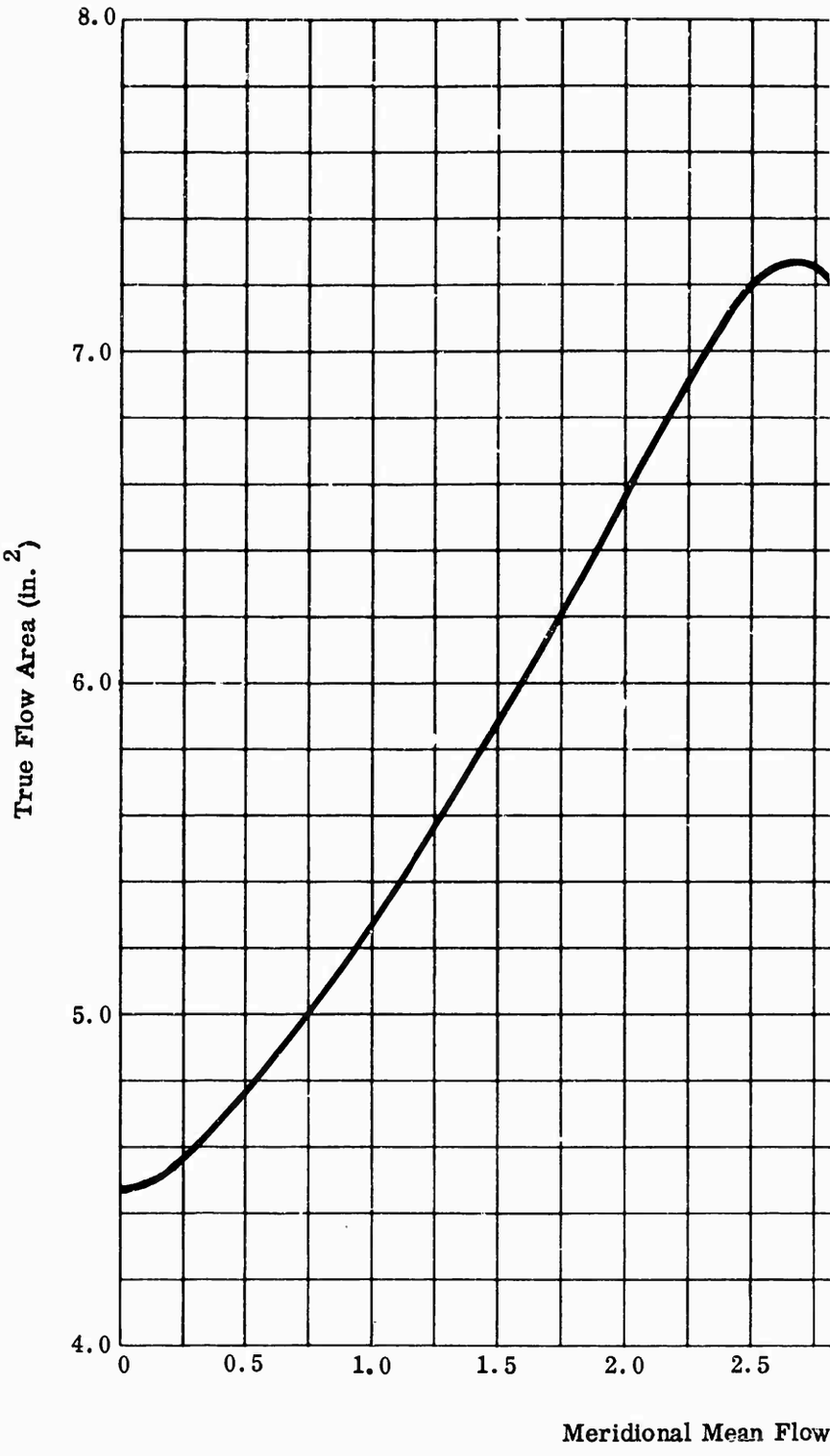


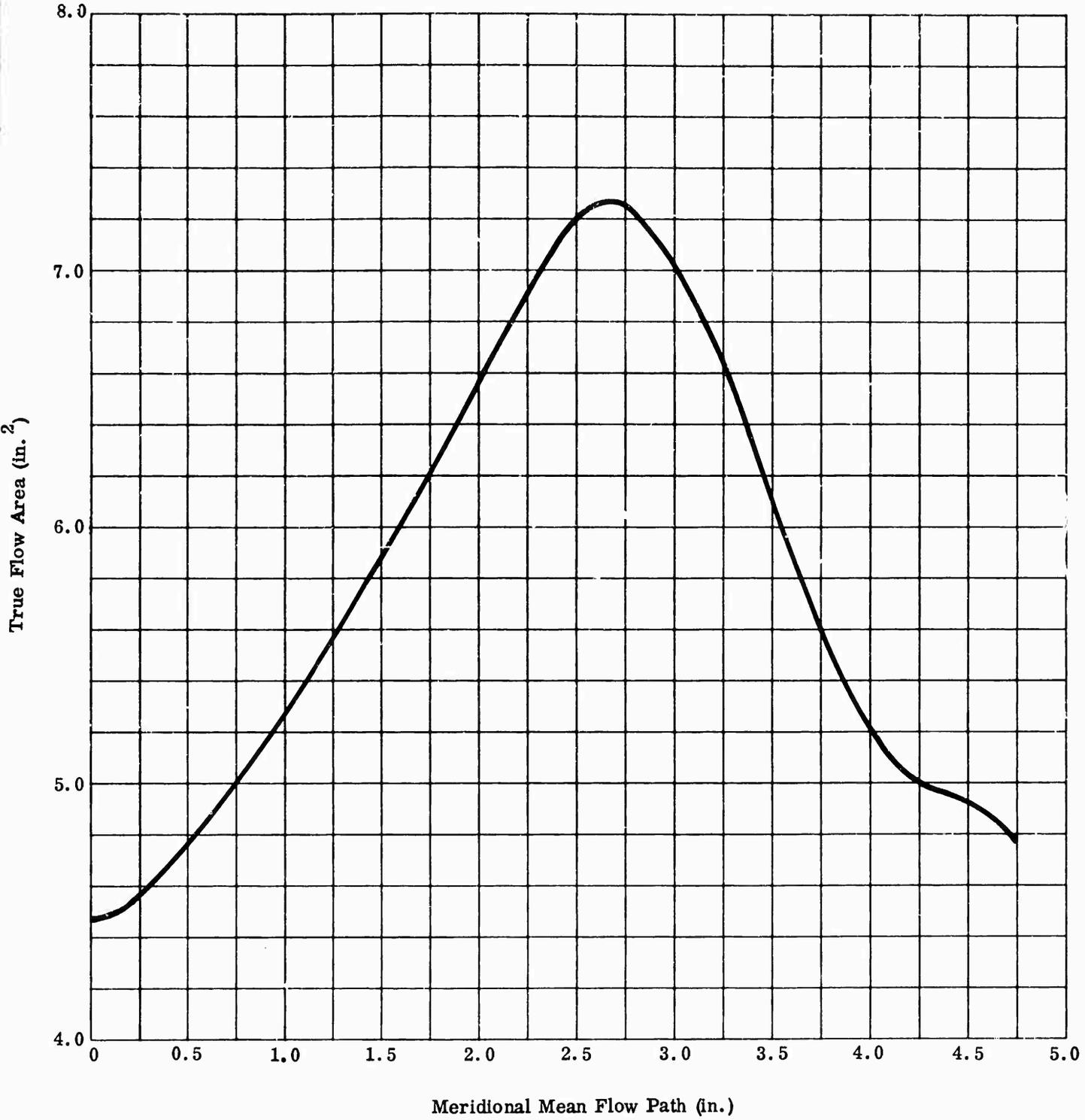
Figure 40. Blade-Root Stress, Temperature, and Safety Factor for RF-1.

Flow Area Calculation											
Sec.	h	r_1	r_2	A_T $\pi h (r_1 + r_2)$	h'	t_t	t_r	A_B $\frac{N}{2} h' (t_t + t_r)$	A' $(A_T - A_B)$	ϕ	Cos
A	0.789	1.968	1.129	7.8005	0.769	0.045	0.054	0.837	7.0225	50.0	0.(
B	0.790	1.972	1.182	7.8277	0.770	0.043	0.079	1.033	6.7947	48.2	0.(
C	0.790	1.980	1.190	7.8675	0.770	0.038	0.111	1.262	6.6055	44.7	0.7
D	0.783	2.000	1.220	7.9208	0.763	0.035	0.146	1.519	6.4018	37.9	0.7
E	0.770	2.046	1.285	8.0578	0.750	0.032	0.159	1.576	6.4818	31.8	0.8
F	0.747	2.120	1.396	8.2512	0.727	0.030	0.167	1.576	6.6752	25.8	0.9
G	0.708	2.222	1.560	8.4121	0.688	0.028	0.162	1.436	6.9761	19.7	0.9
H	0.653	2.357	1.791	8.5094	0.633	0.026	0.148	1.213	7.2964	13.6	0.9
I	0.563	2.526	2.097	8.1767	0.543	0.026	0.124	0.896	7.2807	7.6	0.9
J	0.455	2.737	2.446	7.4086	0.435	0.025	0.116	0.675	6.7336	1.5	0.9
K	0.346	3.008	2.835	6.3513	0.326	0.025	0.105	0.466	5.8853	0.0	1.(
L	0.268	3.330	3.239	5.5307	0.248	0.025	0.093	0.322	5.2087	0.0	1.(
M	0.243	3.512	3.438	5.3057	0.223	0.025	0.087	0.275	5.0307	0.0	1.(
N	0.226	3.697	3.629	5.2014	0.206	0.025	0.078	0.233	4.9684	0.0	1.(
O	0.194	4.042	3.984	4.8916	0.174	0.025	0.048	0.140	4.7516	0.0	1.(

Figure 41. Impeller Flow Area of RF-1.

A' $(A_T - A_B)$	ϕ	Cos ϕ	A A' Cos ϕ
7.0225	50.0	0.64279	4.476
6.7947	48.2	0.66653	4.529
6.6055	44.7	0.71080	4.695
6.4018	37.9	0.78908	5.052
6.4818	31.8	0.84989	5.509
6.6752	25.8	0.90032	6.010
6.9761	19.7	0.94147	6.568
7.2964	13.6	0.97196	7.092
7.2807	7.6	0.99122	7.217
6.7336	1.5	0.99966	6.731
5.8853	0.0	1.000	5.885
5.2087	0.0	1.000	5.209
5.0307	0.0	1.000	5.031
4.9684	0.0	1.000	4.968
4.7516	0.0	1.000	4.752




8.0
7.0
6.0
5.0
4.0
True Flow Area (in.^{2})
0
0.5
1.0
1.5
2.0
2.5
3.0
3.5
4.0
4.5
5.0
Meridional Mean Flow Path (in.)

Disk Tangential Force, Cross-Sectional Area, Weight, Mass Moment of Inertia, and Failure Force

Material: Titanium 6Al-4V

I_{ts} 3.57 x 10^{4} lb-in.-sec^{2}

Speed, N 62,700 rpm (10% overspeed)

F_{sr} 7,310 lb

Density, γ 0.160 lb/in.^{3}

Number of Blades, n = 22

W_{ts} 3.53 x 10^{-2} lb

Segment No.	r in.	Δr in.	t in.	ΔA in.^{2}				Failure Stress @ .2% Yield: T F	Failure Stress @ .2% Yield: S_f psi		Failure Stress Ultimate: T F	Failure Stress Ultimate: S_f psi	
1	3.897	0.286	0.115	0.033				455	80,000		455	93,500	
2	3.611	0.286	0.185	0.053				440	80,500		440	94,000	
3	3.325	0.286	0.260	0.074				424	81,300		424	94,700	
4	3.039	0.286	0.360	0.103				408	82,000		408	95,300	
5	2.753	0.286	0.465	0.133				390	83,000		390	96,200	
6	2.467	0.286	0.565	0.162				370	84,000		370	97,200	
7	2.181	0.286	0.710	0.203				356	84,800		356	97,900	
8	1.895	0.286	0.940	0.269				338	86,000		338	98,600	
9	1.609	0.286	1.310	0.375				318	87,000		318	100,000	
10	1.323	0.286	2.040	0.583				286	88,000		286	101,500	
11	1.0175	0.325	3.030	1.180				248	90,000		248	104,000	
12	0.975	0.315	3.740	1.178				232	93,500		232	105,000	
13	0.455	0.170	4.690	0.797				240	92,800		240	104,300	
14	0.3375	0.065	1.675	0.109				180	98,500		180	108,500	

Computer Calculated

A_{td}	10.50	in.^{2}
F_{td}	387,570	lb
F_{ts}	51,180	lb
F_{tw}	438,750	lb
W_{tw}	7.20	lb
I_{tw}	0.0699	lb-in-sec^2
η_y $F_{fy} \div F_{tw}$	1.99	—
η_u $F_{tu} \div F_{tw}$	1.74	—
S_{tan} $F_{tw} \div A_{td}$	41,800	psi
S_{tan} Average Tangential Disk Stress		

F_{fy} = 763,500 F_{fu} = 871,300

S_f = Failure Stress at Temperature, T

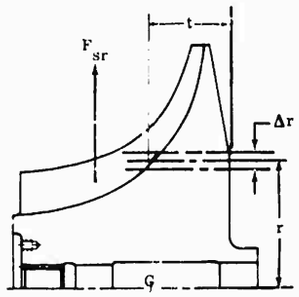


Figure 42. Disk Calculations for RF-1.

6.0 WORKHORSE IMPELLER ANALYSIS

This impeller is satisfactory for steady-state operation to 50,000 rpm. The intersection of the first mode and eighth order shown at 34,000 rpm on the Campbell diagram, Figure 44, must be avoided for steady-state operation. A complete blade stress survey should be made in the test rig before prolonged aerodynamic tests are performed.

The flow areas were not calculated for this design because the blade configuration was already defined by a prior design.

The calculated minimum safety factors for steady-state operation at 50,000 rpm and for an impeller inlet temperature of 60° F are as follows:

1) Blade safety factor is 1.91 to minimum 0.2-percent yield stress including ± 12,000 psi vibratory stress.

2) Disk safety factors are 1.86 to minimum 0.2-percent yield stress and 2.08 to minimum ultimate stress.

The calculated minimum safety factors for momentary operation at 60,000 rpm and for an impeller outlet temperature of 60° F are as follows:

1) Blade safety factor is 1.73 to minimum 0.2-percent yield stress.

2) Disk safety factors are 1.29 to minimum 0.2-percent yield stress and 1.44 to minimum ultimate stress.

The weight of the impeller is 13.51 pounds, and the mass moment of inertia is 0.187 lb-in.-sec^2.

Figures 43 through 50 present the results of stress and vibration analyses for the workhorse impeller.

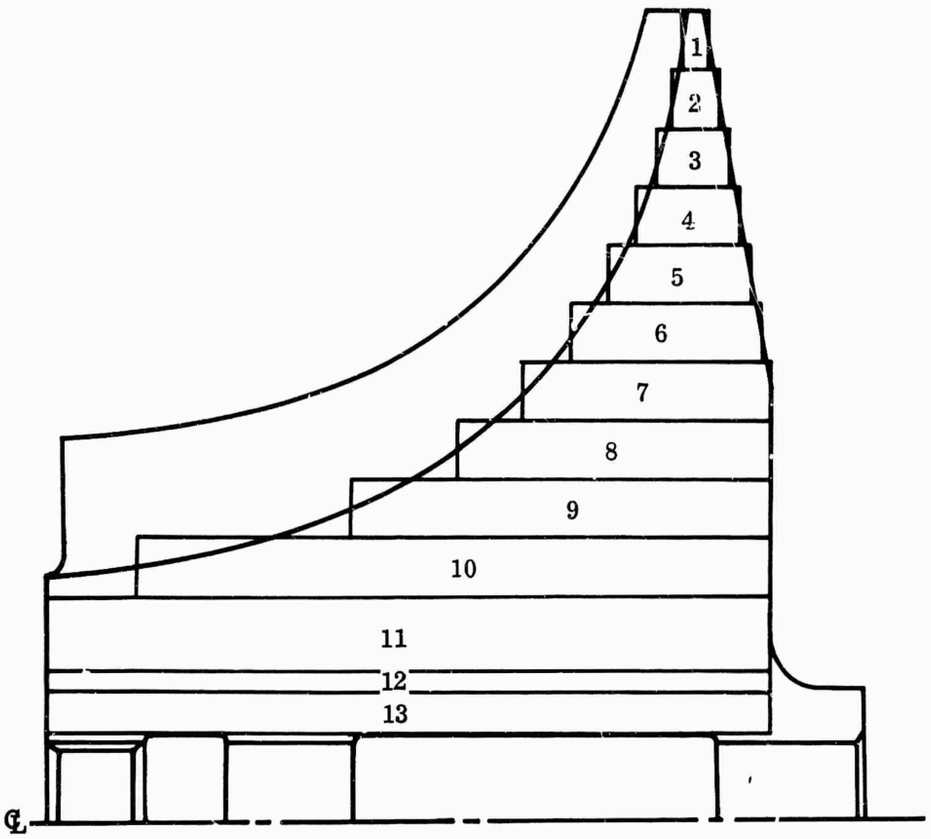


Figure 43. Disk and Blade Profile of Workhorse Impeller.

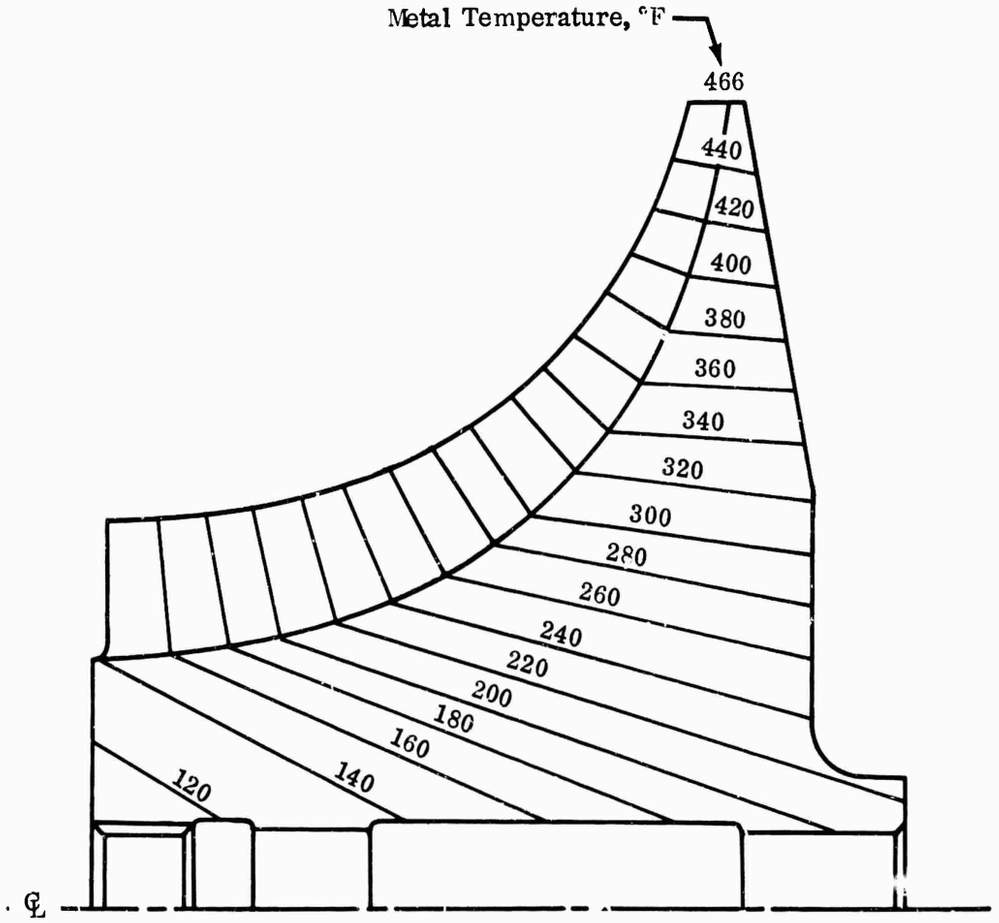


Figure 44. Temperature Distribution of Workhorse Impeller.

Computer Input Data:

Title

Workhorse Impeller Blade Natural Frequencies
(Nominal Blade)

Number of Drawing Stations	Material Const.		Blade Profile	Number of Nodes at General Z Station	Required Number of Modes
	Density γ	Modulus of Elasticity E			
	($lb/in.^3$)	(psi)			
17	0.16	15,500,000	Linear	5	5

Computer Output Data:

Mode No.	Frequency, cps
1	4,495
2	8,673
3	10,803
4	13,253
5	16,980

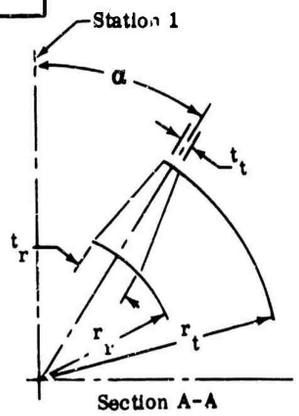
Information From Drawing :

Station No.	Axial Dist. Z	Tip Rad. r_t	Root Rad. r_r	Inclination α	Tip Thickness t_t	Root Thickness t_r
	in.	in.	in.	Degree	in.	in.
1	0	0.910	0.910	0	0.031	0.031
2	0.100	1.806	0.913	5.4	0.050	0.063
3	0.200	1.815	0.919	10.5	0.050	0.093
4	0.392	1.830	0.935	19.4	0.051	0.133
5	0.600	1.847	0.969	27.9	0.053	0.152
6	0.794	1.865	1.015	34.5	0.054	0.163
7	1.000	1.887	1.079	40.8	0.057	0.168
8	1.183	1.912	1.141	45.6	0.056	0.171
9	1.559	1.994	1.294	52.9	0.053	0.169
10	1.905	2.127	1.487	56.7	0.045	0.153
11	2.235	2.338	1.738	58.2	0.040	0.129
12	2.524	2.601	2.030	58.5	0.034	0.107
13	2.773	2.900	2.344	58.5	0.030	0.090
14	2.991	3.219	2.694	58.5	0.025	0.073
15	3.191	3.105	3.105	58.5	0.054	0.054

13 Required Number of Node Distances

Z Distances for Node Stations, (In.)

0.0	0.2	0.4	0.6	0.8	1.2	1.6	2.0	2.4	2.8
3.2	3.5	3.71							



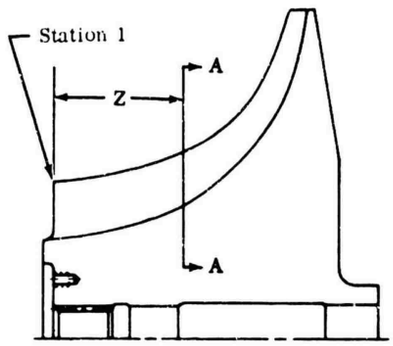


Figure 45. Natural Frequencies of Workhorse Impeller Blades.

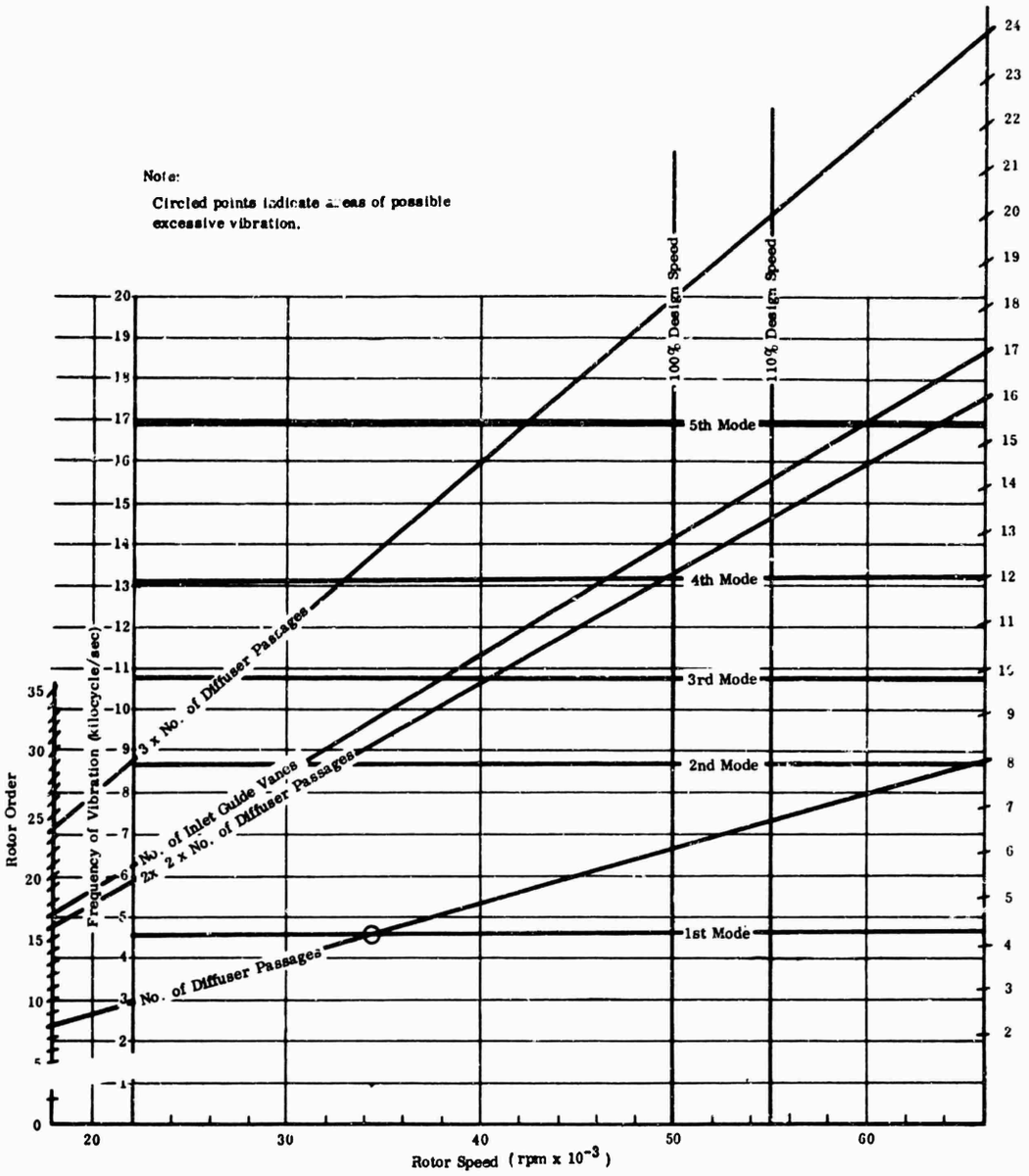
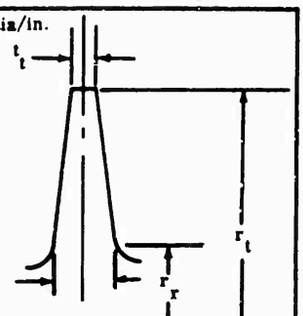


Figure 46. Campbell Diagram for Workhorse Impeller.

Radial Flow Blade Root Stress, Force/in., Weight/in., and Mass Moment of Inertia/in.



Material: Titanium, 6Al-4V

Speed, N = 50,000 rpm Density, γ = 0.160 lb/in.^{3}

Blade Station No.			1	5	9	13	14	15	16
Computer Input									
1	r_t	in.	2.21	2.415	3.025	3.860	4.220	4.600	4.600
2	r_r	in.	1.40	1.56	2.32	3.07	3.34	3.68	4.02
3	t_t	in.	0.075	0.065	0.056	0.069	0.055	0.040	0.045
4	t_r	in.	0.080	0.095	0.084	0.101	0.090	0.077	0.068
Computer Output									
1	F'	lb/in.	1,280	1,380	1,490	2,620	2,720	2,500	1,460
2	S_{root}	$\frac{lb/in.^2}{lb-in.-sec^2/in.}$	16,050	14,550	17,690	25,990	30,170	32,500	23,110
3	I' x 10^4		0.86	1.03	1.44	3.31	3.72	3.75	2.28
4	W' x 10^2	lb/in.	1.00	0.97	0.79	1.07	1.02	0.86	0.48

Figure 47. Blade Stress Calculations for Workhorse Impeller.

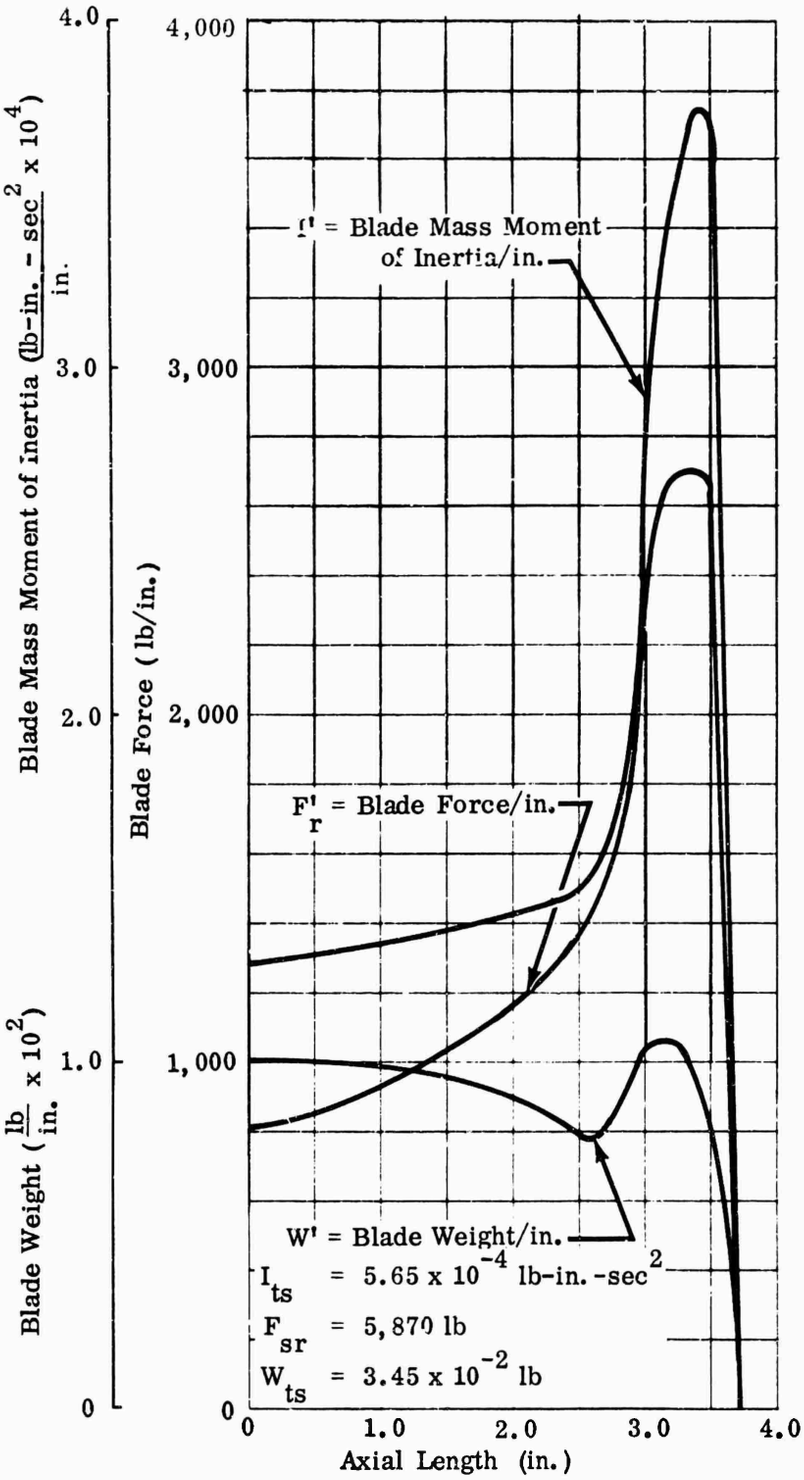


Figure 48. Workhorse Impeller-Blade Force, Weight, and Inertia.

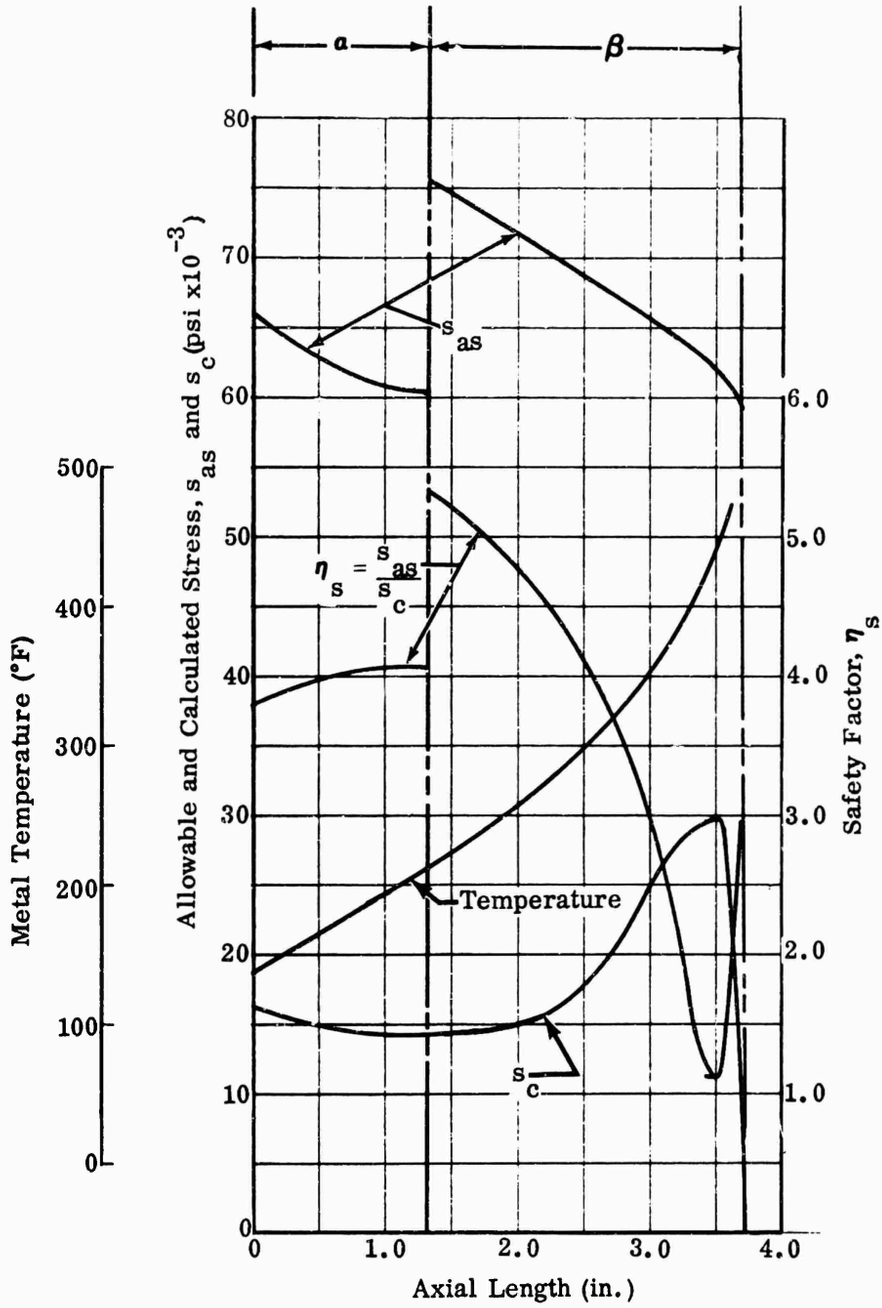


Figure 49. Blade-Root Stress, Temperature, and Safety Factor for Workhorse Impeller.

Disk Tangential Force, Cross-Sectional Area, Weight,
Mass Moment of Inertia, and Failure Loads

Material: Titanium 6Al-4V

I_{ts} 5.64 x 10^{-4} lb-in.-sec^2

Speed, N 50,000 rpm

F_{sr} 5,87 lb

Density, γ 0.160 lb/$in.^3$

Number of Blades, n 23

W_{ts} 3.45 x 10^{-2} lb

Segment No.	r	r	t	ΔA				Failure Stress 0.2% Yield (8) T	(9) S_f	(10) (4) x (9)	Failure Stress Ultimate (8) T	(9) S_f	(10) (4) x (9)
	in.	in.	in.	$in.^2$				F	psi	lb	F	psi	lb
1	4.433	0.333	0.15	0.04995				450	80.100	4.001	450	93.100	4.6[illegible]
2	4.100	0.333	0.28	0.09324				420	81.000	7.553	420	94.300	8.[illegible]11
3	3.767	0.333	0.43	0.14319				410	82.800	11.853	410	95.700	13.712
4	3.434	0.333	0.60	0.19980				390	82.800	16.542	390	96.600	19.313
5	3.101	0.333	0.83	0.27639				370	84.240	23.283	370	97.200	26.865
6	2.768	0.333	1.12	0.37296				346	85.500	31.887	346	99.000	36.927
7	2.435	0.333	1.45	0.49284				320	87.300	43.020	320	99.540	49.054
8	2.102	0.333	1.87	0.62271				300	88.290	54.923	300	100.500	62.559
9	1.769	0.333	2.49	0.82917				260	91.800	76.118	260	103.500	85.819
10	1.436	0.333	3.79	1.26207				210	95.400	120.401	210	106.560	134.486
11	1.062	0.430	4.30	1.84900				180	98.100	181.387	180	108.540	200.690
12	0.805	0.130	4.30	0.55900				160	100.260	56.046	160	109.980	61.479
13	0.620	0.240	4.30	1.03200				150	101.250	104.490	150	111.150	114.707

Computer Calculated

A_{td}	15.56	$in.^2$
F_{td}	584.730	lb
F_{ts}	43.000	lb
F_{tw}	637.730	lb
W_{tw}	13.51	lb
I_{tw}	0.187	lbs-in-sec^2
η_y = $F_{fy} \div F_{tw}$	1.86	—
η_u = $F_{fu} \div F_{tw}$	2.05	—
S_{tan} $F_{tw} \div A_{td}$	40.980	psi
S_{tan} Average Tangential Disk Stress		

$F_{fy} = 1.62 \times \Sigma(7) = 1,185,000$ $F_{fu} = 1.62 \times \Sigma(7) = 1,327,300$

S_f - Failure Stress at Temperature, T

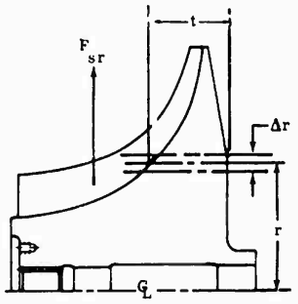


Figure 50. Disk Calculations for Workhorse Impeller.

(U) APPENDIX III

TEST RIG DEVELOPMENT

ABSTRACT

This appendix covers the design development of test rigs required for the Army centrifugal-compressor research program. It provides information relative to methods used in correcting initial operational difficulties encountered with the test sections. The appendix is intended to supplement the discussions given in Section 2.4 in the body of this report.

SYMBOLS

C_c critical damping coefficient (lb_m/sec)

C_{inner} inner bearing clearance (in.)

C_{outer} outer bearing clearance (in.)

C_s dynamic radial load rating (lb)

c radial bearing clearance (in.)

c_1 inner bearing-to-journal radial clearance (in.)

c_2 outer bearing-to-journal radial clearance (in.)

D bearing diameter (in.)

D_i bearing inner diameter (in.)

D_{mean} bearing mean diameter (in.),

$$D_{mean} = \frac{D_i + D_o}{2}$$

D_o bearing outer diameter (in.)

K_n spring rate (lb/in.)

L bearing length (in.)

m damper mass (lb_m)

N, N_o journal speed (rps)

N_1 bearing speed (rps)

n	journal bearing attitude, $n = \frac{\text{eccentricity}}{\text{radial clearance}}$
P	bearing load (psi)
R_H	static radial load (lb)
R_S	dynamic radial load (lb)
r, r_1	journal radius (in.)
r_2	outer film radius (in.)
S	Sommerfeld number, $S = \left(\frac{r}{c}\right)^2 \left(\frac{\mu N}{P}\right)$
T	thrust load (lb)
T_n	spring rate $\frac{\text{(lb-sec)}}{\text{in.}}$, $T_n = \frac{K_n}{\omega_n}$
W	design load (lb)
X, Y	imbalance bearing load coefficients
μ	absolute viscosity $\left(\frac{\text{lb-sec}}{\text{in}^2}\right)$
ω_n	angular velocity $\left(\frac{\text{radians}}{\text{sec}}\right)$

1.0 INTRODUCTION

Two basic test rigs were required to evaluate performance and structural characteristics of the various compressor component configurations. The diffusers were tested in a rig equipped with a workhorse impeller operating at a maximum speed of 55,000 rpm. A second rig was used for evaluation of the impellers at speeds of up to 57,000 rpm. The contractor's concept for compressor rigs was modified to accommodate the diffuser components, and a new rig was designed to accommodate the impeller rotors. This appendix presents the design analyses and subsequent modifications of these test rigs.

2.0 DIFFUSER TEST SECTIONS

The design of the diffuser test rig included provisions for monitoring mechanical operation. The rotor system was an adaptation of an existing rig, but with higher speed requirements (55,000 rpm). Operating temperatures ranged from ambient at the inlet to 750°F at the diffuser exit. The unit was to be operated at various back pressures at a number of constant speed increments of from 33,000 through 55,000 rpm. Instrumentation was to be provided for measurement of static and dynamic pressures and temperatures. A schlieren optical system for evaluating flow patterns near the diffuser vanes was also to be incorporated in the design.

The configuration selected from preliminary studies was a cantilevered-rotor system with the shaft passing through the impeller. All bearing supports were flexible to provide versatility in controlling the critical speeds to be encountered. Thrust loads were limited by providing a labyrinth seal at the rear face of the impeller at the tip. The seal was designed to prevent high pressures at the impeller backface.

2.1 BEARING SYSTEM

The rotor system was designed as a stiff shaft assembly supported by 2 hydrodynamic floating-sleeve bearings. A titanium impeller was precision fit to the shaft. In a similar manner, a thrust balance disk was attached to the aft or coupling end of the shaft.

Thrust load was carried in both the forward and aft directions by hydrodynamic-slipper bearings. A damped, resilient support for the forward radial bearing was incorporated during the operational development of the unit to accommodate excessive radial loads due to shaft vibration. A reverse-thrust slipper bearing was also replaced during this period so that the arrangement was capable of carrying both radial and thrust loads in a 3-bearing rotor system.

Hydrodynamic full-floating journal bearings were used to support the rotor system and to provide maximum capacity for radial loads that might result from rotor imbalance or operation near critical speeds. The operating characteristics of the full-floating journal bearing compensate for a number of disadvantages encountered at high speeds with conventional journal bearings. High-speed journal bearings require more clearance than a conventional journal type to induce the proper amount of oil flow. Increased clearance, however, reduces the load carrying capacity of a bearing and increases the tendency for oil-film whirl. The full-floating bearing provides 2 paths through which the oil will flow, which permits operation at an acceptable temperature without increased clearance. Because the forces acting on the inner and outer oil films of the full-floating bearing are in equilibrium, the rotational speed of the bearing may be 25 to 70 percent of the shaft or journal speed and is independent of the Sommerfeld number. The Sommerfeld number, S, defines the operating characteristic of a journal bearing as a function of attitude (n),

where:
$$n = \frac{\text{eccentricity}}{\text{radial clearance}} \tag{166}$$

For a conventional journal bearing:

$$S = \left(\frac{r}{c}\right)^2 \left(\mu \frac{N}{P}\right) = \frac{(2 + n^2)\sqrt{1 - n^2}}{12\pi^2 n} \tag{167}$$

where:

S = Sommerfeld number (dimensionless)

r = journal radius (in.)

c = radial clearance (in.)

μ = viscosity, reyns (1 reyn = 68,850 poise)

N = journal speed (revolutions per second)

P = bearing load (psi)

The above equation applies to a bearing of infinite length with no end leakage. However, in a full-floating bearing the Sommerfeld number may be used to compare two bearings of the same finite length. The attitude of a full-floating journal bearing is the same as though the journal alone were to rotate at a speed equal to the sum of the journal- and floating-bearing speeds. Therefore, the Sommerfeld number for the inner film of a floating bearing becomes:

$$S = \left(\frac{r_1}{c_1}\right)^2 \frac{\mu\left(N_o + N_1\right)}{P} \tag{168}$$

where:

N_o = journal speed (revolutions per second)

N_1 = bearing speed (revolutions per second)

r_1 = journal radius (in.)

c_1 = bearing-to-journal radial clearance (in.)

and for the outer oil film:

$$S_1 = \left(\frac{r_2}{c_2}\right)^2 \left(\frac{\mu N_1}{P_2}\right) \tag{169}$$

where the subscript 2 applies to outer film dimensions.

The bearing analyses are based on the Sommerfeld number for a bearing capable of supporting a 500-pound radial load. A bearing is considered to be lightly loaded when the Sommerfeld number is longer than 0.16, moderately loaded when the Sommerfeld number is between 0.16 and 0.035, and heavily loaded when the Sommerfeld number is less than 0.035.* Sommerfeld numbers for the inner and outer oil film are determined as follows.

*M.C. Shaw and F. Mack, Analysis and Lubrication of Bearings, McGraw-Hill Book Company, Inc., New York, 1949.

Given:

W = design load = 500 lb

N_o = journal speed = 50,000 rpm

S = Sommerfeld No. > 0.16 (lightly loaded bearing)

r_1 = journal radius = 0.845 in.

r_2 = bearing outside radius = 1.000 in.

C_1 = journal to bearing clearance = 0.00125 in.

C_2 = bearing to retainer clearance = 0.0025 in.

L = bearing length = 0.80 in.

μ = absolute viscosity = 3.94×10^{-7} Reyns (MIL-L-7808 oil)

from Figure 51 at $\frac{C_2}{C_1} = 2.0$ $\frac{N_1}{N_o} = 0.45$

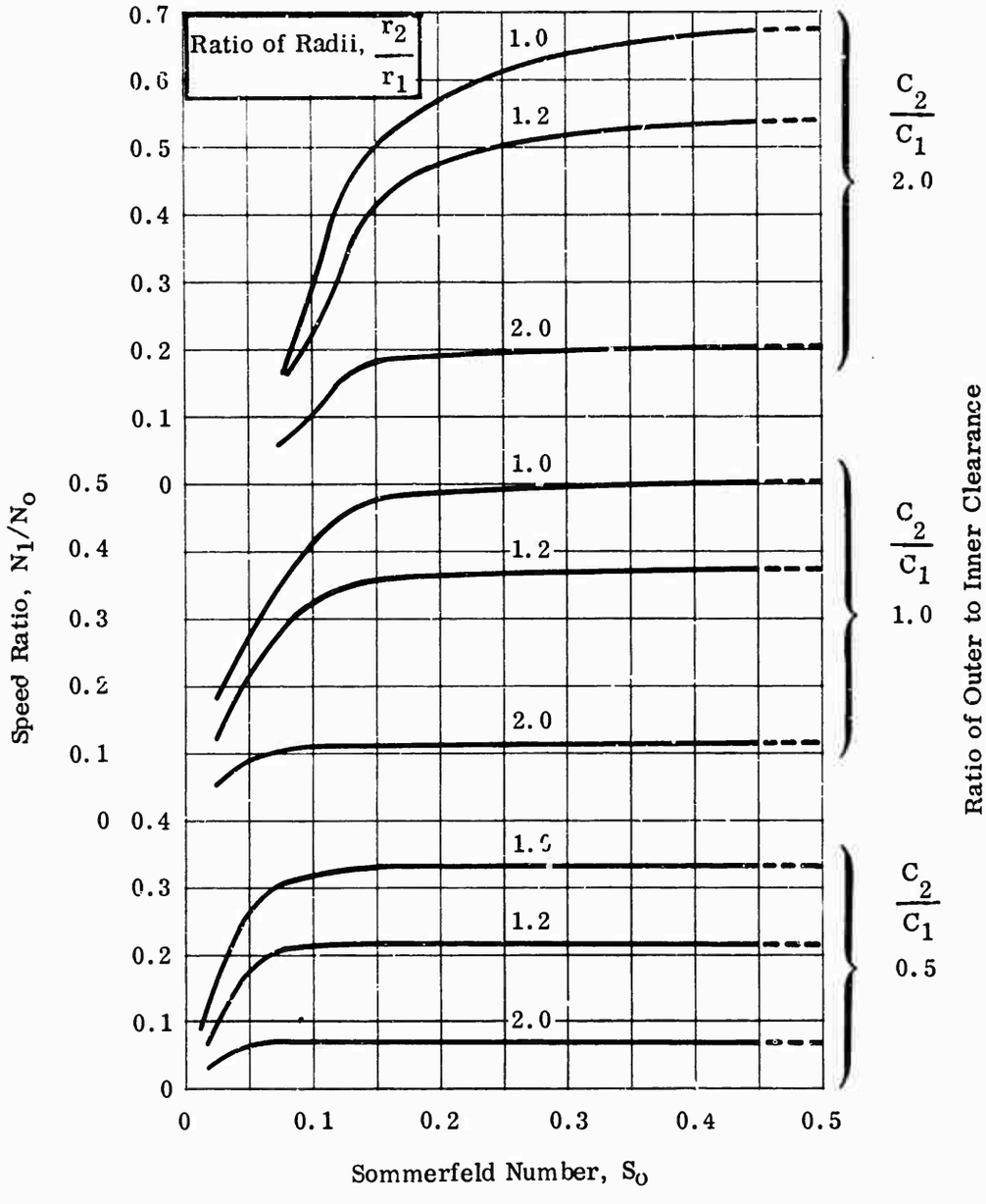
where:

N_1 = speed of floating sleeve

For inner film:

$$S_1 = \left(\frac{r_1}{C_1}\right)^2 \left[\frac{\mu (N_o + N_1)}{\frac{60W}{2r_1 L}}\right] \qquad (170)$$

$$S_1 = \left(\frac{0.845}{0.00125}\right)^2 \left[\frac{3.94 \times 10^{-7} (50,000 + 22,500)}{\frac{500 \times 60}{(2)(0.8)(0.845)}}\right] = \underline{\underline{0.588}}$$



*See footnote, Page 192.

Figure 51. Variation of Speed Ratio with Sommerfeld Number for Full-Floating Journal Bearing.*

For outer film:

$$S_2 = \left(\frac{r_2}{C_2}\right)^2 \left[\frac{\mu N_1}{\frac{60W}{2r_2 L}}\right] = \left(\frac{1.0}{.0025}\right)^2 \left(\frac{(0.394 \times 10^{-6})\,(2.25 \times 10^{4})}{\frac{(500)\,(60)}{(0.8)\quad(2.0)}}\right) = \underline{\underline{0.0755}}$$

The Sommerfeld numbers for the inner and outer films are 0.588 and 0.0755, respectively, with the result that the inner film is lightly loaded and the outer film is moderately loaded. This margin in the oil film loads indicates that the chosen 500-pound radial load was reasonable for the bearing.

2.2 ROTOR DYNAMICS ANALYSIS

The critical speeds of synchronous-whirl modes and the respective mode shapes were determined through use of a mathematical model consisting of 10 mass points and 8 coincident hinged joints with rotational springs. The mathematical model was represented by a linear differential equation. Solution of the equation involved matrix methods and iteration to obtain the eigenvalue for shaft-critical frequencies and the eigenvector for the corresponding mode shapes. Bearing supports were considered to be ideal massless springs. The effect of the gyroscopic-stiffening moment (the difference between gyroscopic moment and rotational inertia) was considered. The bearing supports were simulated by conventional spring constants, K_n (lb/in.), with the radial oil-film stiffness defined as a function of the absolute viscosity of the oil, bearing geometry, and rotor speed by empirical relationship:

$$K_n = \frac{\mu L^3 DN}{6.08\, C^3} \tag{171}$$

where:

N = rotor speed (revolutions per second)

μ = absolute viscosity $\left(\frac{\text{lb-sec}}{\text{in.}^2}\right)$

L = bearing length (in.)

D = bearing diameter (in.)

C = total bearing clearance (in.)

When spring rate, K_n, is divided by ω_n, the spring rate can be expressed as a linear function of rotor speed, so that:

$$T_n = \frac{K_n}{\omega_n} \left(\frac{\text{lb-sec}}{\text{in.}} \right) \tag{172}$$

$$T_n \left(\frac{\text{lb-sec}}{\text{in.}} \right) = \frac{K}{\omega_n} \left(\frac{\text{lb/in.}}{\text{rad/sec}} \right) = \frac{\mu L^3 D}{(6.08) C^3 (2\pi)} = \frac{\mu L^3 D}{(38.2) C^3} \tag{173}$$

where:

$$\mu \text{ (at } 210^\circ \text{F)} = 0.394 \times 10^{-6} \frac{\text{lb-sec}}{\text{in.}^2}$$

$$D_{mean} = \frac{1.690 + 2.000}{2} = 1.845 \text{ inches}$$

$$C_{inner} = 1.6895 - 1.6875 = 0.0020 \text{ inch}$$

$$C_{outer} = 2.0015 - 1.9975 = 0.0040 \text{ inch}$$

$$C_{mean} = \text{mean radial clearance}$$

$$C_{mean} = \frac{0.0040 + 0.0020}{2} = 0.0030 \text{ inch}$$

$L = 0.775$ inch

$D_i = 1.69$ inches

$D_o = 2.00$ inches

$$T_n \text{ (inner)} = \frac{(0.394 \times 10^{-6})\ (0.775)^3\ (1.690)}{(6.08)\ (0.0010)^3\ (2\pi)} = 8.15 \text{ lb-sec/in.}$$

$$T_n \text{ (outer)} = \frac{(0.394)\ (0.466)\ (2.00 \times 10^{-6})}{(6.08)\ (0.002)^3\ (2\pi)} = 1.2 \text{ lb-sec/in.}$$

If the inner and outer film stiffnesses are assumed to be 2 springs in series, the overall film stiffness will be:

$$T_n \text{ (overall)} = \frac{\left(T_n \text{ outer}\right)\ \left(T_n \text{ inner}\right)}{\left(T_n \text{ outer}\right) + \left(T_n \text{ inner}\right)} = \frac{(8.15)\ (1.2)}{(8.15) + (1.2)} \tag{174}$$

$$= 10.45 \text{ lb-sec/in.}$$

Equivalent oil-film stiffness at 46,000 rpm will be:

$$K = T_n\ \omega_n$$

$$= (10.45)\ \frac{(46,000)\ (2\pi)}{60}$$

$$= 50,400 \text{ lb/in.} \tag{175}$$

The results of the rotor analysis, showing variation in the critical speeds as a function of bearing stiffness, T_n, is presented in Figure 52 with the corresponding mode shapes shown in Figure 53.

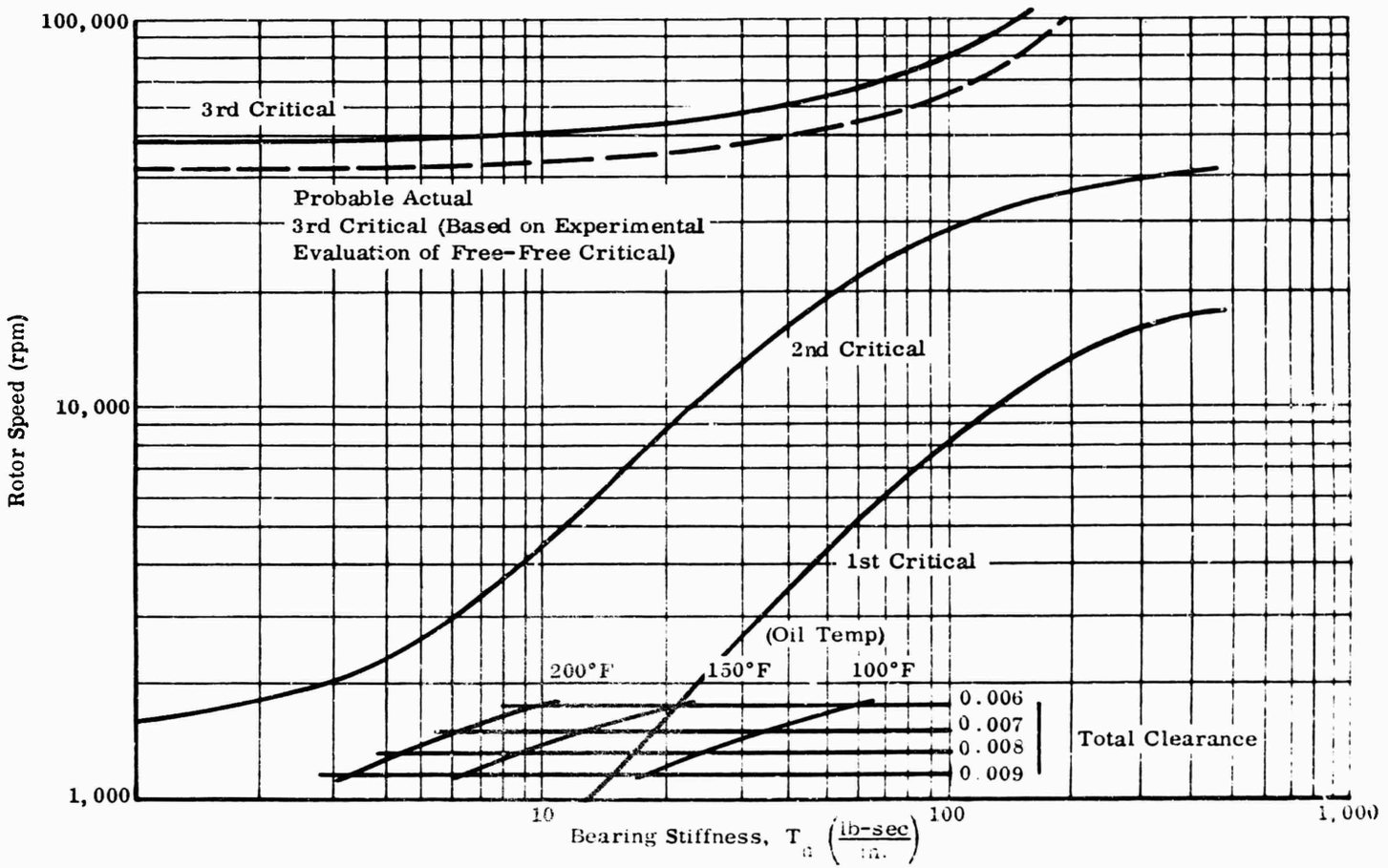
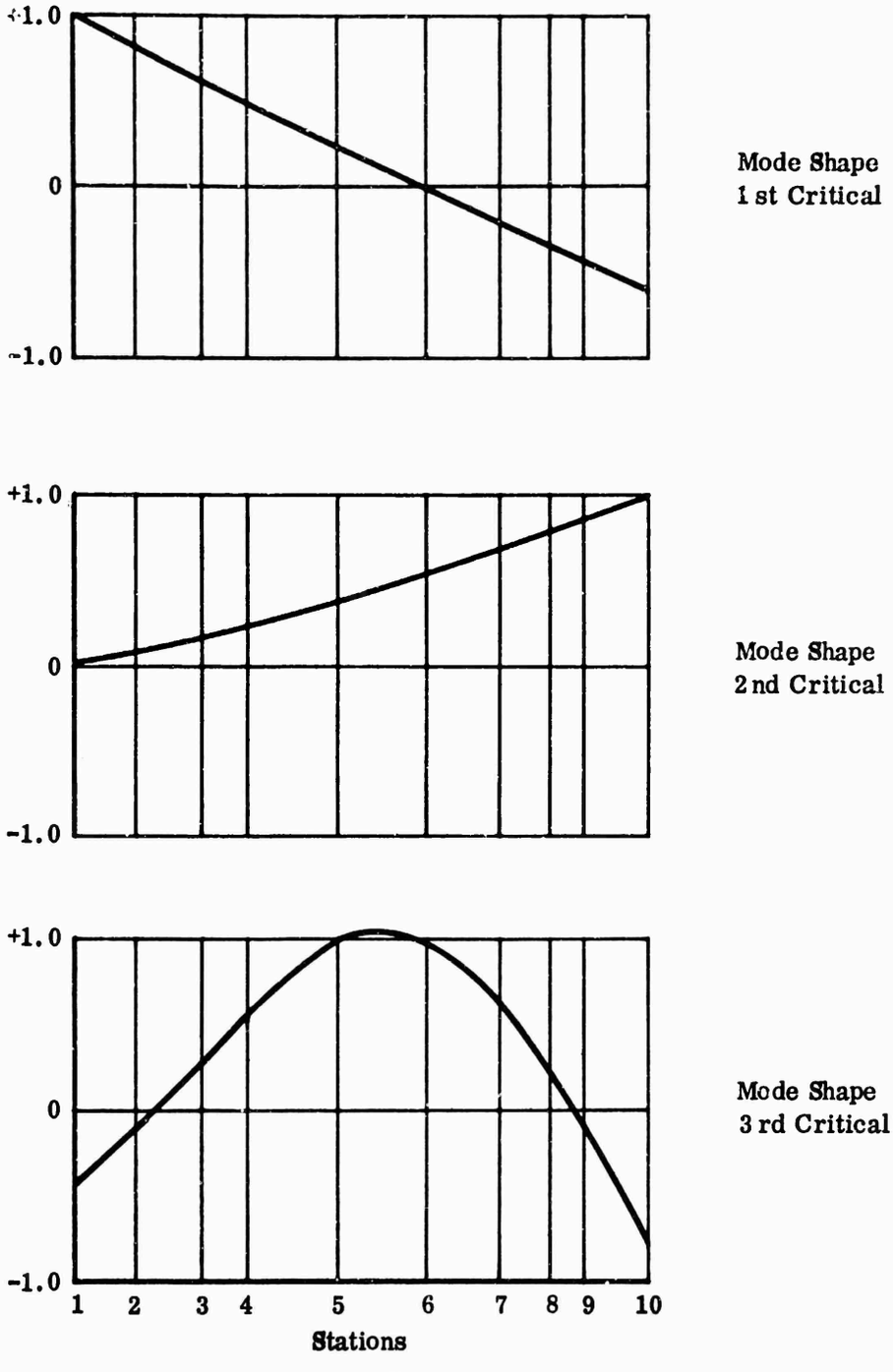


Figure 52. Bearing Stiffness Versus Rotor Speed.



$$T_n = 25 \frac{\text{lb-sec}}{\text{in.}}$$

Figure 53. Shaft Mode Shapes.

The first and second critical speeds were noted to be essentially nonbending modes at K values up to 100,000 lb/in. and to be at speeds below 20,000 rpm. Operational experience with a similar rotor system indicated that these modes would not be troublesome, and the shaft displacement resulting from them would be easily accommodated by the clearance of the journal bearings. The third critical, however, was the first bending mode and was noted to occur between 48,000 and 80,000 rpm, depending on the true stiffness of the bearing system (principally the radial stiffness of the oil film). Only limited experimental and analytical data were available to provide an accurate method of determining the fluid-film radial stiffness, since this parameter varies with speed, oil viscosity, temperature, clearance, and rate of oil feed. For a previous turbine rotor design of the contractor, it was noted that the predicted values of critical speeds for comparable journal-bearing systems were approximately 25 percent high when the flexibility of the oil film was neglected. Therefore, with $K = 10^8$ lb/in., it was estimated from Figure 52 that the actual third critical speed would be approximately 67,000 rpm. Since this speed was 22 percent above the maximum design speed, the design was considered to be satisfactory. Subsequent experimental evaluations, however, proved this assumption to be erroneous, with the critical speed actually occurring at approximately 46,000 rpm.

2.3 MODIFICATIONS

The initial mechanical checkout testing revealed a critical-speed condition of the rotor system at 46,000 rpm. Additional testing near the 46,000 rpm speed revealed that the rotor system could not be operated at or above this speed and could not be accelerated through it. A soft-mount bearing design which incorporated an oil-damping system was added. The soft-mount bearing made little change in the critical speed because the bearing stiffness was already below the $K = 10^8$ value originally assumed. However, it did limit the displacement at the resonant condition by damping. The kinetic energy generated by the forced excitation from the rotor imbalance at resonance was dissipated in a damped-bearing-support system.

A flexible bearing support (Figure 54) with spring-loaded disk-type dampers was designed and implemented into the rotor system. This arrangement permitted operation through the critical speed with a minimum change to the rig design.

Testing to evaluate the degree of success attained with the modified bearing support resulted in satisfactory operation throughout the desired range. Analysis of the test data showed 2 new vibration-amplitude peaks at resonant conditions — 1 at 37,000 rpm and the other at 40,000 rpm. The maximum shaft displacements at these resonant speeds were 0.0007 and 0.0005 inch, respectively. However, operation at the previous critical speed of 46,000 rpm was smooth. The new critical speeds were narrow in speed-band width, and the rotor accelerated through them easily.

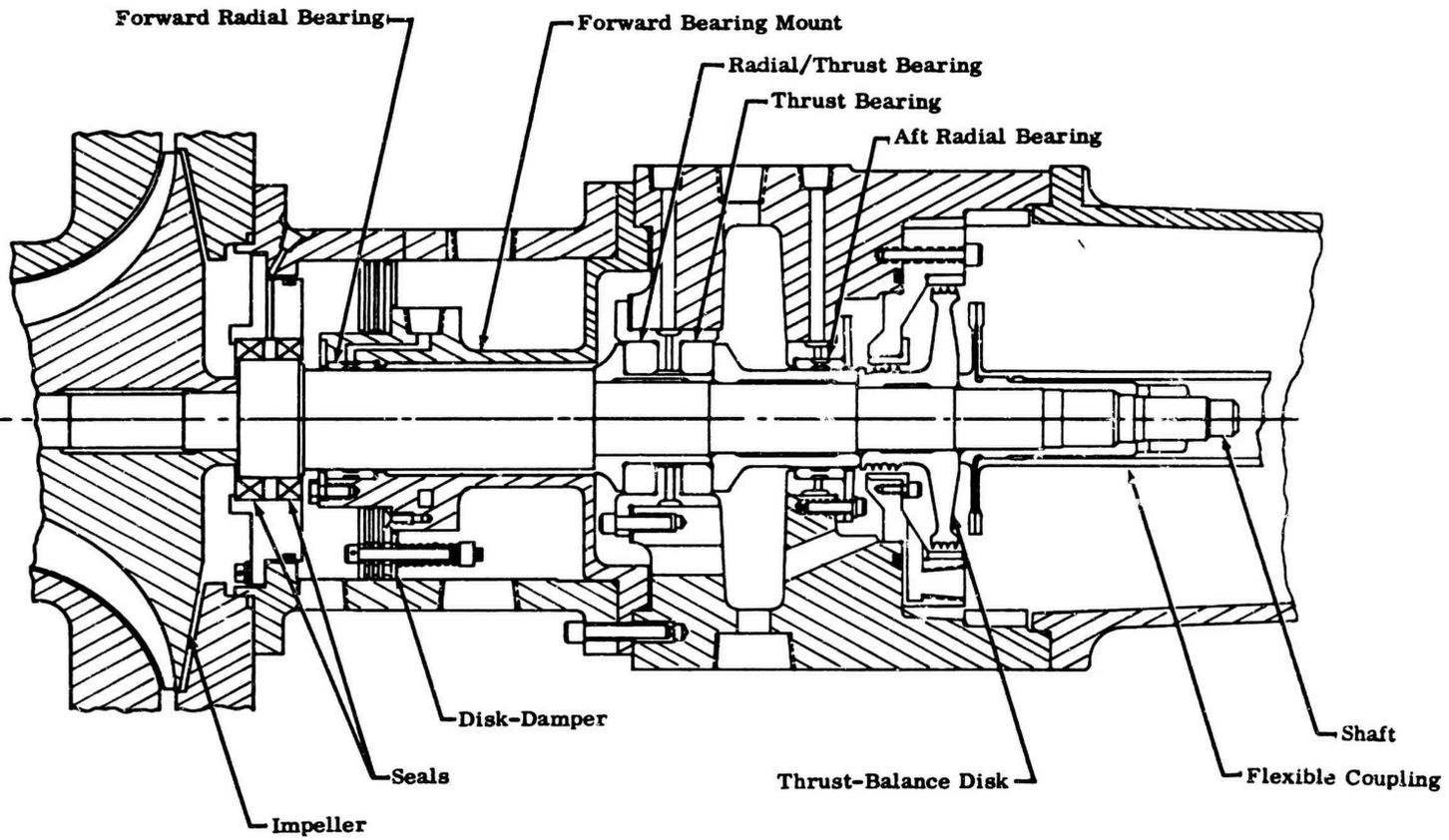


Figure 54. Diffuser Rig Rotor System.

2.4 CONCLUSIONS

It was determined that rig difficulties were caused principally by unpredicted rotor-dynamic characteristics. All bearings were found to be moderately loaded and capable of long-term operation at the design conditions.

Approximately 280 hours of operation under varying speed and surge conditions have been completed successfully with this rig. The rig can be modified readily to accommodate various impellers and compressor systems without appreciably upsetting the existing dynamic characteristics. A smaller mass impeller will very likely increase the current speed limit of 54,000 rpm. A heavier impeller would reduce it in proportion to the 1/2 power of the mass. With proper maintenance to ensure minimum bearing wear, the system should continue its currently displayed operational capability indefinitely.

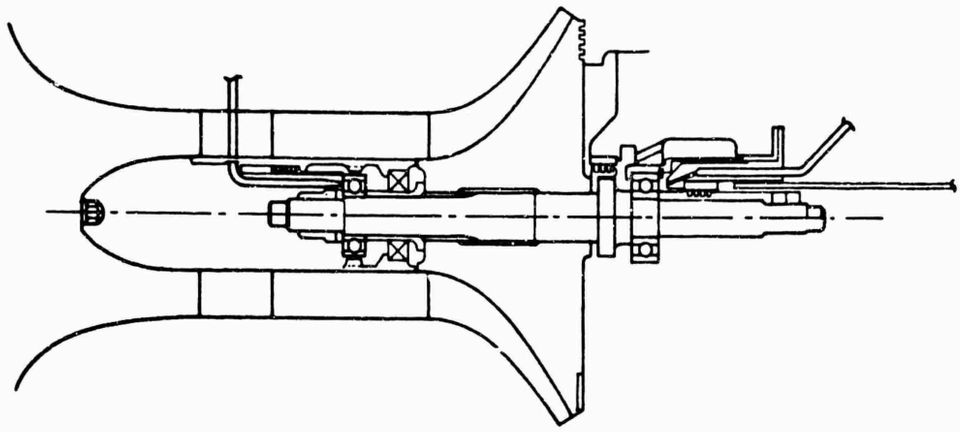
3.0 IMPELLER TEST SECTIONS

Requirements were defined for a test rig capable of accommodating four different impeller configurations of various diameters operating at 2,000 fps tip speed. Three of the impellers were mixed-flow configurations, designated as MF-1, MF-2, and MF-3; and the fourth was a radial-flow unit, designated as RF-1. It was desirable that a single test rig with detachable test sections be provided to reduce fabrication, assembly, and installation time. Three of the impellers (MF-1, MF-3 and RF-1) were required to operate at maximum speeds (10 percent above design speeds) of 63,000, 71,000, and 63,000 rpm. One unit (MF-2) had a maximum speed requirement of 80,000 rpm. The designs consisted of a single housing-collector assembly with a common bearing system for the MF-1, the MF-3, and the RF-1, and with a second bearing system for the high-speed MF-2 unit. A separate turbodrive unit for powering the test sections was provided as a Boeing facility.

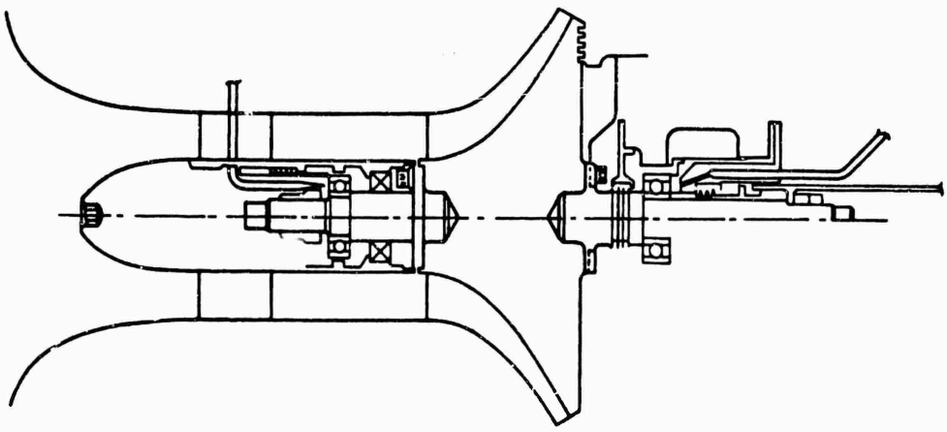
Design analyses were conducted to evaluate three different shaft and housing configurations, as shown in Figure 55. Configuration A consisted of a straddle-mounted bearing system with the impeller mounted on a stub shaft. Configuration C was a cantilevered system with the shaft through the impeller. All bearing supports were flexible to provide versatility in controlling the critical speeds to be encountered. Thrust loads were limited by a labyrinth seal at the rear face of the impeller at the tip.

3.1 BEARING SYSTEM

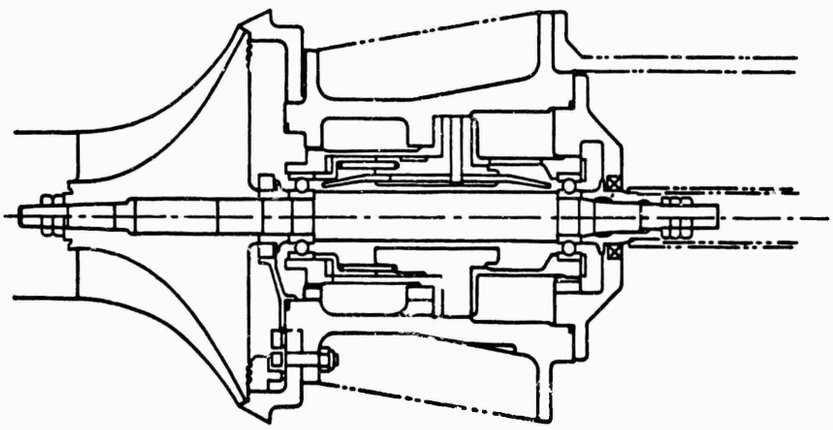
Precision ball bearings, preloaded to reduce axial and radial movement, were selected for the high speed rotors. Bearing sizes of 17 and 20 mm were considered in pairs and combinations to carry the expected radial and thrust loads. Variations in thrust load were expected because of differences in diameters of the



Configuration A



Configuration B



Configuration C

Figure 55 . Impeller Shaft Arrangements.

impellers. It was anticipated that radial loads could be minimized by precision balance of the rotating masses to 0.005 ounce-inch. Design criteria of 500-hour bearing life were established to meet operating requirements. (Design life of 500 hours was projected by bearing manufacturers to 2,500-hour average life.)

Thrust-load calculations showed that a maximum of 60 pounds could be expected at design speed for the MF-1 rotor. A 20 mm bearing most nearly satisfied this design criterion with a projected design life of 500 hours. Maximum radial loads were expected with the MF-2 rotor. Assuming a 0.005 ounce-inch imbalance, a 55-pound radial load was anticipated at 80,000 rpm. A 17 mm bearing met these conditions. Axial loads for the MF-2 rotor were calculated to be approximately 60 pounds, or an equivalent radial load of 147 pounds. Rotating speed limits for a 20 mm bearing, which was capable of carrying the load with a projected design life of 500 hours, were marginal because of the centrifugal load of the balls. A trade between speed limit and bearing life at these loads resulted in selection of the 17 mm bearing for both radial and thrust loads for the MF-2 configuration. The selections, which were based on recommendations of a bearing manufacturer, were high-speed, deep-groove precision bearings with aluminum-phenolic retainers and SAE 52100 chrome steel balls.

The MF-1 and RF-1 sections were designed for a common shaft with 20 mm bearings and the MF-2 and MF-3 rotor for 17 mm bearings. A preload of 40 pounds was specified for each bearing. Air-oil mist lubrication, with MIL-L-7808 synthetic oil being used, was specified, and a positive scavenge system was believed to be unnecessary. Operating temperatures for these bearings were predicted at about 300°F for the design life. Air-oil mist was considered to be adequate to remove the heat generated and to hold bearing temperatures to this limit. A microfog lubrication system was used to provide a feed rate of 4 ounces per hour. The ball-bearing design-life calculation was based on the bearing design data supplied by the bearing manufacturer. An imbalance of 0.005 ounce-inch at 60,000 rpm will produce an unbalance centrifugal force of 32 pounds at the rotor center of gravity. This dynamic load will be 43 pounds at the forward bearing and 11 pounds at the aft bearing. The total thrust load, consisting of a 40-pound bearing preload and a 60-pound impeller thrust, is 100 pounds. The C_s value for the 20 mm bearings (see Figure 56) running at 60,000 rpm is 160.* The equivalent radial load, with the rotor forces shown in Figure 56, is:

$$P = X\ (R_H + 1.2\ R_S) + YT \qquad (176)$$

*Engineering Catalog G-3, The Barden Corporation, Danbury, Connecticut, 1962.

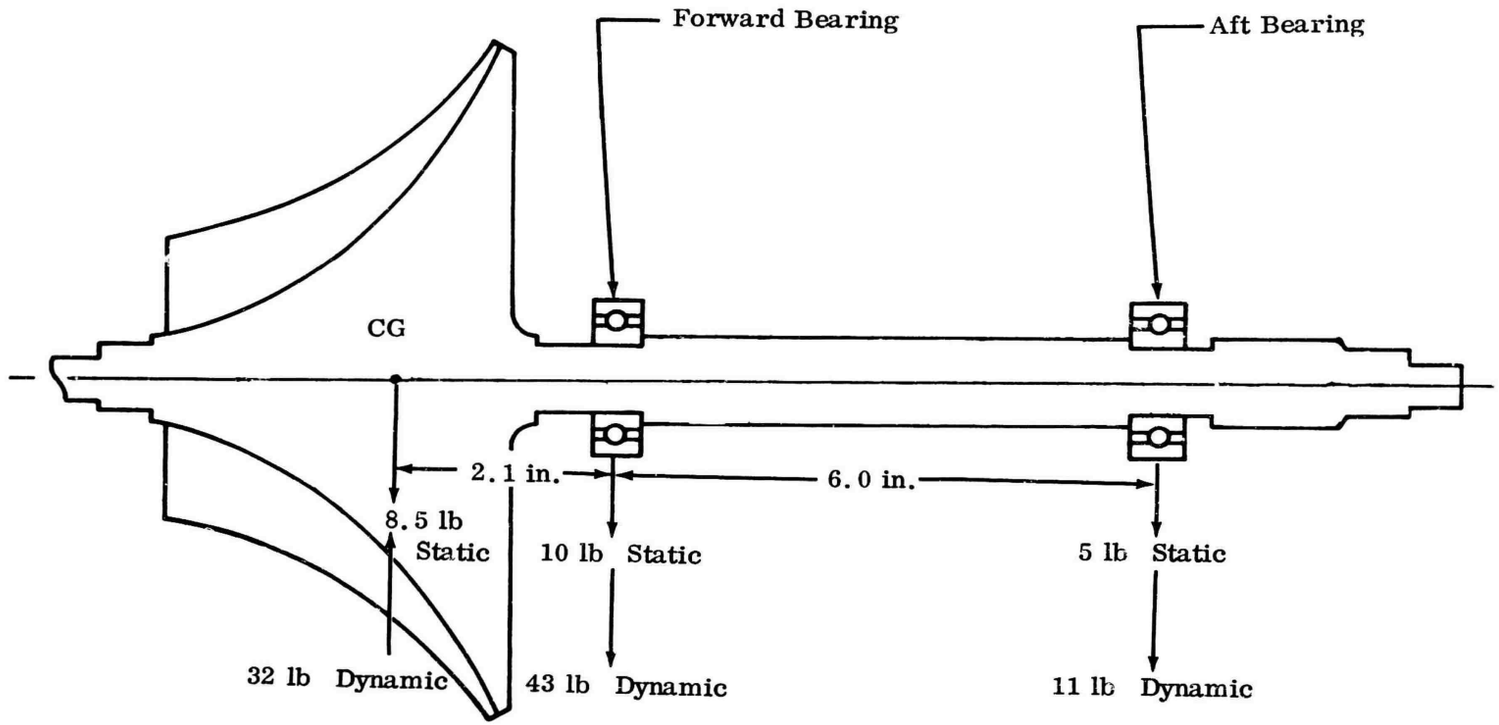


Figure 56. MF-1 Rotor Force Diagram.

where:

C_s = dynamic radial load rating, 160 lb

X = 0.47 for contact angle of 10 degrees

Y = 1.3 for thrust/ZD^2 of 228

R_H = 10-pound static radial load

R_s = 43-pound dynamic radial load

T = 100-pound thrust load

P = 0.47 (61.5) = 1.3 (100) = 159 pounds

Bearing design life for the 204 (20 mm diameter) bearing is:

$$\text{life in hours} = 500 \left(\frac{C_s}{P}\right)^3 \tag{177}$$

$$= 500 \left(\frac{160}{159}\right)^3 \approx 500 \text{ hours}$$

The equivalent average life for the 500-hour bearing design life is 2500 hours. Similarly, the bearing design life for the 203 (17 mm diameter) bearing, with the rotor forces shown in Figure 57, is 280 hours, and the equivalent average bearing life is 1400 hours. The projected test-rig time was only 100 hours.

3.2 ROTOR DYNAMICS ANALYSES

Analyses of the dynamic characteristics of the rotor system with various bearing support stiffnesses were conducted. The cantilevered-shaft configuration shown in Figure 55 was investigated. The resulting first, second, and third critical speeds are shown in Figure 58.

The selected forward and rear bearing-mount spring rates of 10,000 lb/in. permitted operation between the second and third critical speeds, which were 17,000 and 80,000 rpm, respectively.

The typical configuration studied above did not apply directly to the rotor system for the MF-2 impeller, since limiting bearing size to 17 mm precluded use of a shaft with the same diameter and stiffness. An investigation of the effect of shaft

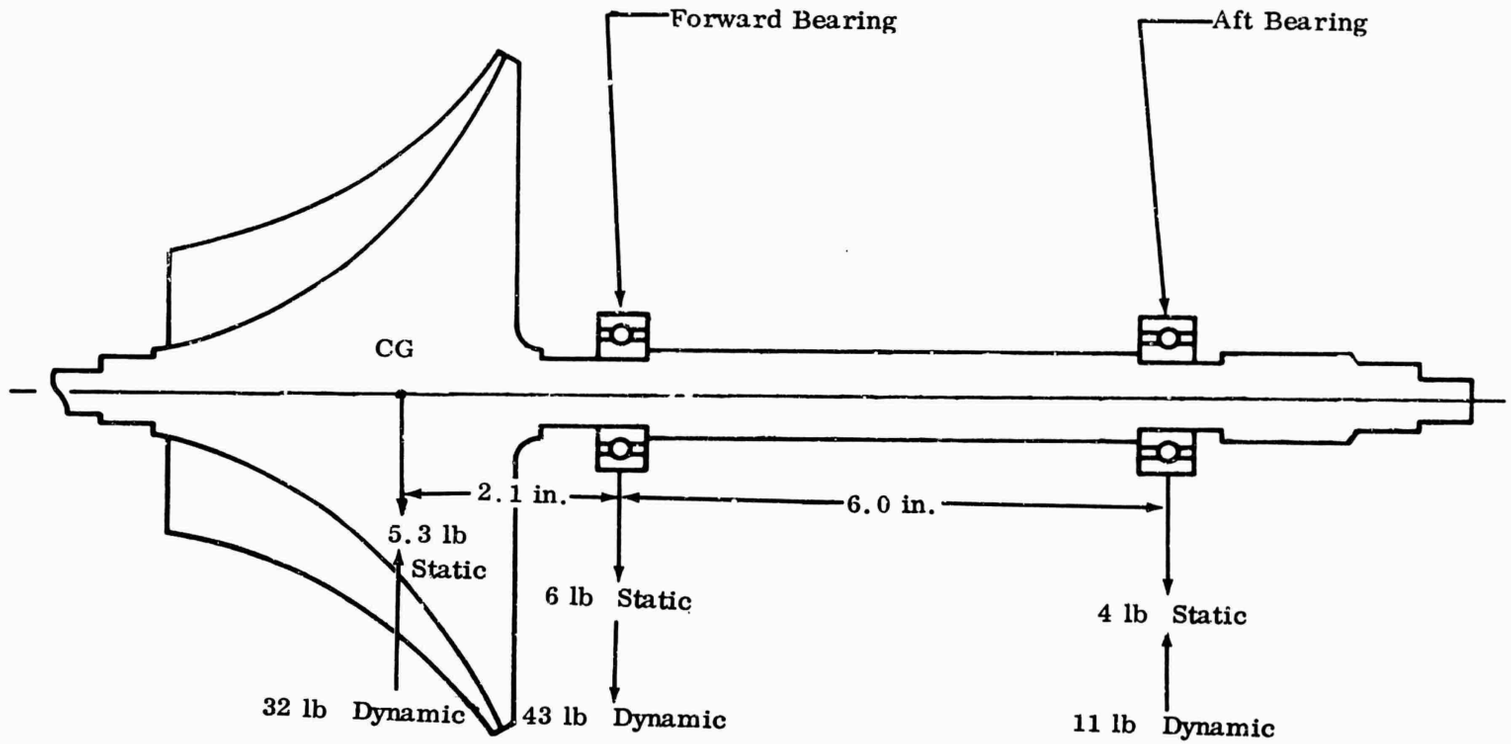


Figure 57. MF-2 Rotor Force Diagram.

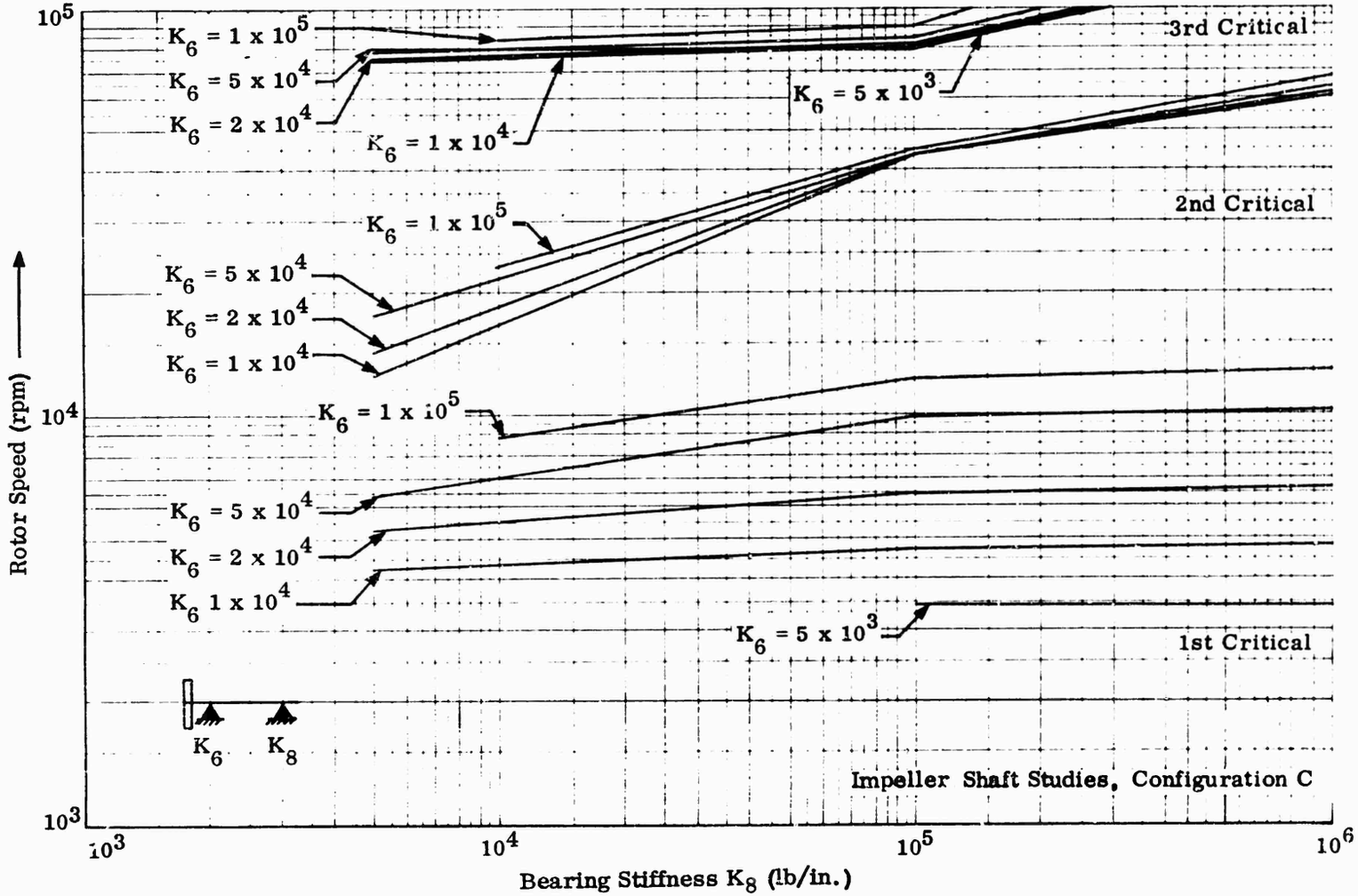


Figure 58. Critical Speed Versus Bearing Stiffness.

diameter and forward bearing stiffness, and assessment of critical speeds as a function of rear bearing stiffness was made. The 17 mm bearing established the shaft diameter to be between 0.65 and 0.80 inch. The first and second criticals presented no problems, but the third and fourth criticals transcended the operating range. The configuration selected was a shaft diameter of 0.70 inch and a bearing stiffness of 10,000 lb/in., projecting the first through fourth criticals at 4,700, 12,999, 36,000 and 102,000 rpm, respectively.

3.3 MODIFICATIONS

A shakedown test to evaluate the structural and operational integrity of each compressor unit was planned.

3.3.1 MF-1 CONFIGURATION

Accelerometers were mounted on the turbodrive and compressor-unit housings to measure the vibration, and thermocouples were installed to monitor bearing outer-race temperatures. The turbodrive unit was tested to 78,000 rpm as a free turbine with no load. Maximum bearing temperatures of 160°F and vibration levels of 2 g at rotor frequency were recorded at the maximum speed. These conditions were considered to be satisfactory for long-term use of the unit.

The dynamic characteristics of the combined units were initially checked with a dummy impeller, with the mass moment of inertia of the test impeller installed. This allowed operation with a minimum of torsional and thrust loads. With the rotor balanced to within 0.002 ounce-inch,test runs were completed successfully to 63,000 rpm. Resulting vibration levels versus speeds are shown in Figure 59. Maximum bearing temperatures encountered were 300°F. The dummy impeller was removed, and the test impeller was installed for the next phase of the test.

Several mechanical problems were encountered with the test impeller assembly:

1) The positive contact bearing seals failed to function above 30,000 rpm due to lack of lubrication from the air-oil-mist system;

2) The labyrinth seal at the impeller tip did not provide a sufficient pressure drop to limit the thrust load at the back face of the impeller;

3) The air-oil-mist system provided adequate lubrication but failed to remove excessive heat generate . in the bearings;

4) The splined coupling between the compressor and drive units was considered to be the source of forced excitation to the shaft above that incurred by the imbalance of the rotor system;

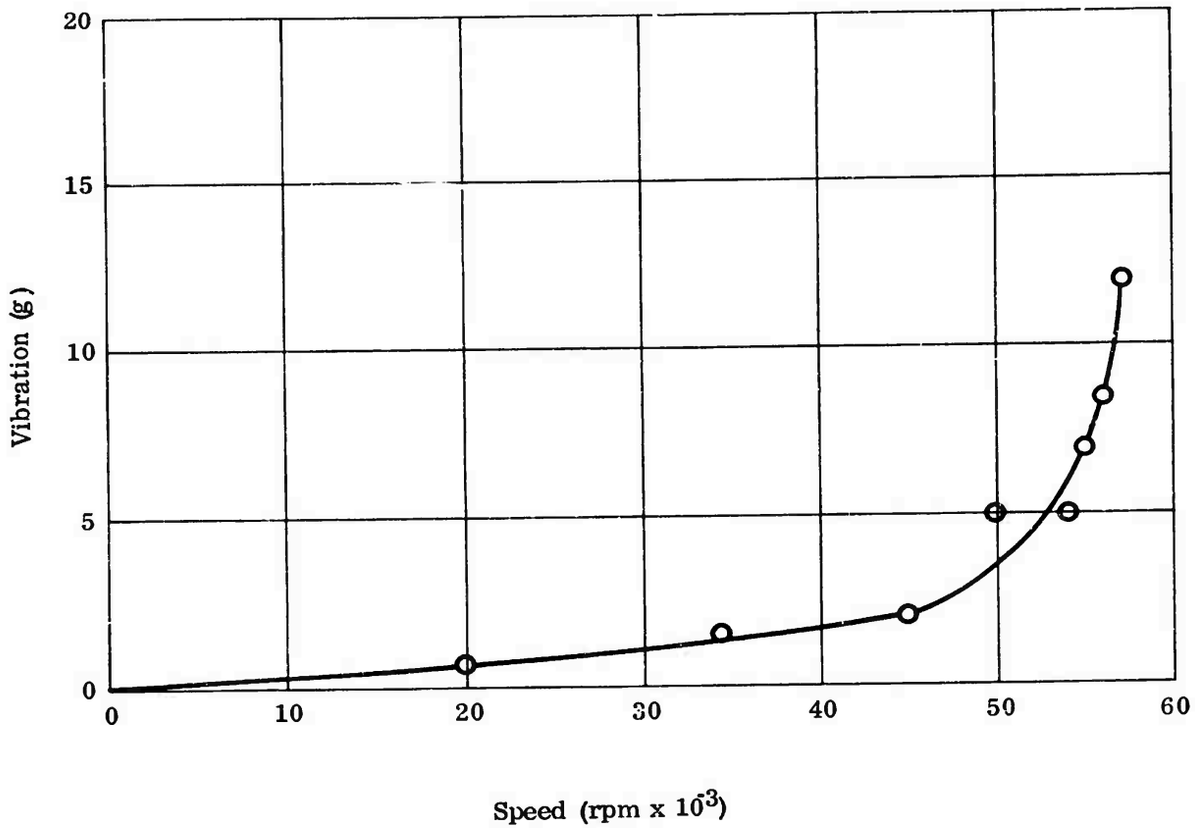


Figure 59. MF-1 Vibration Levels.

5) Several instances of contact between the impeller blades and shroud indicated that a change in the clearance between the blade tip and shroud took place with an increase in speed.

Initial evaluations on clearance changes attributed this condition to distortion caused by thermal gradients in the shroud; however, a detailed analysis (Figure 60) revealed that only 40 percent of the distortion was due to thermal growth and 60 percent to elastic growth of the impeller disk. The projected change in clearance as a function of speed was calculated, and further rubs were eliminated by spacing the shroud to allow for the change with speed.

Design modifications were implemented to correct the above problems. Test data indicated that a maximum thrust load of approximately 1700 pounds was produced by the static pressure acting on the back of the impeller disk, which showed that the labyringh seal at the impeller tip was ineffective. An antithrust disk, with a controlled pressure cavity, was installed at the coupling end of the shaft to balance the thrust and to reduce bearing loads to the capacity of the bearing. The air-oil mist lubrication system was replaced with a jet-spray system. The carbon-seal support was modified to ensure adequate lubrication of the contact surfaces without excessive oil flow into the impeller cavity. This correction reduced bearing operating temperatures from a maximum of 300° to 160°F at the design speeds. The splined coupling was replaced with a flexible-disk frictionless coupling, capable of sustaining a total misalignment of 0.002 inch.

These modifications served to correct the mechanical operating difficulties of the rig and made possible a complete run through the design speed. The dynamic characteristics of the compressor unit with the rotor balanced to within 0.001 ounce-inch were then investigated to check the computed critical speeds.

The level of vibration above 55,000 rpm increased rapidly, which indicated that a rotor- or support-system resonance occurred in the immediate range above this speed. This resonance was not predicted from the initial calculations, which indicated that the third critical would not occur until 80,000 rpm. It was necessary to modify the rotor system to allow operating the test rig at speeds between 55,000 rpm and the design speed. The original design utilized soft bearing mounts similar to these of the diffuser-test-rig modification, but no damping system was used. Therefore the design was modified to incorporate a viscous damper for the bearing mounts.

It was believed that if the clearance between the flexible bearing support and the housing frame were pressurized with lubricating oil, damping effectiveness would increase with frequency. This revision reduced the shaft displacement and bearing loads and allowed safe operation at speeds of up to 59,000 rpm, as shown in Figure 61. At this point the MF-1 rig was considered to be satisfactory.

Curve A, Shroud and Backplate Distortion
Curve B, Axial Thermal Expansion Differential
Curve C, Impeller Centrifugal Force Distortion
Curve D, Dynamic Tip Clearance (sum of A, B, & C)

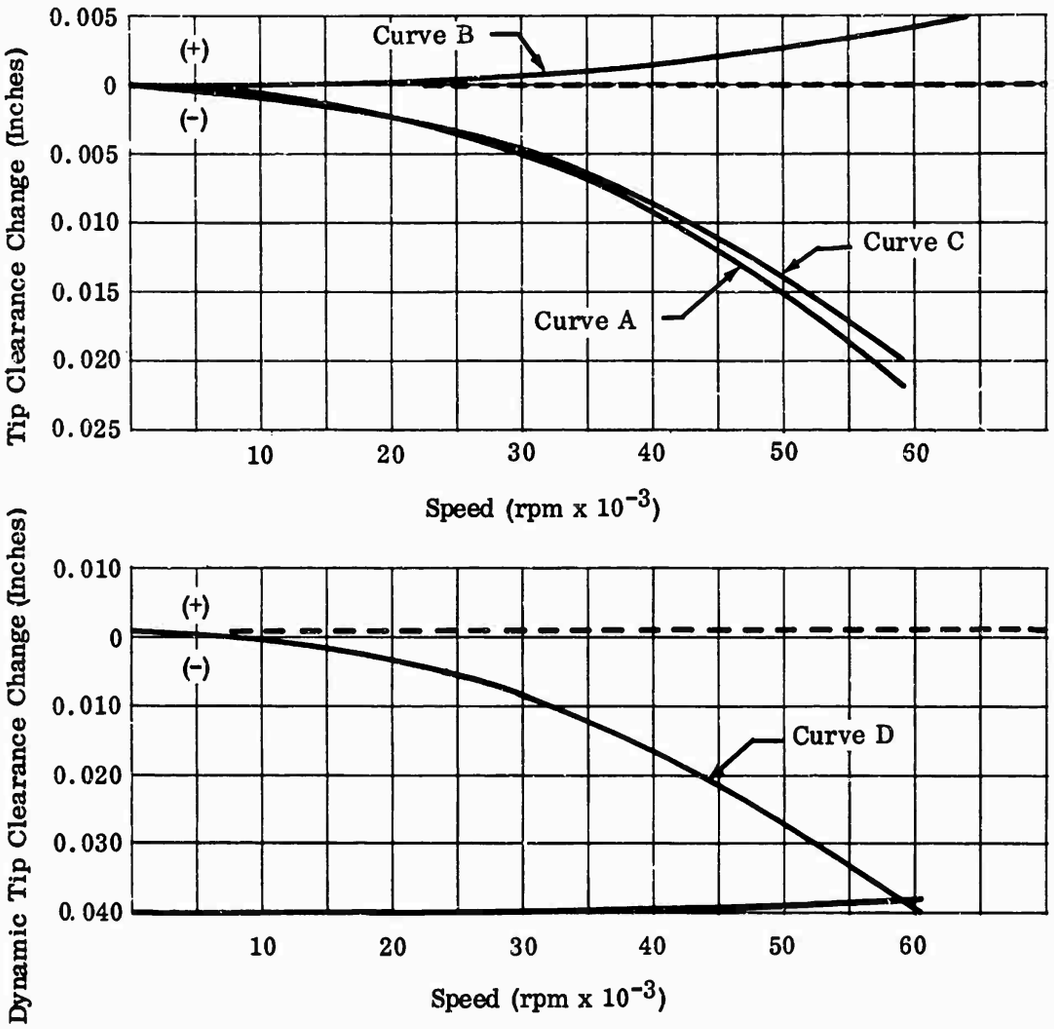


Figure 60. MF-1 Clearance Changes.

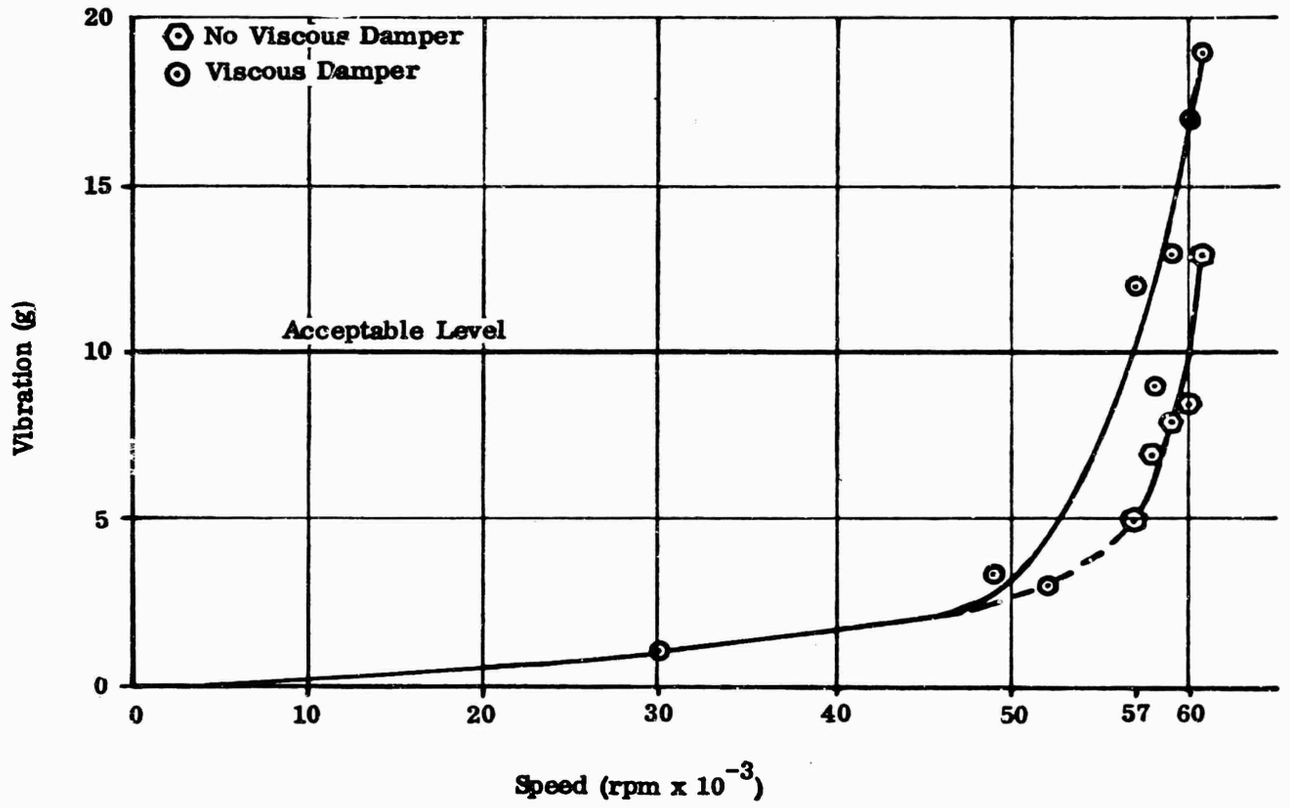


Figure 61. Effects of Viscous Damping.

3.3.2 RF-1 CONFIGURATION

The initial run of the RF-1 was successful at speeds of up to 44,000 rpm as a result of improvements implemented from the MF-1 experience. However, a substantial increase in the vibration level was encountered at speeds above 44,000 rpm. A critical speed was found at 48,000 rpm by accelerating rapidly to 50,000 rpm, at which speed a rub between the impeller and shroud occurred. These dynamic characteristics of the RF-1 rotor assembly were not predicted by the original analysis.

Another preliminary test, similar to the one performed on the MF-1 rig, was planned for the RF-1. Because of the more symmetrical disk shape of the RF-1, its elastic growth at high speeds was less than that encountered with the MF-1. Probes were installed to measure the movement of the related structures and the blade clearances at various speeds. In addition, improved rub sensors were installed to detect contact and to prevent damage to the impeller blades.

Relative to the critical speed, a study was made to evaluate the computer program input parameters. Twenty-eight variations in the input parameters were made in an attempt to correct the previous input variables and to establish improved prediction techniques. The results showed that the best correlation with the test was attained by lumping the large masses and by increasing the number of sections used to define the more flexible part of the shaft. Accordingly, the first, second, and third critical speeds were recalculated for the MF-1 to be 3,239, 8,959, and 56,142, respectively. Additional refinements were made by adjusting the mass in the disk in proportion to the effect of the polar moment of inertia on gyroscopic stiffening.

With the above refinements being made, the critical speeds were recalculated for the RF-1; the results are shown in Table I.

TABLE I
COMPRESSOR CRITICAL SPEEDS

Compressor Unit	Critical Speeds			
	First	Second	Third	Fourth
MF-1	3,239	8,959	56,142	
RF-1	3,262	8,784	48,286	155,440

The third criticals for the MF-1 and RF-1 were within the operating range. Positive resolution of this problem would involve substantial modifications to the rig and rotor hardware. Damping was proved to be only partly effective, since space was not available to provide a damping system with a critical damping factor. Therefore, it was considered that, if each of these units could be balanced for the third mode, the displacement could be reduced to a safe operating level and operation at or through this critical speed would be permitted.

A modal balance technique, as described in Appendix V, was subsequently adopted on the RF-1 unit with rewarding results. An 80-percent reduction in the shaft displacement at the previously determined critical speed was noted without an increase in the displacement at the other speeds. The problem of operating in the critical speed range was therefore resolved without need for further modification of the hardware. The rig was subsequently run up to 59,000 rpm through the third critical without excessive bearing load. Thermal growth of the housing and elastic growth of the rotor disk were compensated by adjusting the shroud position to provide the desired clearance between the impeller blades and the shroud contour at various speeds.

Modal balance of the MF-1 rig was similarly successful. Operation of both impeller sections at speeds of up to 59,000 rpm was demonstrated without further malfunctions.

3.4 CONCLUSIONS

The problems encountered with the impeller test rigs were associated with critical speed, thermal distortion, and elastic deformation. Correlated experimental and analytical evaluations provide an improved technique for predicting dynamics of the rotor system.

The heavy sections used to provide the structure and rotor system housing accommodated the heavy saturation of aerodynamic and rotor dynamics sensors and facilitated fabrication of one-only components with a minimum of tooling. However, temperature gradients across irregularly shaped sections made it difficult to predict the distortion which resulted. Uniform cross sections and flexible structures comparable to the conventional designs used in gas-turbine engine would have provided better assurance of dimensional stability. Accurate prediction of critical speed is largely dependent on previous experimentally confirmed inputs. The correlated experimental and analytical evaluations made with the impeller rig revealed the following specific factors:

1) Forced excitation of the rotor system by friction-type couplings, imbalance, and aerodynamic pulsations will prevent operation in the critical-speed range unless compensating factors are provided to minimize or dissipate the energy being generated. Damping can be effective if the geometry and design speed make it possible to provide a damper with critical damping coefficient (C_c) where $C_c = 2\ m\ \omega_n$. Modal balance was proven to be most effective for operation at or near a shaft critical speed. With the forced excitation caused by built-in imbalance, counteracted by an equal and opposite imbalance at the point of maximum shaft deflection, the exciting force in the rotor is held to a minimum and results in smooth operation at or near resonance. The method is especially effective if some damping can be provided, since it is possible to attain critical balance only for specific modes of vibration. The process was relatively simple for the subject rotor but would become increasingly more complex if compensation for additional modes of vibration were necessary.

2) The magnitudes of thermal distortions and elastic deformations, due to the dynamic behavior of a rotor system, are difficult to predict accurately. Experimental systems which are designed to accommodate rotors with minimum shroud clearances should be equipped with proximity probes for continuous monitoring of the clearances.

3) High-speed antifriction bearing systems should be designed with spray- or jet-lubrication system. Air-oil-mist systems may not remove the heat generated in the bearings at high speed. Although bearings are designed for operation at up to 300°F, the design life is substantially reduced by dimensional changes which will alter the bearing design clearances and will result in operation at various contact angles.

(U) APPENDIX IV

SPIN-PIT TESTING

ABSTRACT

Research impellers tested by the contractor for the Army compressor research program were proof-spun in a high-speed spin pit before assembly in the aerodynamic test rig. This appendix describes the high-speed spin-pit facility and discusses its operation. General recommendations are made that should contribute to a successful high-speed spin-pit operation.

1.0 BACKGROUND AND INTRODUCTION

The impellers associated with the Army centrifugal-compressor research program were designed for high blade-tip speed (2000 feet per second compared to 1600 feet per second in previous contractor applications). In minimizing the risk of damage to the aerodynamic test rig, proof of material integrity was important. This was accomplished by running the impellers overspeed in the spin pit. The RF-1 and MF-1, as well as a workhorse impeller used for diffuser research, were successfully proof-spun. The MF-2 impeller was damaged in the spin pit because of a combined failure in a bent drive quill shaft, a severely scored bearing race in the drive turbine, and a broken test-rotor arbor.

2.0 BOEING SPIN-PIT FACILITY

The Boeing spin pit has a design maximum speed of 100,000 rpm and can accommodate rotors up to 16 inches in diameter or 17 inches in length. The chamber was constructed of armor plate with a replaceable 4-inch-thick hardwood inner liner. The test rotor was positioned with the rotational axis vertical and was suspended from the air-drive turbine on a long, slender quill shaft. Figure 62 is a photograph of the spin-pit facility.

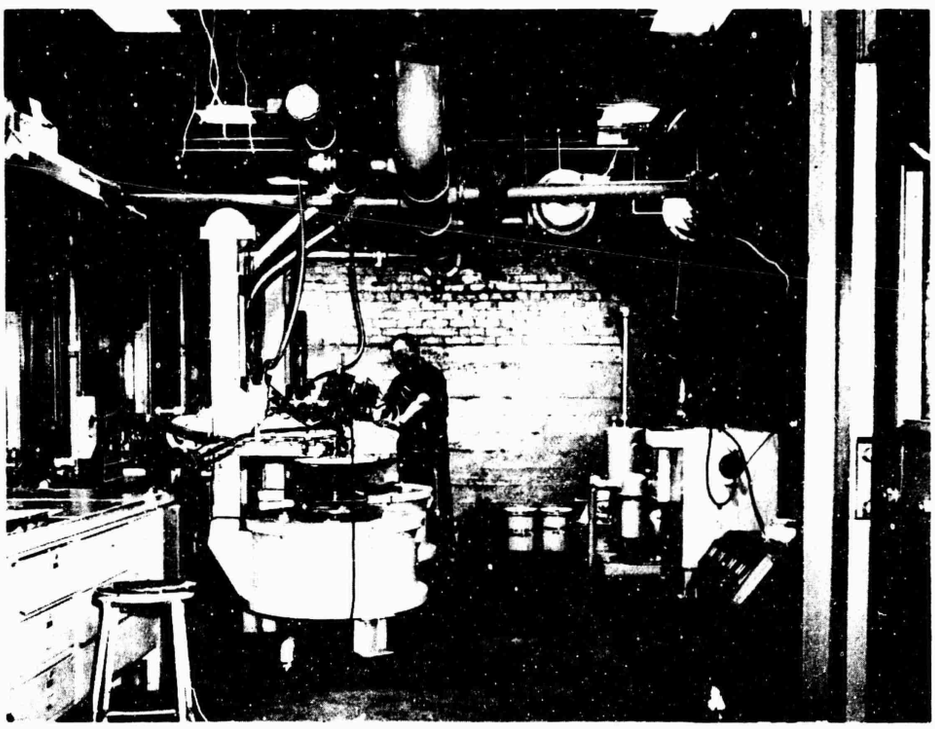


Figure 62. Spin-Pit Facility.

Figure 63 is a cross section of the drive system with the MF-2 impeller installed. The ends of the quill shaft were attached with shear pins to the test-rotor arbor and to the drive-turbine shaft. Snubber bushings with approximately 0.005-inch diametric clearance were provided to contain the quill shaft. This arrangement was intended to permit the test rotor to rotate about its own mass center and to isolate it from the drive turbine if a test-rotor failure occurred. In such an event, shearing of the pins would allow the lower end of the test-rotor arbor to drop into the bearing-mounted catch cup, while gyrations of the upper end of the arbor would be limited by the clearance between the arbor and the upper catch ring.

The drive turbine was mounted on preloaded ball bearings, which were oil-mist lubricated. Devices for controlling, indicating, and recording speed were used.

Proof-spinning was accomplished by bringing the impeller up to speed as rapidly as possible. For this application, the drive-turbine bearing selections were based on short-operating-life considerations. Operating limits of the spin pit are as follows:

1) Rotor-shaft displacement, 0.010 inch;

2) Bearing temperature, 250°F;

3) Lubrication, one drop oil per 10 seconds (gravity feed);

4) Spin-pit vacuum, 0.5 inch Hg;

5) Spin-pit temperature, 1800°F;

6) Speed limit, 100,000 rpm.

The test-rotor assembly on the arbor had to be balanced within 0.001 ounce-inch about the axis on which it will spin in the pit.

3.0 IMPELLER SPIN TESTS

The first 3 impellers proof-spun in this program were the RF-1, the MF-1, and the diffuser-test-rig workhorse impeller. Proof-spinning of these impellers was accomplished satisfactorily. However, an instability was encountered when an attempt to proof-spin impeller MF-2 was made.

Of the impellers proof-spun, including the impeller of the T50-BO-10 engine, the MF-2 had the lowest equivalent diameter length.

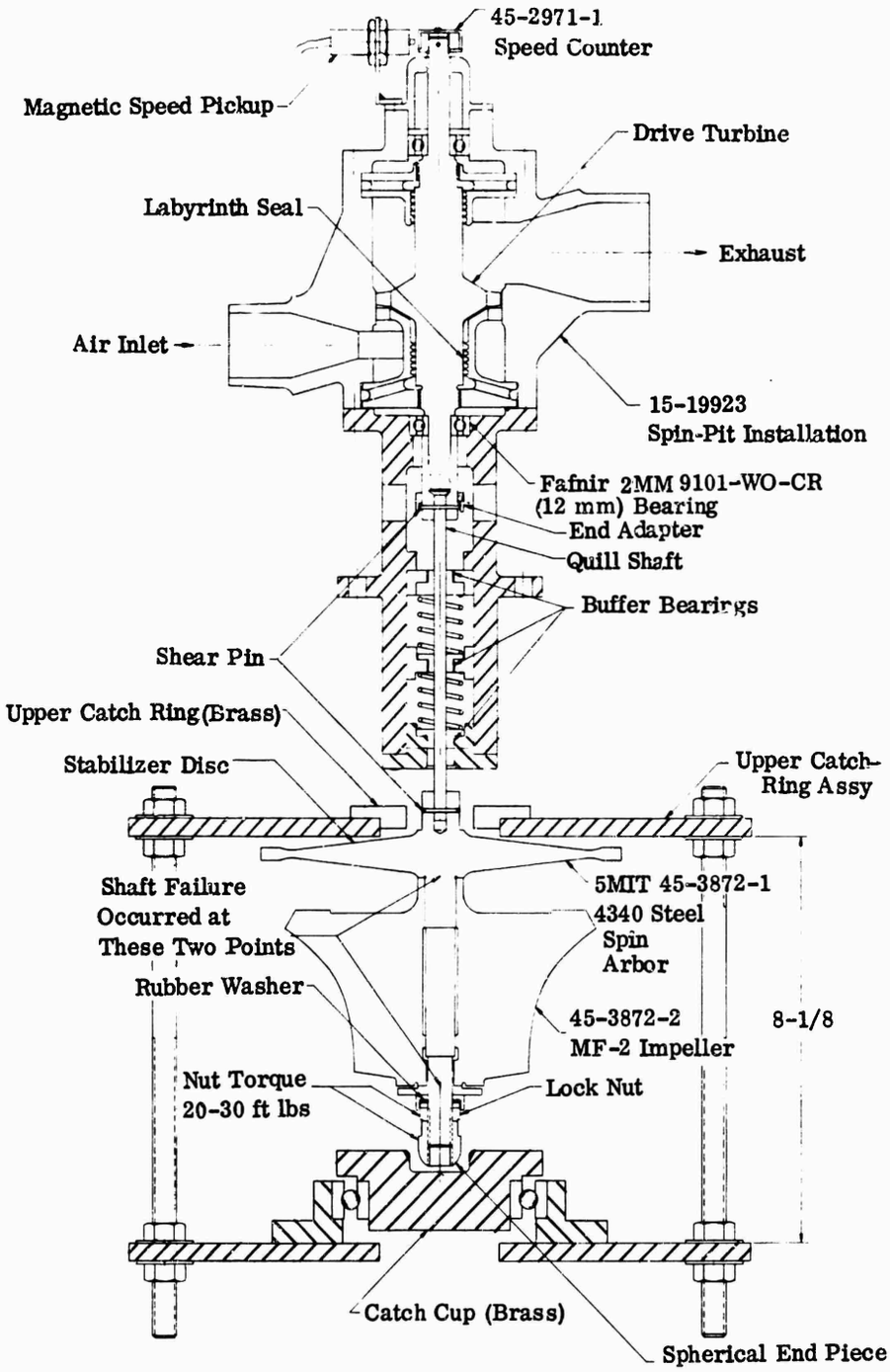


Figure 63. MF-2 Impeller (Spin-Pit Installation).

Impeller	D/L
T-50	3.55
MF-1	3.10
RF-1	2.85
MF-2	2.22

Den Hartog* states that as the D/L ratio approaches the theoretical minimum stable ratio of 1.1, varying degrees of instability may be encountered. In this case, an impeller may be excited readily by extraneous forces such as residual imbalance, rubbing of the quill-shaft bushings, or turbine bearing-induced vibrations. A rotor that has an unfavorable D/L ratio will tend to seek another axis of rotation when spun.

To increase the D/L ratio, a stabilizer disk was added (Figure 63). This raised the equivalent D/L ratio to 3.33.

4.0 DISCUSSION

The instability in the test-rotor assembly could have been triggered by a number of conditions, singly or in combination, as described in the following sections.

4.1 RESIDUAL IMBALANCE

The assembly was balanced to an accuracy of 0.0005 ounce-inch, which was adequate. However, if a misalignment or eccentricity existed in the counterbore where the drive quill was attached, unstable operation could occur with the resulting imbalance. The accompanying forces vary in amplitude as a function of the square of the speed.

The final balancing correction of the impeller and stabilizing disk assembly was made in 2 planes normal to the rotational axis (i.e., at the impeller inlet end and at the stabilizer disk). Because the imbalance to be corrected did not lie in either of these planes, the correction produced force couples between the actual imbalance and the 2 correction planes which increased in magnitude as a function of the square of the speed.

If the hub connection between impeller and stabilizing disk were sufficiently flexible, it was expected that these 2 main elements of the assembly could be

*J.P. Den Hartog, Mechanical Vibrations, McGraw Hill Book Co., New York, 1956.

deflected from the axis of rotation. This effect was minimized by balancing the impeller and the disk individually before final assembly and balancing.

4.2 IMPELLER-TO-SHAFT FIT

The spin arbor was sized to provide 0.0002-inch diametrical interference in the impeller bore at both ends to ensure positive alignment on center. Analysis of the deflection in the impeller bore due to centrifugal force at 66,000 rpm showed that the lower (inlet) end would increase in diameter by 0.0009 inch allowing 0.0007-inch diametrical or 0.00035-inch radial clearance. The diameter of the hub extension at the upper end contracts 0.0005 inch, which increases the effective diametrical interference to 0.0007 inch. While the interference occurring at the upper end would tend to hold the impeller centered, the clearance at the lower end could have permitted a radial shift, with a possible resultant force (imbalance) of 58 pounds at 66,000 rpm.

4.3 AXIAL CLAMPING LOAD

The axial clamping load of the impeller on the arbor could tend to deter a radial shift, such as that indicated above, or it could force the shift in one direction as a result of squareness tolerance between the nut and the impeller clamping surface. An analysis of the arbor stretch (due to retainer nut torque) versus axial contraction of the impeller-hub dimension (due to centrifugal load) showed a clamping load of approximately 3100 pounds at 66,000 rpm, compared to an initial load of 5640 pounds.

4.4 EXTRANEOUS EXCITATIONS

A high-speed rotating system such as the MF-2 in the spin pit could have been excited by various external vibrations or cyclic loads. Those excitations most likely to have affected the system are:

1) Residual imbalance in the drive-turbine rotor and quill shaft;

2) Dynamic action in the drive-turbine bearings, including motion of ball bearings and cages relative to the races, which could have been affected by axial preload and radial clearance in the bearings;

3) Dynamic behavior of the drive quill in the buffer bearings. If the rotor system encountered a dry rub while whirling in a backward, nonsynchronous fashion, the whirl could have become self-excited and would have been catastrophic.

This combination was subjected to a spin test, and it sustained a failure at 65,940 rpm as indicated by the speed recording reproduced in Figure 64. The

speed trace showed essentially constant acceleration of the drive turbine up to the point of failure, then 400 rpm drop in speed followed by a rapid acceleration to the overspeed cutoff point of 71,000 rpm.

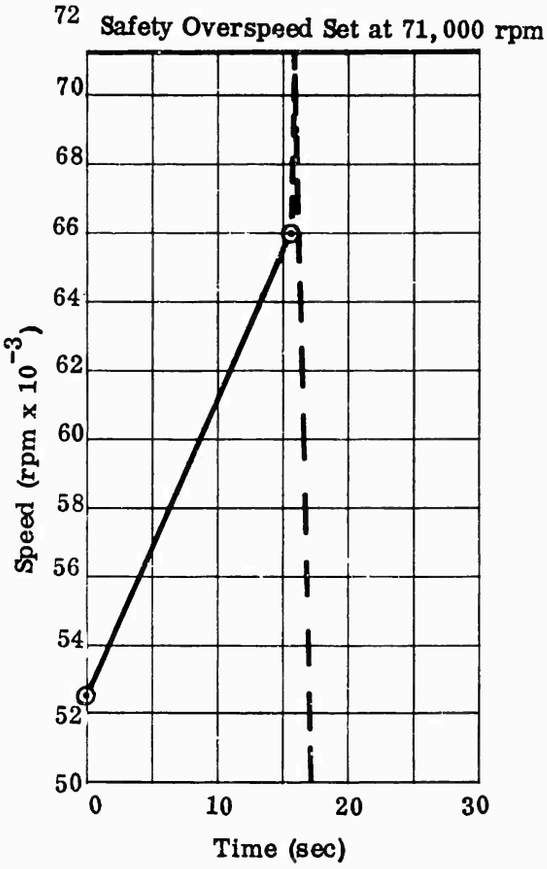


Figure 64. MF-2 Impeller (Spin-Pit Speed Record).

Post-test examination of the parts revealed the following points.

1) The drive quill shaft was bent at the lower end, indicating a substantial lateral displacement of the test-rotor arbor (Figure 65). Both pins had sheared. The bent quill shaft had worn the bushings oversize and there had been relative rotation between the quill and the drive-turbine shafts after the quill shaft was bent.

2) The inner race of the lower bearing in the drive turbine was severely scored, indicating a heavy side load similar to imbalance (Figure 66). The phenolic

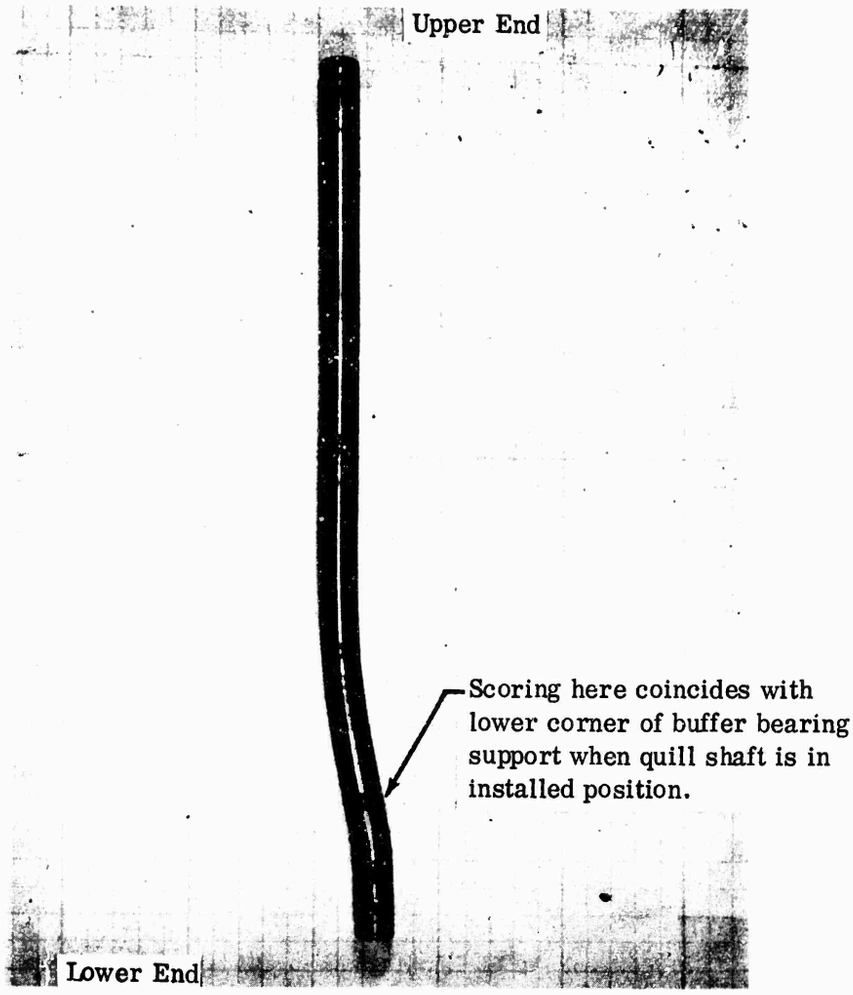


Figure 65. Spin-Pit Drive Quill Shaft After Attempted Proof Spin of Impeller MF-2.

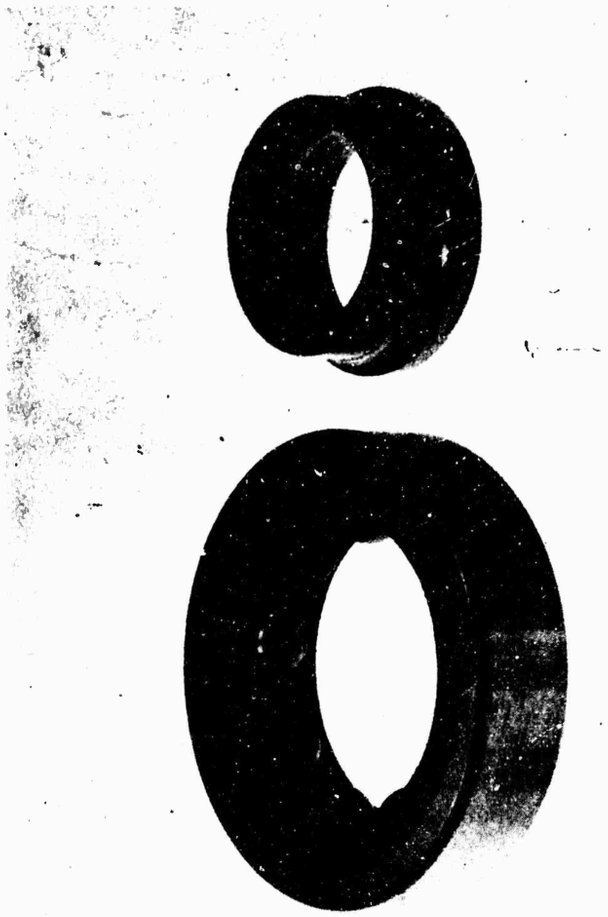


Figure 66. Spin-Pit Drive Turbine Lower Bearing After Attempted Proof Spin of Impeller MF-2.

cage and the balls in the outer race of the bearing were relatively undamaged, indicating that the load which damaged the inner race did not persist for any substantial interval.

3) The spin-test arbor was broken in 2 places, at the upper and the lower side of the impeller. The impeller sustained blade damage from random contact with the walls of the chamber (Figures 67 and 68). Examination of the fractured arbor ends in the impeller (Figures 69 and 70) indicated that the arbor had broken at the upper end first, then was pulled downward about 0.060 inch as the lower end of the arbor broke off. Closer scrutiny of the score marks in Figure 69 shows that the impeller was probably rotating faster than the stabilizing disk as the 2 pieces separated. The probable sequence of events in the failure was as follows:

   a) The rotor and arbor assembly lost stability at 65,940 rpm, causing lateral movement of the spin-arbor axis and bending of the quill shaft.

   b) The quill shaft jammed in its buffer bearings, momentarily causing an excessive rotating radial load on the lower drive-turbine bearing.

   c) The shear pins then failed, permitting the turbine to accelerate relative to the quill shaft and allowing the impeller to drop into the catch cup.

   d) The upper hub of the arbor was not constrained by the upper catch ring. (There were no marks on the upper hub to indicate contact with the upper catch ring. It was concluded that the ring must have been positioned too high to be effective.)

   e) With no restraint at the upper end, the impeller with the stabilizing disk tumbled in the spin chamber, breaking the arbor in 2 places as described above.



Figure 67. Impeller MF-2 After Attempted Proof Spin.

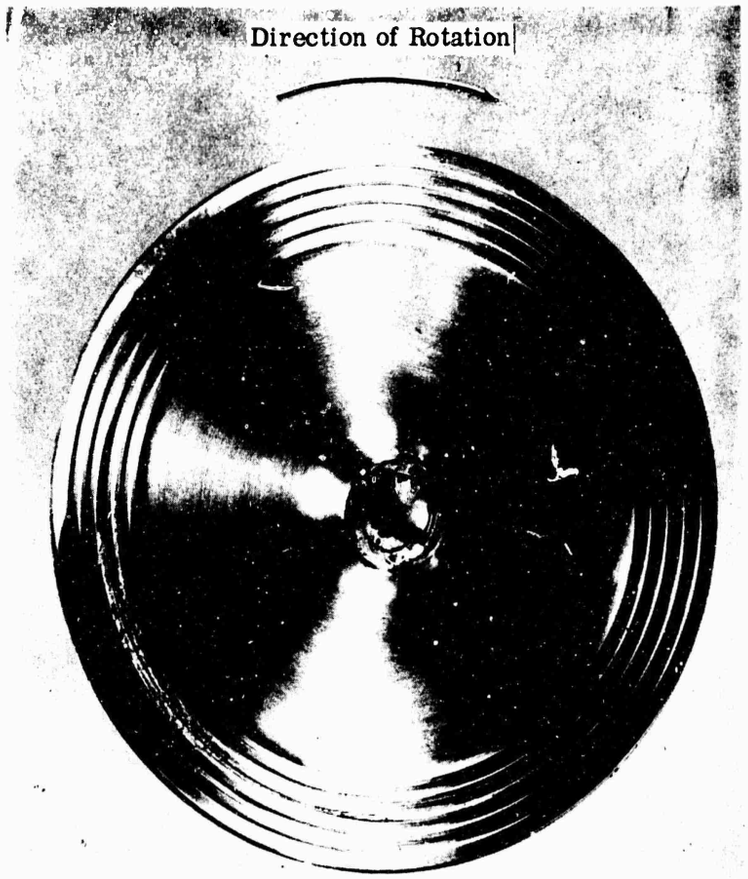


Figure 68. Upper (Rear) Face of Impeller MF-2 After Attempted Proof Spin.

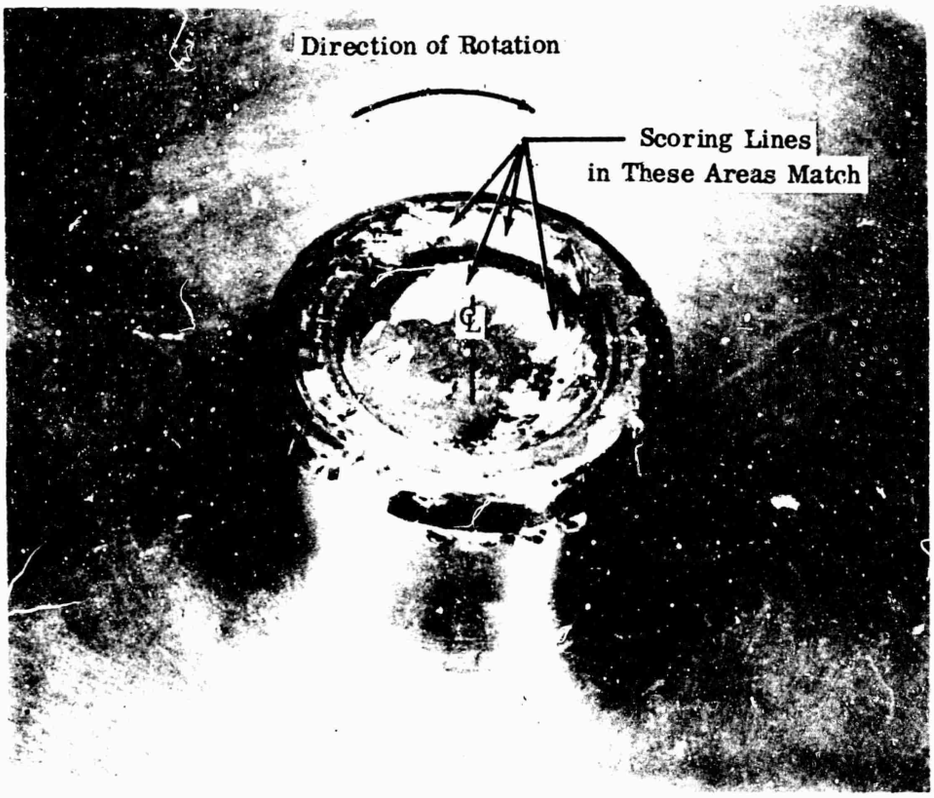


Figure 69. Broken Arbor at the Upper End of Impeller MF-2 After Attempted Proof Spin.

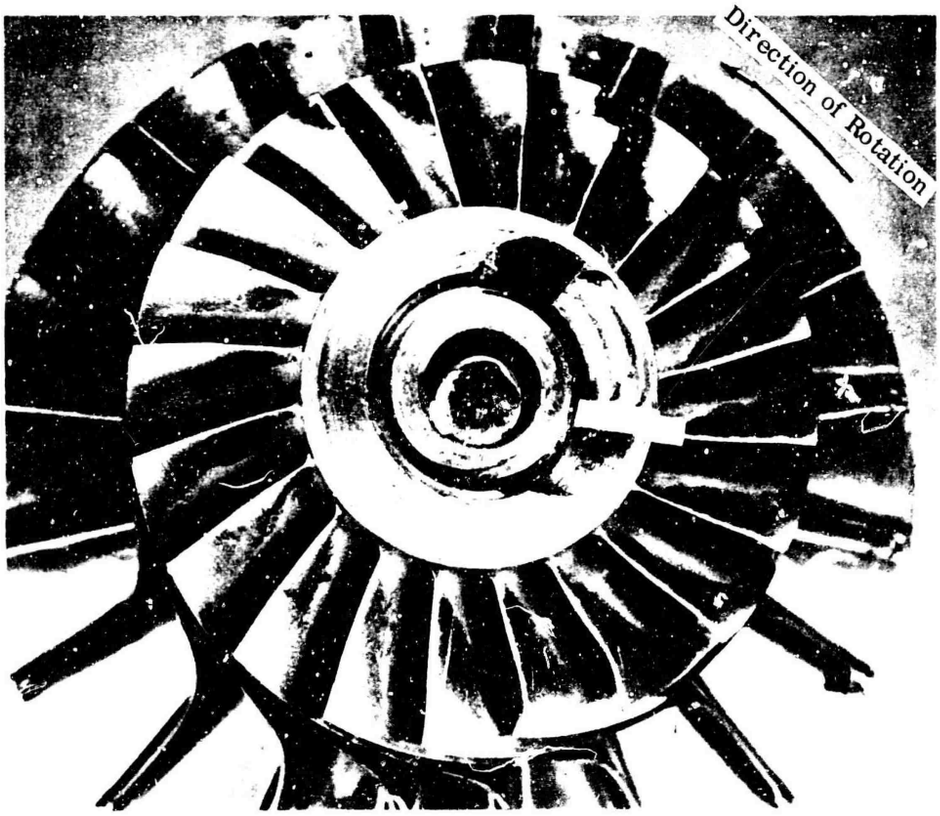


Figure 70. Broken Arbor at the Lower End of Impeller MF-2 After Attempted Proof Spin.

5.0 CONCLUSIONS AND RECOMMENDATIONS

Of the considerations discussed above, indications were that a radial shift of the MF-2 impeller on the spin arbor was the most likely explanation for the sudden instability that caused failure. As the rotor accelerated, the gradual reduction in axial clamping load, accompanied by increasing internal force couples, could have permitted the shift, possibly triggered by a cyclic vibration transmitted from the drive quill shaft on the drive turbine, or both.

The following recommendations should ensure successful high-speed spin-pit operation:

1) Consult with a reliable bearing manufacturer in the selection, installation, and operation of drive-turbine bearings;

2) Dynamically balance the drive turbine and the spin-pit-test rotor to less than 0.001 ounce-inch;

3) If the spin-pit-test rotor is comprised of more than 1 disk or wheel, dynamically balance the separate parts before assembly, and then dynamically balance the assembly;

4) If the rotative speed is such that the bore fit of the spin-pit-test rotor will be lost due to centrifugal load, provide for holding the rotor on center;

5) When the axial length of the test rotor permits, undercut the spin arbor to reduce the tensile spring rate, thus minimizing the variation of axial clamping load with speed.

(U) APPENDIX V

MODAL BALANCE

ABSTRACT

This appendix presents the balancing method used to reduce the vibration amplitude of the first shaft-flexure mode. This technique is commonly known as modal balancing and is useful if excessive vibrations are encountered when accelerating rotating machinery through a shaft critical speed.

SYMBOLS

A_1	displacement amplitude
CW	calibration weight
M_1	modal balance weight
θ_1	phase angle (degrees)
ϕ	phase angle (degrees)
W	base speed (rpm)

1.0 GENERAL INFORMATION

Static and dynamic balancing operations of a rotor system will result in smooth operation at speeds below the first shaft-bending critical (the third shaft critical for soft-mounted bearings). The balance corrections are made in 2 planes, regardless of how the imbalance is distributed. As the rotational speed of the shaft is increased, elastic deflections due to centrifugal forces occur and the condition of balance is upset. The changes in balance caused by these deflections can become large and prohibit running at certain speeds. The forces caused by the eccentricity of the shaft and the resultant forces for particular shapes of elastic deflections can be determined. As a result, small correcting masses which introduce imbalance (static and dynamic) can produce vibration-free operation at all speeds. This process of counterbalancing a dynamically unstable rotor system is termed modal balancing.

The process of modal balancing was experimentally tried when the MF-1 rotor system was discovered to be operating at a critical speed. The success of the first application of this technique led to modal balancing the RF-1 rotor system to improve its acceleration through the shaft critical speed.

The basic theory of modal balance technique shows that a rotor assembly can be balanced (i.e., made to operate through a critical speed with little or no vibration amplitude) by the addition of small weights to the shaft.* The number of weights and corresponding planes of application required equals the number of shaft-vibration modes in the operating range. Most shafts can be designed to operate below the third critical; thus only 1 plane is required for the correction weight. For high-order criticals, the modal balance method becomes increasingly difficult because it is necessary to position the correction weights in such a manner that their combination will balance but that it will not excite other criticals as the speed is advanced through the operating range. The discussion here will be limited to the first critical-speed modal balance solution.

The first mode of vibration is excited by an inherent imbalance due to manufacturing tolerances of the rotor assembly. In this mode, the shaft will bend in a plane that passes through the axial centerline of the rotor assembly. As long as the rotor remains assembled, this bending plane will remain at the same phase angle on the shaft. To modal balance the rotor, a compensating, small imbalance weight is used. This weight is placed in the bending plane, but at 180 degrees out of phase with the initial bend (Figure 71). The weight can be positioned arbitrarily along the shaft. Thus, this small weight counteracts the original imbalance that caused the large amplitudes at the critical speed. The added weight also produces equal but opposite forces and cancels the bending.

---

*Jon Parkinson, Critical Speed Vibration-Modal Balance, SAE Paper 928A, October 1964.

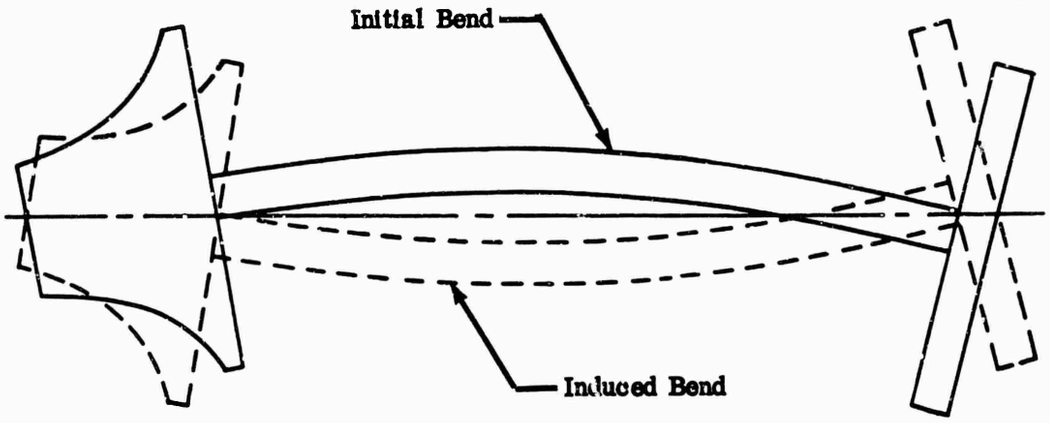


Figure 71. Shaft-Bending Schematic.

2.0 INSTRUMENTATION

The modal balance technique required running the rotor assembly in the rig near the critical speed. Therefore, instrumentation for monitoring the shaft deflection was provided. Electronic induction-type proximity probes had proved to be accurate and reliable for measuring shaft displacement at high rpm during previous tests and were used for these runs. A typical probe of this type is shown in Figure 72, and its installation is shown in Figure 73. The probe was installed in a threaded screw to allow setting the head at various distances from the shaft for the purpose of calibration. This probe was connected to an oscillograph paper recorder for a permanent data record.

3.0 PROCEDURE

Two different methods of modal balancing are presented and were used for different test-rig modal balance operations. The results were identical for either procedure. One procedure uses a trial and error solution of placing the weights while the other uses a single trail and an analytical solution.

3.1 TRIAL AND ERROR METHOD

The trial and error balance operation is a fast and simple procedure. The first operation is to establish definitely that the vibration problem is due to the first shaft-bending critical. This can be done by analysis or by experimental measurement with shaft proximity probes. These investigations also give a fair indication of the rpm at which the critical occurs. A base speed was next established just below the critical speed at which the rig will operate safely while the modal balance operation is performed. This speed was selected at approximately

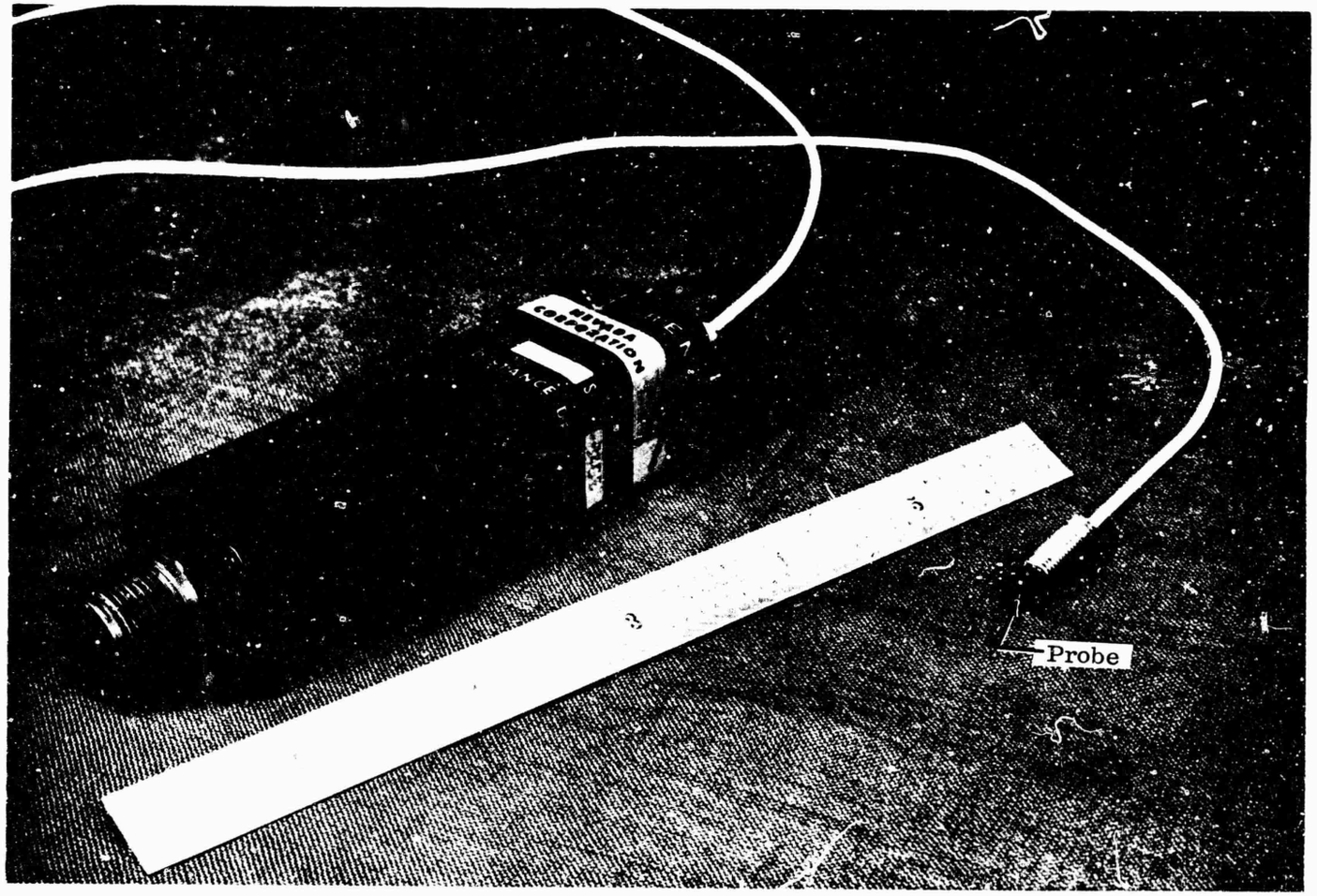


Figure 72. Proximity Probe.

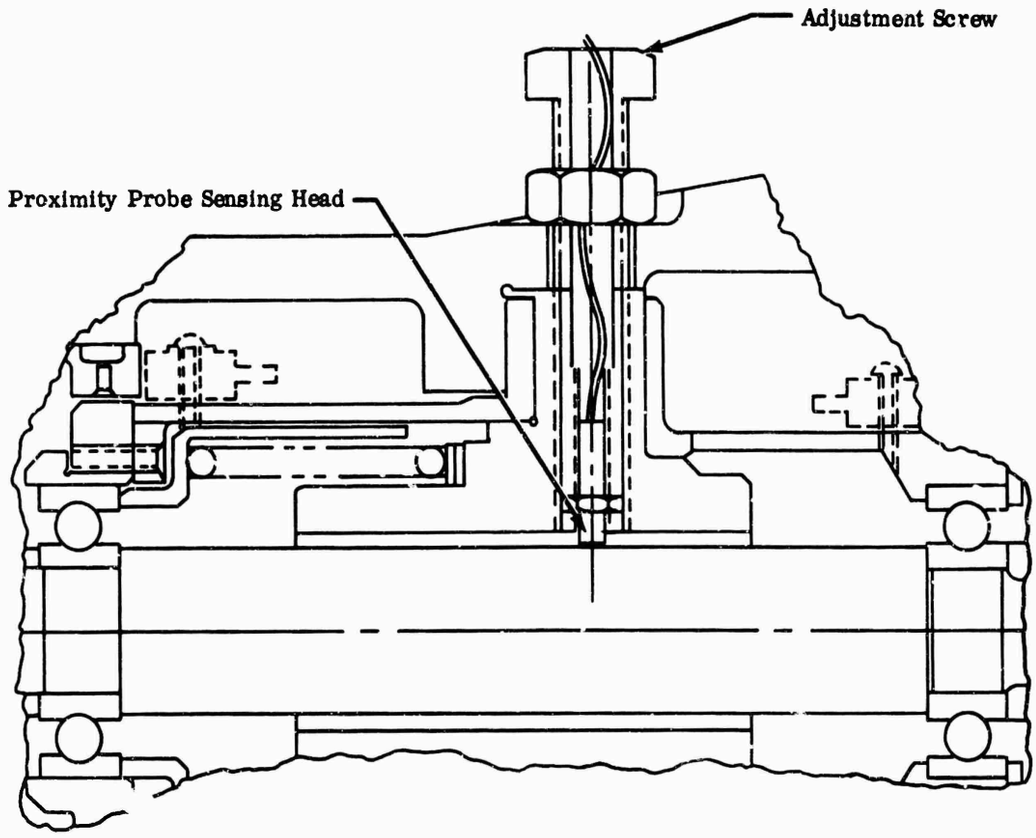


Figure 73. Proximity-Probe Installation.

10 percent below the critical speed. At this rpm, the base displacement of the shaft was plotted as shown in Figure 74. A small imbalance weight (Figure 75) was installed at the forward end of the impeller shaft, Figure 76. The angular location on the shaft for the imbalance weight was chosen to coincide with the angular location of maximum displacement. The test rig was then rerun at the same base speed with the weight attached. The shaft amplitude was recorded, and this value was plotted at the 0-degree phase angle (see Figure 74). The same imbalance weight then was rotated 90 degrees, and the test was repeated at the base speed. The shaft amplitude was again recorded and plotted. This process was repeated with the imbalance weight rotated 180 and 270 degrees. The resultant data were plotted and the points were connected by a sinusoidal curve. The desired phase angle for the imbalance weight was the point of minimum amplitude. With the correct phase angle known, the amount of im-

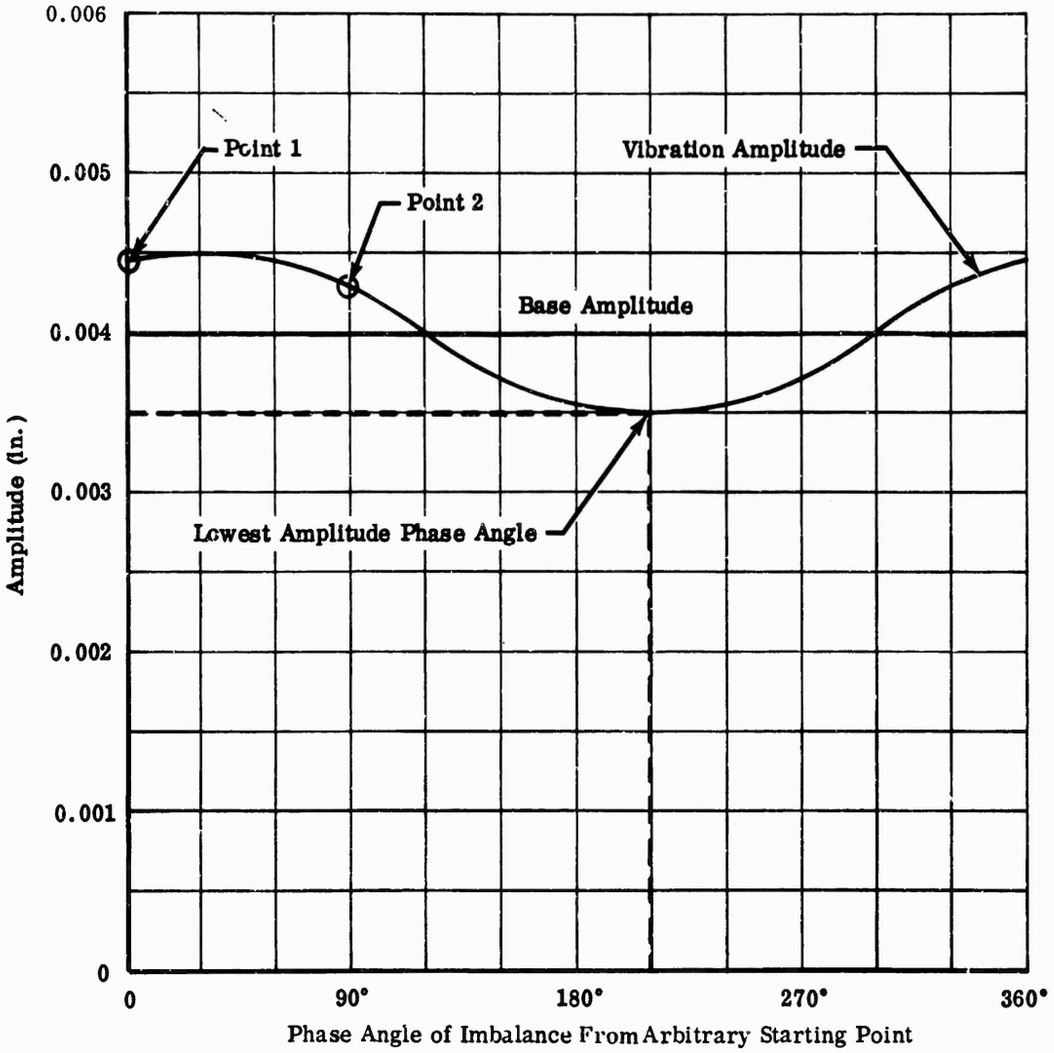


Figure 74. Amplitude-Phase Relationship.

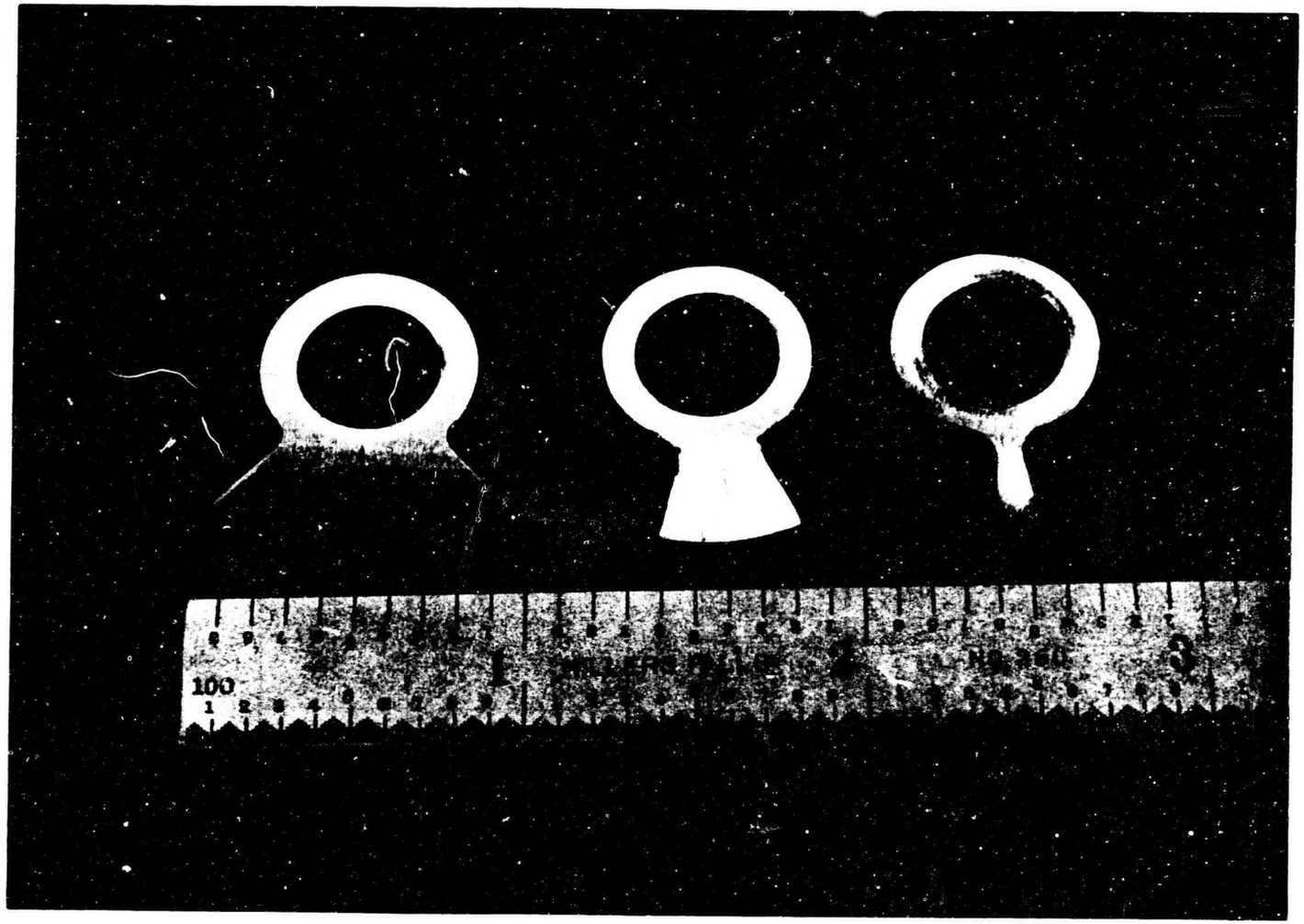


Figure 75. Typical Modal-Balance Weights.



Figure 76. Impeller With Modal-Balance Weight.

balance was varied at this angle until the amplitude at the base speed was a minimum. The rig then was able to accelerate through the critical speed safely.

This method was used on the impeller test rig with the MF-1 impeller. The design speed of the rig was 57,000 rpm. To run this speed, it was necessary to accelerate through the first shaft-bending mode critical speed (48,000 rpm). Near this speed the shaft-vibration amplitude was 0.007 inch, peak-to-peak. This amplitude would have imposed a high bearing load while accelerating through the critical speed. The base speed was set at 43,000 rpm, and the base amplitude of 0.004 inch peak-to-peak was observed. After the modal balance procedure was performed, the amplitude was less than 0.001 inch peak-to-peak. The rig was then able to operate safely through the 48,000 rpm critical speed at less than 0.002 inch peak-to-peak vibration amplitude.

3.2 ANALYTICAL METHOD

The analytical method required additional instrumentation to that which was available for the initial trial and error method of modal balancing the impeller test rig with the MF-1 impeller. The analytical solution was vectorial: it required measurement of the shaft-displacement amplitude and displacement phase relative to a fixed reference on the shaft. The simplest method was to notch the shaft in the area of the displacement pickup and to display the signal on an oscilloscope. Figure 77 is a sketch of a typical oscilloscope recording.

A base speed (ω) was established as in the previous trial and error solution. It was necessary to repeat the speed accurately because of a 180-degree shift in the phase angle (Figure 78) as the rotor passes through the critical speed. An initial plot of the displacement amplitude (A_1) and phase angle (θ_1) was made on polar coordinates (Figure 79) for the rotor system at the base speed. A known calibration weight (CW) was installed, and the resultant displacement amplitude (A_2) and phase angle (θ_2) were measured at the base speed (ω_1). These values were plotted (Figure 79), and the correct modal balance weight (M_1) and phase angle (ϕ) were computed by vector subtraction.

$$\left|M_1\right| = \frac{\left|A_1\right|}{\left|AB\right|} CW_1 \tag{178}$$

Vector AB (Figure 79) was the vector due to the calibration weight (CW_1), and ϕ was the location of M_1 from the position of CW_1.

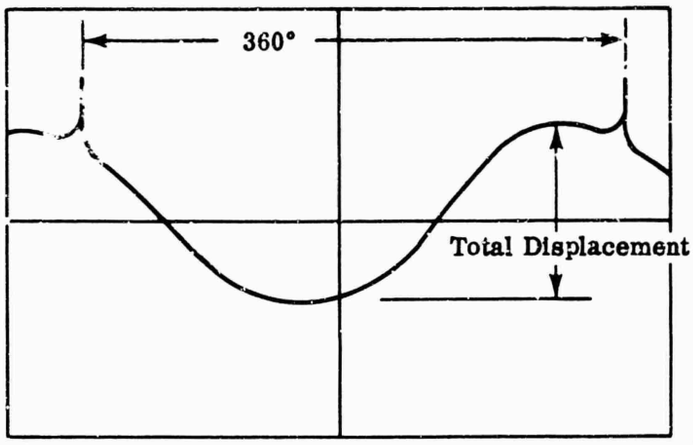


Figure 77. Shaft-Displacement Sketch.

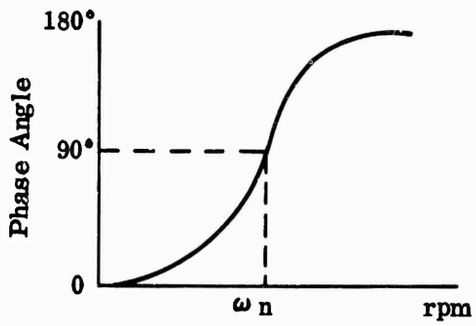


Figure 78. Phase Angle Versus Rotational Speed.

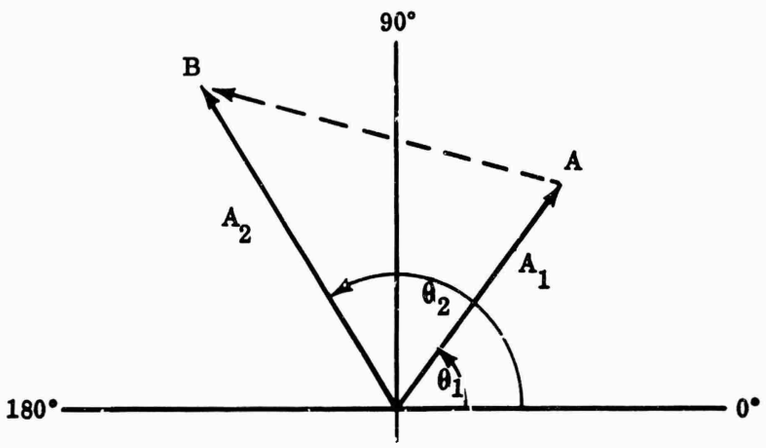


Figure 79. Shaft-Displacement Diagram.

(U) APPENDIX VI

VIBRATORY-STRESS TEST OF WORKHORSE IMPELLER

ABSTRACT

This report covers the vibratory-stress test of a titanium impeller. The objectives were to corroborate calculated blade natural frequencies and to determine whether conditions existed which would prevent operation of the compressor in any area required for performance tests. Results are presented in terms of blade natural frequencies and stresses at the various speeds.

SYMBOLS

a	peak-to-peak amplitude (in.)
c	gage calibration factor (psi/in.)
f	frequency (cps)
K	gage factor
K'	gage factor sensitivity compensation
N	rotor speed (rps)
n	number of oscillations per time period (cycles)
P_S	static-pressure tap, wall
P_R	total-pressure rake
P_T	total-pressure probe, fixed
$P_{T\phi}$	total-pressure probe, directional
R_L	lead resistance (ohm)
R_S	shunt resistance (ohm)
Rg'	strain gage resistance after installation (ohm)
T	temperature probe, unshielded
T_{SH}	temperature probe, shielded
T_T	total-temperature probe, stagnation
t	time period (sec)

1.0 SUMMARY

The test was considered to be successful in that all major objectives were met. The blade frequencies determined from this test were compared with the predicted values. Differences between predicted and test frequencies were generally within 500 cps. Therefore, the speeds at which these critical vibrations actually occurred necessitated correcting the predicted Campbell diagram. With this small change in the Campbell diagram, there were only minor restrictions for operation in the test rig. Vibratory-stress levels in nearly all regions were below the allowable of ±20,000 psi. As expected, the vibratory stresses in surge exceeded the design allowable for about half of the speed range. However, the levels of steady stress and metal temperature provided enough margin to permit operation in all regions along the surge line except in the range of from 39,000 to 41,500 rpm. This range must be avoided entirely for steady-state operation at reduced-flow conditions. In addition, the accumulated number of surges in the speed ranges between 49,200 and 50,100 rpm, and between 51,500 and 55,000 rpm, must be limited to 30 with the surge-relief valve in operation. The inlet guide vane angles do not affect the vibratory-stress level.

2.0 DISCUSSION

The purpose of this test was to determine the natural frequencies and vibratory-stress levels of the workhorse impeller under varying conditions of compressor operation. In addition, the investigation was directed toward establishing all critical vibration conditions to be used as an operating guide in future performance testing of this impeller. The testing was to be accomplished by use of a strain-gage instrumented impeller running under the same environmental conditions that would be encountered during performance testing.

2.1 RIG COMPONENTS AND INSTRUMENTATION EQUIPMENT

The following special equipment was used for the test:

1) Inlet guide vane assembly;

2) Diffuser islands;

3) Eight strain gages (1/8 inch);

4) One 8-channel water-cooled slip-ring assembly;

5) Bridge completion and signal conditioning equipment;

6) One frequency-modulated tape recorder and support equipment;

7) Three light-beam-type oscillographs.

All strain gages on the impeller had a gage factor of 1.99 ±3 percent. The strain gages had been used previously on impellers and axial compressors.

2.2 PROCEDURE

Extension lead wires were attached to the strain gages before they were cemented on the impeller. The leads were No. 32 AWG solid conductors with baked-on enamel insulation. Leads were attached to the strain gages by first removing about 0.25 inch of insulation from the lead ends. The ends were twisted together with the strain-gage leads, and the lead ends were then fused by using a heli-arc-welding process.

A preliminary test specimen of titanium was prepared to verify the strain-gage installation procedure before instrumenting the impeller. Strain gages were mounted on the specimen to test the cement in shear and tension under actual centrifugal loads and temperatures. Preparation of titanium for strain-gage installation required careful evaluation of the chemicals used. The common degreaser, trichloroethylene, could not be used because of halogenation. However, the standard metal conditioners and neutralizer solutions supplied by most strain-gage manufacturers could be used where the temperature of the titanium parts was less than 700° F. Beyond 700° F, titanium is subject to hydrogen embrittlement.

For the impeller-stress test, the impeller surface was degreased by soaking the areas to be instrumented in Dow Chemical Company 19AC E-Z Strip, followed by repeated washings in household ammonia. The surface was then sanded lightly and washed with metal-conditioner and neutralizer solutions. Because titanium oxidizes rapidly, a base coat of cement about 0.001-inch thick was applied to the areas on which the strain gages and lead wires were to be placed. The surface protection was sufficient for cementing the strain gages. The cement used was Budd Company GA-60 2-part epoxy. Curing of the cement took 5 hours at 350° F.

Because only dynamic strain-gage data were required, potentiometric circuitry was used. A 1200-ohm ballast resistor was used in series with each 120-ohm strain gage, and the outputs were capacitively coupled to the amplifiers.

2.2.1 BENCH TEST

Resistance of the strain gages after installation (R_g') and strain-gage and lead-wire resistance ($R_g' + R_L$) were measured to the nearest 0.1 ohm. Gage-factor sensitivity compensations (K') were computed by:

$$K' = \frac{R_g'}{R_g' + R_L} (K) \qquad (179)$$

where:

K is the gage-factor nominal value specified by the manufacturer.

Strain gages were calibrated with resistors using:

$$\text{Strain (microinches/inch)} = \frac{R_g' + R_L}{(R_g' + R_L + R_s)} (K') \qquad (180)$$

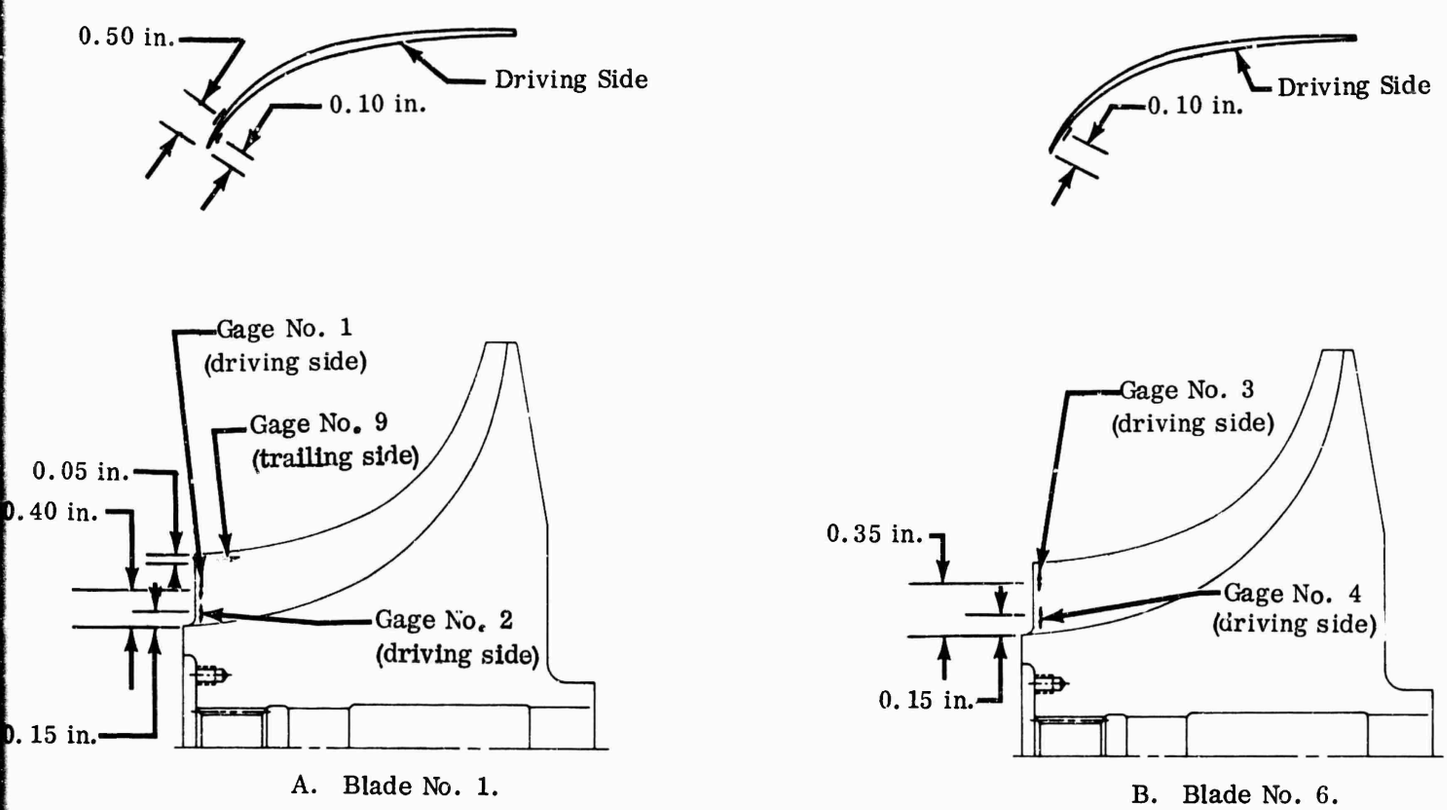
where:

R_s is the calibration shunt resistance.

Gage-factor sensitivity compensation for temperature was not necessary because the metal temperature was below 300° F in the areas where strain gages were installed; strain gages were not necessary in the higher temperature regions near the impeller tip because of the shorter, stiffer blade sections in this region.

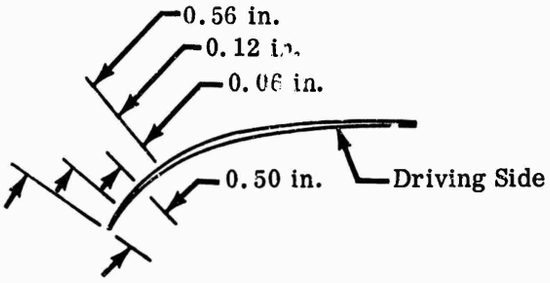
A bench test of the impeller blades was made to determine natural frequencies and areas of maximum stress that corresponded to each of the first 3 modes of vibration. The frequencies were determined first with the use of an electromechanical excitor and were rechecked with a pulsed-air rig (siren) by reading the output frequency of the strain gages attached at critical areas of the blades (Figure 80). The strain signals read from these gages were recorded on magnetic tape and on an oscillograph for subsequent data reduction.

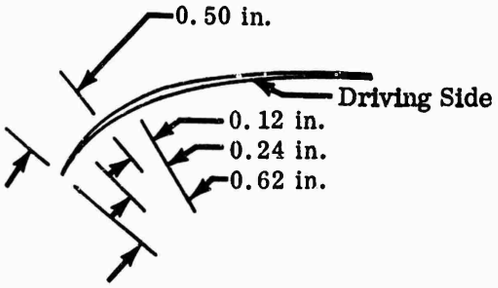
The recording system was calibrated for frequency response throughout the test range, and correction factors were computed for each recorded blade natural frequency. The strain signals were corrected and were compared to each other to obtain the relation between the amplitude and strain-gage location on each instrumented blade. These bench-test data were then used to correct the analytically predicted frequencies on the Campbell diagram. In addition, regions of maximum stress were identified for each of the first 3 modes. This information was used to select the locations of strain gages to be used in the compressor-rig test. The gages were located where the greatest number of modes could be read

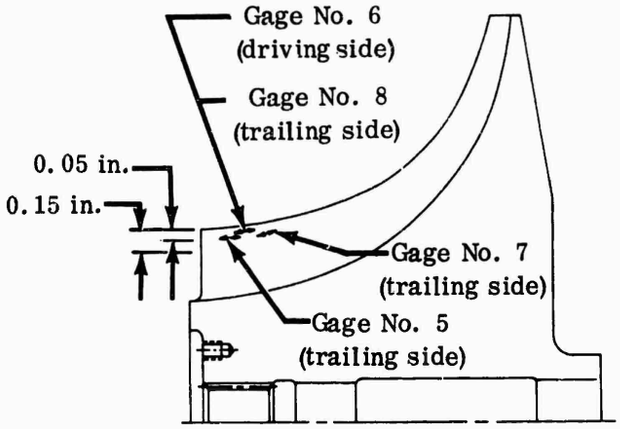


No Scale

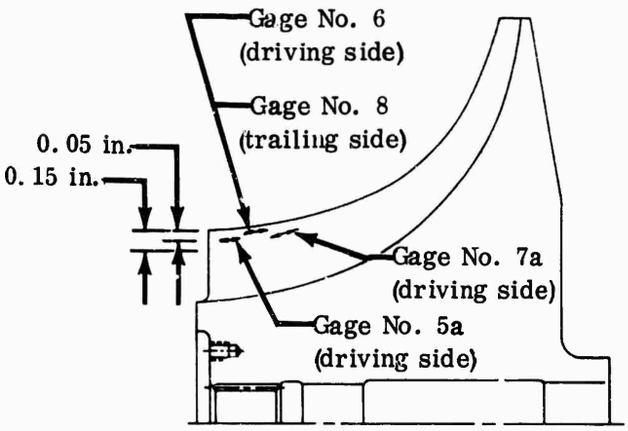
Figure 50. Bench-Test Strain-Gage Locations.







C. Blade No. 13.



D. Blade No. 13.
(alternate instrumentation)

from each gage and were not necessarily at points of maximum stress. The results of these preliminary tests are given in Figures 81 through 83.

2.2.2 COMPRESSOR-RIG TEST

The impeller was tested in a compressor test rig in which the turbodrive unit was independent of the impeller test section; thus, maximum flexibility was permitted in selecting airflow rate versus compressor pressure ratio throughout the operating range. The test setup and data sensors are shown in Figure 84.

A slip-ring connector assembly was fabricated, and the receptacle was designed to shrink-fit within the impeller hub face. The connector-assembly plug was mounted directly on the slip-ring flexible-drive shaft. Two threaded studs held the plug-receptacle assembly together — 16 female pins were installed on the impeller receptacle and 8 male pins on the slip-ring plug. The pin-pattern design enabled repositioning of the slip-ring connector (180 degrees with respect to the impeller) so that a different set of pins could be mated if desired. This design permitted installing twice the number of strain gages that could be handled by an 8-ring system and increased its utility.

The slip-ring assembly was cradled in an enclosed support duct at the diffuser-rig inlet. The duct was tapered to prevent airflow restrictions, and the core of the duct, which supports the slip ring, was held in place by 4 thin vanes. Two of the vanes carried cooling water and instrumentation leads to the slip-ring assembly.

The typical test procedure was as follows:

1) The rig was brought up to design speed with the flow valve in the full-flow position;

2) The magnetic tape recorder and oscillograph were started;

3) The flow valve was closed slowly until surge while the rotor speed was held constant;

4) Repeat 2) and 3) at 500 rpm decrements from the design speed of 50,000 rpm to 25,000 rpm.

Cycle duration was approximately 1 minute for each of the first 63 runs. The test was rerun at speeds offset from the first series by 250 rpm to collect additional data. This second test included runs in the 50,000 to 55,000 rpm range. The inlet guide vane setting was 0 degrees for all runs except at 35,000 and 50,000 rpm, where the guide vanes were varied from +40° to -20° with the impeller operating at the knee of the constant-speed line. Positive angle is defined as moving the vane trailing edge in the direction of rotor rotation.

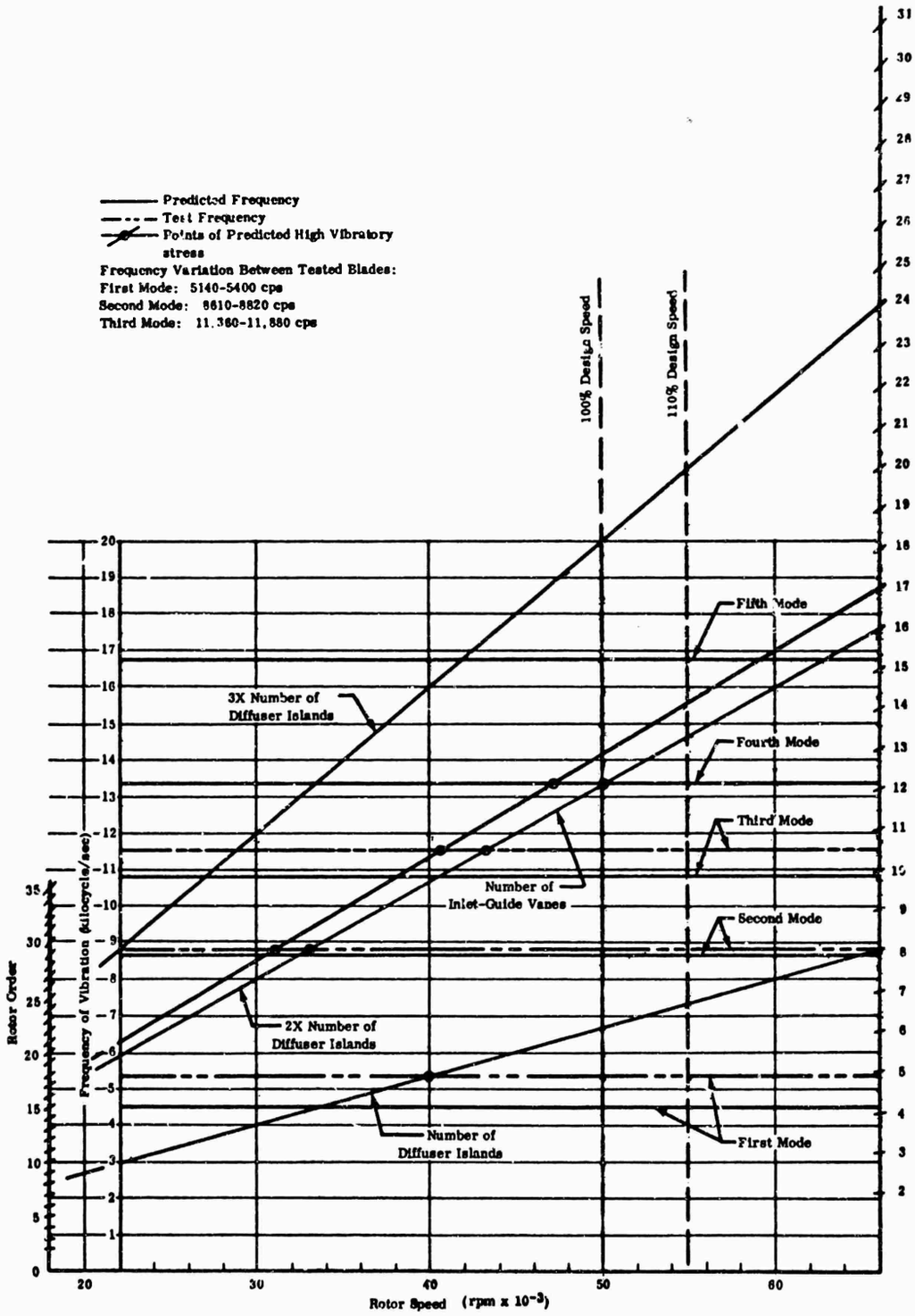


Figure 81. Campbell Diagram.

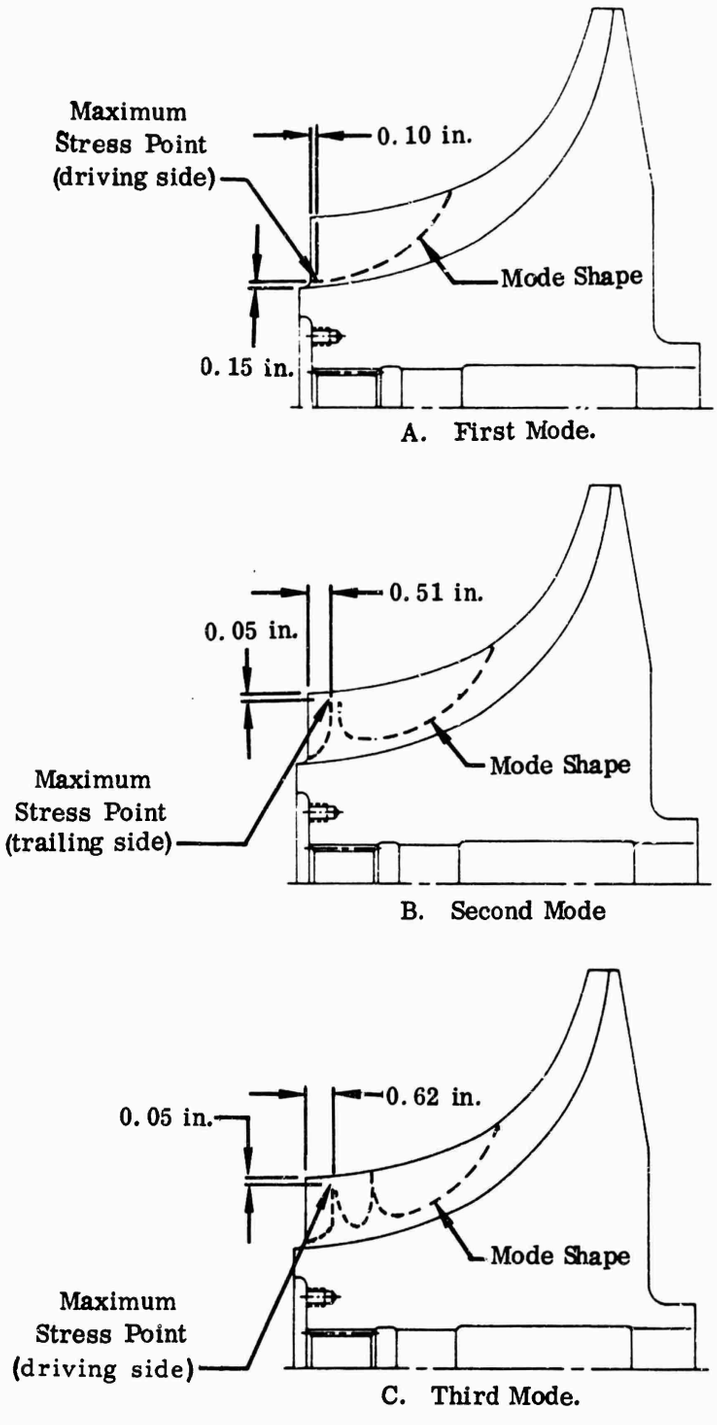


Figure 82. Maximum Vibratory-Stress Points.

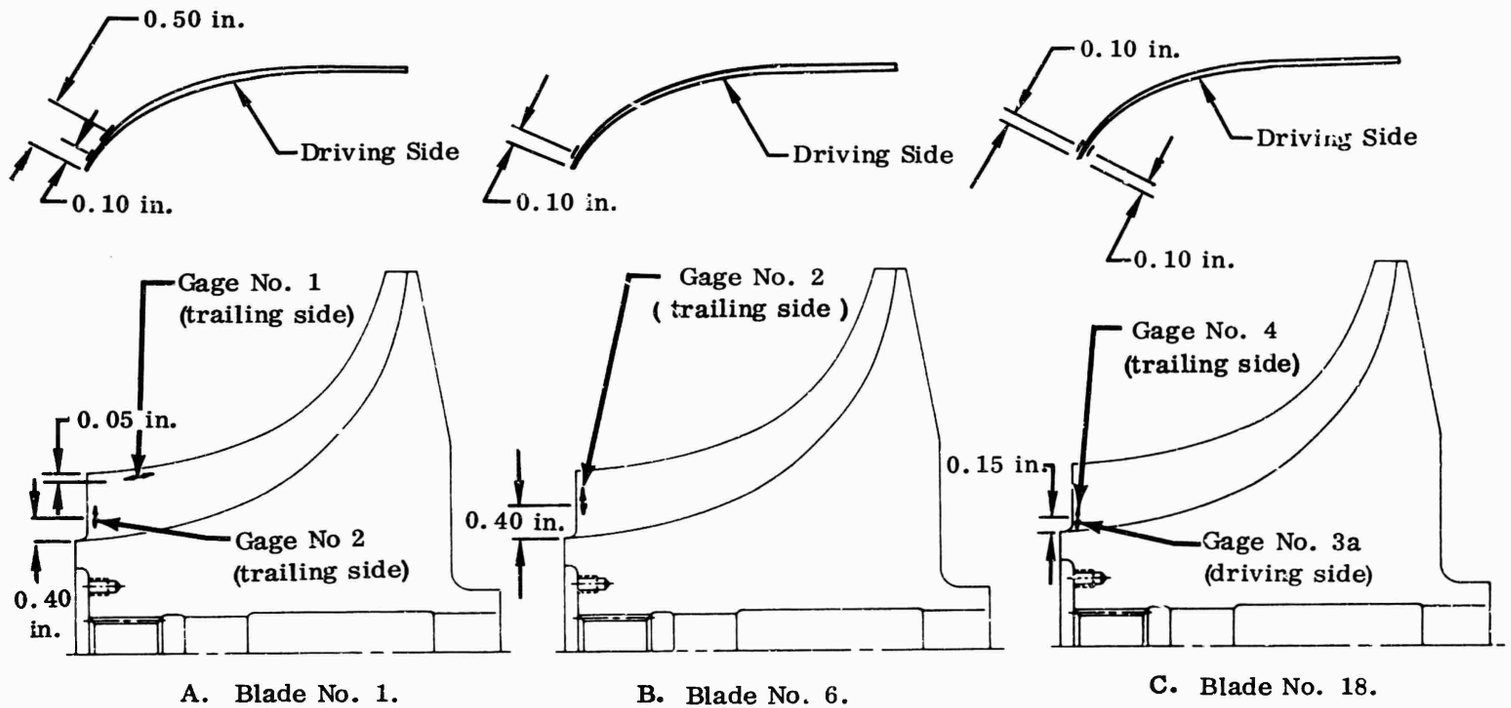


Figure 83. Rig-Test Strain-Gage Locations.

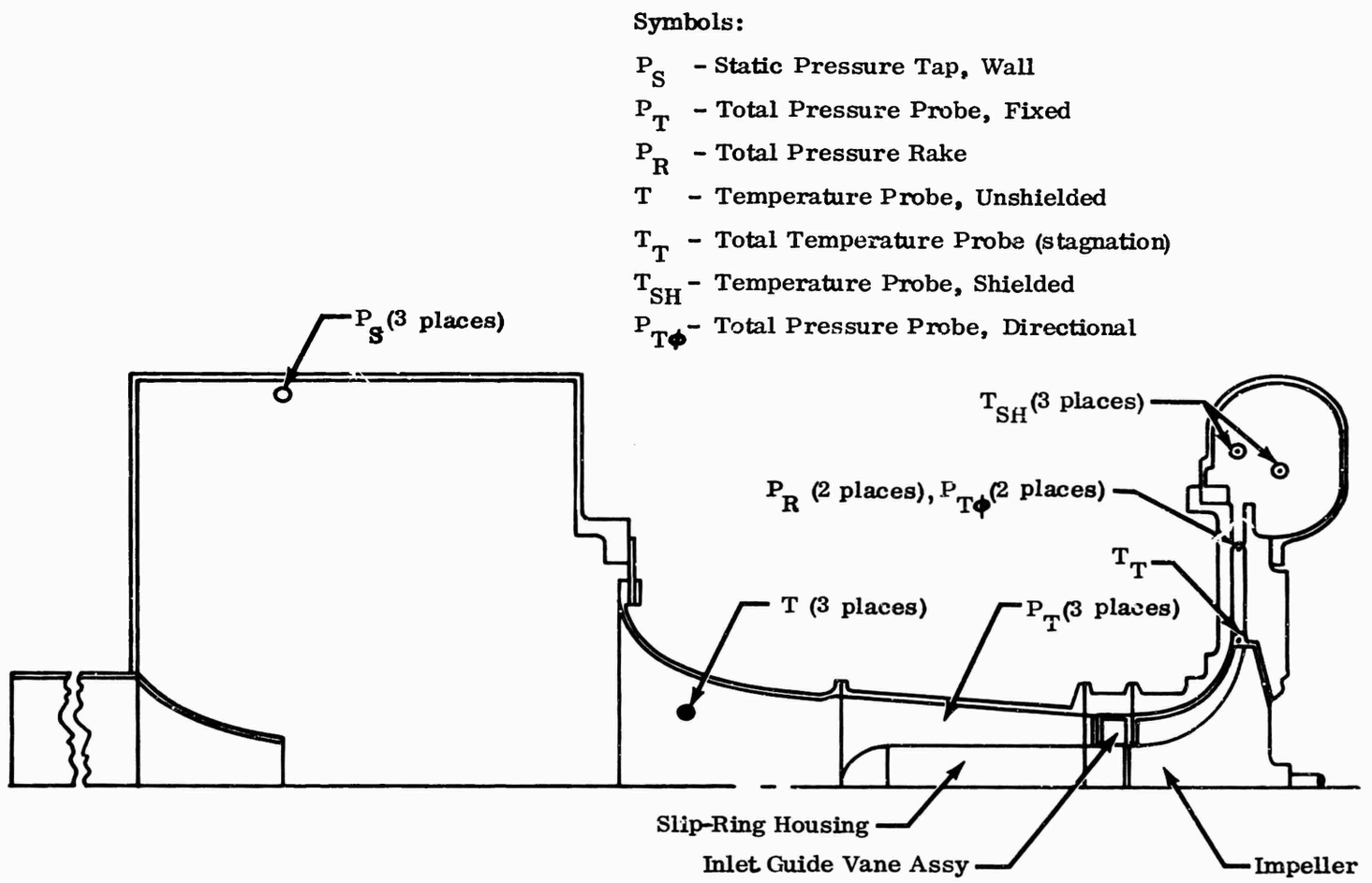


Figure 84. Test Equipment Instrumentation.

After the first 5 runs, 3 strain channels were found to be inoperative. The malfunctioning channels affected signals from gages 1a, 3, and 4. However, backup (and redundant) instrumentation was incorporated in the buildup as a safeguard against such an occurrence.

From run No. 6 and on, 5 strain signals and 1 rotor-speed signal were recorded on the magnetic tape. Simultaneously, signals were recorded for inlet-duct temperature, collector temperature, impeller-exit pressure, inlet pressure, flow-nozzle pressure, and rotor speed on the oscillograph. The magnetic-tape recording was synchronized with the oscillograph by picking up a prerecorded binary-coded time signal from the tape and by recording it simultaneously on the oscillograph. This technique allowed comparison of instantaneous aerodynamic data with strain data.

The strain recordings for the entire test were reproduced on an oscillograph with a low paper speed to produce a condensed version of the data so that resonances could be scanned easily. Each trace that showed a resonance was checked with the calibration values for that channel to determine if the indicated stress exceeded ±4000 psi (vibratory stresses below ±4000 psi were considered negligible). All resonance points with indicated vibratory stresses greater than ±4000 psi were identified on the tape; with a speed reduction of 8:1, they were reproduced on the oscillograph at a paper speed of 100 inches per second. This method of expanding the data allowed frequency resolution of vibratory signals to over 30,000 cps.

Resonances to be studied were selectively chosen at a level of ±7,300 psi and were analyzed in detail for frequency, amplitude, and excitation orders, as shown in Figure 85.

Vibratory stresses at the surge point were considered separately from the vibratory stresses at steady-state conditions. The surge stresses were analyzed in the same manner as the steady-state vibratory stresses, but were plotted against rpm on a scale adjacent to the compressor map. This method for displaying the surge stresses allows simultaneous comparison with the surge line on the compressor map.

2.3 RESULTS

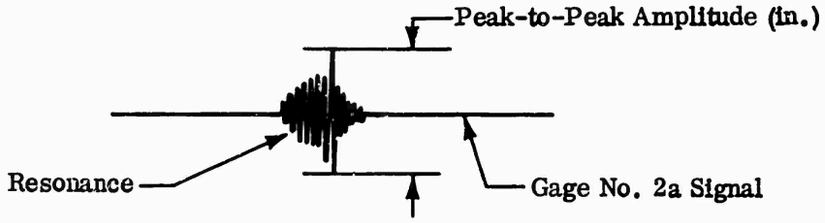
An example of a typical expanded oscillograph trace is shown in Figure 86. It shows run number, binary-location number, the numbers of the recorded strain-gage signals, and the rpm. In addition, any significant strain signal is marked with the indicated vibratory-stress level (i.e., the stress level measured from the trace without correction for system-frequency response or gage location), the frequency, and the rotor-speed order.

Sample

Calibration Factor for Gage No. 2a:
± 10,000 psi/in. Peak-to-Peak Amplitude

Sample

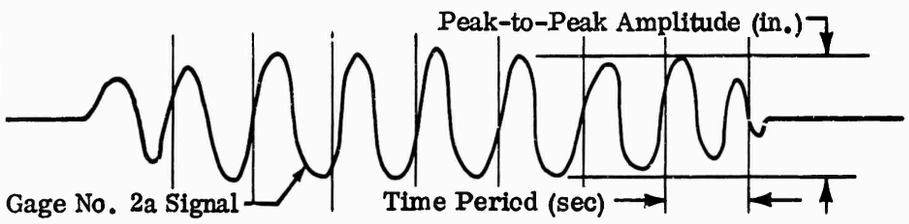
Frequency Response and Gage Location Correction for Gage No. 2a:
K = 2.0 (for First Mode of Vibration)



Indicated Vibratory Stress = a x c
= ± a x 10,000 psi;

where a = Peak-to-Peak Amplitude (in.)
c = Gage No. 2a Calibration Factor (± psi/in.)

A. Condensed Oscillograph Trace.



Corrected Vibratory Stress = a x c x K
= ± a x 20,000 psi,

where a and c are as above
K = 2.0

Frequency = n/t; where n = Number of Oscillations Per Time Period (cycles)
t = Time Period (sec)

Order = $\frac{f}{N}$; where f = Frequency (cps)
N = Rotor Speed (rps)

B. Expanded Oscillograph Trace.

Figure 85. Data Reduction Method.

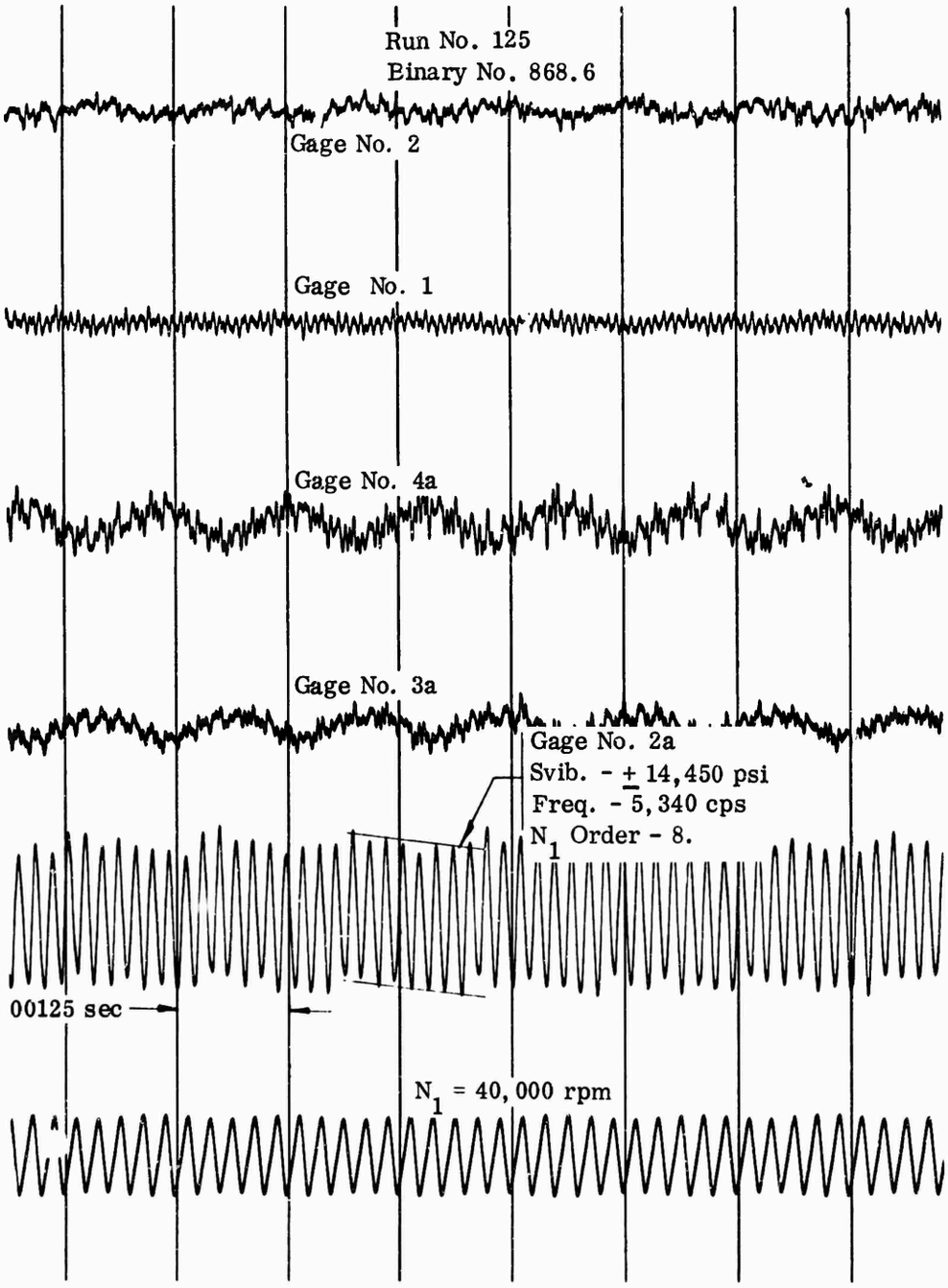


Figure 86. Expanded Oscillograph Trace.

The frequencies determined during the test varied slightly from the predicted frequencies, but the first mode showed the maximum deviation (18 percent high). The second mode showed the least deviation (2.3 percent high). The frequency spread of the tested blades was not more than ±3 percent from the mean frequency for a given mode. This information is shown on the Campbell diagram in Figure 81.

All indicated vibratory stresses (outside of surge) in excess of ±7300 psi appear on the Campbell diagram in corrected form in Figure 87. One point below this stress level is plotted (±7000 psi resonance point at the 9th mode and the 34th order). The point is unique because of its unusually high frequency at the upper limit of the speed range. It should be noted that all major disturbances are related to the number of inlet guide vanes or diffuser islands.

Vibratory stresses occurring at surge are identified on the stress map in Figure 88 and correspond to the surge line shown in the adjacent compressor map. Those stresses occurring during a rapid approach to surge are marked as triangles on the stress map. Because the surge vibratory-stress levels through much of the speed range are above ±20,000 psi, consideration of temperature and centrifugal stress at a given speed was used to obtain the allowable vibratory-stress level from a Goodman diagram. Vibratory stress from the Goodman diagram was divided by 2 to obtain the allowable and was plotted on the stress map (shaded). Only 3 areas in the speed range exceeded the limit. One critical area (Area A) for steady-state operation is marked on the compressor map between 39,000 and 41,500 rpm. The maximum recorded stress in this range is marked for reference at the pressure ratio and weight flow where it occurred. Other highly stressed rpm ranges are between 49,200 and 50,100 rpm, and between 51,500 and 55,000 rpm. In these 2 ranges, all high stresses occur in surge (Figure 88).

At the test speeds of 35,000 and 50,000 rpm, no variation in stress level was observed when the inlet guide vane angles were changed.

3.0 CONCLUSIONS

The test was considered to have met all of its objectives. Natural frequencies and associated stress levels were determined during actual rig testing, and an operating map was prepared.

The actual and predicted frequencies did not coincide as close as had been shown in previous tests using aluminum impellers. However, this test was the first with titanium, and this new experience should form a basis for improved predictions. The reasons for the deviation were not explored beyond the scope of this test.

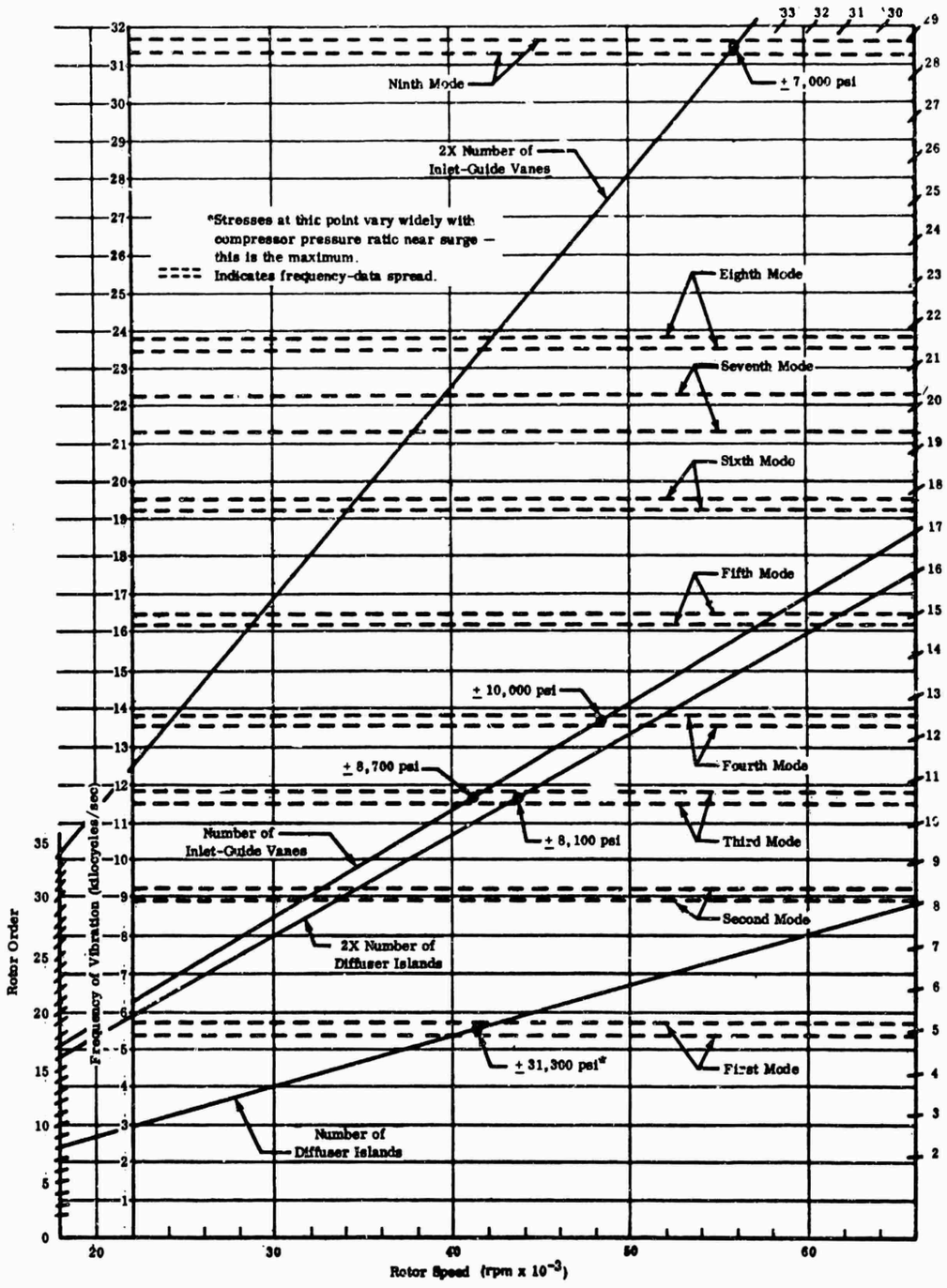


Figure 87. Campbell Diagram.

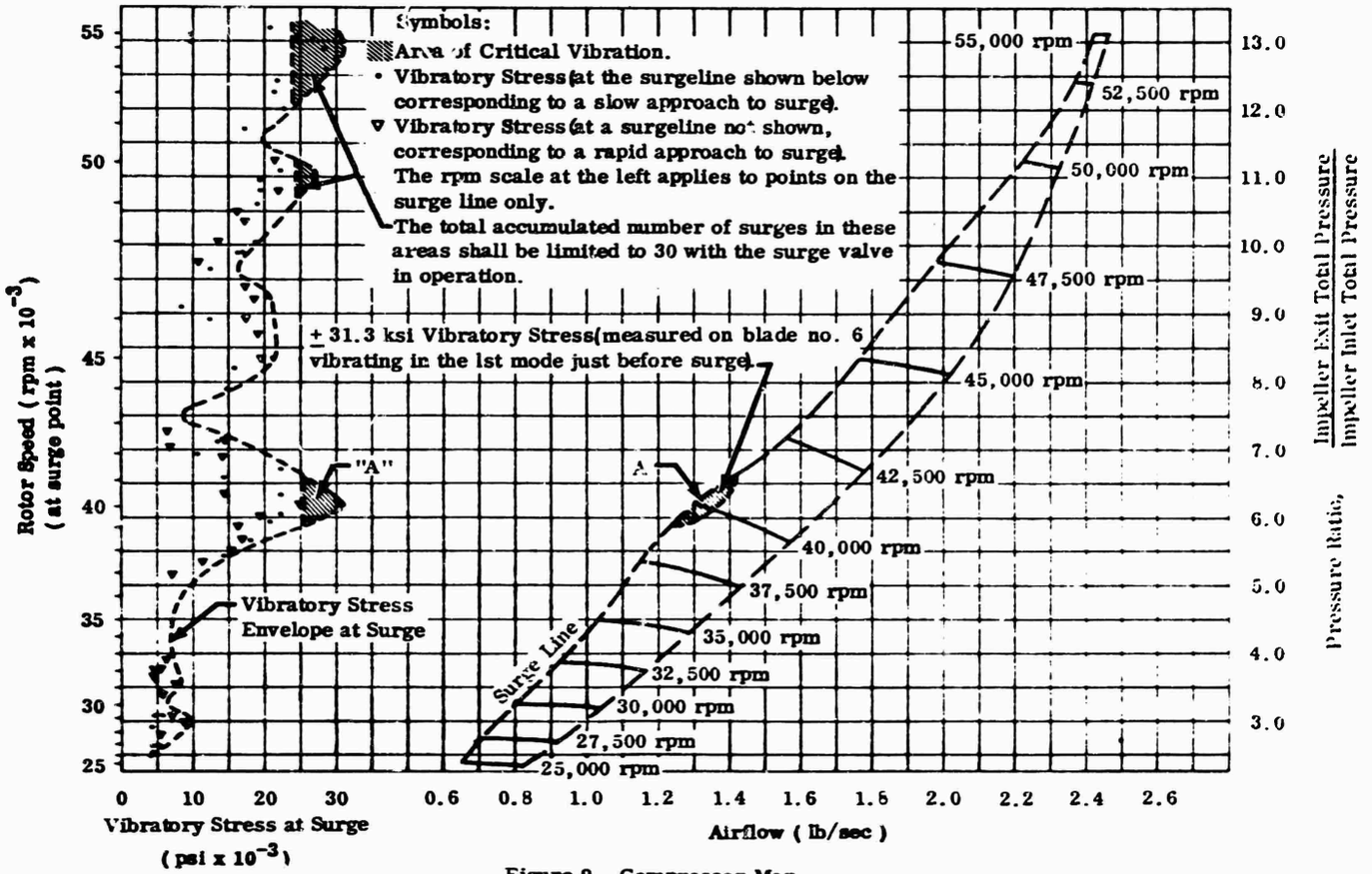


Figure 9. Compressor Map

Figure 88. Compressor Map.

The impeller should not be operated for prolonged periods near the surge region between 39,000 and 41,500 rpm. In the speed ranges of from 49,200 to 50,100 rpm and from 51,500 to 55,500 rpm, the total number of surges should be limited to 30 (surge is defined as one audible pop). The surge-relief valve should be in operation at all times. By limiting the number of surges, the total number of cycles at the high stress levels will not become excessive.

Because the inlet guide vane angle did not affect the stress level, guide vane use is not restricted.

(U) APPENDIX VII

WAKE INTERACTION EFFECTS AND PERFORMANCE CHARACTERISTICS OF STAGNATION-TYPE THERMOCOUPLE

ABSTRACT

This appendix presents the results of a study sponsored by the contractor aimed at (1) Determining the wake interaction on the accuracy of the thermocouple measurements near the rim of a high-speed, separated-flow rotor; and (2) Estimating the performance characteristics of a stagnation-type thermocouple probe. The studies were based on temperature measurements taken during centrifugal-compressor research programs. The purpose was to resolve differences in temperature measured between the impeller tip and the collector. A complete mathematical treatment of effects on a typical probe is presented.

The work was conducted by Robert J. Moffat (Associate Professor of Mechanical Engineering, Stanford University) with assistance from Dr. Robert C. Dean (Creare, Incorporated, Hanover, New Hampshire).

SYMBOLS

A = apparent overall recovery factor of the probe, including the effects of internal conduction but with no losses to the walls by conduction or by radiation

A_i = area of the control volume at the impeller exit (in.^{2} or ft^2)

A_o = area of the control volume at the outer diameter (in.^{2} or ft^2)

C_p = coefficient of specific heat at constant pressure (Btu/lbm — °F)

D = diameter (inches or feet)

E = error introduced by heat transfer from thermocouple

f_1 = the fraction of one blade period during which the probe is exposed to the jet-fluid portion of the blade spacing

g_c = gravitational constant (32.17 ft/sec^2)

h = heat-transfer coefficient (Btu/hr-ft^2 — °F)

h_1 = average heat-transfer coefficient between jet fluid and thermocouple (Btu/lb-ft^2 — °F)

h_2 = average heat-transfer coefficient between the wake fluid and thermocouple (Btu/lb-ft^2 — °F)

J = mechanical equivalent of heat (778 ft — lb/Btu)

k = thermal conductivity (Btu/hr-ft^2 — °F/ft)

L = characteristic length (feet or inches)

N_{nu} = Nusselt number

P_j = static pressure of the jet (psia)

P_w = static pressure of the wake (psia)

SYMBOLS (Continued)

R = radius (inches or feet)

Re = Reynolds number

T = temperature (°R)

T_m = average system temperature (°R)

$\overline{T}$ = average temperature (°R)

$\overline{T}_{f,p}$ = average temperature of fluid swept past the probe position (°R)

$\overline{T}_1$ = average static temperature of the jet fluid (°R)

$\overline{T}_2$ = average static temperature of the wake fluid (°R)

V = fluid velocity (fps)

α = thermal diffusivity of the solid, $k/\rho \ C_p$ (ft^2/hr)

α_B = recovery factor of the base, referenced to free stream

α_j = recovery factor of the junction, referenced to local condition

α_s = recovery factor of the shield, referenced to free stream

ϵ = emmissivity

ϵ_s = surface-temperature variation

ϵ_G = gas-temperature variation

$\rho_1 V_1$ = average mass velocity of the jet fluid with respect to the stationary probe

$\rho_2 V_2$ = average mass velocity of the wake fluid with respect to the stationary probe

σ = Stefan-Boltzmann constant (0.1713×10^{-8} Btu/hr-ft^2 -$°R^4$)

τ = time (hour)

τ_o = period of disturbance (hour)

Subscripts

a = adiabatic

abs = absolute component

B = base

c = heat transfer by convection

f = fluid

j = thermocouple junction

M = mean

o = stagnation conditions

P = junction-shield combination

r = heat transfer by radiation

rel = relative component

s = thermocouple shield

w = wall

1 = jet

2 = wake

∞ = free-stream conditions

1.0 SUMMARY, CONCLUSIONS, AND OUTLINE OF ANALYSIS

1.1 SUMMARY

Thermocouple probes placed near the rim of a compressor rotor operating in the jet-wake mode may be seriously in error with respect to the true bulk-fluid temperature of the fluid leaving the compressor. For a typical case, considered in this report, the error is between 45° and 60°F.

The error is caused by the fact that the wake fluid affects the thermocouple temperature, but not the temperature of the through-flow fluid, and it is assumed that the wake is more or less permanently attached to the rotor. Redesign of the probes can in no way affect this behavior.

If the wake fluid is hotter than the jet fluid, then the thermocouple will read high. The amount of the error will depend on the jet-wake width ratio, the jet-wake radial-velocity ratio, and the difference in temperatures of the jet and the wake.

Experimental results from compressor tests at Boeing support the trends deduced from this analysis.

1.2 RECOMMENDATIONS AND CONCLUSIONS

1) Thermocouple probes should not be installed close to the rim of the rotor.

2) Schlieren studies suggest that the flow is steady and well mixed at a radius ratio of 1.06 for typical cases, and thermocouples should be located no nearer than 1.06 radius ratio from the rim.

3) The error may be on the order of 50°F for typical cases, and cannot be reduced by modifying the probe geometry. The error may be calculated, although much of the input for this equation can only be estimated.

1.3 OUTLINE OF ANALYSIS

The steady-state recovery factor of the contractor's temperature probe is first calculated based on its geometry. The effects of the fluctuating-velocity field on this probe are then investigated, using conventional heat-transfer relationships. It is shown that the thermocouple assumes a quasi-steady state when the fluctuations are of compressor frequency. The relationship to gas temperature is then developed by using low-velocity heat-transfer relations. Introduction of the adiabatic wall temperature as the effective gas temperature for heat transfer in a

high-velocity environment allows the low-velocity results to be used directly and rigorously in the high-velocity case. The effect of the wake-fluid temperature on the thermocouple temperature is then determined,as is the effect of the wake-fluid temperature on the temperature of the fluid leaving the compressor. Comparison of the two reveals that the probe is always affected by the wake-fluid temperature, while the discharge-fluid temperature is only affected by the wake fluid when there is an appreciable radial velocity in the wake region. Thus the temperature sensed by the probe cannot reflect the temperature which is significant in evaluating the compressor performance.

2.0 STEADY-STATE PROBE BEHAVIOR

The behavior of the thermocouple probe must be understood under steady-flow conditions before the unsteady problem can be discussed reasonably.

The following represents an estimate of the performance of the probe (see Figure 89) based on its geometry and on the characteristics of its components: cylinders parallel to and perpendicular to the flow. The probe-analysis procedure is straightforward. Any uncertainty in the final result is the result of estimating (rather than calculating) the conduction relationships which govern the behavior. These links were estimated (based on approximate calculations of Reynolds numbers) and the data of Figure 9* were used.

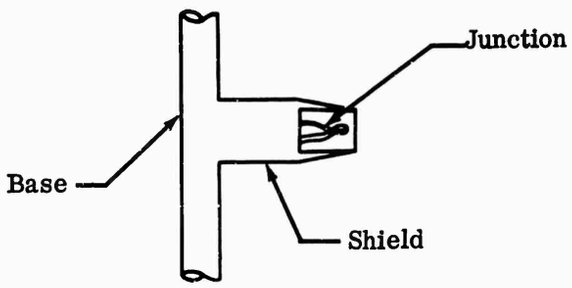


Figure 89. Sketch of Temperature Probe.

*R. J. Moffat, "Gas Temperature Measurement," Temperature, Its Measurement and Control in Science and Industry. Vol. 3, Part 2, 1962, p. 553.

The junction is 0.063/0.058 inch long, measured to the weld bead. It should be noted that the twisted-wire junction is not well suited to this type of probe design, since the effective thermocouple junction will be at the location of the first point of electrical contact and thus may be very close to the base of the apparent junction. Such an accidental junction would greatly increase the susceptibility to conduction errors and cause the probe to read lower than its design capabilities.

The wire diameter is not specified, but it is reasonable to suppose that it is between 0.010 and 0.013 inch, in keeping with general commercial practice in the 0.0625 swaged MgO thermocouple stock. The junction is between 4.6 and 6.3 wire diameters long (assuming no accidental junctions closer to the base than the weld bead).

The shield-bleed slots have a total area of 0.00151 square inch, and the shield-entrance area is 0.00247 square inch. At the entrance plane, then, the air velocity is approximately 0.6 times the free-stream velocity just ahead of the probe (behind the shock, if one exists).

The thermocouple junction is assumed to have a recovery factor of 0.86, similar to that of a tent-type or steeple junction. While twisted junctions may have slightly lower recovery factors, the assumption greatly simplifies the analysis.

The following notation will be used:

$T_{j,a}$ = junction temperature with no conduction or radiation loss

T_s = shield temperature

T_o = gas-stream stagnation temperature

V = velocity at the junction location (inside the shield)

V_∞ = velocity of the free-stream gas

α_j = recovery factor of the junction, referenced to local condition

α_s = recovery factor of the shield, referenced to free stream

α_B = recovery factor of the base, referenced to free stream

α_P = apparent recovery factor of the junction-shield combination; no conduction or radiation losses

A = apparent overall-recovery factor of the probe, including the effects of internal conduction, but with no losses to the walls by conduction or by radiation

The adiabatic junction temperature can be written as:

$$T_{j,a} = T_o - (1 - \alpha_j) \frac{V^2}{2g_c J C_p} \tag{181}$$

In terms of the apparent recovery factor of the junction-shield combination,

$$T_{j,a} = T_o - (1 - \alpha_P) \frac{V_\infty^2}{2g_c J C_p} \tag{182}$$

The relationship between the junction-recovery factor and that of the junction-shield combination is:

$$\alpha_P = 1 - (1 - \alpha_j) \left(\frac{V}{V_\infty}\right)^2 \tag{183}$$

The analysis has so far dealt only with adiabatic systems. The junction does, in fact, lose heat by conduction to the shield, and the shield loses heat, in turn, to the base. Even if the base were sufficiently long so that there was no heat transfer to the duct walls by conduction, the internal conduction problem would persist, and would link the junction temperature to that of the base. The base, being a cylinder in cross-flow, has a much lower recovery factor than the junction-shield combination, about 0.75 compared to 0.92. This internal-conduction link is one of the chief problems in the design of accurate probes.

Assuming no conduction to the walls, the base temperature is:

$$T_B = T_o - (1 - \alpha_B) \frac{V_\infty^2}{2 g_c J C_p} \tag{184}$$

The shield, taken alone as a cylinder parallel to flow, has a recovery factor of about 0.85. The conduction link between the shield and base is estimated (Figure 9)* to be 0.25 for the purposes of illustrating the analysis. A more accurate calculation does not seem warranted for this study. The shield temperature is thus given by:

$$T_s \cong T_{s,a} - 0.25\,(T_{s,a} - T_B) \tag{185}$$

The adiabatic shield temperature is:

$$T_{s,a} = T_o - (1 - \alpha_s)\,\frac{V_\infty^2}{2\,g_c\,J\,C_p} \tag{186}$$

The base temperature, assuming no conduction to the walls, is:

$$T_B = T_o - (1 - \alpha_B)\,\frac{V_\infty^2}{2\,g_c\,J\,C_p} \tag{187}$$

Combining these relationships yields:

$$T_s \cong T_o - (1 - \alpha_s)\,\frac{V_\infty^2}{2\,g_c\,J\,C_p} - 0.25\,(\alpha_s - \alpha_B)\,\frac{V_\infty^2}{2\,g_c\,J\,C_p} \tag{188}$$

$$T_s \cong T_o - (1 - 0.75\,\alpha_s - 0.25\,\alpha_B)\,\frac{V_\infty^2}{2\,g_c\,J\,C_p} \tag{189}$$

---

*(See footnote, page 272.)

The junction-recovery factor is quite near that of the shield, and will be taken to be exactly equal, for convenience. The adiabatic junction temperature can be written:

$$T_{j,a} = T_o - \left[(1 - \alpha_j) \left(\frac{V}{V_\infty}\right)^2 \right] \frac{V_\infty^2}{2 g_c J C_p} \tag{190}$$

The conduction link between the junction and the shield is estimated to be 0.20*, and is used to determine the actual junction temperature from the adiabatic junction temperature and that of the shield.

$$T_j \cong T_{j,a} - 0.2 (T_{j,a} - T_s) \tag{191}$$

$$T_j \cong T_o - \left\{ \left[1-\alpha_j \right] \left(\frac{V}{V_\infty}\right)^2 \frac{V_\infty^2}{2 g_c J C_p} + 0.2 \right.$$

$$\left. \left[\left(\left[1 - 0.75 \alpha_s - 0.25 \alpha_B \right] - (1 - \alpha_j) \left(\frac{V}{V_\infty}\right)^2 \right) \frac{V_\infty^2}{2 g_c J C_p} \right] \right\} \tag{192}$$

$$T_j \cong T_o - \left\{ 0.8 (1 - \alpha_j) \left(\frac{V}{V_\infty}\right)^2 + \right.$$

$$\left. 0.2 (1 - 0.75 \alpha_s - 0.25 \alpha_B) \right\} \frac{V_\infty^2}{2 g_c J C_p} \tag{193}$$

---

*(See footnote, page 272.)

Define an overall-probe factor, A , by the following equation:

$$T_j = T_o - (1 - A) \frac{V_\infty^2}{2 g_c J C_p} \tag{194}$$

The factor, A , can be evaluated from:

$$A = 1 - \left\{ 0.8 \left(1 - \alpha_j \right) \left(\frac{V}{V_\infty} \right)^2 + 0.2 \left(1 - 0.75 \alpha_s - 0.25 \alpha_B \right) \right\} \tag{195}$$

Substituting the values assumed for the present probe yields:

$$\begin{aligned} \alpha_B &= 0.75 \\ \alpha_s &= 0.85 \\ \alpha_j &= 0.85 \\ \frac{V}{V_\infty} &= 0.60 \\ \text{and } A &= 0.928 \end{aligned} \tag{196}$$

As the velocity of the gas in the main stream goes down, the conduction links between the shield and the base, and between the junction and the shield, become more important in determining the performance of the probe. This is the natural result of decreasing the convective-heat input at the surface while maintaining the same conduction path through the solid.

At approximately 30 percent of design flow the conduction links will have nearly doubled, and the value of the factor (A) is given by:

$$A = 1 - \left\{ 0.6 \left(1 - \alpha_j \right) \left(\frac{V}{V_\infty} \right)^2 + 0.4 \left(1 - 0.5 \alpha_s - 0.5 \alpha_B \right) \right\} = 0.88 \tag{197}$$

Note that the component-recovery factors of the assembly are not changed; only the conduction links are affected.

At extremely low flows, conduction will dominate, and if the base is large enough to act as a heat sink, the factor (A) will approach the recovery factor of the base:

$$A \longrightarrow 0.75 \tag{198}$$

The variation in the overall-probe-recovery factor, A , is shown qualitatively on the sketch in Figure 90.

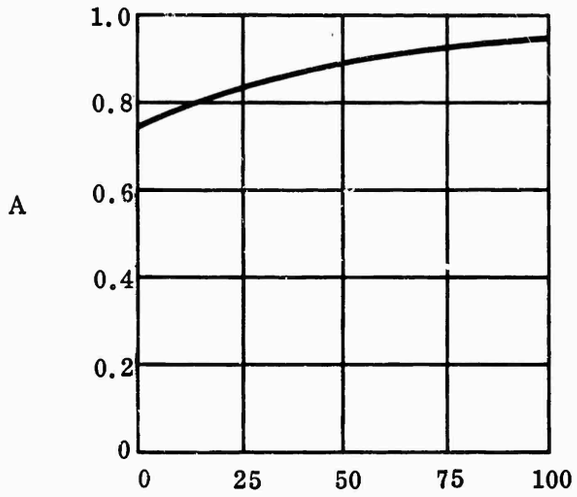


Figure 90. Variation in Overall Probe-Recovery Factor.

This probe performance map is predicated on zero heat transfer to the duct walls by conduction or radiation, and serves only to describe the recovery-factor aspects of the probe design.

The relationship between the probe indicated temperature (T_j) and true gas-stream stagnation temperature must also account for the effects of conduction and radiation to the walls.

The radiation effect can be estimated by using a linearized radiation-heat-transfer coefficient, defined by:

$$h_r \triangleq 4\sigma\epsilon \quad T_m^3 \tag{199}$$

where: σ = Stafan-Boltzmann constant, 0.1713×10^{-8} Btu/hr-ft^2-°R^4

ϵ = emissivity (estimated at 0.75)

T_m = average system temperature (°R)

The radiation causes the shield temperature to go down. The junction then radiates and conducts to the shield, attaining a new stable temperature.

$$T_s - T_{s,a} = \frac{h_r}{h_c} \quad (T_s - T_w) \tag{200}$$

If the errors are assumed to be small, then $(T_s - T_w) \cong (T_{s,a} - T_w)$ and the radiation problem can be written:

$$\frac{T_s - T_{s,a}}{T_{s,a} - T_w} = \frac{h_r}{h_c} \tag{201}$$

The heat-transfer coefficient, h_c, can be evaluated from the Reynolds number, based on shield diameter (Re = 50,000) (using Figure 3 of the reference by extrapolation).* The value of the Nusselt number is found to be $\cong$ 130. The values of h_r and h_c are then (for T_m = 1200°R):

$$h_r = 4\sigma\epsilon \quad T_m^3 = 7.34$$

$$h_c = \frac{N_{nu}\,(k_f)}{D} = 748$$

*(See footnote, page 272.)

The radiation of the shield is then:

$$\frac{T_s - T_{s,a}}{T_{s,a} - T_w} \cong 0.01 \qquad (202)$$

For each 100°F difference between the wall temperature and the adiabatic shield temperature, the shield temperature will drop about 1°F.

The junction is linked to the shield, both by radiation and by conduction. Conduction is by far the stronger link, estimated to be 0.25 for the present problem. The junction temperature will drop 0.25° for each 100°F wall-temperature depression.

The wall conduction effect is also related to the difference between the shield temperature and the wall temperature. Assuming a passage .5 inch wide, with the probe centered, the shield can be approximated by a fin having an effective immersion of 4 diameters (2 diameters in the base and 2 diameters in the shield itself). Using the previously determined value of h_c in the conduction-error equation (Equation 3 of the reference*) yields:

$$\frac{T_s - T_{s,a}}{T_{s,a} - T_w} = \frac{1}{\cosh\left\{\frac{L}{D}\sqrt{\frac{4\,h_c}{k_s}}\,D\right\}} = 0.01 \qquad (203)$$

The effects of conduction and radiation are of approximately equal importance, each resulting in about 0.25°F drop in probe indicated temperature per 100°F wall-temperature depression.

As the free-stream airflow goes down, the conduction and radiation errors will increase.

---

*(See footnote, page 272.)

The probe performance is summarized as:

$$\left.\begin{aligned} A &= 0.928 \\ \frac{E_r + E_c}{\Delta T_w} &= 0.50/100 \end{aligned}\right\} \text{Design Point}$$

$$\left.\begin{aligned} A &= 0.88 \\ \frac{E_r + E_c}{\Delta T_w} &= 1.00/100 \end{aligned}\right\} \text{30-Percent Flow}$$

2.1 CONCLUSIONS

The performance of the adiabatic probe can be described in terms of a single probe-performance factor, A , which serves to define the adiabatic junction temperature of the probe. This value will be used in the high-velocity heat-transfer analysis in Section 3.0 of this appendix.

The probe, at design-flow conditions, is essentially adiabatic, having losses of less than 0.5°/100°F. The treatment of the probe as an adiabatic body is justified.

2.2 RECOMMENDATIONS

The performance of the probe would be considerably improved if the junction were made longer, up to 10-15 wire diameters, and if it were of the tent or steeple type, instead of the present twisted junction. The shield, of course, should also be extended in length. Bleed holes drilled in the shield at the base of the junction (area ratio set for $V/V_\infty = 0.5$) would then be recommended in place of the milled bleed slots.

3.0 EQUILIBRIUM TEMPERATURE OF AN ISOLATED PROBE IN A HIGH-FREQUENCY INTERMITTENT FLOW

It will first be shown that the frequencies encountered in testing of radial-flow compressors are sufficiently high that only negligible fluctuating components are induced in the thermocouple temperature. The quasi-steady thermocouple-equilibrium temperature will then be determined as a function of the jet-wake area, velocity, and temperature ratios using incompressible-flow heat-transfer relationships. The solution to the heat-transfer problem is then expressed for compressible-flow conditions by substitution of stagnation temperature for static temperature in each of the heat-transfer-rate equations.

3.1 THE EFFECT OF HIGH-FREQUENCY FLUCTUATIONS

When a solid body is immersed in a fluid whose temperature is cyclically varying with time, the surface temperature of the solid varies cyclically also, and at the same frequency as the disturbances in the fluid temperature. The amplitude of the surface-temperature disturbance is less than that of the fluid temperature, as a result of the resistance to heat transfer in the boundary layer between the fluid and the surface. This reduction is calculable by the following:

Let the fluid temperature oscillate about its average temperature according to:

$$T_f = \overline{T}_f + \epsilon_G \cos\left(\frac{2\pi\tau}{\tau_o}\right) \tag{204}$$

A nonsinusoidal variation can be resolved, by a Fourier analysis, into a sum of sinusoidal terms (each term follows the above description).

Then the surface temperature oscillates about the same mean temperature with an amplitude less than that of the fluid temperature. The ratio given by Eckert and Drake* is:

---

*E. R. G. Eckert and R. M. Drake, Heat and Mass Transfer, McGraw-Hill Book Co., New York, 1959, pp. 103-107.

$$\frac{\epsilon_s}{\epsilon_G} = \frac{1}{\left(1 + 2\sqrt{\frac{\pi k^2}{\alpha \tau_o h^2}} + 2\frac{\pi k^2}{\alpha \tau_o h}\right)^{1/2}} \qquad (205)$$

where:

k	=	thermal conductivity of the solid, Btu/hr-ft^2-°F/ft
τ_o	=	period of the disturbance (hour)
α	=	thermal diffusivity of the solid, $k/\rho c$
h	=	heat-transfer coefficient (Btu/hr-ft^2-°F)

Taking typical properties for thermocouple materials,

k	=	16 Btu/hr-ft^2-°F/ft
α	=	0.50 ft^2/hr
h	=	1160 Btu/hr-ft^2-°F (using velocity inside probe as 400 fps and wire diameter as 0.012 inch)*

Considering a 15-blade rotor at 20,000 rpm,

$$\tau_o = 5.5 \times 10^{-8} \text{ hr}$$

The amplitude ratio is thus found to be:

$$\frac{\epsilon_s}{\epsilon_G} = 0.0048$$

Estimates of the jet-wake temperature differences (from the contractor's compressor-test data, see Table II) indicate that it can be equal to or less than 66°F for a typical installation. The surface-temperature variation is thus seen to be:

$$\epsilon_s = 0.88°\text{F}$$

---

*(See footnote, page 282.)

The thermocouple may be assumed to produce an output based on the average temperature of its cross section (radial nonuniformity in temperature will cause radially flowing electrical currents), which will further reduce the amplitude, since the fluctuation observed at the surface will be attenuated more and more at increasing depths beneath the surface. This attenuation can also be calculated, by methods given in the reference.* Using the values listed above shows that the disturbance would be reduced to less than 1 percent of its surface value at the centerline of a wire size of 0.012 inch in diameter. The decline is more rapid than a linear variation with radius.

TABLE II

COMPRESSOR DATA FOR THE GENERAL TEST CASE OF THE WORKHORSE IMPELLER SUPPLIED BY THE CONTRACTOR

Jet	Wake
$P_j = P_w$	$P_w = P_j$
T_j = 777°R (static)	T_w = 850°R (static)
$T_{j_{rel}}$ = 850°R (total)	$T_{w_{rel}}$ = 850°R (total, assume $V_R = 0$)
$T_{j_{abs}}$ = 1127°R (total)	$T_{w_{abs}}$ = 1175°R (total)
$V_{j_{abs}}$ = 2050 fps	$V_{w_{abs}}$ = 2000 fps
$V_{j_{rel}}$ = 931 fps	$V_{w_{rel}}$ = 0
Discharge angle, rel. = 10 degrees	Discharge angle, rel. = 0 degrees

As an approximation, the average temperature across the section might be taken to be constant to within 0.4°F. This 0.4°F fluctuation would be evidenced by an A.C. component of the thermocouple output, at a frequency of 5000 cps. Most thermocouple-recording systems would not be capable of interpreting this component.

*(See footnote, page 282.)

The thermocouple will be considered to indicate a quasi-steady temperature equal to the mean temperature under the above conditions; i.e., constant h and equal duration of the positive and negative half-cycles of the temperature fluctuation.

A problem arises when conditions are such that the values of h are not the same on the positive and negative half-cycles. The problem is then one of determining the relationship between the mean temperature of the thermocouple and the mean temperature of the fluid. It is apparent that the heat-transfer coefficient acts as a weight factor in determining the mean temperature of the thermocouples. This effect can cause the thermocouple to establish a mean temperature, which is different from the time averaged fluid temperature.

In the specific case considered in this report, another problem arises; i.e., that of defining the mean temperature of the fluid. When a thermocouple is installed very close to the tip of a rotor operating in the jet-wake mode, the thermocouple is alternately exposed to jet fluid and to wake fluid, and it assumes an average temperature based on these two components. However, if the wake fluid does not leave the rotor, but is simply carried around with it, then that fluid is not part of the through-flow fluid of the compressor, and its temperature should not be permitted to affect the temperature of the thermocouple. This problem will be treated in more detail in Section 4.0.

3.2 THE LOW-VELOCITY HEAT-TRANSFER PROBLEM — ENERGY-BALANCE RELATIONS

$\overline{T}_{f,p}$ = average temperature of fluid swept past the probe position

T_j = temperature of thermocouple junction (indicated temperature)

$\overline{T}_1$ = average static temperature of the jet fluid

$\overline{h}_1$ = average heat-transfer coefficient between jet fluid and thermocouple

$\overline{T}_2$ = average static temperature of wake fluid

$\overline{h}_2$ = average heat-transfer coefficient between the wake fluid and the thermocouple

$\rho_1 V_1$ = average mass velocity of the jet fluid with respect to the stationary probe

$\rho_2 V_2$ = average mass velocity of the wake fluid with respect to the stationary probe

f_1 = the fraction of one blade period during which the probe is exposed to the jet-fluid portion of the blade spacing

Applying an energy balance to the isolated probe over the duration of one cycle of the gas flow (assuming no heat transfer by conduction or by radiation) yields:

$$\bar{h}_1 \left(\bar{T}_1 - T_j \right) f_1 = \bar{h}_2 \left(T_j - \bar{T}_2 \right) \left(1 - f_1 \right) \tag{206}$$

Solving for T_j yields:

$$T_j = \frac{\bar{T}_1 + \frac{\bar{h}_2}{\bar{h}_1} \left(\frac{1 - f_1}{f_1} \right) \bar{T}_2}{1 + \frac{\bar{h}_2}{\bar{h}_1} \left(\frac{1 - f_1}{f_1} \right)} \tag{207}$$

An expression describing the average temperature of the fluid passing the stationary probe will now be presented, in terms of the absolute velocities of the jet and wake regions:

$$\bar{T}_{f,p} = \frac{\overline{\rho_1 V_1} f_1 C_p \bar{T}_1 + \overline{\rho_2 V_2} (1 - f_1) C_p \bar{T}_2}{C_p \left[\overline{\rho_1 V_1} f_1 + \overline{\rho_2 V_2} (1 - f_1) \right]} \tag{208}$$

Based on data from Table II for a typical case, the absolute velocity of the jet fluid might be taken as 2050 fps, while that of the wake, having no slip relative to the rotor (but also no radial component), might at the same time be on the order of 2000 fps. Estimating the temperatures of the jet and wake, considering the wake to exchange heat with the rotor and equilibrate at jet-relative-stagnation temperature (rotor recovery factor of unity),indicates that the wake would

probably be hotter than the jet. Estimates from the table were, specifically, T_j (static) = 777°R and T_w (static) = 845°R. Under the assumption, then, of uniform static pressure around the periphery of the rotor, the jet-wake mass-velocity ratio (based on absolute velocity) is unity, within 11 percent:

$$\frac{\rho_1 V_1}{\rho_2 V_2} = \frac{2050 \times 845}{2000 \times 777} = 1.112$$

Thus the average temperature of the fluid swept past the stationary probe can be approximated by:

$$\overline{T}_{f,p} = f_1 \overline{T}_1 + (1 - f_1) \overline{T}_2 \tag{209}$$

The relationship of the probe temperature to the mean fluid temperature at the probe position is given by:

$$T_j - \overline{T}_{f,p} = \left(\frac{1}{1 + \frac{\overline{h}_2}{\overline{h}_1}\left(\frac{1 - f_1}{f_1}\right)} - f_1 \right) \overline{T}_1 + \left\{ \frac{\frac{\overline{h}_2}{\overline{h}_1}\left(\frac{1 - f_1}{f_1}\right)}{1 + \frac{\overline{h}_2}{\overline{h}_1}\left(\frac{1 - f_1}{f_1}\right)} - (1 - f_1) \right\} \overline{T}_2 \tag{210}$$

Some special cases can be examined to illustrate the behavior described by the above equation:

1) When $\overline{h}_1 = \overline{h}_2$, $T_j = \overline{T_{f,p}}$ for all values of f_1;

2) When $f_1 = 0.5$, the probe temperature will be unbalanced toward that of the jet fluid when $\overline{h}_1$ exceeds $\overline{h}_2$ and toward the wake temperature when $\overline{h}_2$ exceeds $\overline{h}_1$.

Examination of the special case (2) shows clearly that the heat-transfer coefficient acts as a weight factor by which the thermocouple determines its equilibrium temperature in terms of the jet and wake temperatures. The true mass-flow-averaged temperature of the gas stream is determined by using the individual

mass velocities as weight factors; in the present case, these are equal. When the heat-transfer coefficients are not in the same ratio as the mass velocities, the thermocouple cannot make a true-average interpretation of the gas temperature. In the most general case (unequal mass velocities in the two streams) the heat-transfer coefficients will not be equal. The heat-transfer coefficients vary, in general, either with the square root of the mass velocity (laminar heat transfer) or with the fifth root (turbulent heat transfer). It can also be seen from Equation 210 that the jet-wake fraction is of importance in determining the measurement error $(T_j - \overline{T_{f,p}})$ whenever the heat-transfer coefficients are not equal.

It is also important to recognize that the average temperature of the fluid swept past the probe may not be the proper temperature to use in evaluating compressor performance. In the simplest model of the jet-wake mode of operation, the wake can be thought of as a rigid body rotating with the rotor. If the probe is mounted close to the rotor, it will be affected by the wake-fluid temperature as the wakes are swept by the probe. The wake fluid, however, does not leave the rotor, under this simplest model, and its temperature should not be allowed to affect the reading of the probe. It would be more pertinent, under this simple model, to compare the thermocouple temperature to the temperature of the jet fluid alone, since that is the fluid which actually leaves the rotor. This comparison is given by the following relationship:

$$\overline{T}_j - \overline{T}_1 = - \frac{\dfrac{\overline{h}_2}{\overline{h}_1} \left(\dfrac{1 - f_1}{f_1} \right)}{1 + \dfrac{\overline{h}_2}{\overline{h}_1} \left(\dfrac{1 - f_1}{f_1} \right)} \left(\overline{T}_1 - \overline{T}_2 \right) \qquad (211)$$

Note that the thermocouple cannot correctly indicate jet-fluid temperature unless the heat transfer to the wake is zero.

When the heat-transfer coefficients are equal, Equation 211 reduces to:

$$\overline{T}_j - \overline{T}_1 = - (1 - f_1) (\overline{T}_1 - \overline{T}_2) \qquad (212)$$

3.3 ESTIMATE OF THE JET- AND WAKE-FLOW CONDITIONS AFFECTING THE TEMPERATURE-MEASURING PROBLEM

It must be borne in mind, in considering the values of Table II, that they are estimates based on plausible models of the fluid-rotor interaction. They do not have the certainty of experimental data, but serve only to provide estimators of the problems discussed in this report. Nor is it felt worthwhile to conduct experiments solely for the purpose of improving these estimates unless there is a considerable amount of data already gathered which might be reinterpreted based on this analysis. Wake-temperature profiles could be measured by instrumenting a special rotor, as could the jet-wake width ratio, but the experiments would be time-consuming and costly.

As will later be brought out, a more effective way of avoiding the errors described in this report is simply to relocate the thermocouples so they are no longer affected by the wake region.

3.4 THE EFFECT OF VELOCITY FLUCTUATIONS ON THE HEAT-TRANSFER COEFFICIENT

The heat-transfer coefficient is not sensitive to velocity alone, but is also sensitive to the mass velocity, ρV, as it occurs in the Reynolds number of the probe-flow situation. From the estimates provided, it can be seen that while the velocities and densities of the jet and wake are not respectively equal, it is true that the mass velocities are equal to within 11 percent. This point was previously demonstrated. Thus the Reynolds numbers of the 2 flow regimes are equal within 1 order of magnitude. Steady-state heat-transfer literature and experiments both suggest that this is a sufficient condition for the heat-transfer coefficients to be substantially equal (h varying either with the square root or the fifth root of the Reynolds number). On the assumption that pulsating flows at steady Reynolds numbers yield the same results as steady flows, then the heat-transfer coefficients in the 2 flow regimes would remain the same within 1.25 percent.

Since probe-to-probe variations in heat-transfer coefficient may be on the order of 5 percent, and since experiments indicate an uncertainty of 5-10 percent in repeating heat-transfer data under supposedly identical, steady-state conditions, it does not appear warranted to try to account for variations on the order of 1.25 percent.

3.5 THE EFFECT OF FLUCTUATIONS IN THE ANGLE OF INCIDENCE OF THE STREAM

The angle of incidence of the air stream on the probe will fluctuate ± 12.5 degrees about the mean, as the jet and wake regions pass the probe.

A probe of the type under consideration will typically have a yaw plateau of ± 15 degrees for a 1-percent drop-off in recovery factor, or a 2-percent drop-off in heat-transfer coefficient.

Comparing the above figures indicates that there should be no significant effects due to the fluctuating angle of incidence, providing that the probe is aligned with the mean-incidence angle.

3.6 THE HIGH-VELOCITY HEAT-TRANSFER PROBLEM

High- and low-velocity heat transfer differ chiefly due to the shear-work dissipation in the boundary layer. This causes even an adiabatic wall to achieve a temperature different than the gas-stream temperature. In fluids whose Prandtl number is unity, the adiabatic wall temperature is equal to the stagnation temperature of the free-stream fluid. For air (Pr = 0.68), the adiabatic wall temperature is usually referred to by means of the recovery factor, referenced to the stagnation state of the free stream. It is this phenomenon of boundary-layer-shear work which is responsible for the recovery factors of 0.86 and 0.75 used in Section 1.0 of this appendix for cylinders parallel and perpendicular to the flow.

It is apparent that the temperature potential for heat transfer in a high-velocity flow should be based on the difference between the actual wall temperature and the adiabatic wall temperature.

In many respects it is more useful to think of the adiabatic wall temperature as the effective gas temperature. This is the temperature which an adiabatic system will reach when immersed in the stream. It must be borne in mind, however, that this effective gas temperature is not a property of the gas stream only, but of the system of a particular body immersed in the stream (recall that cylinders parallel and perpendicular to the stream see different effective gas temperatures even though they are in the same stream).

With the substitution of the effective gas temperature for the actual gas temperature, the high-velocity heat-transfer problem can be handled by the low-velocity results; the same Reynolds number dependent relationships which determined the heat-transfer coefficient for the low-velocity, nigh-density problem can be used.

To convert the low-velocity results of Section 2.0 to high-velocity information it is only necessary to make the following substitutions for T_1 and T_2 :

$$T_1 = T_{o,1} - (1 - A) \frac{V_1^2}{2g_c JC_p} \tag{213}$$

$$T_2 = T_{o,2} - (1 - A) \frac{V_2^2}{2g_c JC_p} \tag{214}$$

$T_{o,1}$ is the stagnation temperature of the jet flow; $T_{o,2}$ is the stagnation temperature of the wake flow; and A is the overall probe recovery factor described in Section 2.

Thus Equation 210 becomes:

$$T_j - \left(T_{f,o} - [1-A]\frac{V^2}{2g_c JC_p} \right) = \left\{ \frac{1}{1 + \frac{h_2}{h_1}\left(\frac{1-f_1}{f_1}\right)} - f_1 \right\} \left\{ T_{o,1} - [1-A]\frac{V_{\infty,1}^2}{2g_c JC_p} \right\} +$$

$$\left[- \frac{\frac{h_2}{h_1}\left(\frac{1-f_1}{f_1}\right)}{1 + \frac{h_2}{h_1}\left(\frac{1-f_1}{f_1}\right)} - [1-f_1] \right] \left(T_{o,2} - [1-A]\frac{V_{\infty,2}^2}{2g_c JC_p} \right) \tag{215}$$

and Equation 211 becomes:

$$T_j - \left(T_{1,o} - [1-A]\,\frac{V_1^2}{2g_c JC_p}\right) = \left\{ - \frac{\frac{h_2}{h_1}\left(\frac{1-f_1}{f_1}\right)}{1 + \frac{h_2}{h_1}\left(\frac{1-f_1}{f_1}\right)} \right\}$$

$$\left\{\left(T_{o,1} - [1-A]\frac{V_1^2}{2g_c JC_p}\right) - \left(T_{o,2} - [1-A]\frac{V_2^2}{2g_c JC_p}\right)\right\} \qquad (216)$$

3.7 SIMPLIFICATIONS BASED ON $h_1 = h_2$ AND $\rho_1 V_1 = \rho_2 V_2$

Sections 3.3 and 3.4 produced the information that the above assumptions are reasonable (probably within 1 or 2 percent). Thus, Equations 210 and 212 can be used.

Equation 210 (comparison of T_j with average fluid temperature, $h_1 = h_2$):

$$T_j = T_{f,o} - \left(1 - A\right)\frac{V^2}{2g_c JC_p} \qquad (217)$$

Equation 212 (comparison of T_j with jet-fluid temperature, $h_1 = h_2$):

$$T_j - \left(T_{o,1} - [1 - A]\,\frac{V_1^2}{2g_c JC_p}\right) = - \left(1 - f_1\right)\left(T_{o,1} - T_{o,2}\right) \qquad (218)$$

4.0 THE EFFECT OF WAKE-FLUID ENTRAINMENT AND PROBE POSITION

The mass-flow-averaged total temperature is defined as that which should be used in determining the efficiency of the compressor. The first question which might be asked is: Where should the thermocouple be placed so as to measure this

temperature? The answer is, obviously, that it should be far enough away from the rotor so that the fluid has been well mixed and has established a uniform temperature. R. C. Dean, commenting on the draft of this appendix, says:

> "The mixing outside the impeller apparently takes place in a very small distance; i.e., a radius ratio around 1.05..... In experimental work the total-temperature probe may be placed very close to the tip of the impeller so that in estimating errors, it would probably be best to assume that it is at the tip, before mixing occurs. High-speed schlieren movies have shown no significant unsteadiness of the flow at the leading edge of the vaned diffusers which lie in a radius ratio of 1.06. One obvious means for avoiding these temperature errors due to fluctuating flow would be to place the probe at radius ratios greater than 1.05....."

The second question which might be asked is: Can the thermodynamically significant temperature be measured by a probe close to the rotor? To answer this, one must propose a model of the flow near the rotor.

Consider the simplest model, where the wake fluid forms a rigid, radially extending node of fluid (at rest with respect to the rotor). When the probe is close to the rotor, it is swept by these nodes as they rotate, and the thermocouple seeks some temperature between that of the jet fluid and that of the wake fluid. If the heat-transfer coefficients in the 2 regions are equal, and it has been shown that they are for practical purposes, the thermocouple will read the average temperature of the jet and wake fluids. Is this the thermodynamically significant temperature? No, because the wake fluid does not leave the rotor under this simplest model (only the jet fluid leaves the rotor); therefore, the thermodynamically significant temperature is the temperature of the fluid leaving the rotor (the jet fluid only). The relationship between the thermocouple temperature and the jet-fluid temperature is given by Equations 211 or 212.

It seems apparent that the wake-fluid region cannot be exactly at rest with respect to the rotor. When the wake fluid has a radial-velocity component, some of the wake fluid will be mixed with the jet fluid in determining the thermodynamically significant temperature. An energy balance, performed on an annular-control volume around the rotor, can be used to describe the mixed-mean temperature of the discharge fluid in terms of the entering flows of jet and wake fluids and to describe their individual temperatures.

The thermocouple temperature will be relatively unaffected by small changes in the radial-velocity component of the wake region; whether or not the wake fluid leaves the compressor, it is still swept past the thermocouple and affects the temperature of the thermocouple.

The probe temperature, close to the rotor, is given by Equation 207. In high velocity form,

$$T_j = \frac{T_{o,1} - (1 - A)\frac{V_1^2}{2g_c JC_p} + \left(\frac{1 - f_1}{f_1}\right)\left[T_{o,2} - (1 - A)\frac{V_2^2}{2g_c JC_p}\right]}{1 + \left(\frac{1 - f_1}{f_1}\right)} \tag{219}$$

For purposes of this analysis, the difference in velocities of the jet and wake will be ignored. The differences are about 11 percent; the term is then squared (21 percent) and multiplied by (1 - A), where A is about 0.928. Therefore, the error is about 1.4 percent of the kinetic temperature. This is on the same order as the uncertainties in the value of A . Under this simplification, the kinetic temperature terms can be combined, yielding:

$$T_j = \frac{T_{o,1} + \left(\frac{1 - f_1}{f_1}\right) T_{o,2}}{1 + \frac{1 - f_1}{f_1}} - \left(1 - A\right)\frac{V^2}{2g_c JC_p} \tag{220}$$

With the thermocouple-indicated temperature described in terms of the jet-wake conditions at the tip diameter of the rotor, the mixed-mean fluid temperature actually leaving the rotor can be determined.

Consider an annular-control volume around the rotor, extending radially outward far enough to permit the assertion that the fluid leaving the control volume is at a uniform temperature given by $T_{M,o}$ (stagnation temperature, mixed-mean discharge) (see Figure 91).

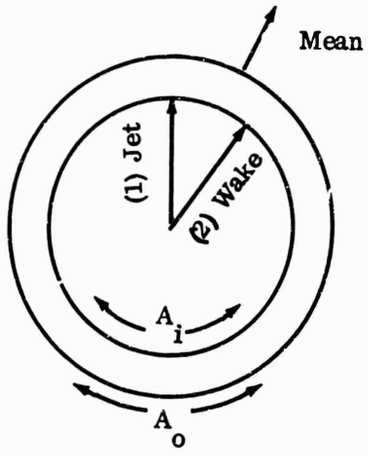


Figure 91. Annular-Control Volume (Jet and Wake).

Fluid entering from the jet region (1) carries with it energy in the amount:

$$\text{Jet Contribution:} \quad \rho_1 V_{R,1} f_1 A_i C_p T_{o,1}$$

For fluid entering from the wake region (2):

$$\text{Wake Contribution:} \quad \rho_2 V_{R,2} f_2 A_i C_p T_{o,2}$$

The mixed-mean fluid temperature at the outer diameter of the control volume is defined to account for all of the energy inputs:

$$\rho_M V_{R,M} A_o C_p T_{o,M} \tag{221}$$

The control volume is also subject to the Conservation of Matter Principle, which relates the mean radial velocity at the outer diameter to the inner-diameter conditions:

$$\rho_1 V_{R,1} f_1 A_i + \rho_2 V_{R,2} (1-f_1) A_i = \rho_M V_{R,M} A_o \tag{222}$$

If the control volume is shrunk to zero radial width (instantaneous mixing) and the fluid density is assumed uniform, then:

$$f_1 V_{R,2} + (1 - f_1) V_{R,2} = V_{R,M} \tag{223}$$

Applying the Conservation of Energy Principle to Equations 220 through 222 and assuming no heat transfer from the gas to the compressor case yields:

$$\rho_M V_{R,M} A_o C_p T_{o,M} = \rho_1 V_{R,1} f_1 A_i T_{1,0} + \rho_2 V_{R,2} (1-f_1) A_i C_p T_{o,2} \tag{224}$$

Introducing the same simplification used in Equation 223 yields:

$$V_{R,M} T_{o,M} = f_1 R_{R,1} T_{o,1} + (1-f_1) V_{R,2} T_{o,2} \tag{225}$$

Substituting Equation 223 into Equation 225,

$$T_{o,M} = \frac{f_1 V_{R,1} T_{o,1} + (1 - f_1) V_{R,2} T_{o,2}}{f_1 V_{R,1} + (1 - f_1) V_{R,2}} \tag{226}$$

Dividing through by $f_1 V_{R,1}$ yields:

$$T_{o,M} = \frac{T_{o,1} + \left(\frac{1 - f_1}{f_1}\right) \left(\frac{V_{R,2}}{V_{R,1}}\right) T_{o,2}}{1 + \left(\frac{1 - f_1}{f_1}\right) \frac{V_{R,2}}{V_{R,1}}} \tag{227}$$

Equations 227 and 220 combine to present:

$$T_j - T_{o,M} = - \frac{\left(\frac{1-f_1}{f_1}\right)\left(1 - \frac{V_{R,2}}{V_{R,1}}\right)\left(T_{o,1} - T_{o,2}\right)}{\left(1 + \frac{1-f_1}{f_1}\right)\left(1 + \left(\frac{1-f_1}{f_1}\right)\left(\frac{V_{R,2}}{V_{R,1}}\right)\right)} - (1 - A)\frac{V^2}{2g_c JC_p} \tag{228}$$

Two special cases may be considered:

1) If $V_{R,2} = 0$, then $T_{o,M} = T_{o,1}$, and the high-velocity form of Equation 212 is:

$$T_j - T_{o,1} = - (1 - f_1)(T_{o,1} - T_{o,2}) - (1 - A)\frac{V^2}{2g_c JC_p} \tag{229}$$

2) If $V_{R,2} = V_{R,1}$ the high-velocity form of Equation 210 for equal heat-transfer coefficients is determined, since $T_{o,M} = T_{f,p,o}$ in that case (mixed-mean stagnation temperature at the probe location).

$$T_j - T_{o,1} = - (1 - A)(T_{kinetic}) = - (1 - A)\frac{V^2}{2g_c JC_p} \tag{230}$$

It would appear that Equation 228 provides the most flexible and general form for considering the problem of measuring the bulk temperature of the discharge fluid, using a thermocouple located close enough to the rotor to be affected by the wake temperature.

Equation 228 will be used to estimate effects, based on estimates of f_1 and $V_{R,2}/V_{R,1}$ shown in the table.

Take:

$$f_1 = 0.25$$

$$\frac{V_{R,2}}{V_{R,1}} = 0;\ 0.15 \text{ (estimated to be 0 based on the impeller model)}$$

Then, taking A = 0.928 (typically), we have

$$T_j - T_{o,M} = -0.75\,(T_{o,1} - T_{o,2}) - 0.072\left(\frac{V^2}{2g_c JC_p}\right) \text{for the case of } \frac{V_{R,2}}{V_{R,1}} = 0 \tag{231}$$

$$T_j = T_{o,M} = -0.44\,(T_{o,1} - T_{o,2}) - 0.072\left(\frac{V^2}{2g_c JC_p}\right) \text{for } \frac{V_{R,2}}{V_{R,1}} = 0.15 \tag{232}$$

If the wake and jet stagnation temperatures differ by as much as 50° to 70°F, as has been estimated, and if the other estimates of jet width and radial-velocity ratios are correct, then a probe mounted close to the rotor will be reading between 45° and 60°F higher than the value it would have read had it been placed far enough from the rotor to sense the mixed-fluid condition.

From the way in which this mixing error is introduced, by sensing the temperature of fluid which does not actually leave the system, it can be seen that the effect is exaggerated by low radial velocities in the wake and goes to zero when the wake fluid has the same radial velocity as the jet. In this case, all of the fluid sensed by the probe influences the temperature of the fluid leaving the system.

Contractor's note:
Significant differences have been observed in the past between collector temperature (at the end of the compressor) and that measured at the rim of the impeller. Part of this difference has been ascribed to heat transfer, but not all of it (nor even the largest fraction of it) can be accounted for in that way. Thus the effects predicted by this analysis seem to be borne out by experience in testing compressors.

(U) APPENDIX VIII

INSTRUMENTATION RESEARCH

ABSTRACT

This appendix describes instrumentation research conducted in 1966 by the contractor in support of other engine and component development programs. Specifically investigated were methods of measuring (1) blade-to-shroud running clearance, (2) total pressure in the presence of unsteady flow fields, (3) torque at rotational speeds up to 60,000 rpm, and (4) total temperature utilizing miniature probes.

A system was evaluated that would measure blade-to-shroud running clearance with an accuracy of ±0.002 inch. An analysis of existing typical total-pressure-measuring installations indicated that no errors were being introduced due to the unsteady flow fields encountered. Several methods of torque measurement were investigated, but all required major modifications to the test rigs. A calibration facility was constructed to determine temperature-recovery ratio of existing miniature total-temperature probes.

The above research was conducted in a company-funded program.

SYMBOLS

B	=	shape factor
D	=	probe internal diameter (feet)
f	=	minimum frequency for which probe will give true average readings
f_m	=	minimum permissible square wave frequency (cps)
L	=	probe tube length (feet)
P	=	pressure (psia)
P_f	=	fluctuation pulse amplitude (psia)
P*	=	root-mean-square average pressure (psia)
$\overline{P}$	=	true average pressure (psia)
S	=	pulse duration period (sec)
T	=	time period between pulses (sec)
ν	=	kinematic viscosity (ft-sec)
ρ	=	mass density of fluid (lbm/ft^3)

1.0 INTRODUCTION

1.1 OBJECTIVE

The objective of the research program was to investigate instrumentation hardware and application techniques to provide an accurate definition of performance characteristics of turbine engines and components.

The instrumentation technology developed has application to several of the contractor's engine and component development programs, such as the T50-BO-10 improvement and the Army centrifugal-compressor research program.

1.2 SCOPE

The research was divided into 4 parts:

1) Blade-to-shroud running clearance measurement;

2) The influence of unsteady flow fields on total-pressure measurement;

3) Torque measurement at high rotational speeds;

4) More accurate measurement of total temperature in diffuser passages.

2.0 MEASUREMENT OF BLADE-TO-SHROUD RUNNING CLEARANCE

2.1 GOALS

A monitor of impeller blade-to-shroud clearance during rig operation is necessary in order to avoid mechanical rub of the impeller and shroud as they expand thermally and distort under centrifugal forces. In addition, a knowledge of clearance allows clearance losses to be calculated,which contributes to a more accurate definition of performance. The measurement accuracy goal was 10 percent of the clearance. An operating range of 0 to 0.060 inch and an ability to withstand temperatures up to 700°F were necessary.

2.2 RESEARCH AND DEVELOPMENT EFFORT

Specifications of several commercially available distance measuring systems were studied. Two systems were selected for evaluation: the gated-beam proximity detection and sensing system and the eddy-current clearance detection system.

2.2.1 GATED-BEAM PROXIMITY DETECTION AND SENSING SYSTEM

System Description

The proximity detection and sensing system was procured on a 3-month lease. The system was received by the contractor on 11 April 1966.

This system is basically a gated-beam detector, a circuit commonly employed in later generation television receivers. The circuit provides an output which is a function of the difference in frequency between 2 parallel resonant circuits. These circuits are designed to operate at a frequency between 10 and 14 MHz, providing an essentially flat response to changes in capacitance occurring between 0 and 1 MHz.

In this system, shown schematically in Figure 92, the sensor and its capacitance to its surroundings comprise one of the resonant circuits, while a conventional inductor and capacitor make up the reference circuit. Variation in the capacitance between the sensor and its surroundings changes the operating frequency of the active (sensor) circuit. This difference in frequency causes a change in output of the gated-beam tube. The output of this tube is amplified in several stages and is indicated on a panel meter or on an oscilloscope.

System Evaluation

Initial checkout and evaluation of the system indicated that successful operation demanded that calibration be carried out with the sensor installed in the actual hardware to be measured.

The sensor assembly was mounted in the diffuser-rig frontplate, which in turn was clamped to the work table of a layout-drilling machine. The impeller was mounted on a spare balancing arbor and chucked in the machine spindle. The parts were aligned and checked for concentricity between the impeller and plate. The initial attempt was made to obtain a static calibration, that is, with a blade positioned over the sensor. It soon became obvious that the short-term drift of the system electronics was great enough to cause nearly a ± 10-percent uncertainty in the calibration. Static calibration attempts were abandoned; however, satisfactory calibrations were obtained by measuring the alternating component of the system output while driving the impeller at 1500 rpm.

The calibrations thus obtained were satisfactory from a standpoint of short-term repeatability; however, long-term drift remained a problem. Long-term drift is estimated to be ± 10-percent full scale per day.

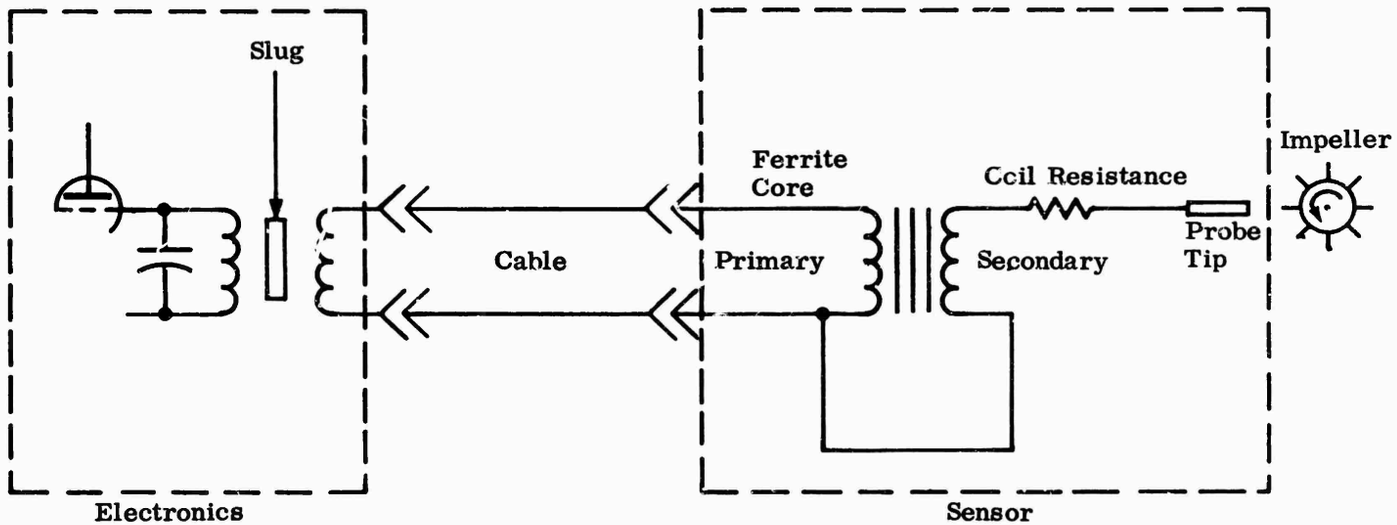


Figure 92. Gated-Beam Proximity Detection System (Schematic Diagram).

The calibrated system was immediately moved to the test rig where elapsed time for assembly and installation was about 1.5 hours. This delay was tolerable for long-term drift. Measurements taken during rig operation soon led to the conclusion that the temperature change of the probe during operation was causing excessive signal drift.

Several checks were made with the sensor in the operating position, while monitoring the temperature of the probe body. It was observed that an increase in sensor body temperature of 60°F caused the system output to decrease to zero, equivalent to 100-percent drift. An attempt was made to cool the sensor by surrounding it with a simple shroud and directing an air blast at it. This proved to be insufficient cooling. The sensor body temperature still increased approximately 25°F during the run, causing an estimated 30-percent error in system output. Analysis of these results indicated that the error primarily was a result of the change in resistance of the sensor inductor.

It was obvious that a means of protecting the sensor from the high temperatures encountered in the compressor test rigs was necessary. A flush-mounted, water-cooled mounting adapter, Figure 93, was designed and built. First attempts to calibrate the sensor-adapter assembly revealed several shortcomings:

1) The area of the adapter center conductor was 0.0002 square inch (0.016-inch diameter). This was too small an area and resulted in a small change in capacitance when an impeller blade was moved under the sensor.

2) The attempt to build the adapter with a flush center conductor (no protrusion into the diffuser passage) resulted in excessive stray capacitance to the surrounding frontplate surface. This lowered the self-resonant frequency of the sensor assembly below the capability of the electronics.

3) The method of insulating the center conductor of the adapter resulted in destruction of the sensor when disassembly was attempted.

The following changes were incorporated in the reassembly of the adapter with a new sensor:

1) The adapter center-conductor area was increased to 0.003 square inch (0.062-inch diameter) to increase the capacitance change when an impeller blade moved past the sensor. A loss in blade shape definition resulted from this configuration. It was believed that this loss had no effect on the application of the system to the immediate task.

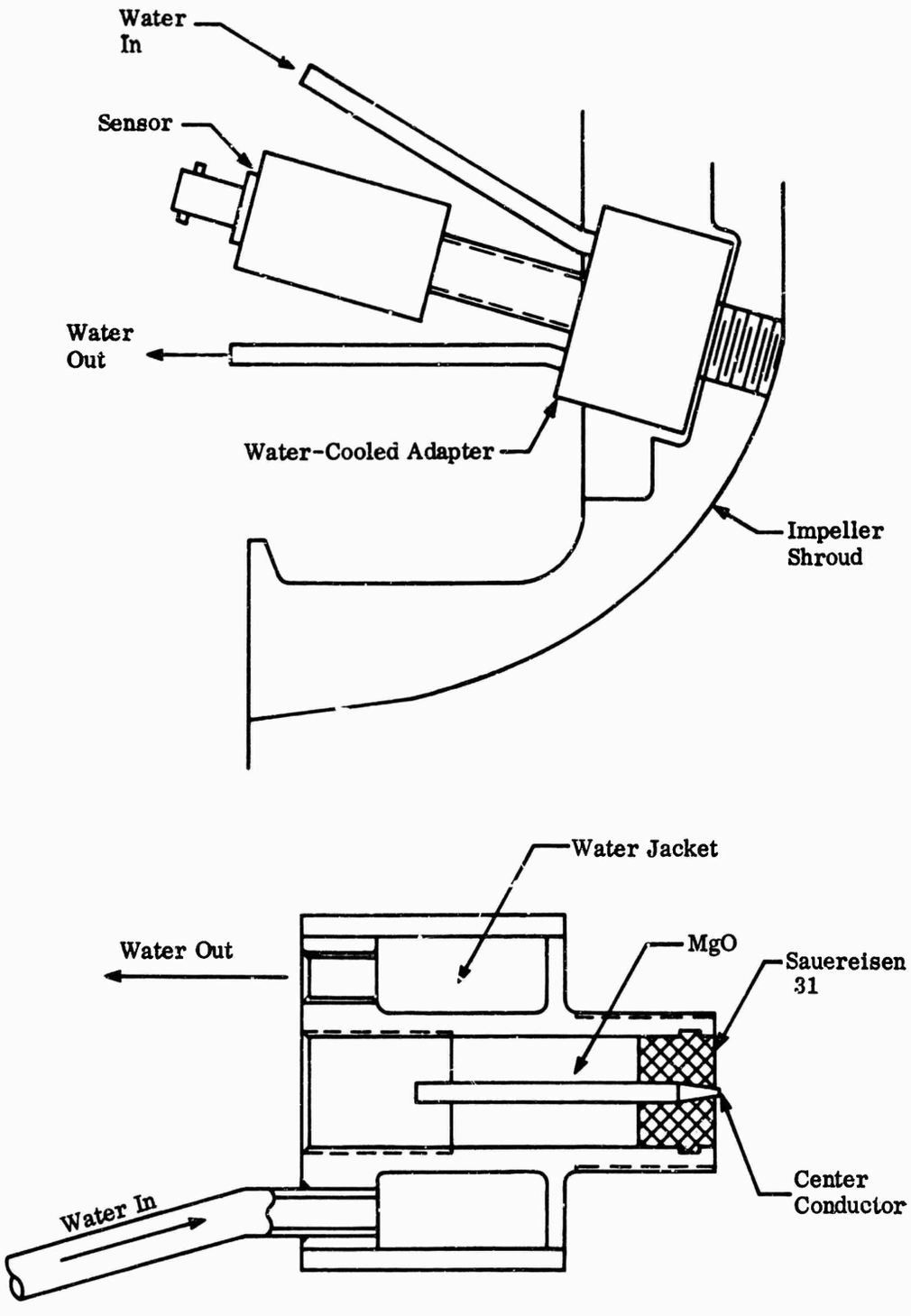


Figure 2. Detail of Water-Cooled Sensor Adapter.

2) The adapter center conductor was allowed to stand approximately 0.050 inch salient of the rig frontplate when installed. This was later decreased to bring the protrusion below the point that would cause it to be the first point to rub if running clearance decreased to the minimum. This decrease in protrusion left the center conductor approximately 0.022 inch salient of the frontplate. This change decreased the stray capacitance to the point that the self-resonant frequency of the sensor assembly was raised to 10.5 MHz: well within the operating range of electronics.

3) The annular space between the adapter body and its center conductor was packed with an hydrous magnesium oxide (MgO) to within 0.2 inch of full. A thin layer of Sauereisen No. 31 cement was laid over the MgO and cured at approximately 250°F for 8 hours. The cement was trimmed away from the center conductor to further minimize stray capacitance. Chipping or grinding away the thin cement layer should permit easy disassembly with little risk of damage to the sensor proper.

Proposed Improvements

It was proposed to surround the sensor completely with a water jacket; however, the center conductor was still the most direct path of heat transfer between the diffuser passage and the sensor inductor. Any attempt to cool the center conductor would almost certainly increase the leakage capacitance.

Some improvement was possible by a redesign of the electronics. The possibility of making the reference oscillator circuit into a compensating dummy sensor was an avenue of improvement which could be explored by the system manufacturer.

System Application

Contact with 2 other companies who have had experience with probes of this type disclosed that 1 company had rejected the system as unworkable. The other company is employing a gated-beam detector system for obtaining qualitative information on rotor behavior. No attempt was being made to obtain static displacement information.

Conclusions

This application of the capacitance-type proximity-measurement system was limited mainly by its sensitivity to temperature. The possibility of holding the sensor at a constant temperature was remote. A means of introducing temperature compensation into the electronics appeared to be the only workable way to

overcome temperature sensitivity. Design of the electronics, including manufacturing and testing, to evaluate means of temperature compensation will necessitate an extensive development effort. The system was not usable in its present stage of development for the intended purpose, i.e., measurement of clearance between a high-speed rotor and its surroundings at elevated temperatures. The system is usable for observing qualitative dynamic behavior of a high-speed rotor.

2.2.2 THE EDDY-CURRENT CLEARANCE-DETECTION SYSTEM

System Description

A turbine blade-tip clearance monitor system was acquired by the contractor, on a temporary loan basis, for evaluation in the compressor test rigs.

The system arrived on 11 July 1966, and consisted of a calibration fixture, a chassis of electronics, a modified oscilloscope with calibrated bezel, cables, and two water-cooled transducers. The system operating principle was based on an eddy-current sensitive transducer. The transducer consisted of a coil of fine wire, usually wound in pancake form and mounted on the probe tip. A high-frequency current is passed through the coil, and the resultant magnetic field induces eddy currents in a nearby conducting body (in this case, the impeller blade). A. C. loading of the coil, by the secondary magnetic field created by these eddy currents, causes the coil impedance to vary, depending on the proximity of the coil to the surface under observation. The system electronics senses this impedance change and provides readout.

Previous correspondence and discussion with instrumentation personnel of another company indicated that the system had been used successfully over a measurement and temperature range similar to the contractor's requirements, but with turbine wheels with more blades and operating at lower rotational speeds than the contractor's test rigs.

System Evaluation

One of the water-cooled transducers was installed in the RF-1 test rig impeller shroud. The shroud was set up in a layout-drilling machine with the impeller mounted on an arbor and chucked in the machine spindle. The static calibration thus obtained indicated excellent linearity and repeatability. Warm air from a hair dryer was used to check the temperature sensitivity of the transducer. The heat did not affect the calibration.

The impeller and shroud were then installed in the RF-1 test rig. The results of runs in the RF-1 test rig are shown in Figures 94 and 95. A total of 18 actuated-rub-sensor probes were used during the test for comparative data. Data were taken at 30,000 rpm through 57,000 rpm. Several minutes were allowed at each speed for the hardware to stabilize thermally.

Conclusions

The eddy-current system is relatively easy to set up, holds its calibration well, and is not affected by the temperatures involved in the compressor test rigs. The eddy-current-type transducers require a large (0.75-inch-diameter) mounting hole.

The data indicate that the actuated probe is not repeatable enough for use as a calibration reference. However, the repeatability band of the eddy current probe data was ± 5 percent of the impeller-shroud clearance in the tests run. No test data were obtained at clearances below about 0.028 inch. It is felt from the data taken that the long-term system measurement uncertainty would be about ± 0.002 inch. Therefore, at clearances above 0.020 inch, the accuracy goal of 10 percent of the gap was attained.

Figure 94. Eddy-Current Clearance-Probe Data.

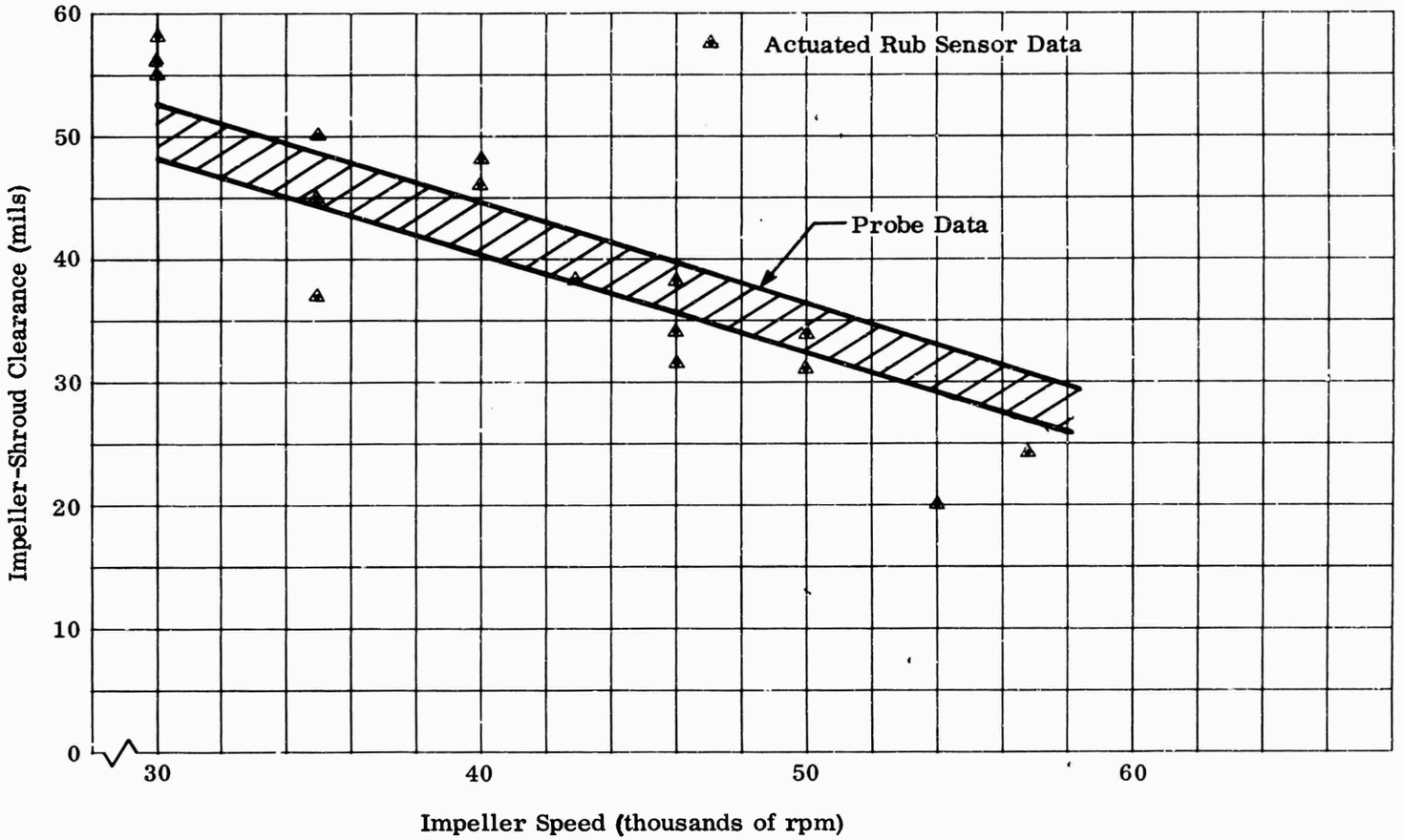


Figure 95. Actuated Rub Sensor Data and Eddy-Current Clearance-Probe Data.

3.0 MEASUREMENT OF TOTAL PRESSURE IN THE PRESENCE OF UNSTEADY FLOW

3.1 GOALS

Pressure fluctuations generated by the motion of impeller blades are superimposed on the stream total pressure in compressor diffuser passages.

A study was made to determine if true average total pressure could be measured with pitot probes and venturi-shrouded (Kiel) probes under these fluctuating conditions. Of particular interest was a determination of the performance of total-pressure-measuring systems in current test use.

3.2 RESEARCH EFFORT

Considerable information was already available; therefore, the study was confined to a literature survey and the compilation of a bibliography covering the general subject of pressure measurement in the presence of fluctuating flow.

3.2.1 FINDINGS

In general, the authors of all the entries in the bibliography, References 1 to 25 inclusive, agree that in turbulent or pulsed flow, total-pressure probes and their associated receiver and sensor systems (i.e., manometer, bourdon tubes, or transducers, along with their interconnecting tubing) will tend to give readings lying between true average and root-mean average. The difference between true average and root-mean average can be as much as 15 percent of the fluctuation pulse amplitude, depending upon wave shape.

Considering the rectangular wave of Figure 96 and the following equations, derived from Reference 14,

$$(P + P_f - P^*)^{1/2} S = (P^* - P)^{1/2} (T - S)$$

$$P + P_f - P^* = (P^* - P) \left(\frac{T - S}{S}\right)^2$$

$$P^* = P + P_f \left(\frac{(S/T)^2}{(S/T)^2 + (1 - S/T)^2}\right) \qquad (233)$$

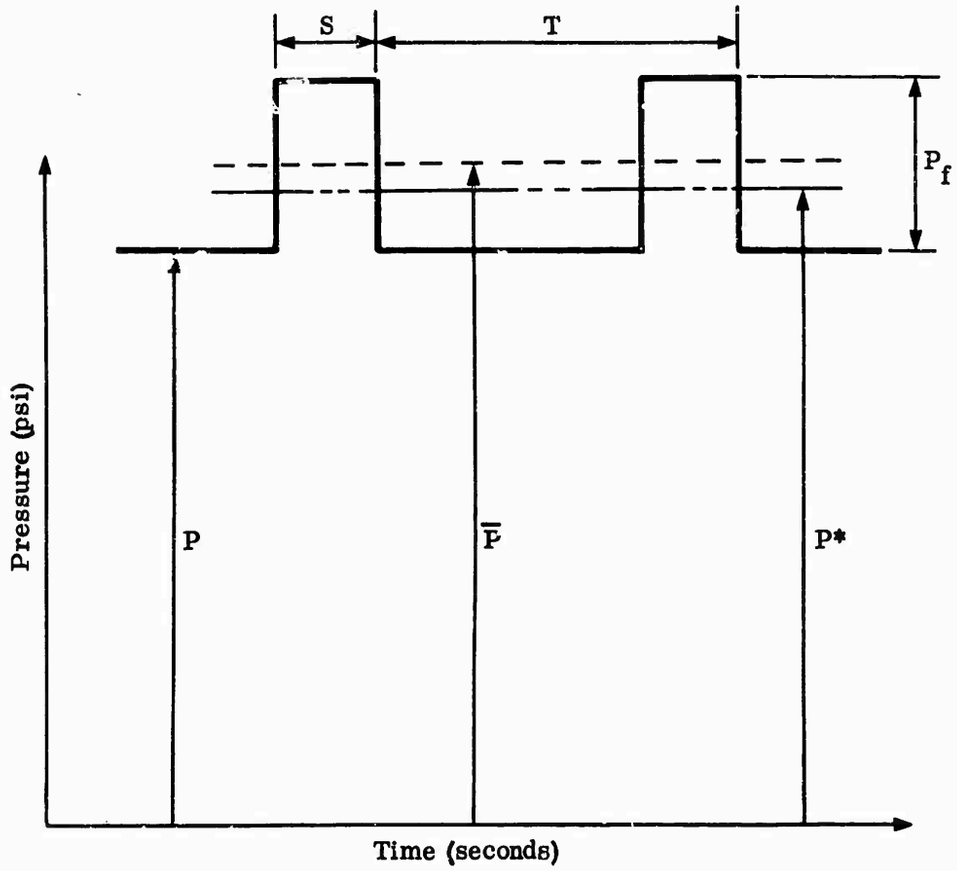


Figure 96. Rectangular-Wave Pressure Pulsation.

$$\bar{P} = \frac{P\,T + P_f\,S}{T} = P + P_f \frac{S}{T} \tag{234}$$

Combining equations 233 and 234:

$$\frac{\bar{P} - P^*}{P_f} = \frac{S}{T} - \frac{(S/T)^2}{(S/T)^2 + (1 - S/T)^2} \tag{235}$$

where:

P	=	pressure, psi
P^*	=	root-mean-square average pressure, psi
$\bar{P}$	=	true average pressure, psi
P_f	=	fluctuation pulse amplitude, psi
S	=	pulse duration period, sec
T	=	time period between pulses, sec

It is clear that the shape of the pulse, S , will affect the difference between true average and root-mean average pressures. Figure 97 shows that when the wave is truly symmetrical, i.e., when S is 50 percent of the period T , there is no difference in these average pressures. The maximum difference is 15 percent, when S is 25 percent of period T .

Reference 14 discusses 3 ways in which nonlinearity may arise and cause pressure readings to be different from true average pressures. First, unsymmetrical ends of the probe may cause unsymmetrical losses, depending on flow direction in the probe. The authors conclude that this effect is small and, further, that it can be eliminated by making the aft end of the probe tube empty abruptly into a chamber whose diameter is large compared with the probe diameter, essentially duplicating the total pressure probe tip configuration. Second, compressibility may result in higher density in the probe during inflow than outflow, or vice versa. Reference 16 reports that compressibility can account for a deviation from true average of up to 2 percent of pulsation amplitude depending upon wave form, 2 percent being a likely occurrence at low frequencies.

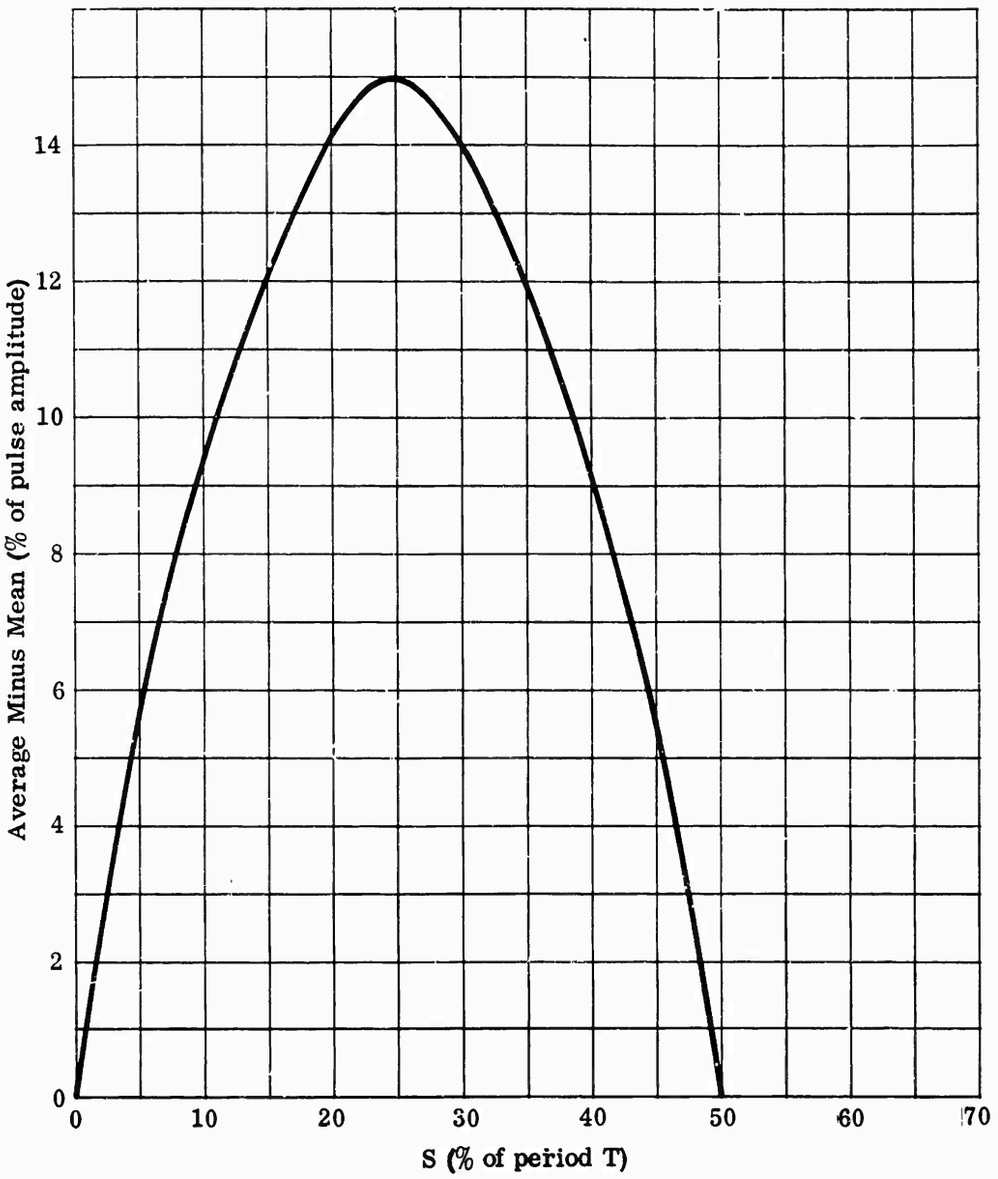


Figure 97. Effect of Pressure Pulse Shape on Root-Mean Balance Pressure.

This deviation diminishes at higher frequencies (several thousand H_z) where the flow inside the probe is very small. Third, turbulent flow in the probe can cause deviations from true average pressure up to a theoretical maximum of 15 percent of the pulse amplitude for an unsymmetrical rectangular wave.

Pertinent to the turbulent flow problem, Reference 14 discusses fluid dynamic analyses, supporting laboratory experiments, and compressor impeller-blade wake tests. Two equations were derived for relating probe dimensions to conditions which produce laminar flow in the probe hole. One equation gives the maximum permissible pressure fluctuation amplitude at low frequencies, and the other, which is reproduced below, gives the minimum permissible square-wave frequency.

$$f_m = \left[\left(\frac{P_f}{\rho L}\right)^3 \frac{\nu}{D^5} (0.317)^4\right]^{1/7} \left[S/T\,(1 - S/T)\,\frac{(S/T)^2 + (1 - S/T)^2}{(S/T)^{8/7} + (1 - S/T)^{8/7}}\right]^{4/7} \quad (236)$$

where:

D = probe internal diameter, ft

f_m = minimum permissible square-wave frequency

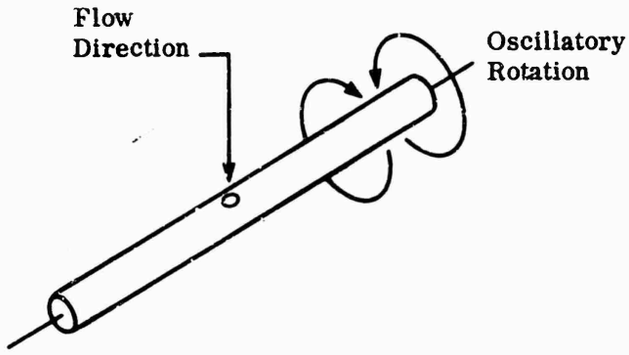
L = probe tube length, ft

ρ = mass density of fluid, lb-mass/(foot)^3

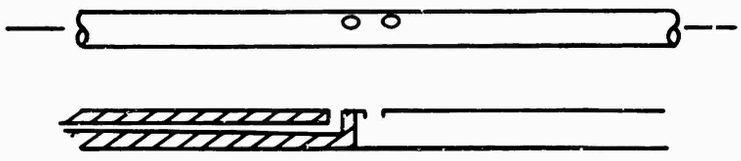
ν = kinematic viscosity, ft-sec

This equation was derived by solving simultaneously the classic textbook equation for incipient turbulent flow in a tube with an equation derived for maximum theoretical nonviscous inertial flow per pulsation cycle.

Laboratory experiments on pressure probes, as shown in Figure 98a, were subjected to a known steady flow. To simulate modulated pressure, the probe was rotated ±90 degrees at rates up to 400 Hz. Probes with various internal geometries were compared with each other.



98a. Oscillatory Probe.



98b. Stationary Probe.

Figure 98. Pressure Probes Tested.

A similar stationary probe (Figure 98b), having 2 sensing holes close together, was placed in the fluctuating airstream behind a rotating axial-flow-compressor blade row. Fluctuating frequencies of up to 3,300 Hz were thus studied. Hot-wire anemometers were used to determine instantaneous flow direction and pressure wave form.

As predicted by the equation above, pressure readings of probes were affected by probe-hole geometry. Probes with holes opening directly into a cavity gave readings which closely matched root-mean average pressure. Probes with long small-gage holes tended to give true average pressure readings. True average pressure was read when probe length, probe-hole gage, fluctuation amplitude, and fluctuation frequency were in accord with the limits set by the equation.

The equation for the minimum permissible square-wave frequency was solved with a set of conditions applicable to the contractor's compressor tests.

Rewriting Equation 235:

$$f = \left[\left(\frac{P_f}{\rho L}\right)^3 \frac{\nu}{D^5} (0.317)^4\right]^{1/7} (B) \tag{237}$$

where: B = shape factor

$$= \left[S/T\,(1 - S/T)\,\frac{[(S/T)^2 + (1 - S/T)^2]}{(S/T)^{8/7} + (1 - S/T)^{8/7}}^{4/7}\right] \tag{238}$$

Typical Test Conditions:

Assume:

Probe Length L = 0.5 foot

Probe Diameter D = 0.01 inch = 0.00083 foot

Density ρ = 0.0141 lb mass/(foot)^3

(air at 1000°R and 340 in. Hg Abs)

Kinematic Viscosity ν = 0.0000485 ft-sec

(air at 1000°R and 340 in. Hg Abs)

Pulse Ratio S/T = 0.25 (worst case per Figure 6)

Assume Pressure Amplitude P_f = 20 psi

Calculations:

Solve for f = minimum frequency for which probe will give true average readings under conditions stated

$$B = \left[S/T\,(1 - S/T)\, \frac{\left[(S/T)^2 + (1 - S/T)^2\right]^{4/7}}{(S/T)^{8/7} + (1 - S/T)^{8/7}} \right] = 0.155$$

$$f = \left\{ \left[\frac{(20)\,(144)}{(.0141)(0.50)} \right]^3 \frac{0.0000485}{(0.00083)^5}\,(0.317)^4 \right\} \times 0.155$$

f = 790 cycles/sec

The results indicate that roughly 800 Hz is the minimum frequency for which inertial effects dominate in limiting flow inside the probe. Above this frequency, flow is laminar, the condition required for obtaining true average pressure. Fluctuation frequencies caused by impeller-blade motion in the contractor's compressor tests range between 10,000 Hz and 23,000 Hz.

3.2.2 CONCLUSIONS

In pulsating flow, deviations of indicated pressure from true average pressure are caused chiefly by a combination of turbulent flow inside the probe and asymmetrical wave shape. If the pulsation frequency is high enough for a particular pulsation amplitude and set of probe dimensions, inertia prevents the air inside the probe from reaching velocities which cause turbulence. At pulsation amplitudes of 5 or 10 psi, frequencies generated in the contractor's compressor tests by motion of impeller blades are much higher than the highest frequency

which can cause turbulent flow inside currently used total-pressure probes. Although no measurements have been made by the contractor of pressure fluctuations occurring at the impeller exit, it is felt that fluctuation amplitudes of 5 to 10 psi are possible. Literature surveys indicate that mixing is quite complete within a radius ratio of 1.02 to 1.05. Therefore, fluctuation amplitudes become less significant as the pressure-probe location is moved downstream. Total-pressure probes are typically located at a radius ratio of 1.02 to 1.025 in the contractor's compressor tests.

A worst-case calculation for the contractor's tests, assuming a pressure pulsation amplitude of 20 psi, showed that typical operating frequencies were 12 to 35 times higher than the frequency at which the probe indicated that pressure would be expected to deviate from the true average pressure. Therefore, for the conditions stated, true average total pressure is obtained with current probe design.

4.0 MEASUREMENT OF TORQUE AT ROTATIONAL SPEEDS TO 60,000 RPM

Accurate means of measuring torque in engine and component research and development programs is desirable for performance evaluations. Torque measurement allows a better determination of work done than measurement of temperature differences alone. A measurement of turbodrive torque on the compressor test rigs would be useful as a cross-check on work absorbed by the compressor (usually determined by measurement of inlet and outlet temperatures).

4.1 RESEARCH EFFORT

Several methods of torque measurement were studied. Primary considerations were high accuracy, ability to operate at speeds up to 60,000 rpm, and adaptability to compressor test rigs without major rig modification.

Four of the methods studied showed promise upon initial examination. These methods were:

1) Variable Reluctance (noncontacting);

2) Electronic Vernier (noncontacting);

3) Strain Gage (contacting);

4) Optical Torquemeter (noncontacting).

4.1.1 VARIABLE RELUCTANCE (NONCONTACTING)

This method of torque measurement makes use of the Vallari effect. In a cylindrical shaft under pure torsion, the principal stress lines are 45-degree helices around the axis, 1 for tension and the other for compression. These are also the directions of maximum and opposite permeability changes for a shaft of magnetostrictive material.

Devices utilizing this effect have been built and are commercially available. These devices are accurate within ± 2 percent, if shaft runout and radial vibration are held to within acceptable limits. Radial shaft displacements measured on compressor test rigs have been as great as 0.005 inch peak-to-peak. The combined effects of a large pole piece to shaft air gap necessitated by this radial displacement and the lightly stressed shafts used in the test rigs would result in an output signal smaller than the minimum required for acceptable resolution and accuracy. Further study of the system was not warranted in view of the required rig changes.

4.1.2 ELECTRONIC VERNIER (NONCONTACTING)

This method of torque measurement uses two toothed wheels or other pulse generating devices mounted along the shaft and separated, as far as possible, within limitations of space and shaft dynamics. The 2 pulse generators produce a different number of pulses per revolution. The 2 frequencies are heterodyned and the resultant frequency is analyzed by means of servomechanism techniques. This method requires dynamic calibration. Space and shaft length limitations preclude the use of this method without major modification to the compressor test rigs.

4.1.3 STRAIN GAGE (CONTACTING)

The strain gage method is probably the most desirable method from the standpoint of accuracy and ease of calibration. Liquid-cooled sliprings of the type presently used by the contractor could be used for picking the signal off the shaft. However, the high rotational speeds involved require the use of a hollow shaft with the strain gages mounted on the inner surface. For satisfactory signal strength, the shaft would have to be highly stressed under operating conditions. To be usable over a moderately wide range of speed and load conditions, the shaft would have a low safety factor at maximum load. In addition, some loss in axial stiffness could be expected. This method also was considered unsatisfactory, since major rig modification would be necessary.

4.1.4 OPTICAL TORQUEMETER (NONCONTACTING)

An optical torquemeter was under development prior to the establishment of this research program. The system consisted of a torque shaft with a system of optics and associated servomechanisms to provide readout of torsional displacement. The principal factors that motivated the prototype design and development were the projected accuracy and ability to calibrate the system statically.

In mid-1966, it was considered inadvisable to continue evaluation and development of the optical torquemeter. The torque shaft and coupling showed intolerable hysteresis (0.7 to 5 percent). In addition, the design configuration initially was intended for use in measuring turbine-power output and was not adaptable to the compressor test rigs. The principle, however, showed promise. Further development of this system could lead to a satisfactory high-speed, noncontacting-type, torque-measuring device.

4.2 CONCLUSIONS

Of the 4 methods investigated, only the variable reluctance method appeared usable, but only with major compressor test-rig modifications. This method required a shaft operating highly stressed and with very small radial displacement. The shafts used in compressor test rigs did not meet these requirements.

5.0 ACCURATE MEASUREMENT OF TOTAL TEMPERATURE IN COMPRESSOR DIFFUSER PASSAGES

Due to the small (0.25 inch) width of the diffuser passage in the compressor test rigs, probes installed to measure diffuser gas temperature were very small. In addition, probe immersion was low enough that conduction errors could be expected. It was felt that a check on probe temperature recovery was necessary, since the probes were smaller than previously reported upon in the literature and since individual probes differed somewhat due to the difficulty of fabricating and assembling small pieces.

5.1 RESEARCH EFFORT

To validate the accuracy in total-temperature measurements, the possible sources of probe error were investigated:

1) Uncertainty of probe total-temperature recovery;

2) Conduction errors due to the short immersion lengths made necessary by rig hardware;

3) Radiation errors;

4) Thermocouple wire calibration.

5.1.1 PROBE RECOVERY

A test facility (Figure 99) was fabricated for the determination of total-temperature-probe recovery ratio. The facility consisted of a supersonic duct with test stations located along its length. A controlled flow of compressed air was supplied through a heat exchanger to the test section. Calibration was accomplished by insertion of the probe under test into one of the various test stations along the length of the duct. Airflow was established; Mach number was determined from pressure data, and probe indicated temperature was measured. This procedure was repeated as the probe was inserted in each of the nine test stations along the duct. Reference air total temperature was measured in a plenum upstream of the duct. From these data, temperature recovery versus Mach number characteristics of a particular probe were established. The duct was capable of calibration over the range of Mach 0.2 to 1.35 at temperatures from ambient to 700°F.

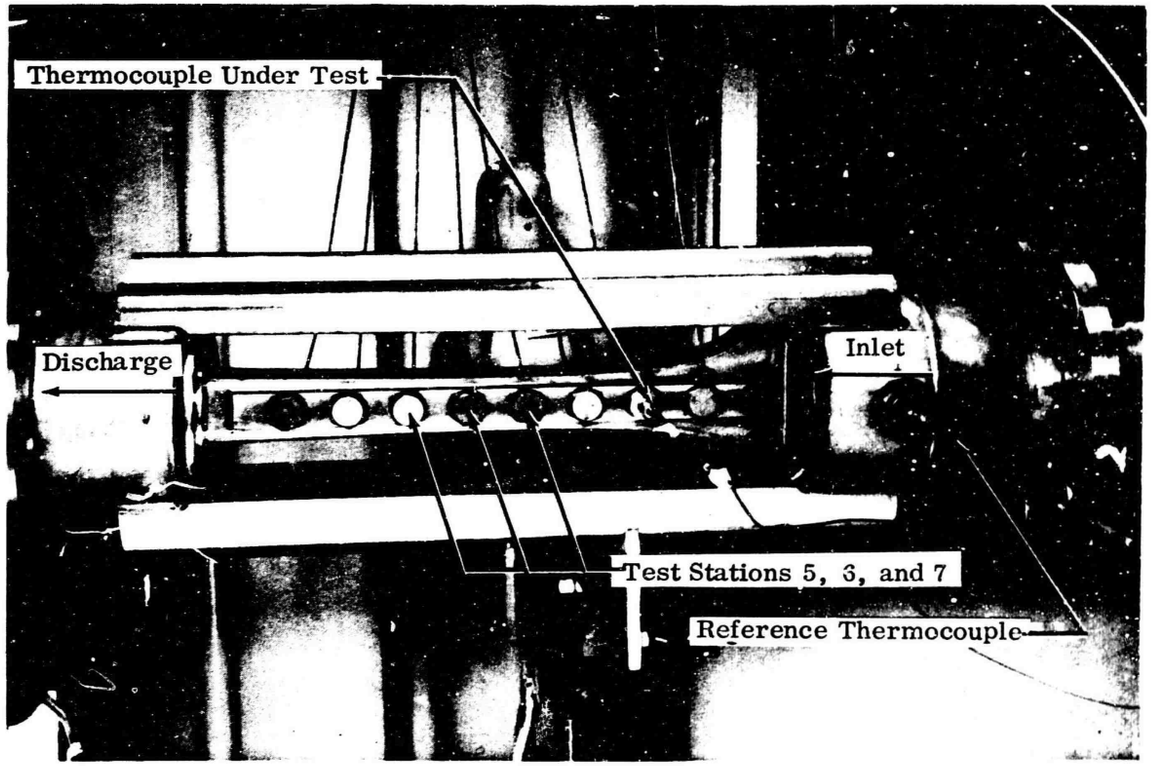


Figure 99. Supersonic Duct (Temperature-Recovery Calibration Facility).

The duct was checked with a 24-gage bare-wire thermocouple probe built per Reference 26 (Figure 100a). The test results compared favorably with data reported in Reference 26 up to Mach 0.9. A scatter of 1 percent recovery-ratio data was noted in the Mach 1.0 to 1.35 range (Figure 100b).

Three of the slotted-shield total-temperature probes (Figure 101), typical of those used in the compressor development program, were calibrated in the duct. Test results (Figure 102) indicate that the true recovery ratio agreed within ± 1/4 percent with the assumed ratio (0.995) used in previous data reduction. This uncertainty in recovery ratio is equivalent to a ± 2.3°F uncertainty in total temperature at 700°F. The variation in probe recovery ratio as a function of pitch angle is also shown in Figure 102.

Several of the miniature (0.032 inch in diameter) total-temperature probes were calibrated (Figure 103). A probe of this type was used to measure temperature profile in the diffuser passage. In the Mach number range of 1.0 to 1.35, a maximum uncertainty in recovery ratio equivalent to 4.1°F at 700°F was obtained. Due to the extremely small size of this type probe, construction tolerances contributed to the scatter in recovery data.

5.1.2 CONDUCTION ERRORS

Several methods have been devised and used in the compressor development program to minimize conduction errors in gas temperature measurements. Testing done by the contractor indicated that a minimum insertion of 25 times the thermocouple probe outside diameter was desirable in order to reduce the conduction error to 2 percent of the difference between gas temperature and probe base (wall) temperature at Mach 0.25 and less. As gas velocity increases, immersion requirements become less (Reference 27).

When space was available, immersion of 25 diameters was accomplished with no problems. In the diffuser passage, however, a thermocouple probe mounting tower (Figure 104) was devised such that the effective exposure to gas temperature met the required minimum.

5.1.3 RADIATION ERRORS

A literature study indicated that with the hardware and the temperatures involved in the compressor program, radiation errors were not significant. A bare-wire probe in the collector would have a radiation error of only about 3°F if the gas and wall temperatures differed by 100°F (Reference 28), which is unlikely. The

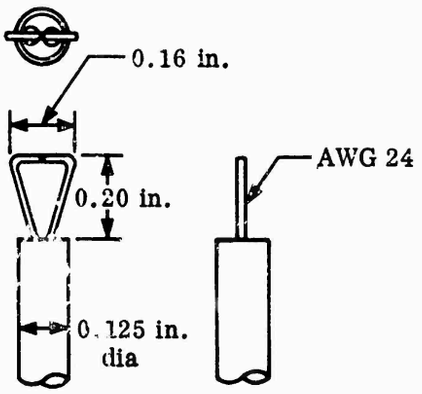


Figure 100a. Thermocouple Probe Built (per Reference 26).

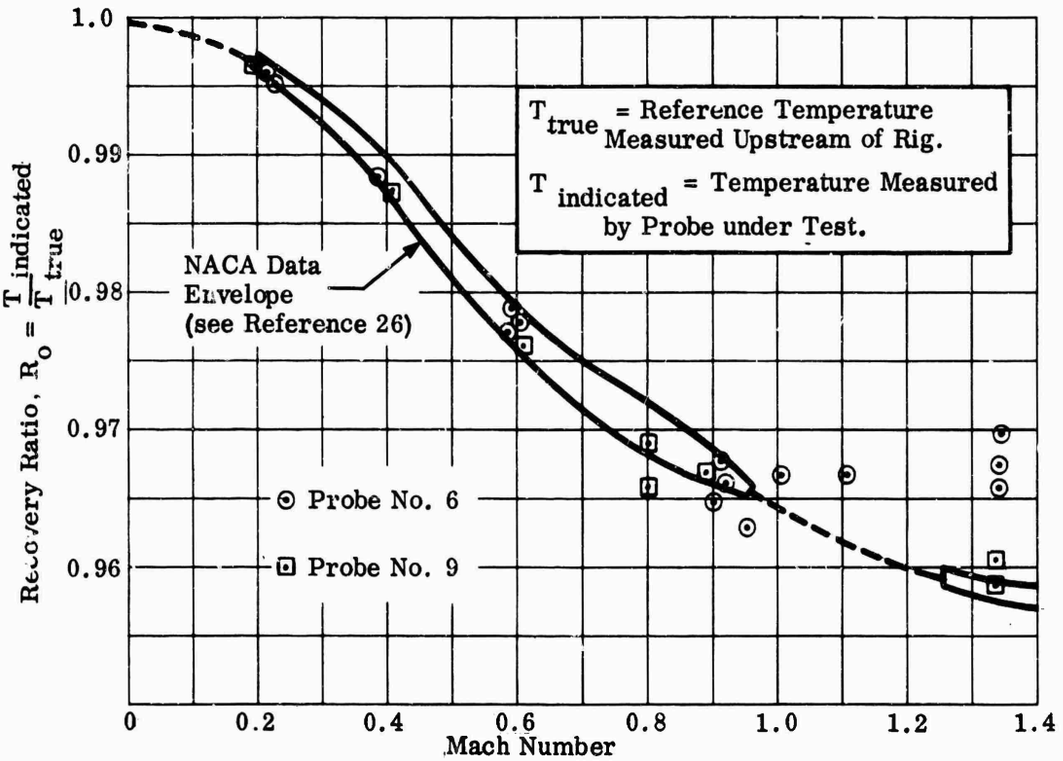


Figure 100b. Temperature Recoveries.

Figure 100. Temperature Recovery Data.

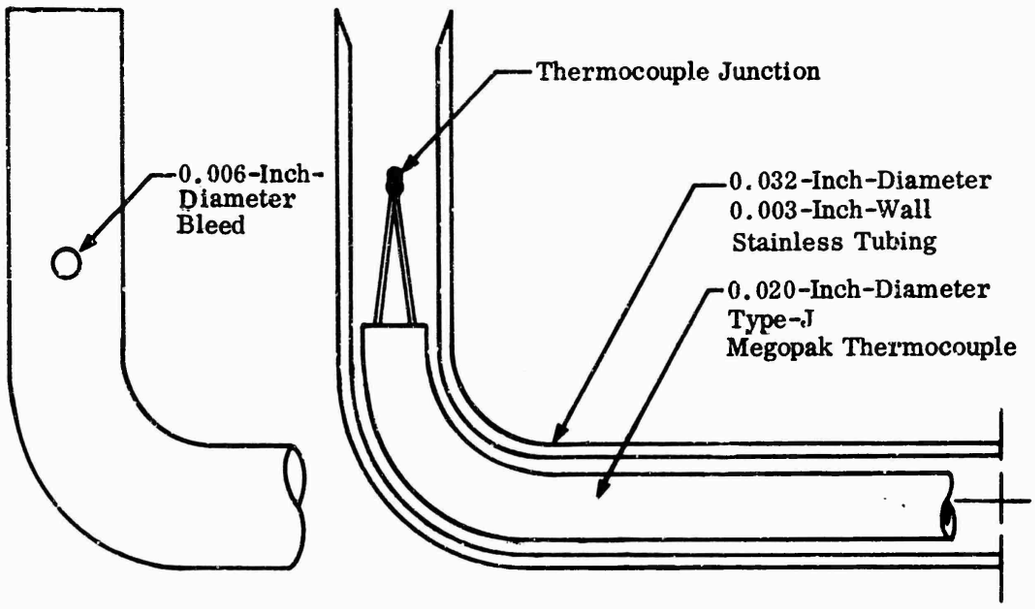


Figure 101a. Miniature Total-Temperature Probe.

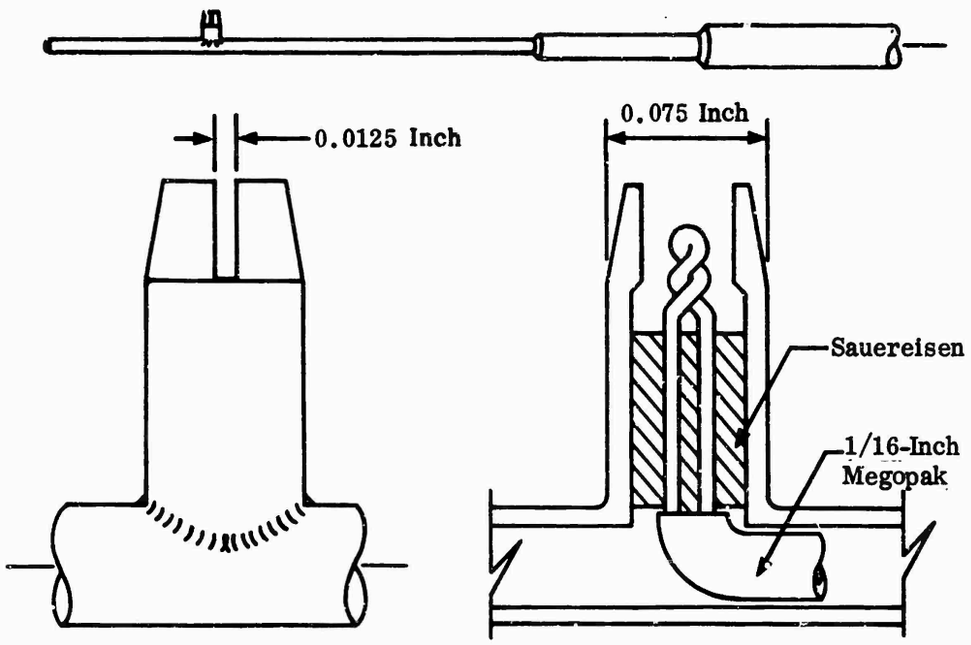


Figure 101b. Slotted-Shield Probe.

Figure 101. Temperature Probes.

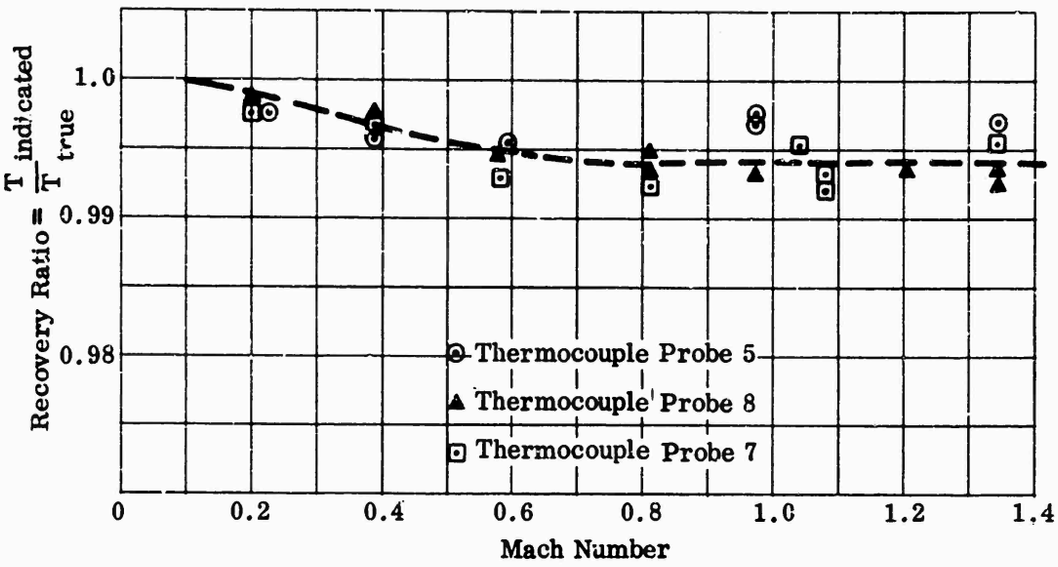


Figure 102a. Temperature-Recovery Ratio Versus Mach Number.

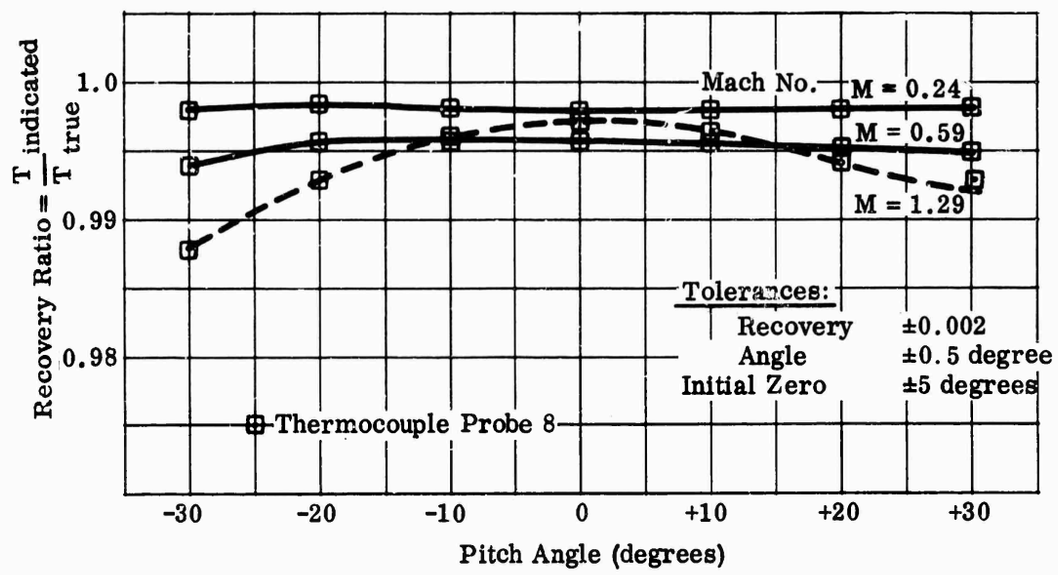


Figure 102b. Temperature-Recovery Ratio Versus Pitch Angle.

Figure 102. Slotted-Shield Total-Temperature-Probe Data.

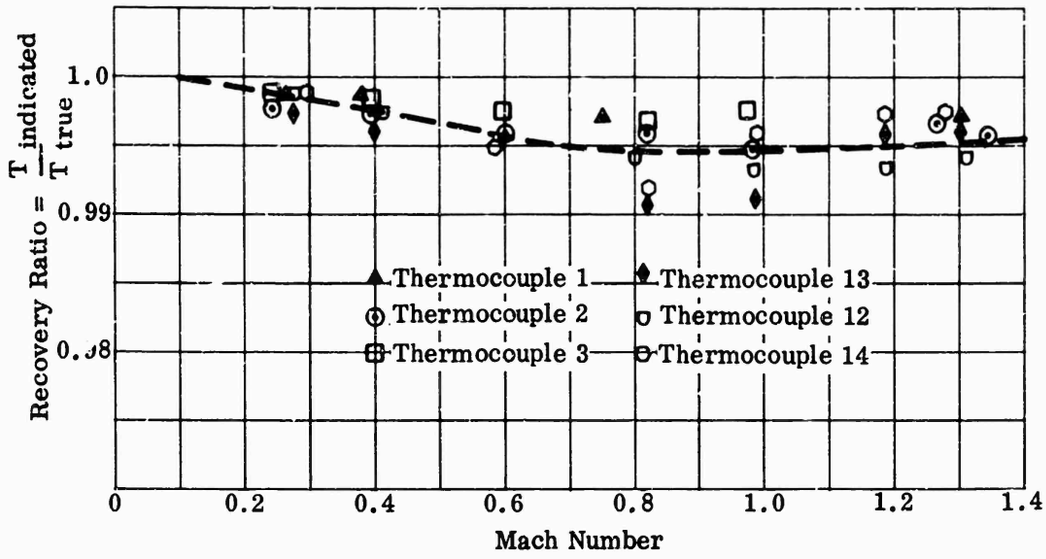


Figure 103a. Temperature-Recovery Ratio Versus Mach Number.

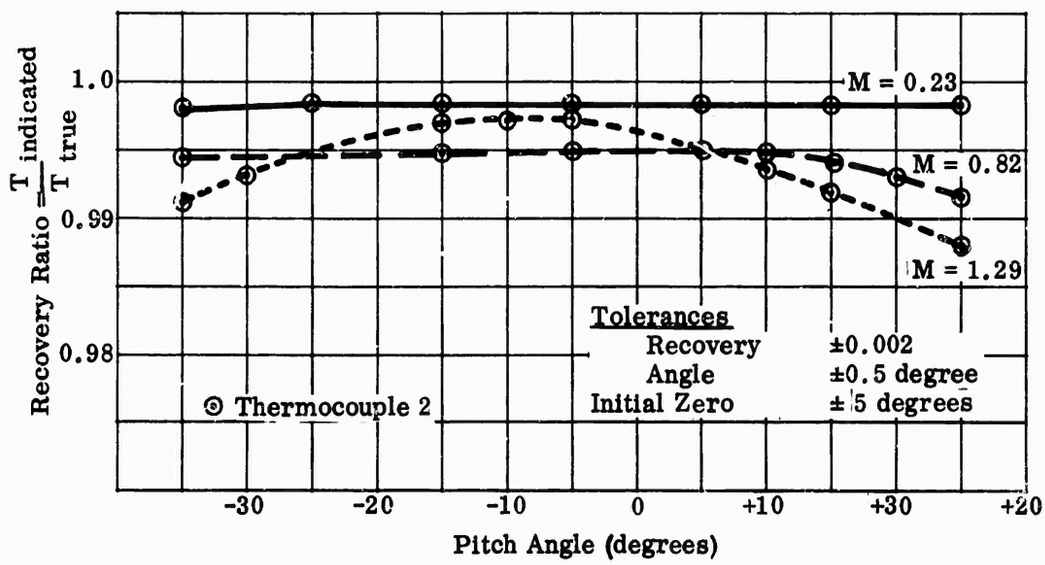


Figure 103b. Temperature-Recovery Ratio Versus Pitch Angle.

Figure 103. Miniature Total-Temperature-Probe Data.

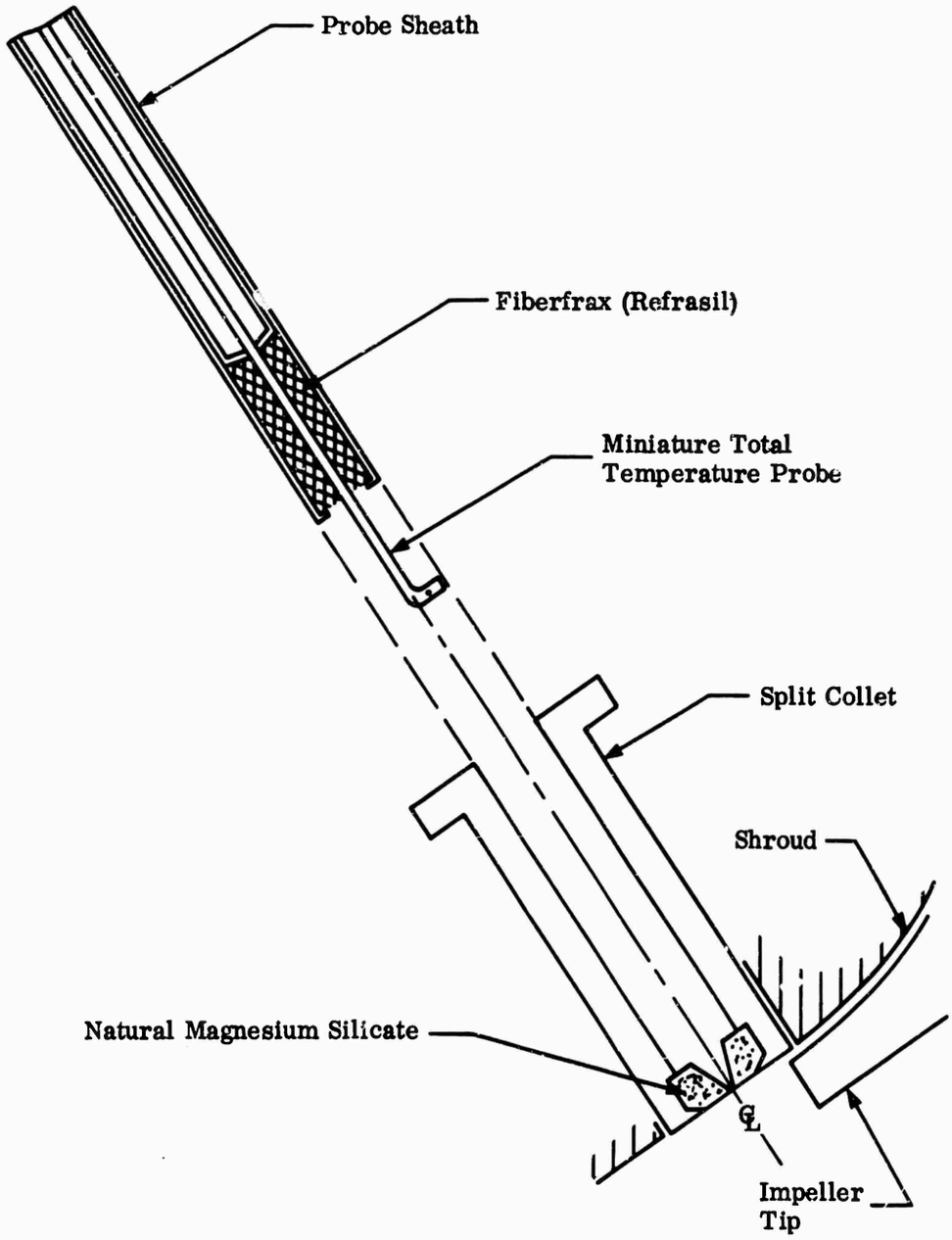


Figure 104. Total-Temperature-Probe Mounting Tower.

total-temperature probes used had 1 shield which reduced the radiation error by approximately two-thirds (Reference 29).

5.1.4 THERMOCOUPLE WIRE CALIBRATION

All thermocouple probes were fabricated from premium grade iron-constantan type-J wire. In addition, thermocouple probes used in test work were calibrated by the Pyrometrics Laboratory of the contractor. Calibration error, at or near observed points, was quoted as ± 0.5°F over the temperature range of 500° to 700°F.

5.2 CONCLUSIONS

Utilizing the slotted-shield total-temperature probes, a measurement uncertainty of ± 3.5°F was determined for the diffuser passage, provided that conduction errors were minimized.

The miniature total-temperature probes were very difficult to fabricate due to small size of the pieces of material involved. In addition, the probes tested showed a greater spread in recovery data than the slotted-shield type, and an overall measurement uncertainty of ± 5.5°F was determined.

A study of the data taken indicated that a probe can be designed that has a nearly constant recovery ratio over the flow range involved in diffuser passages. Design would involve an increase in the thermocouple junction length exposed to the gas. The data indicated that a short, stubby junction effects a dip in the recovery ratio between Mach 0.6 and 1.0. Probe numbers 1, 2, and 3 (Figure 103) were built with long thermocouple junctions. Probes 13 and 14 had very short, stubby junctions. Probe 12 had a medium length junction. It can be seen from the recovery data, Figure 103, that probes 1, 2, and 3 had a more constant recovery factor as the Mach number changed than probes 12, 13, and 14.

(U) REFERENCES

1. Bailey, N. P., Pulsating Air Velocity Measurement, Transactions of the ASME, May 1939.

2. Bietler, S. R., The Effect of Pulsations on Orifice Meters, Transactions of the ASME, May 1939.

3. Bietler, S. R., Lindahl, E. J., and McNichols, Developments in the Measuring of Pulsating Flows with Inferential-Heat Meters, Transactions of the ASME, May 1943.

4. Bruer, L. J. F., and DeHann, R. E., "Total-Head Measurements in Fluctuating Flows", Journal of Applied Mathematics and Physics (ZAMP), Vol. IXb (1958, p. 162).

5. Corcos, G. M., Pressure Measurements in Unsteady Flows, ASME Symposium on Measurement in Unsteady Flow, Worcester, Massachusetts, May 1962, T15-19-1962, pp. 15-21.

6. Corcos, G. M., Pressure Measurements in Unsteady Flows, University of California, Institute of Engineering Research, Report Series No. 183, Issue No. 1 (Jan. 1962).

7. Delio, G. J., Schwent, G. V., and Cesaro, R. S., Transient Behavior of Lumped Constants System for Sensing Gas Pressures, NACA TN 1988, 1949.

8. Earles, S. W., and Zarek, J. M., Use of Sharpe-Edged Orifices for Metering Pulsating Flow, Institute of Mechanical Engineers, Proceedings, Vol. 177, No. 37, 1963, pp. 997-1024.

9. Goldstein, S., A Note on the Measurement of Total Head and Static Pressure in a Turbulent Stream, Proceedings of the Royal Society of London, Series A, Vol. 155, No. 886 (July 1936), pp. 570-575.

10. Hubbard, P. G., Interpretation of Data and Response of Probes in Unsteady Flow, ASME Symposium on Measurement of Unsteady Flow, Worcester, Massachusetts, May 21-23, 1962, pp. 3-8, T15-19-1962.

11. Iberall, A. S., Attenuation of Oscillatory Pressures in Instrument Lines, National Bureau of Standards Research Paper RP2115, Vol. 45, 1950.

12. Johnson, R. C., Averaging of Periodic Pressure Pulsations by a Total-Pressure Probe, NACA TN 3568, Lewis Flight Propulsion Laboratory, Cleveland, Ohio, October 1955.

13. Kastner, L. J., and Williams, T. J., Pulsating Flow Measurement by Viscous Meters, with Particular Reference to the Air Supply of Internal-Combustion Engines, Proceedings of the Institute of Mechanical Engineers, Vol. 169, Number 26, 1955.

14. Kronauer, R. E., and Grant, H. P., Pressure Probe Response in Fluctuating Flow, Proceedings of the 2nd U. S. National Congress of Applied Mechanics, 1954.

15. Kuelte, A. M., and Dryden, H. L., Effect of Turbulence in Wind Tunnel Measurements, NACA TR 342, 1929.

16. Nesbitt, M. V., The Measurement of True Mean Pressures and Mach Numbers in Oscillatory Flow, Memo No. M. 180 British N.G.T.E., March 1953.

17. Rose, W. G., Corrections to Average Measurements in Unsteady Flow, ASME Symposium on Measurement in Unsteady Flow, Worcester, Massachusetts, May 1962, pp. 85-89, T15-19-1962.

18. Sparks, C. R., Pulsation Effects on Flow Metering of Compressible and Non-Compressible Fluids, Annual Symposium on Instrumentation for Process Industries, 17th Proceeding, 1962, pp. 42-46.

19. Strasberg, M., Measurements of the Static and Total-Head Pressures in a Turbulent Wake, Boeing Turbine Division library file No. ST 81, December 1963.

20. Taback, I., The Response of Pressure Measuring System to Oscillating Pressures, NACA TN 1819 (February 1949).

21. Ury, J. F., "Pulsation Errors of Rotameters", Israel Journal of Technology, Vol. 1., No. 1, July 1963, pp. 19-31.

22. Walshe, D. E. and Garner, H. C., Usefulness of Various Pressure Probes in Fluctuating Low-Speed Flow, Aeronautical Research Council, A.R.C. 21, 714, February 1960.

23. Weidemann, Hans, Inertia of Dynamic Pressure Arrays, NACA TM 998, July 1940.

24. Wildhack, W. A., Pressure Drop in Tubing in Aircraft Instrument Installations, NACA TN 593, February 1937.

25. Williams, T. J., Pulsation Errors in Manometer Gages, ASME paper 55-A-92, January 1955.

26. Stickney, T. M., Recovery and Time Response Characteristics of Six Thermocouple Probes in Subsonic and Supersonic Flow, NACA TN 3455, Figure 4a, July 1955.

27. Moffat, R. J., Gas Temperature Measurement, GMR-329, pp. 19-23.

28. Glawe, Simmons, and Stickney, Radiation and Recovery Corrections and Time Constants of Several Chromel-Alumel Thermocouple Probes in High-Temperature, High-Velocity Gas Streams, NACA Tech. Note 3766, p. 4.

29. Moffat, R. J., Gas Temperature Measurement, GMR-329, p. 28.

(U) APPENDIX IX

COMPUTER PRINTOUT OF DIFFUSER DATA — STATIC PRESSURES

SUMMARY

This appendix contains the static-pressure measurements on the sidewalls of the diffuser in the vaneless space, the semivaneless space, and the channels for the 8-vane-island diffuser configurations that were tested. Only the data necessary for analysis are presented.

Since this appendix supplements the data of Section 6, the line number, which locates the test point on the speed line, is given to facilitate cross referencing. Line 3 is near surge airflow and Line 7 is near maximum airflow as shown in Figure 105. The data are presented in tabular form and the location of each pressure tap with respect to the vanes is shown in Figures 106 through 114. The sketch shows the basic DI-1 configuration in all cases. The dashed lines show the surfaces that deviated from the DI-1 configuration.

The pressures given are in psia and are not corrected to a standard day. The δ correction is listed for each test on the respective computer printout. The speed given is corrected ($N/\sqrt{\theta}$) in rpm, and airflows are corrected ($Wa\sqrt{\theta}/\delta$) in pounds per second. Inlet guide vane (IGV) settings are in degrees, and throat areas are given in percent of design throat area.

Some taps were covered by the diffuser islands when vane configurations were changed. Although these measurements were recorded, and shown on the printout, their location is not shown on the figures. These pressures should be disregarded.

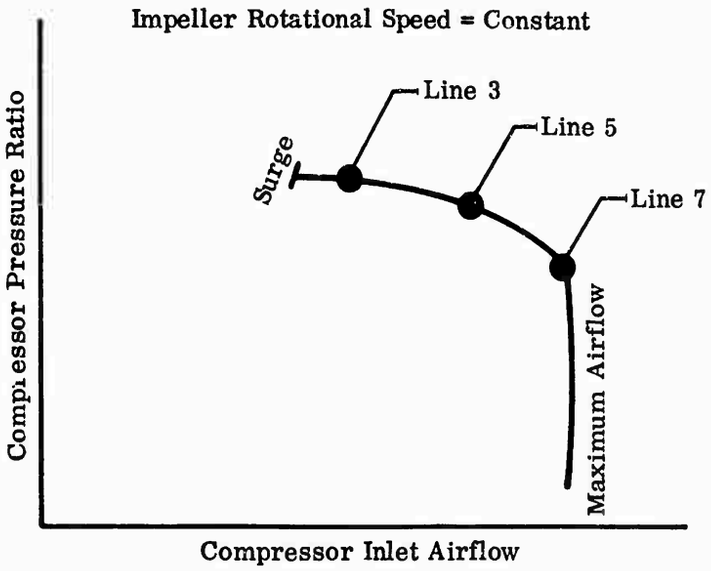


Figure 105. Test Points.

DI 1 PRESSURE SURVEY

TEST NO. 3306 F SPEED = 50000 AIR FLOW = 2.36

IGV = 0 THROAT AREA = 100% RADIUS RATIO = 1.10

LINE NO. 5 δ = 1.000

ALL PRESSURES ARE IN PSIA

TAP NO.	STATIC PRESSURE	TAP NO.	STATIC PRESSURE	TAP NO.	STATIC PRESSURE	TAP NO.	STATIC PRESSURE	TAP NO.	STATIC PRESSURE	TAP NO.	STATIC PRESSURE
1	64.1	2	65.7	3	65.1	4	70.0	5	69.0	6	69.7
7	65.6	8	69.3	9	62.0	10	67.1	11	64.5	12	70.3
13	64.9	14	63.0	15	66.6	16	71.7	17	64.9	18	70.5
19	69.8	20	74.4	21	74.2	22	71.6	23	75.2	24	71.6
25	77.5	26	71.1	27	77.1	28	71.4	29	77.9	30	68.2
31	75.5	32	64.6	33	68.9	34	65.7	35	74.2	36	69.9
37	63.0	38	76.9	39	73.2	40	68.2	41	63.2	42	64.7
43	67.2	44	63.8	45	68.4	46	67.0	47	65.7	48	61.2
49	60.4	50	78.6	51	82.5	52	60.2	53	71.7	54	58.4
55	63.9	56	70.0	57	58.2	58	61.7	59	63.8	60	93.5
62	106.2	63	112.6	64	115.5	65	94.4	66	117.2	67	118.3
68	119.1	69	118.4	70	117.7	71	117.3	72	115.9	73	114.2
74	112.7	75	112.5	77	95.4	78	71.4	79	63.3	80	62.9
81	62.3	82	53.7	83	63.9	84	23.1	85	0.0	87	68.0
88	21.4	89	0.0	90	69.1	91	69.2	92	64.8	93	69.1
94	58.2	95	65.9	96	75.1	97	86.1	98	79.2	99	74.1
100	70.9	101	66.0	102	69.8	103	63.0	104	67.7	105	55.9
106	62.2	107	64.5	108	65.0	109	34.4	110	70.9	112	68.3
113	21.9	114	34.9	115	73.7	116	75.0	117	74.5	118	77.4
119	71.1	120	76.0	121	73.6	122	79.8	123	75.6	124	81.0
125	75.2	126	80.0	127	76.2	128	78.7	129	71.8	130	76.0
132	73.7	133	67.5	134	72.9	135	66.3	136	76.8	137	72.0
139	94.8	140	94.4	141	107.2	142	107.9	144	113.5	146	106.9
147	112.7	148	115.3	149	117.1	150	118.3	151	119.0	152	119.1
153	118.2	154	116.5	155	118.1	156	116.5	157	120.2	158	120.8
159	120.8	160	120.9								

DI-1 PRESSURE SURVEY

TEST NO. 3317 SPEED = 50000 AIR FLOW = 2.37

IGV = 0 THROAT AREA = 100% RADIUS RATIO = 1.06

LINE NO. 5 δ = 0.995

ALL PRESSURES ARE IN PSIA

TAP NO.	STATIC PRESSURE	TAP NO.	STATIC PRESSURE	TAP NO.	STATIC PRESSURE	TAP NO.	STATIC PRESSURE	TAP NO.	STATIC PRESSURE	TAP NO.	STATIC PRESSURE
1	64.4	2	64.7	3	63.9	4	71.9	5	70.3	6	61.1
7	67.7	8	68.1	9	68.7	10	70.3	11	66.1	12	70.1
13	65.1	15	66.6	16	72.0	17	59.0	19	68.9	20	72.2
21	74.4	22	70.7	23	75.8	24	70.8	25	77.6	27	74.9
28	73.3	29	77.3	30	70.0	31	76.2	32	66.0	33	70.0
34	69.8	35	77.2	36	79.2	37	80.2	38	76.1	39	74.1
40	66.5	41	62.3	42	64.3	43	66.1	44	67.4	45	68.3
46	68.1	47	65.8	48	61.4	49	64.1	50	22.4	51	84.3
52	66.7	53	80.2	54	62.8	55	60.5	56	62.4	57	64.1
58	62.7	59	66.7	60	75.0	62	92.7	63	100.8	64	105.4
65	76.9	66	108.4	67	110.3	68	111.5	69	109.8	70	108.7
71	107.8	72	105.8	73	105.0	74	101.7	75	101.1	77	73.1
78	72.9	79	63.1	80	65.5	81	64.4	83	63.6	86	64.4
87	66.9	90	68.6	91	68.4	92	64.7	93	69.3	95	66.8
96	78.6	97	87.3	98	78.1	99	83.7	100	70.9	102	70.1
104	60.9	105	62.7	106	62.9	107	63.0	108	63.7	110	69.2
112	69.6	115	72.9	116	74.9	117	73.0	118	71.9	118	75.7
119	70.1	120	75.5	121	72.7	122	78.6	123	74.8	124	79.0
125	73.4	127	76.2	128	78.6	129	72.6	131	70.4	132	74.4
134	79.2	135	82.0	136	78.0	138	76.4	139	69.7	140	0.0
142	95.3	144	102.0	146	92.8	147	101.3	148	105.3	149	108.3
150	110.3	151	111.5	152	110.6	153	109.0	154	106.3	155	109.1
156	106.3	157	113.0	158	113.6	159	113.7	160	113.7		

DI-1* PRESSURE SURVEY

TEST NO. 3339 SPEED = 50000 AIR FLOW = 2.45

IGV = REMOVED THROAT AREA = 100% RADIUS RATIO = 1.06

LINE NO. 3 δ = 0.989

ALL PRESSURES ARE IN PSIA

TAP NO.	STATIC PRESSURE	TAP NO.	STATIC PRESSURE	TAP NO.	STATIC PRESSURE	TAP NO.	STATIC PRESSURE	TAP NO.	STATIC PRESSURE	TAP NO.	STATIC PRESSURE
2	67.1	3	66.6	4	91.9	5	82.4	6	54.5	7	63.8
8	69.9	9	66.3	10	71.1	11	65.4	13	66.8	15	67.5
17	61.3	19	68.9	20	72.3	21	73.3	24	73.8	25	80.1
27	80.9	28	74.5	29	81.1	31	78.8	32	66.0	33	68.9
34	83.4	35	94.8	35	86.0	36	80.6	37	81.8	38	81.0
39	79.1	40	66.9	41	61.4	42	65.6	43	68.3	44	69.1
45	71.8	46	69.5	47	68.2	48	62.9	49	70.9	50	84.8
51	92.6	52	61.3	53	82.1	54	58.2	55	65.2	56	64.9
57	63.2	58	63.9	59	63.1	60	94.8	62	109.9	63	116.5
64	119.8	65	97.6	66	121.4	68	113.6	69	122.9	70	121.8
71	121.9	72	119.7	73	119.8	74	116.3	75	116.6	77	97.8
78	77.9	84	67.9	115	0.0	118	73.0	122	94.5	127	75.0
156	0.0	157	124.6	158	125.3	159	125.4	160	125.4		

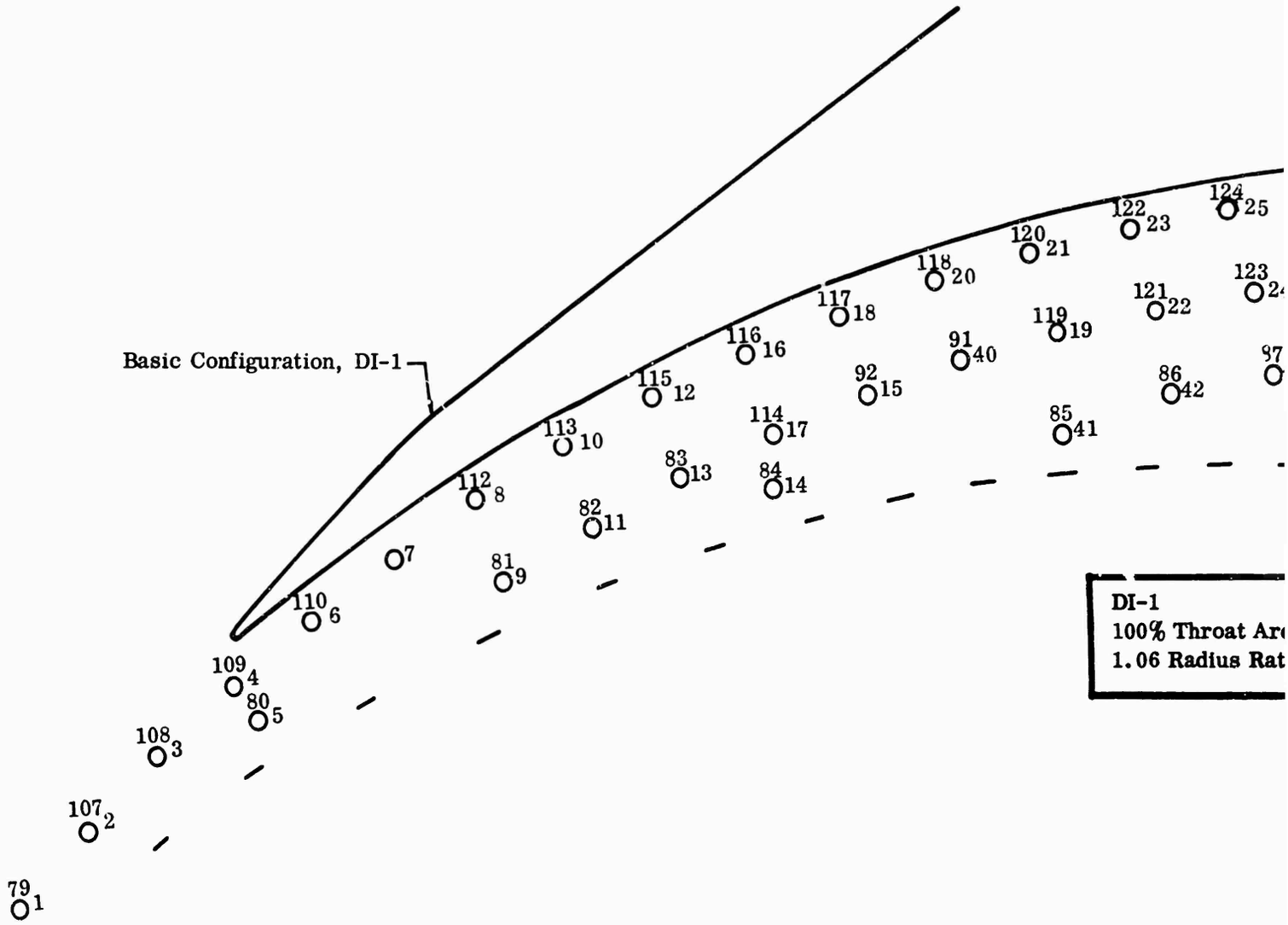
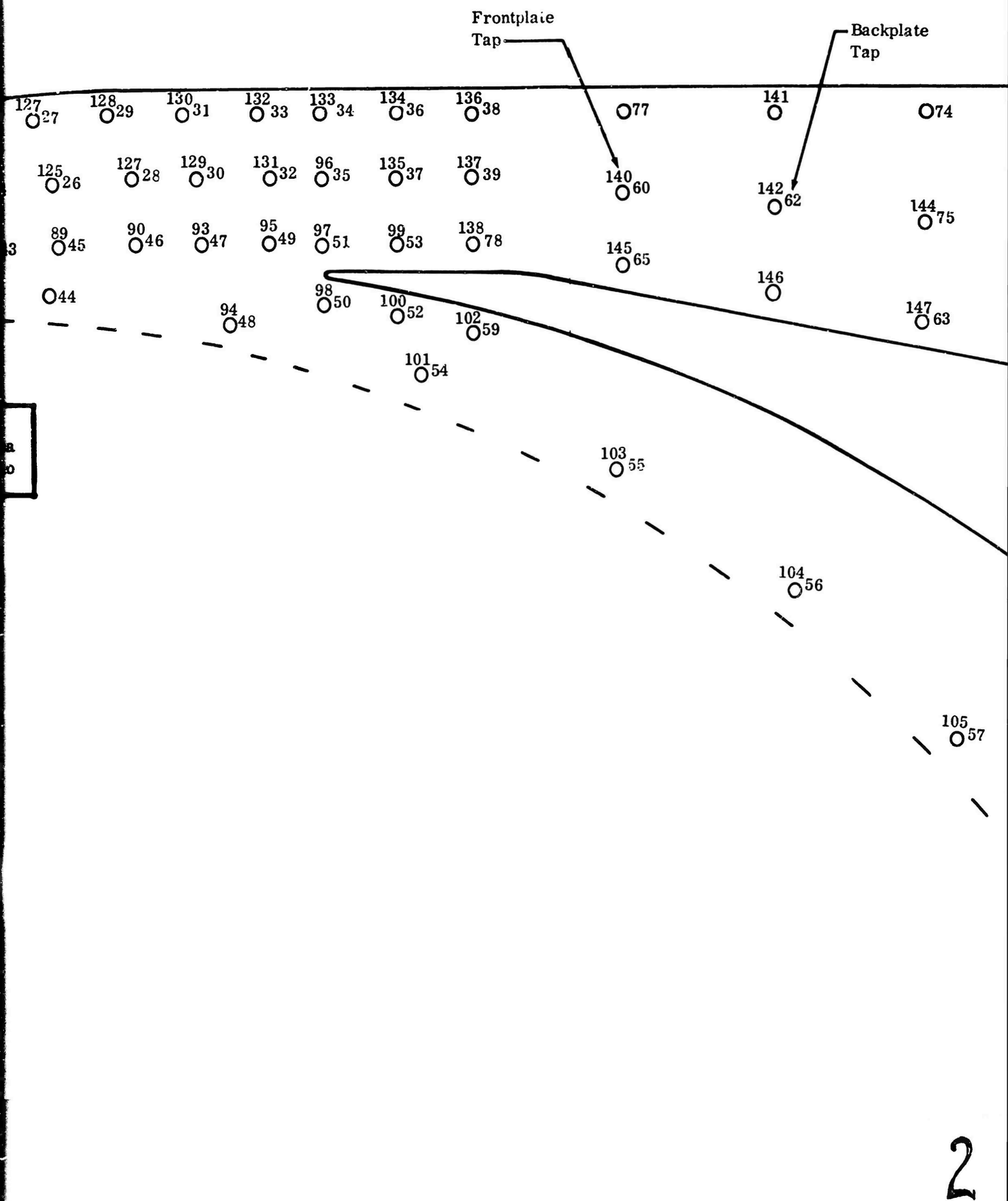
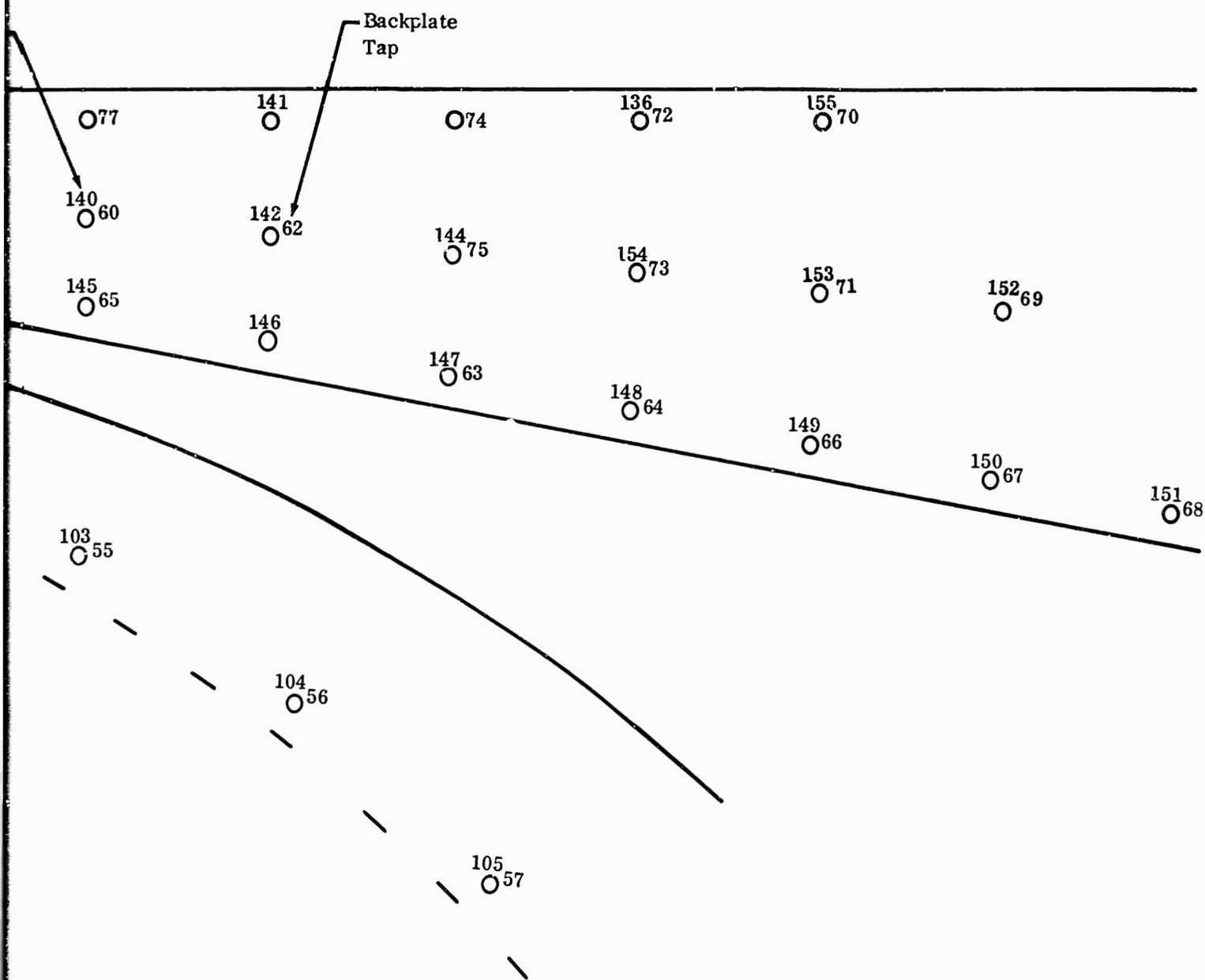


Figure 106. Diffuser Static-Pressure Instrumentation, DI-1.


Frontplate Tap
Backplate Tap
127 27
128 29
130 31
132 33
133 34
134 36
136 38
77
141
74
125 26
127 28
129 30
131 32
96 35
135 37
137 39
140 60
142 62
144 75
89 45
90 46
93 47
95 49
97 51
99 53
138 78
145 65
146
44
98 50
100 52
102 59
147 63
94 48
101 54
103 55
104 56
105 57

2


Backplate
Tap
77
141
74
136
72
155
70
140
60
142
62
144
75
154
73
153
71
152
69
145
65
146
147
63
148
64
149
66
150
67
151
68
103
55
104
56
105
57

DI 1 PRESSURE SURVEY

TEST NO. 3309 F SPEED = 50000 AIR FLOW = 2.48

IGV = 0 THROAT AREA = 100% RADIUS RATIO = 1.10

LINE NO. 3 δ = 0.998

ALL PRESSURES ARE IN PSIA

TAP NO.	STATIC PRESSURE	TAP NO.	STATIC PRESSURE	TAP NO.	STATIC PRESSURE	TAP NO.	STATIC PRESSURE	TAP NO.	STATIC PRESSURE	TAP NO.	STATIC PRESSURE
1	66.3	2	66.5	3	66.5	4	67.2	5	63.9	6	66.2
7	64.3	8	73.4	9	68.8	10	66.1	11	60.4	12	67.8
13	64.7	14	62.8	15	67.4	16	71.6	17	66.1	18	71.8
19	70.3	20	72.8	21	74.6	22	71.6	23	75.7	24	72.1
25	77.2	26	22.8	27	76.6	28	76.2	29	80.3	30	74.7
31	79.2	32	75.3	33	80.2	34	77.8	35	73.9	36	72.6
37	69.5	38	80.7	39	81.8	40	68.6	41	64.2	42	65.5
43	67.5	44	64.8	45	67.1	45	0.0	46	71.5	47	69.9
48	65.5	49	70.8	50	65.1	51	68.9	52	62.7	53	66.5
54	63.2	55	55.4	56	64.7	57	64.7	58	64.7	59	76.9
60	89.5	62	95.7	63	109.0	64	115.5	65	88.8	66	119.1
67	120.6	68	123.1	69	121.6	70	120.8	71	119.0	72	37.1
73	114.7	74	47.7	75	107.8	77	90.4	77	0.0	78	83.9
79	66.8	80	62.4	81	72.5	82	49.8	83	64.2	84	32.2
85	64.2	86	66.7	87	69.1	88	23.3	89	0.0	90	77.0
91	70.0	92	67.7	93	73.0	94	65.8	95	0.0	96	0.0
97	71.7	98	68.8	99	0.0	99	71.1	100	67.9	102	78.6
104	0.0	105	64.7	106	65.1	107	66.6	108	66.5	109	23.1
110	67.5	112	76.1	113	0.0	114	38.4	115	70.2	116	73.2
117	73.6	118	75.2	119	71.3	120	75.6	121	73.0	122	79.1
123	75.3	124	79.6	125	74.1	126	69.1	127	78.7	128	80.8
129	77.1	130	79.5	132	82.1	133	79.6	134	74.9	135	72.7
136	77.9	137	0.0	140	90.7	141	95.6	142	97.9	144	108.5
145	92.0	146	97.0	147	109.4	148	115.5	149	119.5	150	122.7
151	123.4	152	122.1	153	119.2	154	115.6	155	120.1	156	115.3
157	125.7	158	126.2	159	126.4	160	126.2				

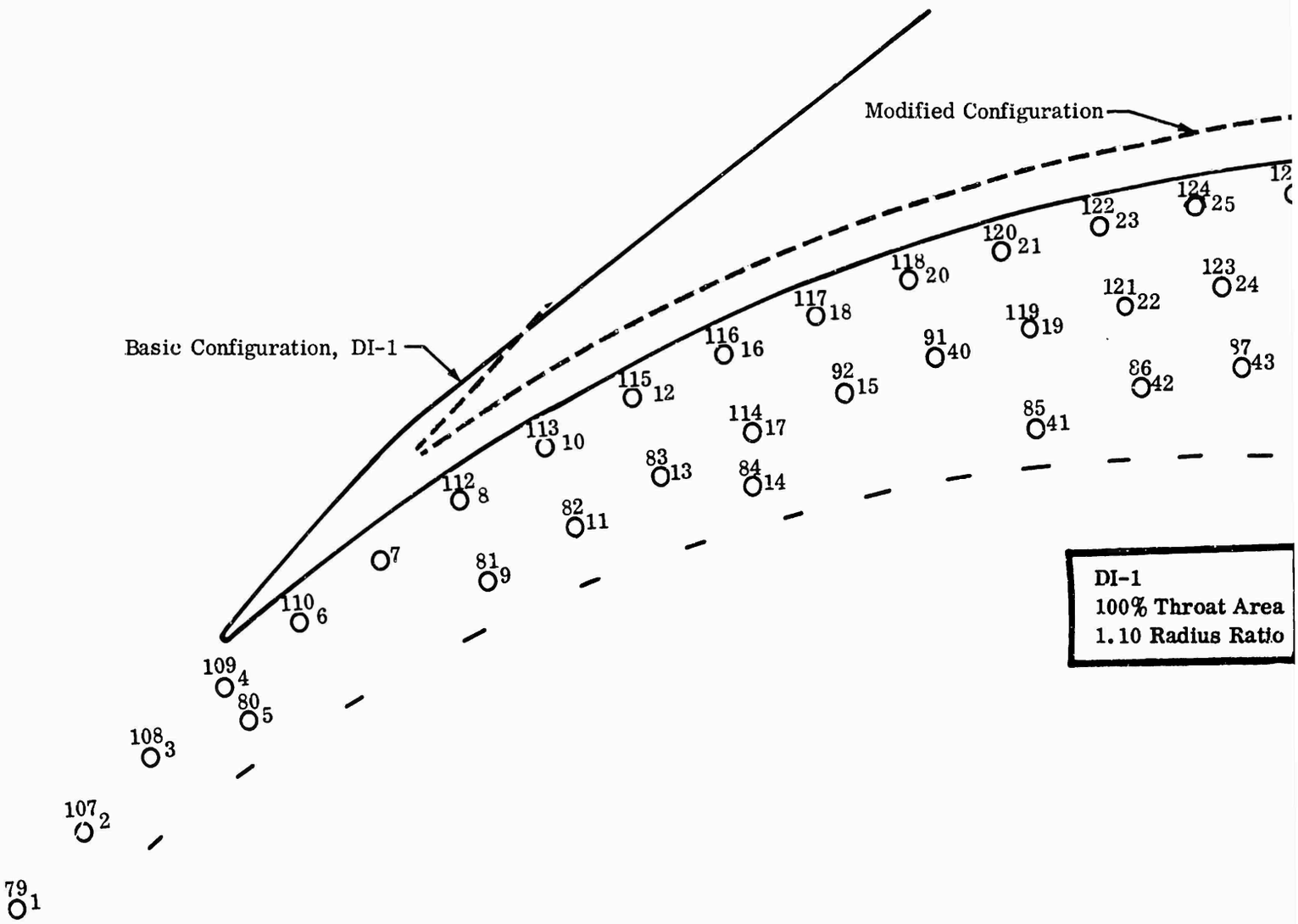
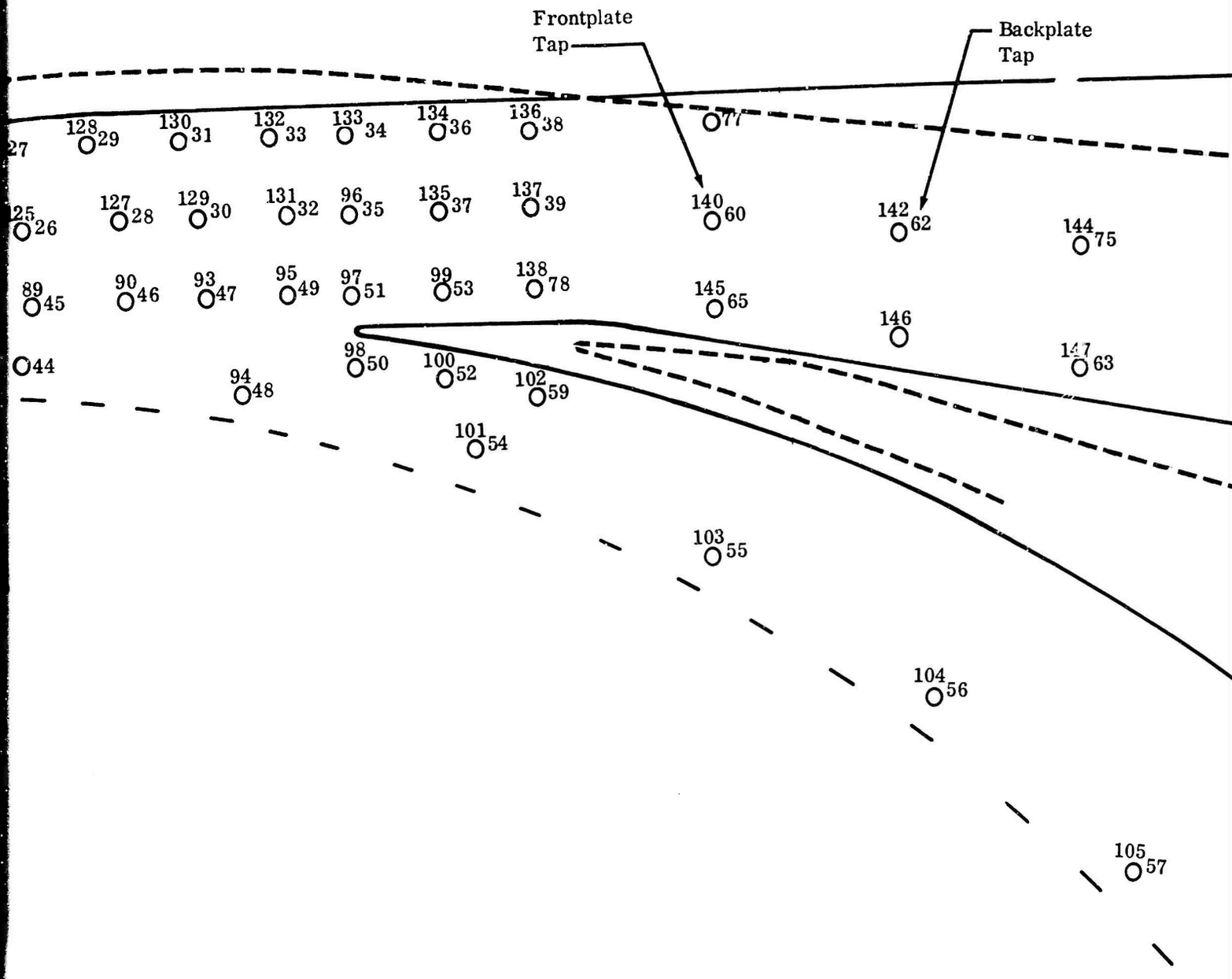
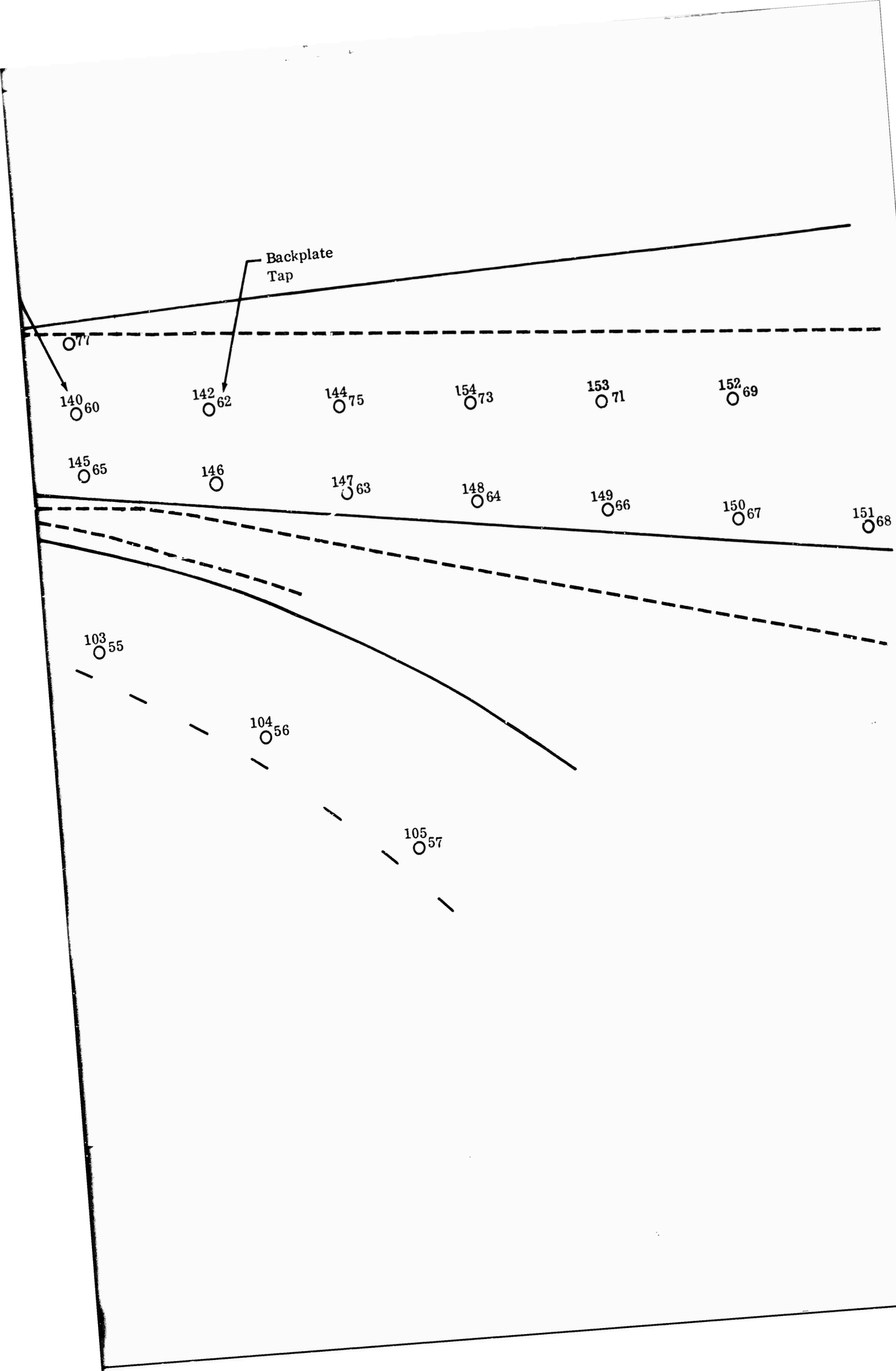


Figure 107. Diffuser Static-Pressure Instrumentation, DI-1.


Frontplate
Tap
Backplate
Tap
27
128 29
130 31
132 33
133 34
134 36
136 38
77
125 26
127 28
129 30
131 32
96 35
135 37
137 39
140 60
142 62
144 75
89 45
90 46
93 47
95 49
97 51
99 53
138 78
145 65
146
44
98 50
100 52
102 59
147 63
94 48
101 54
103 55
104 56
105 57


Backplate
Tap
77
140 60
142 62
144 75
154 73
153 71
152 69
145 65
146
147 63
148 64
149 66
150 67
151 68
103 55
104 56
105 57

DI 1 PRESSURE SURVEY

TEST NO. 3309 G SPEED = 50000 AIR FLOW = 2.48

IGV = 0 THROAT AREA = 125% RADIUS RATIO = 1.06

LINE NO. 5 δ = 1.00

ALL PRESSURES ARE IN PSIA

TAP NO.	STATIC PRESSURE	TAP NO.	STATIC PRESSURE	TAP NO.	STATIC PRESSURE	TAP NO.	STATIC PRESSURE	TAP NO.	STATIC PRESSURE	TAP NO.	STATIC PRESSURE
1	53.4	2	55.0	3	55.2	4	75.3	5	64.8	6	44.0
7	48.9	8	52.1	9	48.5	10	56.8	11	53.3	12	59.3
13	56.0	14	52.5	15	56.7	16	60.3	17	53.4	18	59.6
19	57.7	20	60.6	21	62.0	22	59.6	23	63.5	24	61.1
25	65.6	26	22.3	27	64.5	28	64.7	29	67.6	30	70.4
31	72.1	32	80.6	33	79.8	34	86.8	35	86.8	36	90.0
37	90.0	38	91.9	39	90.4	40	56.3	41	51.6	42	53.4
43	56.4	44	54.2	45	57.1	45	0.0	46	59.1	47	67.0
48	67.2	49	80.0	50	68.5	51	89.9	52	44.5	53	90.7
54	43.7	55	53.9	56	55.0	57	54.5	58	59.6	59	45.5
60	95.6	62	101.4	63	105.1	64	107.1	65	96.0	66	109.0
67	109.2	68	107.7	69	111.4	70	110.1	71	109.9	72	108.1
73	107.8	74	105.4	75	105.2	77	96.8	77	0.0	78	89.8
79	53.7	80	64.4	81	47.3	82	44.8	83	54.9	84	27.5
85	51.6	86	54.5	87	57.5	88	21.3	89	0.0	90	87.4
91	57.4	92	55.5	93	68.0	94	65.6	95	0.0	96	0.0
97	90.4	98	69.9	99	0.0	99	92.3	100	48.3	102	48.6
104	0.0	105	54.5	106	59.0	107	55.0	108	54.8	109	30.3
110	46.7	112	52.0	113	0.0	114	32.3	115	61.6	116	62.6
117	61.4	118	62.4	119	58.3	120	63.0	121	60.3	122	65.9
123	63.3	124	67.5	125	61.9	126	54.3	127	66.2	128	68.8
129	72.2	130	72.1	132	80.9	133	86.9	134	90.7	135	91.1
136	92.1	137	0.0	140	96.2	141	102.0	142	102.5	144	105.7
145	96.7	146	101.9	147	104.7	148	104.1	149	107.1	150	110.6
151	111.3	152	111.5	153	110.0	154	108.2	155	110.1	156	108.4
157	114.4	158	114.8	159	115.1	160	115.0				

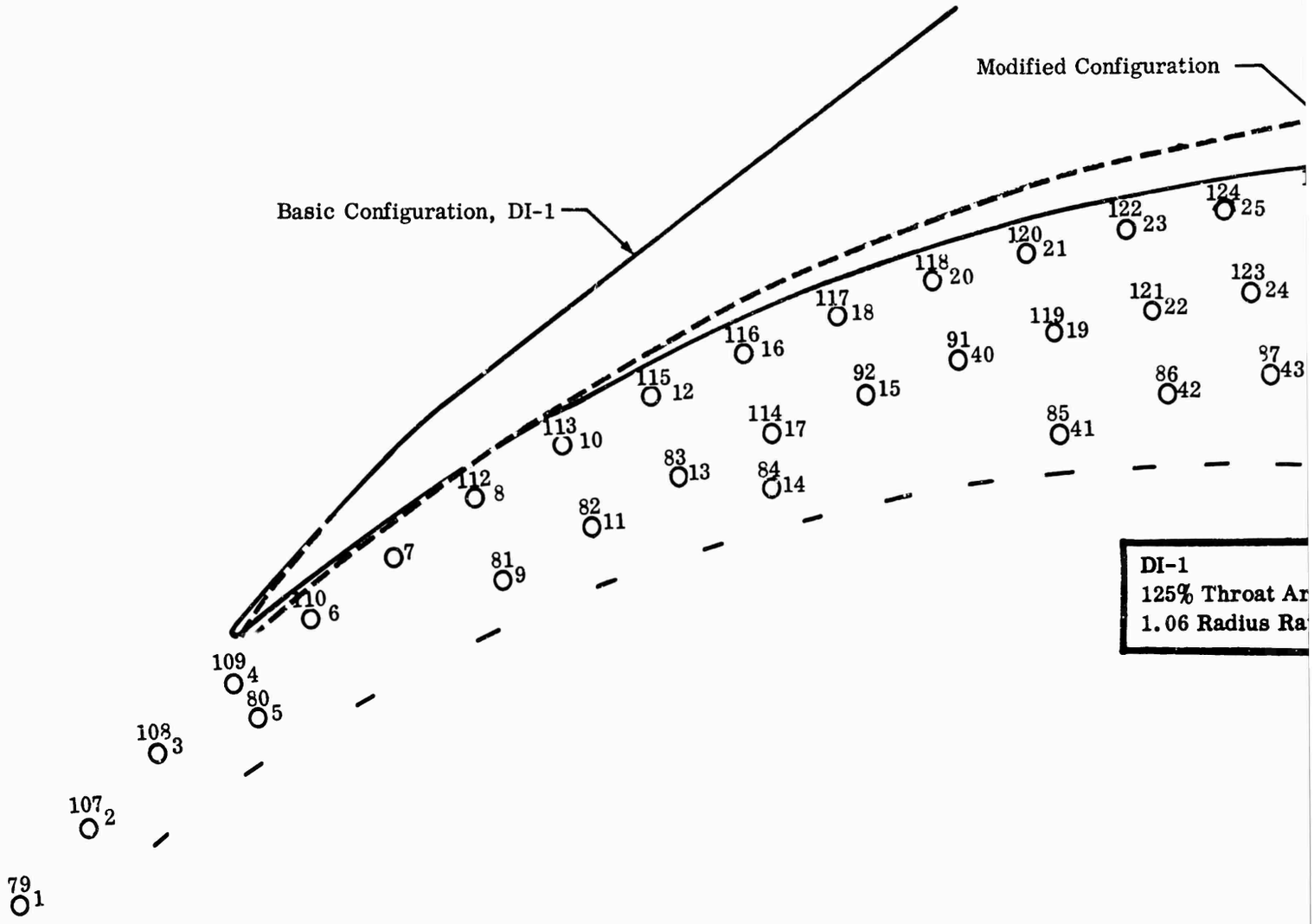
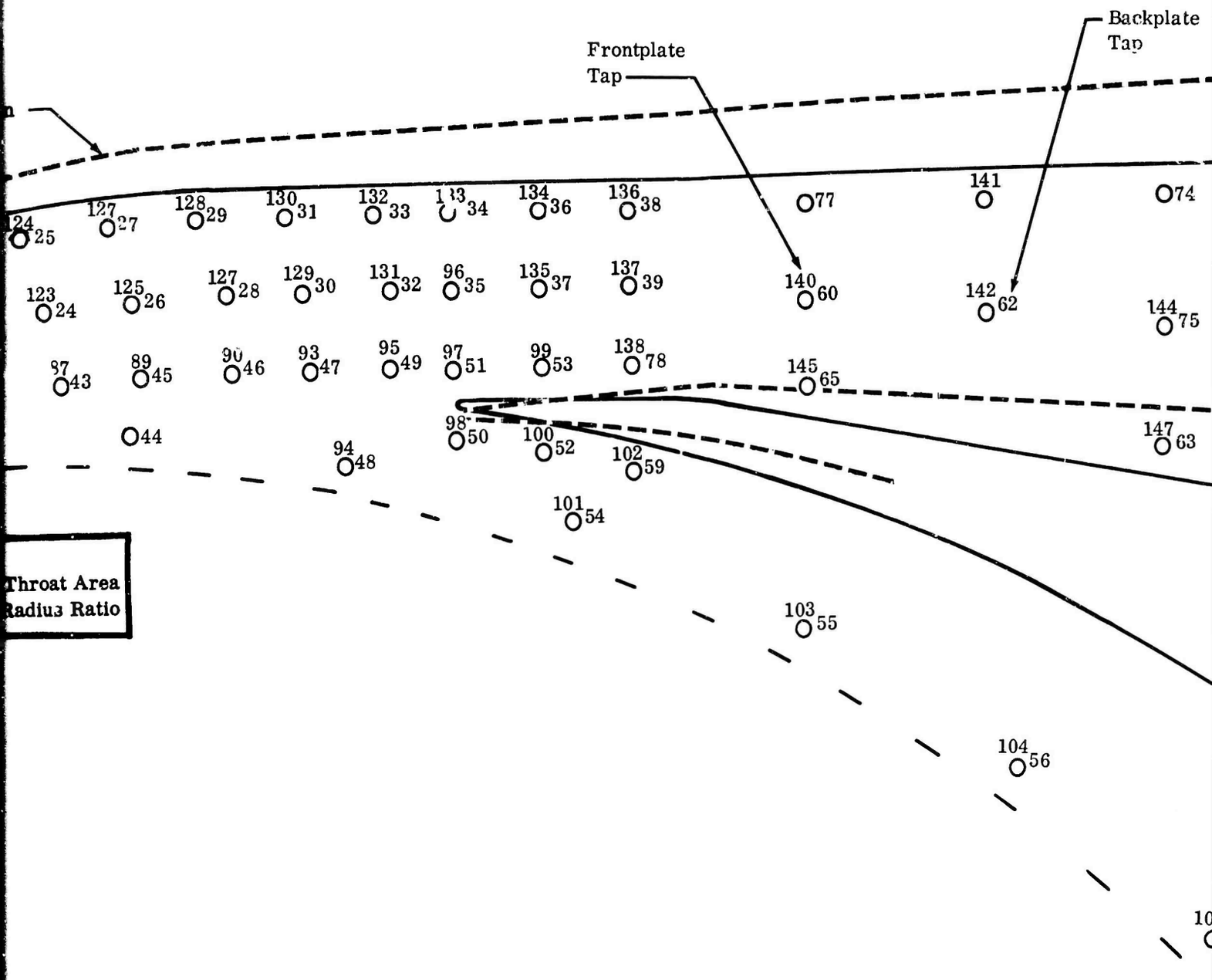
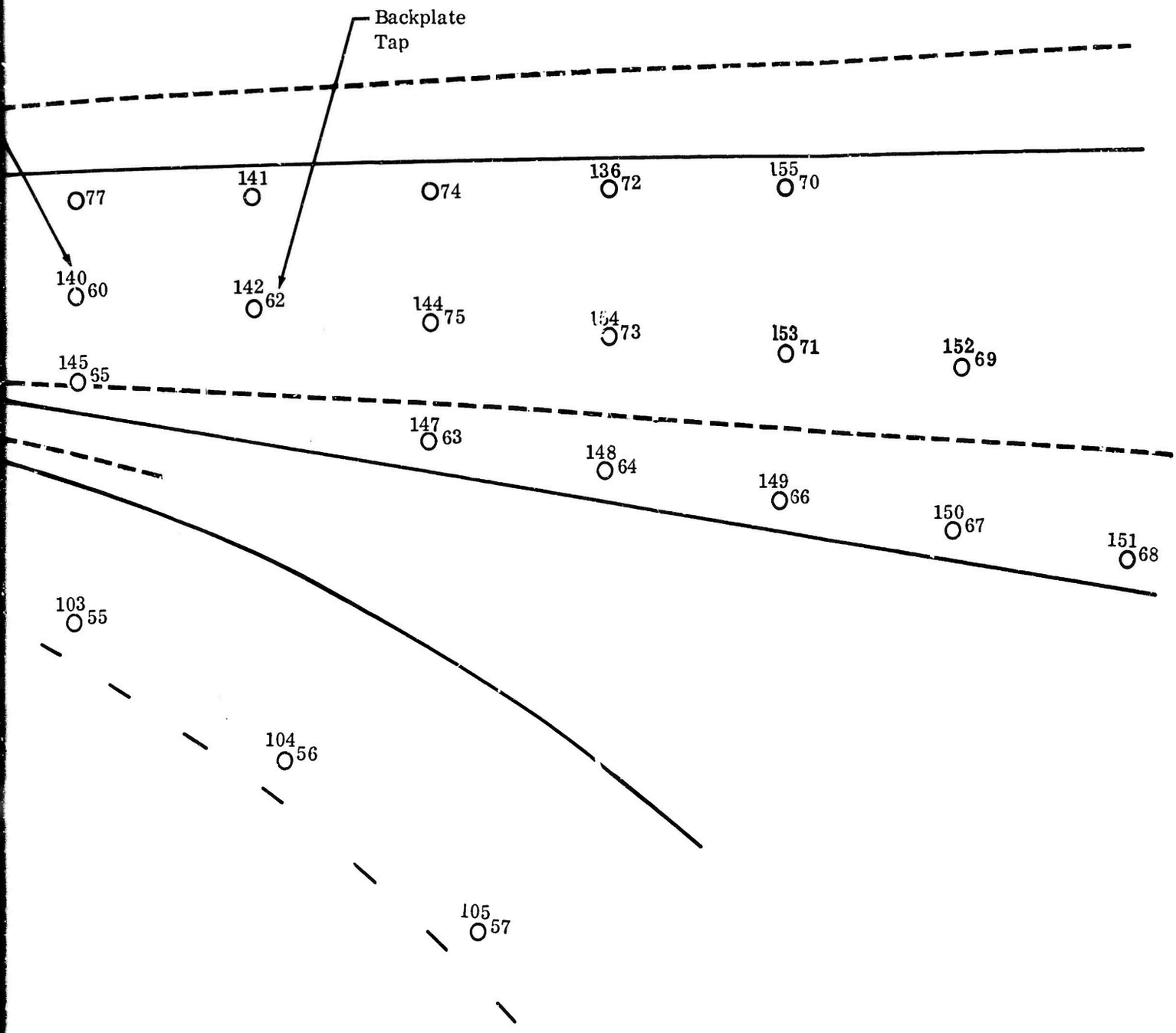


Figure 108. Diffuser Static-Pressure Instrumentation, DI-1.


Backplate
Tap
Frontplate
Tap
Throat Area
Radius Ratio


Backplate
Tap
77
141
74
136
72
155
70
140
60
142
62
144
75
154
73
153
71
152
69
145
65
147
63
148
64
149
66
150
67
151
68
103
55
104
56
105
57

DI-1-2 PRESSURE SURVEY

TEST NO. 3334 SPEED = 50000 AIR FLOW = 2.35

IGV = REMOVED THROAT AREA = 100 % RADIUS RATIO = 1.06

LINE NO. 3 δ = 0.990

ALL PRESSURES ARE IN PSIA

TAP NO.	STATIC PRESSURE	TAP NO.	STATIC PRESSURE	TAP NO.	STATIC PRESSURE	TAP NO.	STATIC PRESSURE	TAP NO.	STATIC PRESSURE	TAP NO.	STATIC PRESSURE
2	68.6	3	69.7	4	89.7	5	79.4	6	59.8	7	64.2
8	69.8	9	77.7	10	73.0	11	68.1	13	67.2	15	67.3
17	61.6	19	73.3	20	73.6	21	78.2	24	74.2	25	80.6
27	79.3	28	75.6	29	81.2	31	79.5	32	87.3	33	82.7
34	97.7	35	94.7	35	97.4	36	104.7	37	104.1	38	110.2
39	109.0	40	68.8	41	65.1	42	68.5	43	67.8	44	70.7
45	71.8	46	70.9	47	69.0	48	70.2	49	87.6	50	82.9
51	100.2	52	64.2	53	103.3	54	61.2	55	64.1	56	67.0
57	65.1	58	66.6	59	61.6	60	116.2	62	123.1	63	0.0
64	131.5	65	115.1	66	132.9	68	99.2	69	134.5	70	133.0
71	133.4	72	131.3	73	131.3	74	128.0	75	128.4	77	117.1
78	108.7	84	68.2	115	0.0	118	73.0	122	94.5	127	74.3
156	0.0	157	135.8	158	136.3	159	136.5	160	136.5		

DI-1-2 PRESSURE SURVEY

TEST NO. 3334 SPEED = 50000 AIR FLOW = 2.41

IGV = REMOVED THROAT AREA = 100 RADIUS RATIO = 1.06

LINE NO. 5 δ = 0.990

ALL PRESSURES ARE IN PSIA

TAP NO.	STATIC PRESSURE	TAP NO.	STATIC PRESSURE	TAP NO.	STATIC PRESSURE	TAP NO.	STATIC PRESSURE	TAP NO.	STATIC PRESSURE	TAP NO.	STATIC PRESSURE
2	67.7	3	67.2	4	88.1	5	79.1	6	61.4	7	65.9
8	69.2	9	77.6	10	73.3	11	68.4	13	67.4	15	67.3
17	61.5	19	72.8	20	73.3	21	77.7	24	74.1	25	80.7
27	79.3	28	75.1	29	81.1	31	79.3	32	82.2	33	76.9
34	94.9	35	94.7	35	94.6	36	102.1	37	101.2	38	108.0
39	106.8	40	68.3	41	63.5	42	68.6	43	67.6	44	70.6
45	72.0	46	70.8	47	68.9	48	66.5	49	84.7	50	83.9
51	97.1	52	66.7	53	100.4	54	62.5	55	63.8	56	67.0
57	65.1	58	65.2	59	63.0	60	114.6	62	121.8	63	0.0
64	130.6	65	113.4	66	132.0	68	112.2	69	133.5	70	132.1
71	132.5	72	130.3	73	130.4	74	127.0	75	127.3	77	115.5
78	106.5	84	68.2	115	0.0	118	73.0	122	94.4	127	74.4
156	0.0	157	135.0	158	135.5	159	135.7	160	135.7		

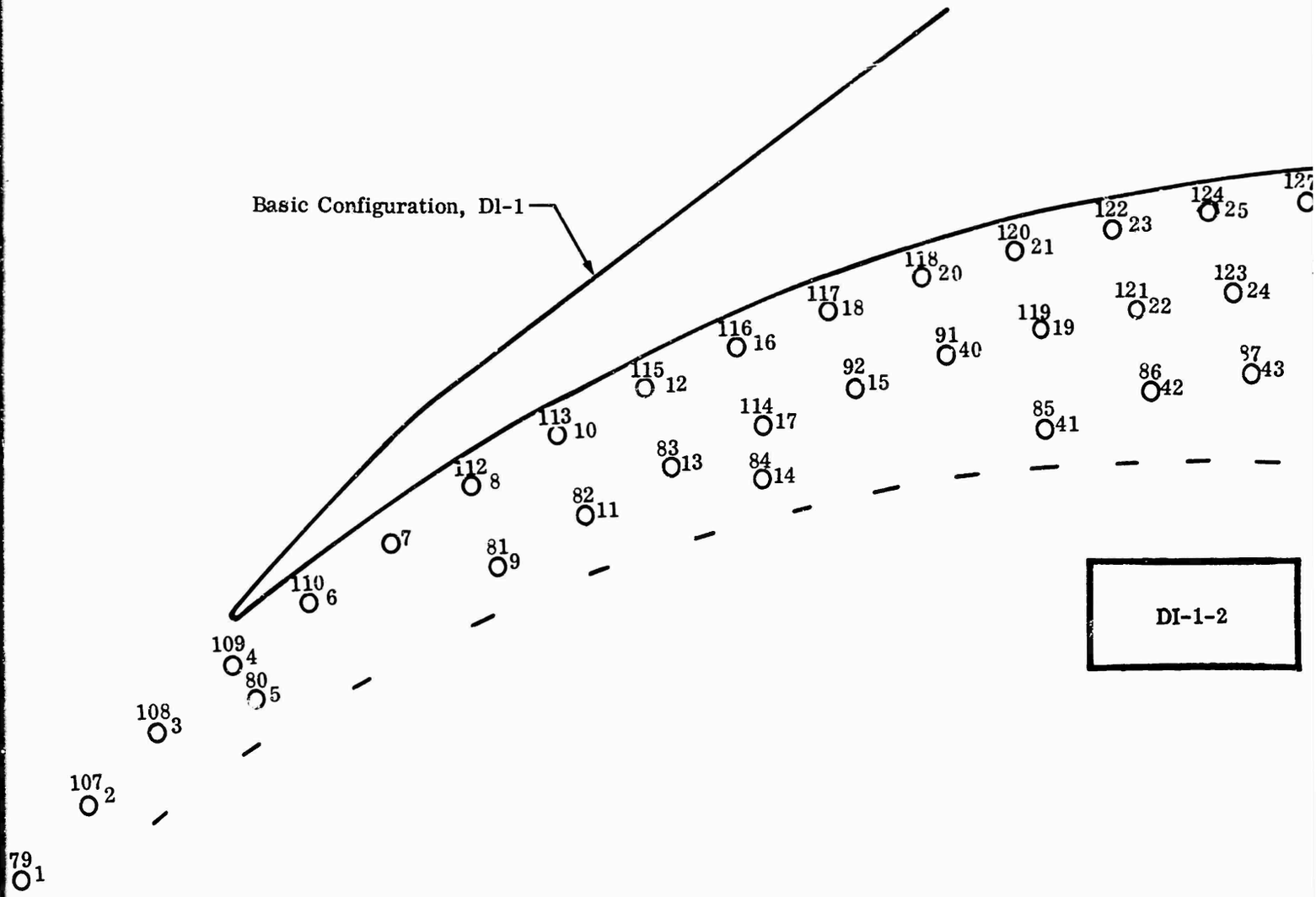
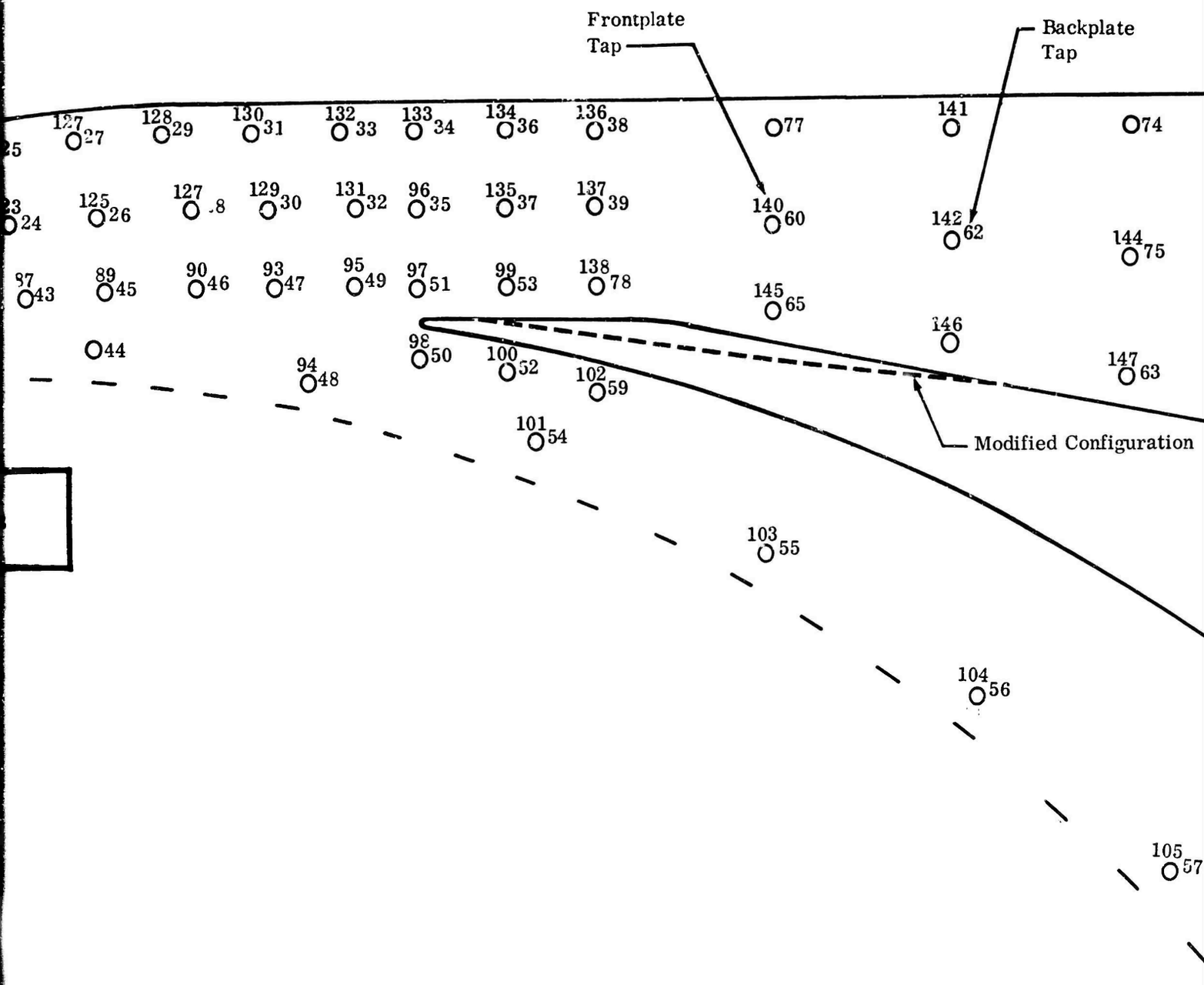
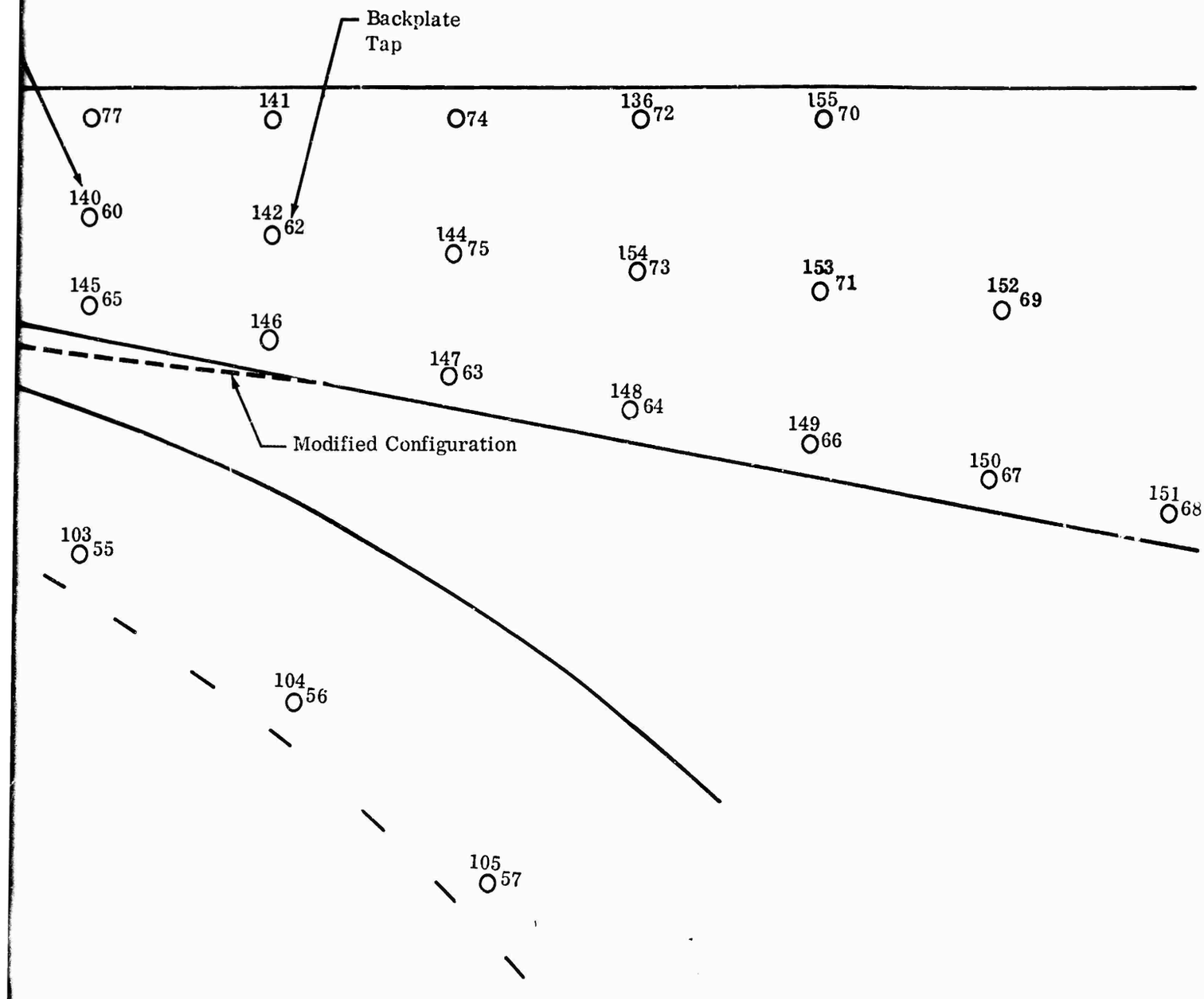


Figure 109. Diffuser Static-Pressure Instrumentation, DI-1-2.


Frontplate Tap
Backplate Tap
Modified Configuration
127 27
128 29
130 31
132 33
133 34
134 36
136 38
77
141
74
25
23 24
125 26
127 28
129 30
131 32
96 35
135 37
137 39
140 60
142 62
144 75
97 43
89 45
90 46
93 47
95 49
97 51
99 53
138 78
145 65
146
147 63
44
94 48
98 50
100 52
102 59
101 54
103 55
104 56
105 57


Backplate
Tap
77
141
74
136
72
155
70
140
60
142
62
144
75
154
73
153
71
152
69
145
65
146
147
63
148
64
149
66
150
67
151
68
Modified Configuration
103
55
104
56
105
57

DI-1-3 PRESSURE SURVEY

TEST NO. 3340 SPEED = 50000 AIR FLOW = 2.43

IGV = REMOVED THROAT AREA = 100^{6} RADIUS RATIO = 1.06

LINE NO. 3 δ = 0.990

ALL PRESSURES ARE IN PSIA

TAP NO.	STATIC PRESSURE	TAP NO.	STATIC PRESSURE	TAP NO.	STATIC PRESSURE	TAP NO.	STATIC PRESSURE	TAP NO.	STATIC PRESSURE	TAP NO.	STATIC PRESSURE
2	66.2	3	64.5	4	62.5	5	62.0	6	79.6	7	72.6
8	71.3	9	63.9	10	71.2	11	66.5	13	66.5	15	67.6
17	61.6	19	70.1	20	73.0	21	75.3	24	74.3	25	79.9
27	80.3	28	75.2	29	82.0	31	77.9	32	65.5	33	68.8
34	68.8	35	95.0	35	67.1	36	88.2	37	87.4	38	97.6
39	95.6	40	68.4	41	63.9	42	66.4	43	69.2	44	71.5
45	72.1	46	70.5	47	67.4	48	63.0	49	63.7	50	68.2
51	72.0	52	67.3	53	83.8	54	63.1	55	64.2	56	66.9
57	64.2	58	63.7	59	67.5	60	104.0	62	114.2	63	120.3
64	124.3	65	105.3	66	126.3	68	126.7	69	128.1	70	126.3
71	126.7	72	124.1	73	124.3	74	120.0	75	120.6	77	107.5
78	95.4	84	68.1	115	0.0	118	72.3	122	94.8	127	74.3
156	0.0	157	130.0	158	130.6	159	130.8	160	130.7		

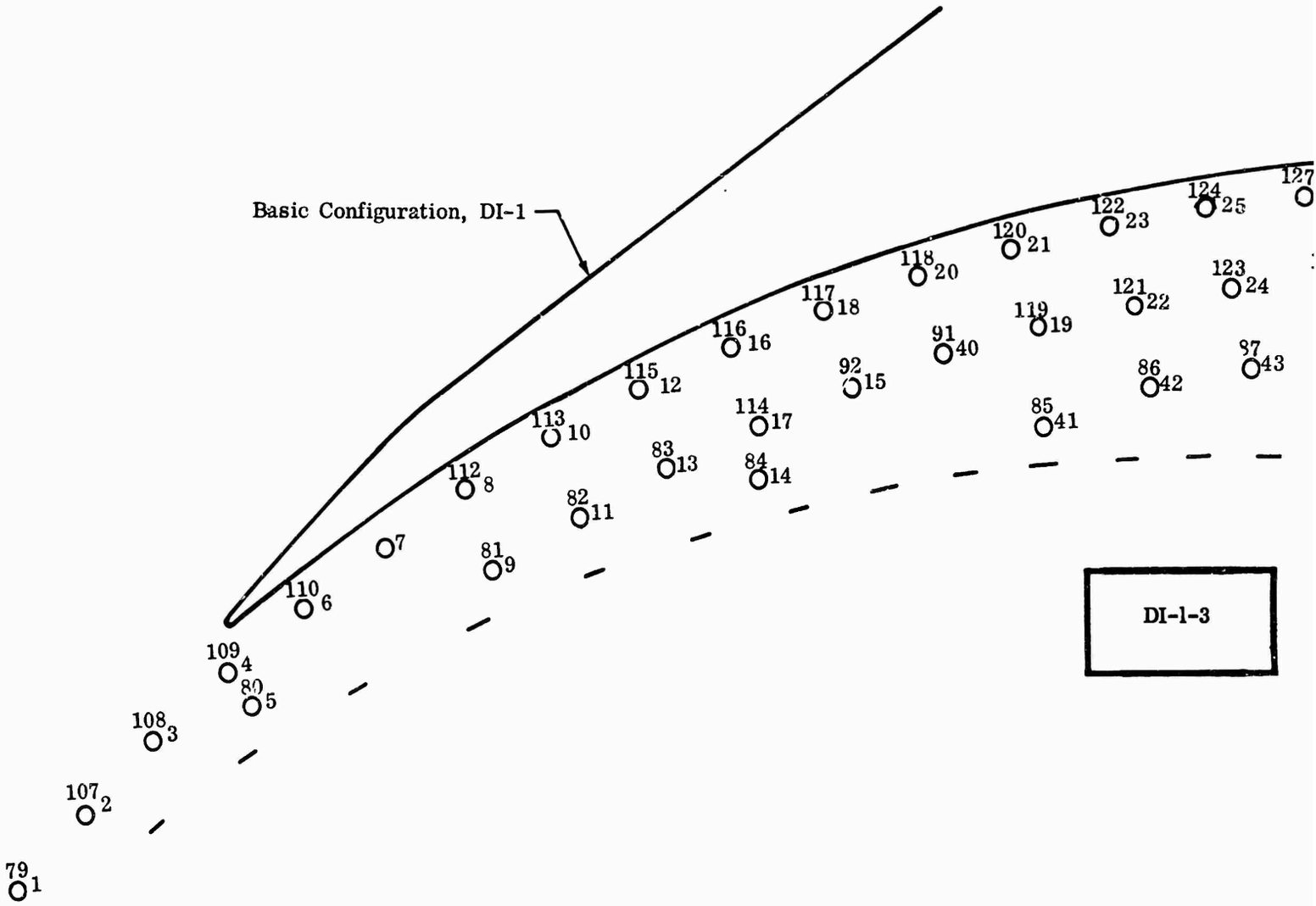
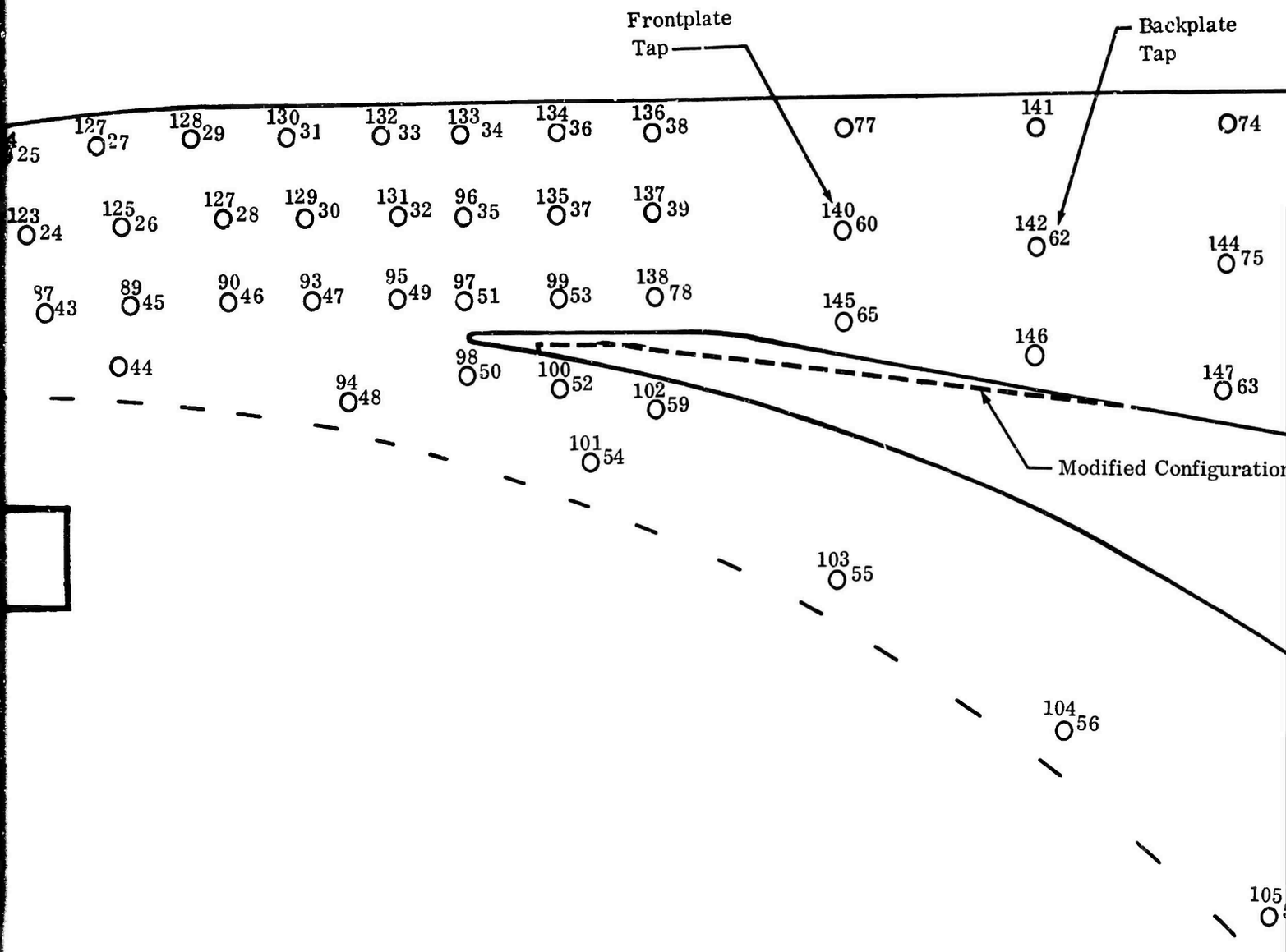
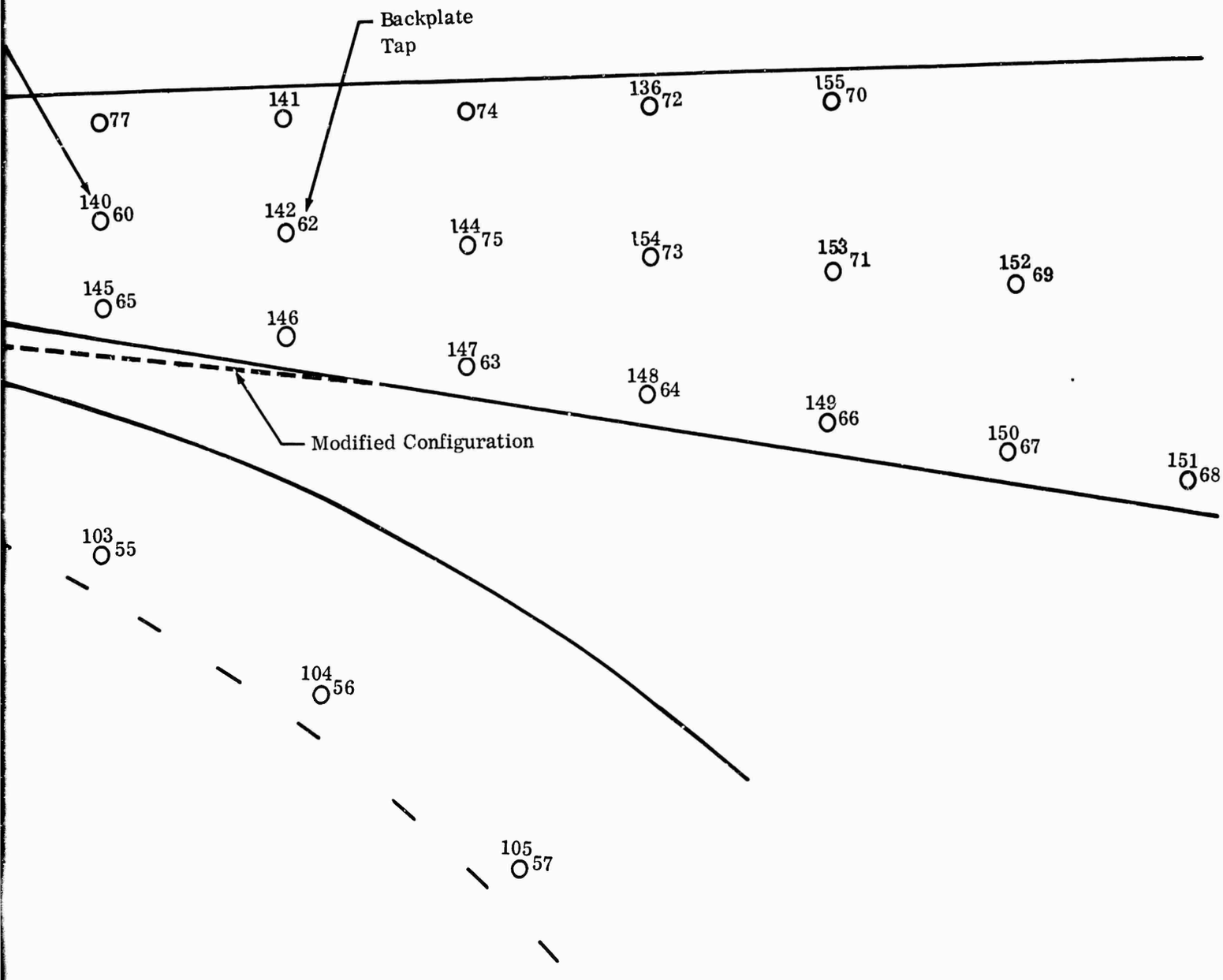


Figure 110. Diffuser Static-Pressure Instrumentation, DI-1-3.


Frontplate
Tap
Backplate
Tap
Modified Configuration


Backplate
Tap
77
141
74
136 72
155 70
140 60
142 62
144 75
154 73
153 71
152 69
145 65
146
147 63
148 64
149 66
150 67
151 68
Modified Configuration
103 55
104 56
105 57

DI-2 PRESSURE SURVEY

TEST NO. 3310A SPEED = 50000 AIR FLOW = 2.38

IGV = 0 THROAT AREA = 100% RADIUS RATIO = 1.06

LINE NO. 3.1 δ = 0.997

ALL PRESSURES ARE IN PSIA

TAP NO.	STATIC PRESSURE	TAP NO.	STATIC PRESSURE	TAP NO.	STATIC PRESSURE	TAP NO.	STATIC PRESSURE	TAP NO.	STATIC PRESSURE	TAP NO.	STATIC PRESSURE
1	64.6	2	62.7	3	59.3	4	77.0	5	70.9	6	61.9
7	65.0	8	70.7	9	64.0	10	70.9	11	65.3	12	70.8
13	64.5	14	61.5	15	65.0	16	69.4	17	61.2	18	69.1
19	70.1	20	73.8	21	76.0	22	72.0	23	77.3	24	71.7
25	78.1	26	20.4	27	77.6	28	68.5	29	70.9	30	0.0
31	67.2	32	62.9	33	62.3	34	84.8	35	87.0	36	91.8
37	91.1	38	95.1	39	92.9	40	67.0	41	63.2	42	65.5
43	66.9	44	62.3	45	67.5	45	0.0	46	64.9	47	60.6
48	57.3	49	71.4	50	78.0	51	91.2	52	62.9	53	90.9
54	60.1	55	61.9	56	0.0	57	65.1	58	72.1	59	62.4
60	104.2	62	113.2	63	117.4	64	120.4	65	105.2	66	123.1
67	124.8	68	126.1	69	126.3	70	124.5	71	124.7	72	122.3
73	122.3	74	118.7	75	118.8	77	105.4	77	0.0	78	91.2
79	65.0	80	65.0	81	64.9	82	56.2	83	64.4	84	29.4
85	62.7	86	66.9	87	68.3	88	23.4	89	0.0	90	87.6
91	68.1	92	64.9	93	63.9	94	56.7	95	0.0	96	0.0
97	90.4	98	80.7	99	0.0	99	92.9	100	64.6	102	65.9
104	62.2	105	65.0	106	72.5	107	63.3	108	59.8	109	35.4
110	62.5	112	70.9	113	0.0	114	39.4	115	73.2	116	72.2
117	73.0	118	76.0	119	71.2	120	76.8	121	73.3	122	80.0
123	75.1	124	80.1	125	74.6	126	66.7	127	71.4	128	74.2
129	65.4	130	66.9	132	64.0	133	83.0	134	92.3	135	93.0
136	95.3	137	0.0	140	105.0	141	113.6	142	114.7	144	119.5
145	105.3	146	113.4	147	118.4	148	120.3	149	122.0	150	124.7
151	126.0	152	126.4	153	124.9	154	122.8	155	124.7	156	122.4
157	128.9	158	129.3	159	129.4	160	129.5				

CI-2 PRESSURE SURVEY

TEST NO. 331CA SPEED = 39000 AIR FLOW = 1.88

IGV = 0 THROAT AREA = 100% RADIUS RATIO = 1.06

LINE NO. 5 δ = 1.00

ALL PRESSURES ARE IN PSIA

TAP NO.	STATIC PRESSURE	TAP NO.	STATIC PRESSURE	TAP NO.	STATIC PRESSURE	TAP NO.	STATIC PRESSURE	TAP NO.	STATIC PRESSURE	TAP NO.	STATIC PRESSURE
1	39.1	2	37.4	3	37.1	4	45.6	5	42.2	6	42.6
7	42.0	8	42.7	9	39.8	10	42.8	11	40.5	12	43.9
13	41.1	14	39.3	15	42.1	16	43.5	17	41.4	18	44.2
19	42.4	20	44.9	21	45.0	22	42.7	23	45.0	24	42.5
25	45.1	26	0.0	27	44.0	28	39.9	29	41.7	30	38.8
31	39.9	32	42.4	33	41.5	34	43.6	35	43.8	36	43.3
37	42.8	38	42.4	39	41.4	40	42.3	41	40.2	42	40.4
43	41.0	44	38.5	45	39.4	45	0.0	46	38.6	47	38.0
48	39.6	49	43.4	50	44.8	51	45.9	52	42.0	53	42.6
54	38.8	55	40.8	56	0.0	57	40.9	58	37.4	59	41.3
60	47.8	62	53.7	63	55.9	64	57.7	65	47.6	66	59.0
67	59.8	68	60.4	69	61.2	70	60.3	71	60.4	72	58.6
73	59.1	74	57.1	75	57.1	77	48.6	77	0.0	78	40.7
79	39.6	80	43.2	81	40.4	82	37.1	83	41.8	84	22.7
85	40.2	86	41.0	87	41.9	88	0.0	89	0.0	90	44.8
91	43.2	92	42.8	93	39.3	94	38.7	95	0.0	96	0.0
97	47.9	98	46.8	99	0.0	99	44.3	100	44.1	102	43.4
104	41.7	105	40.8	106	37.3	107	37.6	108	36.7	109	0.0
110	42.7	112	43.1	113	0.0	114	28.0	115	45.7	116	44.8
117	45.7	118	46.0	119	43.1	120	45.3	121	43.5	122	45.8
123	43.9	124	45.7	125	42.3	126	40.4	127	41.2	128	42.7
129	40.0	130	40.3	132	42.0	133	44.3	134	44.1	135	44.0
136	43.0	137	0.0	140	48.1	141	54.0	142	54.1	144	57.3
145	48.5	146	53.9	147	56.4	148	57.3	149	57.8	150	59.0
151	59.8	152	61.2	153	60.4	154	59.3	155	60.3	156	59.1
157	62.4	158	62.7	159	62.7	160	62.9				

DI-2 PRESSURE SURVEY

TEST NO. 3320 SPEED = 50000 AIR FLOW = 2.23

IGV = 0 THROAT AREA = 100 % RADIUS RATIO = 1.06

LINE NO. 3 δ = 0.990

ALL PRESSURES ARE IN PSIA

TAP NO.	STATIC PRESSURE	TAP NO.	STATIC PRESSURE	TAP NO.	STATIC PRESSURE	TAP NO.	STATIC PRESSURE	TAP NO.	STATIC PRESSURE	TAP NO.	STATIC PRESSURE
1	65.2	2	62.8	3	58.9	4	56.9	5	58.0	6	74.1
7	74.4	8	67.1	9	66.9	10	65.9	11	62.3	12	68.1
13	63.2	15	66.1	16	69.8	17	58.3	19	69.8	20	73.4
21	75.5	22	72.5	23	77.5	24	72.2	25	78.7	27	77.2
28	67.8	29	69.7	30	62.0	31	65.7	32	58.0	33	58.7
34	54.0	35	64.1	36	66.4	37	62.9	38	68.1	39	65.3
40	67.0	41	63.0	42	65.5	43	67.4	44	67.3	45	68.2
46	64.9	47	59.5	48	55.9	49	54.8	50	21.5	51	78.4
52	62.6	53	61.0	54	60.3	55	59.9	56	60.3	57	62.0
58	57.7	59	64.4	60	88.3	62	100.1	63	106.6	64	109.0
65	89.6	66	110.7	67	112.7	68	113.9	69	113.3	70	112.5
71	111.9	72	110.2	73	109.7	74	106.9	75	106.6	77	89.7
78	63.1	79	63.9	80	54.4	81	62.2	83	61.7	86	66.1
87	68.4	90	65.8	91	68.2	92	64.2	93	63.2	95	56.9
96	61.8	97	79.8	98	61.4	99	62.7	100	56.4	102	58.6
104	59.4	105	61.0	106	58.3	107	62.5	108	59.2	110	73.0
112	68.1	115	70.9	116	71.9	117	72.5	118	70.9	118	76.4
119	70.8	120	76.9	121	74.0	122	80.9	123	75.9	124	81.1
125	74.7	127	70.6	128	73.5	129	64.6	131	59.8	132	63.7
134	68.5	135	63.6	136	65.6	138	67.0	139	89.0	140	0.0
142	101.9	144	107.2	146	100.6	147	106.4	148	108.9	149	109.2
150	101.7	151	95.5	152	0.0	153	112.3	154	110.4	155	112.8
156	110.7	157	116.3	158	112.4	159	117.0	160	116.3		

DI-2 PRESSURE SURVEY

TEST NO. 3331 SPEED = 50000 AIR FLOW = 2.41

IGV = REMOVED THROAT AREA = 100% RADIUS RATIO = 1.06

LINE NO. 3 δ = 1.003

ALL PRESSURES ARE IN PSIA

TAP NO.	STATIC PRESSURE	TAP NO.	STATIC PRESSURE	TAP NO.	STATIC PRESSURE	TAP NO.	STATIC PRESSURE	TAP NO.	STATIC PRESSURE	TAP NO.	STATIC PRESSURE
2	65.8	3	60.2	4	77.7	5	73.7	6	70.2	7	68.4
8	71.5	9	61.6	10	72.5	11	67.8	13	68.6	15	67.9
17	61.2	19	72.8	20	74.3	21	79.0	24	75.0	25	81.1
27	81.5	28	72.5	29	76.1	31	81.0	32	99.3	33	98.6
34	109.1	35	95.1	35	108.6	36	114.0	37	113.9	38	116.8
39	115.4	40	70.9	41	67.6	42	70.0	43	70.6	44	73.4
45	73.1	46	69.1	47	83.3	48	86.0	49	99.3	50	78.8
51	111.5	52	56.6	53	114.6	54	54.7	55	65.8	56	69.2
57	67.6	58	63.1	59	59.7	60	121.5	62	126.6	63	42.4
64	131.0	65	121.6	66	132.9	68	134.2	69	134.5	70	133.4
71	133.5	72	132.2	73	132.0	74	129.2	75	129.9	77	122.0
78	114.6	84	68.4	115	0.0	118	73.2	122	94.6	127	74.6
156	0.0	157	135.8	158	136.3	159	136.5	160	136.5		

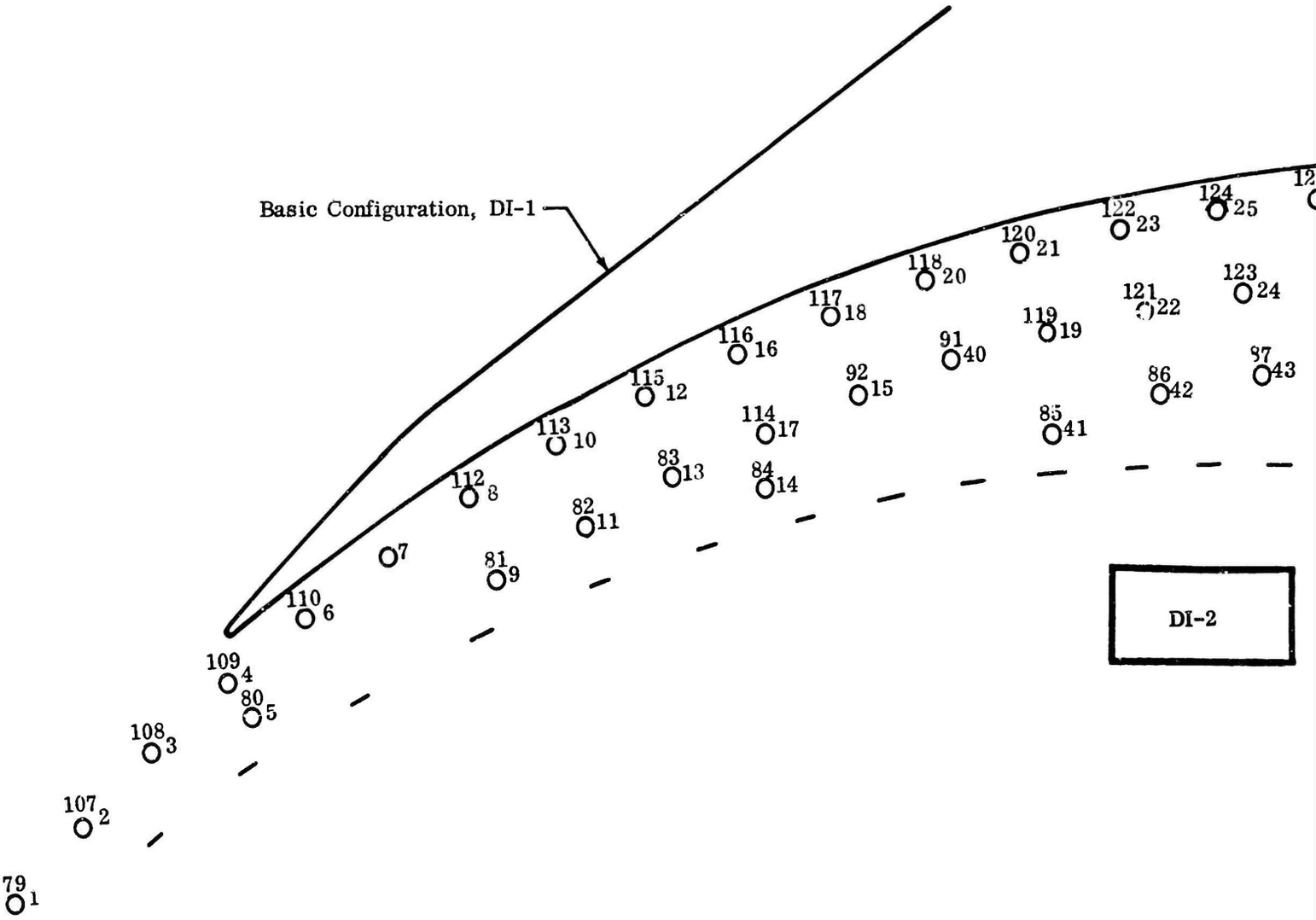
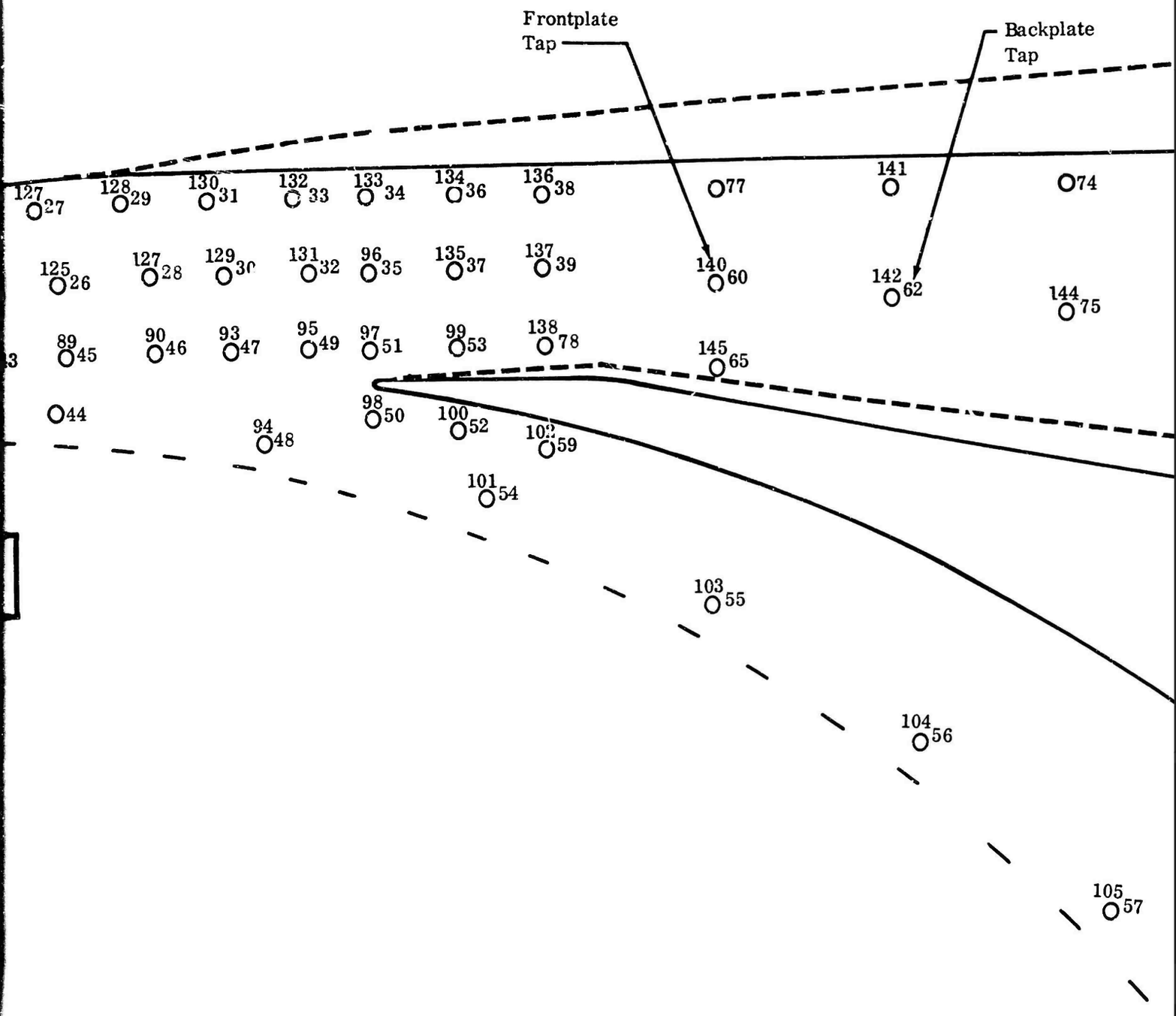
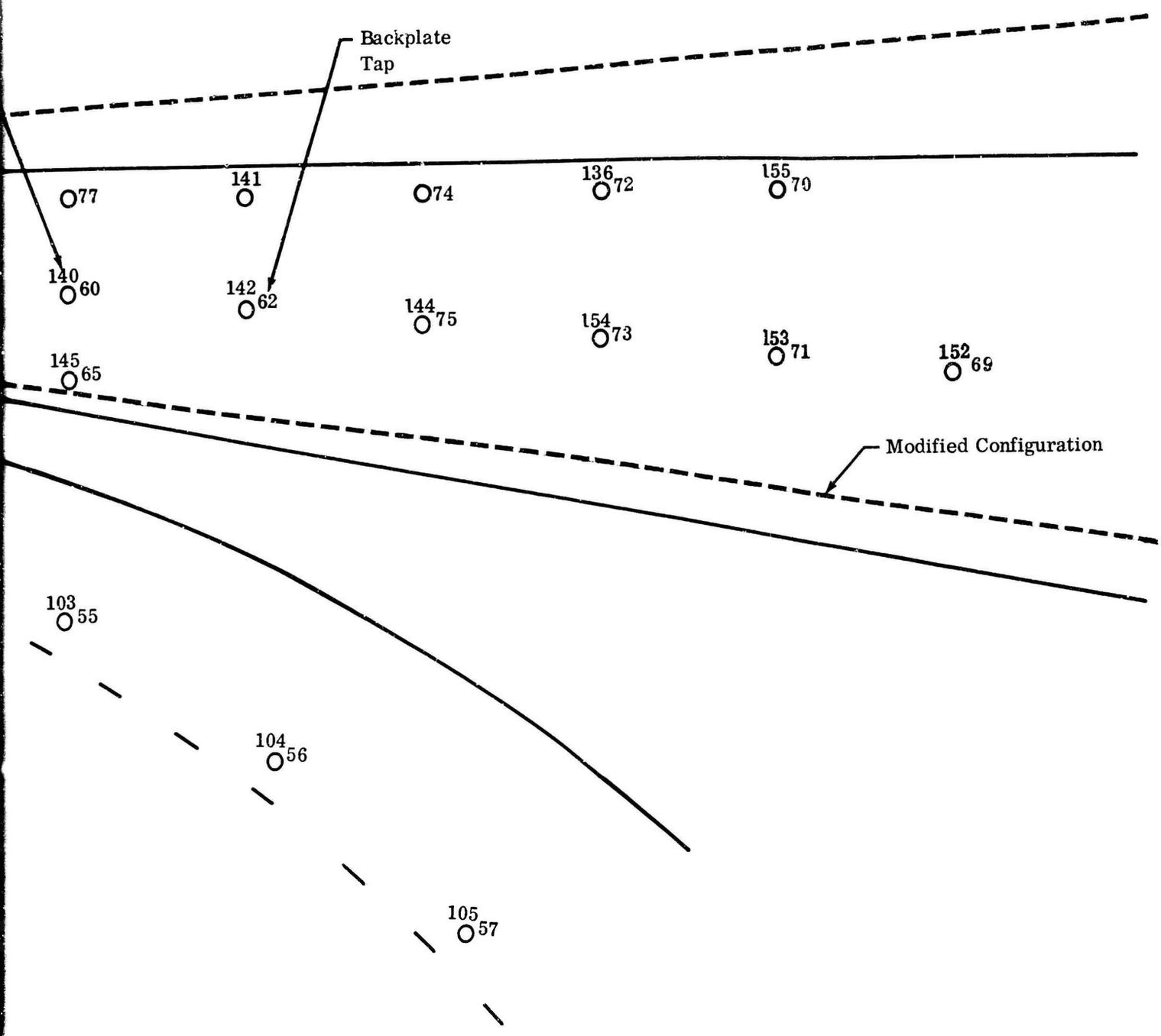


Figure 111. Diffuser Static-Pressure Instrumentation, DI-2.


Frontplate
Tap
Backplate
Tap
127 27
128 29
130 31
132 33
133 34
134 36
136 38
77
141
74
125 26
127 28
129 30
131 32
96 35
135 37
137 39
140 60
142 62
144 75
89 45
90 46
93 47
95 49
97 51
99 53
138 78
145 65
44
94 48
98 50
100 52
102 59
101 54
103 55
104 56
105 57


Backplate
Tap
77
141
74
136
72
155
70
140
60
142
62
144
75
154
73
153
71
152
69
145
65
Modified Configuration
103
55
104
56
105
57

CI-X1 PRESSURE SURVEY

TEST NO. 3338 SPEED = 50000 AIR FLOW = 2.48

IGV = REMOVED THROAT AREA = 100% RADIUS RATIO = 1.06

LINE NO. 5 δ = 0.989

ALL PRESSURES ARE IN PSIA

TAP NO.	STATIC PRESSURE	TAP NO.	STATIC PRESSURE	TAP NO.	STATIC PRESSURE	TAP NO.	STATIC PRESSURE	TAP NO.	STATIC PRESSURE	TAP NO.	STATIC PRESSURE
2	63.9	3	59.2	4	74.6	5	71.3	6	63.2	7	68.9
8	71.5	9	72.0	10	68.1	11	63.4	13	63.6	15	65.3
17	59.1	19	67.6	20	70.9	21	72.4	24	72.8	25	78.1
27	78.7	28	72.0	29	77.7	31	68.0	32	57.4	33	58.4
34	79.7	35	94.8	35	82.1	36	86.9	37	87.0	38	87.8
39	87.6	40	65.4	41	60.9	42	64.2	43	67.2	44	69.4
45	71.1	46	67.7	47	62.1	48	58.0	49	58.8	50	80.1
51	85.9	52	66.1	53	87.0	54	62.2	55	63.0	56	63.7
57	61.8	58	59.9	59	66.5	60	99.5	62	110.2	63	37.1
64	87.9	65	101.2	66	108.2	68	121.6	69	125.2	70	123.1
71	123.3	72	120.4	73	120.2	74	116.1	75	116.4	77	102.2
78	87.1	84	64.8	115	0.0	118	70.6	122	94.6	127	74.3
156	0.0	157	129.7	158	130.2	159	130.4	160	130.5		

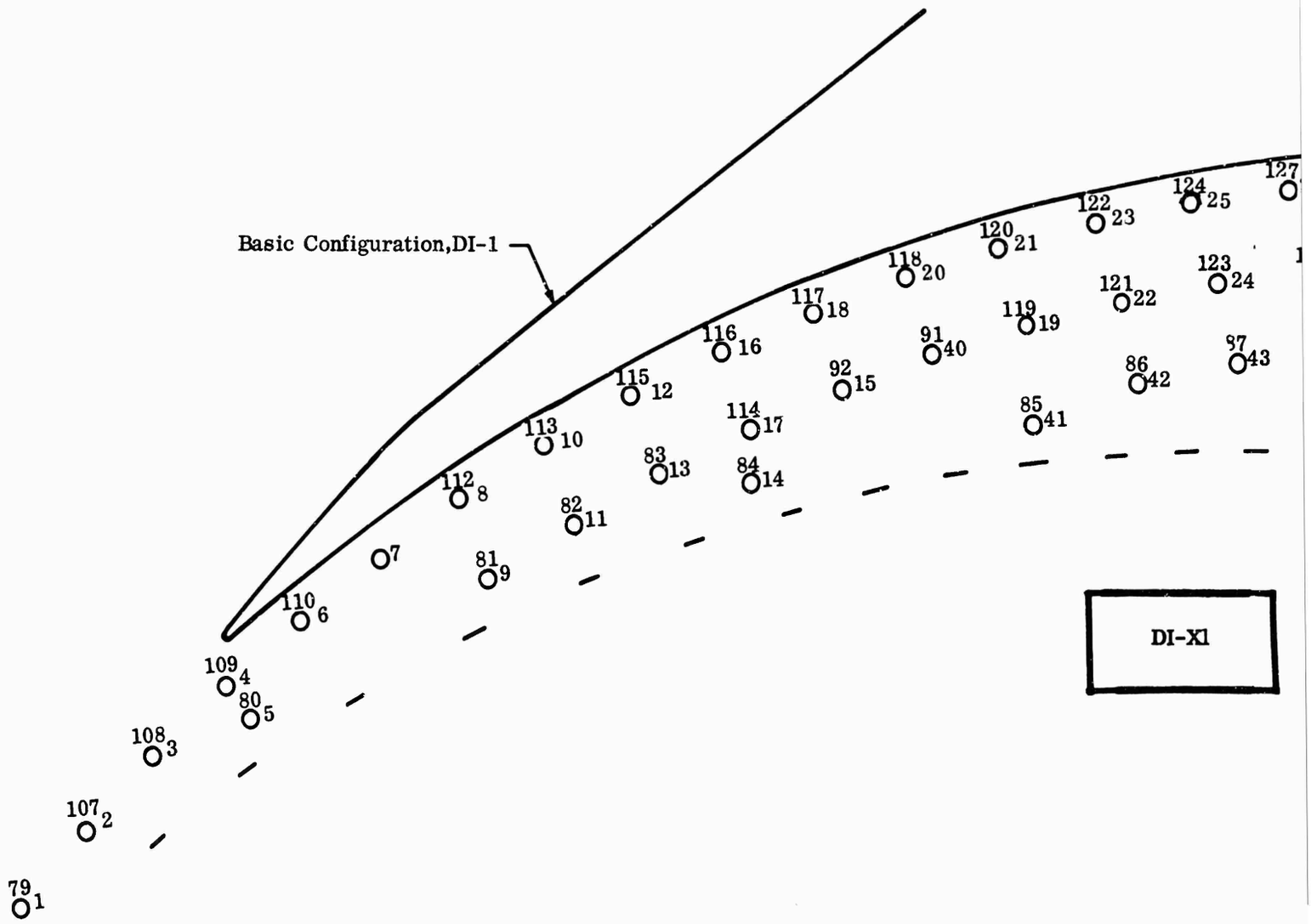
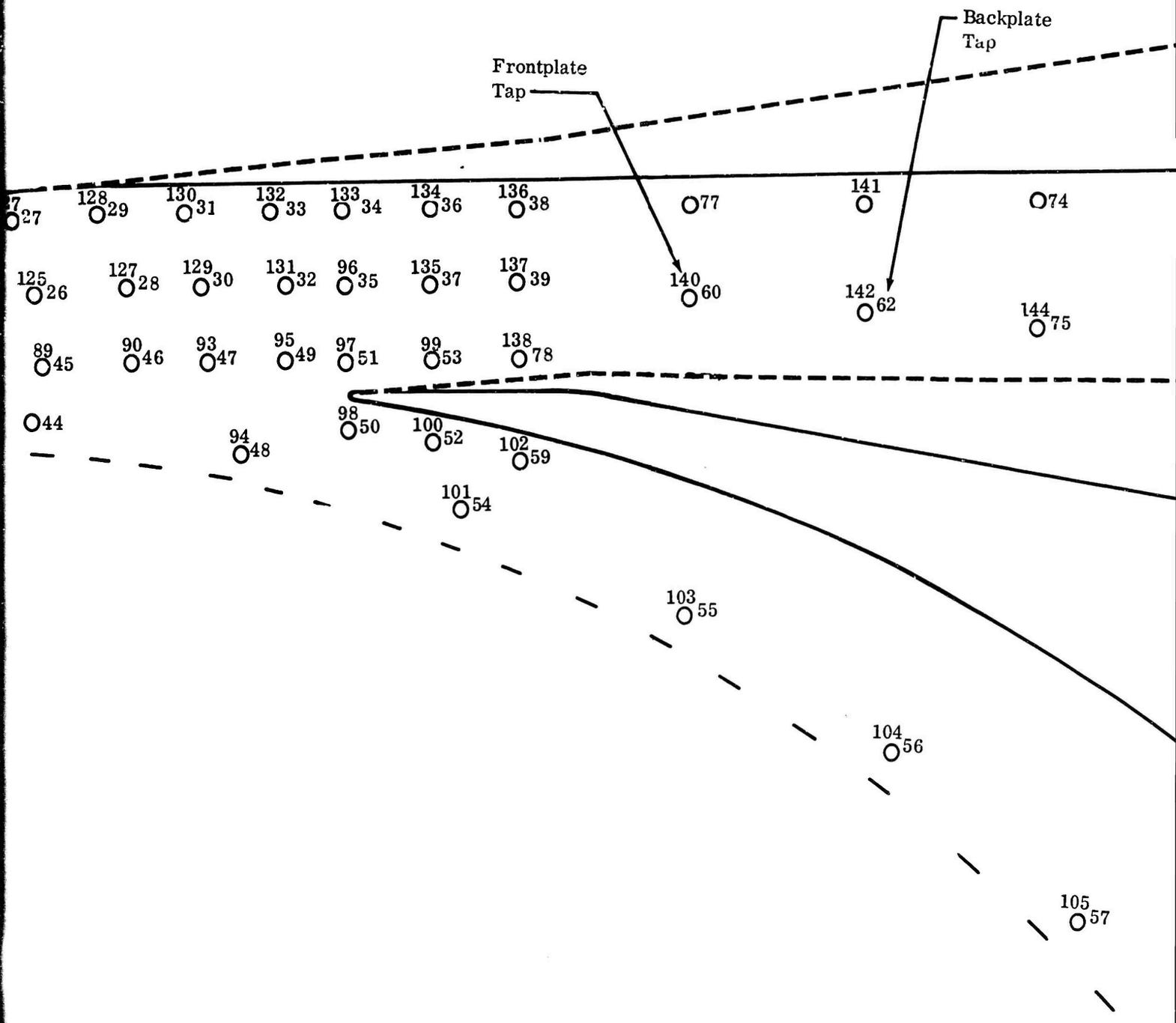
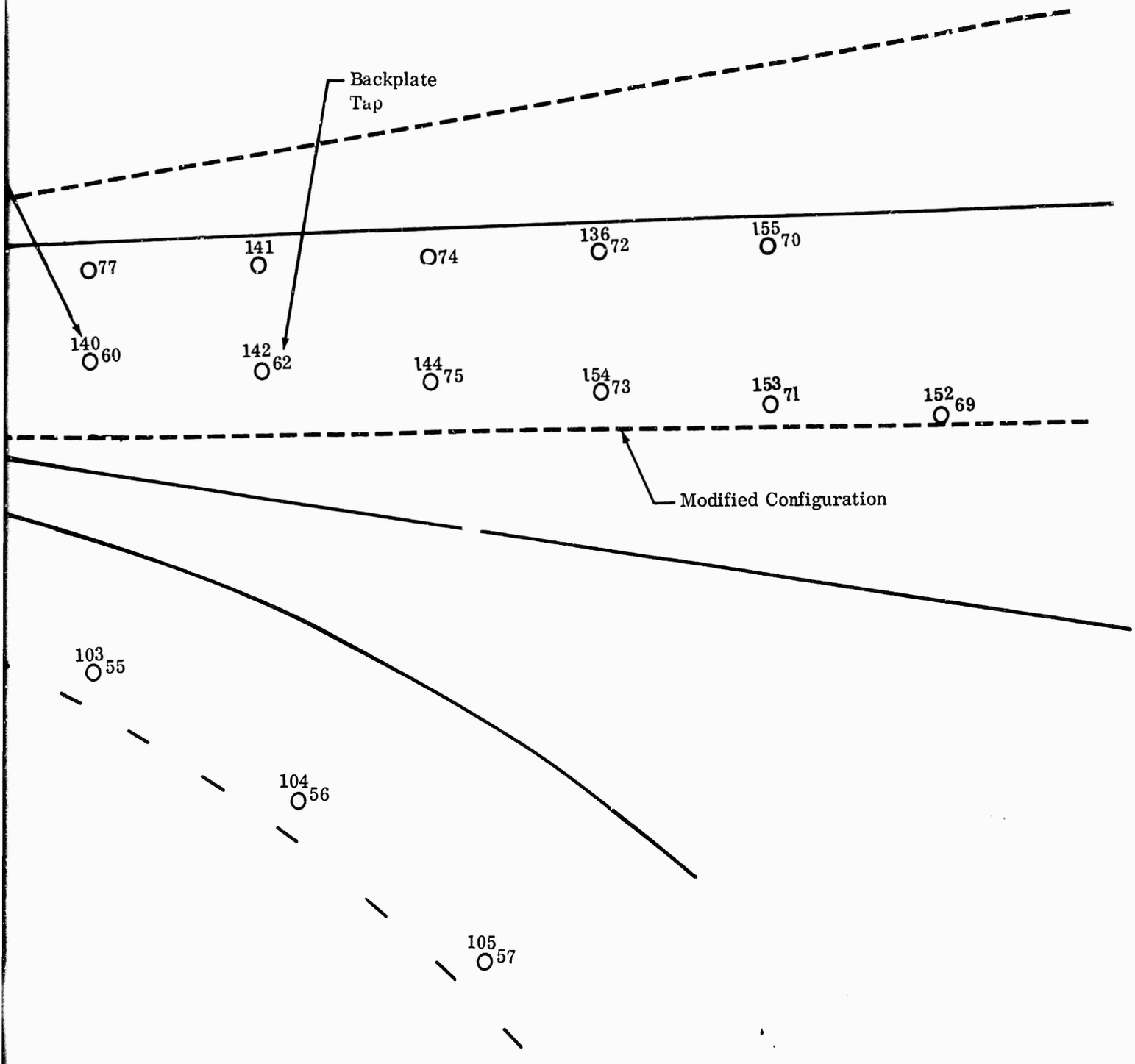


Figure 112. Diffuser Static-Pressure Instrumentation, DI-X1.


Backplate
Tap
Frontplate
Tap
27
128 29
130 31
132 33
133 34
134 36
136 38
77
141
74
125 26
127 28
129 30
131 32
96 35
135 37
137 39
140 60
142 62
144 75
89 45
90 46
93 47
95 49
97 51
99 53
138 78
44
94 48
98 50
100 52
102 59
101 54
103 55
104 56
105 57


Backplate
Tap
77
141
74
136
72
155
70
140
60
142
62
144
75
154
73
153
71
152
69
Modified Configuration
103
55
104
56
105
57

DI-X1-2 PRESSURE SURVEY

TEST NO. 3341 SPEED = 50000 AIR FLOW = 2.49

IGV = REMOVED THROAT AREA = 100% RADIUS RATIO = 1.06

LINE NO. 3 δ = 0.988

ALL PRESSURES ARE IN PSIA

TAP NO.	STATIC PRESSURE	TAP NO.	STATIC PRESSURE	TAP NO.	STATIC PRESSURE	TAP NO.	STATIC PRESSURE	TAP NO.	STATIC PRESSURE	TAP NO.	STATIC PRESSURE
2	62.9	3	59.3	4	64.1	5	65.2	6	69.3	7	70.6
8	70.6	9	70.9	10	67.6	11	63.2	13	63.1	15	64.5
17	58.6	19	67.1	20	70.3	21	71.8	24	72.2	25	77.1
27	78.7	28	71.1	29	77.0	31	67.2	32	57.6	33	59.0
34	74.8	35	94.8	35	77.7	36	84.2	37	84.7	38	86.2
39	86.2	40	65.1	41	60.5	42	63.6	43	67.0	44	68.7
45	70.2	46	67.1	47	61.6	48	57.4	49	57.4	50	78.4
51	82.9	52	67.8	53	84.8	54	62.7	55	62.0	56	63.1
57	61.3	58	59.4	59	67.6	60	100.0	62	111.3	63	116.1
64	117.5	65	102.6	66	117.9	68	124.6	69	125.9	70	123.7
71	124.1	72	121.4	73	121.4	74	117.4	75	117.6	77	102.7
78	85.5	84	63.9	115	0.0	118	70.1	122	94.4	127	73.2
156	0.0	157	129.3	158	129.8	159	129.9	160	130.0		

CI-X1-3 PRESSURE SURVEY

TEST NO. 3333 SPEED = AIR FLOW = 2.50

IGV = REMOVED THROAT AREA = 100% RADIUS RATIO = 1.06

LINE NO. 3 δ = 0.997

ALL PRESSURES ARE IN PSIA

TAP NO.	STATIC PRESSURE	TAP NO.	STATIC PRESSURE	TAP NO.	STATIC PRESSURE	TAP NO.	STATIC PRESSURE	TAP NO.	STATIC PRESSURE	TAP NO.	STATIC PRESSURE
2	63.0	3	59.9	4	80.4	5	72.6	6	58.1	7	64.0
8	69.8	9	72.6	10	69.9	11	64.6	13	63.0	15	63.2
17	57.2	19	66.3	20	69.1	21	71.2	24	68.0	25	74.3
27	76.0	28	70.2	29	75.2	31	68.6	32	82.3	33	76.5
34	91.0	35	94.9	35	92.1	36	95.0	37	95.4	38	96.3
39	96.6	40	63.8	41	59.3	42	62.9	43	61.6	44	65.5
45	67.6	46	66.2	47	61.6	48	61.9	49	84.0	50	80.7
51	96.4	52	60.5	53	96.0	54	59.9	55	62.7	56	62.6
57	61.5	58	60.9	59	63.8	60	107.6	62	115.6	63	0.0
64	121.0	65	108.7	66	122.9	68	56.5	69	128.5	70	126.6
71	126.8	72	124.4	73	124.3	74	120.0	75	120.9	77	108.1
78	95.8	84	64.0	115	0.0	118	68.8	122	94.5	127	70.9
156	0.0	157	132.1	158	132.6	159	132.7	160	132.8		

DI-X1-3 PRESSURE SURVEY

TEST NO. 3326 SPEED = 50000 AIR FLOW = 2.50

IGV = REMOVED THROAT AREA = 100% RADIUS RATIO = 1.06

LINE NO. 3 δ = 0.990

ALL PRESSURES ARE IN PSIA

TAP NO.	STATIC PRESSURE	TAP NO.	STATIC PRESSURE	TAP NO.	STATIC PRESSURE	TAP NO.	STATIC PRESSURE	TAP NO.	STATIC PRESSURE	TAP NO.	STATIC PRESSURE
1	58.1	2	60.8	3	53.9	4	61.5	5	61.9	6	64.7
7	65.4	8	67.6	9	55.5	10	64.8	11	59.8	12	64.9
13	61.0	15	62.7	16	66.9	17	56.1	19	63.3	20	65.9
21	57.7	22	65.4	23	66.5	24	66.6	25	71.5	27	71.5
28	67.4	29	42.5	30	58.2	31	67.1	32	51.7	33	54.6
34	79.2	35	79.6	36	83.0	37	83.1	38	83.3	39	83.6
40	61.6	41	58.0	42	58.8	43	60.8	44	64.7	45	65.3
46	63.6	47	59.9	48	56.5	49	55.8	50	0.0	51	82.9
52	59.1	53	83.1	54	61.0	55	62.0	56	61.1	57	58.9
58	61.1	59	58.3	60	97.7	62	107.2	63	112.7	64	116.1
65	99.0	66	117.5	67	118.9	68	120.4	69	120.0	70	118.3
71	118.5	72	116.4	73	116.0	74	112.3	75	112.8	77	98.9
78	82.8	79	0.0	80	0.0	81	0.0	83	0.0	86	0.0
87	0.0	90	0.0	91	0.0	92	0.0	93	0.0	95	0.0
96	0.0	97	0.0	98	0.0	99	0.0	100	0.0	102	0.0
104	0.0	105	0.0	106	0.0	107	0.0	108	0.0	110	0.0
112	0.0	115	0.0	116	0.0	117	0.0	118	66.2	118	0.0
119	0.0	120	0.0	121	0.0	122	0.0	123	0.0	124	0.0
125	0.0	127	0.0	128	0.0	129	0.0	131	0.0	132	0.0
134	0.0	135	0.0	136	0.0	138	0.0	139	0.0	140	0.0
142	0.0	144	0.0	146	0.0	147	0.0	148	0.0	149	0.0
150	0.0	151	0.0	152	0.0	153	0.0	154	0.0	155	0.0
156	0.0	157	123.0	158	123.8	159	124.4	160	124.4		

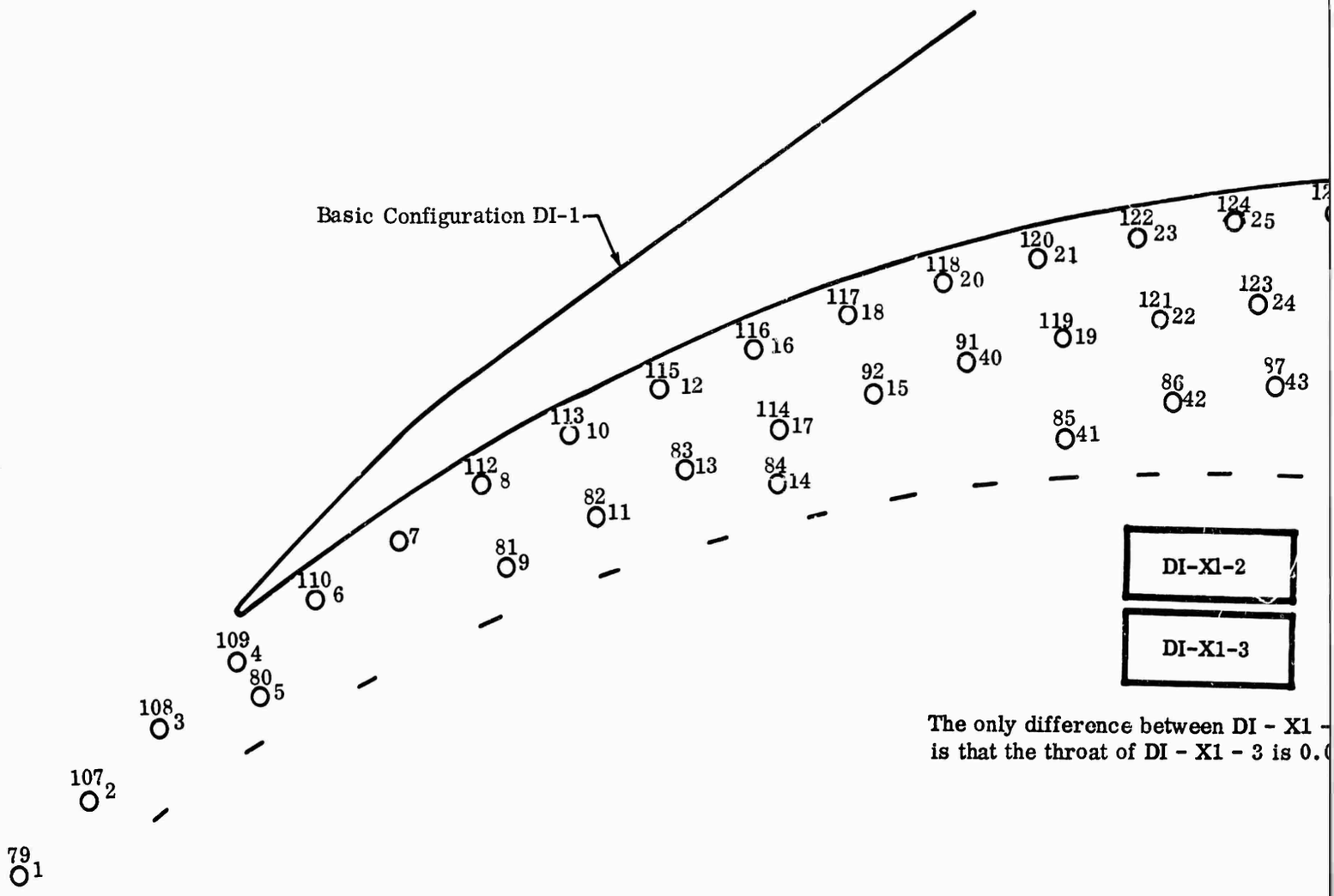
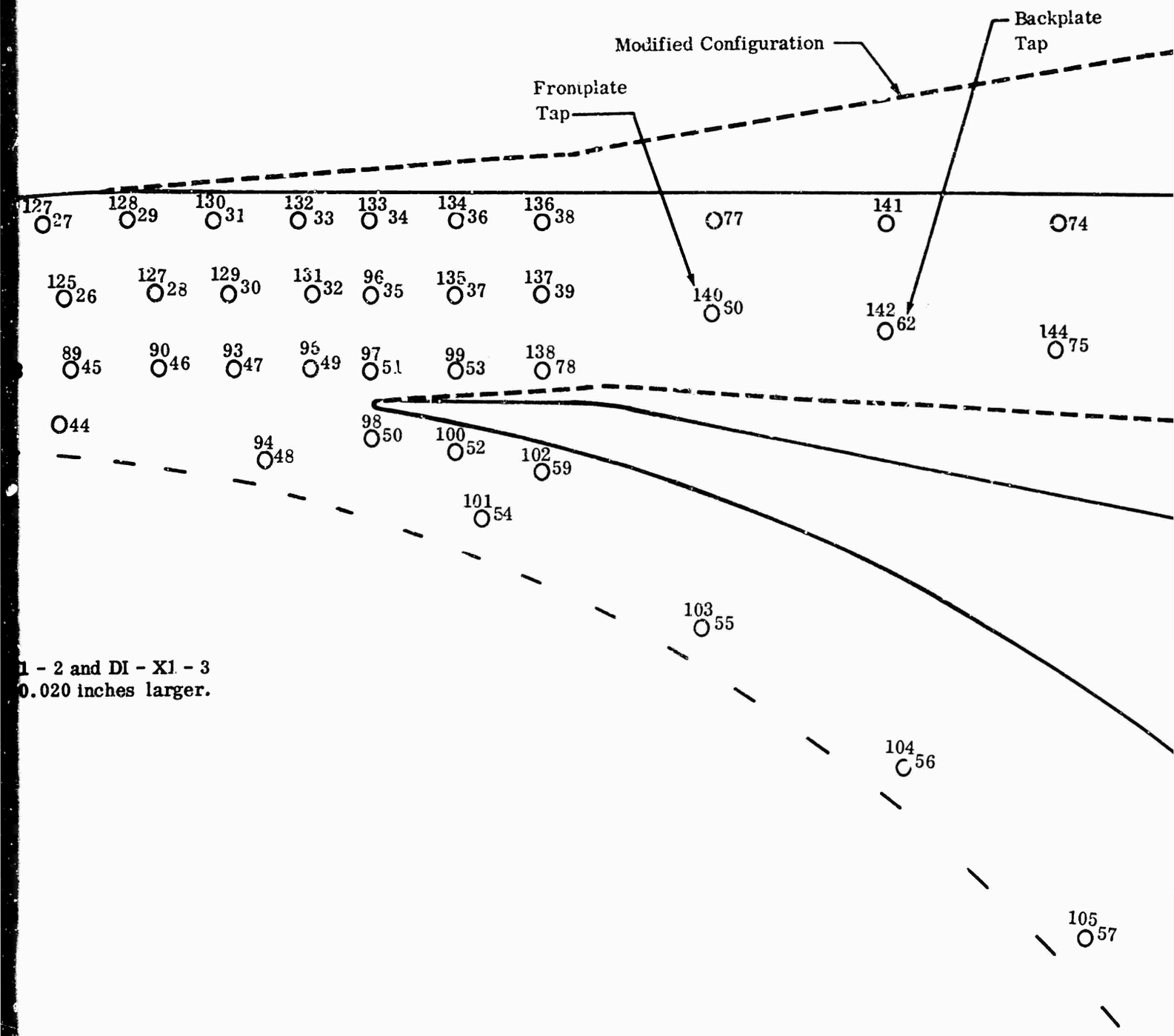
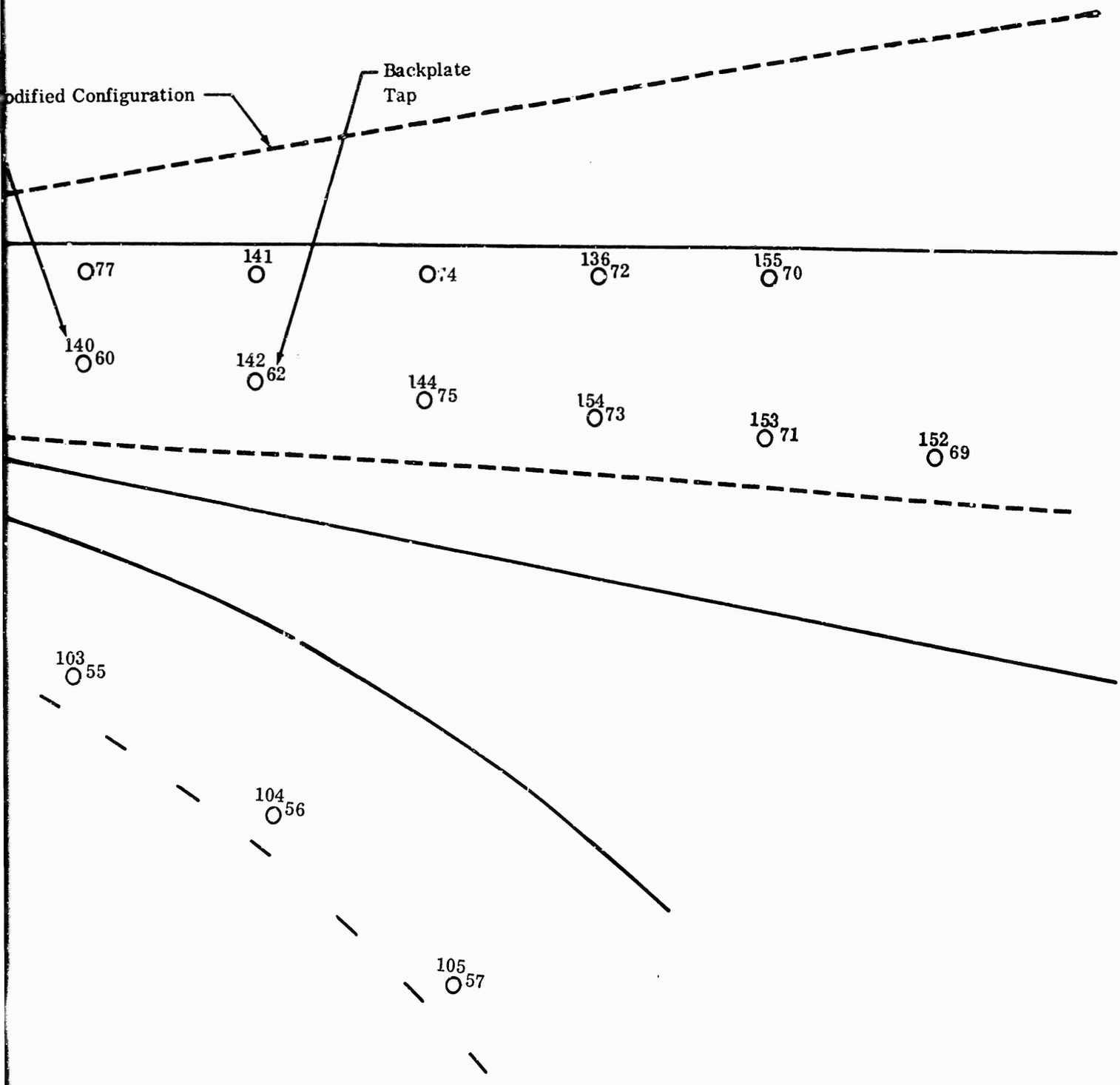


Figure 113. Diffuser Static-Pressure Instrumentation, DI-X1-2 and DI-X1-3.



1 - 2 and DI - X1 - 3
0.020 inches larger.


odified Configuration
Backplate
Tap
77
141
74
136
72
155
70
140
60
142
62
144
75
154
73
153
71
152
69
103
55
104
56
105
57

CI-2-2 PRESSURE SURVEY

TEST NO. 3327 SPEED = 50000 AIR FLOW = 2.51

IGV = REMOVED THROAT AREA = 100 % RADIUS RATIO = 1.06

LINE NO. 3 δ = 0.985

ALL PRESSURES ARE IN PSIA

TAP NO.	STATIC PRESSURE	TAP NO.	STATIC PRESSURE	TAP NO.	STATIC PRESSURE	TAP NO.	STATIC PRESSURE	TAP NO.	STATIC PRESSURE	TAP NO.	STATIC PRESSURE
1	58.0	2	58.4	3	60.4	4	81.5	5	71.2	6	60.4
7	67.0	8	69.1	9	59.8	10	66.4	11	61.7	12	66.7
13	61.9	15	62.2	16	66.9	17	55.7	19	61.9	20	65.0
21	64.3	22	63.5	23	65.5	24	63.6	25	69.9	27	70.6
28	66.7	29	57.5	30	64.3	31	73.1	32	70.5	33	67.7
34	83.6	35	83.9	36	85.1	37	84.8	38	85.8	39	83.3
40	60.8	41	57.0	42	58.2	43	58.5	44	62.2	45	63.1
46	63.1	47	63.3	48	59.6	49	75.0	50	0.0	51	88.7
52	58.7	53	84.8	54	61.7	55	62.1	56	60.2	57	57.5
58	63.4	59	58.3	60	97.3	62	107.5	63	114.1	64	117.4
65	98.8	66	119.3	67	119.4	68	120.7	69	121.0	70	119.5
71	119.6	72	117.5	73	117.1	74	113.6	75	113.6	77	98.5
78	81.5	79	0.0	80	0.0	81	0.0	83	0.0	86	0.0
87	0.0	90	0.0	91	0.0	92	0.0	93	0.0	95	0.0
96	0.0	97	0.0	98	0.0	99	0.0	100	0.0	102	0.0
104	0.0	105	0.0	106	0.0	107	0.0	108	0.0	110	0.0
112	0.0	115	0.0	116	0.0	117	0.0	118	65.0	118	0.0
119	0.0	120	0.0	121	0.0	122	0.0	123	0.0	124	0.0
125	0.0	127	0.0	128	0.0	129	0.0	131	0.0	132	0.0
134	0.0	135	0.0	136	0.0	138	0.0	139	0.0	140	0.0
142	0.0	144	0.0	146	0.0	147	0.0	148	0.0	149	0.0
150	0.0	151	0.0	152	0.0	153	0.0	154	0.0	155	0.0
156	0.0	157	123.1	158	124.0	159	124.5	160	124.6		

CI-2-2 PRESSURE SURVEY

TEST NO. 3332 SPEED = 50000 AIR FLOW = 2.46

IGV = REMOVED THROAT AREA = 100% RADIUS RATIO = 1.06

LINE NO. 3 $\delta = 1.00$

ALL PRESSURES ARE IN PSIA

TAP NO.	STATIC PRESSURE	TAP NO.	STATIC PRESSURE	TAP NO.	STATIC PRESSURE	TAP NO.	STATIC PRESSURE	TAP NO.	STATIC PRESSURE	TAP NO.	STATIC PRESSURE
2	62.8	3	68.4	4	89.0	5	76.7	6	61.5	7	64.2
8	73.4	9	73.4	10	72.7	11	66.9	13	64.9	15	64.4
17	58.4	19	66.3	20	69.2	21	70.8	24	68.8	25	74.0
27	75.6	28	71.7	29	76.6	31	78.4	32	87.6	33	85.7
34	94.7	35	95.1	35	95.3	36	98.4	37	98.1	38	100.5
39	98.7	40	64.2	41	59.5	42	61.9	43	63.2	44	65.4
45	66.7	46	66.7	47	67.6	48	70.5	49	87.2	50	79.4
51	99.6	52	61.9	53	98.2	54	63.3	55	63.8	56	64.8
57	62.8	58	78.9	59	66.9	60	109.7	62	119.1	63	24.3
64	129.1	65	110.4	66	131.1	68	105.4	69	133.1	70	131.2
71	131.4	72	129.0	73	128.7	74	124.7	75	125.1	77	110.6
78	96.4	84	65.6	115	0.0	118	69.3	122	94.8	127	70.6
156	0.0	157	135.9	158	136.4	159	136.5	160	136.6		

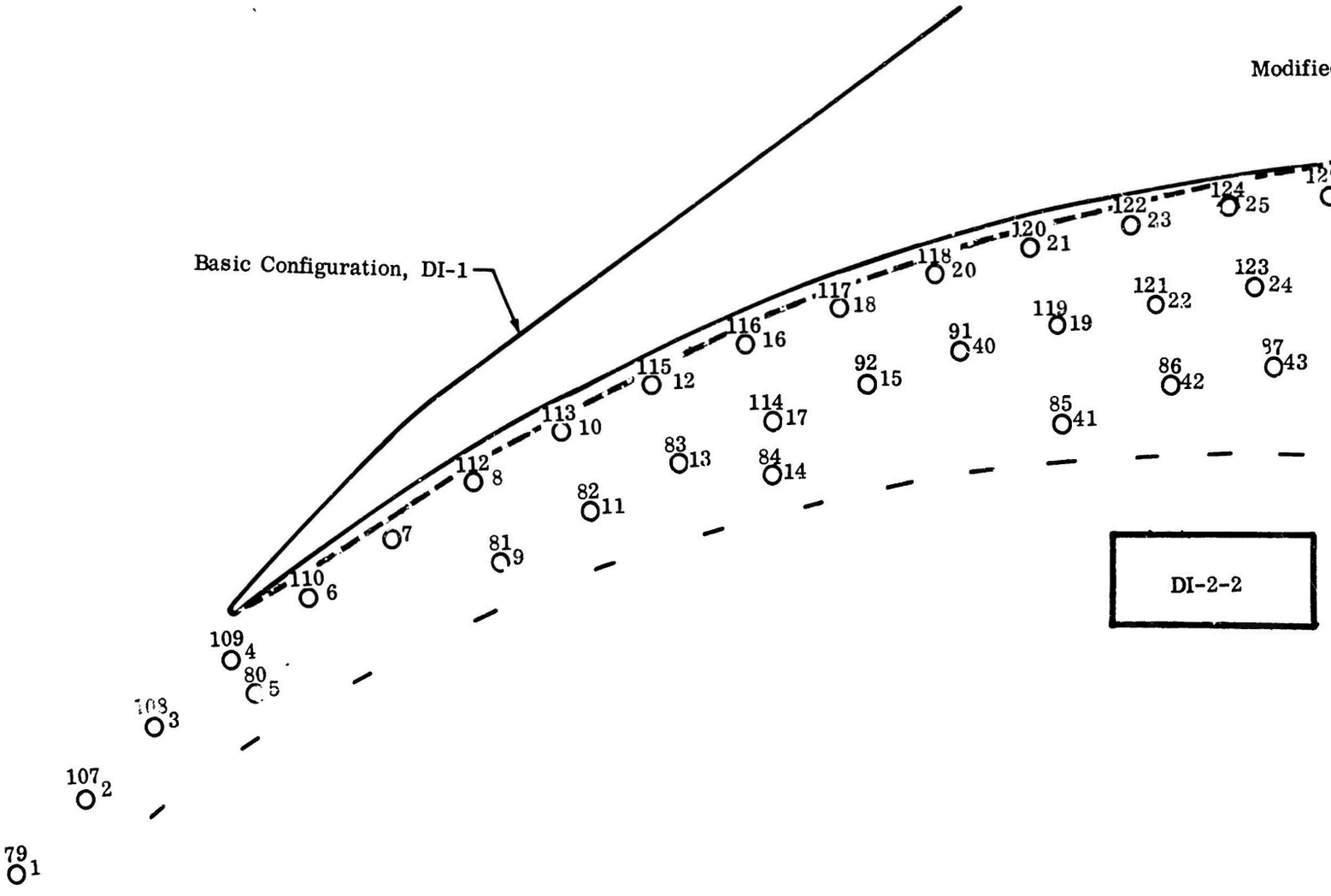
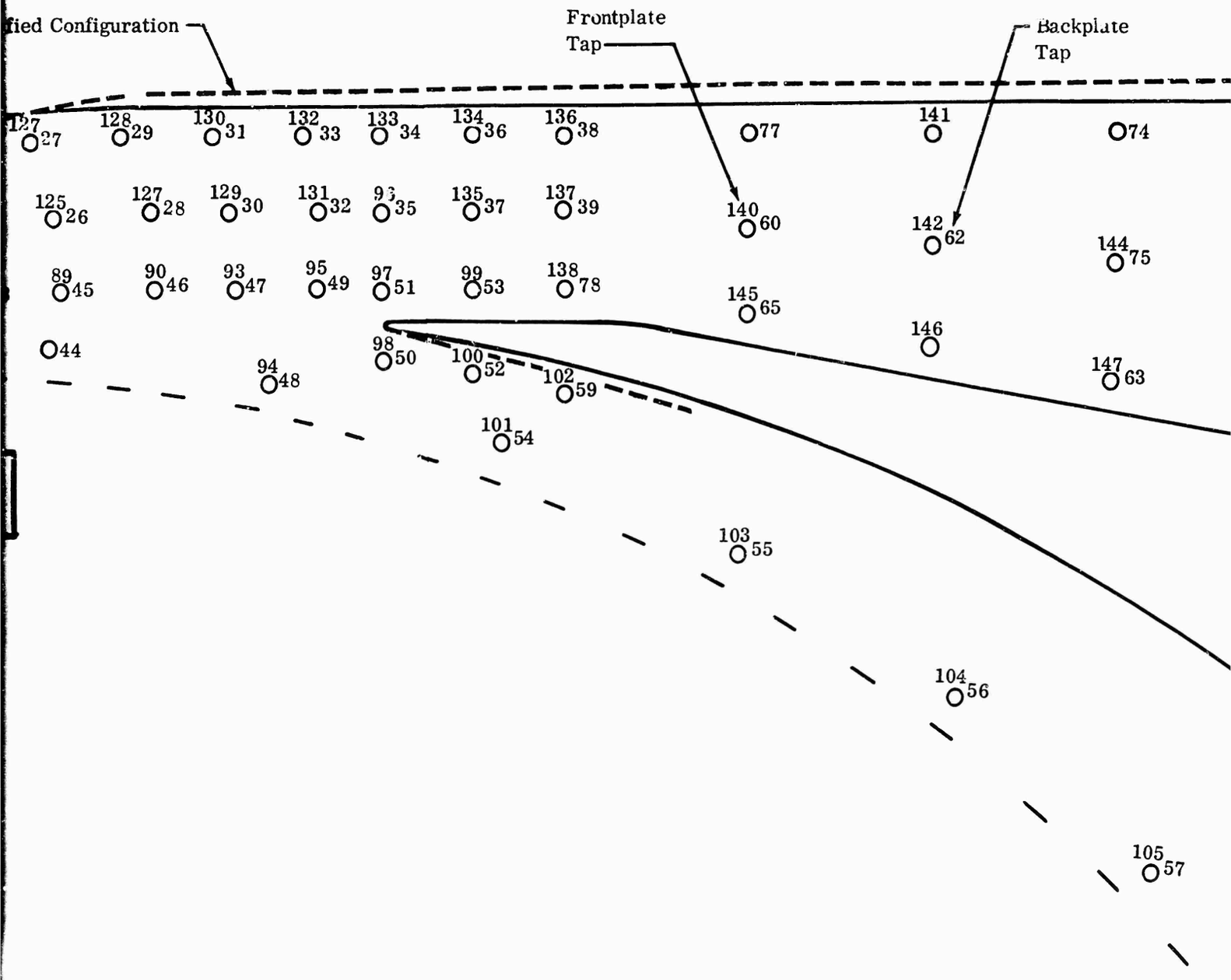
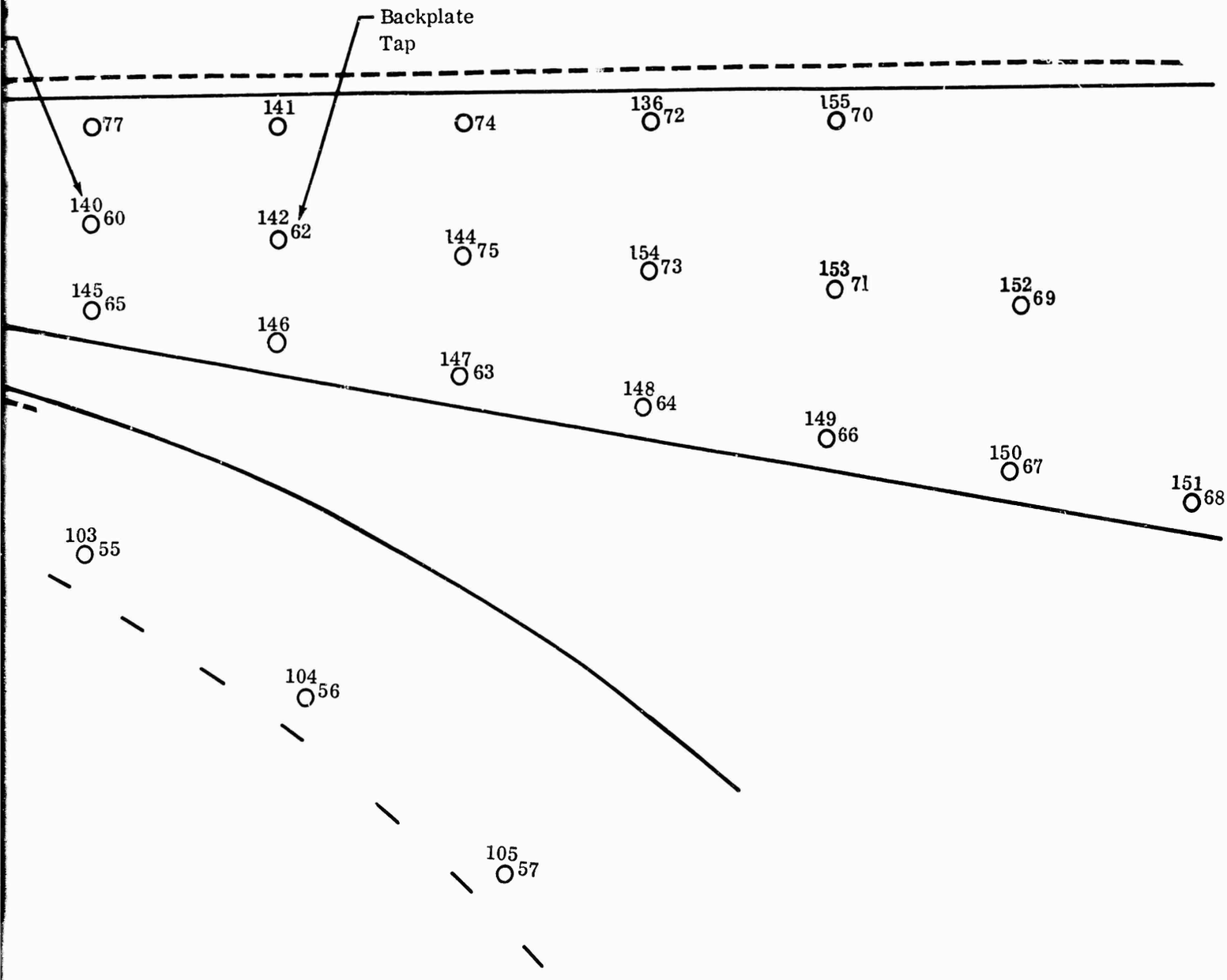


Figure 114. Diffuser Static-Pressure Instrumentation, DI-2-2.


fied Configuration
Frontplate Tap
Backplate Tap
127 27
128 29
130 31
132 33
133 34
134 36
136 38
77
141
74
125 26
127 28
129 30
131 32
93 35
135 37
137 39
140 60
142 62
144 75
89 45
90 46
93 47
95 49
97 51
99 53
138 78
145 65
146
147 63
44
94 48
98 50
100 52
102 59
101 54
103 55
104 56
105 57


Backplate
Tap
77
141
74
136
72
155
70
140
60
142
62
144
75
154
73
153
71
152
69
145
65
146
147
63
148
64
149
66
150
67
151
68
103
55
104
56
105
57

(C) APPENDIX X (U)

SCHLIEREN PHOTOGRAPHS (U)

ABSTRACT (U)

This appendix presents information on the calibration of the schlieren unit and the information obtained from the photographs. The unit was developed on a company-sponsored research program by the contractor to study diffusers for centrifugal compressors. Flow patterns for the diffusers were photographed, and a discussion of results is given in Section 7.0 of the body of this report.

1.0 OBJECTIVES

Schlieren photographs were obtained for the basic research diffusers in the compressor test rig. The objectives were to:

1) Determine whether flow at the diffuser throat entrance is steady or pulsating and relate the flow conditions to position of the impeller blades;

2) Determine shock strength and variations in shock pattern as the compressor back pressure changes (flow changes) at a constant impeller rotational speed;

3) Determine variation in shock-strength pattern with impeller rotational speed change;

4) Compare flow-pattern, shock-strength, and shock-pattern variations for the three diffuser designs.

2.0 METHOD

The schlieren unit was calibrated to obtain photographs at desired impeller blade positions (see Figure 1). Impeller movement was effectively stopped every 4 degrees (within an arc of 16 degrees), with an instantaneous light source of 1-microsecond duration. The light source for the schlieren photographs was triggered by an indexed pointer on the shaft, which actuated a magnetic proximity pickup on a stationary support. A variable time-delay device in the circuit between the light and the magnetic pickup permitted the photographs to be obtained at the desired impeller-blade position. The time-delay calibration was obtained by removing the impeller front housing and photographing the impeller at various settings (see Figure 116). Time-delay values for the desired rotational speeds and impeller-blade position are given in Table III. Schlieren photographs were obtained by opening the camera lens and energizing the circuit between the magnetic proximity pickup and light source. An automatic reset circuit prevented multiple exposures by allowing only one light source trigger impulse per frame.

Tests were run at several operating conditions for the selected impeller rotational speeds. These operating conditions are shown in Figure 117 and were selected to be near surge (Line 3), near full flow (Line 7), and midway between the extremes (Line 5).

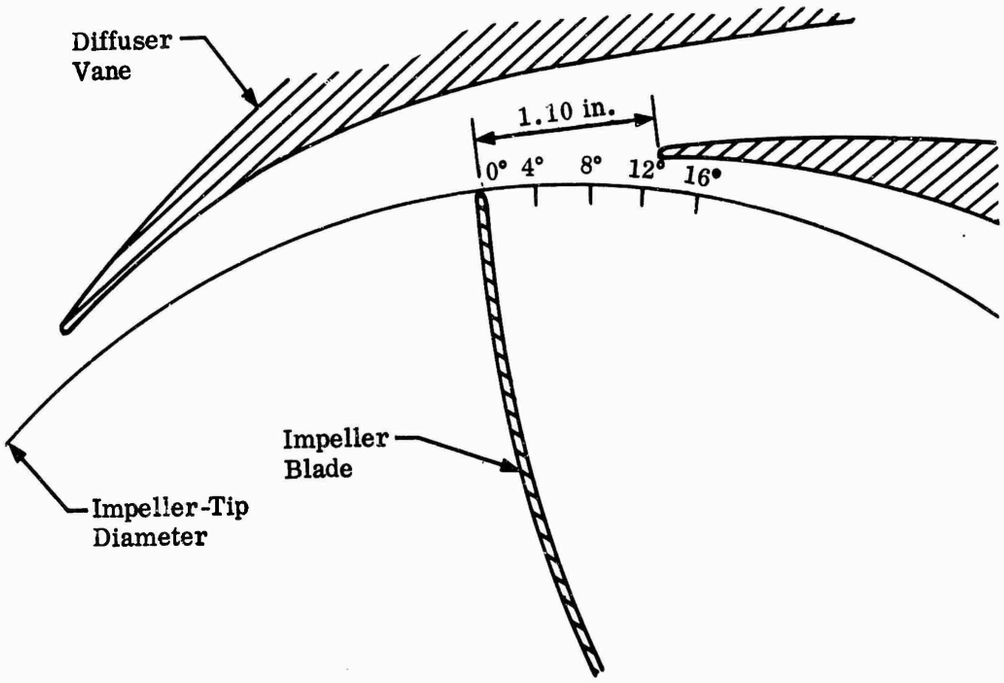
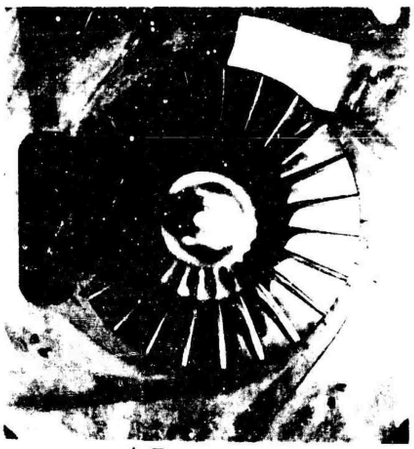


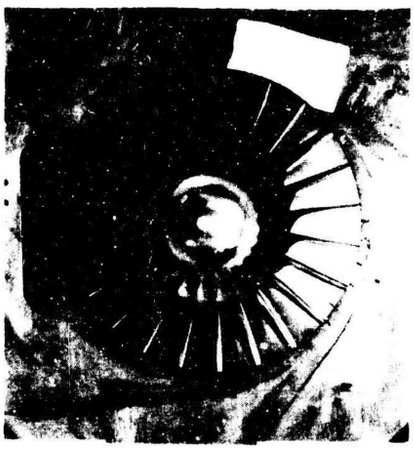
Figure 115. Impeller-Blade Positions for Schlieren Photographs.



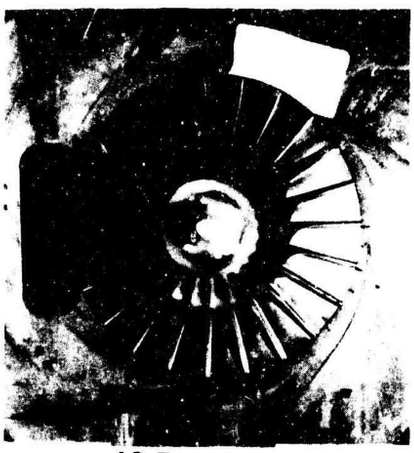
0 Degrees



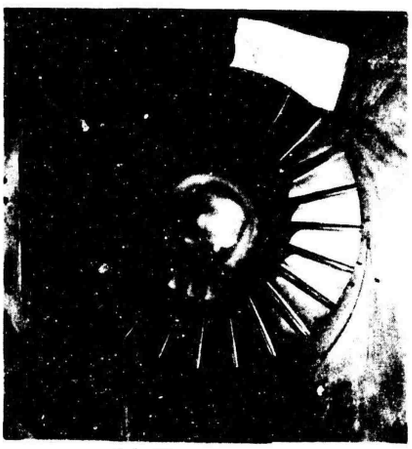
4 Degrees



8 Degrees



12 Degrees



16 Degrees

Figure 116. (C) Time-Delay Calibration. (U)

TABLE III

TIME DELAY IN MICROSECONDS

Impeller Rotational Speed (rpm)	Impeller-Blade Position (degrees)				
	0	4	8	12	16
30,000	66.7	88.9	111.1	133.3	155.5
31,000	64.5	86.1	107.5	129.0	150.5
32,000	62.5	83.3	104.2	125.0	145.8
33,000	60.6	80.8	101.0	121.2	141.3
34,000	58.8	78.5	98.0	117.6	137.2
35,000	57.1	76.2	95.2	114.2	133.3
36,000	55.5	74.2	92.6	111.1	129.6
37,000	54.1	72.2	90.1	108.1	126.1
38,000	52.7	70.2	87.7	105.3	122.8
39,000	51.2	68.3	85.5	102.5	119.6
40,000	50.0	66.7	83.3	100.0	116.6
41,000	48.8	65.1	81.3	97.6	113.8
42,000	47.7	63.5	79.3	95.3	111.1
43,000	46.5	62.0	77.5	93.0	108.5
44,000	45.4	60.7	75.7	90.9	106.0
45,000	44.4	59.3	74.0	88.8	103.7
46,000	43.4	57.9	72.4	87.0	101.4
47,000	42.6	56.7	70.9	85.2	99.2
48,000	41.7	55.5	69.4	83.3	97.2
49,000	40.8	54.4	68.0	81.7	95.2
50,000	40.0	53.3	66.7	80.0	93.3

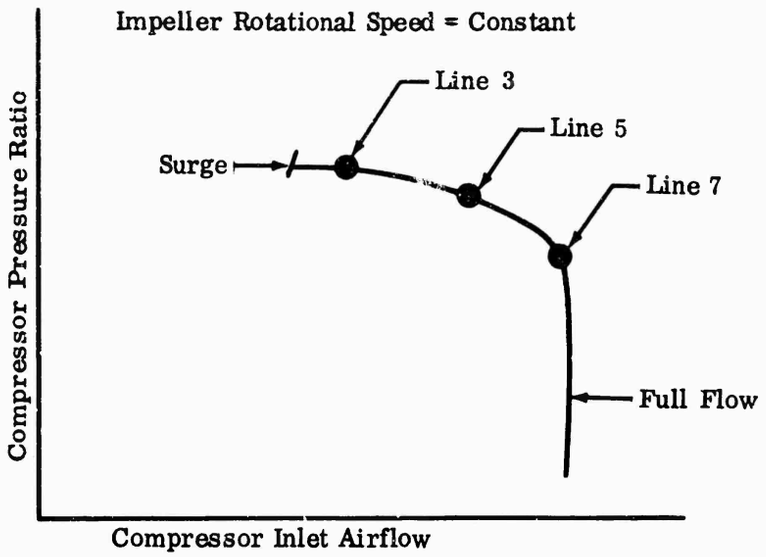


Figure 117. Test Points.

3.0 RESULTS

In light of the objectives, schlieren photographs of the basic diffuser models, showing blade positions, shock locations, and test points, are listed below.

1) Figures 118 through 122 show that the flow is steady and does not pulsate at the throat inlet.

2) Figures 122 through 124 show the variation of shock strength and pattern as compressor back pressure changes at a constant impeller rotational speed.

3) Figures 125 through 131 show the variation of shock strength and pattern as the impeller rotational speed changes.

4) Comparisons of flow patterns, shock strength, and shock patterns of the three diffuser designs are shown in the following figures:

   Figures 125 through 131, Diffuser Design DI-1;

   Figures 118 through 124 and 132 through 137, Diffuser Design DI-2;

Figures 138 through 142, Diffuser Design DI-3;

Figure 143, modification to Diffuser Design DI-1 (DI-1-2);

Figure 144, modification to Diffuser Design DI-2 (DI-X1);

Figure 145, modification to Diffuser Design DI-2 (DI-X1-2).

The diffuser modifications are described in Section 7.0 of the body of the report.

What appears as an isolated airfoil in Figure 131 and Figures 143 through 145 is a permanent etching of the glass caused by prior testing with the 16-channel (DI-3) diffuser.

A photograph of the schlieren unit provided by the contractor for this program is given in Figure 146. The test setup is shown schematically in Figure 147.

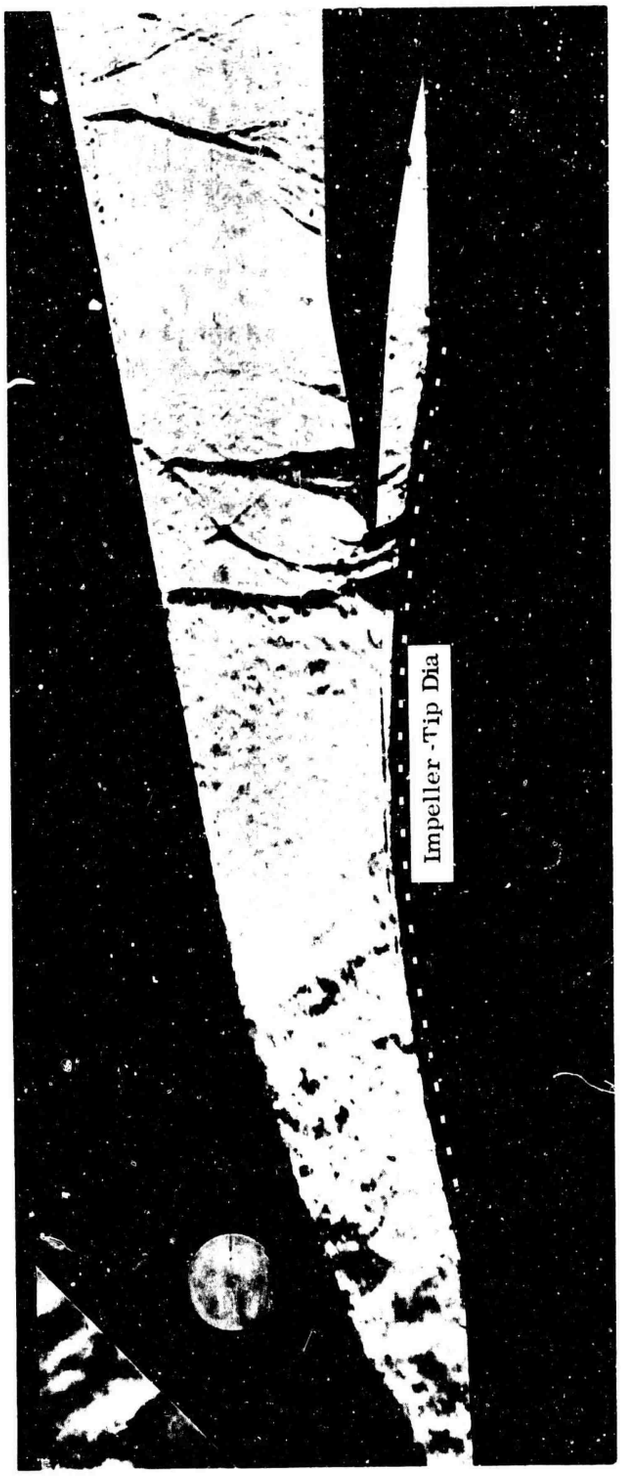


Figure 118. Schlieren Photograph of DI-2 (Test Number 3312, Impeller Position =16 Degrees, Impeller Speed = 46, 000 rpm, Data Point 5).

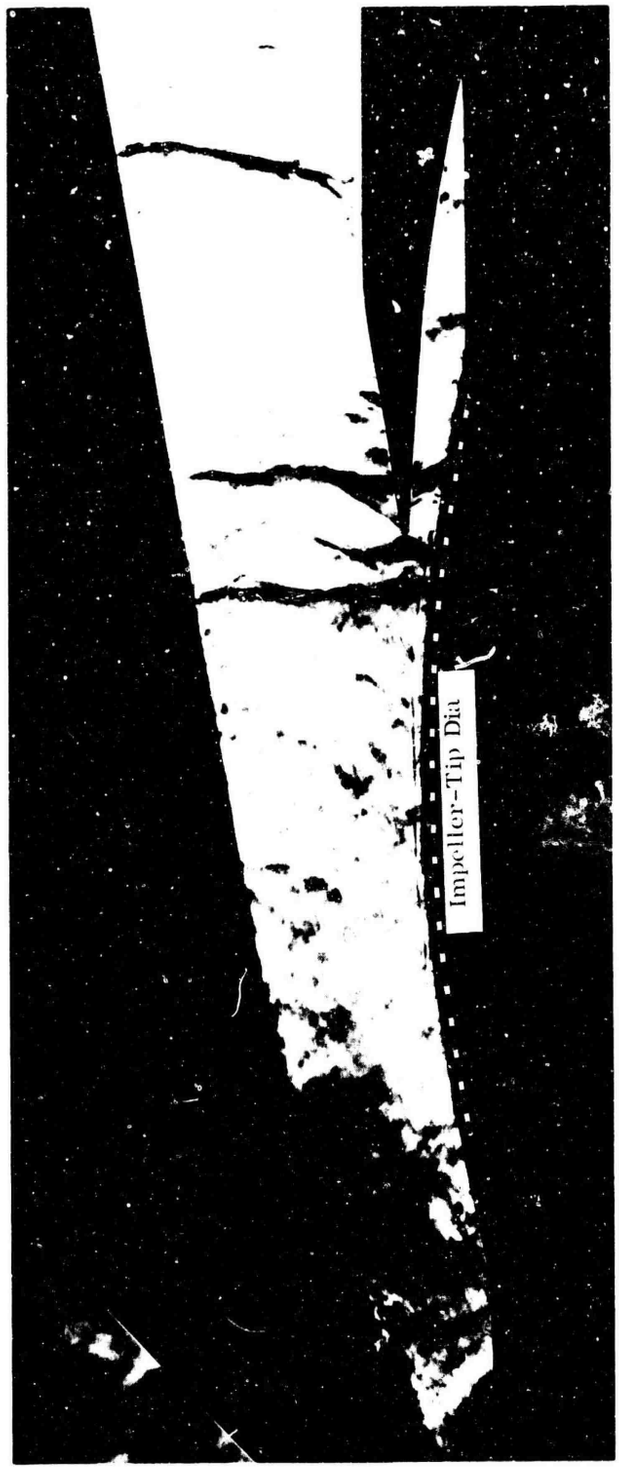


Figure 119. Schlieren Photograph of DI-2 (Test Number 3312, Impeller Position =12 Degrees, Impeller Speed = 46, 000 rpm, Data Point 5).

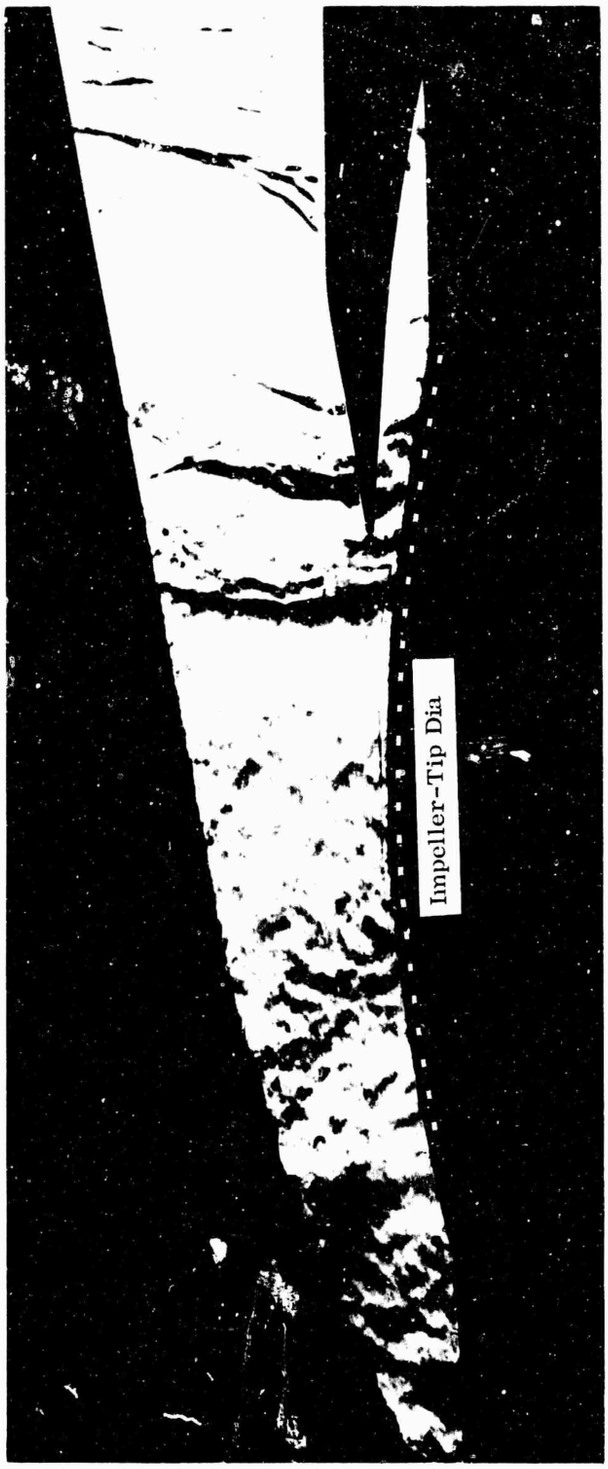


Figure 120. Schlieren Photograph of DI-2 (Test Number 3312, Impeller Position = 8 Degrees, Impeller Speed = 46, 000 rpm, Data Point 5).



Figure 121. Schlieren Photograph of DI-2 (Test Number 3312, Impeller Position = 4 Degrees, Impeller Speed = 46,000 rpm, Data Point 5).



Figure 122. Schlieren Photograph of DI-2 (Test Number 3312, Impeller Position = 0 Degrees, Impeller Speed = 46,000 rpm, Data Point 5).



Figure 123. Schlieren Photograph of DI-2 (Test Number 3312, Impeller Speed = 46,000 rpm, Data Point 3).

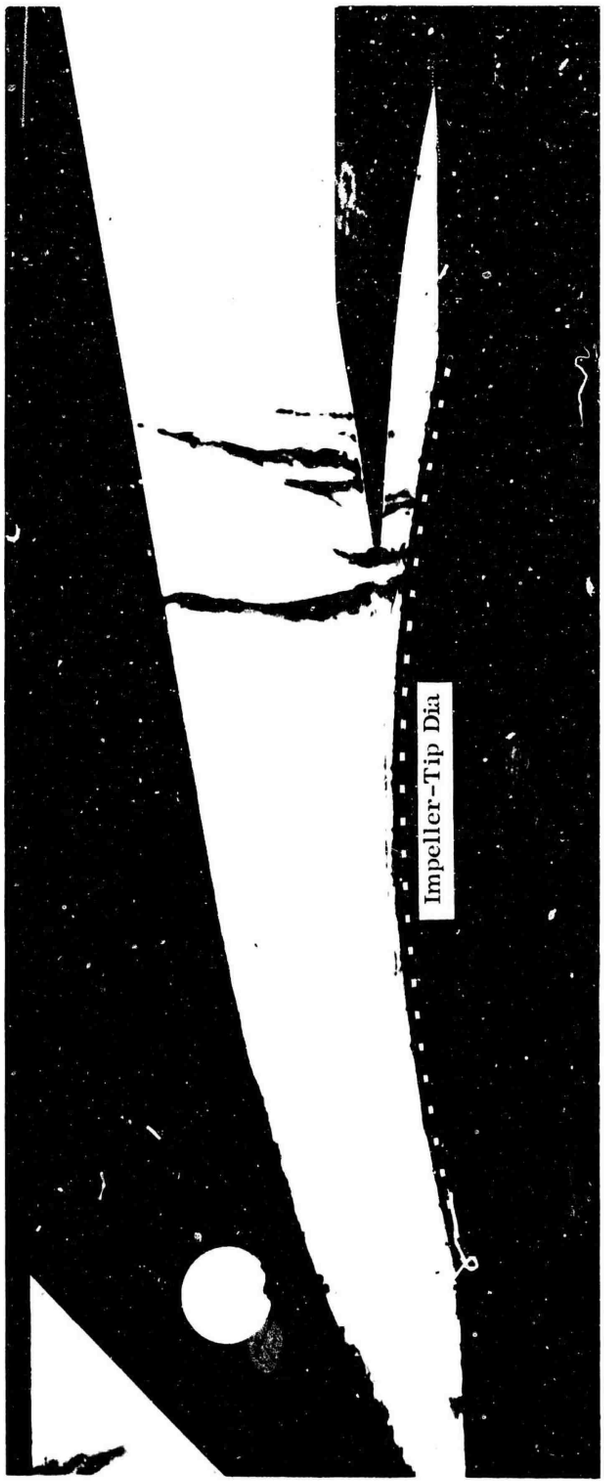


Figure 124. Schlieren Photograph of DI-2 (Test Number 3312, Impeller Speed = 46,000 rpm, Data Point 7).

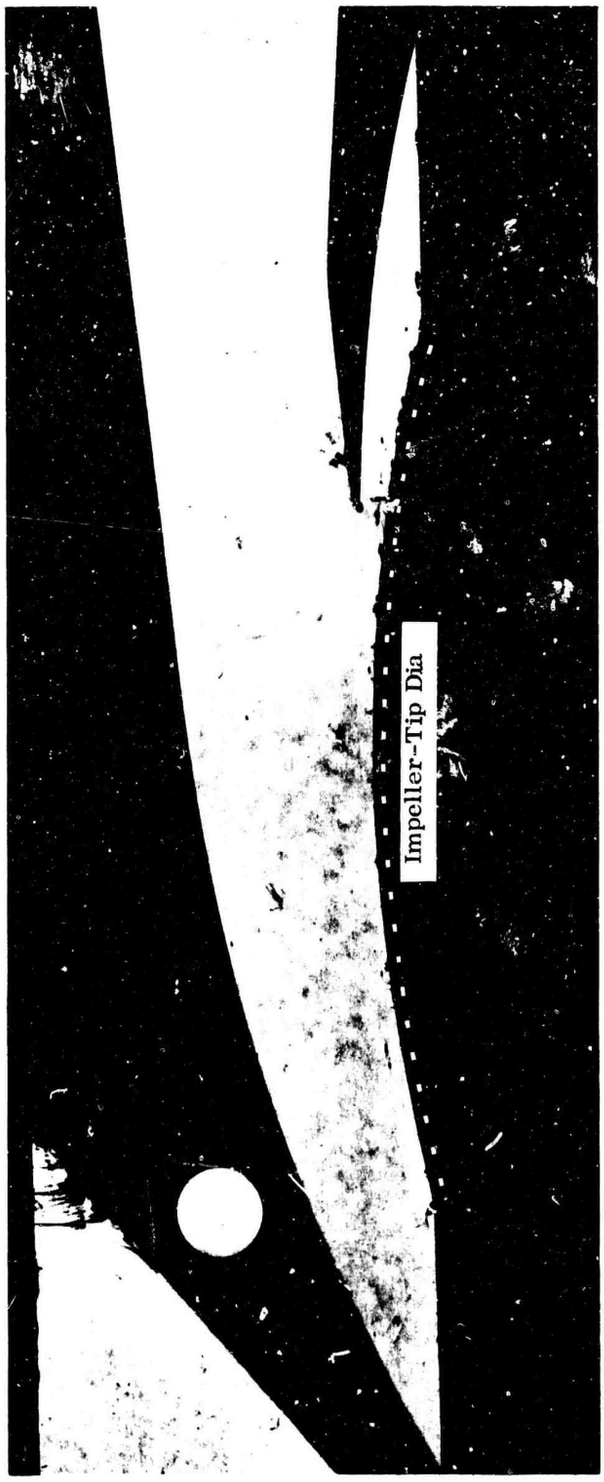


Figure 125. Schlieren Photograph of DI-1 (Test Number 3311, Impeller Speed = 15,000 rpm, Data Point 5).

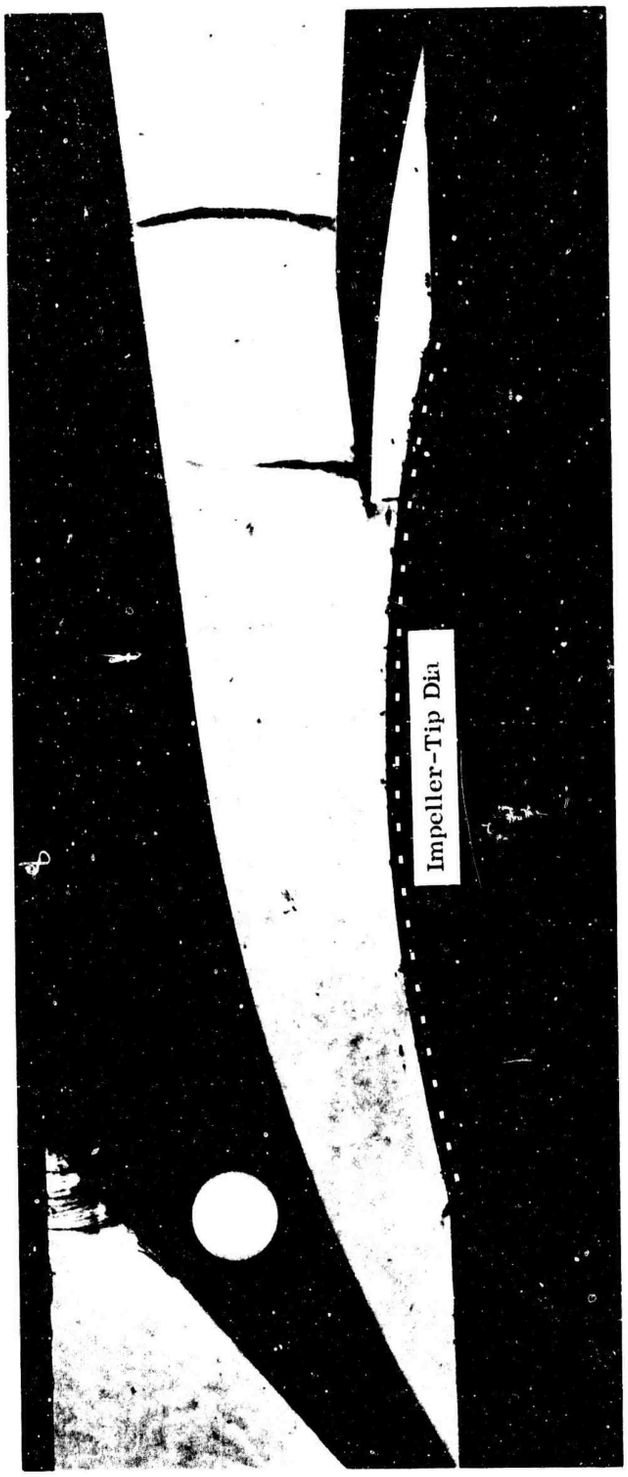


Figure 126. Schlieren Photograph of DI-1 (Test Number 3311, Impeller Speed = 20,000 rpm, Data Point 5).

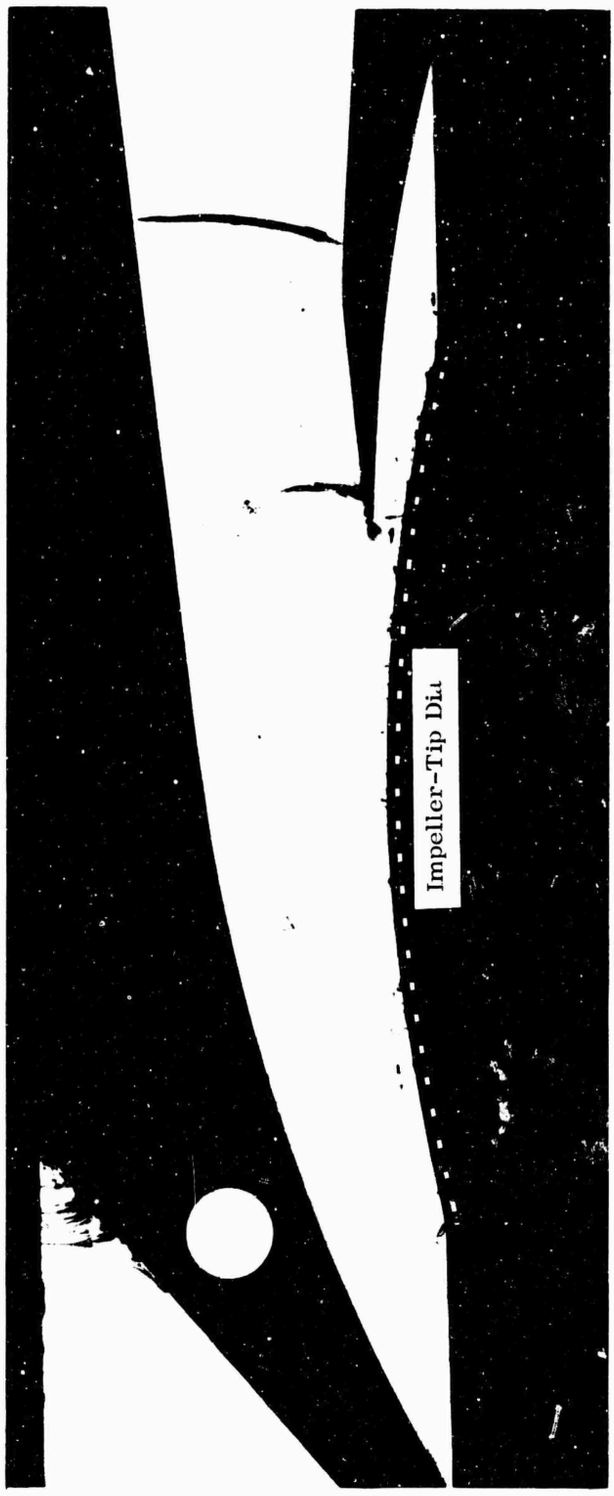


Figure 127. Schlieren Photograph of DI-1 (Test Number 3311, Impeller Speed = 25,000 rpm, Data Point 5).



Figure 128. Schlieren Photograph of DI-1 (Test Number 3311, Impeller Speed = 30,000 rpm, Data Point 5).



Figure 129. Schlieren Photograph of DI-1 (Test Number 3311, Impeller Speed = 35,000 rpm, Data Point 5).

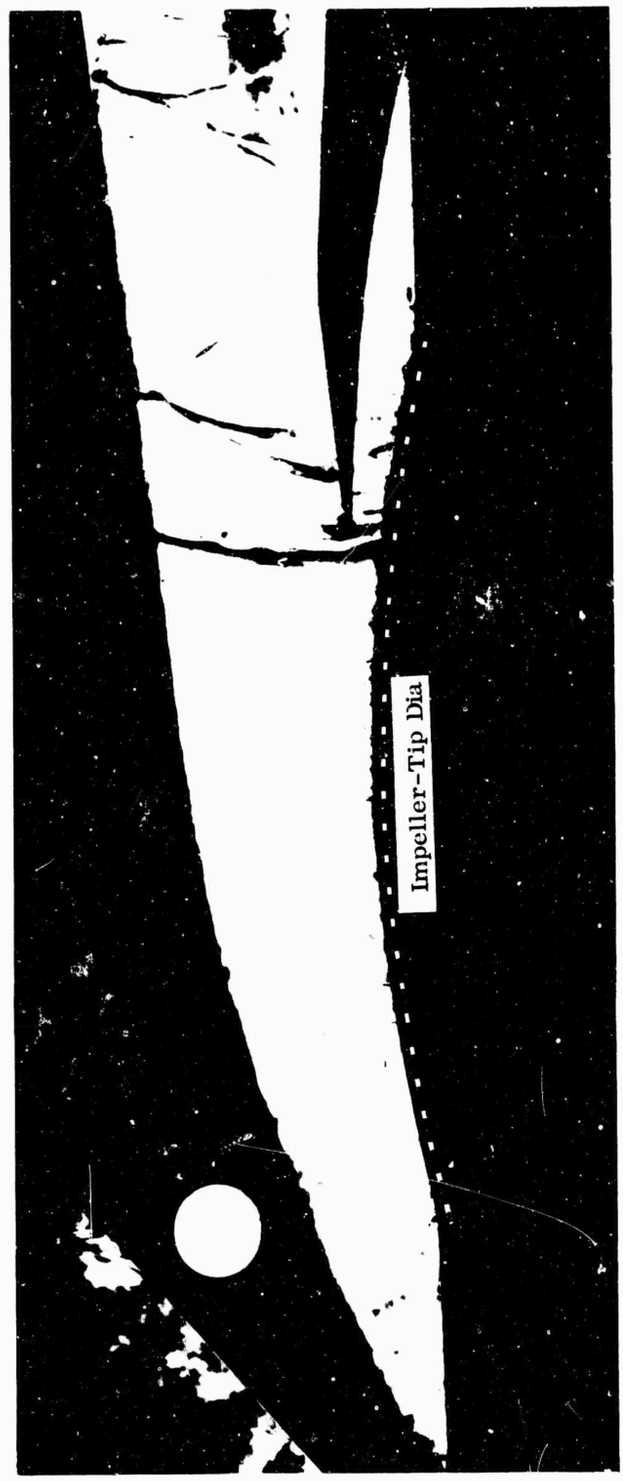


Figure 130. Schlieren Photograph of DI-1 (Test Number 3311, Impeller Speed = 46,000 rpm, Data Point 5).

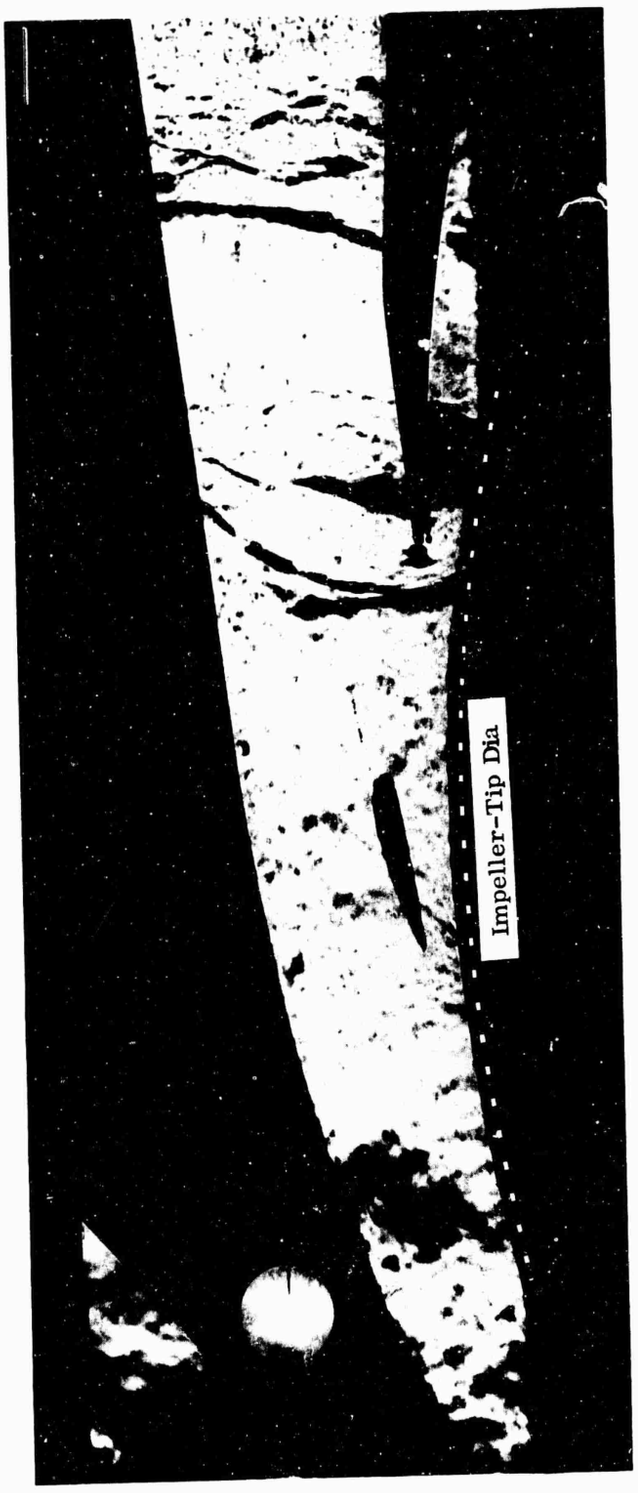


Figure 131. Schlieren Photograph of DI-1 (Test Number 3317, Impeller Speed = 50, 000 rpm, Data Point 5).

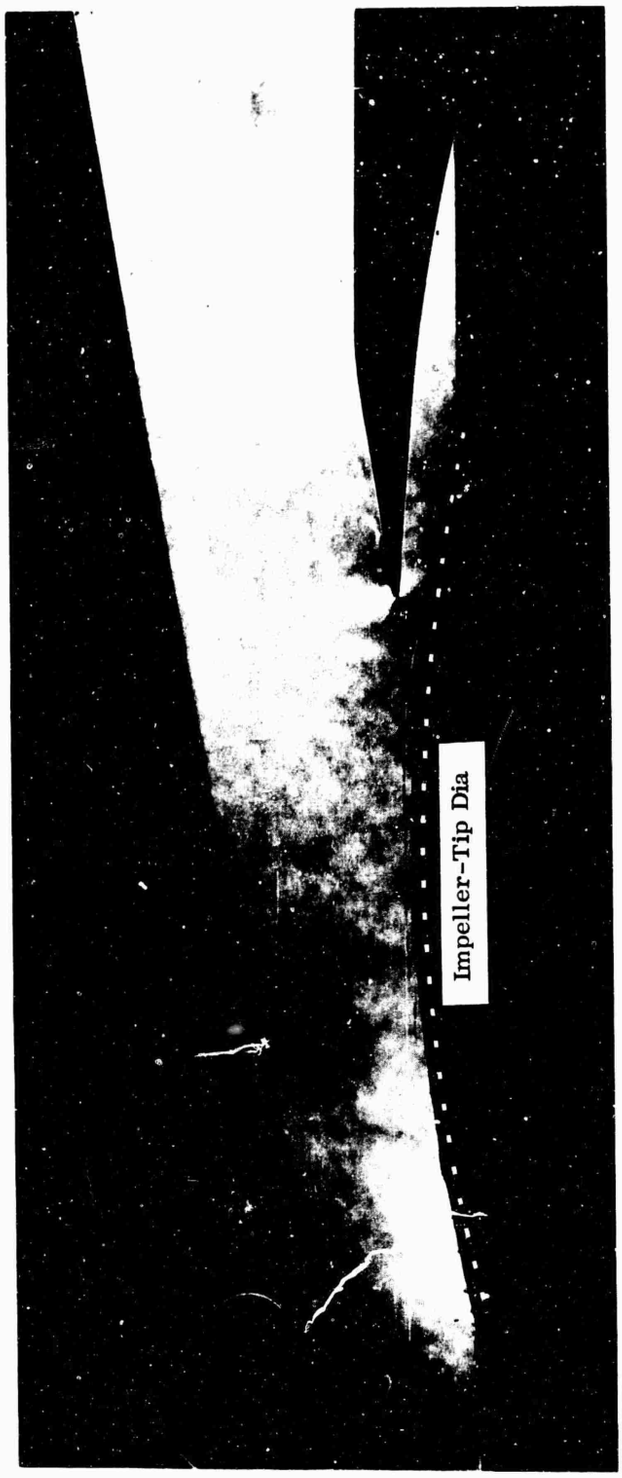


Figure 132. Schlieren Photograph of DI-2 (Test Number 3312, Impeller Speed = 20,000 rpm, Data Point 5).



Figure 133. Schlieren Photograph of DI-2 (Test Number 3312, Impeller Speed = 25,000 rpm, Data Point 5).

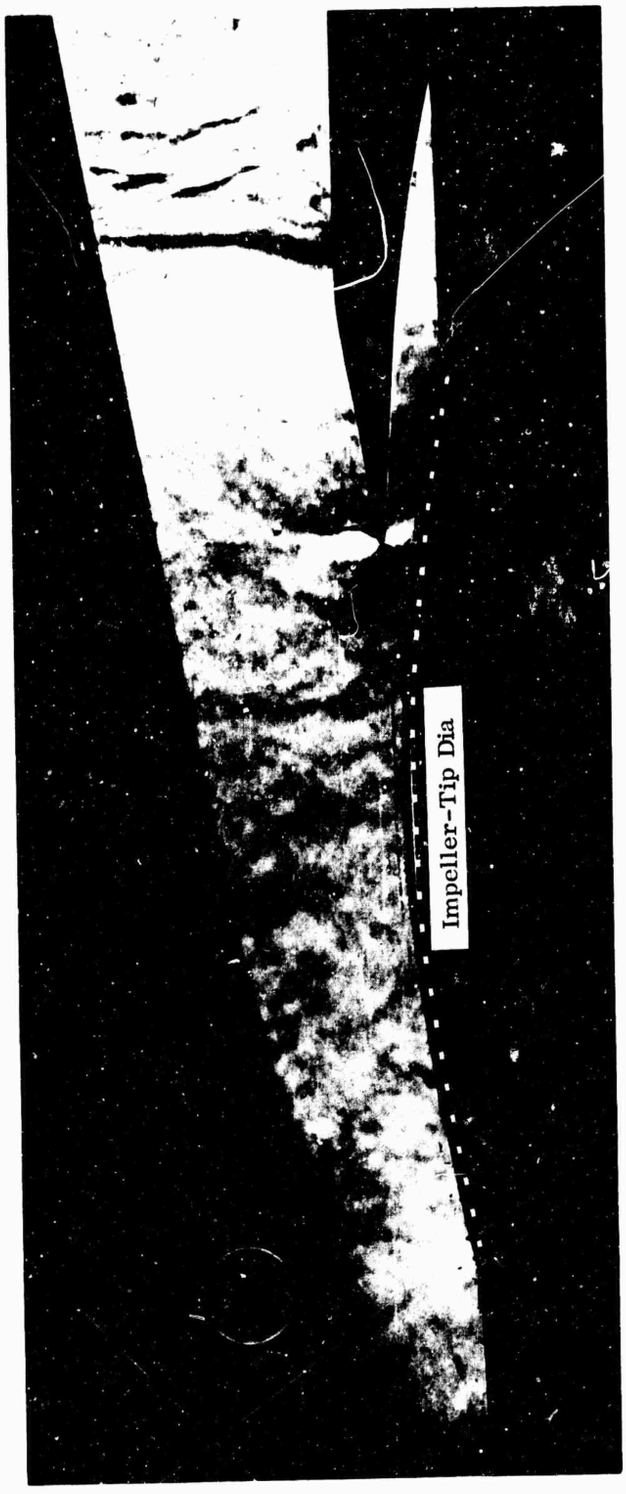


Figure 134. Schlieren Photograph of DI-2 (Test Number 3312, Impeller Speed = 30,000 rpm, Data Point 5).

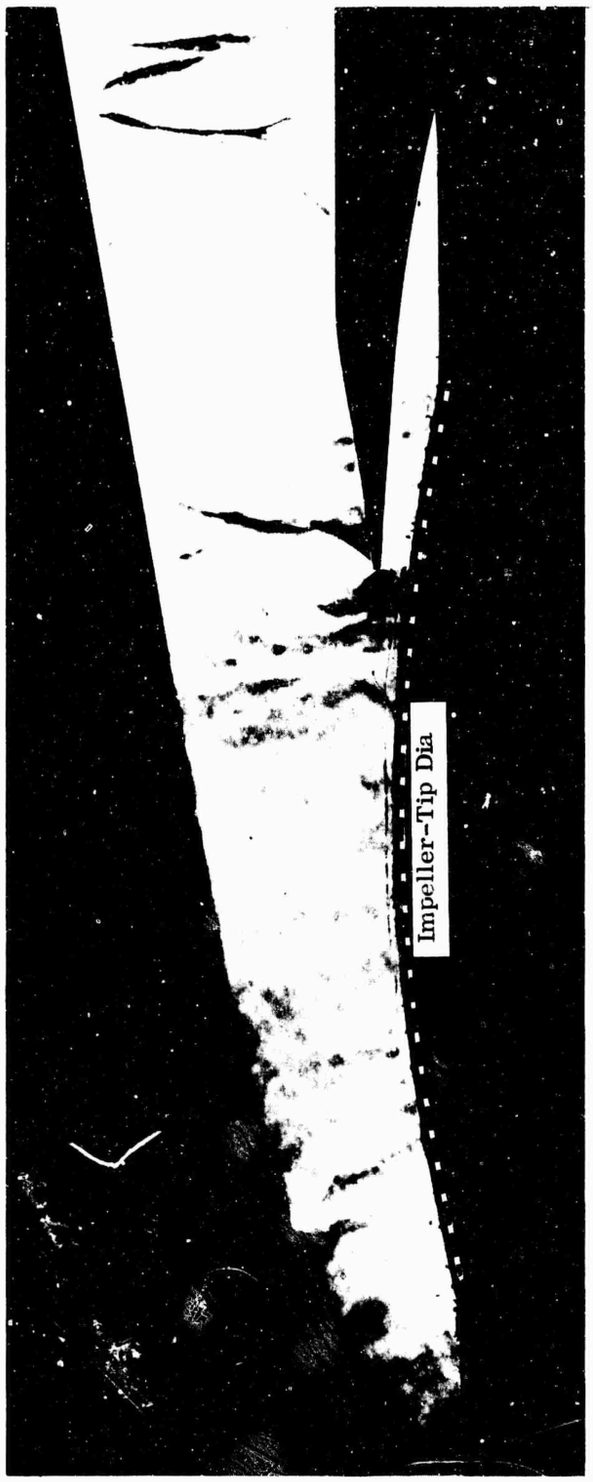


Figure 135. Schlieren Photograph of DI-2 (Test Number 3312, Impeller Speed = 35,000 rpm, Data Point 5).

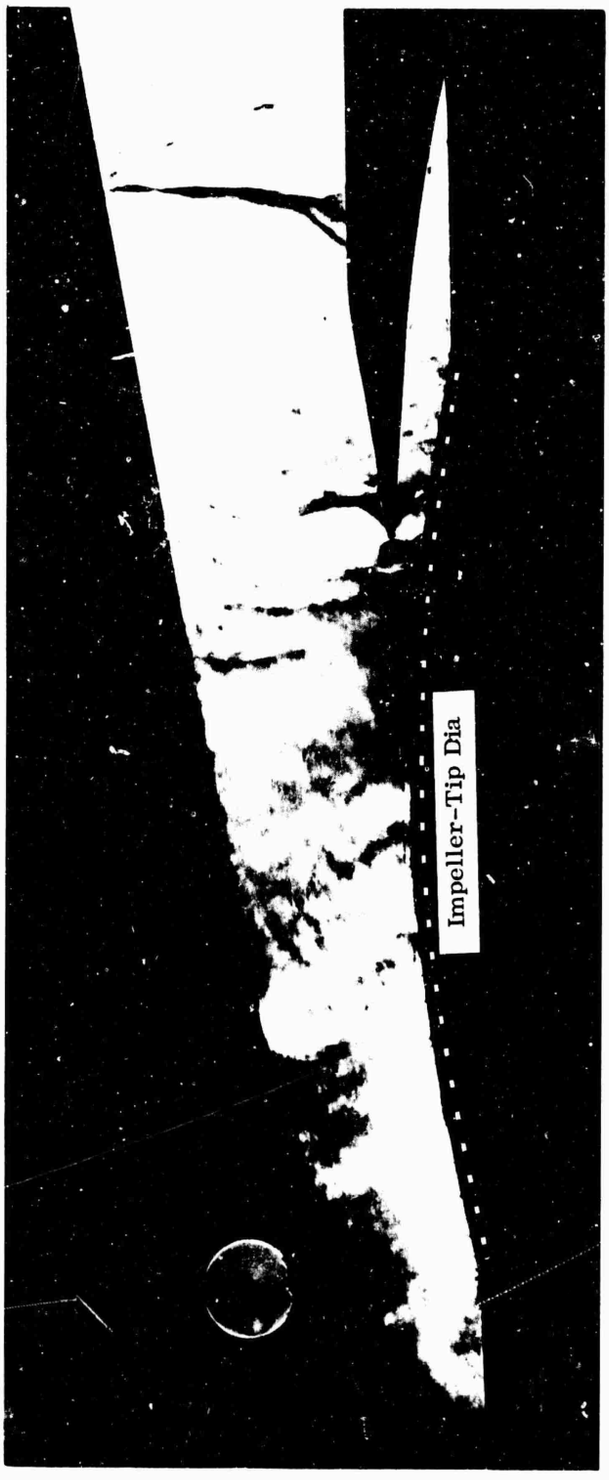


Figure 136. Schlieren Photograph of DI-2 (Test Number 3312, Impeller Speed = 39, 000 rpm, Data Point 5).

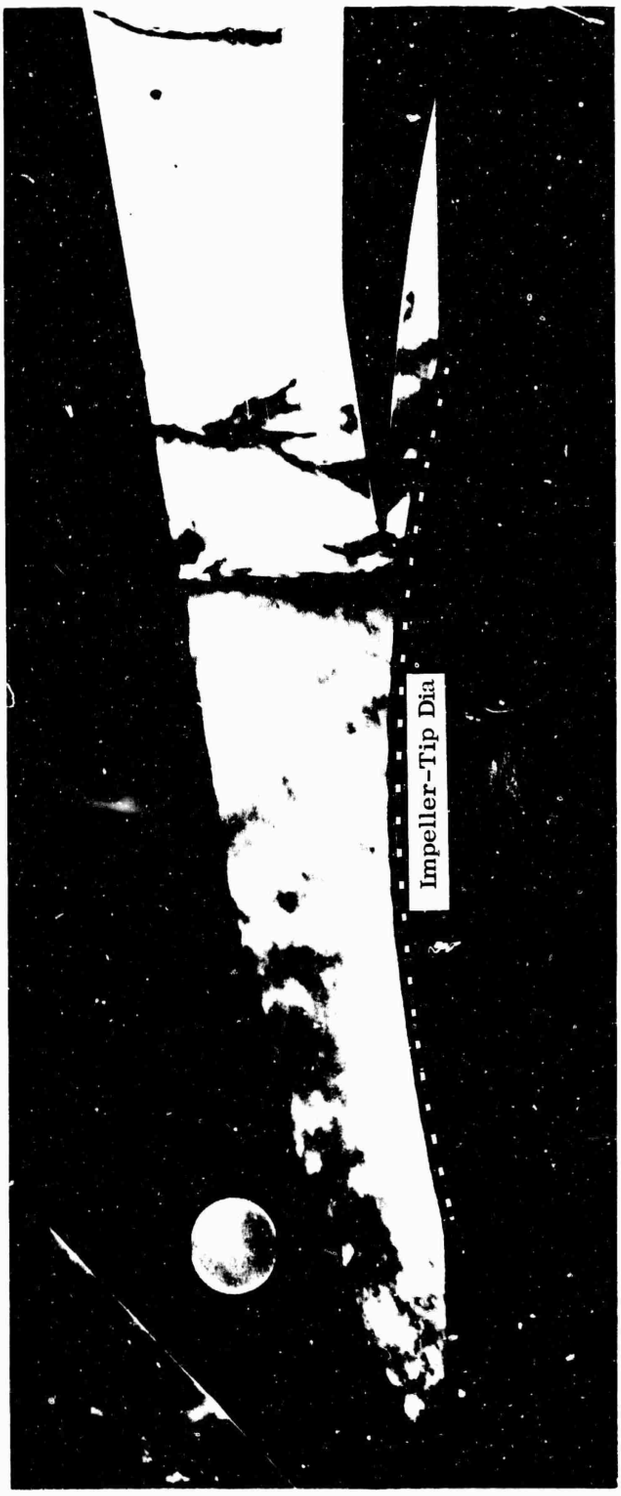


Figure 137. Schlieren Photograph of DI-2 (Test Number 3313, Impeller Speed = 46,000 rpm, Data Point 5).

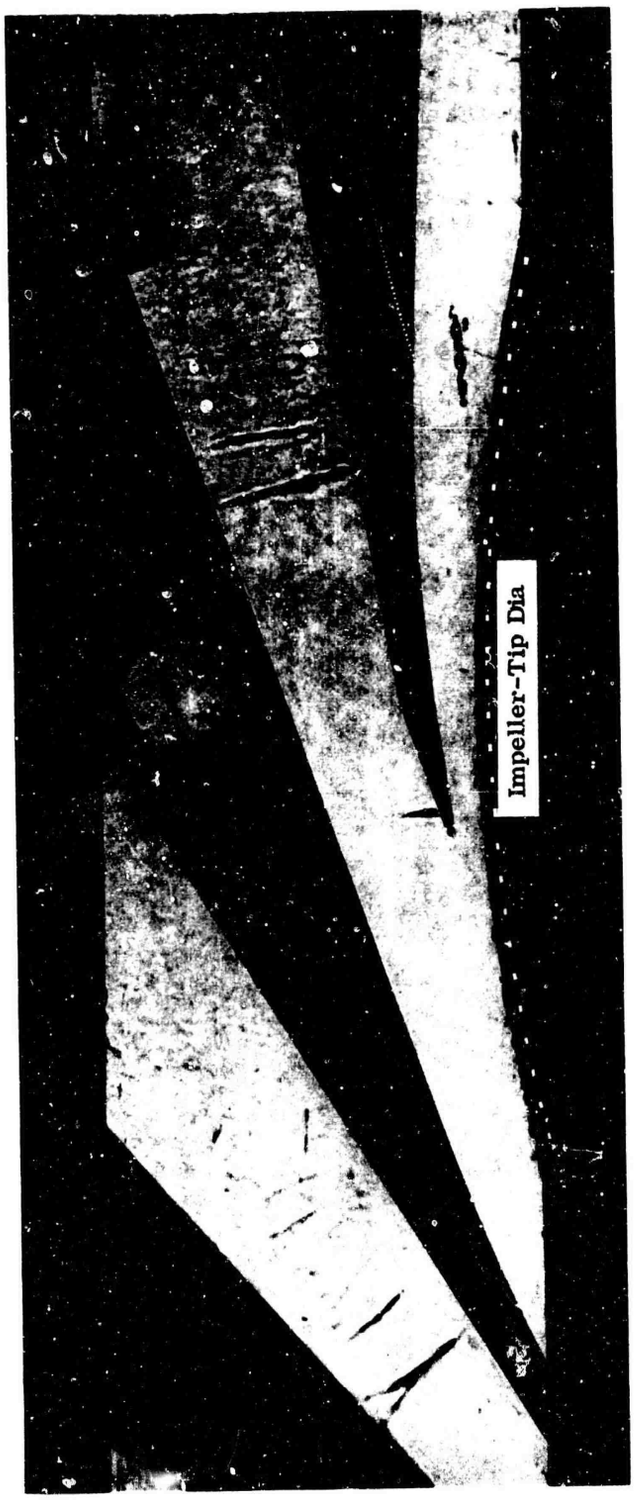


Figure 138. Schlieren Photograph of DI-3 (Test Number 3314, Impeller Speed = 25,000 rpm).

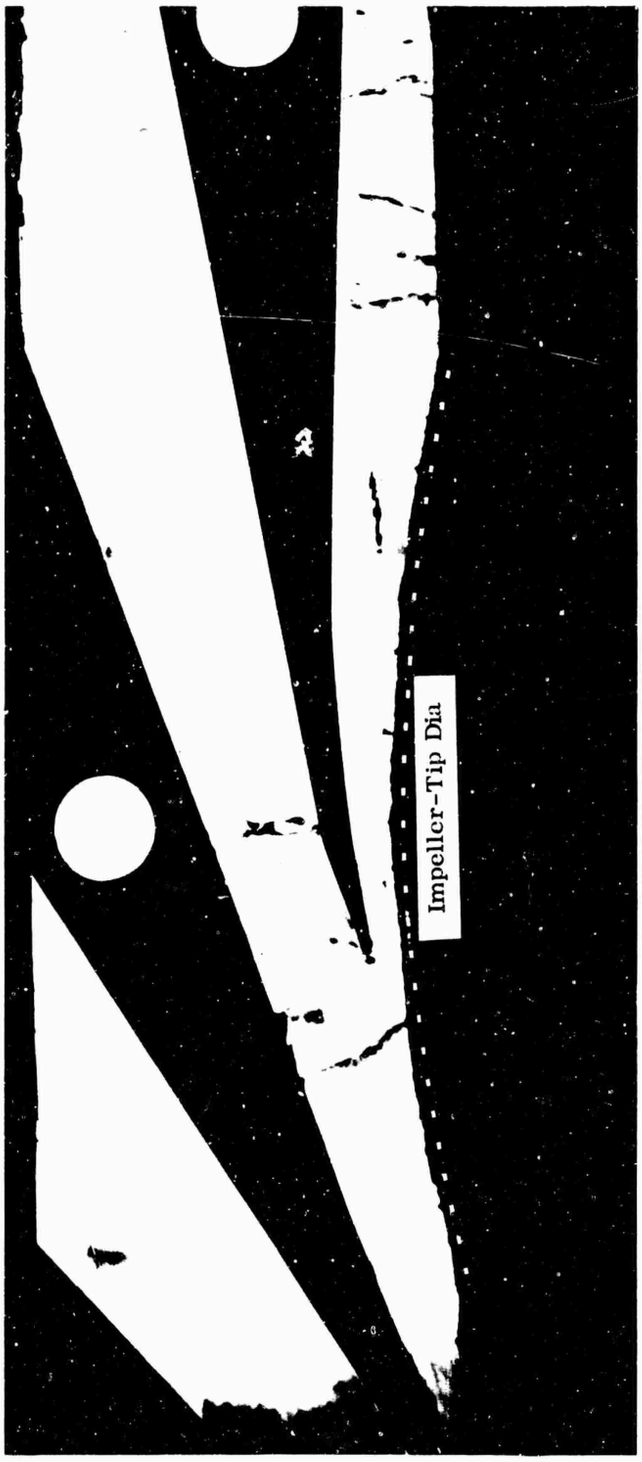


Figure 139. Schlieren Photograph of DI-3 (Test Number 3314, Impeller Speed = 46,000 rpm, Data Point 2).

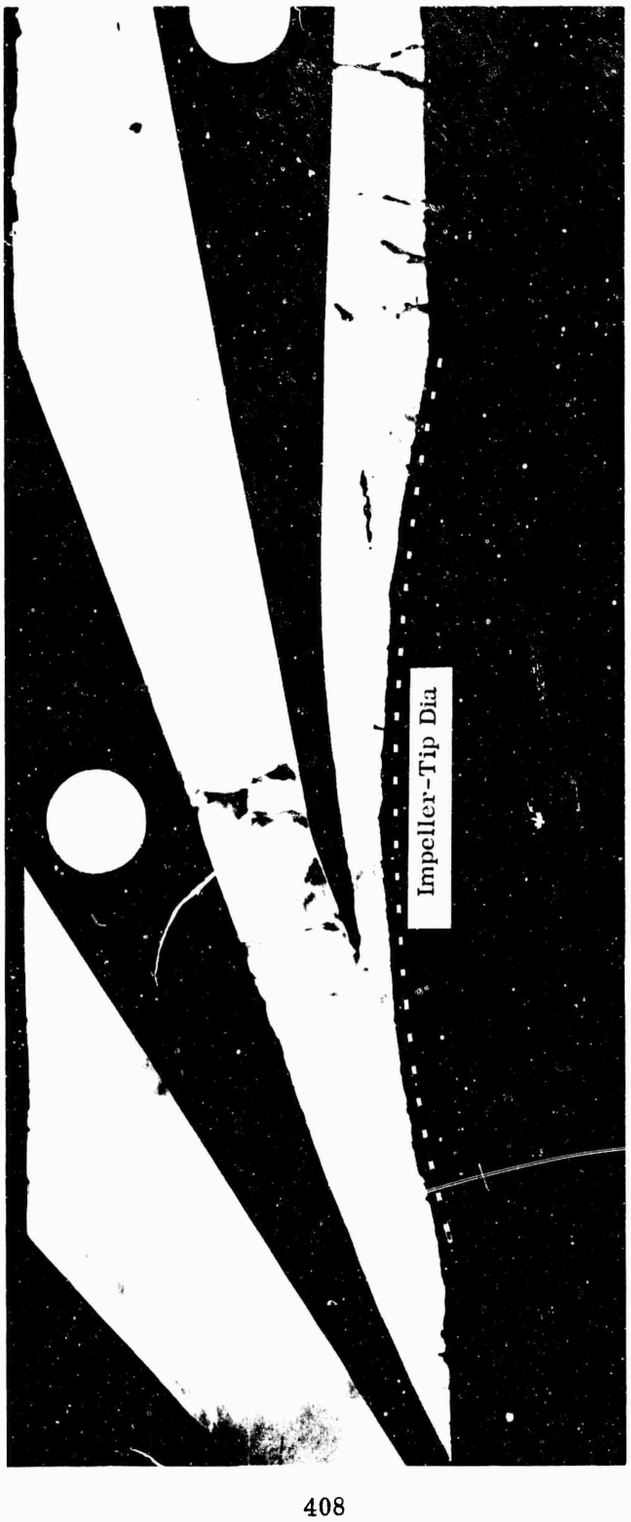


Figure 140. Schlieren Photograph of DI-3 (Test Number 3314, Impeller Speed = 46,000 rpm, Data Point 3).



Figure 141. Schlieren Photograph of DI-3 (Test Number 3314, Impeller Speed = 46,000 rpm, Data Point 5).

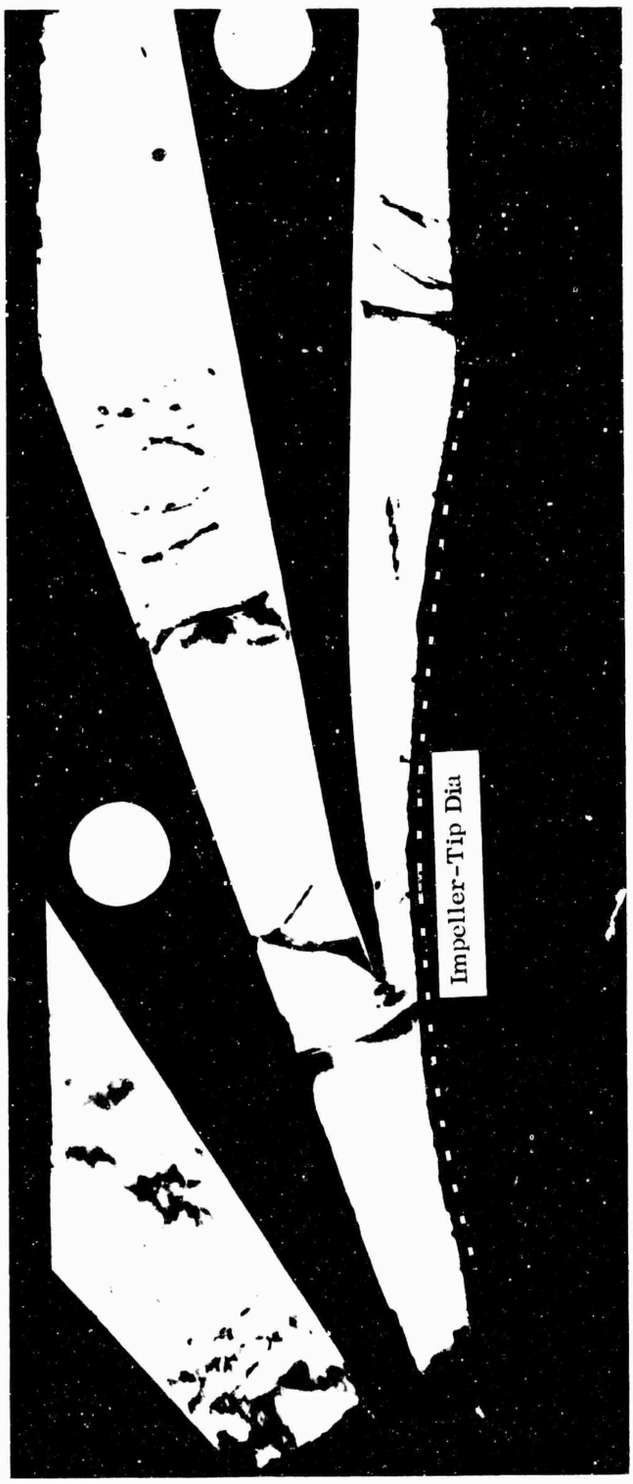


Figure 142. Schlieren Photograph of DI-3 (Test Number 3314, Impeller Speed = 46,000 rpm, Data Point 7).

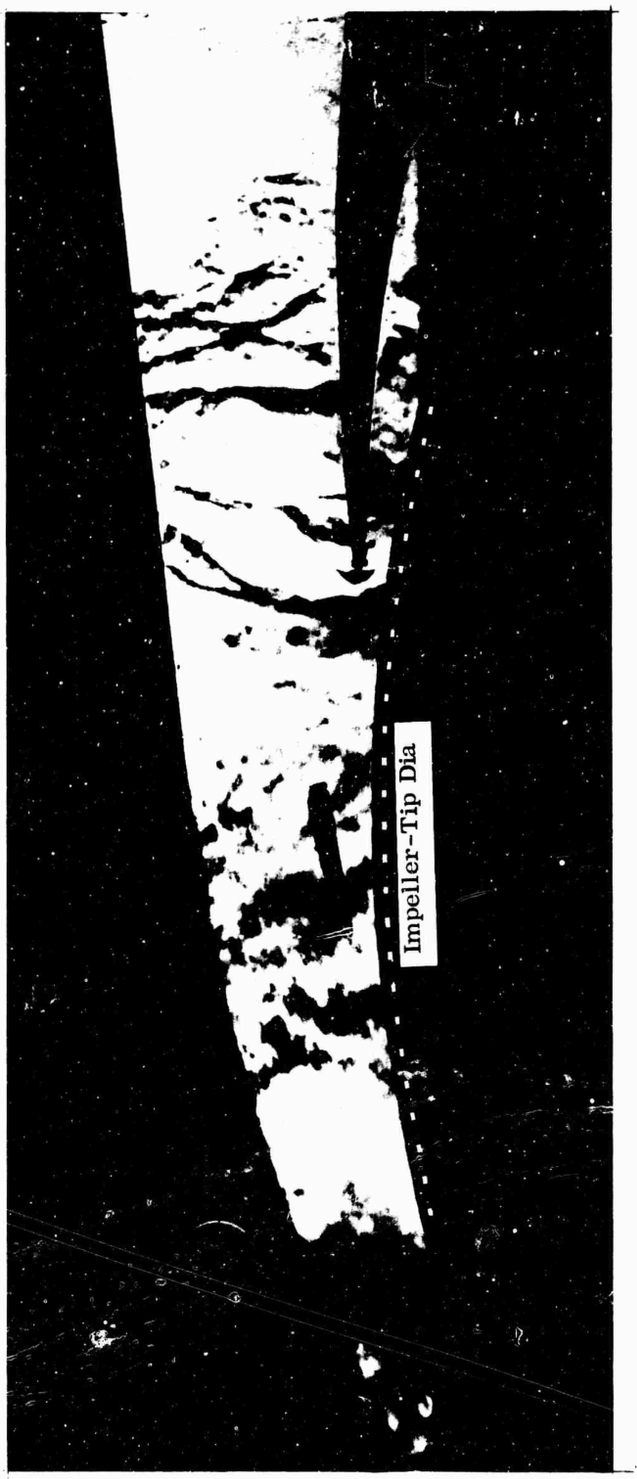


Figure 143. Schlieren Photograph of DI-1-2 (Test Number 3319, Impeller Speed = 50,000 rpm, Data Point 5).



Figure 144. Schlieren Photograph of DI-X1 (Test Number 3315, Impeller Speed = 50,000 rpm, Data Point 5).

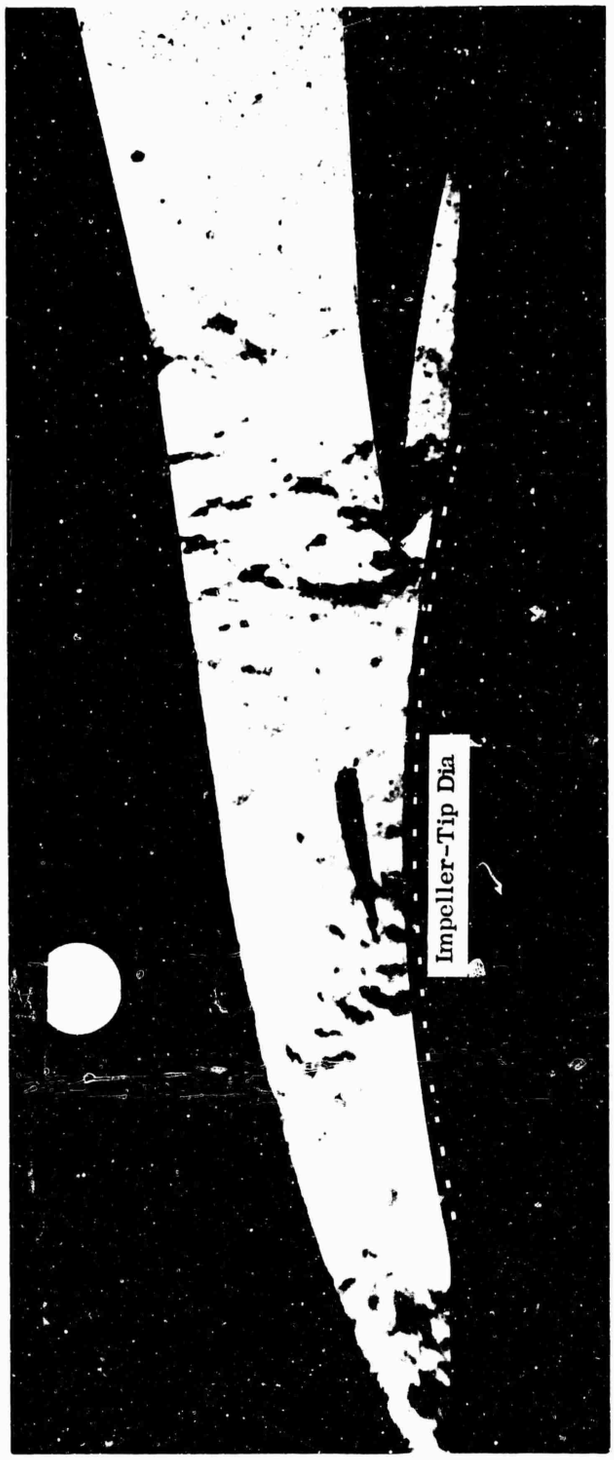


Figure 145. Schlieren Photograph of DI-X1-2 (Test Number 3318, Impeller Speed = 50,000 rpm, Data Point 5).

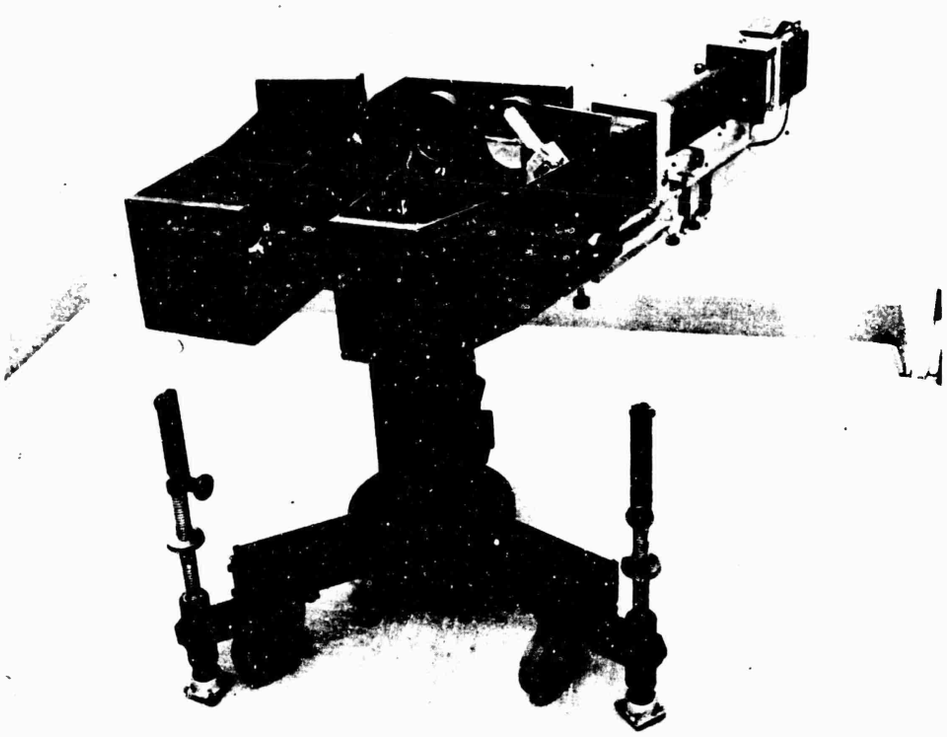


Figure 146. Schlieren Unit.

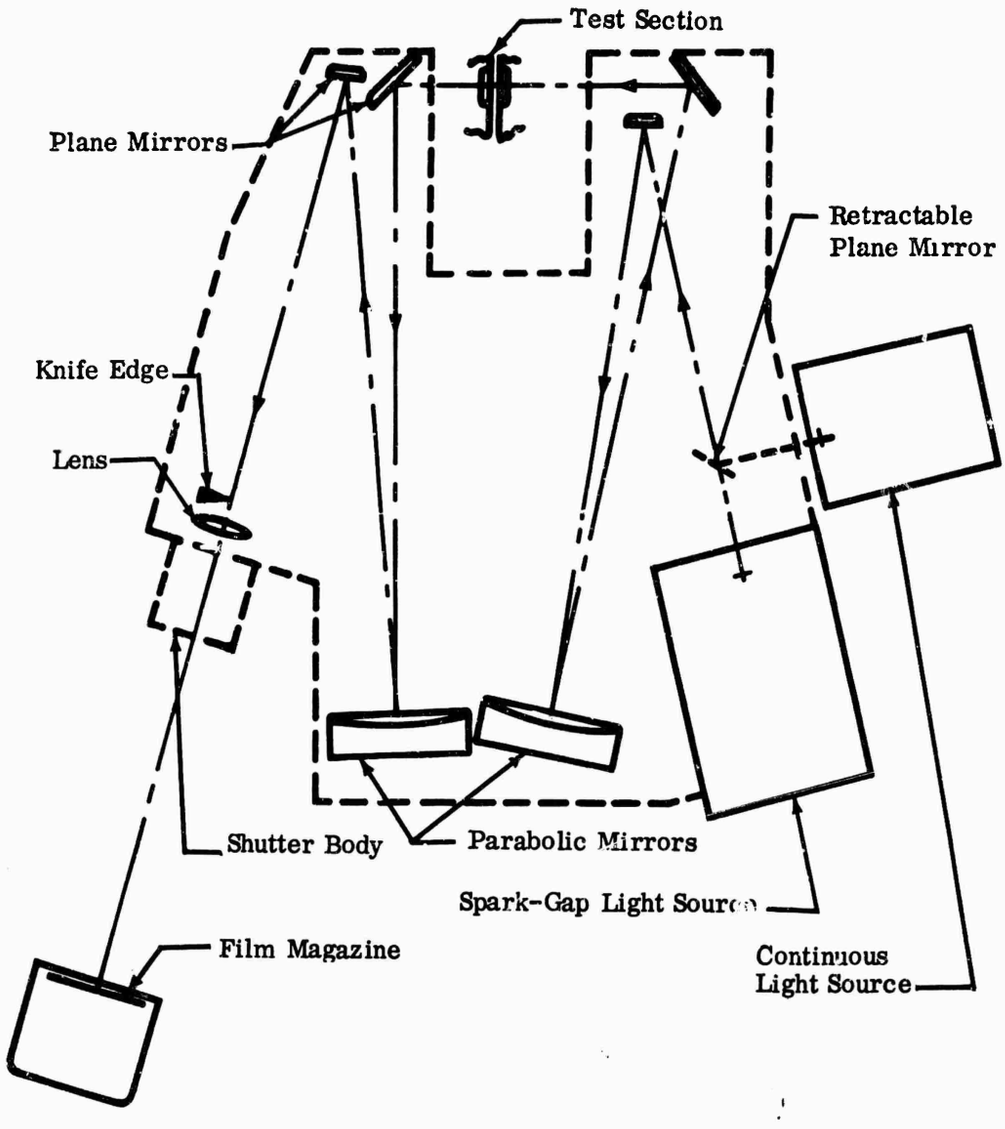


Figure 147. Schlieren Schematic Diagram.

(U) APPENDIX XI

INLET-MACH-NUMBER EFFECTS ON SUBSONIC DIFFUSER PERFORMANCE

ABSTRACT

The following literature survey and data correlation by R. M. Halleen and J. P. Johnston were accomplished by Creare, Incorporated, under a separate contract to The Boeing Company.

The survey results show the design technologies available from the literature on high subsonic diffusers that have stable boundary-layer and uniform conditions at the inlet; they also show various geometric limitations.

SYMBOLS

$\frac{A}{A}$ = area ratio

B_1 = ratio of inlet boundary-layer blockage area to the inlet cross-sectional area (see Reference 11)

C_p = pressure-recovery coefficient — $(P_2 - P_1)/\bar{q}_1$

C_p^* = locus of maximum pressure-recovery coefficient at prescribed nondimensional length (see Reference 11)

C_p^{**} = locus of maximum pressure-recovery coefficient at prescribed area ratio (see Reference 11)

L = axial length

M = Mach number

N = nondimensional axial length: L/R_1 for conical; L/W_1 (two-dimensional); $2L/W$ for square (three-dimensional); $L/(R_o - R_i)_1$ for annular diffusers

P_1 = inlet static pressure

P_2 = exit static pressure

$\bar{q}$ = mass-averaged dynamic pressure

R_1 = radius

u = velocity parallel to wall

W = width

y = perpendicular distance from wall

1.0 LITERATURE SURVEYS OF SUBSONIC DIFFUSERS

Extensive literature surveys on subsonic diffuser performance and other characteristics are available, and some additional experimental studies on diffusers have been reported recently. These studies, with few exceptions, deal essentially with incompressible fluid flow. Design procedures have been developed for particular classes of diffusers. Some experimental information is available that indicates trends in the effect of inlet Mach number on diffuser performance, but generally this information is not satisfactorily correlated. Suggested correlations are given subsequently in terms of limitations and modifications to the incompressible-fluid design procedures.

Three references list the major diffuser studies published through 1963 (see References 4, 7, and 9). Two references on design procedure are available (References 9 and 11). A survey of diffuser literature published since 1963 applicable to the present work on diffuser design procedures was also completed. The significant work heretofore unreported by the previous surveys is found in References 7, 11, and 12. Table IV summarizes the reference data and symbols used in this study.

2.0 EVALUATION OF INLET-MACH-NUMBER EFFECTS

Inlet Mach number is not an important performance parameter when the Mach number is below the range of 0.20 to 0.30. Such performance can be predicted by using incompressible-fluid design procedures (see References 9 and 11). For inlet Mach numbers in excess of 0.20 to 0.30, diffuser performance variation as a function of inlet Mach number can be categorized into three different groups. The typical variation of the pressure-recovery coefficient, C_p, for each group is shown in Figure 148.

When the geometry of the diffusers studied at high subsonic inlet Mach number is plotted on the incompressible flow-regime map (see Figure 150), performance-variation classification — Groups A, B, and C — correlates with the geometric classification of the flow map. All diffusers exhibiting the Group A performance variation characteristic lie to the right of and below the appropriate line of appreciable stall. Those with the characteristic of Group B lie between the line of appreciable stall and Line B-B, and the only diffuser referenced with the characteristic of Group C lies to the left of Line B-B.

This correlation was true in all cases where a normal inlet boundary-layer velocity profile was obtained or could be anticipated. When a separating type of profile occurred at the inlet (Reference 10), Group B variation occurred, whereas the geometry predicts Group A behavior (see Figure 149).

TABLE IV

REFERENCE DATA AND SYMBOLS

Investigator	References	Symbols for Figures 3, 4, 5	$\frac{A}{A}$	N	B_1
Conical Diffusers					
Johnston	5	○	4.0	15.25	0.008 (est)
			4.0	5.39	-
			4.0	3.17	-
Copp	2	◇	2.0	4.72	0.012
			2.0	4.72	0.056
Little & Wilbur	6	△	2.0	2.10	0.038
			2.0	3.92	0.016
			2.0	3.92	0.049
			2.0	4.02	0.007
			2.0	4.02	0.038
Scherrer & Anderson	10	□	1.96	4.30	0.004
			1.96	4.30	0.020
			1.96	6.40	0.004
Annular Diffusers					
Johnston	5	◐	4.0	18.5	0.040 to 0.045 (est)
			3.39	10.8	0.028 to 0.033 (est)
Nelson & Popp	8	◧	1.75	23.2	0.015
			1.75	12.9	0.015
Two-Dimensional Diffusers					
Woollett	13	●	3.0	12.0	-
			3.0	5.5	-
Young & Green	14	■	4.0	21.6	0.030 (est)
			4.0	16.2	0.030 (est)
			4.0	10.8	0.030 (est)
			4.0	8.1	0.030 (est)
			4.0	5.4	0.030 (est)
Friedlich	15	▲	4.0	17.1	-
			3.0	11.4	-
			2.0	5.7	-
Friedlich (Square & Three-Dimensional)	15	▼	4.0	22.9	-
			3.0	16.8	-
			2.0	9.5	-

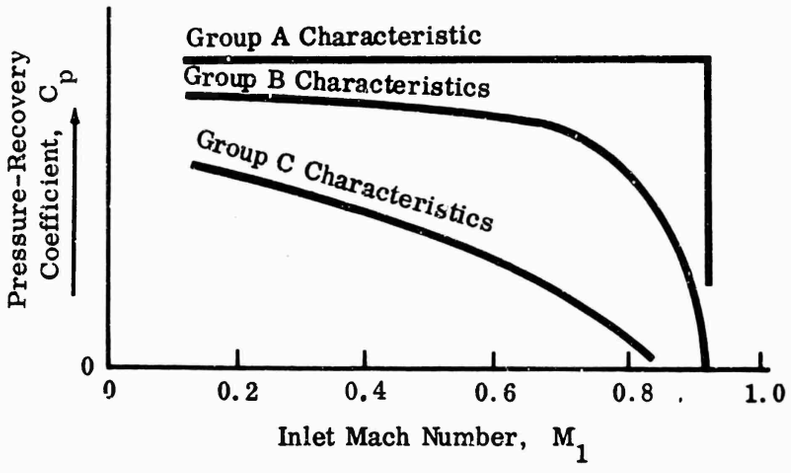


Figure 148. Typical Variation of Pressure-Recovery Coefficient Versus Inlet Mach Number.

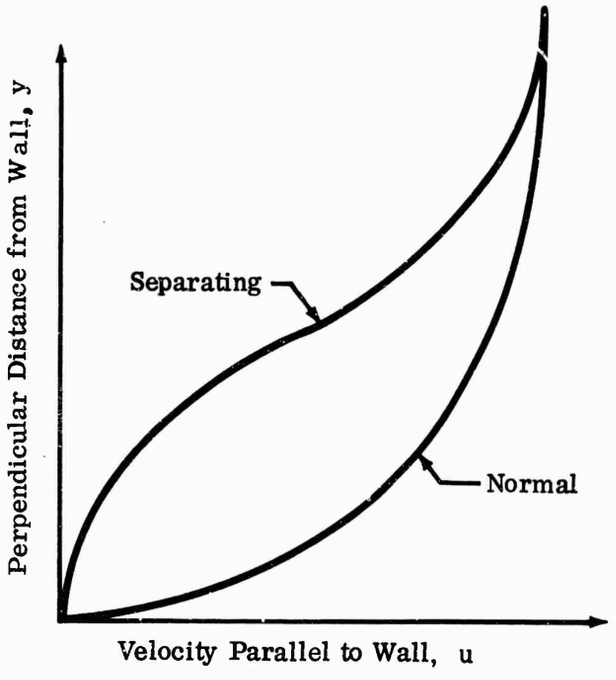


Figure 149. Velocity Profiles of Normal and Separating Boundary Layers.

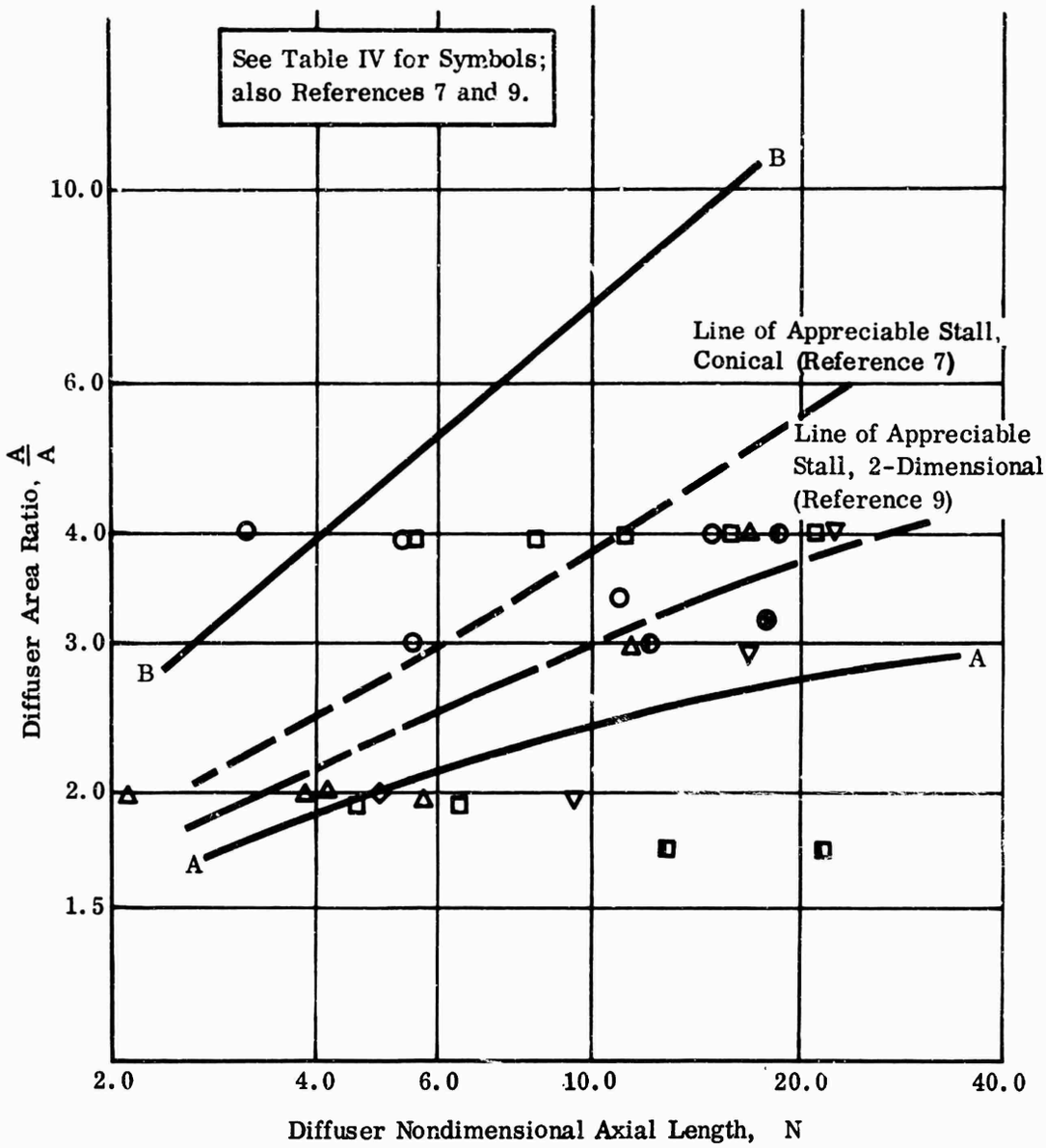


Figure 150. Flow-Regime Map.

The line of appreciable stall is different for conical diffusers from the 2-dimensional case, and Line B-B is from the 2-dimensional data only. Flow-regime information does not exist for the annular case, but the various data correlate on the basis of annular diffuser structure — either 2-dimensional or conical.

A further correlation was attempted using the system geometry and the pressure-recovery coefficients, C_p* and C_p**, from the incompressible data. Figure 151 shows that no apparent correlation is available for subsonic diffusers from the given data.

2.1 EFFECT OF INLET MACH NUMBER ON GROUP A DIFFUSERS

Data indicate that the performance of diffusers in this classification is unaffected, or even slightly improved, by increasing inlet Mach number until some critical value is attained. At the critical value, the performance decreases almost instantaneously to zero. This behavior is generally attributed to the absence of local shocks until the critical value, or choking condition, is reached at the inlet, where local shocks at the inlet cause flow separation and associated stalled flow from the inlet through the diffuser.

The critical inlet Mach number is a direct function of the inlet blockage ratio, B_1. A relation that correlates the available data for Group A diffusers is a straight line, shown in Figure 152. The scatter in the data is due principally to the several methods used in determining the inlet Mach number. The data have not been correlated by a standard method; thus, variation in these values would be expected.

The performance of Group A diffusers below critical Mach numbers can be predicted satisfactorily using a technique similar to that given in References 9 and 11. The analytical procedure would be to consider the core flow on a 1-dimensional compressible basis and the boundary layer on an incompressible basis.

2.2 EFFECT OF INLET MACH NUMBER ON GROUP B DIFFUSERS

Data show that the performance of this group of diffusers is affected adversely by increasing inlet Mach number. The form of the effect is such that the C_p change is relatively small (less than 20 percent) for low Mach numbers (0.2 to 0.6), but decreases more rapidly toward zero in the higher Mach number range. There is no well-defined critical inlet Mach number, as with the Group A diffusers. Insufficient data also prevent correlating the value of inlet Mach number where this parameter will have a major effect on diffuser performance.

See Table IV for Symbols; also Reference 11.

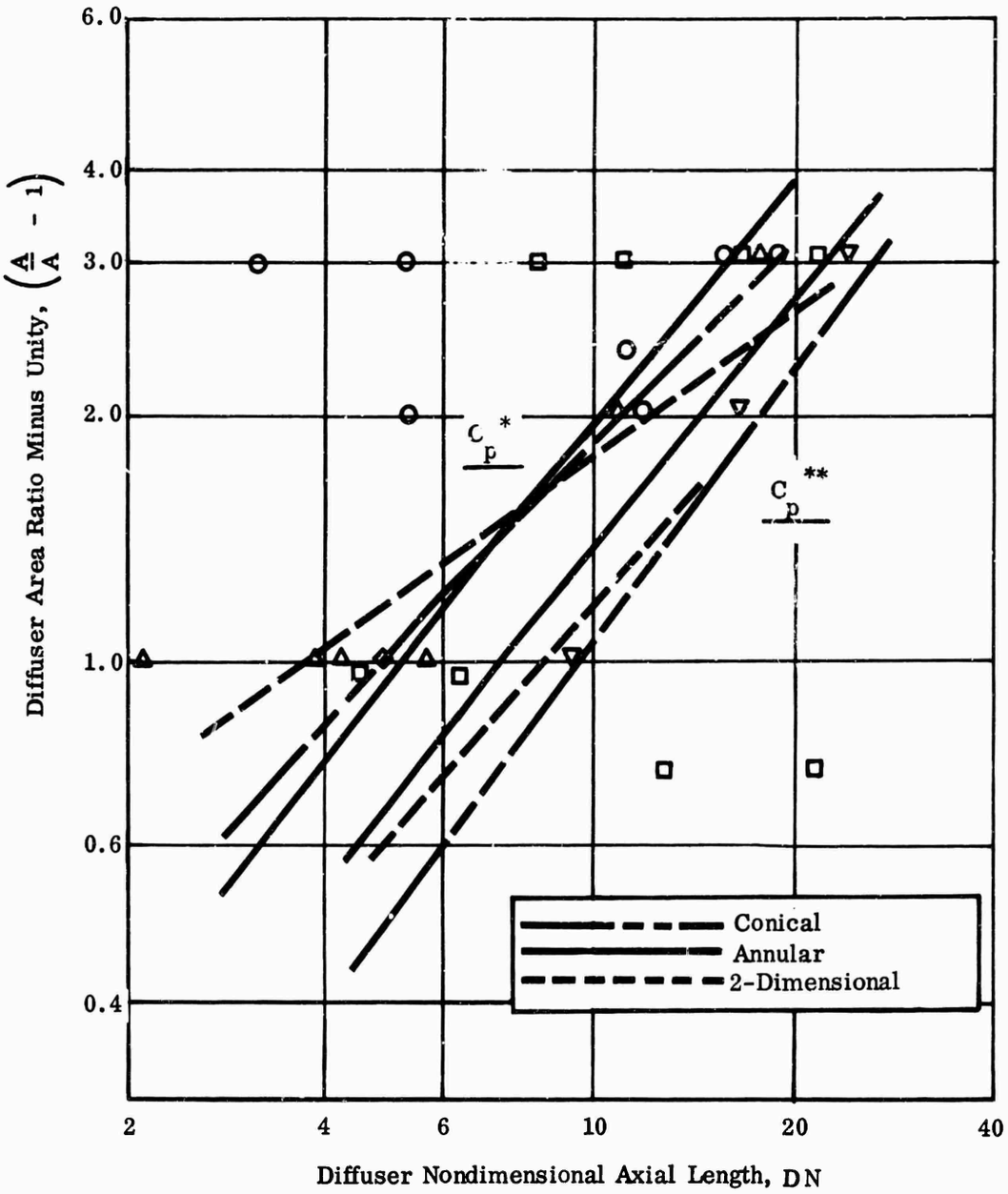


Figure 151. Locus of Maximum Pressure Recovery Versus System Geometry.

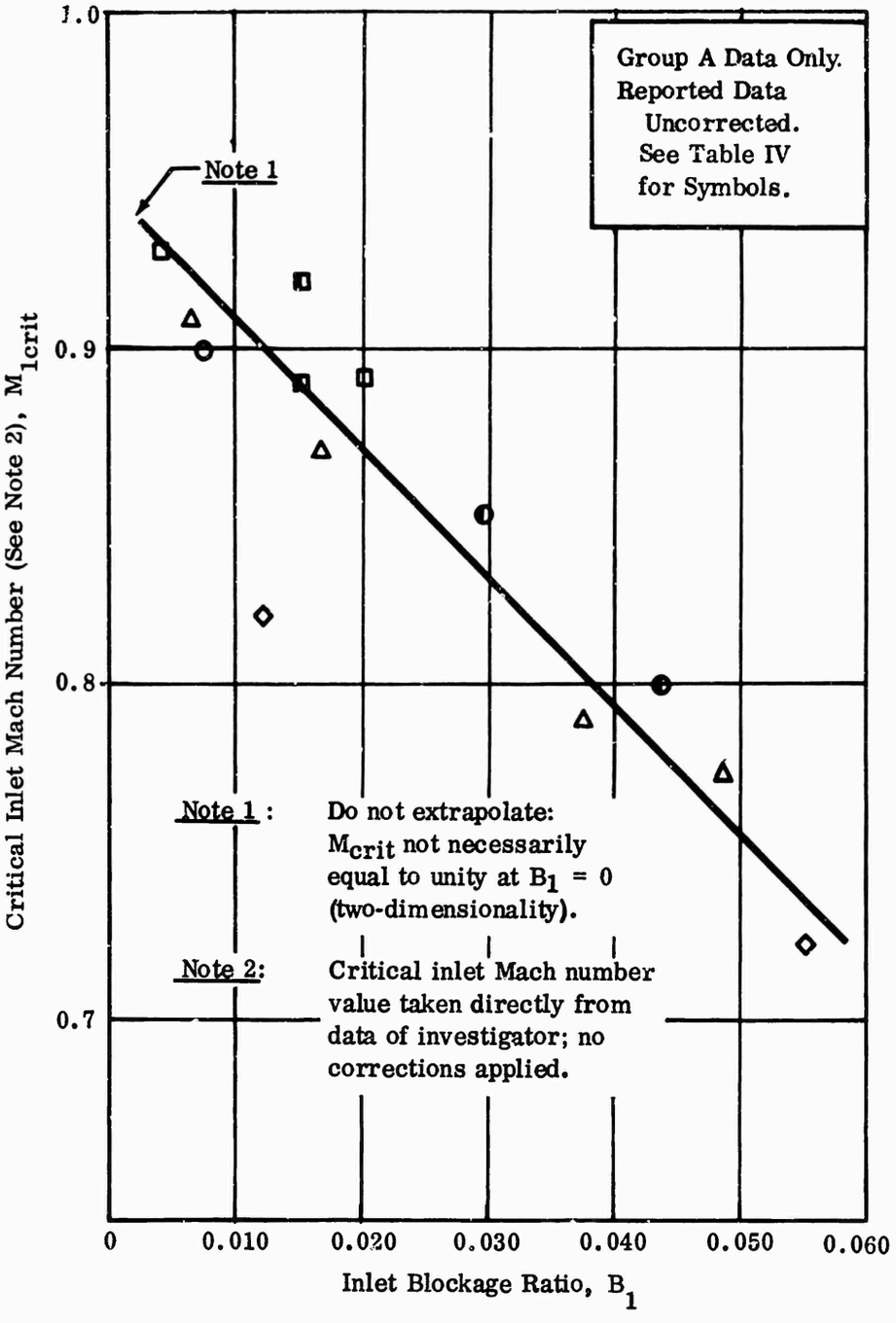


Figure 152. Critical Inlet Mach Number Versus Inlet Blockage Ratio.

Performance, within 20 percent, should be predicted for Group B diffusers with inlet Mach numbers less than 0.6 when a similar scheme to that given for Group A units is used.

2.3 EFFECT OF INLET MACH NUMBER ON GROUP C DIFFUSERS

The performance of this group of diffusers is continuously affected by variation in the inlet Mach number. Major performance reductions are found for small increases in the inlet Mach number over the entire spectrum. No predictive schemes are available for the incompressible case. The only available guides to performance-prediction information for this group of diffusers, and also those of Group B, for high inlet Mach numbers are the correlations given in Reference 4. Caution should be exercised when using these results, as no attempt was made to separate effects, other than inlet Mach number, from the correlation. An example of this can be found in the correlation given in Figure 18 of Reference 4 for critical Mach number as a function of inlet blockage. The resultant correlation, which is more complicated than that shown in Figure 152, was developed by using data from both Group A and B diffusers for curve-fitting.

3.0 SUMMARY

1) The performance variation of subsonic diffusers due to inlet Mach number effects can be classified into 3 groups: A, B, and C.

2) Performance variation classifications correlate directly with the diffuser geometry in the incompressible-flow regimes.

3) The critical inlet Mach number for Group A diffusers is primarily a function of inlet blockage.

4) Prediction of the effect of inlet Mach number on performance can be made for Group A diffusers, but no analytical procedure exists for predicting the critical inlet Mach number.

5) The classification and correlations found are valid for normal inlet boundary-layer velocity profiles, but partial evidence indicates that these results may have to be modified for separating profiles.

REFERENCES

1. Cockrell, D.J., Diamond, M.J., and Jones, G.D., "The Diffuser Inlet Flow Parameter," Journal of Royal Aeronautical Society, Vol. 69, 1965, pp. 350-2.

2. Copp, M.R., Effects of Inlet Wall Contour On the Pressure Recovery of a 10° 10-Inch-Inlet-Diameter Conical Diffuser, NACA RM L51E11a, 1951.

3. Emmons, H.W., The Theoretical Flow of a Frictionless, Adiabatic, Perfect Gas Inside of a Two-Dimensional Hyperbolic Nozzle, NACA TN 1003, 1946.

4. Henry, J.R., Wood, C.C., and Wilbur, S.W., Summary of Subsonic-Diffuser Data, NACA RM L56F05, 1956, Released 1963.

5. Johnston, J.P., Summary of Results of Tests on Short, Conical Diffusers with Flow Control Inserts; as of June 1, 1959, Ingersoll-Rand Company, Philipsburg, N.J., Technical Note No. 71.

6. Little, B.H., Jr., and Wilbur, S.W., Performance and Boundary-Layer Data from 12° and 23° Conical Diffusers of Area Ratio 2.0 at Mach Numbers up to Choking and Reynolds Numbers up to 7.5×10^6, NACA Report 1201, 1954.

7. McDonald, A.T., and Fox, R.W., Incompressible Flow in Conical Diffusers Purdue Research Foundation, Lafayette, Indiana, Project No. 3684, Technical Report No. 1, September 1964.

8. Nelson, W.J., and Popp, E.G., Performance Characteristics of Two 6° and Two 12° Diffusers at High Flow Rates, NACA RM L9H09, 1949.

9. Reneau, L.R., Johnston, J.P., and Kline, S.J., Performance and Design of Straight, Two-Dimensional Diffusers, Stanford University, Stanford, California, Thermosciences Division Report No. PD-8, September 1964.

10. Scherrer, R., and Anderson, W.E., Preliminary Investigation of a Family of Diffusers Designed for Near Sonic Inlet Velocities, NACA TN 3668, 1956.

11. Sovran, G., and Klomp, E.D., Experimentally Determined Optimum Geometries for Rectilinear Diffusers with Rectangular, Conical, or Annular Cross-Section, General Motors Research Laboratories Publication GMR-511, November 1965.

12. Stratford, B.S., and Tubbs, H., "Maximum Pressure Rise Attainable in Subsonic Diffusers," J. Roy, Aero. Soc., Vol 69, No. 652, April 1965, pp. 275-8.

13. Woollett, R.R., Preliminary Investigation of Short Two-Dimensional Subsonic Diffusers, NACA RM E56C02, 1956.

14. Young, A.D., and Green, G.L., Tests of High-Speed Flow in Diffusers of Rectangular Cross-Section, A.R.C.R. & M. No. 2201, 1944.

15. Friedlich, S., Performance Characteristics of Plane Wall Diffuser and Some New Concepts of Diffuser Flow Mechanisms, M.S. Thesis, University of Washington, 1959.

(U) APPENDIX XII

STRAIGHT DIFFUSER PERFORMANCE AT HIGH INLET MACH NUMBERS

ABSTRACT

This test series by Peter W. Runstadler, Jr. was accomplished by Creare, Incorporated, under a separate contract to The Boeing Company.

Measurements have been made of the pressure recovery of straight-wall diffusers with inlet Mach numbers between 0.3 and choking. Two aspect ratios are studied: 5.7 and 0.25. For the 5.7 aspect ratio diffusers, blockages of 0.01 to 0.15 for L/W = 15 and 0.04 for L/W = 10 at choking conditions are reported. For the 0.25 aspect ratio diffusers, blockages range between 0.03 and 0.17 at choking conditions for L/W = 15. Divergence angles, 2θ, from 4 to 12 degrees are covered for both aspect ratios.

There is no critical subsonic inlet Mach number at which a sharp drop in pressure recovery occurs. Evidence in the published literature has previously indicated such a critical subsonic inlet Mach number. There is a severe drop in performance in supercritical flow when the shock Mach number in the diffusing passage exceeds approximately 1.1 to 1.2.

Variation of pressure recovery with inlet Mach number in the subsonic range is observed as a function of divergence angle and blockage.

A significant difference exists between the present data at high inlet Mach numbers and previous data at low Mach numbers to rule out the use of low Mach number data in the design of high inlet Mach number diffusers.

The present data show maximum pressure recovery at a divergence angle of 10 degrees for all blockages up to 0.17 with a diffuser aspect ratio of 0.25, L/W of 15, and inlet Mach number of 1. For an aspect ratio of 5.7, the data indicate maximum pressure recovery for a divergence angle of 6 degrees.

SYMBOLS

AR = aspect ratio

A_t = $A_{geometric}$ = throat geometrical area

A_{flow} = one-dimensional-flow area

B = boundary-layer blockage = boundary-layer displacement area/geometrical area of throat

C_p = diffuser pressure-recovery coefficient = $\frac{P_{exit} - P_{throat}}{P_o - P_{throat}}$

D_H = hydraulic diameter = $\frac{4A_t}{P_T}$

L = diffuser wall length (centerline distance from throat to exit)

m = mass flow rate

M = inlet Mach number on centerline

P = static pressure

P_o = stagnation pressure at diffuser inlet (throat) on centerline

P_T = wetted perimeter

R_e = Reynolds number

$\bar{U}$ = mean velocity = $\frac{m}{\rho A_t}$

W = diffuser throat width

2θ = diffuser divergence angle

ϕ = 1 - B

ρ = density

ν = kinematic viscosity

Subscripts

throat - diffuser throat

exit - diffuser exit

choke - choking conditions at diffuser throat

1.0 INTRODUCTION

A substantial body of data exists in the published literature on the performance of straight-wall diffusers at low inlet Mach numbers. Reneau* has surveyed these data. Diffuser performance (usually in the form of pressure recovery (C_p)) is correlated as a function of divergence angle (2θ), wall length-to-throat-width ratio (L/W), and inlet flow blockage ratio (B). (Reneau reports data in terms of $2\delta^*/W$, which is equivalent to blockage (B) as defined in this report.) There is relatively little information on diffuser performance at high inlet Mach numbers, i.e., M > 0.2 to 0.3. The design of efficient diffusers for high-speed centrifugal compressors depends upon this information.

Halleen and Johnston (Appendix XI) recently surveyed available published data on the performance of straight diffusers at high inlet Mach numbers. They were able to conclude the following:

1) The variation in pressure recovery (C_p) of subsonic diffusers due to inlet Mach number effects can be classified into 3 groups: A, B, and C. The typical variation of pressure recovery for each group is shown in Figure 153.

2) Performance variation in each classification correlates directly with diffuser geometry — the correlation is in agreement with the incompressible flow-regime map of Figure 154.

3) Group A diffusers (conical or 2-dimensional), which are at divergence angles below the line of appreciable stall (conical or 2-dimensional, respectively), exhibit the characteristic of a critical Mach number above which the relatively constant recovery of the diffuser up to this Mach number suffers a drastic drop. This critical Mach number is a function of inlet blockage ratio (B), as shown in Figure 155.

4) Arguments for the existence of a critical Mach number for Group A diffusers can be presented (see Appendix XI), but no analytical procedure exists for predicting the critical inlet Mach number.

5) The classifications and correlations are valid for normal inlet boundary-layer velocity profiles, but partial evidence indicates that these results may have to be modified for separating types of velocity profiles.

---

*L. R. Reneau, et al, Performance and Design of Straight Two-Dimensional Diffuser, Report PD-8, Thermosciences Division, Department of Mechanical Engineering, Stanford University, Stanford, California, September 1964.

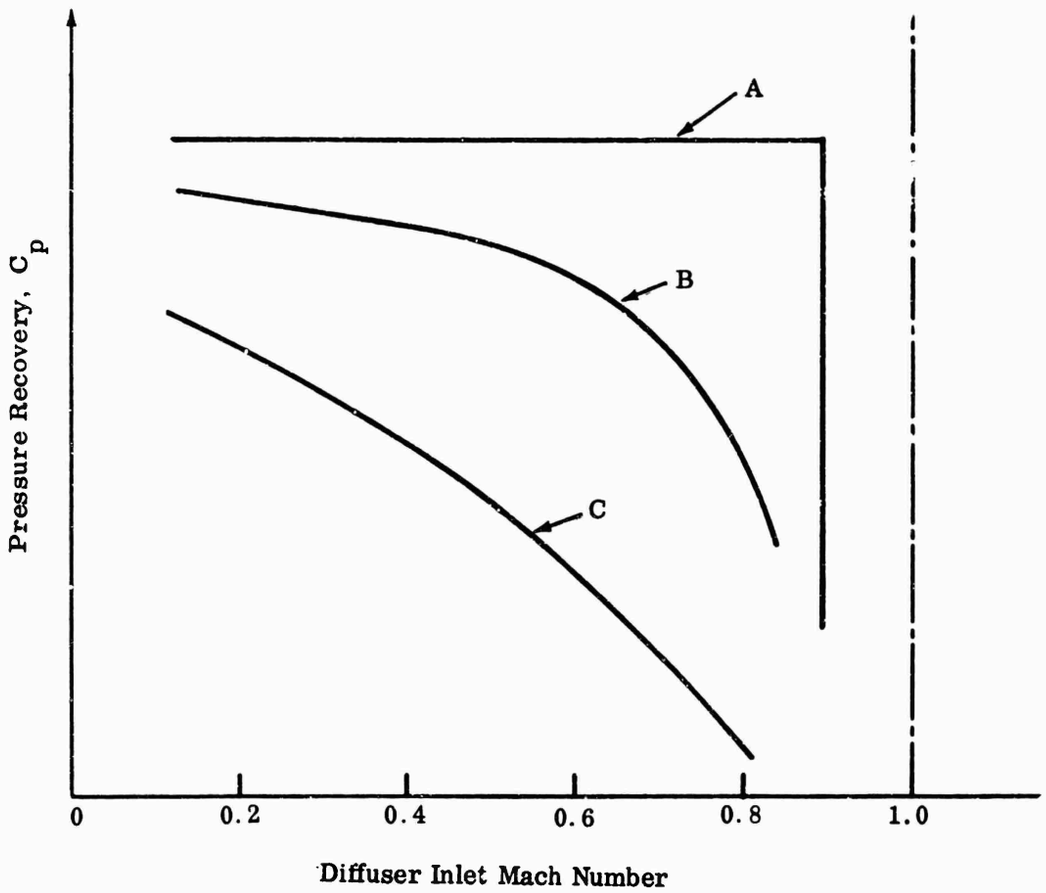


Figure 153. Characteristic Grouping of Diffuser Data, (C_p Versus Inlet Mach Number at Fixed Geometry).

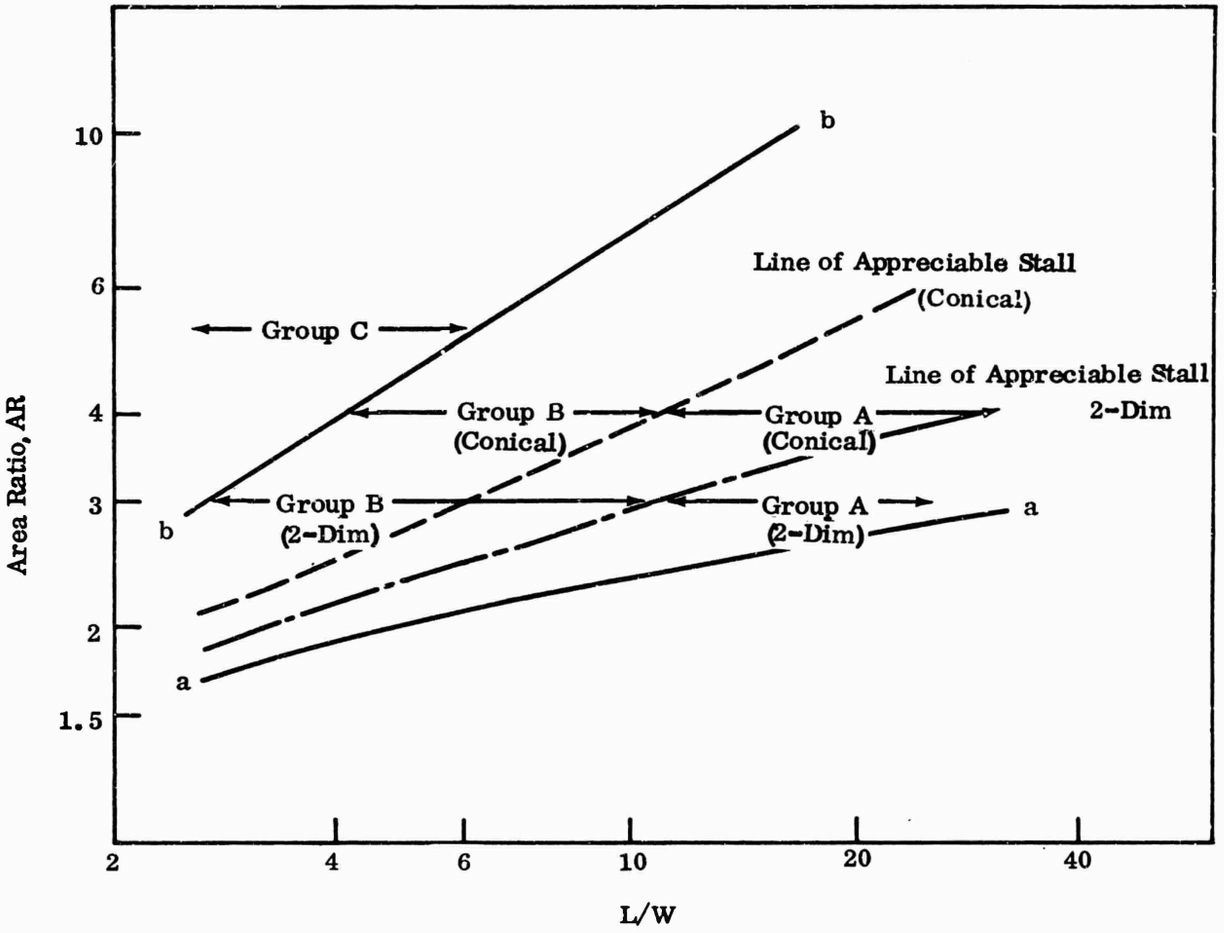


Figure 154. Flow-Regime Map, Inlet Mach Number Group Classification.

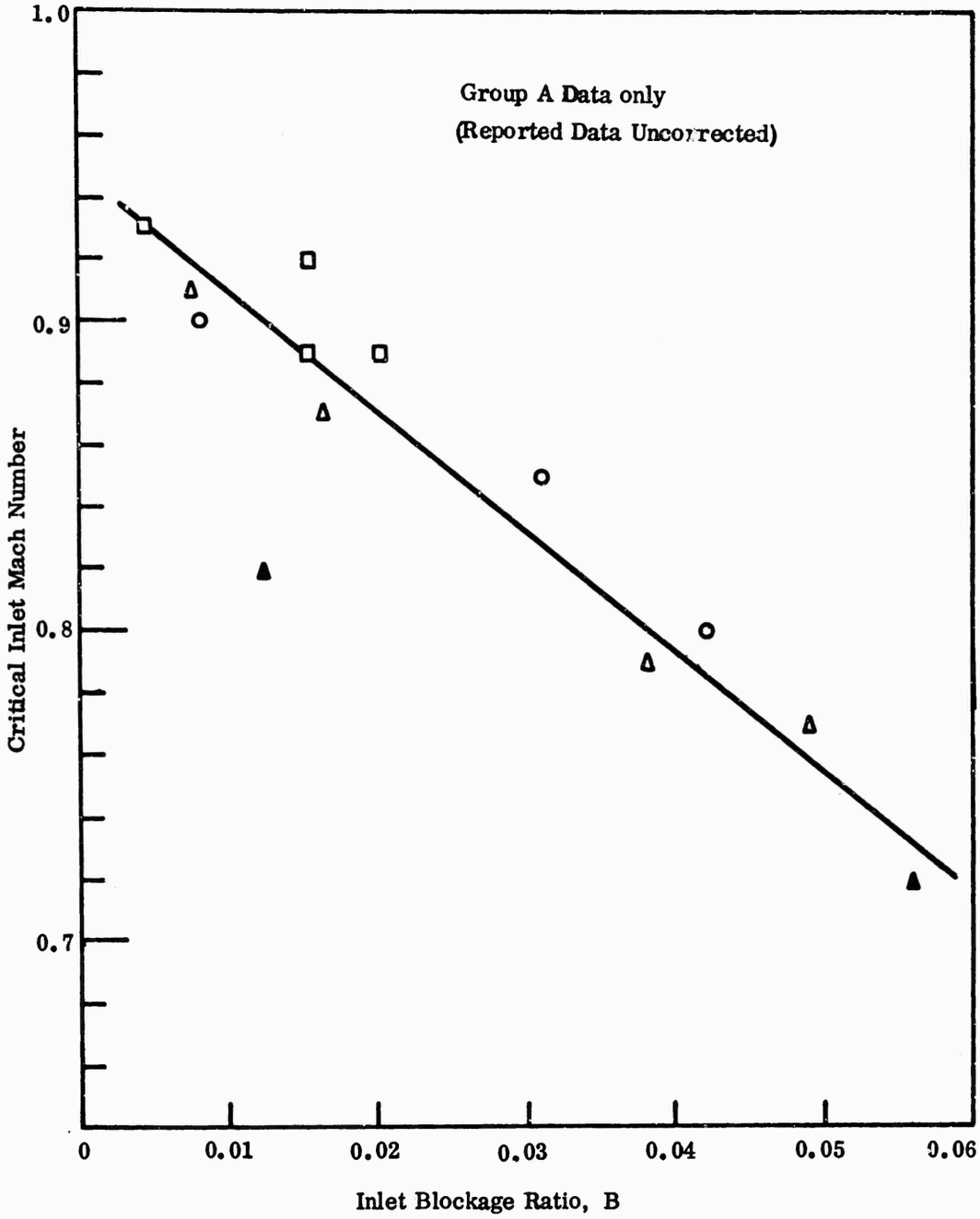


Figure 155. Critical Inlet Mach Number Versus Blockage Ratio.

The aspect ratio, divergence angle, and length-to-width ratio of diffusers for centrifugal compressors yield diffuser geometries which fall largely under the group A classification of Halleen and Johnston. Thus, these diffusers should suffer relatively poor performance at high inlet Mach numbers compared to the performance at low Mach numbers, if conclusions 1, 2, and 3 are correct. However, experimental data on high speed compressors, from the contractor's diffuser research, show that good diffuser performance is obtained, even though throat Mach numbers are higher than the critical values reported in Appendix XI. Two reasons for this discrepancy appear possible:

1) The critical Mach number at subsonic inlet conditions as shown in previously available evidence is not correct*; or

2) A critical Mach number does exist, producing a region of very poor diffuser performance, but this is then followed by a gain in performance at higher Mach numbers; i.e., the C_p versus inlet Mach number characteristic has a "dip" at some high inlet Mach number.

The present work was undertaken (1) to resolve which, if either, of these is correct, and (2) to provide design criteria for high inlet Mach number diffusers with parameters within the range of interest for high-speed centrifugal-compressor applications.

The experimental procedures are considered first, and are followed by a discussion of the results, and major conclusions.

2.0 EXPERIMENTAL PROCEDURE

The pressure recovery for the straight-wall, 2-dimensional diffuser geometry can be correlated on 5 independent parameters:

1) Divergence angle (2θ);

2) Diffuser length-to-throat-width ratio (L/W);

3) Aspect ratio (AR);

4) Flow blockage at the diffuser throat (B);

5) Inlet throat Mach number (M_t).

---

*H. Pearson, J. B. Holiday, S. F. Smith, "A Theology of the Cylindrical Ejector Supersonic Propelling Nozzle," Journal of the Royal Aeronautical Society, 62, 746, 1958.

Design criteria for predicting optimum diffuser performance require a diffuser performance map (C_p) as a function of these 5 variables. The variables were chosen to cover areas of interest to the centrifugal-compressor, vane-island diffuser.

2.1 GEOMETRICAL PARAMETERS

The geometrical configurations of the diffuser and diffuser inlets are shown in Figures 156 through 160. The diffuser test section consists of a series of nozzle blocks and diffuser blocks sandwiched between parallel side plates. The interchangeable nozzle blocks permit the use of different throat lengths preceding the diffuser passage; this allows a range of blockage values to be obtained for a fixed diffuser geometry. Likewise, the different diffuser blocks cover the range of diffuser angles for fixed aspect ratio and length-to-width ratio.

The assembly is bolted together and sealed with RTV sealant. The test section is connected with flanges (Figures 156 and 157) to 4-inch pipe upstream and downstream of the test section. The throat width and diffuser angle are accurately set (< 0.5 percent) with gage blocks at the throat and diffuser exit. The diffuser and throat passages are maintained clean of any residue RTV sealant, etc. The flow exits into the gage space at the end of the diffuser and then into the 4-inch pipe. The exit static pressure is measured in the 4-inch pipe downstream of the diffuser. The difference between the diffuser exit static pressure and the downstream static pressure was less than 0.5 percent.

For convenience of presentation, the tests are divided into two groups; tests with a 5.7 aspect ratio and tests with an 0.25 aspect ratio.

The 5.7 aspect ratio test section had side plates, nozzle,and diffuser blocks of aluminum. The 0.25 aspect ratio test section had one side plate made of 1-inch-thick Lucite, permitting visual observation of the flow. Early in the 0.25 aspect ratio studies it was observed that an oil and water emulsion visible in the flow appeared to produce erratic pressure measurements at the diffuser inlet. (The effect might be caused by any one of a number of factors: an effective increase in the throat blockage caused by water and oil in the flow, a change in sonic velocity as a result of 2-phase flow, the possibility of condensation shock effects, etc.) Since the water and oil came from the compressor supplying air to the test section, 2 centrifugal separators were installed upstream of the test section to assist in reducing the amount of oil and water in the flow. The 0.25 aspect ratio data were only taken when the flow by visual observation was substantially clear of oil and water mist. We suspect that the 5.7 aspect ratio tests (conducted prior to the 0.25 aspect ratio studies) may have had substantial amounts of oil and water vapor in the flow; however, time did not permit these tests to be repeated to determine the possible influence of any mist conditions on the pressure recovery.

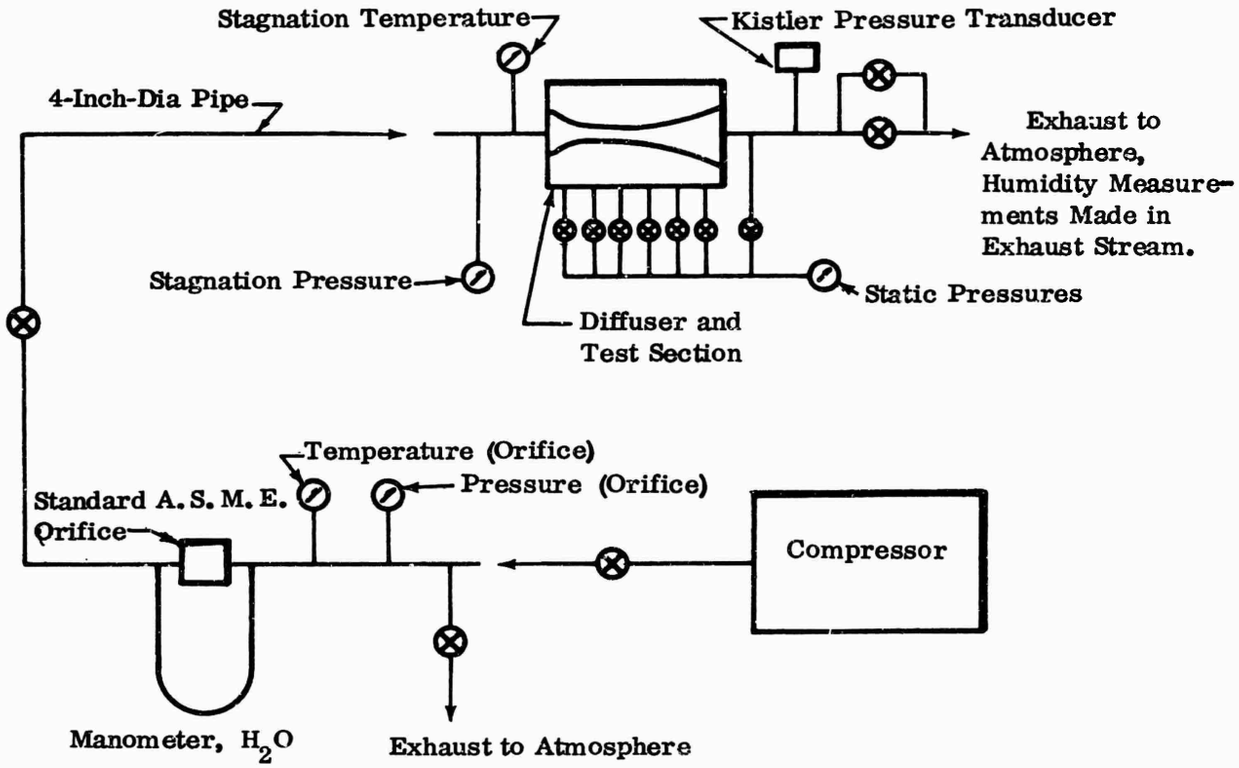


Figure 156. Flow Arrangement and Measurement Techniques.

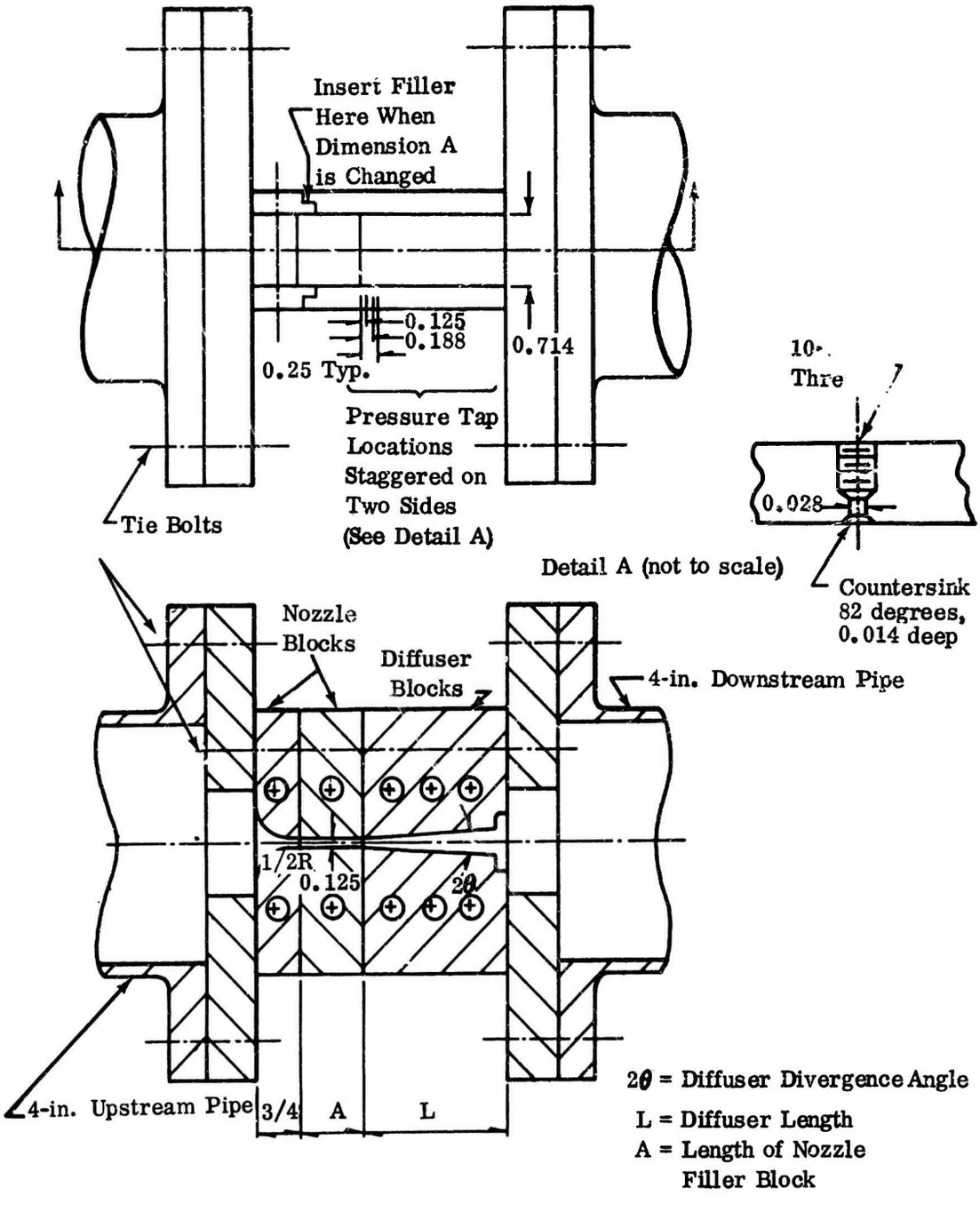
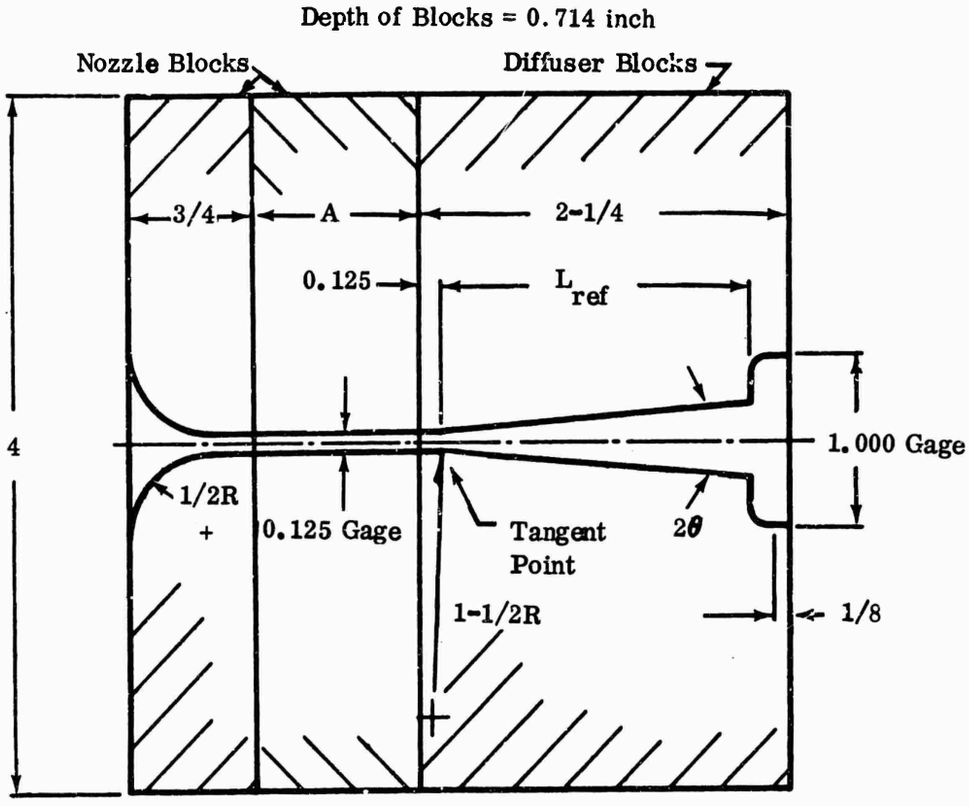


Figure 157. Diffuser Test Section (5.7 Aspect Ratio).



Tolerances: All Fractional Dimensions ± 1/64 inch
All Decimal Dimensions ± 0.005 inch
Except Gage Dimensions ± 0.0005 inch

A = 0
= 1.000 inch
= 2.000 inches
= 4.000 inches

2θ = 4.0 ± 0.1°
= 6.0 ± 0.1°
= 8.0 ± 0.1°
= 10.0 ± 0.1°
= 12.0 ± 0.1°

L = 1.875 for L/W = 15
= 1.250 for L/W = 10
= 2.125 for L/W = 17

Figure 158. Nozzle and Diffuser Block Dimensions (5.7 Aspect Ratio).

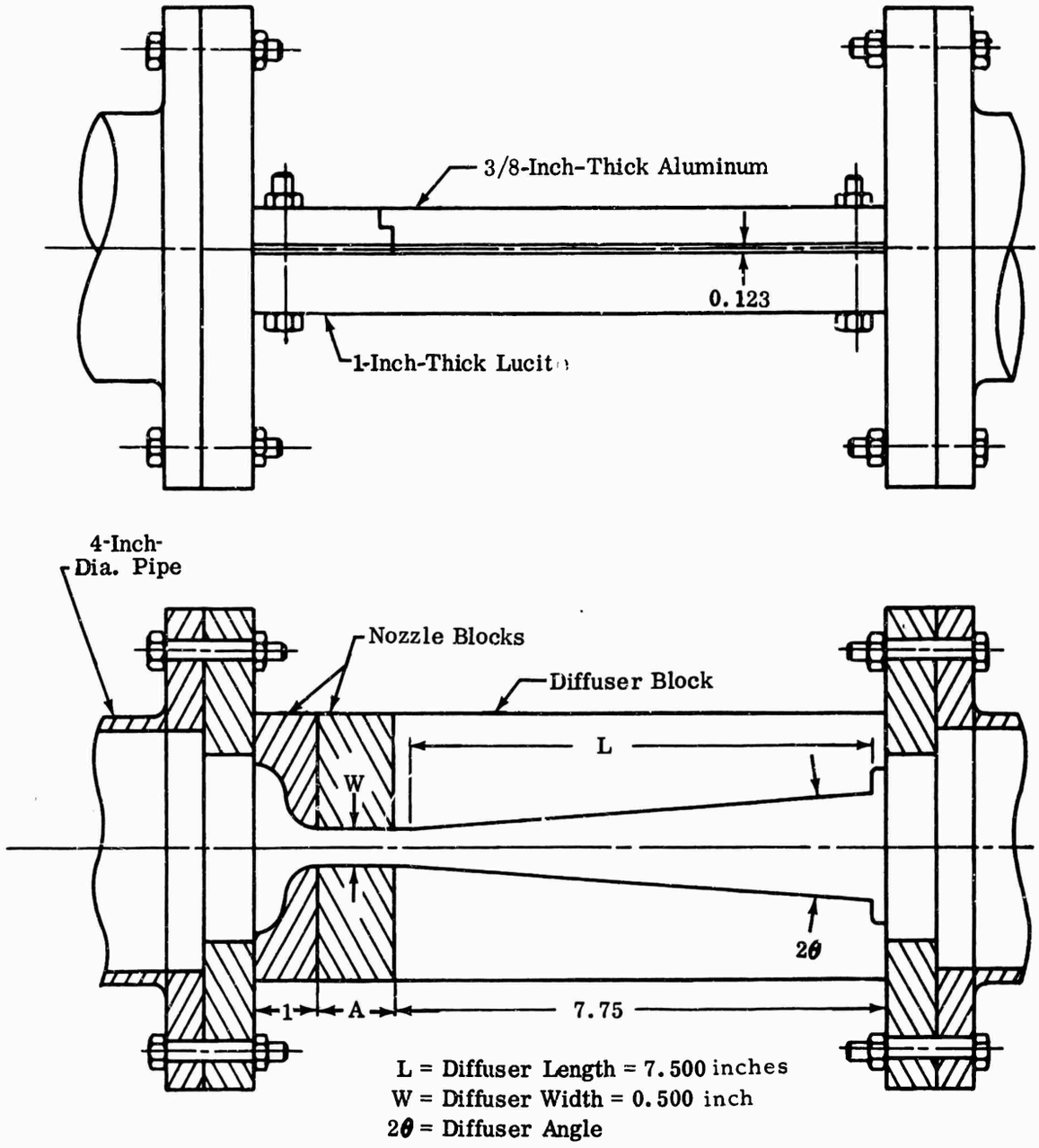
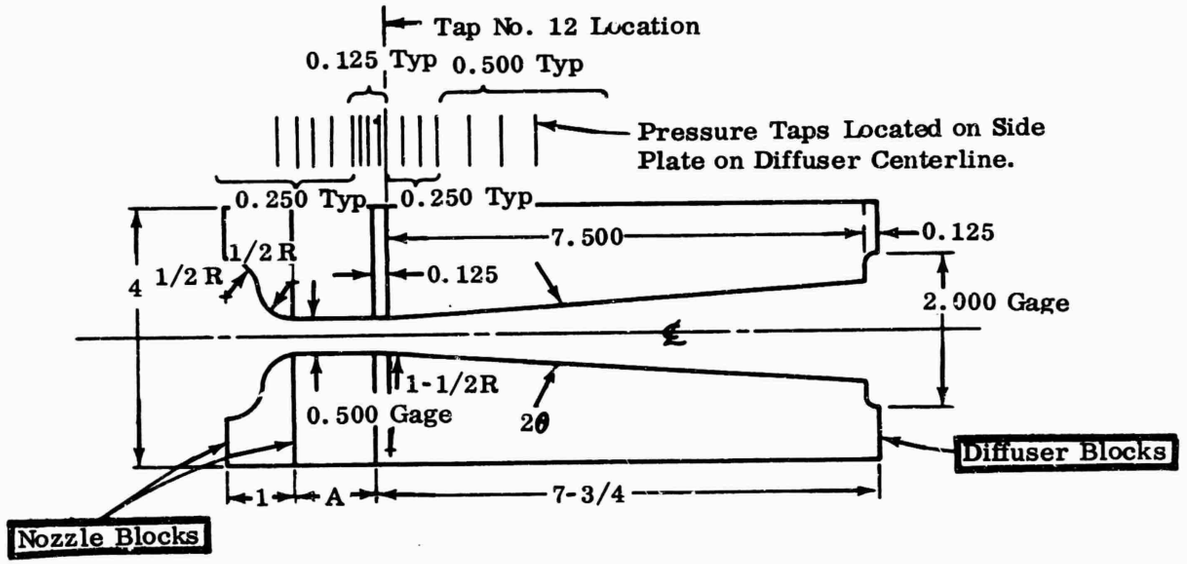


Figure 159. Diffuser Test Section (0.25 Aspect Ratio).



Depth of Blocks = 0.128 Inch
Material: 2024 Aluminum

2θ	=	4.0°	±0.1°	A	=	0
	=	6.0°	±0.1°		=	0.500
	=	8.0°	±0.1°		=	1.500
	=	10.0°	±0.1°		=	3.500
	=	12.0°	±0.1°			

Tolerances:
All Fractional Dimensions ±1/64 inch
All Decimal Dimensions ±0.005 inch
All Gage Dimensions ±0.0005 inch

Figure 160. Nozzle and Diffuser Block Geometry (0.25 Aspect Ratio Tests, L/W = 15).

2.1.1 GEOMETRICAL PARAMETERS, 5.7 ASPECT RATIO

A throat width of 0.125 inch and throat depth of 0.714 inch gave a 5.7 aspect ratio diffuser.

Sets of diffuser blocks provided symmetrical divergence angles (2θ) of 4, 6, 8, 10, and 12 degrees.

Four nozzle blocks gave inlet throat length-to-diffuser-width ratios of 3, 11, 19, and 35.

Two sets of diffuser blocks provided diffuser length-to-width ratios:

$$L/W = 15, 10$$

2.1.2 GEOMETRICAL PARAMETERS, 0.25 ASPECT RATIO

The throat depth of 0.125 inch and throat width of 0.500 inch provided an aspect ratio of 0.25.

Divergence angles covered:

$$2\theta = 4°,\ 6°,\ 8°,\ 10°,\ 12°$$

Inlet nozzle blocks provided inlet throat-length-to-throat-width ratios of 0.25, 1.25, 2.25, 4.25, 7.25.

A single diffuser wall length was used giving a L/W = 15.

2.2 FLOW PARAMETERS

Stagnation pressure ($\sim$ 95 psia) and temperature ($\sim$ 125°F) provided a throat Reynolds number (Reynolds number based on throat hydraulic diameter (D_H) = $\frac{4A_t}{P_T}$ and mean flow velocity $\overline{U}$) of about 6×10^5 at choking conditions for both aspect ratios.

For the largest inlet throat length to diffuser width at 10, this Reynolds number is equivalent to a throat length Reynolds number

$$\left(R_{e_{L_{throat}}} = \frac{\overline{U}\, L_{throat}}{\nu}\right) \text{ of approximately } 1.2 \times 10^{7}.$$

2.3 FLOW MEASUREMENTS

A schematic of the flow arrangement and instrumentation is shown in Figure 156. Static-pressure taps are located along the centerline of the inlet and diffuser blocks (Figures 157 and 160). The mass-flow rate was measured with a standard ASME orifice meter, upstream of the test section. Stagnation pressure and temperatures upstream of the diffuser and static pressure in the pipe downstream of the diffuser were also measured.

The inlet Mach number is defined in terms of the centerline Mach number, i.e.,

1) The potential core flow Mach number, if the throat passage is sufficiently short that the sidewall boundary layers have not met in the center of the throat passage at the entrance to the diffuser;

2) The centerline Mach number, in the case where the sidewall boundary layers have met.

In either case, it is the maximum Mach number of the flow at the diffuser inlet which is used, and not an averaged inlet Mach number obtained from averaging the stagnation pressure across the throat flow. The throat flow is thus treated as a boundary-layer flow where the centerline conditions correspond to the core flow outside the boundary layers.

An equivalent flow area is calculated based on these centerline conditions. This flow area is the area required to pass a 1-dimensional flow with the measured values of stagnation pressure and temperature.

The blockage is the difference between the geometric throat area and the equivalent 1-dimensional flow area. The blockage is expressed in terms of the blockage ratio (B):

$$B = 1 - \phi = \frac{A_{geometric} - A_{flow}}{A_{geometric}} \tag{239}$$

where:

$$\phi = \frac{A_{flow}}{A_{geometric}} \tag{240}$$

When the throat length is sufficiently short to permit a potential core to exist at the diffuser inlet, the use of stagnation conditions upstream of the throat in the 4-inch pipe can be used for calculation of the Mach number and blockage. When the throat is long and the sidewall boundary layers have merged at the throat centerline, it is necessary to measure the throat stagnation pressure at the entrance to the diffuser. A total-pressure probe of 0.040 outside diameter was inserted from downstream along the centerline of the diffuser to the throat location, and total-pressure measurements were made with the 1.5- and 3.5-inch throats in the 0.25 aspect ratio diffuser, Figure 161. For all throat lengths up to 1.5 inch, the total-pressure drop in the throat passage is negligible (0.4 psi out of 95 psia for the 1.5-inch throat). For the 3.5-inch-throat tests, the stagnation pressure at the throat centerline was determined from the measured upstream stagnation pressure and Figure 161.

For the short throat passage lengths (1.5 inches or less) there is a potential core flow at the end of the throat passage; the static-pressure distribution through the diffuser throat should be given by the 1-dimensional isentropic compressible flow relations, since the wall pressure is imposed by the core flow. With choking flow, the ratio of static pressure to upstream total pressure should be 0.528 at the end of the inlet passage (throat). Figures 162 and 163 show the measured static-pressure distributions for $2\theta = 6$ degrees and $L_{throat} =$ 0 and 1.5 inches, respectively (0.25 aspect ratio). If the above remarks are correct, the throat with choking flow is located along the inlet passage where the pressure ratio is 0.528. For the subsonic flow distributions, the throat can be located where the static pressure is minimum. (With the 1/8-inch spacing between pressure taps in the throat region, there is actually ±1/8-inch uncertainty in the location of the minimum pressure in the subsonic distributions). Fitting curves to the measured data (Figures 162 and 163) gives good agreement between the throat location, as determined from the subsonic distributions and the 0.528-pressure-ratio location. The static pressure at the throat (with choking flow) has been obtained by using the measured upstream stagnation pressure and the 0.528-critical-pressure ratio.

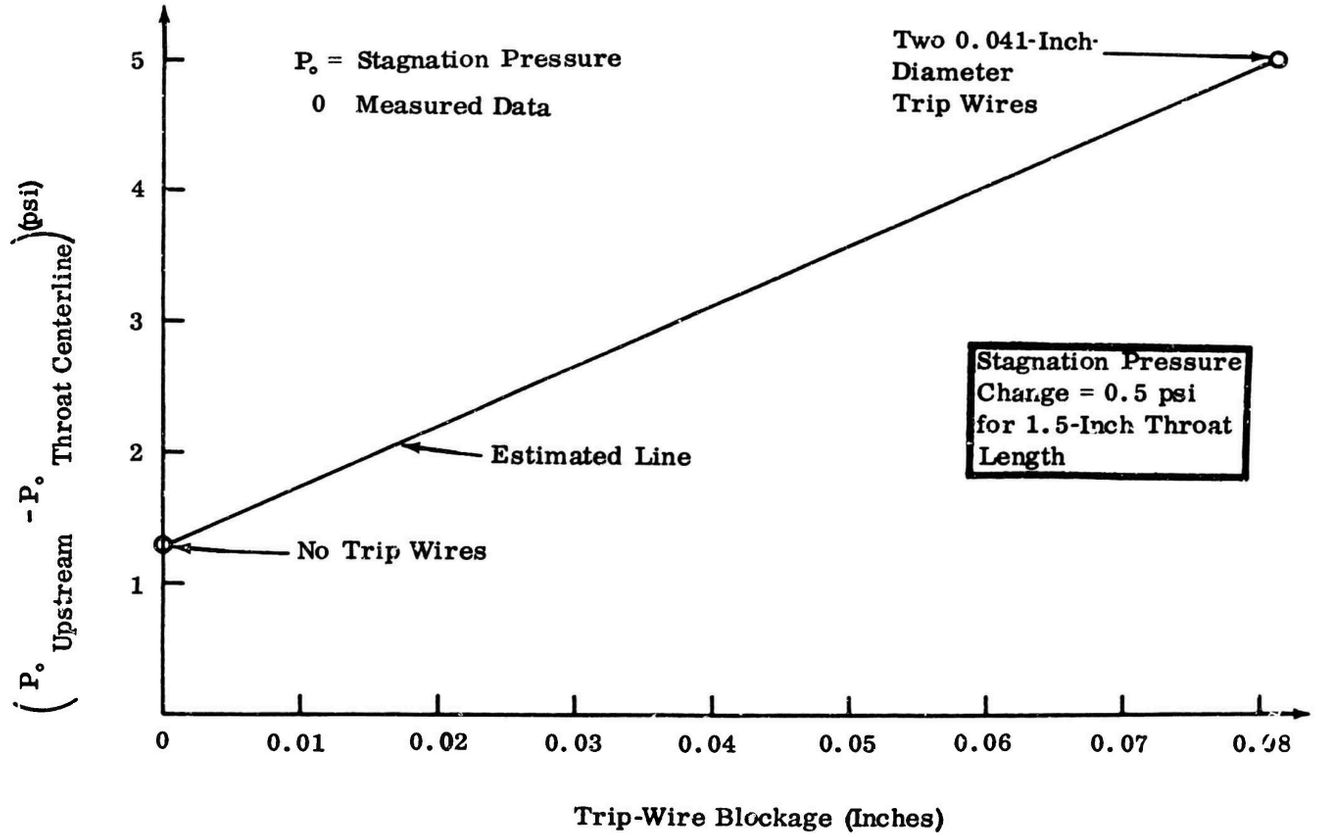


Figure 161. Centerline Stagnation Pressure Change (3.5-Inch-Long Throat).

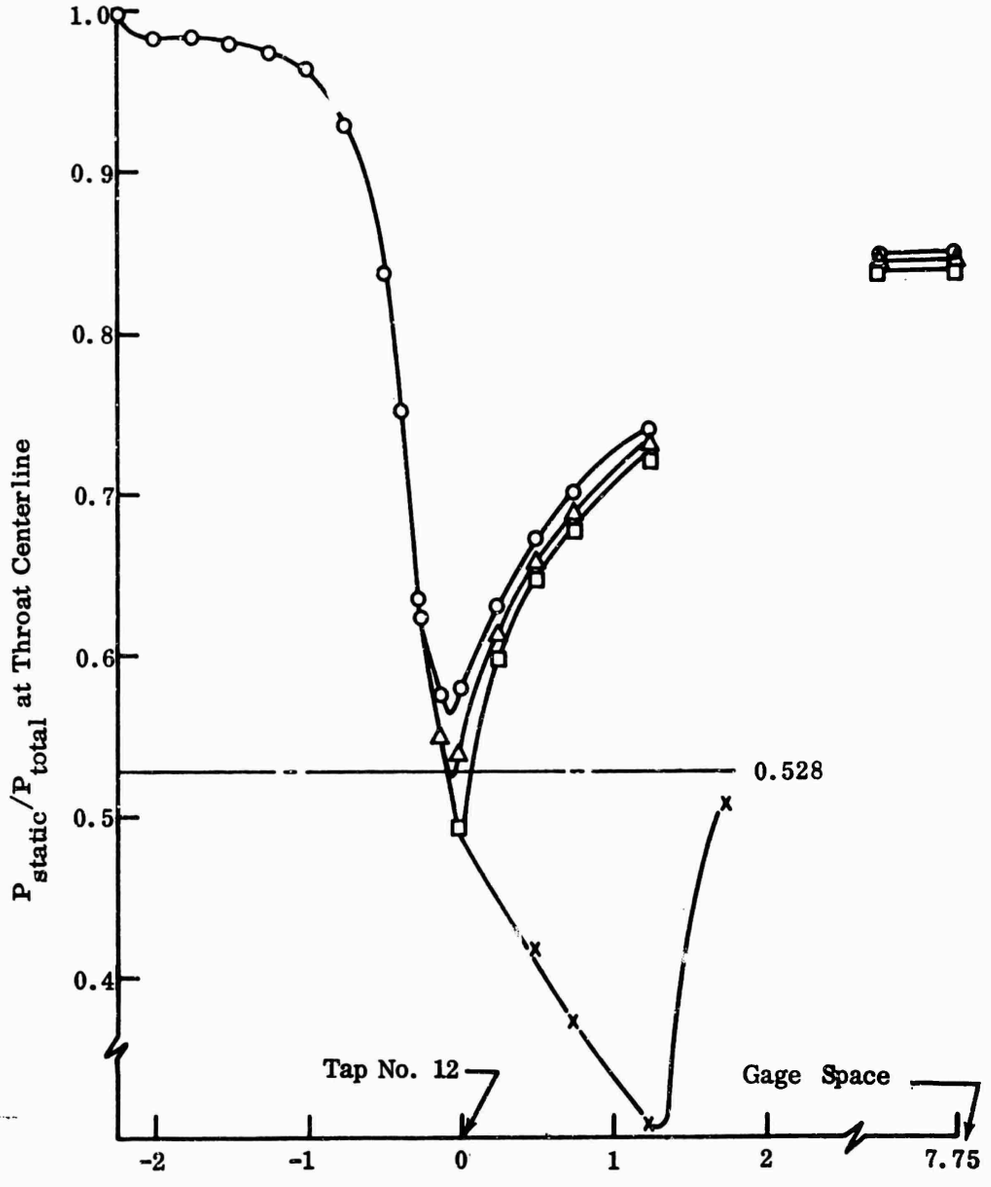


Figure 162. Straight Diffuser Performance (Pressure Ratio Versus Axial Distance For Various Backpressures, 0.25 Aspect Ratio, $2\theta = 6°$, $L_{throat} = 0.125$ Inch).

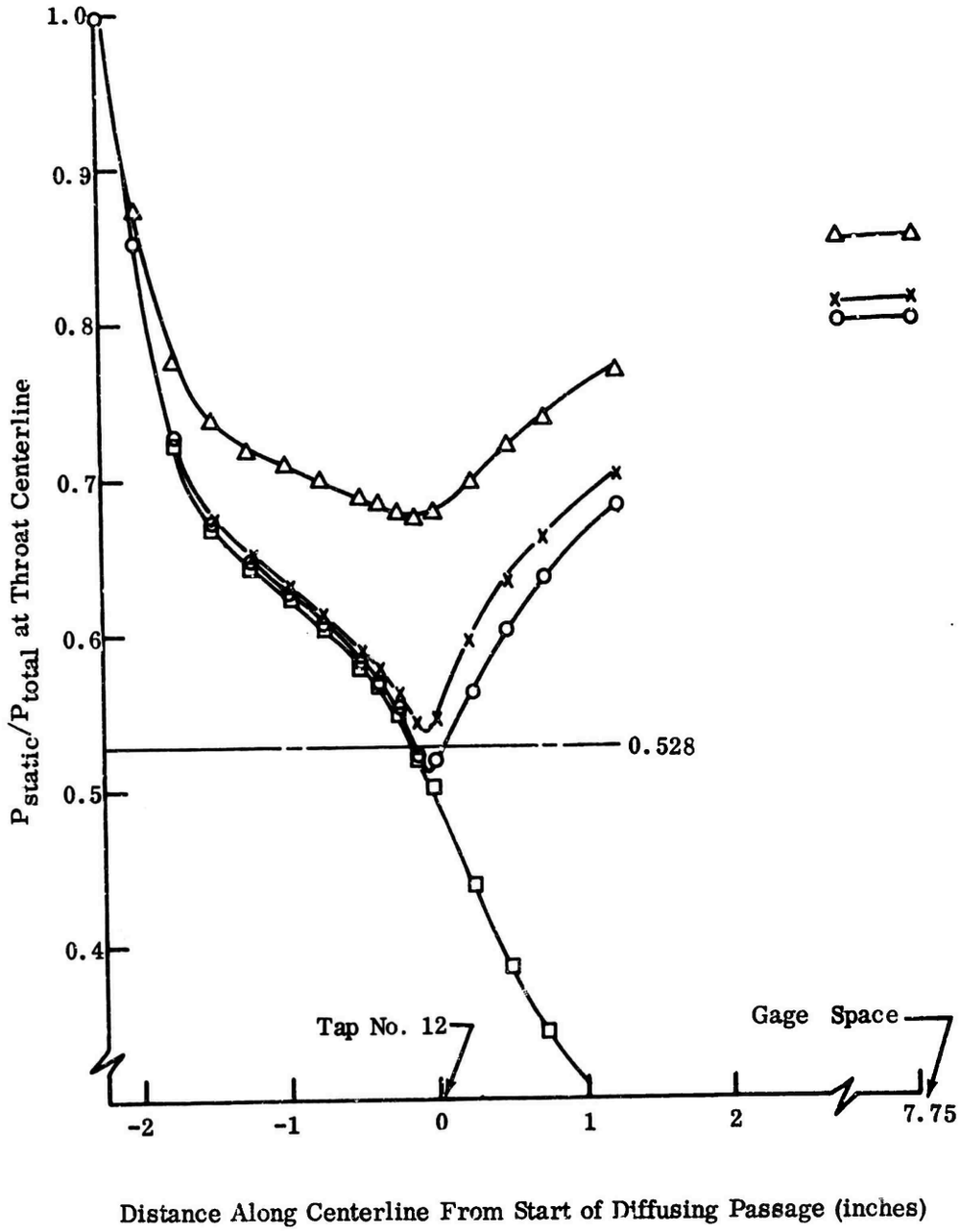


Figure 163. Straight Diffuser Performance (Pressure Ratio Versus Axial Distance For Various Backpressures, 0.25 Aspect Ratio, $2\theta = 6°$, $L_{throat} = 1.625$ Inch.

In the tests with the 3.5-inch throat length, the boundary layers merge before the end of the inlet passage. In these tests, the static pressure at the diffuser inlet (for choking flow) has been found by using the 0.528 critical-pressure ratio and the stagnation pressure measured at the throat (obtained from Figure 161). The flow is thus treated as a 1-dimensional Fanno line flow, with a choking stagnation pressure equal to the measured stagnation pressure at the throat centerline. Static-pressure measurements for $2\theta = 6$ degrees and $L_{throat} = 3.5$ inches are shown in Figure 164. The throat location, as determined by the 0.528-critical-pressure ratio, is 1/4 to 3/8 inch upstream of the location determined from the subsonic distributions. The reasons for this are not entirely clear. The 1-dimensional Fanno calculation should be based upon the proper average stagnation pressure across the throat flow. We have used the centerline, or maximum stagnation pressure, at the diffuser inlet. We have not made measurements to determine the variation in stagnation pressure across the flow, although the high Reynolds number turbulent flow should provide an average stagnation pressure not too much different from the centerline value. Furthermore, a 1-dimensional analysis is only an approximation to the actual flow situation, which in this case is a 3-dimensional developing pipe flow. There has been discussion in recent literature by Pearson, et al,* of the true behavior of compound compressible flows, i.e., compound flows with fluid streams having different stagnation conditions. The passage boundary-layer flow is in actuality such a compound flow, with each streamtube in the boundary layer having a different stagnation pressure, and it does appear possible that alterations in throat location may be possible with this type of passage flow. Further work, however, needs to be done to clarify the behavior of choked flows, which at the same time have significant blockage effects caused by subsonic boundary layers. We have chosen to use the 0.528-critical-pressure ratio to determine the throat static pressure in the 3.5-inch-throat tests. Until a clearer understanding of the behavior of such choked flows with relatively large blockages is obtained, the uncertainty of the pressure-recovery values calculated with the 0.528-critical-pressure ratio for the 3.5-inch-throat data will be open to question. (For example, C_p calculated with the 0.528 pressure ratio yields a value $C_p = 0.52$, while a pressure ratio of 0.475 yields $C_p = 0.54$, a difference of 4 percent. The minimum throat pressure ratio corresponding to choking conditions is apparently 0.475, Figure 164). Note that values lower than 0.528-critical-pressure ratio would produce higher pressure recoveries.

The pressure recovery C_p is calculated from

$$C_p = \frac{P_{exit} - P_{throat}}{P_{stagnation\ throat} - P_{throat}} \tag{241}$$

*(See footnote, page 436.)

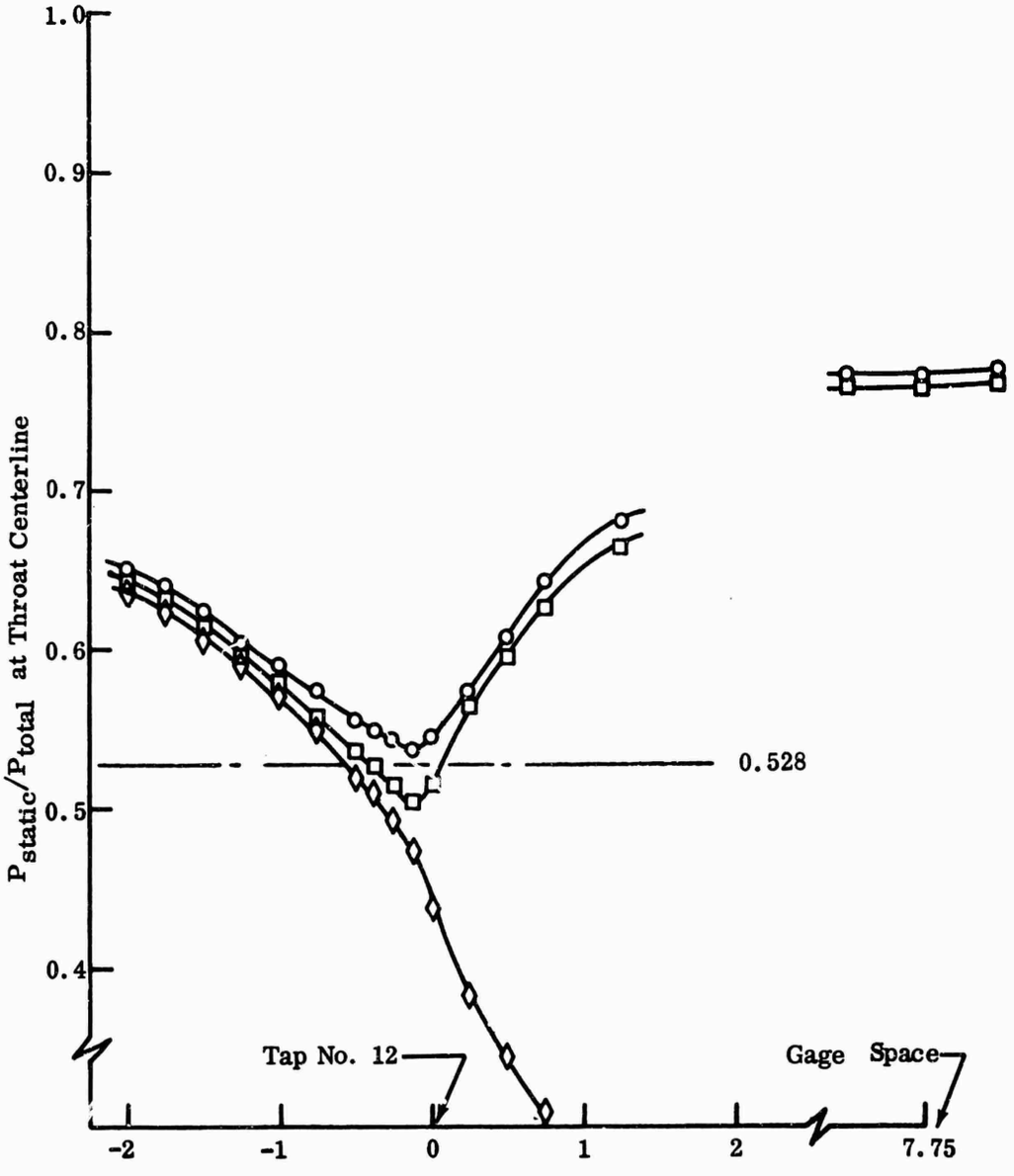


Figure 164. Straight Diffuser Performance (Pressure Ratio Versus Axial Distance For Various Backpressures, 0.25 Aspect Ratio, $2\theta = 6°$, $L_{throat} = 3.5$ Inches).

The data for each test were reduced to the form of Figure 164, pressure ratio versus axial location, and the pressure recovery as a function of Mach number was determined from these plots using the above expression; i.e.,

$$C_p = \frac{\frac{P_{exit}}{P_o} - \frac{P_{throat}}{P_o}}{1 - \frac{P_{throat}}{P_o}} \qquad (242)$$

where:

$$P_o = P_{\text{stagnation throat}}$$

To obtain large values of blockage, some 3.5-inch-throat tests were also made with 0.040-inch-diameter trips glued to the upper and lower nozzle blocks at the entrance to the throat passage. These tests were only run for the 0.25 aspect ratio diffuser.

A pressure transducer was used early in the measurements on the 5.7 aspect ratio diffuser to measure the frequency and amplitude of pressure fluctuations near the throat and in the pipe at the exit of the diffuser. The transducer was coupled closely enough to the flow so that it measured the actual pressure fluctuations with good fidelity. No appreciable difference was noticed between the measurements observed near the throat and in the exit of the diffuser. Some effect on frequency and amplitude of pressure fluctuations was observed as a function of inlet Mach number (increasing amplitude and frequency with increasing Mach number). The transducer was not used for the 0.25 aspect ratio tests.

In the 5.7 aspect ratio studies, the uncertainty in determining pressure recovery was approximately 10 percent for low Mach numbers (Mach numbers approximately equal to 0.3), reducing to approximately 4 percent near choke conditions. For the 0.25 aspect ratio tests, the uncertainty in pressure recovery near choking is approximately ±2 percent. These uncertainty calculations and the uncertainty in determining Mach number, 2θ, and L/W are given in Section 5.

2.4 FLOW UNSTEADINESS

In all tests, pressure measurements were fairly steady (±0.5 percent), although some rather large, unsteady fluctuations were sometimes observed (±1.0 to 1.5 percent). Reasonably long pressure lines were used to reduce the amplitude of observed fluctuations. In practically all of the 5.7 aspect ratio tests, rather large fluctuations in flow rate (manometer reading) were observed at or near choking flow; the manometer reading would fluctuate about some readings (±1.5 percent), then quickly drop in magnitude (-15 percent) and quickly recover to the same random unsteadiness as before the drop.

3.0 RESULTS AND DISCUSSION

There are 2 sets of data at high inlet Mach numbers; the 2 sets of present data at aspect ratios of 5.7 and 0.25, and the collection of low Mach number data reported by Reneau for large aspect ratios from which conclusions may be drawn about the performance of straight-wall diffusers. The data are most usefully presented in the form of contour plots (usually with C_p as a parameter, i.e., a contour plot with C_p appearing as the elevation) from which conditions for obtaining maximum pressure recovery can be graphically seen.

Reneau reports sufficient data to present such contour plots. The data are given in the form of area ratio versus inlet throat-length-to-diffuser-width ratio, with contours of constant pressure recovery (for fixed values of blockage, aspect ratio, and low Mach numbers). From such contour maps (in this case for low inlet Mach numbers) a ridge of maximum pressure recovery can be seen. Along this ridge optimum diffuser performance can be obtained.

The present high inlet Mach number data are insufficient to present the results of diffuser performance in the form given by Reneau. The present data have been obtained at essentailly only a single throat-length-to-width ratio (L/W = 15). However, the range of blockage used in the present tests makes other forms of presentation appropriate. Performance maps will be presented in 2 forms which permit the easiest grasp of the significance of the data:

1) In the form of pressure recovery versus divergence angle with blockage as parameter; or

2) In the form of blockage versus divergence angle with pressure recovery as parameter.

The data of Reneau are compared in these same forms from cross-plots. Some data at L/W = 10 for the 5.7 aspect ratio studies were also obtained. However, the extent of these data is really insufficient for meaningful conclusions to be made.

3.1 C_p VERSUS INLET MACH NUMBER

For the 5.7 aspect ratio studies, diffuser performance was measured over a wide range of subsonic inlet Mach numbers. Over this range of inlet Mach numbers, pressure recovery correlates on diffuser divergence angle 2θ, as follows:

1) At small divergence angles (2θ = 4 degrees) with low blockage ratios (B_{choke} = 0.05), the pressure recovery rises with increasing Mach number; a variation of 25 to 30 percent between Mach number = 0.3 and choking conditions at L/W = 10.

2) At large angles (2θ = 12 degrees) and low blockage ratios (B_{choke} = 0.05), the recovery falls with increasing Mach numbers; a variation of 15 percent between Mach number 0.3 and choking conditions at L/W = 10.

3) For intermediate angles and for all angles at higher blockage ratios (data for B_{choke} = 0.14), the performance remains relatively constant from Mach number = 0.3 to choking.

The interpretation of these trends is subject to the uncertainty in the data discussed earlier; 10 percent (or six to seven points in recovery) at Mach number = 0.3, decreasing to 4 percent (or two to three points in recovery) at choking.

Insufficient data are available at L/W = 15 to draw the same conclusions for the 0.25 and 5.7 aspect ratio tests.

The following results are apparent from an examination of these data (Figures 165 through 173):

1) For the present range of parameters, no critical subsonic inlet Mach number exists in the sense of the conclusions reached in Appendix XI.

2) There is no clear-cut classification, on the basis of performance versus inlet Mach number characteristic, of groupings of diffuser characteristics such as A, B, and C predicated in Appendix XI. The range of the diffuser parameters on the flow-regime map covers the regions common to Groups A and B (Figure 154).

3) Diffuser performance does not suffer a drastic drop until supercritical flow conditions are reached. Performance drops abruptly when the Mach number immediately ahead of the shock in the diffuser passage reaches a value of approximately 1.1 to 1.2. The performance probably suffers

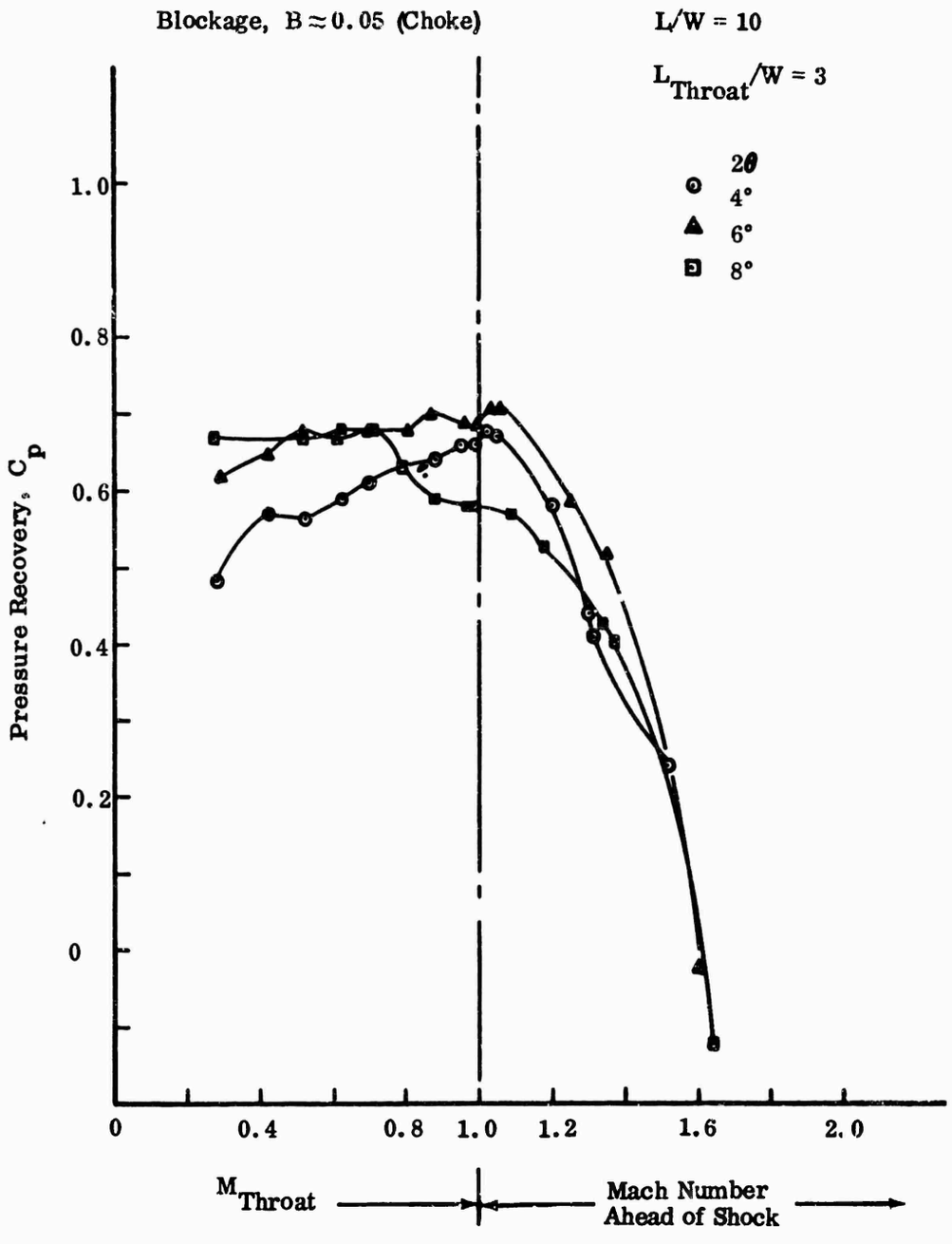


Figure 165. Straight Diffuser Performance (C_p Versus Mach Number).

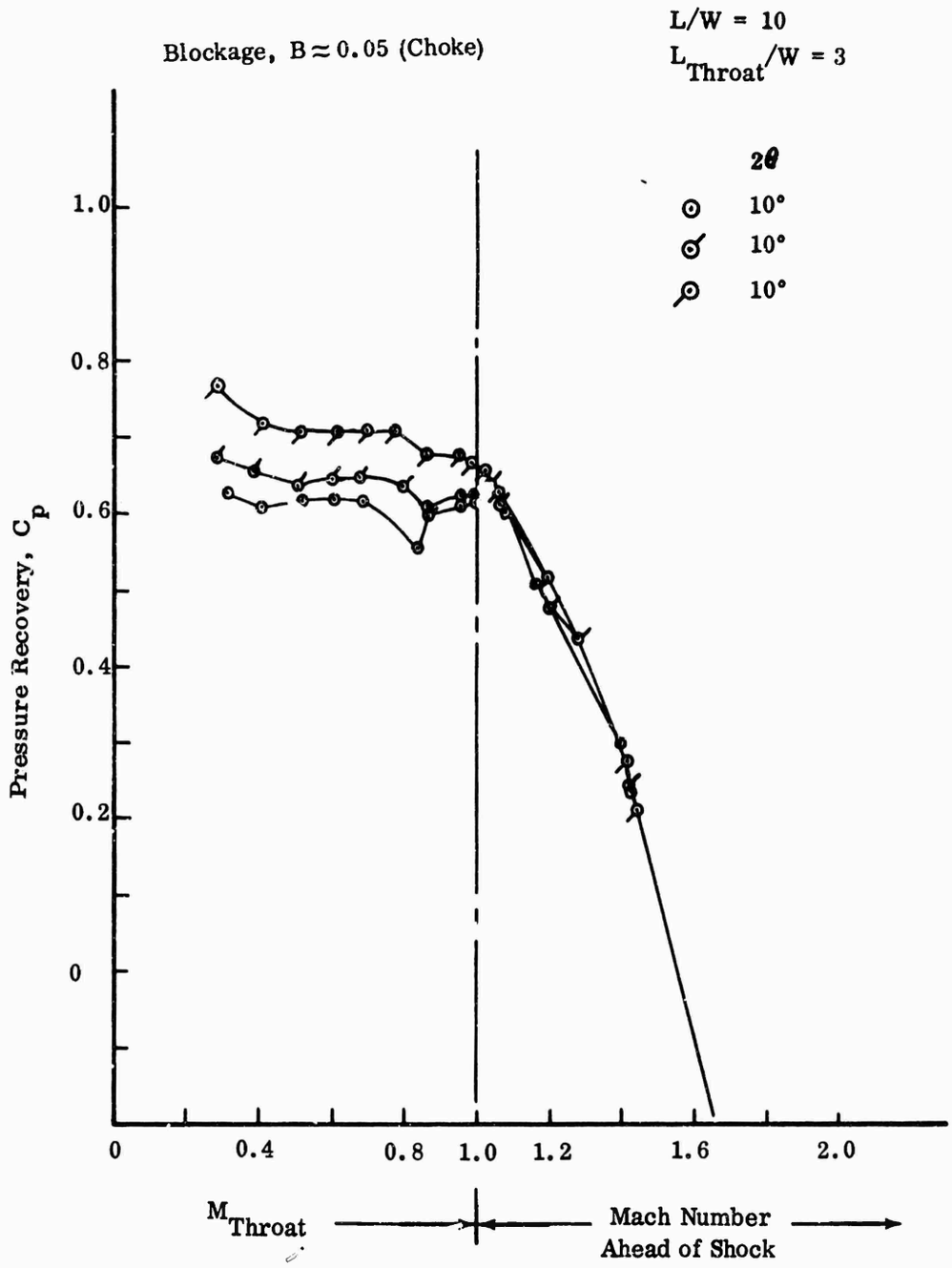


Figure 166. Straight Diffuser Performance (C_p Versus Mach Number).

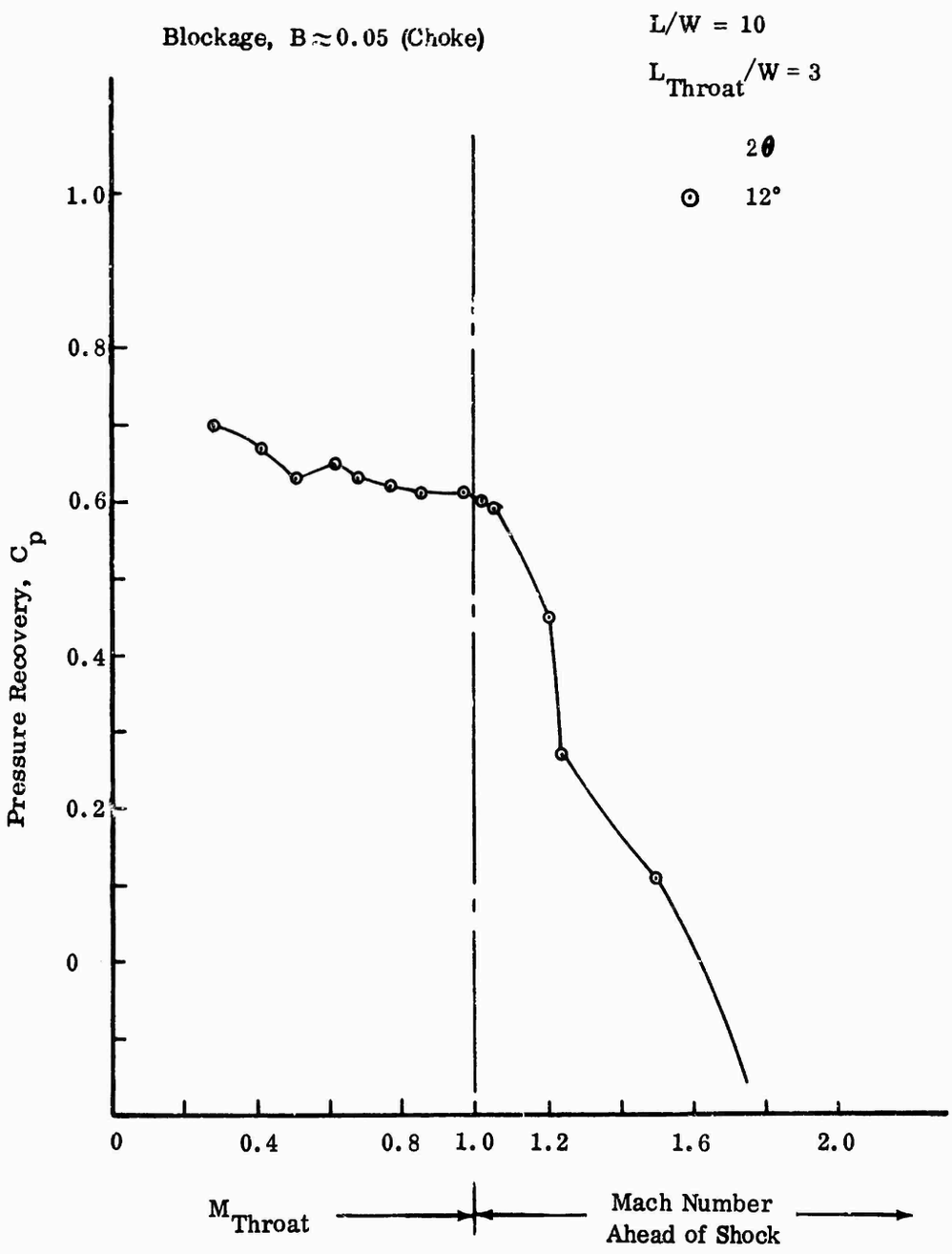


Figure 167. Straight Diffuser Performance (C_p Versus Mach Number).

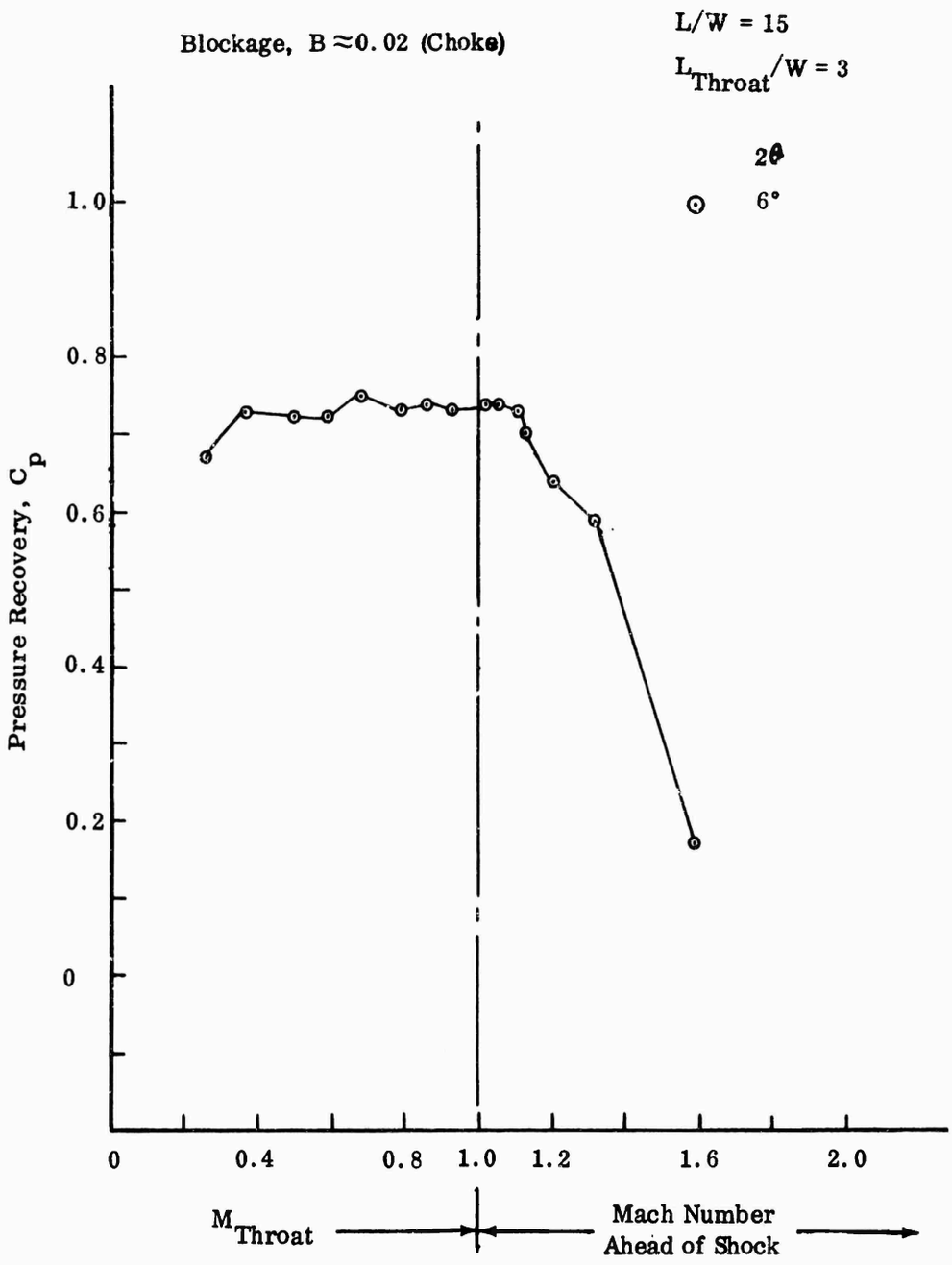


Figure 168. Straight Diffuser Performance (C_p Versus Mach Number).

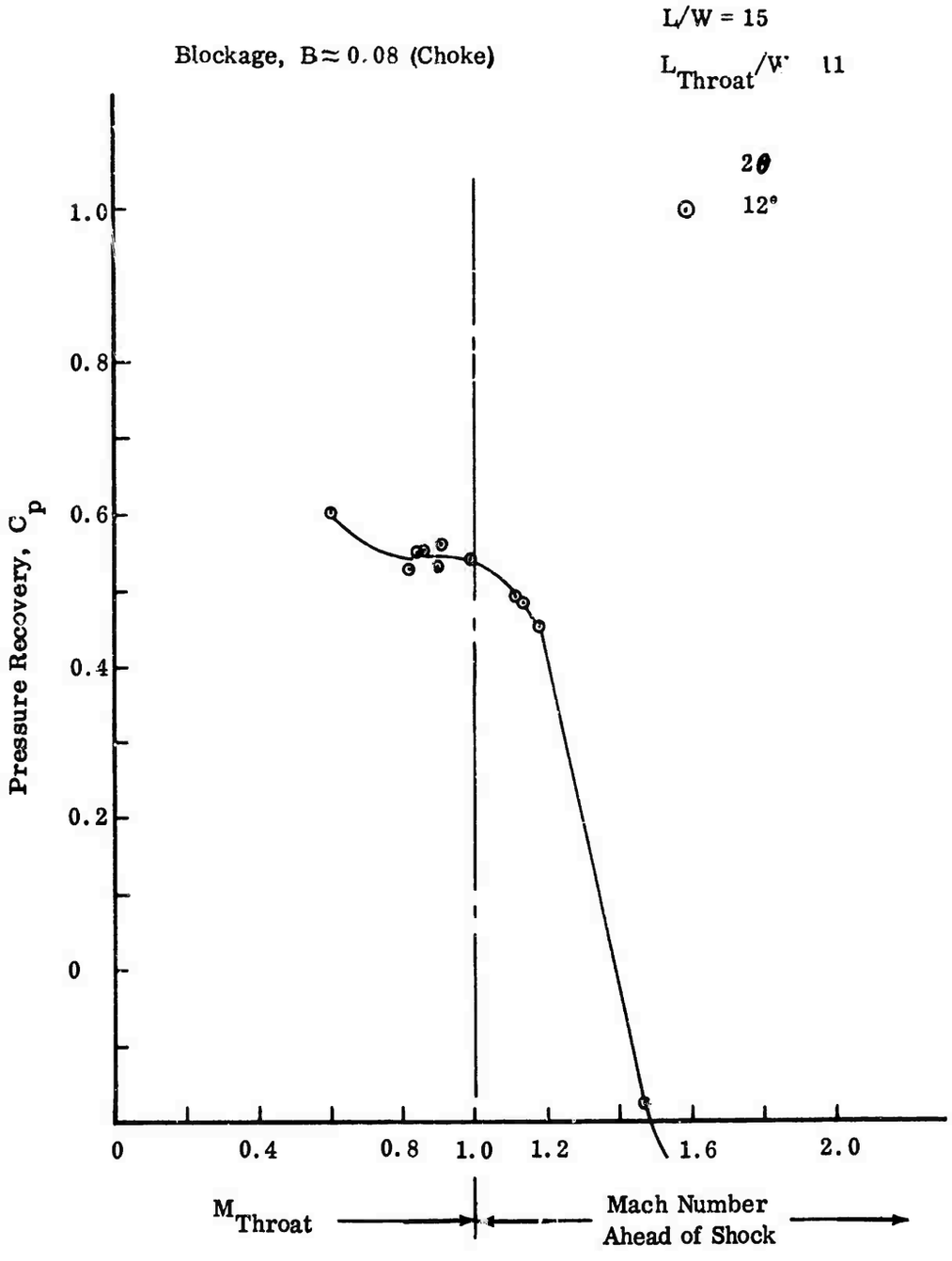


Figure 169. Straight Diffuser Performance (C_p Versus Mach Number).

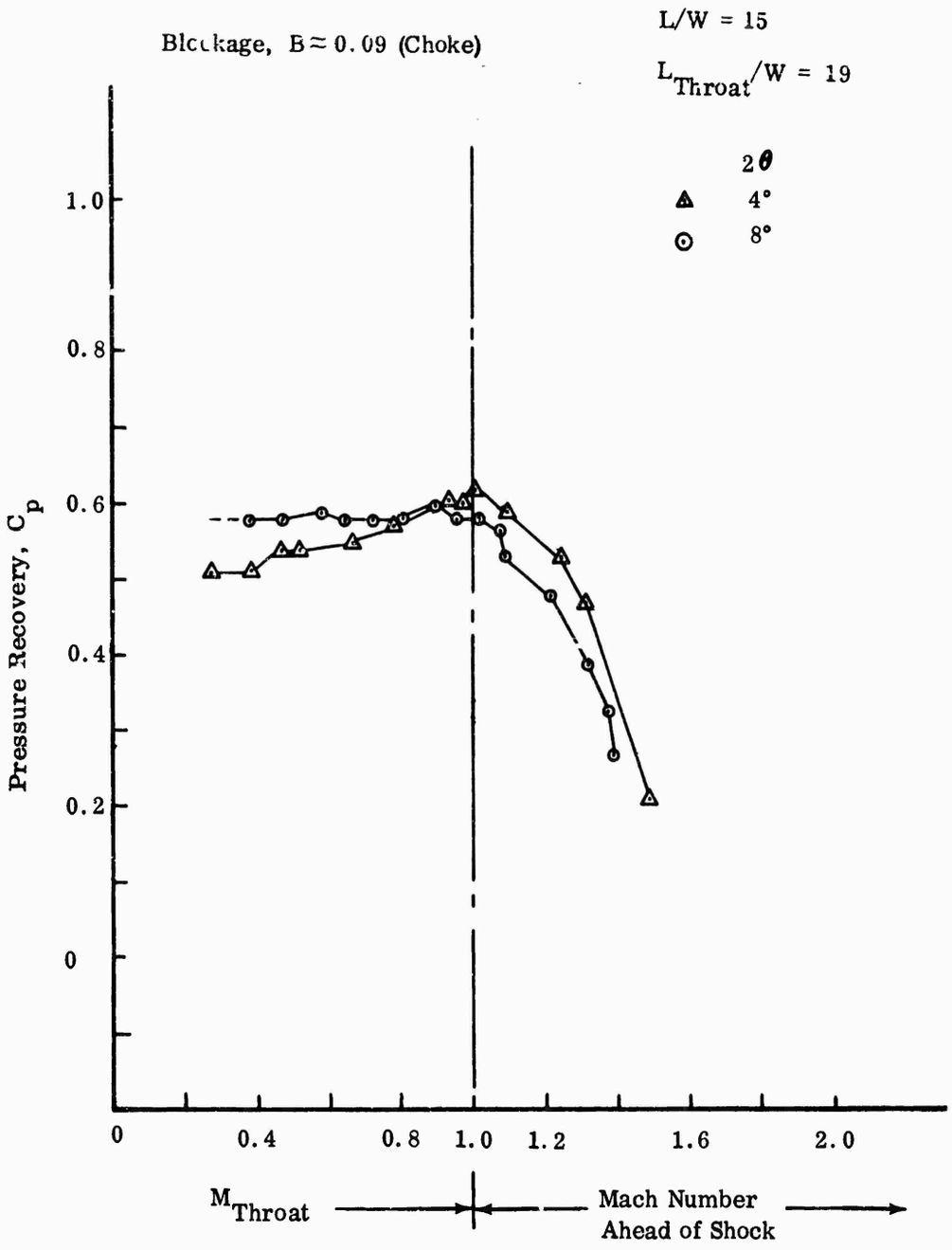


Figure 170. Straight Diffuser Performance (C_p Versus Mach Number).

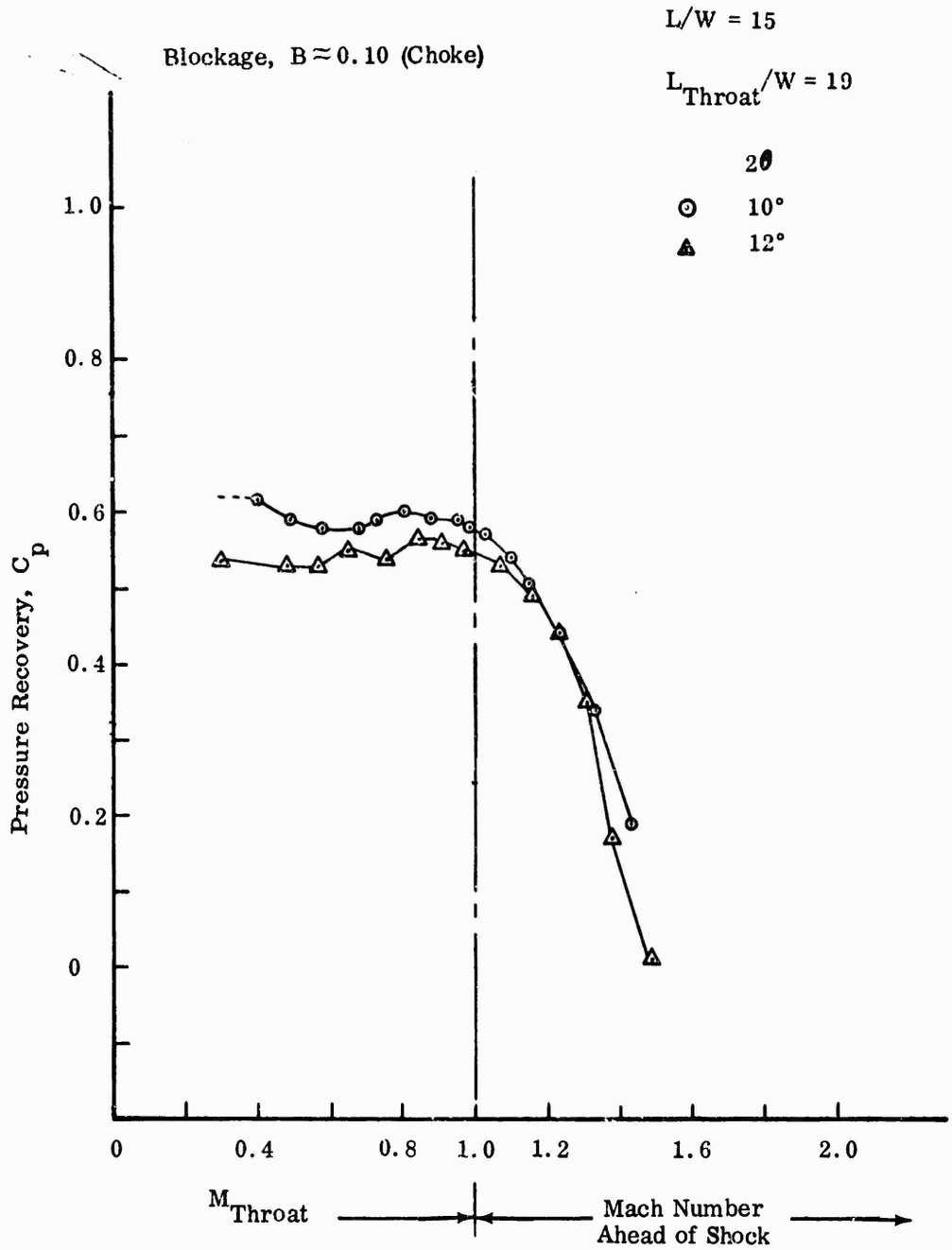


Figure 171. Straight Diffuser Performance (C_p Versus Mach Number).

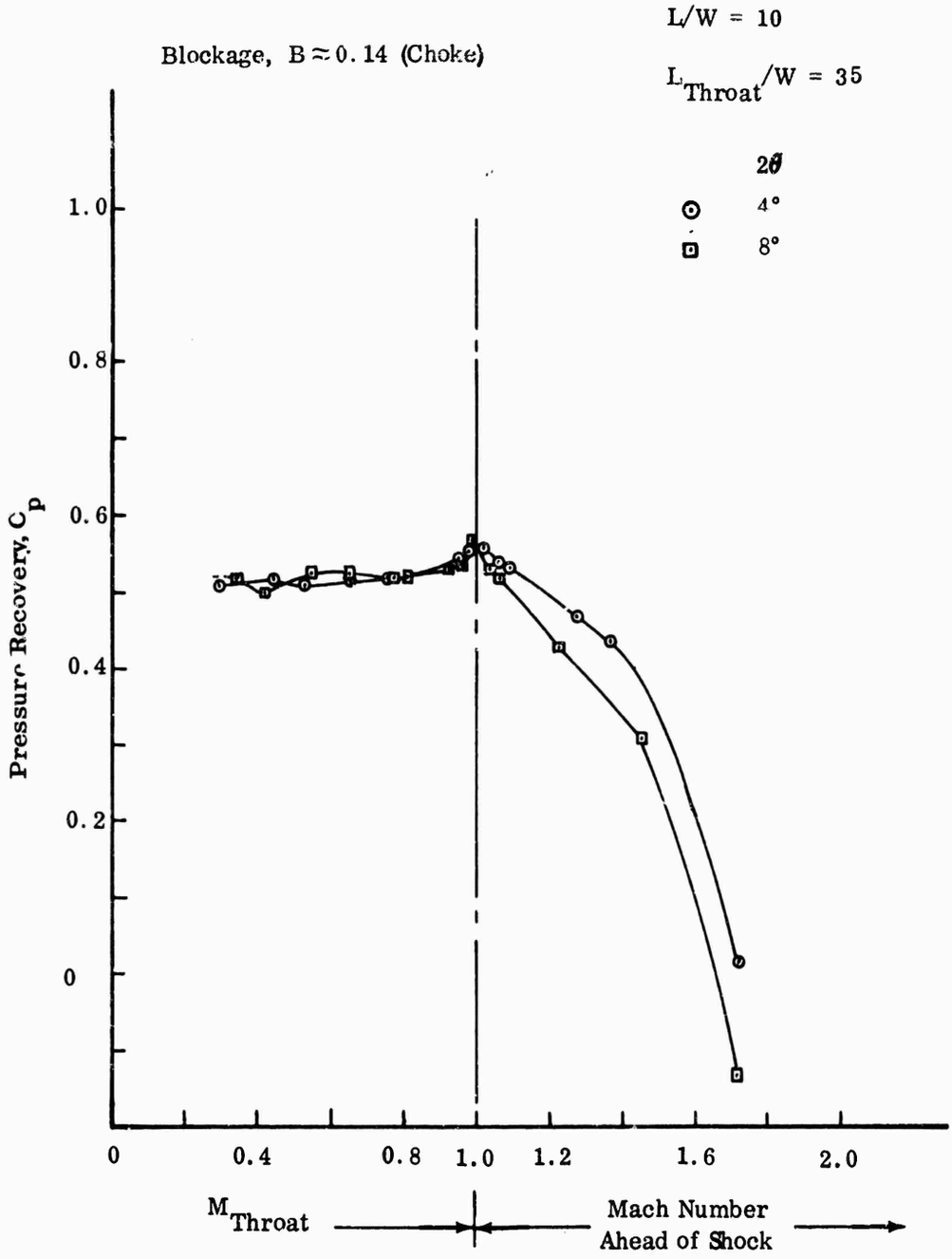


Figure 172. Straight Diffuser Performance (C_p Versus Mach Number).

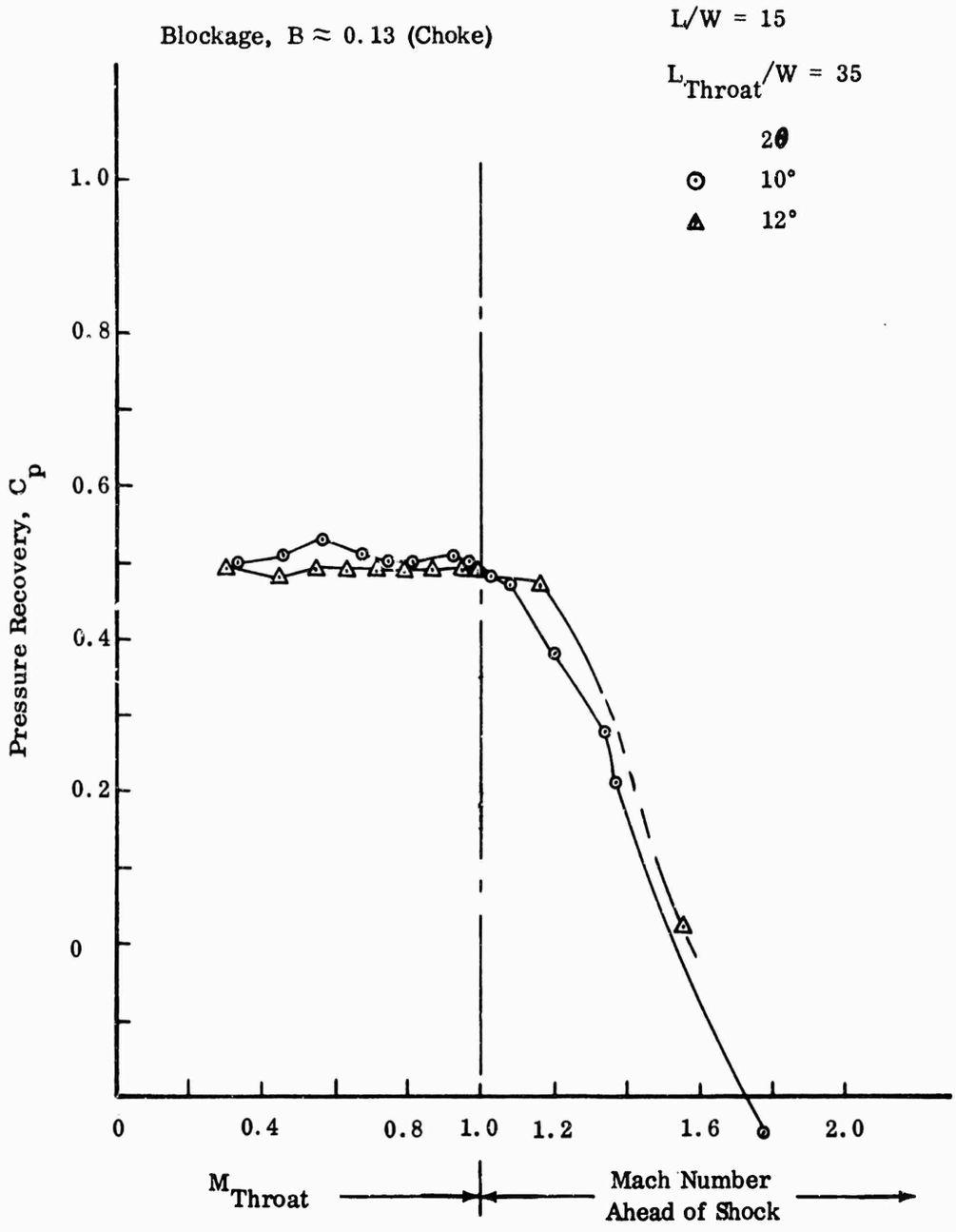


Figure 173. Straight Diffuser Performance (C_p Versus Mach Number).

beyond this point largely because of shock-induced boundary-layer separation, resulting in separated flow throughout the diffuser.

4) Data at low Mach numbers agree with the data of Reneau* ($M < 0.2$), if consideration is made of the rather large uncertainty (approximately 6 to 7 points in performance) in the present data. The data taken at low Mach numbers have this large uncertainty because of the large uncertainty in the pressure readings compared to the pressure difference terms appearing in the expression for the pressure coefficient at these low Mach numbers (see Section 5.0).

These tests show that for the range of diffuser parameters tested, the major conclusions reached in Appendix XI are not correct, at least regarding the Group A characteristics, and that in most cases good performance is maintained over the entire range of subsonic inlet Mach numbers.

3.2 C_p SUPERCRITICAL FLOW CONDITIONS

Supercritical flow conditions are defined as all diffuser back pressure conditions at which choking ($M_{throat} = 1.0$) is maintained at the diffuser throat. In all cases of supercritical conditions, a sudden decrease in recovery is observed when a shock stands in the diffuser with a Mach number immediately upstream of the shock of approximately 1.1 to 1.2. Fair performance can be expected, even at supercritical conditions, if a normal shock in the diffuser is weak enough such that the stagnation-pressure loss through the shock is small and the static-pressure rise across the shock is small enough not to induce separation of the wall boundary layers. Based on an analysis of Stodola's data ** and the results of the present studies, a choked diffuser will produce recovery (approximately the same as its recovery at incipient choking) as long as the shock Mach number in the diffusing passage is less than 1.1 to 1.2. Above a shock Mach number of this value, a precipitous drop in recovery occurs. For optimum performance of a fixed geometry diffuser under supercritical flow conditions, a diffuser should be operated at a back pressure as close to $P_{exit} = P_{exit\ choke}$ as possible.

3.3 COMPARISON OF PRESENT DATA WITH LOW MACH NUMBER DATA OF RENEAU — C_p VERSUS 2θ

The present data are compared with the low Mach number data of Reneau* in Figures 174 through 176 (C_p versus 2θ).

---

*(See footnote, page 432.)

**A. Stodola, and L.C. Loewenstein, Steam and Gas Turbines, Vol. 1, pp 82-105; Peter Smith, New York, 1945.

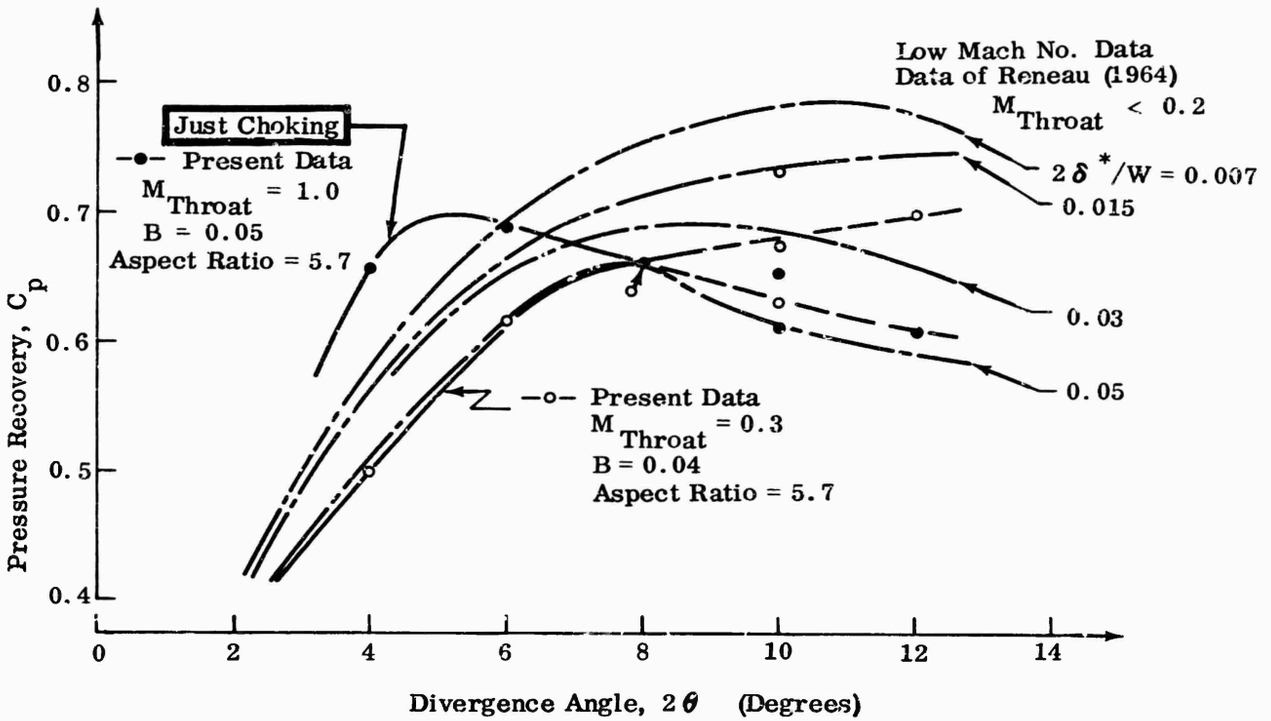


Figure 174. Straight Diffuser Performance (Pressure Recovery Versus Divergence Angle, L/W = 10).

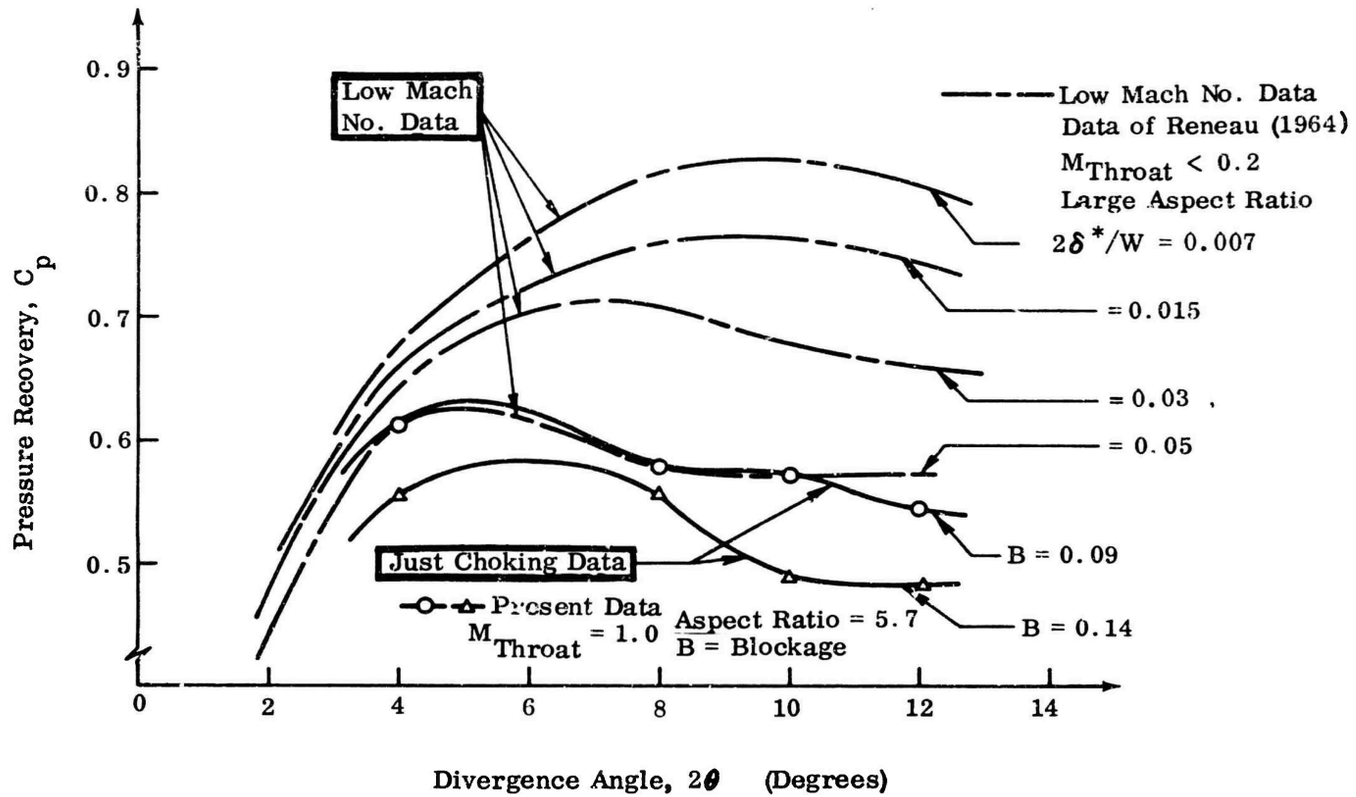


Figure 175. Straight Diffuser Performance (Pressure Recovery Versus Divergence Angle, L/W = 15).

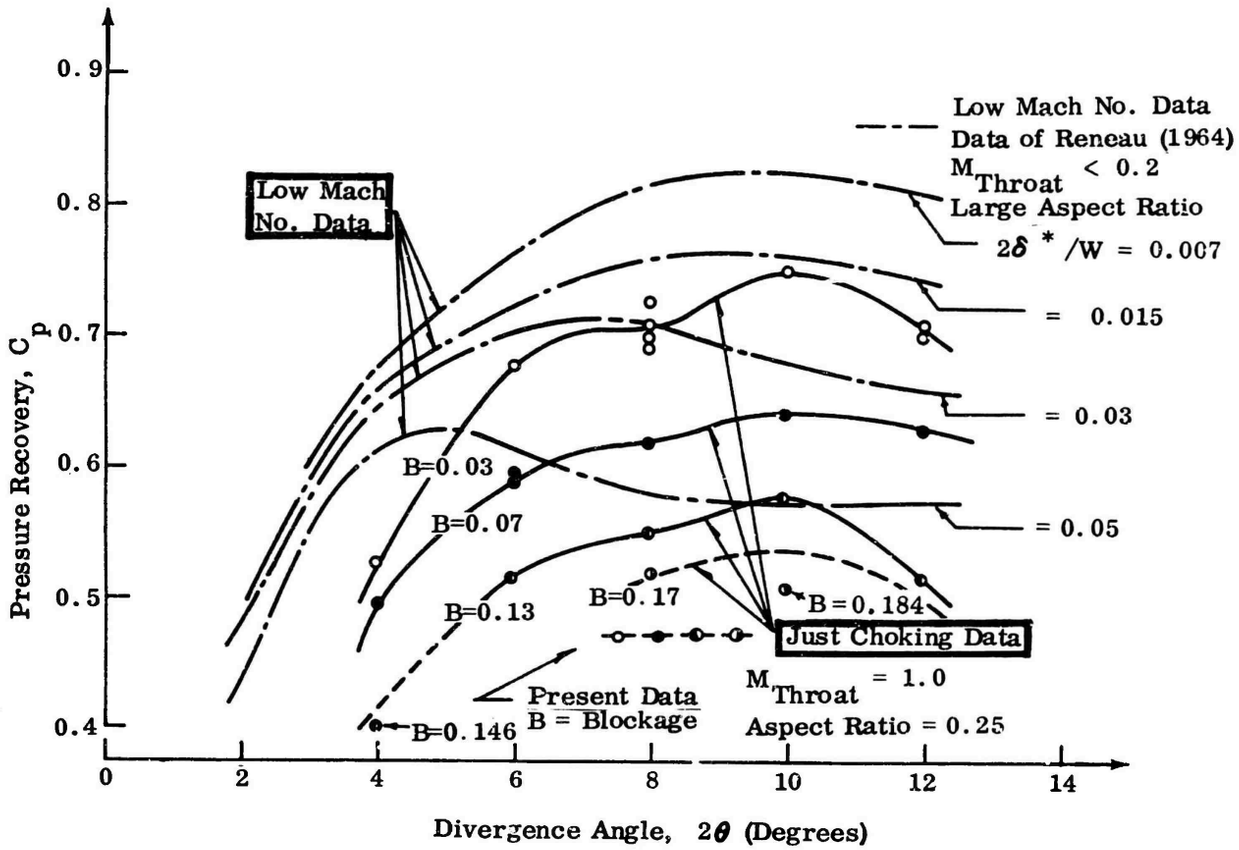


Figure 176. Straight Diffuser Performance (Pressure Recovery Versus Divergence Angle, L/W = 15).

Reneau reports his data to be valid for Mach numbers less than 0.2 to 0.3. Data are reported by Reneau only for blockage ratios less than 0.05. For L/W = 10, only one set of data has been taken at low blockage ratios (B = 0.04) and low Mach numbers (Mach number = 0.3) in the present studies. Within the certainty of the data at this low Mach number, there is agreement between the data of Reneau and the present data except at the higher divergence angles; the present data do not show as early a drop-off in performance with increasing divergence angle at constant blockage as reported by Reneau. The data continue to rise for a 2θ of 8 degrees.

The data for throat Mach number = 1 and blockage B = 0.05 (L/W = 10, aspect ratio = 5.7) show a significant alteration in C_p versus 2θ from that reported for low Mach number flow. Higher values of pressure recovery are obtained at the lower divergence angles studied (2θ = 4 and 6 degrees), while approximately the same pressure recovery is obtained at higher divergence angles. A change in the pressure-recovery characteristic between low inlet Mach numbers and high inlet Mach numbers is observed in all of the data.

For L/W = 15, M = 1.0, aspect ratio = 5.7 (Figure 175), all of the present data are at larger values of blockage than covered by Reneau except for one point at 2θ = 6 degrees and B = 0.04. This 6-degree point agrees with the data of Reneau.

The principal conclusion is that it is not reliable to predict high inlet Mach number performance on the basis of low inlet Mach number data. On the basis of the pressure recovery versus inlet Mach number characteristic results discussed in 3.1, an extrapolation may be made from low inlet Mach number data. However, such extrapolation of data would not be expected to be highly reliable.

3.4 C_p VERSUS B AND ASPECT RATIO AT HIGH INLET MACH NUMBERS

Whereas a survey of low inlet Mach number performance was made for the 5.7 aspect ratio studies, the 0.25 aspect ratio studies only measured pressure recovery at or near choking conditions.

A sufficient amount of data to formulate design criteria at high inlet Mach numbers is only available for L/W = 15. Of these data, the more complete set is available for the 0.25 aspect ratio diffuser: C_p data for blockages of 0.03, 0.07, 0.09, and 0.17 at just choking conditions. For the 5.7 aspect ratio diffuser, data are available only for blockages of 0.09 and 0.14 at just choking conditions. The data, in the form of C_p versus 2θ as a function of blockage, are presented for the 0.25 aspect ratio diffuser in Figure 176 and the 5.7 aspect ratio diffuser in Figure 175. These figures represent a composite of these sets of data overlaid on the L/W = 15 data of Reneau (large aspect ratio, Mach number less than 0.2). From these data, 3 important conclusions may be drawn:

1) The 2 sets of data for large aspect ratio (aspect ratio = 5.7 and data of Reneau) exhibit the same trend in pressure recovery with divergence angle and blockage: a rapidly rising pressure recovery at low angles (with a peak pressure recovery at some angle which is a function of blockage) followed by a gently falling recovery at large 2θ. However, there is a marked shift in the pressure-recovery characteristic (C_p versus 2θ) between the low inlet and high inlet Mach number data; at high inlet Mach numbers, increasing blockage produces higher recovery for a given angle than at low inlet Mach numbers.

2) Entirely different characteristics (C_p versus 2θ) are obtained with low aspect ratios than with high aspect ratios.

3) In spite of the fact that diffuser performance is reasonably well behaved over the entire range of subsonic inlet Mach numbers, i.e., no critical Mach numbers above which performance suffers a drastic decline (Section 3.1), high inlet Mach number data cannot be predicted using low inlet Mach number characteristics. At high inlet Mach numbers there is a drastic alteration in performance characteristics with diffuser aspect ratio. Although data are not available for low Mach number diffusers, the same effect of aspect ratio may hold for low Mach number diffuser performance.

The performance data at L/W = 15 as a function of blockage and divergence angle 2θ (Figures 175, 176, 177, and 179) for high inlet Mach number show the following characteristics:

1) For the 0.25 aspect ratio diffuser, a ridge of maximum recovery exists at a divergence angle 2θ of 10 degrees and recovery decreases with increasing blockage. The functional relationship between pressure recovery and blockage, for aspect ratio 0.25, 2θ = 10 degrees, and L/W = 15, with just choking flow, is shown in Figure 179.

2) For an aspect ratio of 5.7, a ridge of maximum pressure recovery at just choking flow occurs at a divergence angle $2\theta \approx 6$ degrees (Figure 175). Leaky pressure taps invalidated data for B = 0.02 at 2θ = 4, 8, 10, and 12 degrees, and data for 2θ = 6 degrees at B = 0.09 and 0.14. Time has not permitted a recheck of these points.

The trend of pressure recovery with blockage and divergence angle is also conveniently seen on contour maps with pressure recovery as a function of blockage and divergence angle, 2θ. The just choking inlet Mach number data are presented in this form for L/W = 15 and 10 and for the two aspect ratios 0.25 and 5.7 in Figures 177 and 178. Also indicated on these plots are cross-plots of the low Mach number data of Reneau.

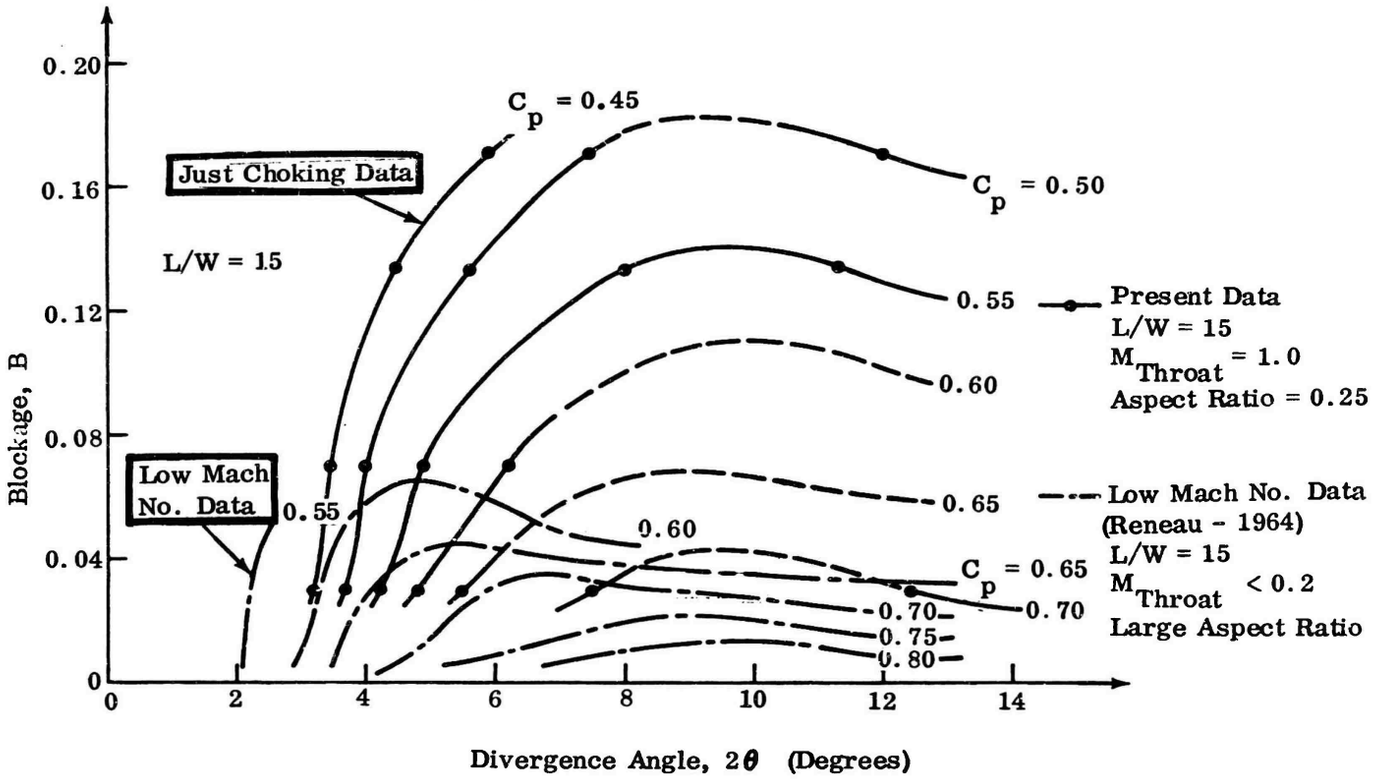
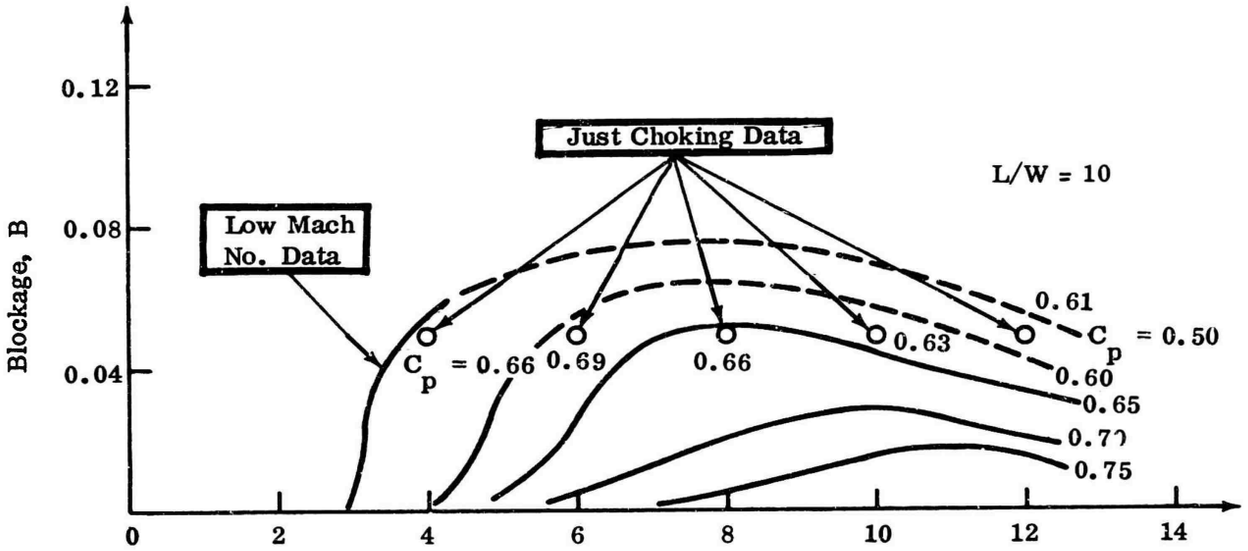


Figure 177. Straight Diffuser Performance (Blockage Versus Divergence Angle With Pressure Recovery as Parameter).



⊖ Present Data
L/W = 10
M_{Throat} = 1.0
Aspect Ratio = 5.7

—— Low Mach No. Data
Data of Reneau (1964)
L/W = 10
$M_{Throat} < 0.2$
Large Aspect Ratio

Figure 178. Straight Diffuser Performance (Blockage Versus Divergence Angle With Pressure Recovery as Parameter).

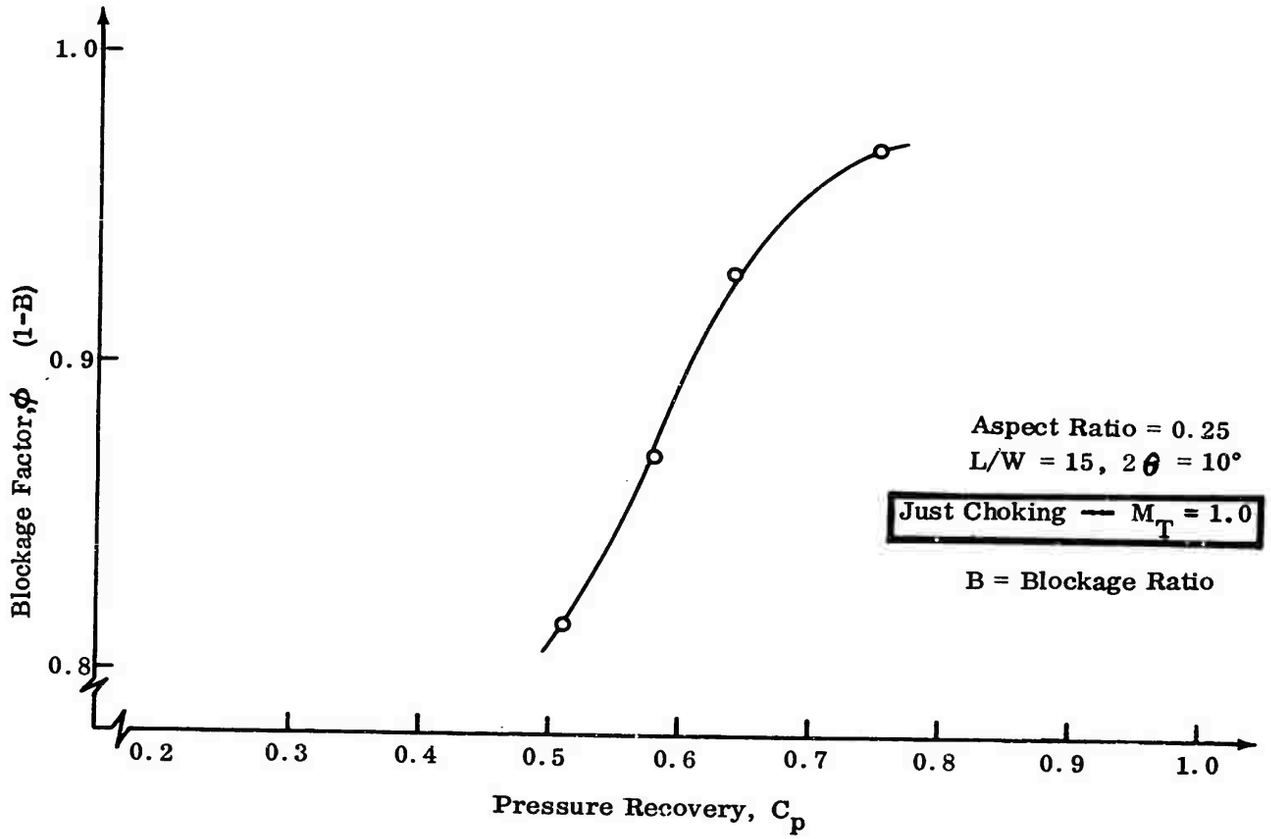


Figure 179. Straight Diffuser Performance.

4.0 RECOMMENDATIONS

Further studies are desirable to:

1) Extend diffuser performance maps at high inlet Mach number over a wider range of L/W and aspect ratio;

2) Extend the present data to low inlet Mach numbers.

4.1 HIGH MACH NUMBER DIFFUSER MAP

In order to map diffuser performance adequately at high inlet Mach numbers, a larger range of geometrical variables (L/W and aspect ratio) is needed. The present high Mach number data for L/W = 15 do not permit the selection of an optimum design at other values of L/W.

The large change in C_p characteristics, as a function of aspect ratio, suggests the importance of further studies to determine the optimum aspect ratio, other variables being fixed.

The selection of the optimum diffuser, i.e., the selection of optimum C_p from maps of C_p as a function of B and 2θ for a range of L/W and aspect ratio, is required for the development of optimum diffuser designs. The development of diffuser performance maps, i.e., C_p as a function of

1) 2θ;

2) L/W;

3) aspect ratio;

4) throat blockage;

5) inlet Mach number;

involves a lengthy experimental program. It is recommended that further investigations of diffuser performance maps be pursued. Immediate studies should be concentrated on L/W ratios surrounding L/W = 15, e.g., L/W = 10 and 20, and for aspect ratios between 0.25 and 5.7, e.g., 1.0.

4.2 LOW MACH NUMBER DATA

As a further cross-check on the data reported here and by Reneau, it may be desirable to repeat and extend data to lower inlet Mach numbers. If such data are taken, more sensitive gages (such as mercury or water manometers instead of

bourdon tube gages, as used in the present study) should be used to obtain more accurate data.

4.3 RESOLVING UNSTEADY CHARACTER OF MASS FLOW RATE

It may be desirable to determine if the shedding of stalled fluid from upstream of the diffuser throat was responsible for large fluctuations in mass flow rate observed in the 5.7 aspect ratio diffuser tests. A single test of a redesigned inlet geometry to eliminate any possible shedding of stalled fluid should determine the effect on measured C_p of any flow unsteadiness (if produced by the shedding of stalled fluid from upstream). If the elimination of flow unsteadiness produces an alteration in C_p, then the 5.7 aspect ratio data should be repeated.

4.4 INLET BOUNDARY-LAYER VELOCITY PROFILE

The shape of the inlet boundary-layer velocity profile producing a given value of blockage may have an important influence on the magnitude of the pressure recovery. The present tests have not made a systematic study of this parameter which may be important in the design of high-speed machines. Future work should survey the importance of this parameter.

5.0 UNCERTAINTY ANALYSIS

1) BLOCKAGE —B

$$\text{At choking, } \dot{m} = \frac{0.532}{\sqrt{T_o}} \quad P_o A_{flow} \tag{243}$$

(at choking conditions $P_{throat} = 0.528 P_o$)

$$\text{Hence, } A_{flow} = \frac{\dot{m}\sqrt{T_o}}{0.532 P_o}$$

$$\text{or } \frac{A_{flow}}{A_{geometric}} = \frac{\dot{m}\sqrt{T_o}}{0.532 P_o A_{geometric}}$$

$$\text{Blockage } B = \frac{A_{flow} - A_{geometric}}{A_{geometric}} = 1 - \frac{A_{geometric} - A_{flow}}{A_{geometric}} = 1 - \phi \tag{239}$$

where: P_o = psia

T_o = °R

A = $in.^2$

From orifice reading, $\dot{m} = \frac{k\sqrt{H\ P_1}}{T_1}$ (244)

where: H = manometer reading = $in.H_2O$

P_1 = orifice pressure = psia

T_1 = orifice temperature = °R

$$\frac{\Delta B}{B} = \frac{\Delta \phi}{\phi} = \left[\left(\frac{1}{2}\ \frac{\Delta H}{H}\right)^2 + \left(\frac{1}{2}\ \frac{\Delta P_1}{P_1}\right)^2 + \left(\frac{1}{2}\ \frac{\Delta T_o}{T_o}\right)^2 + \left(\frac{1}{2}\ \frac{\Delta T_1}{T_1}\right)^2 + \left(\frac{\Delta P_o}{P_o}\right)^2\right]^{1/2} \quad (245)$$

For L_{throat} = 0, 1.5, 3.5 inches

T_o	= 600°R	ΔT_o	$= T_1$ = 1°R
P_o	$= P_1$ = 95 psia	ΔP_o	$= P_1$ = 0.2 psia
H	= 30 $in.H_2O$	ΔH	= 0.07

$\frac{\Delta B}{B}$ = 0.0039 = ± 0.4%

Blockage values at subsonic conditions are calculated in a similar fashion except that account is taken of the 1-dimensional A_{flow} due to subsonic flow, i.e.,

$$\dot{m} = k \frac{P_o}{\sqrt{T_o}} f(M) A_{flow}$$ where: f(M) is a function of Mach number.*

2) L/W

$L = 1.865$ $\quad \Delta L = 0.001$

$W = 0.125$ $\quad \Delta W = 0.001$

$$\frac{\Delta L/W}{L/W} = \left[\left(\frac{\Delta L}{L}\right)^2 + \left(\frac{\Delta W}{W}\right)^2\right]^{1/2} = \left[\left(\frac{0.001}{1.875}\right)^2 + \left(\frac{0.001}{0.125}\right)^2\right]^{1/2} \quad (246)$$

$$= \left[(0.008)^2\right]^{1/2} = 0.008 = .8\% \text{ (maximum)}$$

3) 2θ

$2\theta = 4, 6, 8, 10, 12$ degrees ± 0.1 degree

$$\frac{\Delta 2\theta}{2\theta} = \frac{0.10}{4} = 0.025 = 2.5\% \text{ (maximum)}$$

*A. H. Shapiro, The Dynamics and Thermodynamics of Compressible Fluid Flow, Vol. I, The Ronald Press Company, New York, 1953, p. 84.

UNCLASSIFIED

4) PRESSURE RECOVERY — C_p

$$C_p = \frac{\frac{P_{exit}}{P_o} - \frac{P_{throat}}{P_o}}{1 - \frac{P_{throat}}{P_o}} = \frac{x}{y} \qquad (242)$$

$$\frac{\Delta x}{x} = \left[\left(\frac{\Delta P_{exit}}{P_{exit} - P_{throat}} \right)^2 + \left(\frac{\Delta P_{throat}}{P_{exit} - P_{throat}} \right)^2 \right]^{1/2} \qquad (247)$$

$$\frac{\Delta y}{y} = \left[\left(\frac{\Delta P_o}{P_o - P_{throat}} \right)^2 + \left(\frac{\Delta P_{throat}}{P_o - P_{throat}} \right)^2 \right]^{1/2} \qquad (248)$$

$$\frac{\Delta c_p}{c_p} = \left[\left(\frac{\Delta x}{x} \right)^2 + \left(\frac{\Delta y}{y} \right)^2 \right]^{1/2} \qquad (249)$$

a) Low Inlet Mach Number ($M \approx 0.2$)

(Aspect ratio = 5.7, $L_{throat} = 0$, $L/W = 15$, $2\theta = 4$ degrees)

P_{exit} = 72 psig $\quad \Delta P_{exit}$ = 0.1 psi

P_{throat} = 70 psig $\quad \Delta P_{throat}$ = 0.1 psi

P_o = 75 psig $\quad \Delta P_o$ = 0.2 psi

$$\frac{\Delta x}{x} \approx \frac{\Delta y}{y} \approx 0.07$$

$$\frac{\Delta C_p}{C_p} = \left[2 \times 50 \times 10^{-4} \right]^{1/2} = 0.1 = \pm 10\%$$

UNCLASSIFIED

UNCLASSIFIED

b) High Inlet Mach Number (M = 1.0)

(Aspect ratio = 5.7, L_{throat} = 0, L/W = 15, 2 θ = 4 degrees)

P_{exit}	=	60 psig	ΔP_{exit}	=	0.2 psi
P_{throat}	=	33 psig	ΔP_{throat}	=	0.4 psi
P_o	=	75 psig	ΔP_o	=	0.2 psi

$$\frac{\Delta x}{x} = 0.016 \qquad \frac{\Delta y}{y} = 0.0105$$

$$\frac{\Delta C_p}{C_p} \approx 0.02 = \pm 2\%$$

The above examples of the uncertainty in C_p represent typical examples of test data from these studies. The uncertainty odds in the basic quantities appearing in these estimates is 20:1. Particular tests may have slightly lower or higher uncertainty, depending upon the differences in values of $P_{exit} - P_{throat}$ and $P_o - P_{throat}$.

6.0 CONCLUSIONS

This study has demonstrated that:

1) Performance in terms of C_p as a function of inlet Mach number does not show a critical subsonic inlet Mach number above which performance suffers a drastic drop.

2) Performance of supercritical flow diffusers is approximately the same as diffusers on the verge of choking, if the shock Mach number is about 1.1 to 1.2 or less.

3) The range of present data covers both group A and B diffusers, previously deduced in Appendix XI to depend upon flow-regime behavior based on their available evidence. No such groupings are apparent in the present data.

UNCLASSIFIED

4) There is a strong dependence of diffuser pressure recovery C_p on diffuser aspect ratio. For given blockage and L/W (L/W = 15), maximum pressure recovery occurs at 2θ = 10 degrees for an aspect ratio of 0.25 and at 2θ = 6 degrees for an aspect ratio of 5.7.

   For given values of blockage, higher recovery appears to occur for the larger aspect ratios. This conclusion may not be valid for all values of blockage and aspect ratios, however.

5) In all cases, pressure recovery C_p declines with increasing blockage for fixed values of divergence angle 2θ, L/W, and inlet Mach number.

6) Pressure recovery variation with inlet Mach number appears to be correlated with divergence angle 2θ and blockage ratio B. At low values of blockage (B = 0.04), C_p increases with increasing Mach number at small divergence angles (2θ = 4 degrees). C_p decreases with increasing Mach number at large divergence angles (2θ = 12 degrees). At large values of blockage (B = 0.15), C_p is relatively constant with inlet Mach number for divergence angles 2θ from 4 degrees to 12 degrees.

7) The appearance in the published literature of a critical Mach number for a group of A classification of diffusers is perhaps a miscalculation of true inlet Mach number by other investigators. The reasons for this may be:

   a) Many pressure taps are needed near the throat to determine inlet Mach number, because of the large gradient of static pressure at high subsonic Mach numbers;

   b) The adjustment of diffuser back pressure (and hence setting of throat Mach number) near choking conditions is very sensitive; the mass flow hardly changes as diffuser back pressure is varied;

   c) Other investigators have often used throat pressure taps on curved walls. Wall curvature can produce a false indication of true throat Mach number (the Mach number probably appearing higher than actual). Also, wall curvature in some cases could produce strongly 2-dimensional flows. In this case the throat Mach number would not be uniform and the meaning of obtaining Mach number = 1.0 would not be too clear.

8) The accurate determination of throat stagnation pressure at large values of blockage is necessary to the accurate measurement of pressure recovery in this type of study.

Unclassified

Security Classification

DOCUMENT CONTROL DATA - R&D

(Security classification of title, body of abstract and indexing annotation must be entered when the overall report is classified)

1. ORIGINATING ACTIVITY *(Corporate author)*

The Boeing Company
Seattle, Washington

2a. UNCLASSIFIED

2b. GROUP

3. REPORT TITLE

Element Design and Development of Small Centrifugal Compressor (U) - Volume II

4. DESCRIPTIVE NOTES *(Type of report and inclusive dates)*

5. AUTHOR(S) *(Last name, first name, initial)*

Welliver, A. D.
Acurio, J.

6. REPORT DATE	7a. TOTAL NO. OF PAGES	7b. NO. OF REFS
August 1967	500	44

8a. CONTRACT OR GRANT NO.	9a. ORIGINATOR'S REPORT NUMBER(S)
DA 44-177-AMC-173(T)	
b. PROJECT NO.	USAAVLABS Technical Report 67-30
Task 1M121401D14413	
c.	9b. OTHER REPORT NO(S) *(Any other numbers that may be assigned this report)*
d.	D4-3434

10. AVAILABILITY/LIMITATION NOTICES

In addition to security requirements which apply to this document and must be met, each transmittal outside the agencies of the US Government must have prior approval of US Army Aviation Materiel Laboratories, Fort Eustis, Virginia 23604.

11. SUPPLEMENTARY NOTES	12. SPONSORING MILITARY ACTIVITY
	US Army Aviation Materiel Laboratories Fort Eustis, Virginia

13. ABSTRACT

Contained in this document are appendixes to a report on a research program involving the advancement of single-stage centrifugal compressor technology to attain high pressure ratio (10:1) at a usable efficiency. The main elements, namely, the impeller and the diffuser, were designed, tested, and developed as elements; the results are analyzed and described.

An analysis of the loss of flow through the impeller passage and conditions contributing to early flow separation are discussed as well as suggestions for their prevention. The flow behavior in the vaneless and semivaneless areas and in the channel passage was evaluated from pressure data and schlieric photographs.

DD FORM 1 JAN 64 1473

Unclassified

Security Classification

Unclassified

Security Classification

14. KEY WORDS	LINK A		LINK B		LINK C	
	ROLE	WT	ROLE	WT	ROLE	WT
Compressor: Single-Stage Centrifugal High-Pressure-Ratio						

INSTRUCTIONS

1. ORIGINATING ACTIVITY: Enter the name and address of the contractor, subcontractor, grantee, Department of Defense activity or other organization *(corporate author)* issuing the report.

2a. REPORT SECURITY CLASSIFICATION: Enter the overall security classification of the report. Indicate whether "Restricted Data" is included. Marking is to be in accordance with appropriate security regulations.

2b. GROUP: Automatic downgrading is specified in DoD Directive 5200.10 and Armed Forces Industrial Manual. Enter the group number. Also, when applicable, show that optional markings have been used for Group 3 and Group 4 as authorized.

3. REPORT TITLE: Enter the complete report title in all capital letters. Titles in all cases should be unclassified. If a meaningful title cannot be selected without classification, show title classification in all capitals in parenthesis immediately following the title.

4. DESCRIPTIVE NOTES: If appropriate, enter the type of report, e.g., interim, progress, summary, annual, or final. Give the inclusive dates when a specific reporting period is covered.

5. AUTHOR(S): Enter the name(s) of author(s) as shown on or in the report. Enter last name, first name, middle initial. If military, show rank and branch of service. The name of the principal author is an absolute minimum requirement.

6. REPORT DATE: Enter the date of the report as day, month, year; or month, year. If more than one date appears on the report, use date of publication.

7a. TOTAL NUMBER OF PAGES: The total page count should follow normal pagination procedures, i.e., enter the number of pages containing information.

7b. NUMBER OF REFERENCES: Enter the total number of references cited in the report.

8a. CONTRACT OR GRANT NUMBER: If appropriate, enter the applicable number of the contract or grant under which the report was written.

8b, 8c, & 8d. PROJECT NUMBER: Enter the appropriate military department identification, such as project number, subproject number, system numbers, task number, etc.

9a. ORIGINATOR'S REPORT NUMBER(S): Enter the official report number by which the document will be identified and controlled by the originating activity. This number must be unique to this report.

9b. OTHER REPORT NUMBER(S): If the report has been assigned any other report numbers *(either by the originator or by the sponsor)*, also enter this number(s).

10. AVAILABILITY/LIMITATION NOTICES: Enter any limitations on further dissemination of the report, other than those imposed by security classification, using standard statements such as:

(1) "Qualified requesters may obtain copies of this report from DDC."

(2) "Foreign announcement and dissemination of this report by DDC is not authorized."

(3) "U. S. Government agencies may obtain copies of this report directly from DDC. Other qualified DDC users shall request through _____."

(4) "U. S. military agencies may obtain copies of this report directly from DDC. Other qualified users shall request through _____."

(5) "All distribution of this report is controlled. Qualified DDC users shall request through _____."

If the report has been furnished to the Office of Technical Services, Department of Commerce, for sale to the public, indicate this fact and enter the price, if known.

11. SUPPLEMENTARY NOTES: Use for additional explanatory notes.

12. SPONSORING MILITARY ACTIVITY: Enter the name of the departmental project office or laboratory sponsoring *(paying for)* the research and development. Include address.

13. ABSTRACT: Enter an abstract giving a brief and factual summary of the document indicative of the report, even though it may also appear elsewhere in the body of the technical report. If additional space is required, a continuation sheet shall be attached.

It is highly desirable that the abstract of classified reports be unclassified. Each paragraph of the abstract shall end with an indication of the military security classification of the information in the paragraph, represented as *(TS)*, *(S)*, *(C)*, or *(U)*.

There is no limitation on the length of the abstract. However, the suggested length is from 150 to 225 words.

14. KEY WORDS: Key words are technically meaningful terms or short phrases that characterize a report and may be used as index entries for cataloging the report. Key words must be selected so that no security classification is required. Identifiers, such as equipment model designation, trade name, military project code name, geographic location, may be used as key words but will be followed by an indication of technical context. The assignment of links, rules, and weights is optional.

Unclassified

Security Classification